CHARACTERISATION OF EXTRACELLULAR POLYSACCHARIDES PRODUCED FROM A FUNGAL PATHOGEN OF SUGARCANE

HEIDI DU CLOU
BSc Hons

Submitted in fulfillment of the academic
requirements for the degree of
Doctor of Philosophy in the
School of Chemistry,
University of KwaZulu-Natal.

September 2016

ABSTRACT

The sugarcane fungal pathogen *Phaeocytostroma sacchari* is responsible for sour rot in cane and has been indicated as the producer of sarkaran. Sarkaran has been isolated from poor quality cane affected by drought or frost and is associated with processing problems due its contribution to viscosity. Limited knowledge regarding the structure of sarkaran exists, but it is described as an extracellular polysaccharide (EPS) with a structure similar to pullulan. Incomplete characterisation studies and no physical property investigations have, *hitherto*, been carried out on EPSs produced from *P. sacchari*. The Sugar Milling Research Institute NPC has isolated and identified *P. sacchari* from sugarcane and produced EPSs from this organism under a range of defined conditions. This study explores the structural and physical properties of three EPSs cultured from *P. sacchari* and compares these results with a commercial pullulan and the available literature on sarkaran.

The EPS molecular weights and molecular weight distributions were determined by gel-filtration chromatography with refractive index detection. The monosaccharide composition, absolute configuration and linkage information were established through analysis by gas chromatography-mass spectrometry. The conformation and oligosaccharide repeat units of the biopolymer chains were established by means of one- and two-dimensional nuclear magnetic resonance spectroscopy, as well as with enzymatic hydrolysis and determination by high performance anion exchange chromatography with pulsed amperometric detection. Physical properties explored include the EPS solution behaviour by rheology and the film-mechanical properties by tensile testing.

Structural characterisation revealed that *P. sacchari* EPSs are complex, linear hetero-polysaccharides with molecular weights ranging from 410-1000 kDa. More specifically, the EPSs comprise a variety of α-D-glucopyranose malto-oligosaccharides, predominated by maltotriose and maltotetraose, that are sometimes capped by terminal β-D-mannopyranoses and reducing-end β-D-galactopyranoses. Variations in the *P. sacchari* culture conditions affected the molecular weight distributions, malto-oligomer subunit arrangements, and mannose plus galactose trace component concentrations of the product EPSs. Despite these subtle variations, all the EPSs cultured from *P. sacchari* were found to have essentially the same reported structural features as sarkarans isolated from sugarcane processing matrices.

Physical characterisation revealed that *P. sacchari* sarkarans form structured, shear-thinning solutions of higher viscosity than pullulan as well as clear and transparent films, that are tougher and stronger than pullulan and which are readily plasticised with sorbitol. The differences in *P. sacchari* culture conditions caused subtle structural variations in the sarkarans, which affected both the solution and film-mechanical properties of the EPSs. Hence, tuning the fermentation conditions of *P. sacchari* allows sarkarans with desired characteristics to be produced, which can be tailored for niche applications as either viscosity modifiers, biofilms or bioplastics.

Ultimately, this novel study represents the first comprehensive chemical and physical characterisation of sarkarans produced *in vitro* by *P. sacchari*, and lends new knowledge about a polysaccharide that has plagued the sugarcane industry from time-to-time.

PREFACE

The experimental work described in this thesis was carried out in the School of Chemistry, University of KwaZulu-Natal (UKZN), Durban, the Swedish Institute for Food and Biotechnology (SIK) in Gothenburg, Sweden, and the Chemical Division, Sugar Milling Research Institute NPC (SMRI), Durban. This experimental work was performed from January 2009 to January 2016, under the supervision of Prof. B.S. Martincigh (UKZN).

This study represents the author's original work and has not been submitted in part or in whole for any other degree or diploma to any tertiary institution. Where use has been made of the work of others, it has been duly acknowledged in the text.

Signed: _____

Heidi du Clou
September 2016

DECLARATION 1 – PLAGIARISM

I, Heidi du Clou, declare that

1. The research reported in this thesis, except where otherwise indicated, is my original research.
2. This thesis has not been submitted for any degree or examination at any other university.
3. This thesis does not contain other persons' data, pictures, graphs or other information, unless specifically acknowledged as being sourced from other persons.
4. This thesis does not contain other persons' writings, unless specifically acknowledged as being sourced from other researchers. When other written sources have been quoted, then:
    a. Their words have been re-written but the general information attributed to them has been referenced.
    b. Where their exact words have been used, then their writing has been placed in italics and inside quotation marks, and referenced.
5. This dissertation does not contain text, graphics or tables copied and pasted from the Internet, unless specifically acknowledged, and the source being detailed in the thesis and in the References sections.

Signed: _____

Heidi du Clou
September 2016

DECLARATION 2 – PUBLICATIONS

Publication One

> du Clou H and Walford SN (2010). An introduction to gas chromatography mass spectroscopy for the structure elucidation of polysaccharides from sugar processing streams. *Proceedings of the South African Sugar Technologists' Association.* **83**:392-402.

Publication Two – Refereed Manuscript

> du Clou H and Walford SN (2012). Analytical study of gums found in final molasses from six South African mills for the 2011/2012 milling season. *Proceedings of the South African Sugar Technologists' Association.* **85**:295-311.

Publication Three – Peer Reviewed Manuscript

> du Clou H and Walford SN (2014). A GC-MS study of the structure of gums in South African molasses. *International Sugar Journal*. **116** (1382):105-112.

In all three listed publications, du Clou was responsible for co-developing and executing the research, collecting and analysing the data, and was the lead author in writing up the articles. The carbohydrate isolation, preparation and analysis techniques together with the gas chromatography mass spectroscopy libraries developed for the PhD research were implemented in the research presented in these articles. In the same three articles, Walford was the co-developer of the research and co-author in the writing up of the articles.

Signed: _____

Heidi du Clou
September 2016

TABLE OF CONTENTS

LIST OF SYMBOLS AND ABBREVIATIONS

^{13}C	carbon
1D	one dimensional
^{1}H	proton
2D	two-dimensional
3D	three-dimensional
A	area
Ac	acetyl
BV	bed volume
C	carbon
c	concentration
$CDCl_3$	deuterated chloroform
CH	tertiary carbon
CH_2	secondary carbon
CH_3	primary carbon
COSY	nuclear magnetic resonance correlation spectroscopy
d	doublet
D_2O	deuterium oxide
Da	Daltons
DCM	dichloromethane
dd	doublet of doublets
ddd	triplet of doublets
DEPT	distortionless enhancement by polarisation transfer
DMSO	dimethylsulfoxide
DMSO-d_6	deuterated dimethylsulfoxide
DP	degree of polymerisation
DP3	degree of polymerisation of three/maltotriose
DP4	degree of polymerisation of four/maltotetraose
DP5	degree of polymerisation of five/maltopentaose
DP6	degree of polymerisation of six/maltohexaose
DP7	degree of polymerisation of seven/maltoheptaose
DP8	degree of polymerisation of eight/maltooctaose
DP9	degree of polymerisation of nine/maltononaose
E	Young's modulus
EI	electron ionisation
EPS	extracellular polysaccharide
FID	flame ionisation detector
G'	storage modulus
G''	loss modulus
G^*	complex modulus
Gal	galactose
GC	gas chromatography
GFC	gel filtration chromatography
Glc	glucose
GPa	giga Pascals
GPC	gel permeation chromatography
H	proton
h	height
HCl	hydrochloric acid
HDO	water signal (NMR)
HMBC	heteronuclear multiple bond correlation spectroscopy

HMQC	heteronuclear multiple bond quantum coherence spectroscopy
HPAEC	high performance anion exchange chromatography
HPLC	high performance liquid chromatography
HSQC	heteronuclear single-quantum correlation spectroscopy
IR	infrared
IRF	internal response factor
J	coupling constant
K	consistency coefficient
kDa	kilo Daltons
kPa	kilo Pascals
l	length
l_0	original length
l_f	final length
LVR	linear viscoelastic region
M	mol dm^{-3}
MALDI	matrix assisted laser desorption ionisation
Man	mannose
MeI	methyl iodide
MP	peak-average molecular mass
MPa	mega Pascals
mPa s	milli Pascal seconds
MS	mass spectrometry
ms	mass spectra
mV	millivolt
MW	molecular weight
MWD	molecular weight distribution
m/z	mass-to-charge ratio
M_n	number-average molecular weight
M_w	weight-average molecular weight
M_z	z-average molecular weight
N	number
n	flow index behaviour
N_2	nitrogen
NaOH	sodium hydroxide
NIST	National Institute of Standards and Technology
NMR	nuclear magnetic resonance
NOESY	nuclear Overhauser effect spectroscopy
OAc	acetate
OH	hydroxide
OMe	methoxide/methyl ether
P_2O_5	di-phosphorus pentoxide
Pa	Pascals
PAD	pulsed amperometric detector
PDI	polydispersity index
rad	radians
RF	response factor
RI	refractive index
ROESY	rotating frame nuclear Overhauser effect spectroscopy
RF	response factor
RRT	relative retention time
RSD	relative standard deviation
SEC	size exclusion chromatography

SD	standard deviation
t_1	evolution time
t_2	detection period
t_e	elution time
TIC	total ion current
TLC	thin layer chromatography
TMS	trimethylsilyl
TOCSY	total correlation spectroscopy
UV	ultraviolet
V_{column}	column volume
V_e	elution volume
V_o	void volume
V_t	total permeation volume
W	weight
w_i	weight concentration
ø	diameter
ϕ	dihedral angle
α	alpha
β	beta
γ	shear strain
$\dot{\gamma}$	shear rate
δ	chemical shift or phase angle
$\in$	tensile strain
η	steady-shear or apparent viscosity
$\lvert\eta^*\rvert$	absolute complex viscosity
σ	tensile stress
σ_{M}	maximum tensile stress
σ_y	tensile yield stress
τ_0	yield stress
τ^*	complex stress
ω	angular frequency

ACKNOWLEDGEMENTS

The work detailed in this thesis represents both a significantly challenging, yet deeply rewarding chapter in my academic career. I wish to share my sincerest gratitude to the people and institutions that have contributed to the fulfillment of my PhD degree.

To my supervisor and mentor. I am heartily thankful to my supervisor, Professor Bice Martincigh, for her pearls of wisdom, guidance, and endless support over the years. It is also a pleasure to thank Mr Stephen Walford for mentoring me in many of the analytical techniques that were applied in this study. I am thankful for his faith in me, and for all he has taught me.

To the Nuclear Magnetic Resonance Spectroscopy specialists. Mr Dilip Jagjiven is thanked for all his expertise and assistance with running the NMR experiments, and I am grateful to Dr Maya Makatini for teaching me how to decode two-dimensional NMR spectra.

To the institutions. I am indebted to the SMRI and Dr Janice Dewar for providing me the opportunity and means to undertake this research. I am also grateful to the SMRI and SIK for arranging my visit to conduct analyses at the SIK laboratories in Gothenburg, Sweden, during November-December 2012. I am thankful to Professor Mats Stading of SIK for his expert advice on material characterisation, and to Dr Emma Levenstam Bragd of SIK for mentoring me in the areas of rheology, film preparation and material tensile testing. I am also grateful to all those individuals at SMRI, SIK and UKZN who have assisted me whenever I have needed their guidance.

To my support team. It is a pleasure to thank my dear colleagues Eshara Ramphal, Sanet Nel, Dr Barbara Muir and Dr Katherine Foxon for all their encouragement, assistance, advice and friendship over the years.

To my family. Thank you for your love, patience, understanding and support. This is for you.

The financial assistance of the National Research Foundation (NRF) towards this research is hereby acknowledged. Opinions expressed and conclusions arrived at, are those of the author and are not necessarily to be attributed to the NRF.

Chapter 1
Introduction

Polysaccharides are high molecular weight (MW) carbohydrates that are derived from numerous sources; including, plants, animals, algae and microorganisms (fungi and bacteria) (Lapasin and Pricl, 1995; Yang and Zhang, 2009). They are present in the sugarcane industry, and are associated with sugar processing streams. Sugarcane polysaccharides originate from metabolic processes within the plant or arise due to microbial infection of the cane during harvesting and handling (Bruijn, 1973). Sugarcane polysaccharides include starch, dextran, indigenous sugarcane polysaccharide, Robert's glucan, galactomannan, levans and sarkaran (Imrie and Tilbury, 1972; Kitchen, 1988). Collectively, sugar technologists refer to mixtures of polysaccharides found in processing streams as "*gums*" (Bruijn, 1973). Gums are regarded negatively in the sugar industry. Not only do gums represent a direct loss of recoverable sucrose due to the action of the microbes that produced them, but they also possess physical properties that affect processing and cause a further under-recovery of sucrose. In particular, cane starch, dextran and sarkaran have been linked to increased viscosities and related sucrose losses in sugar processing streams (Cuddihy Jr *et al.*, 2001; Morel du Boil, 2000b; Morel du Boil, 2001; Sahadeo, 1999; Sahadeo, 1998; Sahadeo and Lionnet, 1999). The causes, chemical make-up and effects of cane starch and dextran are well documented and steps to prevent and/or minimise their presence have been instituted in sugar processing practices. For instance, amylase enzymes are dosed in the early stages of sugar processing to reduce starch levels in the raw (unrefined) sugar product (Schoonees, 2004). Dextrans, being of microbial origin, are minimised through reducing delays between harvesting and processing of cane as well as through improved factory sanitation at sugar mills. These practices minimise the action of *Leuconostoc mesenteroides* – the organism identified as a major producer of dextrans in the sugar industry. Furthermore, dextran levels can be minimised by the application of dextranase enzymes (Morel du Boil and Wienese, 2002). Other than dextran and cane starch, other gum polysaccharides are not as well understood, and means for preventing their presence or remedying their effects are not yet available.

In 1966, a polysaccharide first assumed to be similar to dextran (Nicholson and Lilienthal, 1959b) was isolated from the juice of deteriorating cane and further investigated (Bruijn, 1966a; Bruijn, 1966b; Bruijn, 1970). It was established by Bruijn that this was not a dextran, but rather a newly described maltotriose-maltotetraose polysaccharide that he named "*sarkaran*" (Bruijn, 1973). Sarkaran is said to belong to a family of polysaccharides called pullulans (Morel du Boil, 2000a). Pullulans represent a class of polysaccharides predominantly comprising maltotriose repeat oligosaccharides, with variable amounts of maltotetraose interspersed in their structure (Catley *et al.*, 1966; Forabosco *et al.*, 2006). Between 1973–2000, various researchers in the sugar industry further investigated sarkaran, but failed to identify its source (Blake and Clarke, 1984a; Blake and Clarke, 1984b; Blake and Littlemore, 1984a; Blake and Littlemore, 1984b; Bruijn, 1973). It was only in 2005, that the fungal pathogen of sugarcane, *Phaeocytostroma sacchari*, was suggested as the causative agent of sarkaran (Morel du Boil *et al.*, 2005). Sarkaran has been identified from stale cane, stand-over cane as well as burnt cane subjected to post-harvest delays (Blake and Clarke, 1984b; Morel du Boil, 2000a; Morel du Boil, 2006; Morel du Boil *et al.*, 2005). Although sarkaran is mostly associated with the Midlands region of South Africa and was confirmed in various regions of Queensland, Australia (Blake and Clarke, 1984b), more recent monitoring has established its occurrence is widespread. Sarkaran has been identified in all sugar processing streams across the KwaZulu-Natal region and neighbouring countries of South Africa during 1999-2004 (Morel du Boil *et al.*, 2005) and across Jamaica throughout the 2007 milling season at levels between 650-2400 mg kg^{-1} in final molasses (Reece *et al.*, 2008).

Sarkaran, and all the polysaccharides that constitute gums, exhibit physico-chemical properties that negatively affect sugar processing. In particular, dextran and sarkaran both contribute to viscosity in cane processing streams. When the viscosity of sugar processing streams increases, heat transfer is reduced and sucrose crystallisation rates diminish (Morel du Boil, 2000a; Morel du Boil *et al.*, 2005). Hence, sugar technologists investigate gums with the view of prevention and/or elimination from sugar processing streams. On the other hand, many industries exploit polysaccharides for their inherent characteristics (Ge *et al.*, 2009; Lapasin and Pricl, 1995; Yang and Zhang, 2009). Polysaccharides are natural biopolymers that are potentially biocompatible and biologically active – finding favour for specialised applications in the food and medical sectors. Exploitable properties include combinations of gelling, thickening, emulsifying, encapsulating, flocculating, suspending, film-forming and solution stabilising behaviour. Consequently, polysaccharides have also found application in the textile, cosmetics, agricultural, printing, adhesives, coating, paint and oil recovery industries (Dobruchowska *et al.*, 2008; Ge *et al.*, 2009; Lapasin and Pricl, 1995; Ruas-Madiedo and de los Reyes-Gavilan, 2005; Vaningelgem *et al.*, 2004). The discovery of niche applications for any polysaccharide requires a detailed understanding of its structural makeup as well as its useful characteristics.

Polysaccharides are inherently diverse and complex macromolecules. This diversity and complexity makes it challenging to elucidate their structure (Kajiwara and Miyamoto, 2004; Yang and Zhang, 2009). Any elucidation strategy begins with the isolation of the polysaccharide from its source matrix. This process requires one or more steps, to ensure that only the target compound is obtained. The isolate often requires further purification and is subjected to one or more fractionation steps – with the most suitable method selected based on the molecular weight ranges of the isolated polysaccharide (Aspinall, 1982b; Gelders *et al.*, 2003; Janca, 1984; Lindhorst, 2000; Robyt, 1998; Sanz and Martínez-Castro, 2007).

Following the isolation and sufficient purification of the target polysaccharide, structural elucidation and characterisation studies can commence. Traditionally, chemical techniques were used to determine the structure of polysaccharides; including, various total sugar analysis assays, monosaccharide analyses, methylation analyses, periodate oxidation-Smith's degradations, partial depolymerisations (chemical and enzymatic) and fractionation methods (Cui, 2002). Detection in earlier methods relied on ultraviolet (UV) spectroscopy and thin layer chromatography (TLC). The application of these techniques has since been improved upon, or superseded, by the advancement in chromatographic and spectroscopic procedures (Ruas-Madiedo and de los Reyes-Gavilan, 2005; Yang and Zhang, 2009). Modern techniques include the use of:

- high performance anion exchange chromatography (HPAEC) with pulsed amperometric detection (PAD),
- gas chromatography (GC) – especially coupled with mass spectrometry (GC-MS),
- infrared methods such as Fourier transform infrared (FTIR) spectroscopy, and
- one- (1D), two- (2D) and three-dimensional (3D) nuclear magnetic resonance (NMR) spectroscopy.

Together, these various elucidation techniques provide a detailed understanding of a polysaccharide's primary structure. The primary structure of polysaccharides is defined by the (Cui, 2005; Dag, 2005; Kajiwara and Miyamoto, 2004):

- monosaccharide composition (type and ratio),
- monosaccharide ring size, *i.e.*, furanoside (five member) and pyranoside (six member),
- monosaccharide absolute configurations, *i.e.*, dextrorotatory (D) or levorotatory (L),
- monosaccharide sequence,
- glycosidic linkage patterns of both the main chain and branches,
- anomeric configuration of the linkages, *i.e.*, alpha (α) and beta (β), and
- substituents, *i.e.*, any inorganic (or non-carbohydrate) substitutions of the hydroxide (OH) groups.

Depending on the need, an understanding of the primary structure of polysaccharides is important. This need could be for either exploitation or eradication of a particular polysaccharide. For example, cane starch is an undesirable impurity in sugar processing streams. Understanding the primary structure of cane starch led to the development of thermostable α-amylases that are applied in sugar milling streams to reduce starch levels (Schoonees, 2003). Conversely, researchers in the food industry have used the understanding of the primary structure of various starches (*e.g.*, potato, tapioca, *etc*.) to produce a multitude of modified starches with improved qualities (Wurzburg, 2006). The value of a polysaccharide is determined by its qualities, and its qualities are determined by its structure. Valuable qualities of polysaccharides, such as starch and pullulan, include their solution-modifying and film-forming properties.

Morel du Boil and co-workers (2005a), of the Sugar Milling Research Institute NPC (SMRI), have previously isolated and positively identified *P. sacchari* from sugarcane and produced extracellular polysaccharides (EPSs) from this organism (Morel du Boil *et al.*, 2005). EPSs prepared under different shake-flask and bioreactor fermentation conditions from the same *P. sacchari* isolate were subsequently prepared at the SMRI laboratories. Three of the crude EPS isolates were provided for structural, rheological and film-forming property characterisation in this study. The crude EPSs were first examined by gel filtration chromatography (GFC). This technique was used to fractionate one of the crude EPSs into purified fractions. The primary structures of the purified and crude EPSs were determined and compared against each other and against the literature on sarkaran. The physical properties of the *P. sacchari* EPSs investigated include their molecular weights, solution rheological properties, their film-forming capabilities and film-mechanical properties. All the analyses carried out were conducted in conjunction with, and validated against, commercial pullulan. This study set out to explore the variability in both the structure and physical properties of the EPSs produced by this fungal pathogen of sugarcane under different fermentation conditions and to establish a definitive link between *P. sacchari* and sarkaran. This study represents the first comprehensive structure elucidation and physico-chemical study of EPSs produced *in vitro* by *P. sacchari* and lends new knowledge to the sugarcane industry about sarkaran, a gum which plagues the industry from time-to-time.

Chapter 2
Polysaccharides

This chapter introduces the reader to polysaccharides by providing a general definition, basic information on their nomenclature, and describes how they are defined according to their composition and structure; which includes their conformation, configuration, linkage and sequence information. The chapter then concentrates on microbial polysaccharides, discussing their occurrence, industrial importance, production and isolation. Two microbial polysaccharides of highlighted importance include dextran and pullulan.

2.1 Introduction

Polysaccharides are biopolymers composed of more than 10 monosaccharides. Monosaccharides are carbohydrates having the general formula $C_n(H_2O)_n$ and exist as polyhydroxy aldehydes or ketones. The simplest carbohydrates contain three carbons, an aldehyde or ketone group and two OH groups, as illustrated in Figure 2.1. Carbohydrates, such as those depicted in Figure 2.1, have a chiral centre around which the OH group is either to the left (L) or the right (D). D- and L-structures are non-superimposable mirror images, called enantiomers (Robyt, 2012). The absolute configuration of the majority of naturally occurring carbohydrates is in the D-configuration (Stroop *et al.*, 2002). Carbohydrates are either acyclic or exist as furanosides (*f*) or pyranosides (*p*), as illustrated in Figure 2.2 (Lindhorst, 2000).

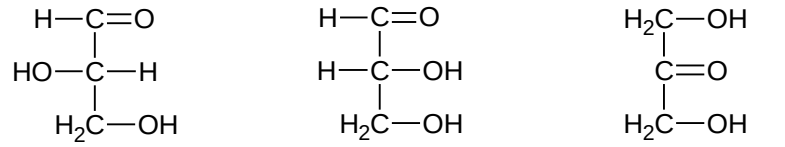

L-glyceraldehyde D-glyceraldehyde dihydroxyacetone

Figure 2.1: Structures of the simplest carbohydrates.

Pyranose structures exist in a chair conformation, with the bulky -CH_2OH group on carbon 5 (C-5). To reduce steric hindrance, this constituent is usually oriented in the more energetically favoured equatorial position in an arrangement known as a $^4C_1$ conformation. In this case, the letter "C" indicates "chair" and the numbers represent which carbon is located either above (superscripted) or below (subscripted) the plane of the chair. This plane is made up of the ring oxygen, C-2, C-3, and C-5 (Lindhorst, 2000). The equilibrium between the $^4C_1$ and $^1C_4$ forms of glucopyranose is illustrated in Figure 2.3.

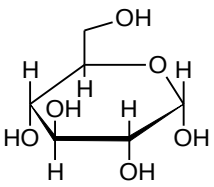

α-D-Glucose
(pyranose)
αGlc*p*

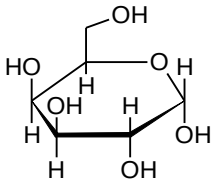

α-D-Galactose
(pyranose)
αGal*p*

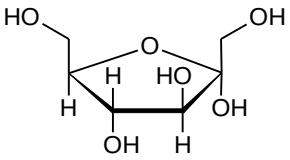

α-D-Fructose
(furanose)
αFru*f*

Figure 2.2: Haworth formulae for some common monosaccharides showing the pyranose (*p*) and furanose (*f*) forms.

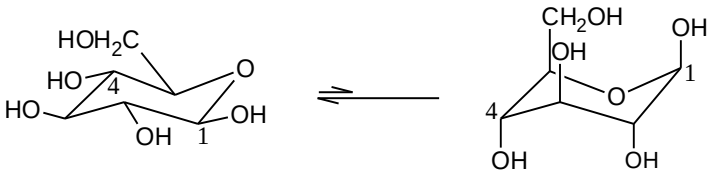

$^4C_1$ $^1C_4$

Figure 2.3: The two chair conformations possible for D-glucopyranose. The equatorial position is more energetically favoured (Lindhorst, 2000).

The remaining OH constituents on a pyranose chair conformer present either axially or equatorially. Isomers of the same pyranoside are distinguishable from the OH in the C-1 position (anomeric carbon). In Figure 2.4, the two anomers of glucopyranose are shown. The α- and β-isomers are distinguished through the stereochemical relationship between the anomeric carbon and the position of the furthest stereogenic centre in the sugar. For glucopyranose, the α-isomer exists when the anomeric OH is axial (or *cis*) at C-1, and the β-isomer exists if the OH presents equatorially (or *trans*) at C-1, with respect to C-5 (equatorial) (Lapasin and Pricl, 1995; Lindhorst, 2000; Robyt, 1998). Figure 2.4 illustrates the mutarotation between these glucose anomers through an acyclic intermediate when in solution (Lindhorst, 2000; Robyt, 1998; Wolf, 2008).

The thermodynamic stability of possible products depends on both the sugar and the solvent system. For example, glucose, mannose and galactose do not form furanoses in water, whereas, arabinose does. The four possible products of arabinose in water are illustrated in Figure 2.5, with α-arabinopyranose having the highest thermodynamic stability (Bhat *et al.*, 2005).

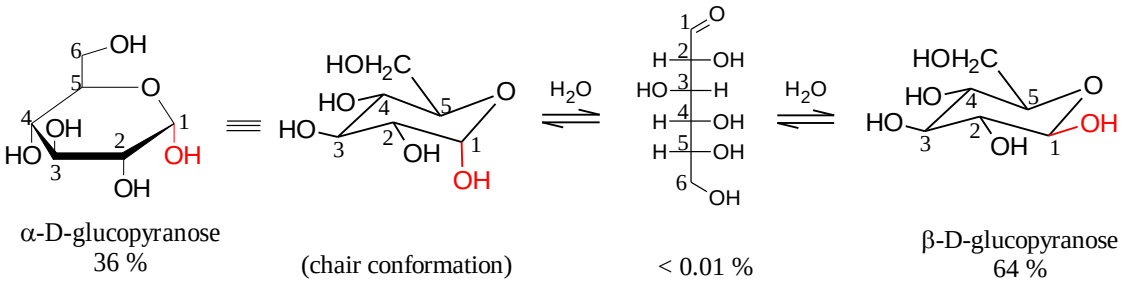

Figure 2.4: Mutarotation equilibrium between the α- and β-anomers of glucopyranose through an acyclic intermediate in an aqueous solution. Some hydrogen atoms have not been shown for clarity. The carbon atoms are labelled 1-5, and the hydroxide group on the anomeric carbon (C-1) is highlighted in red.

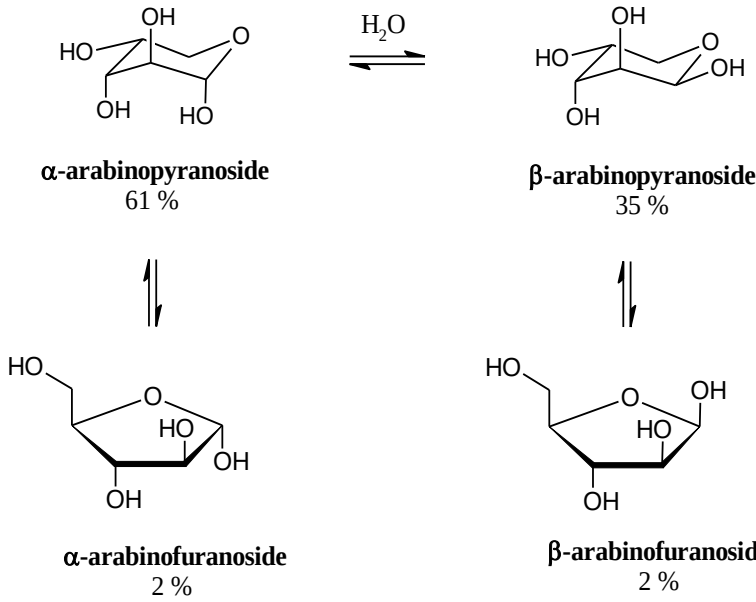

Figure 2.5: The mutarotation between the α- and β-arabinofuranosides and α- and β-arabinopyranosides in water. Note that the acyclic intermediate has not been shown.

When sugar monomers bond they form disaccharides, trisaccharides, oligosaccharides and polysaccharides. For example, sucrose is a disaccharide comprising of glucose and fructose, joined at the C-1 of glucose to the C-2 of fructose. Oligosaccharides consist of up to 10 monosaccharides, and polysaccharides are high MW compounds made up of >10 monomeric sugars.

Polysaccharides vary according to their monosaccharidic composition (*i.e.*, type, ring size and absolute configuration), mode of linkage (α or β), linkage type (*e.g.*, 1,4 or 1,6), and degree of branching (Lapasin and Pricl, 1995; Patamaporn Sukplang, 2000; Robyt, 1998). Figure 2.6 illustrates the types of linkages possible in a hypothetical glucopyranose-type polysaccharide.

In general, polysaccharides consist of between 10 000 to 100 000 monosaccharides, giving rise to substances with MWs that can reach several million daltons (Da). Due to the variety of monomers available, and the differential bonding and branching of monomers possible, polysaccharides compose a very diverse class of compounds. Elucidation of such diversified molecules is challenging, and several techniques are required to determine their structures.

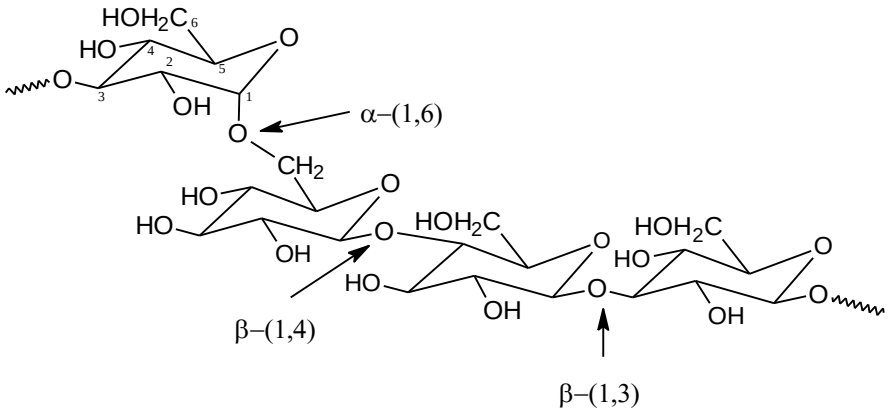

Figure 2.6: Illustration of some of the different linkages possible in a hypothetical polysaccharide comprising of glucopyranoses.

Chapter 3 provides an overview of the various methods used to determine polysaccharide structures, with a particular focus on the methods incorporated in this study to elucidate and characterise the EPSs produced by *P. sacchari*.

2.2 Sources and uses of polysaccharides

This section first provides the reader with a general sense of the ubiquitous nature of polysaccharides and their plethora of uses to man. Then the section focuses on microbial polysaccharide sources and applications, with particular emphasis on dextran and pullulan.

2.2.1 General polysaccharides

Polysaccharides are sourced from plants, microbes (bacteria and fungi), animals, and marine species and their function is either for structure (*e.g.*, cellulose, chitin, *etc.*) or for energy storage (*e.g.*, glycogen, starch, *etc.*) (Aspinall, 1982b; Lapasin and Pricl, 1995; Patamaporn Sukplang, 2000). Polysaccharides have a range of useful physico-chemical properties which lend to their commercial exploitation (Lapasin and Pricl, 1995). They find use in an array of food, pharmaceutical, textile, cosmetic, paint, environmental, oil drilling/recovery, and agricultural applications (Graham, 2008; Kost and Shefer, 1990; Kroon *et al.*, 2008; Lapasin and Pricl, 1995; Patamaporn Sukplang, 2000; Robyt, 1998; Stephen and Churms, 2006).

Polysaccharides that are used in foods and cosmetics must adequately be demonstrated as safe for use under the intended conditions and granted Generally Recognised As Safe (GRAS) status by the Food and Drug Administration in the United States (Bourdichon *et al.*, 2012). In food

products, polysaccharides are used for both processing and preparation. When used as a process aid, a polysaccharide is chosen because it imparts the food product with the correct structure, it acts as an emulsion stabiliser, it increases the product shelf-life, or it increases the products' resistance to melting (*e.g.,* ice-creams). When polysaccharides are chosen to improve the food quality, they usually improve the organoleptic properties of the product (Lopez *et al.*, 2005). For instance, they could be added as a thickening agent to enhance the texture or body of the product. Depending on the chain-chain interactions (tertiary structure), the addition of these polysaccharides can impart a chewy or smooth texture. Sometimes polysaccharides are also added to food to provide non-calorific bulk (Lapasin and Pricl, 1995).

Polysaccharides find favour in the pharmaceutical industry as they are generally biocompatible and non-toxic (Graham, 2008). Pharmaceutical uses for polysaccharides range from simple (bioadhesives) to complex (controlled drug delivery) applications. Pharmaceutical companies have invested extensively into polysaccharide research since the 1960s, which has led to massive diversification of pharmaceutical polysaccharide applications (Lapasin and Pricl, 1995; Prajapati *et al.*, 2013).

In oil recovery applications polysaccharides are exploited for their lubricating and viscosifying properties, taking advantage of their general stability when exposed to high salt concentrations, high temperatures, and the wide pH ranges which are associated with these practices (Baba Hamed and Belhadri, 2009; Lapasin and Pricl, 1995; Robyt, 1998).

Polysaccharides also have favourable gelling, adhesive and film-forming properties. Gelling properties are exploited by the food and cosmetics industries, whilst the paint and paper industries make use of these adhesive properties. The packaging industries exploit certain polysaccharides' film-forming capabilities, especially if the films are impervious to oxygen and moisture (Lapasin and Pricl, 1995).

Whilst the examples of polysaccharides and their important applications are numerous, the following subsection focusses on microbial EPSs, with emphasis on pullulan and dextran.

2.2.2 Microbial polysaccharides

Bacteria and fungi are microorganisms that can produce structural, intracellular or extracellular polysaccharides. Structural microbial polysaccharides, such as murein, are integrated in the bacterial cell wall (Robyt, 1998). Intracellular polysaccharides, such as glycogen, are used for energy storage within the organism (Busuioc *et al.*, 2009). EPSs are excreted to surround the external surface of the cell or the entire organism (Lapasin and Pricl, 1995; Robyt, 1998). EPSs serve a variety of functions including intercellular interactions, adhesion, biofilm formation and cell protection to environmental extremes (Toskoy Öner, 2013). Microbially derived polysaccharides are considerably diverse in composition and structure and used for various applications in many industries (Lapasin and Pricl, 1995; Patamaporn Sukplang, 2000). Microbial polysaccharides are neutral or ionic water-soluble biopolymers that display various rheological and physico-chemical properties. These properties have been exploited for use in drilling muds, wastewater treatment, dredging, detergents, textiles, pharmaceuticals, cosmetics and food products (Singh *et al.*, 2009). Two industrially important microbial EPSs outlined in this section include dextrans and pullulans.

Dextrans

Dextrans are a class of branched polyglucans. Dextran is a bacterial EPS that has a negative association with the beet-sugar, cane sugar, and wine manufacturing industries (Bixler *et al.*, 1953). It is reported that Pasteur investigated dextran as a microbial product in wine as early as 1861 (Pasteur, 1861), however, it was Schiebler who determined its empirical formula $(C_6H_{10}O_5)_n$, and who named the polymeric substance in 1874 (Schiebler, 1874; Jeans, 1977). Dextrans have since been found to be industrially useful due to their viscosifying and flocculating properties (Robyt, 1998). Dextrans are produced by *Leuconostoc mesenteroides*, *Lactobacillus* spp.[1] and *Streptococcus* spp. through fermentation (Mathur and Mathur, 2006; Robyt, 1998). These Gram-positive anaerobic bacteria are capable of producing enzymes which synthesise the EPS from sucrose (Robyt, 1998).

Dextrans are classified as either class-1, class-2, or class-3. They consist of α-1,6-linked D-glucopyranose backbones with either α-(1,2)-, α-(1,3)-, and α-(1,4)-linked branches (Cui and Wang, 2006; Lapasin and Pricl, 1995). The branches can consist of a single glucose monomer or α-(1,6)-linked chains of the D-glucose units (Robyt, 1998). The different classes of dextrans are distinguished by their characteristic branching (Robyt, 1998). A class-1 dextran is depicted in Figure 2.7.

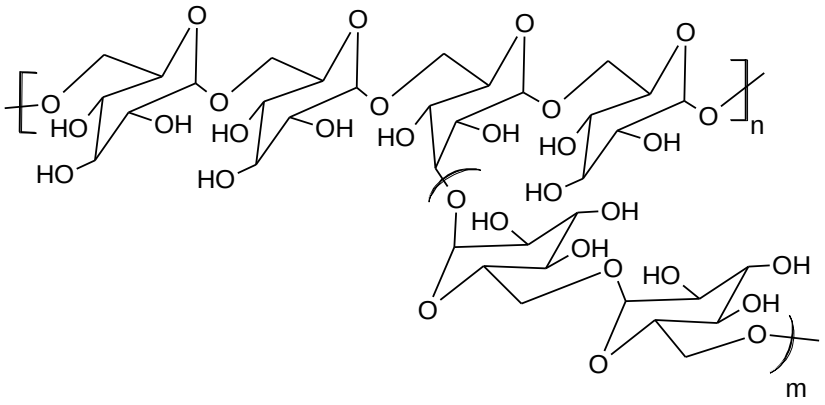

Figure 2.7: Structure of a class-1 dextran with branching at C-3 (adapted from Lapasin and Pricl, 1995).

Dextrans are non-ionic homopolysaccharides (Mathur and Mathur, 2006) which have MWs ranging between 40 Da and several million Da (Cui and Wang, 2006). They are sold according to their average molecular weight distributions (MWDs). Dextran solutions (≤ 50%) are clear and have relatively low viscosities (Cui and Wang, 2006). Dextran finds use in various commercial products, from foodstuffs to pharmaceuticals. This EPS is exploited because of its stabilising, emulsifying and favourable water-holding capacity properties. In confectionary goods, dextran aids in moisture retention and inhibits sugar crystallisation. This polysaccharide has been used in breads to add volume and extend shelf-life and in ice-creams to increase resistance towards heat-shock (Cui and Wang, 2006; Cummins and Sutton, 2005). More commonly, dextran is used as a plasma extender to increase blood volume. Other medicinal applications include tablet binders, water-insoluble vitamin preparation stabilisers and drug taste-

[1] The abbreviation indicates several species in the genus.

masking agents (Cui and Wang, 2006). Dextran is also used in gel filtration chromatography where the porous beads used for the stationary phase are made of derivatised, cross-linked dextran (refer to Section 3.1.2).

Pullulan

Pullulan is a fungal EPS that is produced by certain strains of *Aureobasidium pullulans* (Shingel, 2004). Pullulan is a linear homopolysaccharide comprising of maltotriose units, with a maximum of 7% interspersed maltotetraose units (Robyt, 1998; Shingel, 2004; Singh *et al.*, 2009). Maltotriose is an oligosaccharide with a degree of polymerisation of three (DP3) comprising three α-glucospyranoses joined by two (1,4)-linkages. Maltotetraose is a similar malto-oligomer, with a degree of polymerisation of four (DP4), comprising four α-glucospyranoses linked by three (1,4)-linkages. In pullulan, the maltotriose and maltotetraose repeat oligomers are joined by α-(1,6)-linkages. The representative structure of pullulan is depicted in Figure 2.8 (Delben *et al.*, 2006; Robyt, 1998).

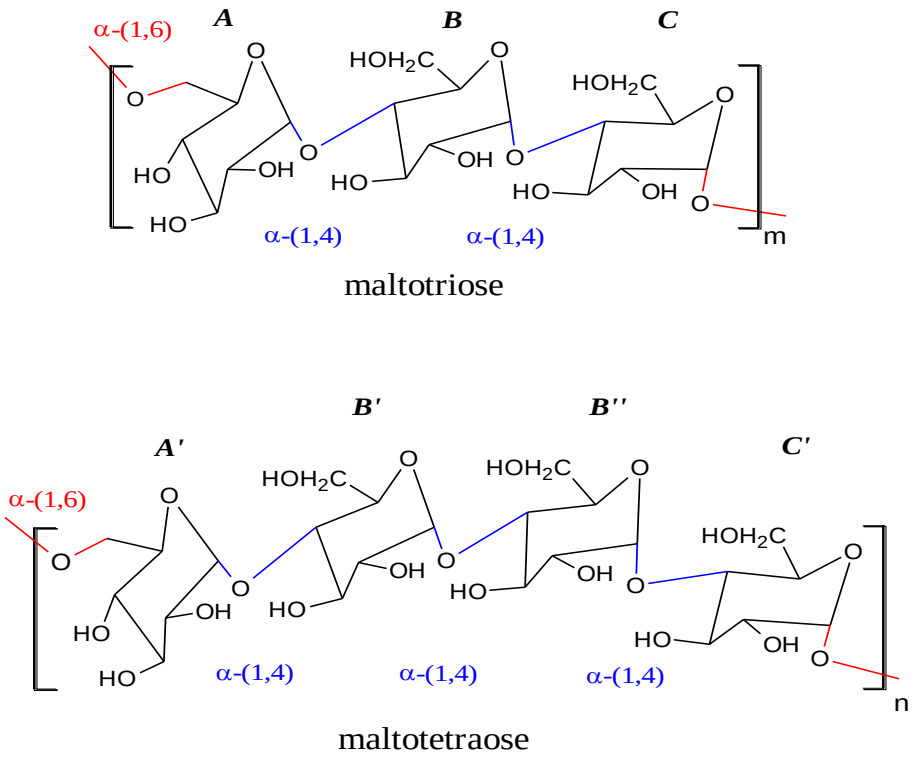

Figure 2.8: A representative structure of pullulan highlighting the α-(1,6)-linkages (red) that join either the maltotriose (A, B and C) or maltotetraose (A', B', B'' and C') repeat units within the biopolymer. Maltotriose and maltotetraose comprise two and three α-(1,4)-linkages (blue) each, respectively (adapted from Delben, *et al.*, 2006).

Over the years, many researchers have found that, depending on the strain of organism and culture conditions used, pullulan can also contain α-(1,3)-, β-(1,3)-, and β-(1,6)-linkages in its backbone (Singh, *et al.*, 2008), as well as galactose (> 5%), traces of mannose (Zajic and LeDuy, 1973) and rhamnose (Wu, *et al*., 2009). Hence, there is no defined unique structure for pullulan (Catley *et al.*, 1986) and it is accepted that the term "pullulan" be used to classify all polymaltotrioses (with or without polymaltotetraoses) produced by various microorganisms. Other microbial sources of pullulans include *Tremella mesenterica*, *Cyttaria harioti*, *Cyttaria darwinii*, *Cryphonectria parasitica*, *Teloschistes flavicans* and *Rhodototula bacarum* (Singh *et al.*, 2008). For example, the pullulan produced by *C. parasitica* is a polymaltotriose EPS that contains substantially high levels of maltotetraose (46-86%) (Delben *et al.*, 2006; Forabosco *et al.*, 2006).

Pullulan has valuable physico-chemical properties including its high water solubility, structural flexibility, and film-forming capabilities. Pullulan's favourable water solubility is different from other linear α-(1,4) polyglucans, such as amylose. This property arises due to the (1,6)-linkages which afford the chain with more flexibility. Pullulan is able to form non-gelling, stable and viscous aqueous solutions (Robyt, 1998). This EPS also forms transparent, colourless and tasteless films which are non-toxic and edible, and used in flavoured mouth patches used to kill plague-producing gums, and promote oral health (Dixon *et al.*, 2006; Singh *et al.*, 2008). Pullulan films are clear, biodegradable and impermeable to oxygen – finding use as coating and packaging materials for dried foods and pharmaceuticals (Dixon *et al.*, 2006; Robyt, 1998; Singh *et al.*, 2009). In the pharmaceutical and biomedical sectors, pullulan and pullulan derivatives find use in tissue engineering and grafting applications, as a carrier for drug and gene delivery, in nanotechnology for medical imaging, in carbon nanotube formulations, as a mucoadhesive ophthalmic vehicle, and as a plasma extender (Prajapati *et al.*, 2013). Some of the numerous food and pharmaceutical applications and related physical properties of pullulan are listed in Table 2.1. The main quality parameters of pullulan are summarised in Table 2.2 (Shingel, 2004; Singh *et al.*, 2008).

Whilst the industrial applications of pullulan and pullulan derivatives are valuable and numerous, maximised use is constrained by the high cost of production of this biopolymer. Pullulan currently costs in the region of three times more than other industrially important polysaccharides, such as dextran. This is primarily due to the additional downstream processing required to remove unwanted melanin pigments[2]. Avenues of pullulan utilisation can only be opened once production strains are improved and/or if engineering innovations can help reduce the costs of pullulan production and purification (Singh *et al.*, 2008).

[2] Melanins are dark brown to black macromolecules produced as metabolites by various microorganisms, including fungi and bacteria. Melanins are produced by microorganisms for antioxidative or other protective reasons via an oxidative polymerisation of phenolic/indolic compounds within fermentation culture media (Manivasagan *et al.*, 2013).

Table 2.1 Food and pharmaceutical applications and related physical properties of pullulan.

Industry	Property
Food	
Dietary fibre	Resistant to mammalian amylases.
Prebiotic	Promotes beneficial bifidobacteria growth.
Dietetic snack	Human enzymes gradually hydrolyse pullulan to glucose. It is a low calorie additive.
Starch replacement	Imparts similar properties to solid and liquid foods including consistency, moisture retention, dispersion, *etc*.
Improve shelf life	Superior water retention properties versus starch.
Films, coatings and packaging	Film forming with oxygen-impermeability and excellent mechanical strength.
Pharmaceutical	
Denture adhesive	Pullulan derivatives have high water solubility and low moisture resistance.
Tablet preparations	Enhances tablet strength without disrupting the disintegration time.
Sugar-coating preparations	Enhanced impact strength and oxygen impermeability.
Oral care products	Film forming, edible and effective plaque-producing gum killers.
Capsules	Soluble, biocompatible films.
Cosmetics, lotions and shampoos	Non-toxic, non-irritating as well as water solubility, moisture absorptivity and tackiness.

Table 2.2 Main quality parameters of pullulan (Singh *et al.*, 2008).

Parameter	Specification
Appearance	White or yellow-white powder
Water solubility at 25 °C	Easily soluble
Specific optical activity $[\alpha]D_2O$ /1% in water	Maximum +160°
Polypeptides /%	Maximum 0.5
pH of solution	5-7
Mineral residue-ash (sulfated) /%	Maximum 3
Moisture (loss on drying) /%	Maximum 6
Molecular weight (range) /kDa	100-250

D_2O = deuterated water, kDa = kilo daltons

2.3 Production of extracellular polysaccharides

EPSs of commercial importance are produced on an industrial scale via fermentations of microorganisms. These microorganisms are typically bacteria, for example, *Leuconostoc* to produce dextran. Industrial use of fungal species, such as *Aureobasidium* to produce pullulan, is still fairly limited (Cheng *et al.*, 2011). Substrates used in industrial fermentations include sugars, syrups, molasses, fruit and vegetable pomace, lignocellulosic biomass, *etc.* (Toskoy Öner, 2013). Fermentation strategies include batch, fed-batch or continuous production. The latter two strategies allow the nutritional and environmental requirements of the microorganism to be carefully controlled (Kim *et al.*, 2006b; Toskoy Öner, 2013). Often variables such as temperature and pH can influence whether biomass or EPS production is favoured by a particular producer-strain of a microorganism. For successful fungal fermentations, the growth characteristics and physiology of the microorganism must be well understood (Papagianni, 2004). Filamentous fungi grown in submerged cultures can exhibit different morphologies, from dispersed mycelial filaments to dense mycelial pellets. This morphology depends on the fungus genetics, the nature of the inoculum, the growth medium constituents (nutrition) and the environmental conditions (temperature, pH, aeration and mixing) (Kim *et al.*, 2006a; Papagianni, 2004; Prajapati *et al.*, 2013). Often, a particular fungal morphology is required to achieve maximum production of the metabolite. In general, EPS fermentations are challenging as the production process often gives rise to highly viscous broths that cause problems with mixing, aeration, oxygen supply and heat transfer. These difficulties can also affect differences in the desired EPS product (Guillouet *et al.*, 1999; Kim *et al.*, 2006a; Toskoy Öner, 2013). This is a common problem in pullulan production (Cheng *et al.*, 2011).

Fermentations, on both a laboratory and industrial scale, use culture media that are designed to optimise the desired metabolite product. Media development and small-scale fermentations are usually carried out in shake-flasks, whilst large-scale and industrial fermentations generally involve fed-batch cultures. Drawbacks with the shake-flask approach include limited control over the dissolved oxygen available and limited control and monitoring of the culture pH. The fed-batch approach allows for larger-scale fermentations, where process variables can be monitored and controlled. In this strategy, the microorganism biomass is generally first established and then one or more nutrients are added to promote product formation (Papagianni, 2004). In the case of EPS production, the culture media generally contain a large carbon to nitrogen ratio. The carbon provided by the substrate is utilised for growth, whilst the nitrogen serves to limit this growth (Sutherland, 1996). Since the nutrients required for product formation may inhibit growth if added in high concentrations at the start of fermentation, adding these later may potentially extend the growth and product formation periods in a fed-batch approach (Kim *et al.*, 2006b).

The three EPSs investigated in this study were produced under two different sets of culture conditions in either shake-flasks or a bioreactor. The microorganism used in these preparations was from the same, positively identified *P. sacchari* isolate that was described by Morel du Boil and co-workers (2005a). The three EPSs were coded FB2, PB2 and PB7. PB2 and PB7 were cultured in shake-flasks, whilst FB2 was cultured under different conditions in a bioreactor. Following cultivation, these EPSs were isolated from their culture media and characterised. Techniques for isolating polysaccharides from culture media are discussed in the next section.

2.4 Isolation of cultivated extracellular polysaccharides

The isolation of any material is carried out in order to obtain a sufficient amount which is as chemically pure as possible (Aspinall, 1982b). The isolation of polysaccharides is complicated by the fact that they are often amorphous and cannot be recrystallised (Lindhorst, 2000). Instead, the isolation of polysaccharides will depend on the source, other materials present in the cultivation medium, as well as the polysaccharide's solubilisation properties (Robyt, 1998). This section looks specifically at methods used for isolating microbial EPSs.

The method chosen to isolate polysaccharides may depend on the type of polysaccharide present, the extent of degradation permissible, and the other materials present in the medium (such as lipids, proteins, nucleic acids, and other polysaccharides) (Ruas-Madiedo and de los Reyes-Gavilan, 2005). In general, a method is chosen to obtain polysaccharides in soluble form so that fractionation methods can then be applied (Aspinall, 1982b). For isolating microbial EPSs, the first step involves removal of the microbial cells (fungi, bacteria, yeasts, etc.) from a culture medium by centrifugation. The second step involves isolation of the EPSs through dialysis or selective precipitation. Dialysis separates the EPS from the culture medium by use of a semi-permeable membrane, whereby, the EPS molecules diffuse through the membrane to a water compartment. The isolated EPS is then freeze-dried (lyophilised) (Ruas-Madiedo and de los Reyes-Gavilan, 2005). EPS precipitation from the culture medium is carried out using a water miscible alcohol (such as ethanol) and/or acetone. Precipitation can be followed by dialysis to further purify the sample (Dobruchowska *et al.*, 2008; Van Geel-Schutten *et al.*, 1999; Vaningelgem *et al.*, 2004). Often an additional purification step is required to remove residual protein and other non-EPS components from the culture. This is achieved by treatment with variable amounts of trichloroacetic acid (TCA) (final concentrations between 4-14%) and/or by digestion with proteases before precipitation. This additional precipitation step is important if the EPS is to have a full physico-chemical evaluation done (Ruas-Madiedo and de los Reyes-Gavilan, 2005).

Once isolated, the crude EPSs are further separated (fractionated) into individual polysaccharide components. This is best achieved through fractionation by chromatographic techniques (refer to Section 3.1). In this study, the provided EPSs were isolated from their cell-free culture media with an acidic-alcohol precipitation method, similar to that used by Morel du Boil (2000a). One of the EPSs (FB2) was fractionated by size exclusion chromatography (SEC) into three further components. The crude and fractionated EPSs were structurally elucidated and their solution rheology, film-forming and film mechanical properties determined and compared. The next chapter provides background to the elucidation and characterisation strategies carried out on the isolated EPSs, beginning with fractionation. The corresponding experimental details are found in Chapter 4.

Chapter 3
Techniques for polysaccharide elucidation and characterisation

There are a number of useful analytical methods for the fractionation and determination of the composition, structure and physical properties of polysaccharides. Detailed polysaccharide characterisation requires the application of several complimentary analyses. This chapter provides a background to the techniques applied in this study to characterise the EPSs produced from *P. sacchari* in both shake-flask (PB2 and PB7) and bioreactor fermentations (FB2).

3.1 Gel filtration chromatography

As outlined in Section 2.4, a polysaccharide can be isolated from its cell-free fermentation medium through an alcohol precipitation method. Since this is a non-specific isolation method, the precipitated product could consist of a number of polysaccharides of various MWs. Therefore, a method is required to fractionate such a product into its different polysaccharide components. One such method is SEC. This section will discuss the types of SEC possible, the column packing materials available, as well as the methods of packing, evaluating and calibrating such columns. The additional benefit of this purification technique is that MWs and MWDs can be determined. These determinations will also be discussed.

3.1.1 Introduction

SEC is a useful technique for both the preparation and purification of biological substances. This technique is also useful in determining the MW and MWDs of natural and synthetic macromolecules such as polysaccharides (Stulík *et al.*, 2003). SEC is a liquid chromatographic technique that separates high MW components with a hydrophobic or hydrophilic packing material in a column (Skoog *et al.*, 2004). In general, SEC with hydrophobic packing materials is referred as gel permeation chromatography (GPC), whilst the use of hydrophilic packing media is known as gel filtration chromatography (GFC) (Mori and Barth, 1999; Skoog *et al.*, 2004).

Separation in SEC is achieved based on a substance's molecular size and dimensions in solution relative to the pores in the column media (Churms, 1996; Stulík *et al.*, 2003). Separation is effected by dissimilar molecules having steric differences, thus affording them varying degrees of access to the matrix pores in the column media (Hagel, 1998). Figure 3.1 illustrates the separation of a sample mixture of large to small molecules. The large molecules (yellow) cannot penetrate the polymeric bead pores and elute first. A totally excluded solute will elute in the void volume (V_o). Intermediate size molecules (green) traverse the column sampling both the voids and the matrix pores, and elute in the selective permeation elution volume (V_e) (Determann, 1969; Pryde and Gilbert, 1979). The smallest molecules (pink) are able to fully penetrate the matrix pores, allowing a longer residence time in the column, and eluting last in the total permeation volume (V_t) (Barth, 2003).

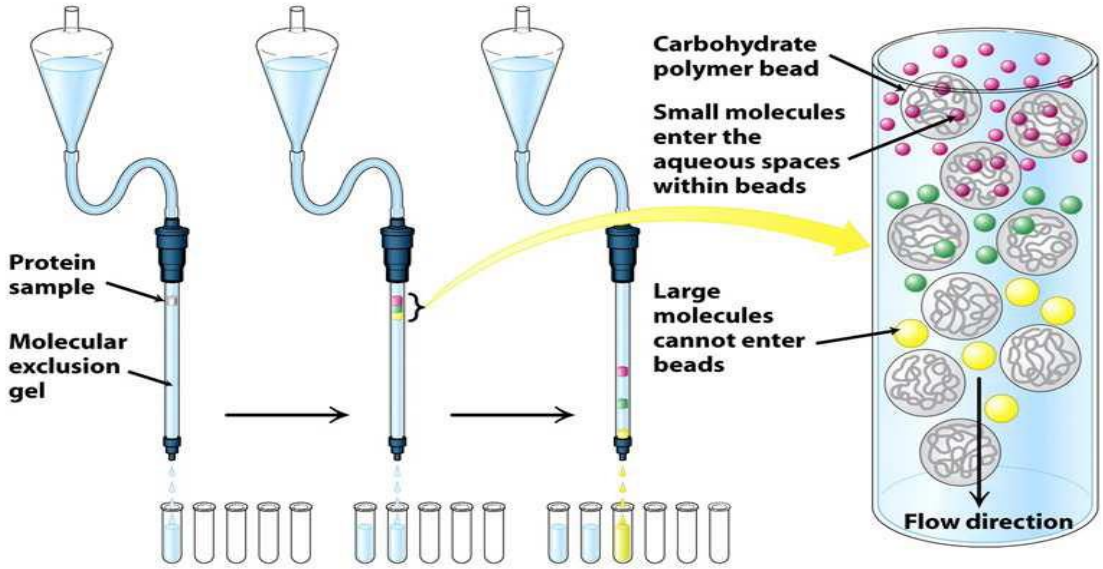

Figure 3.1: Schematic diagram illustrating the principle of how separation of high MW molecules from lower MW molecules is achieved in SEC (Berg *et al.*, 2002).

Since separation in SEC is based on molecular size, conclusions about MW and MWDs are possible. To ensure that the relationship between the solution MWs of the solutes and the output of the system are well-defined and reproducible it is important to consider the type of packing media to be used as well as the column dimensions and packing density. For the packing media, the particle size, -shape, -pore size and -pore volume is considered. For the column bed, the bed width, -height and -density are important. As such, the porous packing media selected should have sufficiently small pores in relation to the void volume. These particles should also be small and regular so that a long, narrow, densely packed column bed is achievable. These considerations are important for maximising separation resolution. Furthermore, unwanted solute and column media electrostatic and hydrophobic interactions must be avoided. These interactions are minimised through altering both the stationary and mobile phases. There are a variety of stationary phases available, which have compositions ranging from modified polysaccharides such as cross-linked dextran (Sephadex®), and highly cross-linked agarose (Superose®), to copolymer gels made from methacrylate (Toyopearl®) (Stulík *et al.*, 2003). The choice of mobile phase will depend on the packing material chosen, and the analytes to be separated. The mobile phase must not interact with the stationary phase, should not denature the analyte, and should suppress hydrophobic interactions between the analyte and the packing media. Three parameters that can be altered in the mobile phase include the pH, the ionic strength and organic additives. The compromise, however, is that any changes in the eluent will affect the hydrodynamic volumes (shape and size) of the solutes, and may affect the column media. In turn, this will influence conclusions drawn on the solute MWs (Stulík *et al.*, 2003). Once all the parameters have been considered, the column has been packed with the chosen media, and the chosen mobile phase is eluted with a reproducible flow, the solute is introduced onto the column (1-4% bed volume, BV) (Hagel, 1998). The column then separates the components into fractions that are collected for further analysis.

There are two approaches for MW and MWD determination by SEC. Either the MW information is derived from the retention of the solutes against calibration of the column with similar standards, or mass spectroscopic detectors can be employed. In-line detectors can measure certain properties of eluting analytes, such as the refractive index (RI), the viscosity, or light scattering. The detector responses and related calibration data enable the MW and MWD of the solutes to be derived (Determann, 1969; Stulík *et al.*, 2003).

In general, SEC coupled with in-line detection, has become a popular chromatographic technique for the purification and determination of the MWs and MWDs of both oligosaccharide and polysaccharide samples (Forabosco *et al.*, 2006; Sanz and Martínez-Castro, 2007; Simas *et al.*, 2008; Yau *et al.*, 2009). SEC was used in this work to determine the MW and MWD of pullulan and all the *P. sacchari* EPS samples. One EPS sample (FB2) was also further purified by this method. The following section discusses the choice of column packing material used in this study, and Section 3.1.4 further explains the how such MWD determinations are made with SEC.

3.1.2 Packing materials

There are several choices available for selecting suitable column media for SEC. In this study, Toyopearl® HW-65F was used. This is a hydrophilic, fine grade (45 µm particle size, 1000 Å pore size) resin comprising a modified hydroxideated methacrylate copolymer which is suitable for the purification of proteins, peptides, nucleic acids and polysaccharides (Anonymous, 2008; Anonymous, 2004). In particular, HW-65F can efficiently resolve dextrans in the MW region of 1000 Da to 1 million Da (Anonymous, 2008). This resin is pH stable (pH 2-13), has good mechanical stability ($\leq$ 700 kPa) and a narrow particle size distribution. These attributes are required for high performance SEC. This resin is also chemically stable against organic solvents, can be used over a range of temperatures (2-60 °C), and offers negligible packing volume changes even under various salt concentrations (Anonymous, 2008).

3.1.3 Packing parameters for Toyopearl® resins

Several steps are required prepare a Toyopearl® column correctly. These steps include de-fining, equilibrating and carefully packing the resin into the column. The resin is packed under constant velocity, semi-constant pressure or assisted gravitational settling methods. The packed column then has to be evaluated, before it can be calibrated and used in SEC analyses. For more details on these packing parameters and column evaluations, refer to Appendix A.

3.1.4 Column calibration and molecular weight determinations

Polysaccharides are generally polydisperse compounds that exhibit a broad range of MWs. Hence, information regarding their composition and molecular size is generally obtained as averages (Aspinall, 1982a). Polysaccharide MW information is determined through either absolute or relative techniques. Absolute techniques do not make suppositions regarding the molecular conformation of the substance, and do not require any calibration with standards. Such techniques include osmometry, static light scattering, equilibrium settling and mass spectrometry. On the other hand, relative techniques rely on assumptions around molecular conformation, and known standards need to be used for calibration purposes. MW determination of polysaccharides by relative methods include: dynamic light scattering, velocity settling, viscometry and SEC (Section 3.1.1) (Wang and Wood, 2005).

SEC it is the only method that allows a compound's complete MWD, including all the statistical averages defining the distribution, to be determined (Mori and Barth, 1999; Skoog *et al.*, 2004; Stulík *et al.*, 2003). These are important determinations for polydisperse substances like polysaccharides (Stulík *et al.*, 2003). These determinations are possible because the V_e of a

substance is proportional to its average solvated MW. Since the total volume required for an analyte to elute remains consistent on the same column, the MW of an unknown can be determined relative to the correlation between its V_e against a set of suitable standards (Determann, 1969). The major pitfall of this method is the assumption that the calibration standards and the polysaccharide samples have the same structure, hydrodynamic volume, and behaviour in the solvent system (Meunier, 1997). Yet, SEC is the only relative technique that allows all the MW statistical averages of a compound to be determined.

Calibration

Column calibration for the SEC analysis of polysaccharides is carried out with a series of different molecular weight pullulan or dextran standards. The V_e values for each standard are used to construct a standard reference curve as depicted in Figure 3.2 (Mohsen *et al.*, 2007; Patamaporn Sukplang, 2000). The analyte solution is then passed through the same column, under the same conditions, and the solute V_e is used to determine the relative MW from the calibration curve.

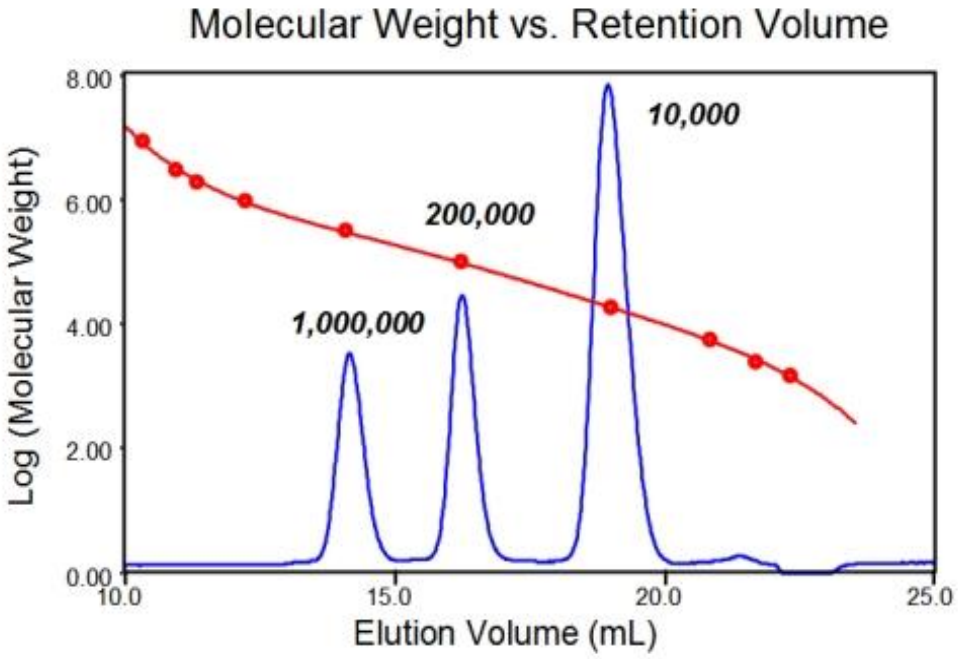

Figure 3.2: Plot showing the correlation between V_e of the peaks for each standard and the corresponding points on the calibration curve (Anonymous, n.a.).

Molecular weight determinations

The MW and molecular size of macromolecules affect the bulk physical properties. In-turn, the mechanical, solution and bulk properties of the material affect the processing and end-product performance. Table 3.1 lists polymer properties influenced by MW or MWDs. Polymers do not have discrete MWs. Instead, they are composed of a mixture of discrete compounds that have different MWs. The grouping of these components makes up the characteristic MWD for that

polymer. Calculation of the statistical averages of these distributions allows for the MWD of such polydisperse substances to be defined (Mori and Barth, 1999).

Table 3.1 Polymer properties influenced by molecular weight (adapted from Meunier, 1997).

Property	
Impact strength	Impact resistance
Melt viscosity	Melt flow
Brittleness	Hardness
Flex life	Pliability
Stress-crack resistance	Glass-transition temperature
Tensile strength	Tear strength
Tackiness	Creep strain
Gas permeability	Compression
Fatigue	Wear

SEC offers a relative technique where the MW, MWD and the MWD statistical averages of polydisperse samples can be determined. The MW provided from the SEC distribution data is more correctly the peak-average MW (MP). The three main statistical averages that can also be determined from SEC data include the number-average MW (M_n), the weight-average MW (M_w), and the z-average MW (M_z). These averages are identified in Figure 3.3 and defined according to Equations 3.1-3.3.

$$M_n = \frac{\sum_i N_i M_i}{\sum_i N_i} = \frac{\sum_i W_i}{\sum_i W_i/M_i} = \frac{\sum_i h_i}{\sum_i h_i/M_i} = \frac{1}{\sum_i w_i/M_i} \tag{3.1}$$

$$M_w = \frac{\sum_i N_i M_i^2}{\sum_i N_i M_i} = \frac{\sum_i W_i M_i}{\sum_i W_i} = \frac{\sum_i h_i M_i}{\sum_i h_i} = \sum_i w_i M_i \tag{3.2}$$

$$M_z = \frac{\sum_i N_i M_i^3}{\sum_i N_i M_i^2} = \frac{\sum_i W_i M_i^2}{\sum_i W_i M_i} = \frac{\sum_i h_i M_i^2}{\sum_i h_i M_i} \tag{3.3}$$

where M_i is the MW, and N_i and W_i are the respective number and weight. The subscript i represents all the MWs present in the fraction. When a mass-sensitive detector (such as a RI detector) is used in SEC, the detector response is proportional to the weight concentration (w_i). Since the detector response of the baseline subtracted height of any slice, h_i, is equal to w_i, the third (Equation 3.1 and 3.2) or fourth (Equation 3.3) term in each equation can be used (Gavilan, 2002; Meunier, 1997).

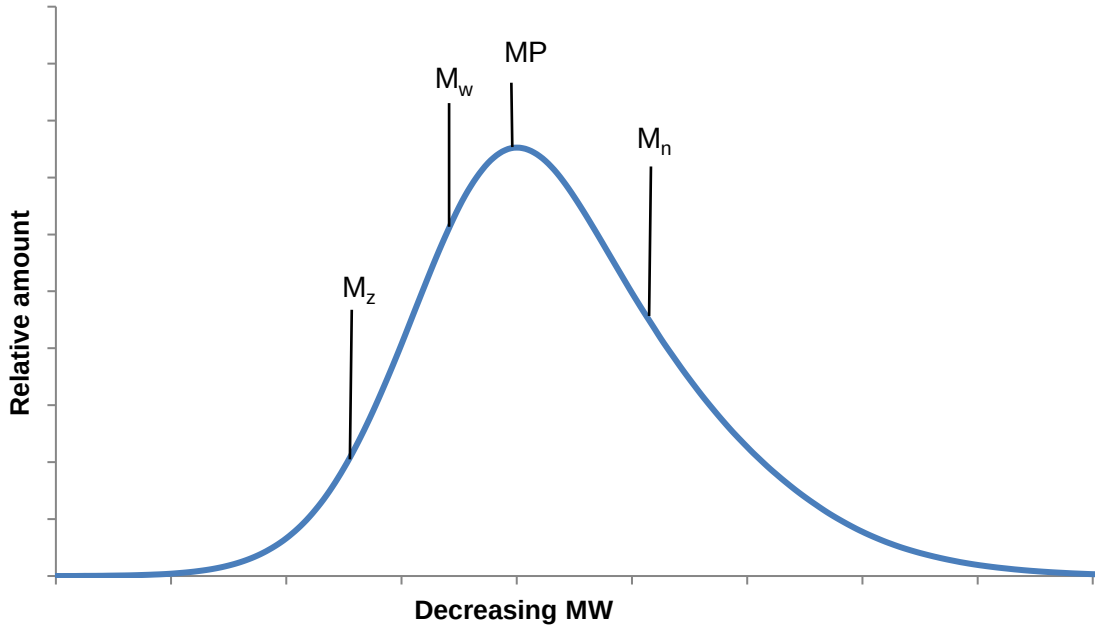

Figure 3.3: An example of a MWD of a polysaccharide showing the relative locations of the statistical moments in relation to the peak-average MW (MP).

Once these statistical averages have been established, the polydispersity index (PDI) of the polymer can be determined by the ratio of M_w:M_n. The higher the PDI the more varied the MWD. If a polymer had a PDI equal to unity, it would consist of a single MW component and it would be classified as monodisperse (Meunier, 1997). The MWD statistical averages are useful in providing insights into a polymer's properties. For instance, M_n relates to brittleness, compression and flow properties, M_w relates to properties of strength (*e.g.*, tensile strength and impact resistance) and the M_z value describes flexibility and elongation properties (Levin, 2002).

In this study, dextran standards were used to equilibrate a Toyopearl® GFC column. The calibration, MW and MWD statistical averages of pullulan were validated, and these values for the *P. sacchari* EPS samples were determined. Where possible, comments on the MWD statistical averages and the EPS physical properties are made. Refer to Section 4.1 for the experimental details, Appendix B for the calibration results, and Chapter 5 for these results.

3.2 Gas chromatography

The previous section describes SEC as a method used to determine the MW data and to further purify isolated polysaccharides. This section details the use of GC to determine the composition and various structural aspects of polysaccharides. Also outlined are the various methods by which polysaccharide samples are treated prior to GC analysis, with emphasis on the methods used to determine the composition and structure of the *P. sacchari* EPSs investigated.

3.2.1 Introduction

Gas chromatography is a method used to separate volatile, thermally stable compounds from one another (Ismail and Nielsen, 2010; Qian *et al.*, 2010). Compounds that do not satisfy these criteria need first to be derivatised. In order to analyse large molecules by GC, they must be appropriately depolymerised and chemically derivatised (Courtin *et al.*, 2000). Before suitable carbohydrate derivatisation methods were devised, the tedious technique of paper chromatography was used to determine their hydrolysate products (Aspinall, 1982a; Hepper, 1972; Smith *et al.*, 1957). Nowadays, GC is routinely used for the high-resolution analysis of polysaccharide structures; enabling the composition, absolute configurations and linkages within their structure to be determined against authentic standards (Aspinall, 1982a; Bleton *et al.*, 1996; Carpita and Shea, 1988; Ciucanu and Caprita, 2007; Gerwig *et al.*, 1978).

Depolymerisation and derivatisation

In order for polysaccharides to undergo GC analysis, they must first be suitably depolymerised and subsequently derivatised. Depolymerisation comes about through cleavage of the glycosidic bonds. This is achieved by enzymatic digestion or acid-catalysed hydrolysis (Aspinall, 1982a; Dag, 2005; Laine *et al.*, 2002; Neeser and Schweizer, 1988; Vuorinen and Alen, 1999; Willför *et al.*, 2009). Polysaccharide enzyme digests are generally analysed by high performance liquid chromatography (HPLC) techniques, for example, by separation on an HPAEC column followed by detection with a PAD (HPAEC-PAD) (refer to Section 3.4) (Willför *et al.*, 2009). On the other hand, acid hydrolysates may also be analysed by GC techniques, provided they are first suitably derivatised. Three possible carbohydrate derivatisation techniques include permethylation, acetylation (acetyl, Ac) or silylation (trimethylsilyl, TMS) (Dag, 2005; Laine *et al.*, 2002).

Derivatisation of acid hydrolysates (including methanolysates)

Polysaccharides can be hydrolysed via mineral or organic acids, or via acid-catalysed methanolysis reactions (Aspinall, 1982a; Svensson *et al.*, 1975). The arising hydrolysates, or methanolysates, require derivatisation prior to GC analysis. The resultant derivatives are identified and quantified by comparing their GC retention times and detector responses against similarly prepared standards. Depending on the carbohydrate derivative formed, one or several peaks arise in the GC chromatogram. Carbohydrates mutarotate to different degrees in different solvents, with derivatisation causing either one, some, or all of the possible isomers and epimers to be retained (refer to Chapter 2 for further detail) (Bhat *et al.*, 2005; Wolf, 2008). Consequently, the more epimers retained, the more complex the arising GC chromatogram. Polysaccharides of diverse composition can give rise to very complex GC chromatograms, depending on the choice of preparation and derivatisation of their hydrolysates. The number of possible derivative peaks appearing in a GC chromatogram may be minimised by appropriate preparation prior to derivatisation. For instance, the carbohydrate hydrolysates can be reduced to alditols or oximated to oximes prior to derivatisation. Alditols form when carbohydrates are reduced with sodium borohydride ($NaBH_4$) (Abdel-Akher *et al.*, 1951; Rumpel and Dignac, 2006). During this

reduction, cyclic monosaccharides are converted to acyclic alditols thus preventing epimers[3] from forming during derivatisation. Reduction provides the simplest GC chromatograms, as only one peak arises per alditol derivative (Vuorinen and Alen, 1999). A hydrolysis-reduction-derivatisation procedure is illustrated in Figure 3.4.

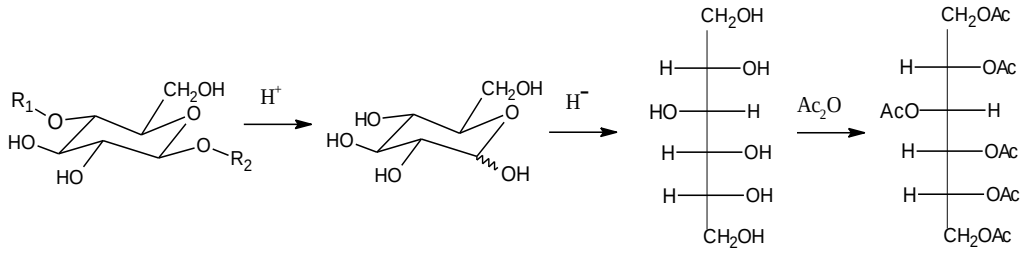

Figure 3.4: Acid hydrolysis (H^+) of a polysaccharide followed by reduction (H^-) and acetylation (Ac_2O) allows the composition to be determined with simplified GC chromatograms. R_1 and R_2 are any remaining carbohydrate chains that compose the polysaccharide (Dag, 2005).

The downside of producing alditols is that the identification of certain carbohydrates can be mistaken. For instance, certain ketoses (*e.g.*, glucose) and aldoses (*e.g.*, fructose) give rise to the same alditols (*e.g.*, sorbitol), making it difficult to unambiguously identify the original sugar (Neeser and Schweizer, 1988). Alternatively, carbohydrates are oximated prior to derivatisation with a reagent such as hydroxideamine hydrochloride ($NH_3OH^-Cl^+$). The resulting oximes give rise to two peaks each in a GC chromatogram: one each for the *syn*- and *anti*-isomers. An oximation-derivatisation reaction is illustrated in Figure 3.5 (Shaffler and Morel du Boil, 1984).

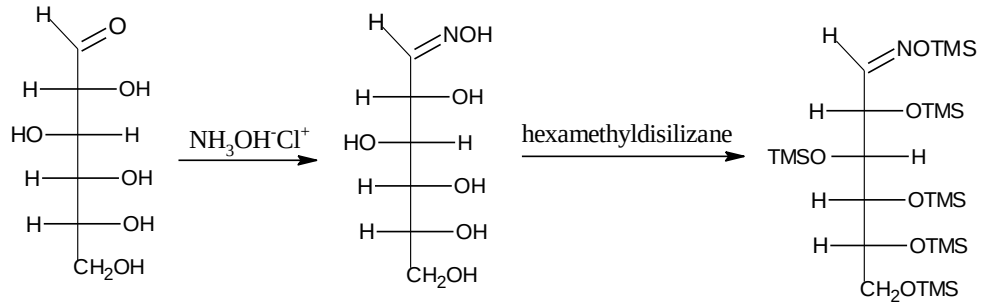

Figure 3.5: Oximation of glucose followed by silylation will provide one peak each for the *syn*- and *anti*-isomers in a GC chromatogram.

Figure 3.6 illustrates the varying GC chromatogram complexity for an equivalent mixture of monosaccharides that have undergone three different treatments before silylation.

[3] Epimers are anomers that arise through mutarotation.

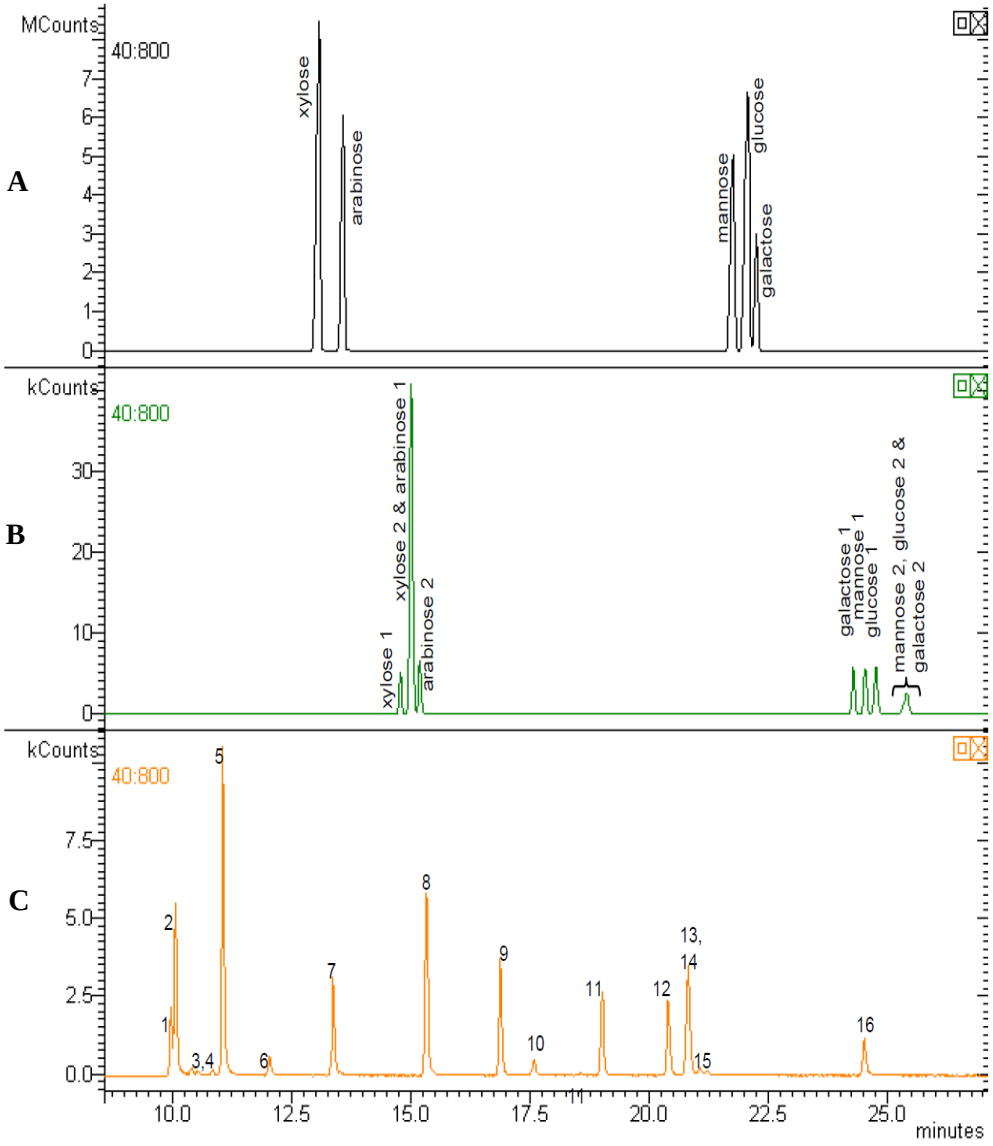

Figure 3.6: The varying complexity of GC chromatograms arising from different preparations of mixtures containing five monosaccharides each is illustrated. Only single monomer peaks appear for sugars reduced before silylation (A). Sugars that are oximated then silylated (B) show two peaks for each of the *syn*- and *anti*-isomers formed – some of which co-elute. Sugars that only undergo silylation (C) provide the most complex chromatograms. Peaks arising in (C) are some, or all, of the α- and β-forms of both the pyranose and furanose isomers. The peaks in (C) correspond to α-, β-Arabinofuranose (1, 6); α-, β-Arabinopyranose (2, 5); α-, β-xylofuranose (3, 7); α-, β-xylopyranose (4, 8); α-, β-mannopyranose (9, 13); α-, β-galactofuranose (10, 14); α-, β-galactopyranose (11, 15); α-, β-glucopyranose (12, 16). Mannose and glucose furanoses were not detected (in pyridine).

Figure 3.6 reveals an increase in chromatogram complexity from A to B to C. These chromatograms correspond to the same monosaccharide mixture first being reduced (one peak per sugar), or oximated (two peaks per sugar) or untreated (up to four peaks per sugar) before silylation, respectively. When analysing polysaccharides, the treatment method chosen will depend on the level of information required of the sample. Whilst reduction may provide simpler chromatograms, these results must be viewed with caution. Reduction is a harsh technique, which can lead to sample degradation and possible loss of sample structure information. Oximation is milder than reduction, however, co-elution of several oximated isomer peaks can make unambiguous determination and quantitation challenging. The most complex chromatograms arise from the mildest of the three techniques, where samples are untreated prior to derivatisation. For example, in Chromatogram C (Figure 3.6), 18 out of a possible 20 peaks for the mixture of five sugars are evident - with some peaks overlapping (1 and 2) and others co-eluting (13 and 14). Although this treatment provides the most complex chromatograms, it is most useful for determining the composition and structure of polysaccharide samples.

It is important to note that methanolysates (produced in an acid-catalysed reaction with methanol) cannot undergo oximation or reduction prior to derivatisation. Oximation or reduction occurs via the reducing-end of a sugar. Methanolysates contain a methoxide group (MeO) at C-1, instead of an OH, rendering them non-reducing. Consequently, GC chromatograms for methanolysates of polysaccharides tend to be complex. Analysis of such GC chromatograms is possible, provided suitable columns and/or detectors are selected. The next subsection discusses these topics in more detail.

Separation and detection

The steps for analysing polysaccharides by GC involve hydrolysis, derivatisation, separation and detection. The type of detector used may influence the choice of sample preparation, and the choice of column depends largely on the type of derivatives that require separating. For example, suitable columns for Ac and TMS derivatives are non-polar dimethyl polysiloxane columns (Willför *et al.*, 2009). Detectors that are suitable for the identification and quantitation of carbohydrate derivatives include a flame ionisation detector (FID) or a MS (Laine *et al.*, 2002; Qian *et al.*, 2010). Quantitation of a component eluting from a GC is possible by a FID, as this detector responds on a mass basis to organic compounds (Qian *et al.*, 2010). In turn, the compound can only be identified based on its relative retention time (RRT) against authentic standards (Laine *et al.*, 2002). However, co-elution in complex mixtures makes identification of the components with a FID ambiguous. Instead, the MS offers a highly sensitive (0.1-100 ng), unambiguous means for identification and quantitation of sugar derivatives in complex mixtures (Hites, 1997).

Interfacing a GC with an MS provides an instrument (GC-MS) that separates vaporised samples into components that can be sequentially measured and identified (Girard, 2010). When a MS is used in electron ionisation (EI) mode, reproducible fragmentation patterns of compounds arise. These EI-MS fragmentation patterns are recorded as mass spectra, which provide the abundance and distribution of fragments arising according to their mass-to-charge (*m/z*) ratios (Kochetkov and Chizhov, 1966). These mass spectra are used to explicitly determine compounds against authentic standards and/or reference libraries (Bleton *et al.*, 1996; Gerwig *et al.*, 1978; Kochetkov and Chizhov, 1966; Vuorinen and Alen, 1999). The National Institute of Standards and Technology (NIST) offers one such reference library (NIST Scientific and technical databases, http://www.nist.gov/data/nist1a.htm) against which mass spectra can be compared. The following section details the use of GC-MS in polysaccharide composition and structure analyses.

3.2.2 Gas chromatography-mass spectrometry for polysaccharide analysis

The GC-MS is a highly versatile tool for determining the composition and structure of oligosaccharides and polysaccharides (Aspinall, 1982a; Robyt, 1998). For structure analysis, the GC-MS allows differentiation between cyclic (furanose or pyranose) or acyclic (aldose or ketose) forms of the components, as well as the mode and conformation (α or β) of linkages between the components within carbohydrate compounds (Bleton *et al.*, 1996; Kochetkov and Chizhov, 1966).

The depolymerisation method used to prepare polysaccharides for GC-MS analysis influences the type of information that can be determined. In this study, the composition of the *P. sacchari* EPSs was determined through depolymerisation in acidic methanol. Similarly, the component absolute configurations were determined through depolymerisation with acidic S-(+)-2-butanol. For structure analysis, the EPSs were permethylated before undergoing acidic methanolysis. In all three cases, the resultant EPS methanolysates were silylated and then identified by GC-MS against the RRTs and mass spectra of similarly prepared authentic standards. Further detail regarding the composition, configuration and structure determination procedures is provided in the following subsections.

Composition analysis

Acidic methanolysis is one of the more gentle depolymerisation techniques used to determine the monosaccharide composition of polysaccharides (Laine *et al.*, 2002). Depolymerisation is carried out in methanol that is acidified with hydrochloric acid (HCl) (Sanz and Martínez-Castro, 2007). The resultant methanolysates are methyl glycosides (Aspinall, 1982a). Methyl glycosides mutarotate to varying degrees in different solvents, consequently, the TMS or Ac derivatives of each give rise to multiple peaks in a GC chromatogram (as discussed in Section 3.2.1).

Configuration analysis

The absolute configuration of polysaccharide components can be determined by adaptation of the composition analysis method described above. Traditionally, absolute configurations were determined by measuring a compound's ability to rotate a plane of polarised light (D-line of sodium). When the optical rotation is to the right, the compound is dextrorotatory (D), and when rotation is to the left, the compound is levorotatory (L) (Robyt, 2012). Pure compounds are required for accurate results. Alternatively, specific enzymes can be used for this determination; however, these are not always available. More conveniently, the enantiomers composing a polysaccharide can be converted into diastereoisomers that can be separated and analysed by GC. This is possible if depolymerisation is carried out with a chiral reagent (Gerwig *et al.*, 1978). Hence, the composition analysis technique can be adapted for absolute configuration determinations by replacing the acidified methanol with an acidified, enantiomerically pure chiral reagent such as S-(+)-2-butanol. In this case, (+)-2-butyl glycoside diastereoisomers arise, instead of methyl glycoside enantiomers, which are separated and differentiated by GC following derivatisation.

Structure analysis

The GC-MS is a powerful tool used to determine polysaccharide structural linkages. Several depolymerisation techniques are suitable to conduct a linkage analysis, for example, sequential degradations or methylation analysis. Sequential degradations, such as the Svensson's degradation (Svensson *et al.*, 1975) and periodate oxidation-Smith degradation (Abdel-Akher *et al.*, 1952), require multiple steps in a tedious procedure to obtain glycerol, ethanediol and/or tetritols (erythritol or threitol) products. These products are specific to certain linkages present in the polysaccharide. For example, in Figure 3.7, the glucan undergoes oxidation, reduction, and

hydrolysis giving rise to an erythritol derivative from regions in the structure where (1,3)-linked glucose is flanked by (1,4)-linked glucoses. What remain are the groups attached to R_1 and R_2. These groups could be low molecular weight glycoside products or degraded polysaccharides – the latter of which are subjected to repeated degradations. Finally, all the information from the generated residues are collated and a linkage profile of the polysaccharide is determined (Aspinall, 1982a).

Methylation analysis is a more convenient procedure to prepare glycosidic linkages for determination by GC and involves a permethylation followed by acidic methanolysis (Ciucanu and Caprita, 2007). Hereinafter, the procedural steps for a methylation analyses are referred to as "the permethylation protocol". Since both permethylated and partially methylated residues arise from the permethylation protocol, derivatisation is required in the final step before GC analysis. Each step in the permethylation protocol is explained in further detail. In the first step, the polysaccharide is completely methylated using Hakomori reagent (Aspinall, 1982a; Hakomori, 1965). This reagent is prepared from dry dimethylsulfoxide (DMSO) treated with sodium methylsulfinylmethanide (sodium dimsyl), which creates the methyl sulfinyl carbanions for the reaction. The carbanions form polyalkoxide ions ($C\text{-}O^-$) with the free OH groups of the dissolved polysaccharide. These alkoxide groups are then treated with methyl iodide (MeI) for methylation to occur (Robyt, 1998). In the second step, the permethylated sample is hydrolysed with acid giving rise to methanolysates (methyl glycosides).

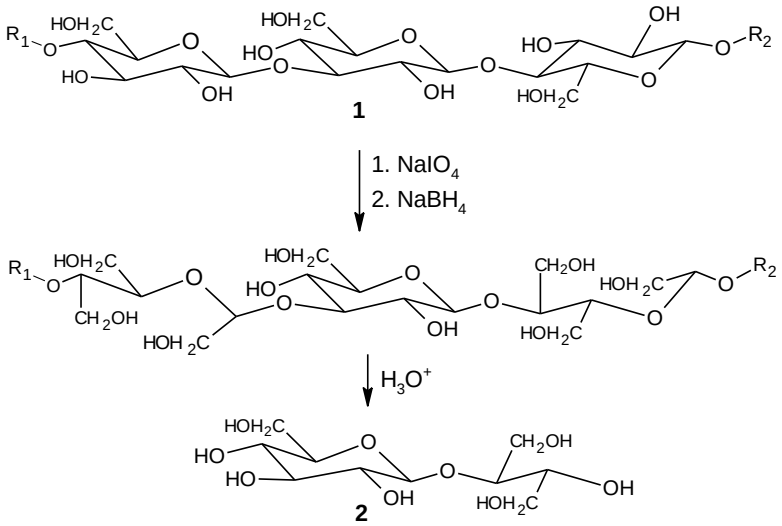

Figure 3.7: The Smith degradation of oat β-D-glucan (1). The glucan undergoes a periodate oxidation then a reduction, followed by a controlled hydrolysis of any acyclic acetal linkages. 2-*O*-β-D-glucopyranosyl-D-erythritol (2) residues arise from regions in the structure where 3-linked residues are flanked on either side by 4-linked residues. The remaining residues containing R_1 and R_2 are analysed or further degraded (Aspinall, 1982a).

More recently, Ciucanu and Caprita (2007) investigated the efficacy of permethylations carried out with powdered sodium hydroxide (NaOH) added directly to DMSO with MeI. In the first step of the permethylation reaction, alkoxide ions and water form in an equilibrium reaction with the NaOH. By adding an excess of this hygroscopic base, it acts as a water scavenger and drives

the deprotonation equilibrium reaction to alkoxide formation. This ensures complete methylations. Hence, it is essential that the conditions are anhydrous and/or that enough excess base is added (> 4 mg NaOH per microlitre of water) (Ciucanu and Caprita, 2007).

Following permethylation, acid methanolysis cleaves the glycosidic bonds giving rise to methyl glycosides. The type of methyl glycoside that arises depends on its mode of linkage in the biopolymeric chain. The linkage information is preserved as only one end across the cleaved glycosidic bond will be methylated (reducing-end) whilst the other will be hydroxideated (non-reducing-end). Consequently, either permethylated glycosides (from the non-reducing terminus of the polysaccharide) or partially methylated methyl glycosides (from the reducing-end, intra-chain and/or branch-point residues) arise. Derivatisation only affects the free OH groups, thus enabling those positions originally involved in the glycosidic linkages to be deduced. The permethylation protocol is illustrated in Figure 3.8, where an oligosaccharide containing a glucose (Glc) backbone of (1,4)-linkages, and having glucose branches linked by (1,6)-glycosidic bonds, is permethylated, methanolysed and silylated. The derivatised methyl glucose residues arising include: methyl 2,3,6-tris-*O*-methyl-4-*O*-(trimethylsilyl)-D-glucose (inner residues of the main chain, Glc-4), methyl 2,3,4,6-tetrakis-*O*-methyl-D-glucose (non-reducing terminus residue of the main chains, Glc-T) and methyl 2,3-bis-*O*-methyl-bis-4,6-(trimethylsilyl)-D-glucose (from the branches off the main chains, Glc-4,6) (Robyt, 1998).

As indicated in Figure 3.8, the permethylation protocol gives rise to an equilibrium mixture of both the α- and β-anomers of pyranoside and/or furanoside isomers of methyl glycosides (refer to Section 3.2.1. for further information). Consequently, complex gas chromatograms arise with each monomer contributing up to four peaks (Dag, 2005; Laine *et al.*, 2002; Vuorinen and Alen, 1999). This phenomenon is useful, as the ratio of isomers in a particular solvent is generally constant for a specific residue. Hence, if peaks from different residues overlap, each residue can be determined from at least one other corresponding peak in the chromatogram (Laine *et al.*, 2002).

Whilst primarily used as a tool for linkage determination, the permethylation protocol can be used to obtain additional structure information. For instance, the eluting order of arising anomers (α or β) can be differentiated (Bleton *et al.*, 1996), and the original ring size of certain residues can be determined. Whilst the original conformation (α or β) of each monosaccharide cannot be determined by this method, the order in which the anomeric residues elute is comparable against authentic methyl glycoside standards. For example, Bleton and co-workers (1996) analysed methyl glycoside standards, including methyl-β-arabinopyranoside, methyl-β-D-xylopyranoside, methyl-α-D-galactopyranoside and methyl-α-D-glucopyranoside to establish that the α-anomer elutes before the β-anomer in all pairs (except for arabinose). They also established that the α-anomer (except for arabinose) is more thermodynamically stable in methanolic HCl. The original ring size of a residue can also be determined from permethylation analysis, provided there are monomers in the polysaccharide chain that are unsubstituted at C-4 (for pyranosides) and C-5 (for furanosides). Substitutions occur in these positions when the methyl glycosides form, preventing isomerisation and causing the original ring shape to be retained (Laine et al., 2002; Vuorinen and Alen, 1999). For example, in Figure 3.8, the terminal, non-reducing Glc residue maintains its pyranose form, whilst the chain Glc residues isomerise between their pyranose and furanose forms.

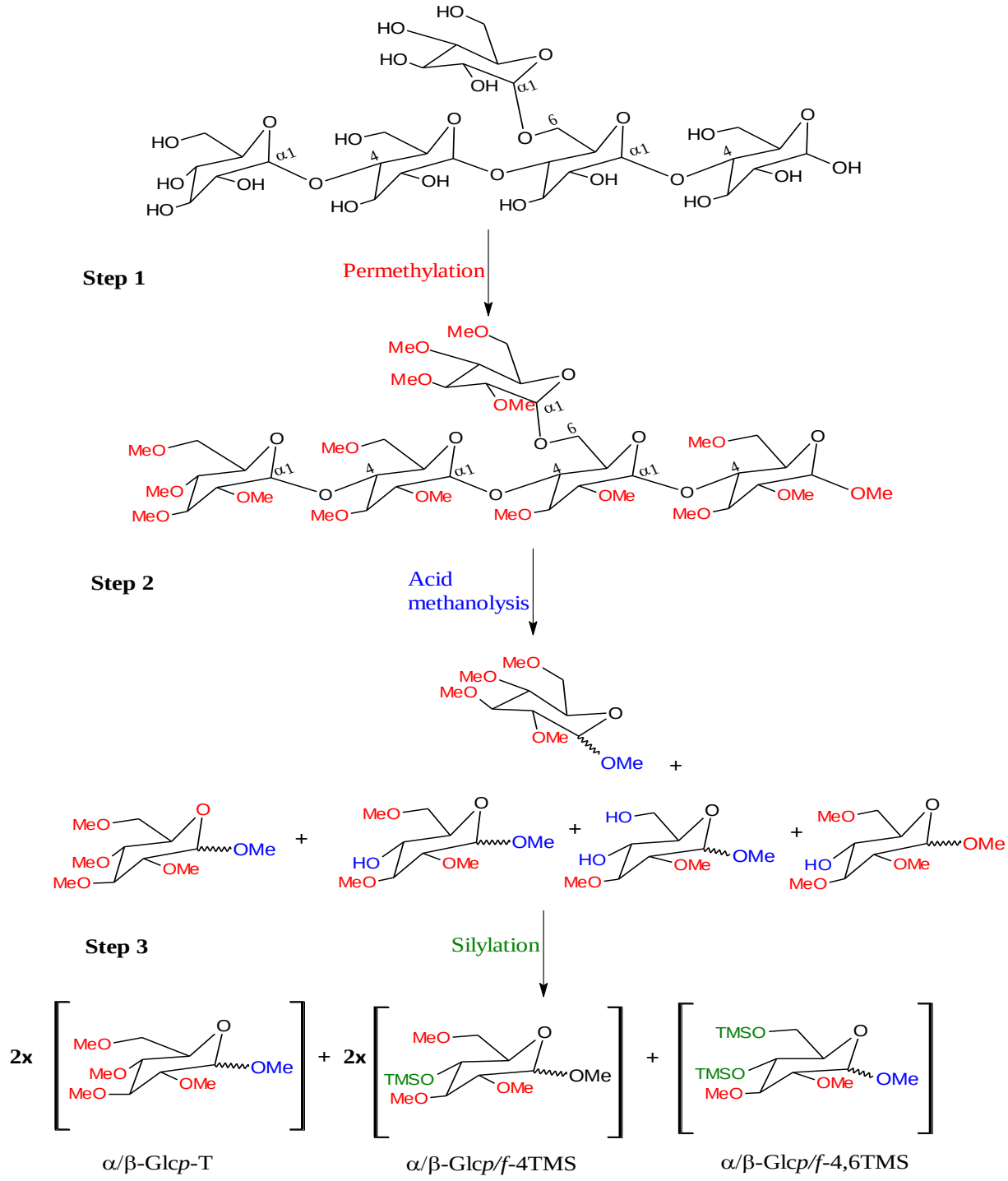

Figure 3.8: Stepwise reactions of the permethylation protocol to determine the structure of a pentasaccharide. Step 1: Quantitative permethylation (red) of the free hydroxide groups. Step 2: Acid methanolysis (blue) of the glycosidic bonds. The α- and β-isomers of the resultant methyl glycosides equilibrate. Step 3: Silylation (green) of the free hydroxide groups. Me = methyl, TMS = trimethylsilyl, T = terminal, p = pyranose, f = furanose (adapted from Laine et al., 2002).

Permethylation followed by GC-MS analysis provides a wealth of information regarding the structure of polysaccharides, but cannot provide all the detail required to describe a polysaccharide as a whole. Various other techniques complement the GC composition and structure methods described herein. These complimentary techniques are discussed in the sections that follow and include the use of NMR and HPLC.

3.3 Nuclear magnetic resonance spectroscopy

The previous section describes GC as the method of choice to determine the composition and linkage information of polysaccharides. This section introduces NMR spectroscopy and its useful application in both anomeric conformation and sequence determination in polysaccharide samples. This section outlines the various non-destructive NMR experiments that are useful in polysaccharide structure characterisation.

3.3.1 Introduction

Historically, polysaccharide sequences were determined by methods incorporating sequential degradations, such as those mentioned in Section 3.2.2. These methods are laborious and destructive. NMR offers an elegant, non-destructive alternative for these determinations. NMR also enables the anomeric conformation of the monosaccharides in the repeat sequence to be determined. NMR spectroscopy has become an especially important tool for elucidating polysaccharide structures (Aspinall, 1982a; Cheng and Neiss, 2012; Cui, 2002; Dag, 2005; Kajiwara and Miyamoto, 2004; Perlin and Casu, 1982).

Generally, NMR is a technique used to determine the carbon and hydrogen framework in organic compounds (Bruice, 2004). The basic principles behind NMR spectroscopy rely on atoms with odd masses (^{1}H, ^{13}C, ^{31}P, *etc.*) having a nuclear spin. This phenomenon allows these atoms to orientate with an applied magnetic field (H_o), with their spins either aligned (low energy state) or opposed (high energy state) to this field. When a radio frequency (RF) signal is then applied, the nuclei resonate at this frequency, causing them to flip between energy states. The energy required to do so, depends on the strength of the magnetic field at the nucleus; which depends on the H_o strength, the type of nucleus in question, and the environment that the nucleus is in (Williams and Fleming, 1987). The output spectral signal is the nuclei's resonance, and the frequency of that signal is called the chemical shift (δ) in parts per million (ppm).

There are several complementary NMR experiments which are useful in the anomeric conformation and sequence determination of polysaccharides; including, proton (^{1}H), carbon (^{13}C), correlation spectroscopy (COSY), heteronuclear single-quantum correlation (HSQC), heteronuclear multiple bond correlation spectroscopy (HMBC), nuclear Overhauser effect spectroscopy (NOESY) and rotating frame nuclear Overhauser effect spectroscopy (ROESY). The first two experiments are described as one-dimensional (1D), whilst the latter are referred as two-dimensional (2D) NMR experiments. Combining two 2D experiments gives rise to a three-dimensional (3D) result.

3.3.2 Proton and carbon nuclear magnetic resonance analysis of carbohydrates

In the ^{1}H NMR spectrum of carbohydrates, the δ_H signals, their integration, and the coupling constants (*J*) of the multiplets are important features that arise from the hydrogen atoms of the sugar rings. Similarly, the δ_C signals are useful for identifying the carbon framework of the sugar rings, however, the low abundance (1.1%) and sensitivity of the ^{13}C nucleus does not always allow accurate integration (Perlin and Casu, 1982). The chemical shift of a monosaccharidic hydrogen

atom depends on whether it is anomeric or non-anomeric, and on the substituents associated on the same and adjacent carbon atoms. The anomeric protons (H-1) appear as a doublet (d), and are further downfield compared with the remaining protons in the sugar ring (see Figure 3.9 for a numbered glucose ring). The splitting patterns for protons H-2, H-3, H-4, H-6a and H-6b are all doublets of doublets (dd), due to each coupling with their two neighbouring protons. The dd-patterns for H-2, H-3 and H-4 of pyranose rings often appear as triplets – especially if the coupling constants are almost the same. Since H-5 couples with H-4, H-6a and H-6b, a ddd-pattern arises (Lindhorst, 2000).

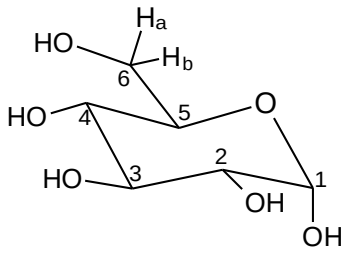

Figure 3.9: A numbered glucose ring is shown for ease of reference. The protons at each numbered position are not shown, except for the geminal H-6 pair (H-6a and H-6b).

For anomeric protons in similar environments, equatorial protons are usually found more downfield compared with axially configured ones. The difference in three bond $^{3}J_{1,2}$ values is caused by the difference in dihedral angles (ϕ) between H-1 and H-2 (α-anomer is ϕ=60° and the β-anomer is ϕ=180°). In Figure 3.10, the ^{1}H spectra for α- and β-penta-*O*-acetyl-glucose are shown, highlighting the anomeric protons in each (Lindhorst, 2000). In general, vicinal $^{3}J_{1,2}$ coupling constants in glucosides are 3-4 Hz for anomers of the α-configuration, whilst β-anomers have $^{3}J_{1,2}$ values of 7-8 Hz (Dag, 2005; Ferreira *et al.*, 1995; Harding *et al.*, 2005; Lindhorst, 2000). Refer to Table 3.2 for a compilation of ^{1}H and ^{13}C resonance values of some structural components of polysaccharides (analogous to the magnetic resonance characteristics of the monosaccharides that they comprise).

As previously discussed, the anomeric configuration of monosaccharides is identified by the ^{1}H chemical shifts and by the coupling constants of vicinal protons. Another method used to aid in the configuration determination of sugars, is to study the ^{13}C-^{1}H coupling information (Perlin and Casu, 1982). For example, ^{13}C-^{1}H coupling is useful for determining the anomers of mannosides. Mannoside configuration is difficult to determine from their ^{1}H NMR spectra alone, as their $^{3}J_{1,2}$ couplings are unresolved. The poor resolution arises because the C-2 hydroxide is in the axial position, forcing the couplings for the α- and β-forms to be less than 3 Hz (ϕ=60° in both cases). To overcome this, the size of the hetero-coupling constant between C-1 and H-1 ($^{1}J_{C1,H1}$) can be used to determine the configuration. There is usually a difference of about 10 Hz in this constant between anomers; with α-glycosides having $^{1}J_{C1,H1}$ of ~170 Hz, and β-glycosides having $^{1}J_{C1,H1}$ of ~160 Hz. For mannosides, both of these values are ~5 Hz smaller (Bock and Pedersen, 1974; Lindhorst, 2000). See Table 3.3 for spin-spin coupling data for the H-1 and C-1 nuclei of polysaccharides and their anomers. The disadvantage of using ^{1}H-coupled spectra is that they are often more complex than decoupled spectra of the same type (Perlin and Casu, 1982).

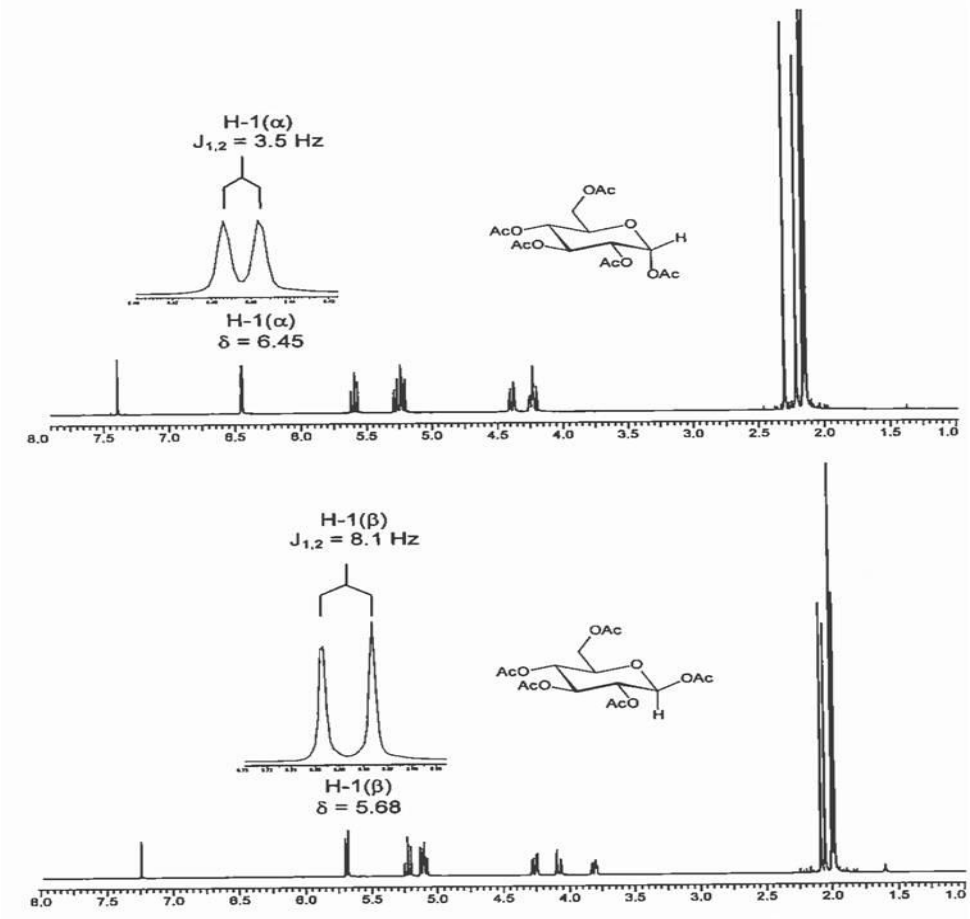

Figure 3.10: ^{1}H NMR (400 MHz, $CDCl_3$) spectra of α- and β-penta-*O*-acetyl-glucose. The doublet for H-1 is expanded in each case and its chemical shift and $^{3}J_{1,2}$ coupling constant are indicated (Lindhorst, 2000).

Table 3.2 Representative ^{1}H and ^{13}C chemical shifts for different nuclei of monosaccharides and polysaccharides in deuterium oxide (Dag, 2005; Perlin and Casu, 1982; Vuorinen and Alen, 1999).

Description	δ_H/ppm	δ_C/ppm
Anomeric region (H-1)		-
α-anomers (equatorial)	4.9-5.9	-
β-anomers (axial)	4.3-4.8	-
Ring protons		
H-2 to H6b	3.5-4.5	-
H-5	4.5-4.6	
Ring carbons (unsubstituted) (C-2 to C-5)	-	65-75
Anomeric region (C-1)		
axial-O, reducing	-	90-95
equatorial-O, reducing		95-98
axial-O, glycosidic		98-103
equatorial-O, glycosidic		103-106
furanoside		106-109
C-O or C-N	-	50-85
CH(NH)		58-61
CH_3O		55-61
CH_2OH		60-65
C-2 to C-5		65-75
C-X[a]		80-87
Glycosidic bond carbons	-	75-85
CH_3C	-	~15
CH_3COH, **C**H_3CO_2	-	20-30
C**H**$_3$C	~1.5	-
C**H**$_3$CON	1.8-2.1	-
C**H**$_3CO_2$	2.0-2.2	-
C**H**$_3$O	3.3-3.5	-
CH_2C	-	38
COOH	-	174-175
HCO_2	5.9	-
HO	5.0-5.4	

[a] Non-anomeric ^{13}C atoms involved in the glycosidic linkage.

Table 3.3 Spin-spin coupling data for ^{1}H-1 and ^{13}C-1 nuclei of polysaccharides and anomeric configuration (adapted from Perlin and Casu (1982)).

	$^{3}J_{1,2}$/Hz		$^{1}J_{C1,H1}$/Hz	
Residue/Polysaccharide	α	β	α	β
Glycopyranosyl				
Amylose	~3			
Dextran	~3		171	
Lichenan		7.5		160
Pustulan				160
Galactopyranosyl				
Klebsiella	~3		172	

^{13}C NMR analyses are complimentary to any NMR study of polysaccharides. Both ^{1}H and ^{13}C analyses allow the number of different residues in a polysaccharide to be determined. The shortfalls of ^{13}C experiments lie in the fact that the integration information is primarily lost – this is because the pulse sequences do not allow for complete ^{13}C relaxation. Consequently, the relative proportions of the signals cannot be estimated. Furthermore, ^{13}C measurements are far less sensitive and require samples that are more concentrated. However, the major advantage of this method is that the superior signal separation allows anomeric resonances to be distinguished from other nuclei. For instance, the chemical shifts of the two carbon atoms involved in a glycosidic linkage (C-1—O—C-X) can be distinguished. The anomeric carbon (C-1) appears most downfield (δ_C 98-110 ppm) from the rest of the ring carbons in the primary carbon region (C-2 to C-5). However, the ring carbon involved in the linkage (C-X) will display a shift of 6-9 ppm downfield from these primary ring carbons.

The ^{13}C analysis of polysaccharides also allows the secondary C-6 carbons to be distinguished through distortionless enhancement by polarisation transfer (DEPT) experiments. Through differential ^{13}C relaxation rates, the DEPT sequences allow for the quaternary, tertiary, secondary and primary carbons to be distinguished. Most often the DEPT sequence is used to suppress the quaternary signals, whilst allowing the CH_2 (C-6) carbons to appear on the negative axis and the CH and CH_3 groups to appear on the positive axis (Perlin and Casu, 1982).

3.3.3 Two-dimensional nuclear magnetic resonance analysis of carbohydrates

Although ^{13}C measurements are useful supplements to the ^{1}H analysis of compounds, the non-anomeric protons of complex carbohydrate samples are often left unassigned due to the high degree of overlapping of the peaks. Subsequently, many other sophisticated NMR pulse sequences have been developed allowing 2D spectra to be recorded. These 2D sequences include COSY, HSQC, HMBC, NOESY and ROESY. Together, 1D and 2D spectra allow complex polysaccharides to be fully assigned (Lindhorst, 2000).

2D Experiments follow a general scheme involving preparation, evolution, mixing and detection periods. The preparation period involves a single pulse (single-quantum coherence) or multiple pulses (multiple-quantum coherence) to generate a transverse magnetism. The coherence generated is then left to evolve over an evolution period (t_1). In the mixing period, the coherence

that has evolved by the end of t_1 is manipulated into a signal which is observable and recordable during the detection period (t_2) (Keeler, 2005). The general scheme for 2D NMR is given in Figure 3.11.

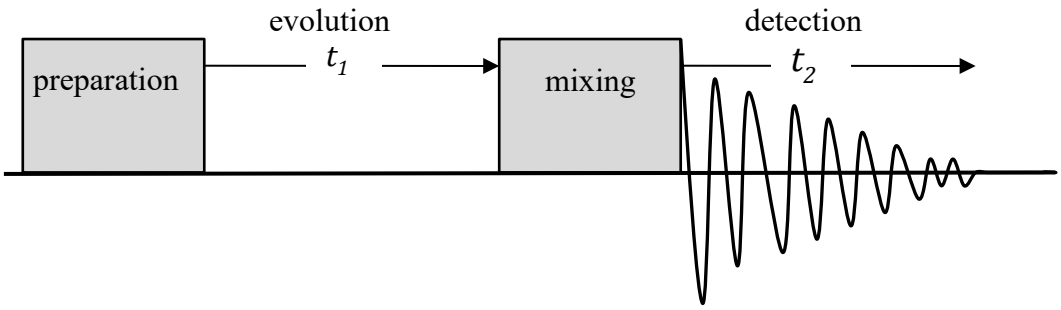

Figure 3.11: The general scheme for 2D NMR is shown. In both the preparation and mixing periods a single pulse without a delay, or complex pulses with a series of delays, is/are applied. Following the preparation period, a coherence is generated, which is allowed to evolve over t_1. There is no detection over this time. Following the mixing period, the signal is detected over t_2.

The ^{1}H-^{1}H-COSY or ^{1}H-^{13}C-COSY spectra are popular and useful 2D tools to facilitate the structural elucidation of large, complex molecules. These experiments identify the chemical shifts of scalar coupled spins. This enables the *J*-coupling network of the molecule to be outlined (Keeler, 2005). The COSY spectrum consists of diagonal peaks and cross-peaks. Cross-peaks are symmetrically located around the diagonal peaks, and indicate correlations between multiplets (Lindhorst, 2000). In the ^{1}H-^{1}H-COSY spectrum the proton spectrum is correlated to itself, thus correlations between protons in the sample can be determined. Therefore, a correlation between cross-peaks perpendicularly across the diagonal indicates a geminal or vicinal coupling between the multiplets (see Figure 3.12). Identification of the various multiplets must begin at a known one. In principle, if each anomeric proton is assigned, they can be connected to the signals for other protons in the same ring structure via *J*-couplings. The H-1 cross-peak will show a correlation to the H-2, H-2 will correlate to H-3, *etc*. In addition, protons such as H-4 should reveal two cross-peaks – one for H-5 and one for H-3. Similarly, the geminal H-6a and H-6b protons should reveal cross-peaks for the coupling between each other. Once all the protons have been assigned, a ^{1}H-^{13}C-COSY spectrum can be used to assign the carbons in the molecule through correlations with the attached protons (see Figure 3.13) (Lindhorst, 2000).

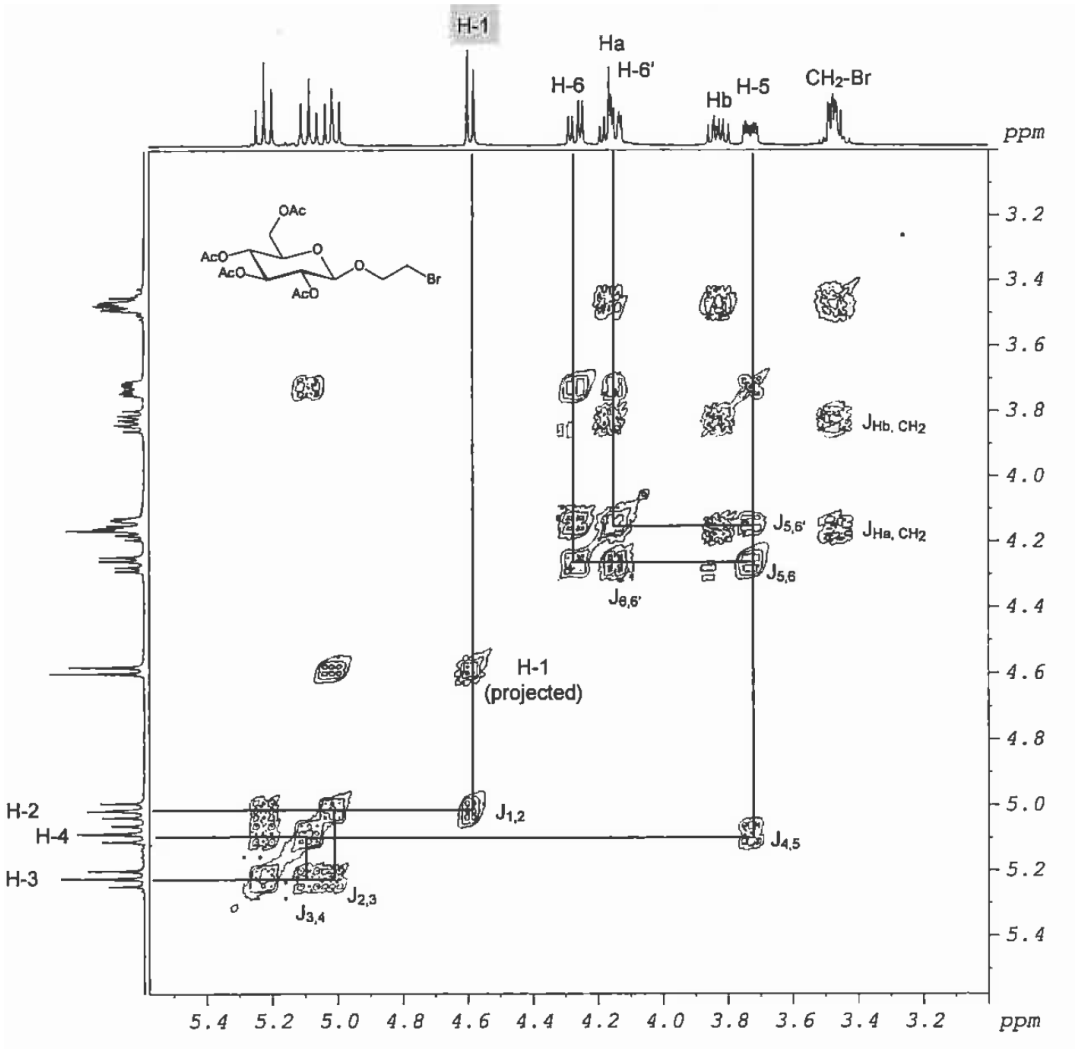

Figure 3.12: ^{1}H-^{1}H-COSY of (2-bromoethyl) 2,3,4,6-tetra-*O*-acetyl-β-D-glucoside. Cross-peak correlations are shown by perpendicular and parallel lines (Lindhorst, 2000).

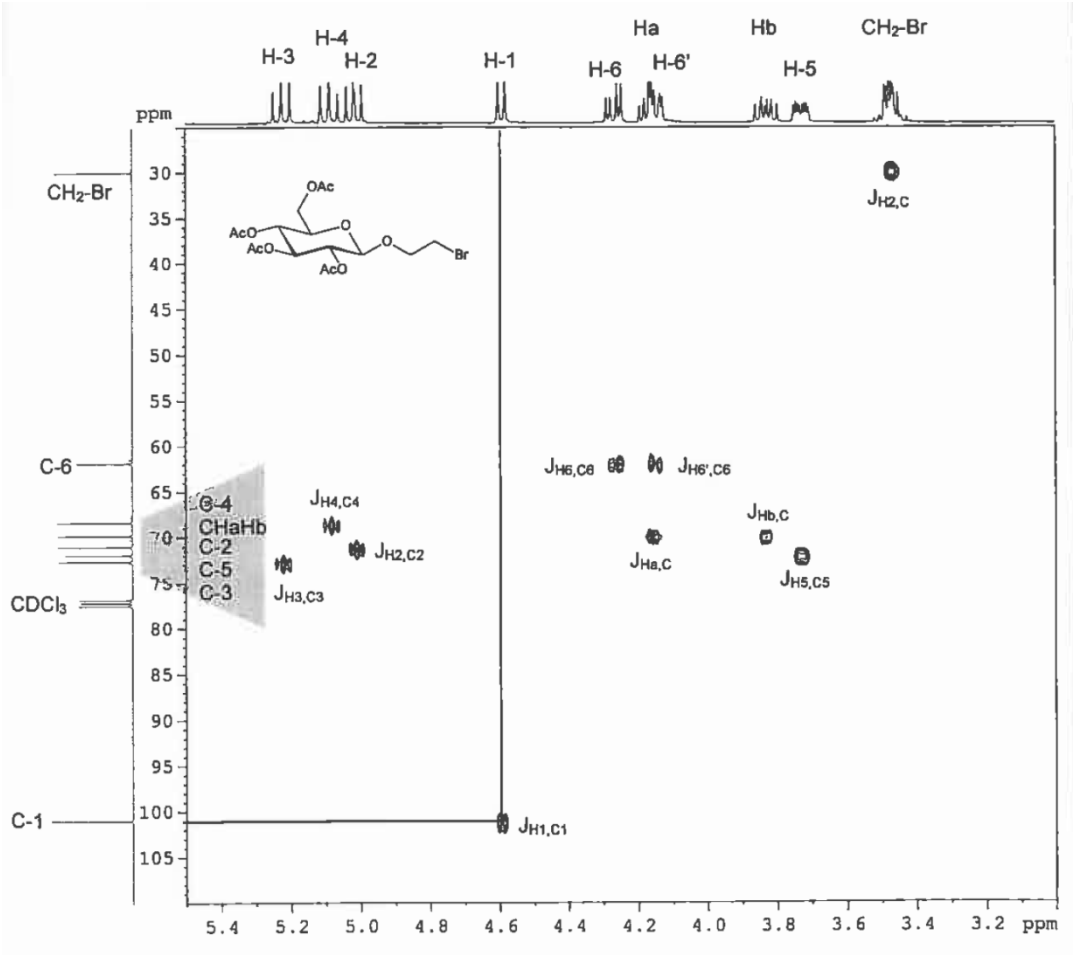

Figure 3.13: ^{1}H-^{13}C-COSY of (2-bromoethyl) 2,3,4,6-tetra-*O*-acetyl-β-D-glucoside. All multiplets recorded in the ^{1}H spectrum of the compound can be cross-peak correlated to the carbon atoms to which these hydrogens are attached. This is indicated in the H-1 – C-1 correlation. This method facilitates the exact assignment of all the ^{13}C peaks (Lindhorst, 2000).

Like ^{1}H-^{13}C-COSY, HMBC and HSQC experiments can be used to assign the carbon framework in carbohydrates. The HSQC experiment requires a greater number of pulses and is susceptible to losses in signal-to-noise ratio due to poor pulse calibration or probe tuning, however, it is an excellent technique for the structure analysis of large polysaccharides (Claridge, 1999; Keeler, 2005; Vliegenthart, 2006). HMBC differs from HSQC in that signals for weak ^{1}H-^{13}C *J*-couplings (two to three bonds away) are generated. The benefit with this technique is that these ^{1}H-^{13}C correlations can extend through the glycosidic linkages, and can provide information regarding the sequence of monosaccharides in polysaccharide structures (Cui, 2002; Dag, 2005; Vliegenthart, 2006).

The NMR techniques discussed thus far all involve scalar couplings. Magnetisation can be transferred in such a way, that through-space dipole-dipole interactions can be measured instead. This dipolar interaction is tensorial; relying on the spatial orientation and interaction of spins between two nuclei in space (Simpson, 2008). This interaction is known as the nuclear Overhauser effect (NOE), and the related NMR experiments are NOESY and ROESY

(Keeler, 2005). A NOESY spectrum resembles a COSY spectrum, except that the cross-peaks generated are through cross relaxation between the spins that are close in space, rather than via through-bond *J*-couplings (Keeler, 2005). Specifically, the NOESY experiments give rise to ^{1}H-^{1}H through-space interactions, correlating pairs of protons which are less than 5 angstroms (Å) apart (and which are not necessarily associated through bonds) (Cui, 2002). Similar to HMBC then, NOESY experiments can provide the sequence information for polysaccharides.

ROESY experiments are analogous to NOESY experiments, and are suitable for distinguishing NOEs in extended spin systems (larger molecules). The difference between the two experiments lies in the mixing time, where a spin-lock[4] is applied to ROESY experiments. This allows NOEs to always be oppositely phased, making them distinguishable from the diagonal and other cross-peaks in the spectrum (Fribolin, 2005; Simpson, 2008).

In order to gather information on both the linkages and sequences within large and complex polysaccharide samples, 1D and 2D experiments may be used (Dag, 2005).

3.3.4 Considerations for nuclear magnetic resonance analysis of carbohydrates

In performing an NMR structural assignment of carbohydrates, about 10 mg of sample is required. The solvents used are deuterated; such as chloroform ($CDCl_3$), DMSO-d_6 or deuterium oxide (D_2O). Deuterium exchanges with protons of hydroxide, carboxyl, amine and amide groups, thus reducing the complexity of the NMR spectrum. There is often a broad, intense signal that results from HDO – as complete deuterium exchange is not possible. At room temperature, this HDO signal may overlap with the anomeric region (δ_{HDO} ~ 4.7 ppm at 25 °C). By increasing or decreasing the temperature the HDO signal shifts upfield (*i.e.*, δ_{HDO} ~ 4.5 at 70 °C) or downfield, respectively (Perlin and Casu, 1982). Temperature changes also affect the solution viscosity, signal line width, and the rate of deuterium/proton exchange (Dag, 2005).

The analysis of carbohydrates begins with the identification of the anomeric protons between δ_H 4.0-5.5 ppm. These are called the "reporter-group" resonances, which are compared to resonances observed for model compounds (Vliegenthart *et al.*, 1981). However, difficulty arises in complex samples when these reporter-group resonances overlap with themselves, or with other signals in the spectrum (such as the solvent peaks). Whilst the complementary ^{13}C spectra may assist with these assignments, the low sensitivity of the ^{13}C nucleus makes analysis difficult or impossible (Goux, 1990). Alternatively, esterified carbohydrates produce less complex NMR spectra that can assist with structure elucidation. The acetylated samples are prepared in DMSO-d_6 or $CDCl_3$ and the signals are assigned through comparison against similarly prepared model compounds, such as, maltose, maltotriose, maltopentaose, and pullulan (Buchanan *et al.*, 1987; Giordano and Trincone, 2002; Heinze *et al.*, 2006; Laignel *et al.*, 1997; Tezuka, 1998). An example of a peracetylated monosaccharide, β-D-galactopyranose pentaacetate, is illustrated in Figure 3.14.

[4] A spin-lock basically removes all magnetisation from the system, causing nuclei to only experience the weak applied radio frequency. This causes spin states to become mixed, and polarisation to be transferred from the particular proton that has been excited in the spin system, to all other scalar and non-scalar coupled protons in the system (Friebolin, 2005).

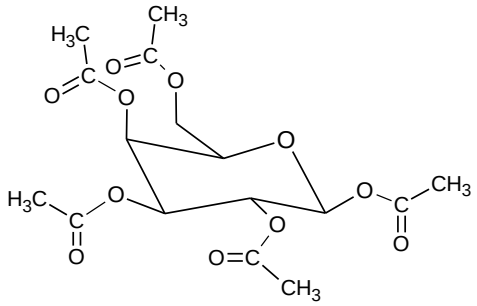

Figure 3.14: β-D-galactopyranose pentaacetate.

In this work, the *P. sacchari* polysaccharides were analysed by both 1D and 2D NMR, in their native and/or peracetylated forms. Refer to Section 4.3 for the experimental details and Section 5.3 for the results of these analyses.

3.4 Enzymatic hydrolysis and high performance liquid chromatography

Traditionally, structural analysis of polysaccharides was carried out with chemical methods including acid hydrolysis, periodate oxidation and methylation analysis (Marshall, 1974). Acid hydrolysis and periodate oxidation have primarily been replaced with enzymatic and spectroscopic methods (Matheson and McCleary, 1985; Tsai, 2007). In this study, pullulan and the EPS samples were treated with pullulanase. This data was used as a complimentary technique to NMR to determine and quantify the repeat oligomers of the EPSs. The following sections introduce enzymatic hydrolysis in its application to polysaccharide structural determinations together with HPAEC-PAD for separation and quantification of the resultant hydrolysates.

3.4.1 Introduction

Enzymatic methods can be used to determine the structure of polysaccharides both qualitatively and quantitatively. Enzymes offer an alternative, more selective, non-degradative method to depolymerise polysaccharides compared to acids (Marshall, 1974). Furthermore, the high specificity of enzymes toward a particular monosaccharide, its anomeric linkage, and neighbouring sugars make them useful for structure analysis (Bochkov *et al.*, 1991). It is due to this specificity that prior structural knowledge of the polysaccharide is required. It is suggested that non-enzymatic compositional and linkage analyses are required before enzymes can be selected (Marshall, 1974; Tsai, 2007). These methods are described in Section 3.2. The products arising from enzymatic hydrolysis may include monosaccharides, oligosaccharides or non-degraded polysaccharides. Chromatographic methods separate enzymatic hydrolysate products before analysis.

Enzymatic hydrolysis of polysaccharides occurs via either an endo- or exo-manner. Endo-enzymes randomly cleave specific glycosidic linkages along the polysaccharide chain, giving rise to oligomers. These oligomers can serve as substrates for further hydrolysis. The factors that affect the degree of hydrolysis and the type of hydrolytic products arising from endo-enzymes include; the composition, sequence, anomeric conformation, solubility, degree of polymerisation, degree of branching, and the type and amount of non-carbohydrate substituents in the

polysaccharide. Exo-enzymes differ from endo-enzymes in that they can only sequentially cleave glycosidic linkages from the non-reducing terminus of polysaccharides. The resultant hydrolysates can be monosaccharides or sequential oligosaccharides (Matheson and McCleary, 1985).

Quantitative determination of the components of more complex polysaccharides may require combinations of enzymes. For instance, galactomannans from legume seeds are measured by treatment with α-D-galactosidase and endo-(1,4)-β-D-mannanase, followed by treatment with galactose dehydrogenase. On the other hand, the major disadvantage of enzymatic procedures is the possible contamination by other enzymes (Marshall, 1974; Matheson and McCleary, 1985). Overall advantages include that enzymes act rapidly, are specific and can be adapted to micro-scale analysis (Matheson and McCleary, 1985).

3.4.2 Enzymatic hydrolysis of pullulan

Pullulan, being an α-(1,4)-linked glucan with α-(1,6)-linkages dispersed every three (and sometimes four) glucose units, can be treated with α-amylase or pullulanase to hydrolyse these glycosidic bonds, respectively. α-Amylase hydrolyses α-(1,4)-glucoses via an endo-manner whilst maintaining the anomeric conformation of the sugars. The α-amylase products arising from amylose include glucose, maltose and maltotriose. Alternatively, when pullulan is treated with α-amylase, glucose, maltose and panose arise instead. Panose is a trisaccharide consisting of an α-(1,6)-linked glucose followed by two α-(1,4)-linked glucoses, and arises due to the repeat maltosyl units in the polysaccharide (Matheson and McCleary, 1985). It should be noted that α-amylases from different sources perform endo-hydrolysis at different points along the pullulan chain, giving rise to some or all of the aforementioned products, and in varying amounts (McCleary and Matheson, 1986).

Pullulanase was discovered by Bender and Wallenfels in 1961 (Marshall, 1974) when an air-borne bacterium (*Aerobacter aerogenes*) grew on pullulan solutions. Pullulanase is a 6-glucanhydrolase endo-enzyme which randomly cleaves α-(1,6)-linkages. Hence, pullulans should give rise to maltotriose subunits when treated with pullulanase (Singh *et al.*, 2010). However, pullulans can contain as much as 7% of maltotetraose oligomers. These segments are found to occur in the interior of the pullulan molecule (Matheson and McCleary, 1985). Through adequate separation and quantification of the arising oligosaccharides, the proportion of maltotriose and maltotetraose units in pullulans can be quantified.

3.4.3 Separation and analysis of enzymatic hydrolysates of polysaccharides

Once a polysaccharide has been debranched by enzymatic treatment, the resulting hydrolysates are separated and analysed. Since the hydrolysates can range from monosaccharides to oligosaccharides, and even small polysaccharides, derivatisation followed by GC separation is not always appropriate. One option for separation is to employ SEC, with a suitable stationary phase able to separate carbohydrates within a lower MW range (i.e. 100-1 000 Da). An example would be BioGel P-2. For detection, either RI or the Dubois phenol-sulphuric colorimetric method are traditionally used (Dubois *et al.*, 1956; Youssef *et al.*, 1999). Since the 1980s a far more efficient and sensitive method has been employed for the separation and detection of carbohydrate compounds. This method includes separation on a HPAEC column with detection by electrochemical means (i.e. PAD) (Cataldi *et al.*, 2000; Huber and Bonn, 1995). In this method, a strongly alkaline eluent is employed and separation of the native carbohydrates (or the enzyme digest) on the column is based on the interaction of the oxyanions of the weakly acidic sugars and the column media. The high resolution of this technique allows for chain length distributions of polysaccharides to be determined. For instance malto-oligosaccharides from amylopectin hydrolysates have been successfully separated to a DP of more than 50 with this

method (Nagamine and Komae, 1996). At the PAD, detection takes place because of the electro-catalytic activity of the gold working electrode under the oxidative, basic conditions. The PAD is relatively specific toward hydroxide-containing compounds, thus the great advantage of this technique is that carbohydrates can be determined from a variety of complex matrices including diary, food, beverages, and biological samples (Cataldi *et al.*, 2000; Huber and Bonn, 1995). The use of an electrochemical detector allows estimation of the molar ratio of carbohydrate species. For this, the detector response is taken into account. For example, it has been found that when the detector response is divided by the moles of saccharide present, this molar unit sensitivity is found to increase with increasing DP (Dudahl-Olesen, *et al*., 2000b; Torto, *et al*., 1997).

In this study, two pullulanases were used to hydrolyse pullulan as well as fractionated (FB2 F1 and FB2 F2) and unfractionated (FB2, PB2 and PB7) EPS samples. HPAEC-PAD was the chromatographic technique employed to determine the malto-oligosaccharides present in the enzyme digests. These data were compared with data gathered from GC-MS and NMR analyses of the same samples.

3.5 Physical properties

Polysaccharides such as pullulan have multiple applications in foods, pharmaceuticals, and cosmetics industries due to their viscosity modifying characteristics and film-forming capabilities (Diab *et al.*, 2001; Lazaridou *et al.*, 2002b; Singh *et al.*, 2008). To maximise the utilisation of polysaccharides, the complexities of their structure must be known and their physicochemical properties need to be explored. In this study, the rheological properties and film-forming characteristics of the *P. sacchari* EPSs were investigated.

3.5.1 Rheological properties

Polysaccharides possess various properties that are important to different industrial sectors. Properties such as thickening, gelling, emulsifying, adhesion and stabilisation are particularly useful in the food and cosmetic industries. These properties are governed by both the polysaccharide structure and solution properties (Timilsena *et al.*, 2015). Various rheological techniques determine the solution properties of polymeric materials.

Rheology is the study of materials and how they respond to an applied stress or strain (Steffe, 1996). These responses include deformation (for solids) or flow (for liquids) (Picout and Ross-Murphy, 2003). The rheology of polysaccharide solutions has been widely studied as it contributes significantly to viscosity (Picout and Ross-Murphy, 2003). In industrial applications, even small additions of polysaccharides control the aqueous phase, due to their high molecular weights and ability to occupy large solution volumes (Dea, 1993; Picout and Ross-Murphy, 2003).

Viscosity is a rheological property that describes an internal resistance to flow when a force is applied to a material (Viswanath *et al.*, 2007). For fluids, viscosity is defined by Equation 3.4:

$$\eta = \frac{\tau}{\dot{\gamma}} \tag{3.4}$$

where η is the viscosity (in Pa s), τ is the shear stress (Pa) and $\dot{\gamma}$ is the shear rate (s^{-1}) (Barnes, 2000; Mezger, 2006; Picout and Ross-Murphy, 2003).

Viscous behaviour is classified as Newtonian or Non-Newtonian. Non-Newtonian behaviour can be further described as being plastic (or Bingham), pseudoplastic (with or without a yield point) or dilatant as illustrated in Figure 3.15 (Bourne, 2002; Viswanath *et al.*, 2007).

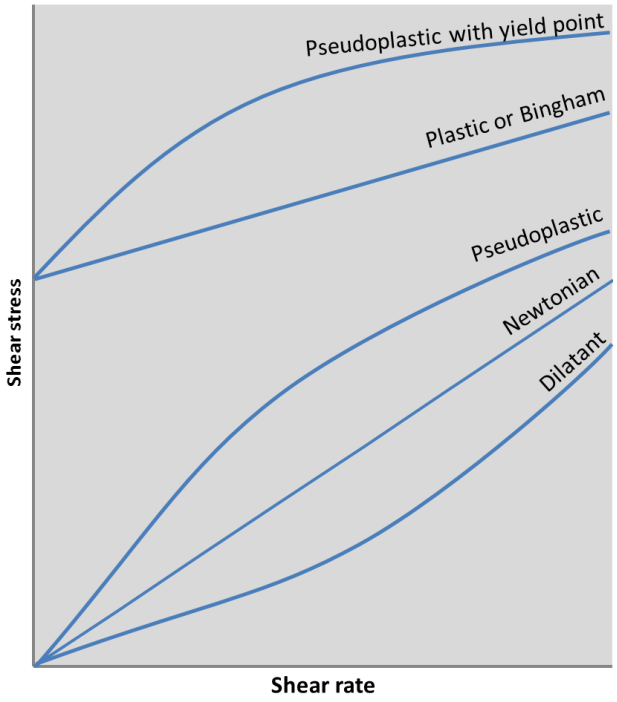

Figure 3.15: Curves for shear stress versus shear rate to illustrate the different types of flow behaviour (Bourne, 2002).

Newtonian flow occurs when the shear rate and shear stress are directly proportional, and the viscosity remains unchanged with changing shear. Newtonian fluids with a high viscosity value are "*viscous*", and those with a low viscosity value are "*mobile*" (Bourne, 2002). Water is an example of a mobile fluid that exhibits Newtonian behaviour. Low molecular weight polysaccharides in solution can also exhibit Newtonian flow (Picout and Ross-Murphy, 2003).

Non-Newtonian dilatant (shear-thickening) and pseudoplastic (shear-thinning) flow describe fluids that experience a shear stress that is either more or less than proportional to the shear rate, respectively. Since the measured viscosity changes depending on the shear rate, it is known as the apparent viscosity. Dilatant flow is less common and can occur in solutions with high levels of suspended solids, for example, in a solution containing 60% cornstarch. Polysaccharide solutions generally exhibit shear-thinning flows (Dea, 1993; Picout and Ross-Murphy, 2003).

Plastic flow describes fluids where the shear rate is directly proportional to the shear stress; however, in order for flow to be initiated, a minimum shear stress must be exceeded. This is known as the yield point (Bourne, 2002). For example, toothpaste requires a certain amount of force before it can be squeezed out of the tube and so exhibits plastic flow (Mezger, 2006).

All the types of flow can be described by the general equation for viscosity, as provided in Equation 3.5:

$$\tau = b\dot{\gamma}^s + C \tag{3.5}$$

where τ is the shear stress, b is the proportionality factor (or viscosity, η, for Newtonian fluids), $\dot{\gamma}$ is the shear rate, C is the yield stress and s is the pseudoplasticity constant. This constant describes the degree of non-linearity in the shear stress versus shear rate curve.

Other flow equations used to describe non-Newtonian flow behaviour include the Power Equation (or Ostwald-de Wael model) and the Herschel-Bulkley Model (Barnes, 2000; Bourne, 2002; Mezger, 2006; Sani *et al.*, 2014; Tao *et al.*, 2016). The Power Equation is a power law function that describes the flow of shear-thinning or shear-thickening behaviours that do not have to overcome a yield stress, whereas the Hershel-Bulkley Model describes the same flows, but for fluids that do have a yield stress.

The power law function is frequently used to describe polysaccharide solutions and is defined by Equation 3.6 (Mitchell, 1979):

$$\tau = K\dot{\gamma}^n \tag{3.6}$$

where τ is the shear stress, K is the consistency index, $\dot{\gamma}$ is the shear rate and n is the flow index. The flow index indicates the deviation from Newtonian behaviour ($n = 1$), where $0 < n < 1$ is shear-thinning, and $n > 1$ is shear-thickening. The further from unity the value of n is, the less Newtonian is the flow. When fluids obey the power law function, plotting the log of the shear stress against the log of the shear rate generates a linear slope equal to n, according to Equation 3.7, (Bourne, 2002; Tao *et al.*, 2016).

$$\log \tau = \log K + n \log \dot{\gamma} \tag{3.7}$$

The Herschel-Bulkley equation describes flow with a yield point, hence Equation 3.6 includes the yield stress (τ_0) per Equation 3.8:

$$\tau = \tau_0 + K\dot{\gamma}^n \tag{3.8}$$

Like the power law equation, the bilogarithmic plot of shear stress against shear rate is linear and the numerical value of n is found from the slope. Deviation of n from unity describes the degree of curvature of the slope when plotted on linear axes. Thus, for $n = 1$, the curve on the shear stress-shear rate plot is also linear (Bourne, 2002).

Viscoelastic measurements

Rheological experiments are time dependent. Over long durations of time, solids under stress begin to flow. Conversely, liquids can behave as solids over very brief periods. Hence, the proportion of the fluid (viscous) and solid (elastic) properties of a material are determined by the timescale of the deformation (Rees *et al.*, 1982). Dynamic viscoelastic measurements involve small deformation oscillations, which are used to determine the storage modulus (G') and loss modulus (G'') components in a polysaccharide network. In turn, these moduli describe the elastic and viscous properties of the system, respectively, over a range of deformation frequencies (Miyoshi and Nishinari, 1999; Timilsena *et al.*, 2015).

Small deformation oscillation tests involve the application of a sinusoidal strain on a sample. This strain induces a sine wave response. For perfectly elastic samples, this response will be exactly in phase with the applied strain. In contrast, purely viscous systems will have a 90° out-of-phase response to the strain wave (Picout and Ross-Murphy, 2003; Rees *et al.*, 1982). When the sample is overstrained, the elastic structure is destroyed. Hence, all oscillation deformation tests are conducted in the linear viscoelastic region (LVR) and the results indicate whether the sample is dominated by elastic or viscous behaviour over a given oscillatory frequency range (Haddarah *et al.*, 2014).

For viscoelastic measurements, the shear strain is defined according to Equation 3.9:

$$\gamma(t) = \gamma_0 \sin(\omega t) \tag{3.9}$$

where ω is the angular frequency. The shear stress is defined according to Equation 3.10:

$$\tau(t) = \tau_0(\omega t + \delta) \tag{3.10}$$

where δ is the phase angle. Then, the shear stress is written in terms of shear strain according to Equation 3.11, and the storage and loss moduli are determined according to Equations 3.12-3.15 (Bui *et al.*, 2012).

$$\tau(t) = \tau_0[\sin(\omega t)\cos\delta + \cos(\omega t)\sin\delta] \tag{3.11}$$

$$\tau(t) = \gamma_0\left[\left(\frac{\tau_0}{\gamma_0}\cos\delta\right)\sin(\omega t) + \left(\frac{\tau_0}{\gamma_0}\sin\delta\right)\cos(\omega t)\right] \tag{3.12}$$

$$\tau(t) = \gamma_0[G'\sin(\omega t) + G''\cos(\omega t)] \tag{3.13}$$

$$G' = \frac{\tau_0}{\gamma_0} cos\delta \tag{3.14}$$

$$G'' = \frac{\tau_0}{\gamma_0} sin\delta \tag{3.15}$$

The measure of the viscous-elastic ratio at a given angular frequency is found according to Equation 3.16 and the complex (dynamic) viscosity (η^*) is determined according to Equation 3.17 (Picout and Ross-Murphy, 2003; Rees *et al.*, 1982):

$$\tan\delta = \frac{G''}{G'} \tag{3.16}$$

$$\eta^* = \frac{G^*}{\omega} \tag{3.17}$$

where the complex shear modulus (G^*) is determined from Equation 3.18.

$$G^* = \frac{\tau^*}{\gamma} = \sqrt{\left(G'^2 + G''^2\right)} \tag{3.18}$$

where τ^* is the complex stress.

Several oscillatory tests are conducted to determine structural properties, including, the structural stability, structural strength and viscoelastic characteristics. Oscillatory amplitude and frequency sweep tests are two examples. The amplitude sweep entails deformation of the sample from small to large oscillation amplitudes whilst maintaining the frequency. This test determines the LVR and the critical amplitude after which the sample is irreversibly deformed. This test provides the structural stability, strength and dynamic yield points for viscoelastic materials. Conversely, the frequency sweep maintains a constant amplitude within the LVR (determined by the amplitude sweep) whilst ramping the oscillation frequency. This test provides the zero shear viscosity and rest structural strength values as well as the characteristic moduli curves for the material (Bui *et al.*, 2012). These characteristics were explored for the pullulan and *P. sacchari* EPS solutions.

3.5.2 Film formation and mechanical properties

Bioplastics and biofilms offer potential alternatives for petrochemical products. In the light of climate change and depleting oil-based carbon reserves polysaccharides and polysaccharide-derivatives have been investigated as suitable replacements for fossil fuel derived synthetic products. The challenge, however, is to produce bio-based alternatives with equivalent characteristics and at a competitive cost (Mekonnen *et al.*, 2013; Persin *et al.*, 2011).

Pullulan and pullulan-derivatives have been extensively studied to produce renewable, bio-based products. In particular, their use in edible films and packaging have been extensively explored. Pullulan forms transparent, colourless, tasteless, edible, non-toxic, biodegradable and oxygen impermeable films that find application in the coatings and packaging markets for both foods and pharmaceuticals (Diab *et al.*, 2001; Dixon *et al.*, 2006; Robyt, 1998; Roukas and Liakopoulou-Kyriakides, 1999; Singh *et al.*, 2008).

Biofilms are classified according to their strength, flexibility, opacity, hydrophobicity, hydrophilicity, and gas permeability (Vieira *et al.*, 2011). Biofilms used for packaging need to be ductile at room temperature and should not rupture during manufacture or use. Often, plasticisers are added to prepare polysaccharide biofilms that do not crack or tear (Mekonnen *et al.*, 2013). Plasticisers are low molecular weight compounds added to polymeric substances that act by disrupting the intermolecular forces (hydrogen bonds, Van Der Waals forces, *etc.*) within the chains, thereby improving the flexibility, workability and processability of the product. The most common biodegradable plasticisers used are water, polyols (*i.e.*, glycerol, sorbitol and mannitol), monosaccharides (*i.e.*, glucose, mannose and fructose) and oligosaccharides (*i.e.*, sucrose) (Vieira *et al.*, 2011).

Linear polysaccharides, such as pullulan and amylose of starch, generally produce tough films and the inflexibility of these films improves with the addition of plasticisers. For instance, the brittleness of starch products is overcome by the addition of glycerol (Rodríguez *et al.*, 2006) and/or sorbitol (Müller *et al.*, 2008). In general, plasticisers allow the mechanical properties of biopolymer films to be tuned according to the desired degree of flexibility, strength and ductility required for end-user applications (Azwar and Hakkarainen, 2012). These mechanical properties of materials are determined through assessment of their stress-strain behaviour. Stress-strain tests are conducted through application of a load over the surface or cross-section area of a material. The load can be applied via compression, shear (torsion) or tension – the latter being the most commonly used mechanical stress-strain test. Tension tests can be used to establish important mechanical properties of materials, including the elasticity, yield strength, maximum tensile strength, ductility and toughness. For polymers, the stress-strain behaviour then allows classification of the polymers as brittle, plastic or elastic. The tension tests used to determine these properties are destructive, since the sample is subjected to a load and deformed until it fractures. During the measurement, the specimen elongation and the applied load (force) are recorded throughout and these parameters are normalised in terms of engineering strain ($\in$) and stress (σ) as described in Equations 3.19 and 3.20, respectively (Callister, 2001):

$$\in = \frac{l_i - l_0}{l_0} = \frac{\Delta l}{l_0} \tag{3.19}$$

$$\sigma = \frac{F}{A} = E \in \tag{3.20}$$

where l_0 is the original length (in meters) of the specimen before any load is applied, l_i is the instantaneous length (in meters), Δl is the change in deformation elongation, F is force (in Newtons, N) and A is the area of the specimen (measured in m^2). Equation 3.20 is also known as Hooke's Law, and E is the constant of proportionality known as Young's modulus or the elastic modulus (in giga Pascal, GPa). The elastic modulus provides a measure of sample stiffness,

where the greater the modulus the stiffer the sample. When an applied load falls within the elastic region, deformation is not permanent and the specimen will retain its original shape on removal of the load. The modulus is determined from the linear region in a stress-strain curve as illustrated in Figure 3.16. This Figure provides the typical stress-strain curves for various types of materials that are deformed beyond the elastic region and until fracture occurs (indicated by ×). Also indicated in the deformation curves are the typical positions for the yield strength (σ_y, in mega Pascals, MPa) and maximum tensile stress (σ_M, indicated by M, and in MPa). The yield strength of a material provides the stress level beyond which elastic deformation ceases, plastic deformation begins and the material is permanently deformed (Davis, 2004). The maximum tensile strength is the stress at the deformation curve maximum and indicates the ultimate stress that the material can sustain under tension and if this stress is maintained the material will eventually fracture. In many instances fracture occurs at the tensile strength maximum, but in other instances "*necking*" can occur where a small constriction forms at some point in the specimen and as strain continues, all subsequent deformation is confined to this region, where fracture will ultimately occur (Callister, 2001). The ductile material represented in Figure 3.16 has undergone this deformation phenomenon beyond the strain where the maximum tensile strength occurred.

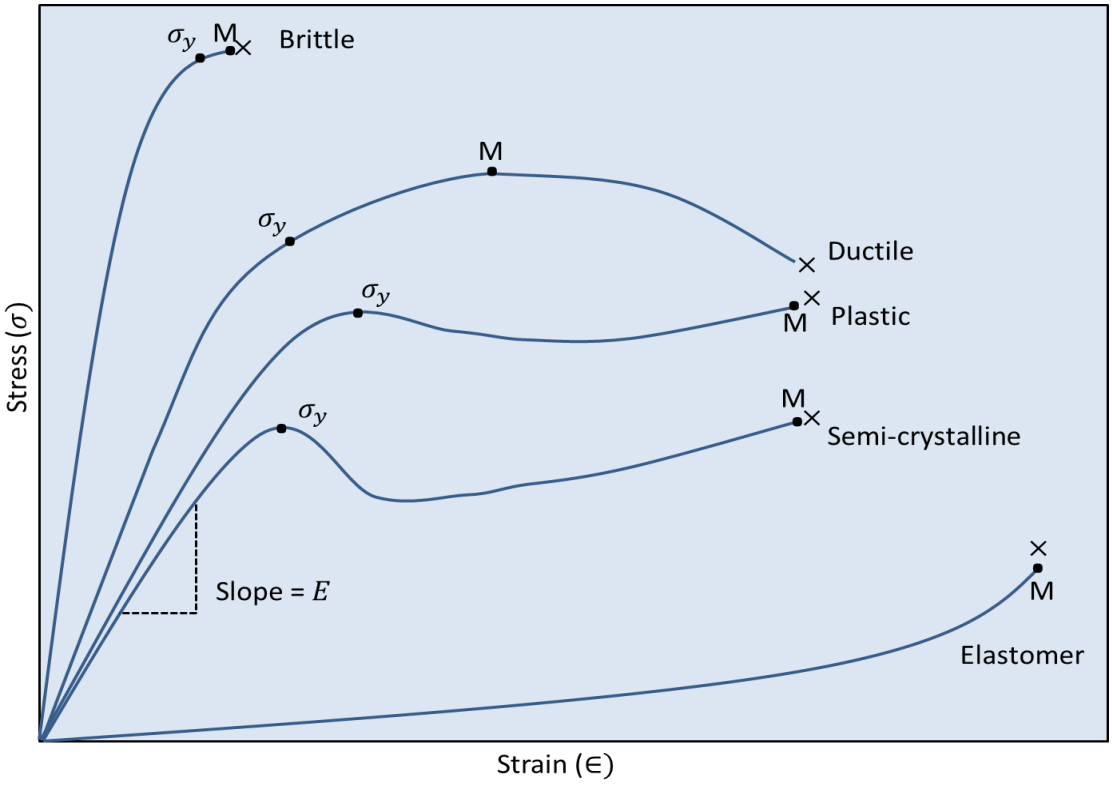

Figure 3.16: Stress-strain curves to fracture (×) illustrating the linear region where the modulus of elasticity (E) is determined from the slope, the point where the yield stress (σ_y) is measured, and the point where tensile strength (M) is measured, together with the typical shapes of the deformation curves for brittle, ductile, plastic, semi-crystalline and elastomer materials.

Ductility is a measure of the degree of plastic deformation a material can undergo before fracturing. Ductility is quantified as a percentage in elongation (%EL) and is calculated according to Equation 3.21 (Callister, 2001):

$$\%EL = \left(\frac{l_f - l_0}{l_0}\right) \times 100 \tag{3.21}$$

where l_f is the final length of the specimen at fracture.

The yield strength, maximum tensile strength and the ductility are important mechanical strength properties used to describe polymeric materials. Furthermore, the shape of the stress-strain curves for polymeric materials are useful for describing their behaviour. Polymers display either brittle, plastic, highly elastic (elastomer) or semi-crystalline stress-strain curves, as illustrated in Figure 3.16. Brittle polymers have a high elastic modulus, and tend to fracture whilst still deforming elastically, or just beyond their yield stress. Plastic polymers, however, have an elastic region, followed by a region of plastic deformation following yielding. The maximum tensile strength coincides with the fracture stress, which may occur at a higher or lower value than the yield strength. Highly elastic polymers do not have a yield strength, as they are completely elastic and are able to recover from large strains at very low stress levels. Finally, semi-crystalline polymers have both an upper and a lower yield point followed by a relatively flat region in their stress-strain curves. In these materials, a neck forms in the specimen following the upper yield point and therein the polymeric chains begin to align. This alignment occurs parallel to the direction of elongation and causes strengthening and resistance to deformation. As the strain increases, elongation and subsequent deformation is confined to the neck region until the specimen eventually fails (Callister, 2001).

The stress-strain curves and the mechanical properties, including, the yield strength, maximum tensile strength and ductility of the pullulan and crude *P. sacchari* EPS films were investigated. Furthermore, the effect of sorbitol as a plasticiser was also determined in these films. The experimental procedures for these tests are described in Section 4.5 and the results thereof are discussed in Section 5.5.

Chapter 4
Experimental

This chapter provides a detailed description of the experimental procedures used in this study. First, all the experimental details are provided for the structural characterisation studies; including, GFC, GC-MS, NMR and enzyme-HPLC analyses. Then, the experimental details are provided for the physical characterisation studies, *i.e.*, for the rheological determinations as well as the film forming and film mechanical property investigations.

4.1 Gel filtration chromatography

As outlined in Section 3.1, GFC was used to determine the MW and MWDs of the isolated *P. sacchari* EPSs. Furthermore, GFC was used to further purify one of the EPSs (FB2) into fractionates for further investigation. This experimental sub-section outlines the methods for the column preparation, evaluation, calibration and MW determinations. During this work, two separate columns (A and B) were prepared. These are both described. This subchapter concludes with the EPS sample preparations and treatments.

4.1.1 Column preparations

A glass Omnifit column (ø = 15 mm), was packed with HW-65F Toyopearl® resin (lot No. 65HWFB22D). To determine the amount of packed resin required, the column volume was first calculated:

$$V_{column} = \pi r^2 h \tag{4.1}$$

In this calculation, the column packed resin volume is V_{column}, the column radius is given as r, and the height of the resin bed is h. According to the manufacturer's specifications, approximately four volumes of supplied resin suspension (in 20% ethanol) is equivalent to three volumes of pure resin. For both columns, 107 cm^3 of resin suspension was transferred to a 1000 cm^3 beaker for de-fining.

For de-fining, four volumes (430 cm^3) of the nitrogen (N_2) degassed, ionic packing solvent (0.1 M $NaNO_3$ in 50 mM tris(hydroxymethyl)aminomethane buffer) was added to the suspension, and the mixture was vigorously stirred with a glass rod. Care was taken not to crush the resin beads. The slurry was left to settle for 45-60 minutes. Thereafter, the supernatant was carefully decanted off and the process repeated until the supernatant was clear (four times).

The resin was left to settle overnight before the slurry concentration was adjusted to 50%. The column was packed using assisted gravity, by means of attaching a peristaltic pump to the column outlet. Solvent was added to the leveled column and the peristaltic pump was set in the down-flow position (flow rate A = 2.3 $cm^3\ min^{-1}$; flow rate B = 3.9 $cm^3\ min^{-1}$). The column was half-filled with solvent before the homogeneous slurry was carefully added (by pouring it down the sides to prevent air bubbles from being trapped). As the resin began to settle, solvent was carefully added to the top of the column to ensure that the resin bed did not run dry. Once the

resin bed had formed, 2-3 cm of solvent was left above the bed and the peristaltic pump was switched off. The flow adapter was carefully placed at the top of the column together with a reservoir of solvent. The peristaltic pump flow was then adjusted to the minimum operating flow rate of 1.0 cm^3 min^{-1}. This flow was incrementally increased over three minutes, to the desired final flow rate (A = 1.9 cm^3 min^{-1}; B = 2.8 cm^3 min^{-1}). After compression of the resin bed was observed, the flow was stopped and the flow adapter was carefully lowered onto the bed (ensuring that the resin did not go past the adapter seal). The peristaltic pump was ramped to the desired flow rate as before and this process was repeated until no further compression of the resin bed was observed (< 0.5 cm). Column A had a final bed height of 42.8 cm and Column B had a bed height of 46.5 cm.

Each packed column was then connected between a pump (LabAlliance™), an auto-sampler (SGE, LS-3200), a RI detector (Erma Inc., ERC-7512) and a fraction collector (Bio-Rad BioLogic BioFrac™). A data system (PeakSimple Chromatography Data System, SRI Model 202) was used to record and process the data. Following the column evaluation tests, the autosampler was replaced with an injector port fitted with a 1 cm^3 loop.

With the pump positioned at the front end of the column, the flow rate was ramped to the desired flow rate (A = 1.0 cm^3 min^{-1}; B = 1.5 cm^3 min^{-1}) in 0.25 cm^3 min^{-1} increments. The operating solvent was deionised, degassed water (Millipore Elix®). The column was left to equilibrate with the minimum five bed volumes (BVs) of water overnight.

4.1.2 Column evaluation

Column efficiency tests were performed with a low MW compound. In this study a 2 M NaCl solution was prepared, and 200 µL was injected with the auto-sampler and eluted at the operating flow rate (A = 1.0 cm^3 min^{-1}; B = 1.5 cm^3 min^{-1}) (Hagel, 1998). The results from the column efficiency tests are found in Appendix A.

4.1.3 Column calibration and molecular weight determinations

This section details the experimental steps taken to calibrate the columns, construct the calibration curves, and determine the sample molecular weight measurements from the acquired data.

Calibration

The prepared Toyopearl® columns (A and B) were calibrated using several GPC grade dextran standards by recording and plotting their elution times against the logarithm ($\log_{10}$) of their respective MWs, synonymous to the illustration in Figure 3.2. The GPC grade dextran standards (Sigma-Aldrich) are described in Table 4.1. To determine the column's separation limits (V_o and V_t)[5] a 0.3 M NaCl and a dextran standard (2 mg cm^{-3}) with a minimum MW of 5 million Da (T5000) were eluted, respectively.

Each dextran standard (~2 mg cm^{-3}) was prepared in deionised water. Before injection onto the column, each standard was filtered through a 0.45 µm Millipore® nitrocellulose membrane syringe filter. All the injections were 1 cm^3 (1.3% BV). The flow rate was kept constant (A = 1.0 cm^3 min^{-1}; B = 1.5 cm^3 min^{-1}).

[5] Since column A was operated with a flow rate of 1.0 cm^3 min^{-1}, the elution time (T) and volume (V) were equivalent. For column B, the elution volumes were 1.5x that of the elution times, since the operating flow rate was 1.5 cm^3 min^{-1}.

Table 4.1 Dextran standards used to calibrate Toyopearl® Column A.

Dextran standard	M_w/Da	MP/Da	M_n/Da
GPC5K[a]	5220	4440	3260
GPC50K	48 600	43 500	35 600
GPC150K	147 600	123 600	100 300
GPC410K	409 800	276 500	236 300
GPC670K	667 800	401 300	332 800

[a] K = 10^3

Three replicates of each standard were eluted through the columns and the corresponding V_es (or T_es) for each peak was recorded. The elution values of each standard were plotted against the corresponding $\log_{10}$MP values to construct the calibration curves. Regression analysis was applied to the data, the residuals plots and curvilinear regression models were assessed, and the best fit polynomial for each calibration was determined using the partial F-test (Miller, 1991).

Molecular weight determinations

To measure the MWs and to determine the MWD statistical averages for the pullulan and EPS samples, the PeakSimple acquisition data and the column calibration equations were required. The calibration equations were determined as described in Section 3.1.4. The PeakSimple acquisition data from each of the samples were saved as ASCII files. The data were acquired at five points per second. For peak slicing, sets of 30 data points were grouped. Each time interval represented a data slice, beginning at zero. For each of the time slices, the corresponding MWs (M_i) were calculated using the polynomial equations generated from the respective calibration curves. The baseline subtracted RI detector response in millivolts (mV) is referred as h_i and the values for M_z, M_w, M_n, MP and the PDI were calculated according to the equations described in Section 3.1.4.

4.1.4 Sample preparation and treatment

Pullulan and the EPS samples were prepared as 2-3 mg cm^{-3} solutions. The pullulan used as a model compound throughout this study is one which was produced by *Aureobasidium pullulans* (Sigma-Aldrich, Product code P-4516, lot number 40K1170). For dissolution of the lyophilised EPSs samples, each were prepared in deionised water and required heating to 80-90 °C for approximately three hours. The cooled solutions were frozen in sachets (~20 cm^3 each) between analyses. Before use, each sachet was thawed and left to equilibrate to room temperature for three hours. Aliquots were filtered through 0.45 µm Millipore® nitrocellulose membrane syringe filters before injection onto the column.

For FB2, the components eluting from the column were collected in 1 cm^3 increments with the fraction collector. Based on the elution profile of the sample, corresponding fractions were pooled. The pooled fractions were then reduced to ~1 cm^3 on a Büchi Rotavapor-R rotary evaporator under vacuum (48 °C, <1 kPa). These fractionates were individually and quantitatively transferred to 2 cm^3 vials and lyophilised (-30 °C, 0.667 kPa). These freeze-dried samples were stored in desiccators with self-indicating silica gel. Before use, the samples were

further dried *in vacuo* over di-phosphorus pentoxide (P_2O_5) (Merck, lot number K29109970146) for a minimum of three hours to remove all traces of water.

4.2 Gas chromatography-mass spectrometry

As outlined in Section 3.2.2, GC-MS is the tool of choice to carry out composition and structure analyses of suitably prepared polysaccharide samples. The following subsections provide the sample preparation and derivatisation steps for analyses carried out by GC-MS, together with the instrument details and settings used to determine the composition and structure of the EPS samples produced by *P. sacchari*.

4.2.1 Composition analysis

For GC-MS composition analysis, the type of monosaccharides arising from the *P. sacchari* EPS samples were determined.

Sample preparation

Pullulan (described in Section 4.1.4) was stored at 4 °C in a sealed container with silica gel desiccant. The lyophilised EPS samples were stored at room temperature in sealed sachets over silica gel desiccant. Standards prepared alongside the samples were dried *in vacuo* over P_2O_5 for a minimum of 6 hours before use to remove any residual water. The RRTs and mass spectra of the standards were compiled into compound tables for processing the sample data and into a mass spectral library for future reference (refer to Appendix D). The sections below describe the sample preparation and instrument analysis parameters used.

Methanolysis

The samples and standards were weighed (0.5-1.0 ± 0.1 mg) into separate Reacti-Vials™. A methanolic HCl (0.500 M) reagent was freshly prepared by adding (35 µL cm^{-3}) acetyl chloride (Merck, lot number 1204450) to dried methanol[6] (Merck, lot number I685107320). An aliquot of this solution (0.5 cm^3) together with D-(-)-sorbitol (Merck, lot number L214259525) internal standard (10 µL, 0.300 g L^{-1} in dried methanol) were added to each of the dried samples. The vials were sealed and placed on a Pierce Reacti-Therm™ III heating module and left at 80 °C for 20 h. After heating, the cooled samples were dried under a flow of dry N_2.

Silylation

Pyridine (0.5 cm^3, Merck, lot number I688465328), hexamethyldisilazane (0.45 cm^3, Merck, lot number S6257624214) and trifluoroacetic acid (50 µL, Merck, lot number 56651360317) were added to each vial of dried methanolysates. The vials were capped with Teflon-lined lids and placed in a sonicator bath (MGW Lauda) at 80 °C for 20 min. The samples were cooled to room temperature, centrifuged at 4800 revolutions per minute (rpm) for 5 min (VWR Himac CT6E), and the supernatant was transferred to 1 cm^3 gas chromatography vials, which were crimped closed.

[6] Methanol was dried over 3 Å molecular sieves, previously activated at 250 °C for 2 hours.

Instrument conditions

The instrument used for analyses was a Varian CP-3800 GC fitted with a factor four capillary column (VF-5ms, 30 m × 0.25 mm × 0.25 µm), coupled to either a Varian 4000 GC-MS/MS or Varian Saturn 2000 GC-MS/MS detector. The injector was set at 280 °C in the standard split/splitless mode. The sample (1 µL) was injected with a split ratio of 1:50 and carried through the column with helium gas set at a flow rate of 1.3 cm min^{-1}. The initial column temperature was set at 140 °C, and this was held for 1.00 min before the temperature was raised to 218 °C at a rate of 2.0 °C min^{-1}. The temperature was then raised to a maximum of 280 °C at a rate of 10 °C min^{-1}, and held for 2.00 min. The total run time was 48.20 min. For detection, the ion source was set in EI mode with an emission current of 10 µA from 5.00-48.20 min. The mass range detected was from 45-650 *m/z*.

For MS/MS confirmation, the same GC parameters were used but detection was split over four segments. From 0.00-5.00 min ionisation was suppressed. From 5.00-13.50 min, full EI at 10 µAmps in the range 45-1000 *m/z* was run. From 13.50-20.00 min, only the precursor ion of 204.0 ± 3.0 *m/z* was ionised. From 20.00-21.50 min, only the precursor ion 217.0 ± 3.0 *m/z* was ionised. The last segment ran from 21.50-48.20 min, with full EI in the range 45-1000 *m/z*.

4.2.2 Absolute configuration analysis

For GC-MS absolute configuration analyses, the enantiomeric (D and L) configuration of the monosaccharides composing the *P. sacchari* EPS samples was determined. The polysaccharides were hydrolysed in S-(+)-2-butanolic HCl (1 M) and silylated, as previously described (Section 4.2.1). The samples were analysed by GC-MS against similarly prepared D and L standards of glucose, galactose and mannose. The RRTs and mass spectra of the (+)-2-butyl glycosides were added to compound tables for processing the sample data (refer to Appendix D and E). The sections below describe the sample preparation and instrument analysis parameters used.

Sample and standard preparation

The standards, pullulan and the EPS samples (FB2, PB2 and PB7) were dried *in vacuo* over silica gel at 40 °C for a minimum of 24 hours, to remove residual water. Standards used in the determination included: D-(+)-glucose (Sigma-Aldrich, lot number 129K0051), L-(-)-glucose (Sigma-Aldrich, lot number BCBP5658V), D-(+)-galactose (Merck, lot number 7517506), L-(-)-galactose (Sigma-Aldrich, lot number 028K1518), D-(+)-mannose (Merck, lot number K21710788), L-(-)-mannose (Sigma-Aldrich, lot number 068K1255) and D-(-)-sorbitol as the internal standard (9.91×10^{-3} g cm^{-3} in dry methanol).

Butanolysis

The method as described by Gerwig and co-workers (1978) was adapted as described. To separate Reacti-Vials™, the sorbitol internal standard solution was added (50 µL) and the vials were evaporated to dryness *in vacuo* overnight. dried pullulan, the standards or the EPS samples were added (1-2 mg ± 0.1 mg) to each of the dry Reacti-Vials™ containing internal standard. S-(+)-2-butanolic HCl (1 M) reagent was freshly prepared by adding acetyl chloride (285 µL cm^{-3}) to S-(+)-2-butanol (Sigma-Aldrich, lot number 91896JJ), which had been dried over powdered potassium carbonate (0.0066 g cm^{-3}). An aliquot of the prepared S-(+)-2-butanolic 1 M HCl (0.5 cm^3) was added to each vial. The vials were sealed, vortexed (YellowLine TTS 2) and placed in a dry bath (MRC Scientific Instruments, DBG-002). Initially, the dry bath was set at 80 °C for 8 h, after which time the standards were removed. The samples were heated at 85 °C for an additional 16 h. After removing the standards or samples from the dry bath, they were left to cool to room temperature. Each was then neutralised with an excess

of solid silver carbonate (BDH, lot number 0359900). The vials were centrifuged (4800 rpm, 5 min) and the supernatants concentrated to dryness *in vacuo* at 40 °C over silica gel in a desiccator for a minimum of 12 h.

Silylation

The same silylation procedure as described in Section 4.2.1 was followed.

Instrument conditions

The instrument used for analyses was a Varian CP-3800 GC fitted with a factor four capillary column (VF-5ms, 30 m × 0.25 mm × 0.25 µm), coupled to a Varian Saturn 2000 GC-MS/MS detector. The injector was set at 280 °C in the standard split/splitless mode. The sample (1 µL) was injected in a split ratio of 1:2 and carried through the column with helium gas, set at a flow rate of 1.0 cm min^{-1}. The initial column temperature was set at 80°C, which was held for 2.00 min before raising to 150 °C at a rate of 30.0 °C min^{-1}. The temperature was then increased at 5.0 °C min^{-1} to 280 °C and held for 1.00 min. Finally, the temperature was raised to 300 °C, at 15.0 °C min^{-1}, where it was held for a further 1.00 min. The total run time was 33.67 min. For detection, the ion source was set in EI mode at 10 µAmps from 5.00-33.67 min. The mass range detected was from 45-650 *m/z*.

4.2.3 Structure analysis – permethylation protocol

For GC-MS structure analyses, the type of linkages present in the *P. sacchari* EPS samples were determined according to the permethylation protocol as described in Section 3.2.2. The sample preparation, permethylation, methanolysis and silylation steps are outlined below, together with the instrument details.

Sample preparation

Pullulan (described in Section 4.1.4) was stored at 4 °C in a sealed container over silica gel desiccant. The lyophilised EPS samples were stored in sealed sachets over silica gel desiccant. Standards and samples were dried *in vacuo* over P_2O_5 for a minimum of 6 h before use, to remove any residual water. The RRTs and mass spectra of the standards were compiled into compound tables for processing the sample data and into a mass spectral library for future reference (refer to Appendix D and Appendix E). The sections below describe the sample preparation and instrument analysis parameters used.

Permethylation

The dried samples and standards were each weighed (0.5-1.0 ± 0.1 mg) into separate 4 cm^3 screw cap vials. To each of these, dry DMSO[7] (0.5 cm^3) and MeI (100 µL) were added. Finely ground, dry NaOH[8] (60 mg) was added in excess[9] to each vial.

The capped vials were vortexed (to mix the suspension), and were then left in the thermo-regulated sonicator bath (50 °C, 30 min). The permethylated samples were cooled to room temperature. Water was added (1 cm^3) to dissolve the NaOH, and the samples were extracted with dichloromethane (1 cm^3), and washed several times with deionised water.

[7] DMSO was dried over 4 Å molecular sieves that were previously activated at 300 °C for 16 hours.

[8] The NaOH pellets were ground with a dry and hot (heated to 120 °C in an oven) mortar and pestle.

[9] An excess of three millimolar equivalents per millimole replaceable hydrogen NaOH was added per vial.

Excess water in the extracted samples was removed by addition of anhydrous sodium sulfate. Following centrifugation (4800 rpm, 5 min) the samples were transferred to 1 cm^3 Reacti-Vials™ containing sorbitol solution (5 µL, 0.3 g cm^{-3} in dry methanol) as the internal standard. The permethylated samples were dried under a flow of dry N_2 and then underwent methanolysis.

Methanolysis

The permethylated samples underwent methanolysis as described before (Section 4.2.1).

Silylation

Following methanolysis, the samples underwent silylation as described before (Section 4.2.1).

Instrument conditions

The instruments and column used were as described in Section 4.2.1. The injector was set at 260 °C in the standard split/splitless mode. The sample (1 µL) was injected, with the split ratio initially set to 1:10, changing to splitless from 0.1-0.75 min, followed by a 1:50 split. The helium gas flow rate was set at 1.0 mL min^{-1}. The initial column temperature was 100 °C, which was held for 2.00 min before being raised to 180 °C, at a rate of 2.0 °C min^{-1}. Thereafter, the rate was increased at 40 °C min^{-1} to a maximum of 300 °C, where it was held for 2.00 min. The total run time was 47.00 min. For detection, the ion source was set in EI mode at 10 µA and run from 5.00-47.00 min. The mass range detected was from 45-600 *m/z*.

4.3 Nuclear magnetic resonance spectroscopy

NMR was used in this study to determine both the anomeric conformation and the repeat sequence within the pullulan model compound and the *P. sacchari* EPS samples. The polysaccharides were analysed by 1D and 2D NMR in either their native form (in D_2O) or after acetylation (and in $CDCl_3$). Table 4.2 summarises the treatments and analyses of each sample, the parameters of which are described in the sections that follow. The sections are divided into two parts. The first part provides the preparation and NMR analysis details for the native polysaccharides. The second part details the preparation and NMR analysis conditions for the polysaccharide peracetates.

Table 4.2 Summary of NMR analyses conducted on the native and/or acetylated pullulan and *P. sacchari* polysaccharides.

Polysaccharide (PS)	NMR analyses of the native PS in D_2O	NMR analyses of the acetylated PS in $CDCl_3$
Pullulan	^{1}H, ^{13}C, Dept90, Dept135, ^{1}H-^{1}H COSY, HSQC, HMBC, NOESY, ROESY	^{1}H, ^{13}C, ^{1}H-^{1}H COSY, HSQC, HMBC, NOESY
FB2 F1	^{1}H, ^{13}C, Dept90, Dept135, ^{1}H-^{1}H COSY, HSQC, HMBC, ROESY	n.a.
FB2 F2	^{1}H, ^{13}C, ^{1}H-^{1}H COSY, HSQC, HMBC, NOESY, ROESY	n.a.
FB2	^{1}H	^{1}H, ^{13}C, ^{1}H-^{1}H COSY, HSQC, HMBC, NOESY
PB2	^{1}H	^{1}H, ^{13}C, ^{1}H-^{1}H COSY, HSQC, HMBC, NOESY
PB7	^{1}H	^{1}H, ^{13}C, ^{1}H-^{1}H COSY, HSQC, HMBC, NOESY

D_2O – deuterated water, $CDCl_3$ – deuterated chloroform, n.a. – not applicable, there was insufficient sample available to prepare this polysaccharide peracetate, DEPT – distortionless enhancement by polarisation transfer, ^{1}H – proton, ^{13}C – carbon, COSY – correlation spectroscopy, HSQC – heteronuclear single-quantum correlation, HMBC – heteronuclear multiple bond correlation spectroscopy, NOESY – nuclear Overhauser effect spectroscopy, ROESY – rotating frame nuclear Overhauser effect spectroscopy.

4.3.1 Polysaccharide preparation and nuclear resonance spectroscopy conditions

Preparation

Pullulan and the lyophilised native *P. sacchari* EPSs were dried *in vacuo* over P_2O_5 overnight to remove any residual moisture. Prior to analysis, the samples were dissolved in D_2O (99.9%) (~17 mg mL^{-1}) at ~80 °C, and transferred to NMR tubes (5 mm, 500 MHz Norell™) to a height of 4.5-5.5 mm.

NMR conditions

The NMR data were recorded on Bruker AVANCE III 400 and 600 instruments. The chemical shifts were referenced to the D_2O solvent peak at $\delta_{H,\ 25\ °C}$ = 4.7 ppm (Gottlieb *et al.*, 1997). The Bruker AVANCE III 400 instrument was fitted with a BBO 400 MHz S1 5 mm probe (with *z*-gradient). The ^{1}H NMR spectra were recorded at a transmitter frequency of 400.2 MHz. The acquisition parameters were as follows: spectral width, 8224 Hz; acquisition time, 1.99 s; 90° pulse width, 10.00 µs; scans, 16; relaxation delay, 1.0 s). The ^{13}C NMR spectra were recorded at 100.6 MHz (spectral width, 34 038 Hz; acquisition time, 1.36 s; 90° pulse width, 8.40 µs; scans, 6400; relaxation delay, 2.0 s).

The Bruker AVANCE III 600 instrument was fitted with a BBO 600 MHz S3 5 mm probe (with *z*-gradient), and all spectra were recorded at 25 °C. The ^{1}H NMR spectra were recorded at a transmitter frequency of 600.1 MHz. The acquisition parameters were as follows: spectral width, 7062 Hz (F1), 5650 Hz (F2); acquisition time, 2.32 s (F1), 2.90 s (F2); 90° pulse width, 13.38 µs (F1),13.60 µs (F2); scans, 16; relaxation delay, 1.0 s). The ^{13}C NMR spectra were recorded at 150.9 MHz (spectral width, 36 000 Hz; acquisition time, 0.91 s; 90° pulse width, 9.00 µs (F1), 12.70 µs (F2); scans, 16 000 (F1), 9600 (F2); relaxation delay, 2.0 s).

The DEPT90 and DEPT135 experiments were run on either the Bruker AVANCE III 400 (pullulan) or the Bruker AVANCE III 600 (FB2 F1) instruments. For pullulan, the acquisition parameters were as follows: spectral width, 24 038 Hz; acquisition time, 1.36 s; 90° pulse width, 8.40 µs; scans, 1600; relaxation delay, 2.0 s. For FB2 F1, the parameters were as follows: spectral width, 36 058 Hz; acquisition time, 0.91 s; 90° pulse width, 9.00 µs; scans, 4800; relaxation delay, 2.0 s.

The acquisition parameters for the 2D experimental data (COSY, HSQC, HMBC, NOESY) obtained on the Bruker AVANCE III 400 for pullulan were as follows: 90° pulse width, 10.00 µs; spectral width for ^{1}H, 1096 Hz (COSY, HSQC, HMBC, NOESY); spectral width for ^{13}C, 16 670 (HSQC) and 22 353 Hz (HMBC); number of data points per spectrum, 2048 (COSY, NOESY), 1024 (HSQC) and 4096 (HMBC); number of time incremented spectra, 256 (COSY, HSQC, HMBC), 512 (NOESY); relaxation delay, 0.74 s (COSY), 1.1 s (HSQC), 0.1 s (HMBC) and 1.3 s (NOESY).

The ROESY data for pullulan was obtained on the Bruker AVANCE III 600 and the acquisition parameters were as follows: 90° pulse width, 13.18 µs; spectral width for ^{1}H, 7212 Hz (COSY, HSQC, HMBC); number of data points per spectrum, 2048; number of time incremented spectra, 512; relaxation delay, 1.5 s.

The acquisition parameters for the 2D experimental data (COSY, HSQC, HMBC, ROESY) obtained on the Bruker AVANCE III 600 for FB2 F1 and FB2 F2 were as follows: 90° pulse width, 13.38 µs (FB2 F1) and 13.60 µs (FB2 F2); spectral width for ^{1}H, 7062 Hz (FB2 F1, COSY) and 5648 Hz (FB2 F2, COSY), 6818 Hz (HSQC), 6887 Hz (HMBC), 7212 Hz (ROESY); spectral width for ^{13}C, 36 059 Hz (HSQC and HMBC); number of data points per spectrum, 2048 (COSY, HSQC AND ROESY), 4096 (HMBC); number of time incremented spectra, 512 (COSY, HSQC AND ROESY), and 256 (HMBC); relaxation delay, 1.0 s (FB2 F1, COSY) and 3.0 s (FB2 F2, COSY), 1.0 s (HSQC), 3.0 s (HMBC), 1.5 s (ROESY).

The spectra acquired in absolute value mode include the ^{1}H, ^{13}C, HMBC and COSY experiments. The HSQC and NOESY experiments were acquired in phase-sensitive mode. Gradients were used on all 2D experiments. All experiments were run at ambient temperature (AVANCE III 400) or at 25 °C (AVANCE III 600). The NMR spectra are found in Appendix F.

4.3.2 Polysaccharide peracetate preparation and nuclear magnetic resonance conditions

Preparation

Pullulan and the lyophilised *P. sacchari* EPSs were acetylated by adaptation of the method used by Tezuka (1996). The pullulan and EPSs (0.05 g) were each weighed into separate Kimax test tubes and 2.5 cm^{3} pyridine (Merck, lot number I642563 224) was added. The tubes were capped and the samples were left to dissolve at 37 °C overnight. To each dissolved sample, 2.5 cm^{3} acetic anhydride (Sigma-Aldrich, lot number SZBA3280V) was added. The test tubes were capped, shaken to mix, and left to react at 37 °C overnight. The acetylated samples were

then poured over 30 cm^3 crushed ice (prepared from deionised H_2O) and left to stand for 30-60 min. The precipitate was isolated by vacuum filtration with the aid of Whatman No. 5 filter papers, and repeatedly washed with aliquots of deionised H_2O to remove any residual solvent. The air-dried precipitate was then quantitatively transferred to a beaker and dissolved in chloroform (PAL Chemicals, lot number not supplied). The dissolved, acetylated samples were decanted into 50 mm plastic petri dishes and left to dry into a film at 37 °C *in vacuo* in a desiccator overnight. The acetyl films were stored in sealed sachets over silica dessicant and dissolved (~17 mg mL^{-1}) in 99.8% $CDCl_3$ (Merck, lot number S5645420 507). Each sample was filtered through cotton wool and transferred to NMR tubes (5 mm, 500 MHz Norell™) to a height of 4.5-5.5 mm.

NMR conditions

The NMR data were recorded on Bruker AVANCE III 400 and 600 instruments. The chemical shifts were referenced to the $CDCl_3$ solvent peak at $\delta_{H,\ 25\ °C}$ = 7.3 ppm and $\delta_{C,\ 25\ °C}$ = 77.4 ppm (Gottlieb *et al.*, 1997).

The Bruker AVANCE III 400 instrument was fitted with a BBO 400 MHz S1 5 mm probe (with *z*-gradient). The ^1H NMR spectra were recorded at a transmitter frequency of 400.2 MHz with the following acquisition parameters: spectral width, 8224 Hz; acquisition time, 1.99 s; 90° pulse width, 10.00 µs; scans, 16; relaxation delay, 1.0 s.

The Bruker AVANCE III 600 instrument was fitted with a BBO 600 MHz S3 5 mm probe (with *z*-gradient), and all spectra were recorded at 25 °C. The ^1H NMR spectra were recorded at a transmitter frequency of 600.1 MHz and the acquisition parameters were as follows: spectral width, 5631 Hz (Pullulan acetate), 6098 Hz (PB2 acetate), 6188 Hz (PB7 acetate), 6466 Hz (FB2 acetate); acquisition time, 2.91 s (Pullulan acetate), 2.69 s (PB2 acetate), 2.65 s (PB7 acetate), 2.53 s (FB2 acetate); 90° pulse width, 7.70 µs pulse; scans, 32; relaxation delay, 1.0 s. The ^{13}C NMR spectra were recorded at 150.9 MHz (spectral width, 36 058 Hz; acquisition time, 0.91 s; 90° pulse width, 9.00 µs; scans, 16 000; relaxation delay, 2.0 s).

The acquisition parameters for the 2D experiments (COSY, HSQC, HMBC, NOESY) obtained on the Bruker AVANCE III 600 are outlined for each sample below.

For Pullulan Acetate: 90° pulse width, 7.70 µs (COSY, HSQC, HMBC) and 15.10 µs (NOESY); spectral width for ^1H, 5631 Hz (COSY, HSQC, HMBC) and 9014 Hz (NOESY); spectral width for ^{13}C, 24 996 Hz (HSQC) and 33 516 Hz (HMBC); number of data points per spectrum, 2048 (COSY, NOESY), 1024 (HSQC) and 4096 (HMBC); number of time incremented spectra, 256; number of scans, 4 (COSY), 8 (HSQC, NOESY), and 64 (HMBC); relaxation delay, 1.0 s.

For PB2 Acetate: 90° pulse width, 7.70 µs (COSY, HSQC, HMBC) and 15.10 µs (NOESY); spectral width for ^1H, 6466 Hz (COSY), 6 097 Hz (HSQC, HMBC) and 9014 Hz (NOESY); spectral width for ^{13}C, 24 996 Hz (HSQC) and 33 516 Hz (HMBC); number of data points per spectrum, 2048 (COSY, NOESY), 1024 (HSQC), and 4096 (HMBC); number of time incremented spectra, 256; number of scans, 4 (COSY), 16 (HSQC), 64 (HMBC), and 8 (NOESY); relaxation delay, 1.0 s.

For PB7 Acetate: 90° pulse width, 7.70 µs (COSY, HSQC, HMBC) and 15.10 µs (NOESY); spectral width for ^1H, 6189 Hz (COSY), 6189 Hz (HSQC, HMBC) and 9014 Hz (NOESY); spectral width for ^{13}C, 24 996 Hz (HSQC) and 33 516 Hz (HMBC); number of data points per spectrum, 2048 (COSY, NOESY), 1024 (HSQC), and 4096 (HMBC); number of time incremented spectra, 256; number of scans, 4 (COSY), 8 (HSQC), 128 (HMBC), and 8 (NOESY); relaxation delay, 1.0 s.

For FB2 Acetate: 90° pulse width, 7.70 µs (COSY, HSQC, HMBC) and 15.10 µs (NOESY); spectral width for ^{1}H, 6466 Hz (COSY), 6466 Hz (HSQC, HMBC) and 9014 Hz (NOESY); spectral width for ^{13}C, 24 996 Hz (HSQC) and 33 516 Hz (HMBC); number of data points per spectrum, 2048 (COSY, NOESY), 1024 (HSQC), and 4096 (HMBC); number of time incremented spectra, 256; number of scans, 4 (COSY), 16 (HSQC), 128 (HMBC), and 8 (NOESY); relaxation delay, 1.0 s.

The spectra acquired in absolute value mode include the ^{1}H, ^{13}C, HMBC and COSY experiments. The HSQC and NOESY experiments were acquired in phase-sensitive mode. Gradients were used on all 2D experiments. All experiments were run at ambient temperature (AVANCE III 400) or at 25 °C (AVANCE III 600). The NMR spectra are found in Appendix F.

4.4 Enzymatic hydrolysis and high performance liquid chromatography

Enzymatic hydrolysis was used as a complementary method to NMR for establishing the sequence information of pullulan, the fractionated EPSs (FB2 F1 and FB2 F2) and the unfractionated EPSs (FB2, PB2 and PB7). The subsections that follow detail the chemicals used, sample preparations and HPLC (HPAEC-PAD) settings.

4.4.1 Chemical details

Two separate pullulanase enzymes were employed over the course of experimentation. The first enzyme experiments were conducted with a Novozyme pullulanase (Promozyme™ 400L, batch number A/GN03032), hereinafter, referred to as E1. The E1 pullulanase is sourced from *Bacillus acidopullulyticus* and has an activity of 400 PUN[10]. The second set of enzyme experiments were carried out with a different pullulanase, as the E1 pullulanase was no longer sufficiently active and the product is discontinued. The second pullulanase (Sigma, lot number SLBB6227) is sourced from *Klebsiella pneumoniae* and, hereinafter, is referred to as E2. The E2 pullulanase is stored in an ammonium sulfate suspension and has a specific enzyme activity of more than 5.00 U/mg protein (as determined by the Biuret-TCA method) (Anonymous, 2015). The E2 enzyme activity was determined by the Somogyi-Nelson method (Nelson, 1944; Somogyi, 1945) and as outlined by Sigma (Anonymous, 1996). The details and results of the enzyme activity assay are available in Appendix G (Section G.2.1).

The standards and pullulan sample used in E1 and E2 were dried *in vacuo* at 40 °C overnight prior to analysis. The lyophilised EPS samples were stored in sealed sachets over silica gel.

Enzyme treatment E1

The E1 experiments were carried out on pullulan, FB2 F1 and FB2 F2, and the conditions as recommended by Singh and co-workers (2010) were followed. The phosphate buffer required was prepared from sodium dihydrogen phosphate ($NaH_2PO_4.H_2O$) (BDH, lot number BB102454R) and the pH was adjusted to 5.0 with 0.05 M NaOH (BDH, lot number 80418A). Maltotriose (DP3) (Merck, lot number 936 K12808863), maltotetraose (DP4) (Sigma, lot number 95F-0433), mannose (Man) (Merck, lot K21710788) and galactose (Gal) (Merck, lot number 7517506) standards were prepared in deionised water and analysed alongside the hydrolysed samples. The details concerning the calibration data are found in Appendix G (Section G.1). The

[10] A pullulanase unit Novo (PUN) is the amount of enzyme that will hydrolyse pullulan to release 1 µmole of reducing sugars per minute at pH 5.0 and 40 ˚C (Tsuchiya *et al.*, 2002).

eluents required were prepared with sodium acetate trihydrate ($NaOAc.3H_2O$) (Saarchem, lot number 1033486) and with NaOH (BDH, lot number 80418A).

Enzyme treatment E2

The E2 experiments were carried out on pullulan, FB2 F2, FB2, PB2 and PB7. The conditions used for the hydrolysis were based on those recommended by Sigma (Anonymous, 1996; Anonymous, 2015). The sodium acetate buffer (20 mM) required was prepared with $NaOAc.3H_2O$ (Merck, lot number 1045573) and adjusted to pH 5.0 at 25 °C with 1 M HCl (Merck, lot number 1041261). Standards were prepared from Gal (Merck, lot number 7517506), Man (Merck, lot number K21710788), maltose (DP2) (Saarchem, lot number 1017380), DP3 (Sigma, lot number 067K1117V), DP4 (Sigma, lot number 030M1683), maltopentaose (DP5) (Supelco, lot number LC10203V), maltohexaose (DP6) (Supelco, lot number LB81802V), and maltoheptaose (DP7) (Supelco, lot number LB81455V). The standard working solutions were prepared in, and the subsequent dilutions were all carried out with, sodium acetate buffer (20 mM). The standards were analysed by HPAEC alongside the samples. The details concerning the calibration data are found in Appendix G (Section G.2.2). The eluents required for the chromatographic system were prepared with $NaOAc.3H_2O$ (Merck, lot number 1045573) and with NaOH (Merck, lot number 1045484).

4.4.2 Sample preparation

The sample preparation for experiment E1 and E2 are provided below.

Enzyme treatment E1

The E1 hydrolysates were obtained by dissolving pullulan (220-400 mg L^{-1}) and each EPS fractionate (480 mg L^{-1} FB2 F1 and 330 mg L^{-1} FB2 F2) in phosphate buffer (0.1 M) and treating with an excess of 10 U of the E1 pullulanase. A total of four pullulan samples and one each of the EPS fractionates were treated. Incubation took place at 50 ºC, with constant shaking at 150 rpm in a shaking incubator (IncoShake, Labotec). After six hours and a total of 19 hours, an aliquot was removed from each sample. The enzyme was deactivated by heating the aliquots at 95 ºC for 2 minutes in a water bath. The aliquots were filtered through a 0.45 µm Millipore® nitrocellulose membrane syringe filter, and injected into the HPAEC column.

Enzyme treatment E2

The E2 hydrolysates were obtained by preparing pullulan (101 mg L^{-1}) and each of the EPS samples (FB2, FB2 F2, PB2 and PB7) (357-379 mg L^{-1}) in $NaOAc.3H_2O$ buffer (20 mM, pH 5.0) and treating with 15 U of E2 pullulanase. Incubation took place at 25 ± 0.1°C, with constant shaking at 95 rpm in a shaking water bath (Fischer Scientific). The samples were treated in duplicate and were incubated for 24 hours to ensure maximum hydrolysis. The enzymes were deactivated by boiling for two minutes on a hotplate. After cooling to room temperature, each sample was quantitatively transferred to a separate volumetric flask and made to the mark (25.0 cm^{-3}) with buffer solution. All standards and samples were filtered through 0.45 µm Millipore® nitrocellulose membrane syringe filters, before being injected into the HPAEC column.

4.4.3 Instrument and settings

HPAEC-PAD was performed with a Perkin Elmer Series 200 pump and autosampler. Detection was with a Dionex PAD set in the range of 3000 nA for E1. For E2, the detector sensitivity had diminished and the sensitivity was increased to 1000 nA and then 300 nA. The hydrolysates were

separated on a Dionex CarboPac™ PA1 pellicular anion-exchange resin column (4 × 250 mm) fitted with a CarboPac™ PA1 guard column (4 × 50 mm). Data was recorded with a PeakSimple Chromatography Data System (SRI model 203). The eluents used include 0.1 M NaOH (A) and 0.1 M NaOH in 0.5 M NaOAc.$3H_2O$ (B), with a flow rate of 1.0 cm^{-3} min^{-1}. The column temperature was 28 °C and the injection volume was 20 µL. The gradient profiles for E1 and E2 are detailed below.

Gradient profile for enzyme treatment E1

The gradient profile for E1 started with eluent A set at 95% and eluent B at 5%, maintained for the first three minutes. Over the subsequent 60 minutes, eluent A was dropped to 5% and eluent B raised to 95%. For the final 11 minutes, eluent A was returned to 95% and eluent B to 5%. The total run-time was 74 minutes.

Gradient profile for enzyme treatment E2

The gradient profile for E2 began with the column equilibrating with eluent A at 95% and eluent B at 5%. Following injection, eluent A was lowered to 5% and eluent B increased to 95%. After 60 minutes, the profile was abruptly changed with eluent A set at 95% and eluent B at 5% over the course of one minute. The final nine minutes of the run were maintained at 5% A and 95% B, with the total run-time being 70 minutes.

4.5 Physical properties

Steady shear viscosity and temperature dependent viscosity measurements were carried out on pullulan and the crude *P. sacchari* EPS solutions. Aqueous-cast films of the polysaccharides were also prepared, both with and without a plasticiser, and the film tensile properties were evaluated. This section provides these experimental details.

4.5.1 Rheological properties

Steady-shear viscosity experiments were performed on a controlled strain rotational Ares-G2 rheometer (TA Instruments, New Castle, DE, USA). A cone (0.04 radians, 40 mm diameter) and plate geometry was used for the steady-shear and dynamic oscillatory measurements. Temperature was controlled at 20 ± 0.03 °C by the Peltier setup. Samples were prepared as 4.00% (m/m), 2.00% (m/m) (1.90% (m/m) for pullulan) and 1.00% (m/m) solutions by dissolving weighed portions of the freeze-dried polysaccharide in deionized water with stirring at room temperature for a minimum of 45 minutes. The solutions were filtered under suction through Whatman 541 filter paper. The rested solutions were loaded onto the sample plate with a plastic dropper, ensuring no air bubbles were present. Once loaded, any excess sample was carefully trimmed with tissue paper, and then the exposed edges were coated with liquid paraffin to prevent evaporation. The apparent viscosity was measured as a function of shear rate from 1-2000 s^{-1}, 1-1000s^{-1} or 1-500s^{-1}, with a 60-second soak time, by using a logarithmic sweep measuring five, eight or ten points per decade, and with a measurement time of five seconds per point. Shear sweeps for pullulan were conducted over 1-1000 s^{-1} for all replicates, except for the second replicate of the 4.00% solution that was measured from 1-500 s^{-1}. FB2, PB2 and PB7 were measured over a shear rate range of 1-2000 s^{-1}. For the dynamic oscillation measurements, both amplitude and frequency sweeps were performed on the samples. The amplitude sweeps were carried out to determine the LVRs of each of the samples at a set angular frequency of 10 rad s^{-1}. Samples were loaded onto the geometry plate as described for the steady-shear measurements, and the edges were coated with liquid paraffin. The logarithmic amplitude sweeps were

performed between strains of 0.1-100.0%, and five data points were collected per second with a cycle delay of 0.5 seconds. The frequency sweeps were carried out on fresh samples (as the amplitude sweeps permanently deform the sample), as described above. The strain for each frequency sweep was determined from the preceding amplitude sweep. This value was the maximum possible strain that still fell within the LVR of the sample (and that was still in phase with the oscillation). The angular frequency range was set from 100.0-0.1 rad s^{-1}. The soak time for all oscillation analyses was 60 seconds.

4.5.2 Film formation and mechanical properties

This section describes the experimental details for preparing the polysaccharide films and their associated mechanical testing.

Film preparation

Films were aqueous cast from 4.00% (m/m) polysaccharide solutions with or without 10.0% (on a dry mass basis) of sorbitol as plasticiser. Solutions were prepared by stirring the weighed polysaccharide in deionised water at room temperature for a minimum of 45 minutes. The solutions were filtered under suction through Whatman 541 filter paper. The filtered solutions were pipetted into 55 mm diameter plastic petri dishes before being degassed *in vacuo*. Films were dried in an oven at 50 °C for a minimum of three hours. The dry films were conditioned at 25 °C and 18.7% relative humidity for a minimum of two days in a constant climate room before mechanical testing was carried out in the same environment. The moisture content of the films was determined by mass difference after drying in an oven at 105 °C for 24 hours. The films containing sorbitol are referred to as the plasticised films.

Mechanical testing of films

The tensile properties of the films were studied with an Instron 1122 instrument (Instron Ltd., High Wycombe, UK). The film thickness was measured by using a digital micrometer (Mitutoyo IDC-112CB, Mitutoyo Corp., Japan) with an accuracy of ± 3 µm. Film strips of 2 × 40 mm and 4 × 40 mm were cut with a stamp tool containing parallel blades fixed at the required widths. The ends of the films were secured with instant adhesive (Loctite® 401) between cardboard strips, 20 × 20 mm in size, and 20 mm apart. The instrument load was balanced with the card before the film was attached. Thereafter, the card-secured ends of the measured film strips were placed between the rubberised pneumatic grips on the instrument and the gauge length was reset before each measurement. The film width and gauge length were measured with a digital caliper with an accuracy of ± 0.01 mm. Force and elongation were recorded to a load maximum of 10 N during extension, with an extension rate of 10% per minute up to the break point. The stress and strain were calculated and the parameters measured were the Young's modulus (E), the maximum stress/tensile strength (σ_M), the tensile percent strain at the maximum tensile stress, and the percent strain at break/percent elongation.

Chapter 5
Structure elucidation of the *P. sacchari* polysaccharides

This chapter details the structure elucidation results for pullulan and the *P. sacchari* EPSs studied. The chapter first presents the GFC results. GFC was used as a means to determine the molecular weight information of all the polysaccharide samples, and to purify the crude FB2 EPS into discrete fractions. The subsequent characterisation analyses detailed in this chapter were carried out on pullulan, the purified FB2 fractionates as well as the crude polysaccharides (FB2, PB2 and PB7). Hence, the outline of this chapter begins with the GFC results. Thereafter, the composition, configuration and linkage information derived from the GC-MS analyses of the crude and purified EPSs is provided. The chapter then details the NMR and enzymatic-HPLC results used to confirm the carbohydrate sequence information of pullulan and to ascertain the same from the purified and crude EPSs. The chapter ends with a summary of the conclusions drawn from each of the analyses carried out, and comparisons are drawn between the *P. sacchari* EPS and the available literature on the structure of sarkaran.

5.1 Gel filtration chromatography

GFC is a chromatographic technique that allowed for the purification of the crude *P. sacchari* EPS samples (FB2 only) as well as the determination of the MWs, MWDs and MW statistical averages of pullulan and the EPSs (FB2, PB2 and PB7).

Pullulan and the crude EPSs were separately eluted through a GFC column packed with Toyopearl® HW-65F resin. Pullulan revealed a unimodal profile (Figure 5.1), the EPS prepared in the bioreactor showed a trimodal distribution (FB2, Figure 5.2) and the two shake-flask prepared EPSs both displayed bimodal distributions (PB2 and PB7, Figure 5.3).

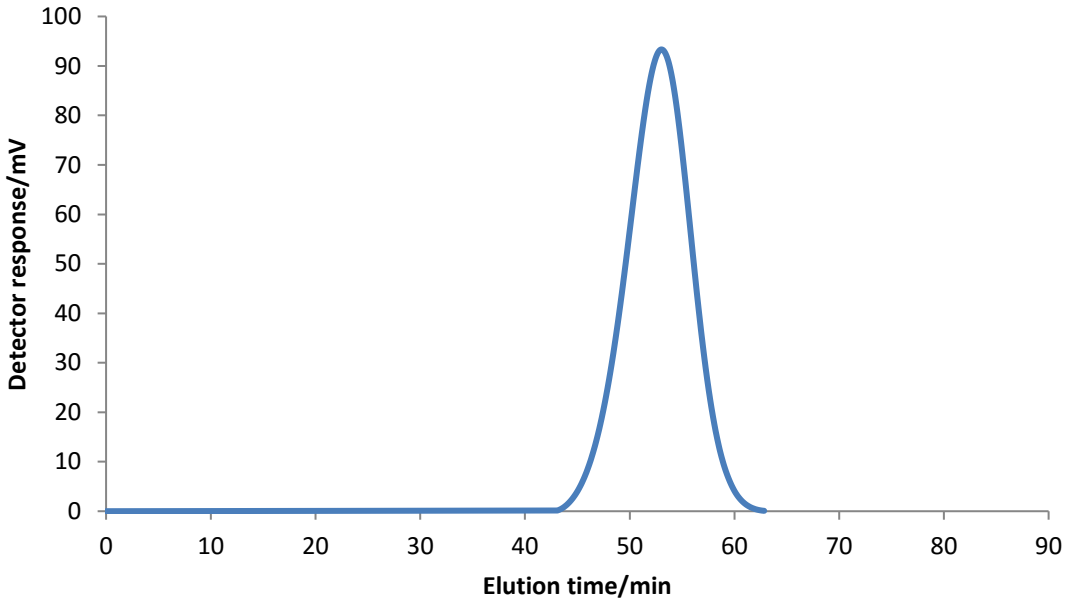

Figure 5.1: GFC elution profile of pullulan at a flow rate of 1.0 cm^3 min^{-1}.

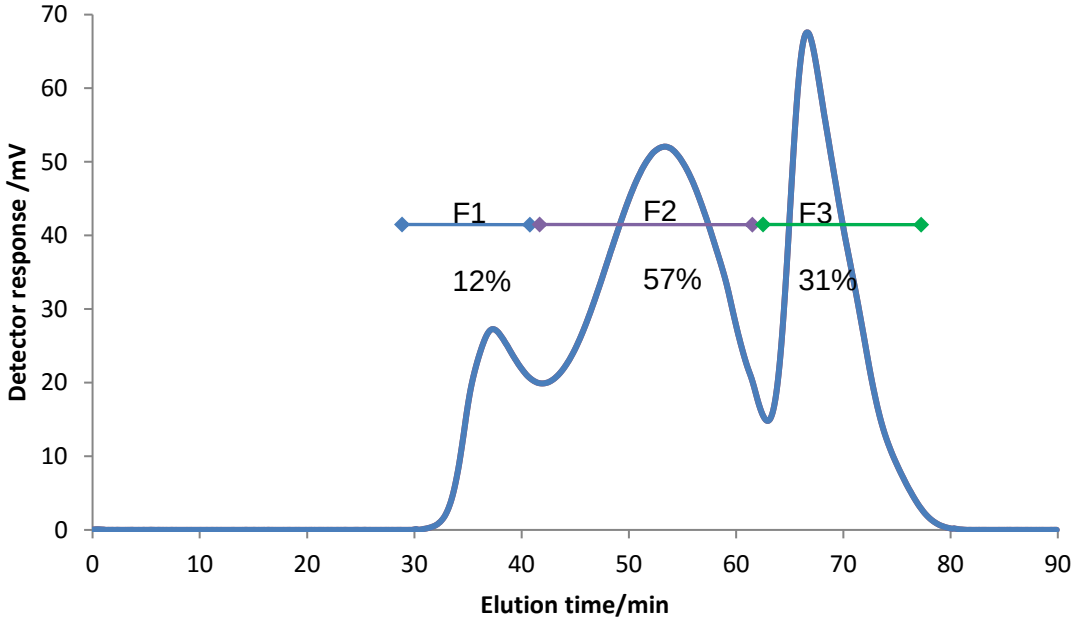

Figure 5.2: Elution profile of the bioreactor prepared EPS (FB2) showing three distinct fractions. Fraction 1 (FB2 F1), fraction 2 (FB2 F2) and fraction three (FB2 F3) were collected, pooled and freeze-dried for further analysis. The elution flow rate was 1.0 cm^3 min^{-1}.

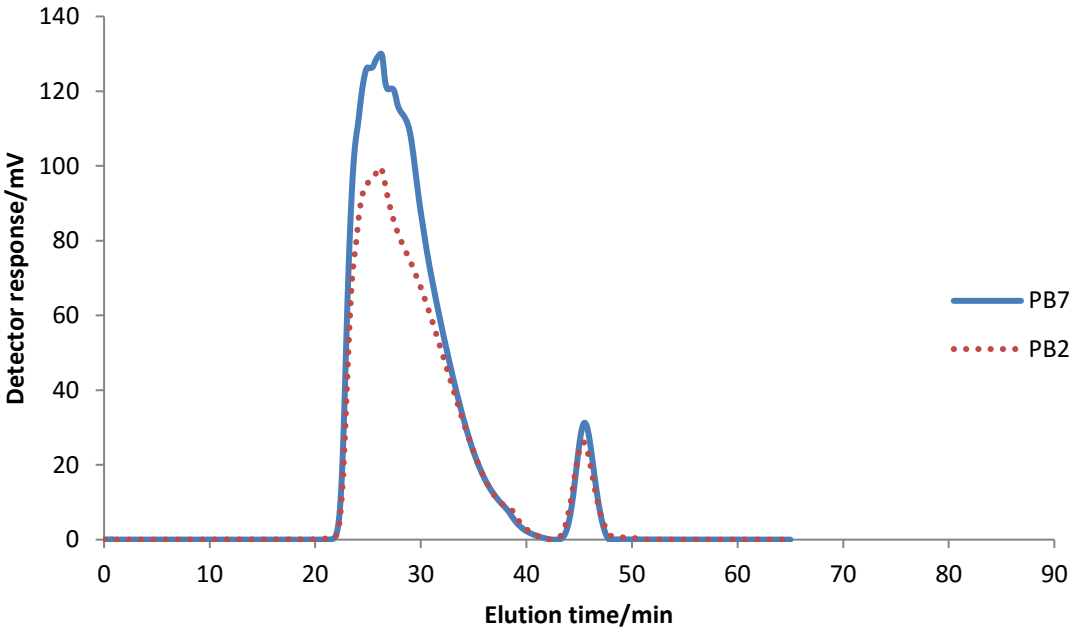

Figure 5.3: Elution profiles for the two shake-flask preparations of the EPSs; PB2 (dotted red line) and PB7 (solid blue line). The elution flow rate was 1.5 cm^3 min^{-1}.

The pullulan and FB2 samples were analysed on Column A, whilst PB2 and PB7 were analysed on Column B. Hence, the molecular weight information for pullulan and FB2 were assessed with Equation 5.1, whilst the same parameters for PB2 and PB7 were assessed with Equation 5.2. These polynomials were determined as the best-fit models from the calibration data, based on the regression analyses and partial F-test determinations for each column. These determinations are found in Appendix B together with the raw data in Appendix C. The resultant MW and MWD statistical averages determined for each of the polysaccharides are presented in Table 5.1

$$y = -3.980\times10^{-3}x^2 + 3.127\times10^{-1}x + 0.02663 \qquad (5.1)$$

$$y = -1.141\times10^{-4}x^3 + 4.905\times10^{-3}x^2 - 4.891\times10^{-2}x + 5.917 \qquad (5.2)$$

Table 5.1 Molecular weight statistical averages, peak-average molecular weight and polydispersity indices determined by gel filtration chromatography for pullulan and the *P. sacchari* EPSs.

Sample	Peak	Molecular weight statistical averages (±%RSD)/Da			MP (±%RSD) /Da	PDI (±%RSD)	Amount /%
		M_z	M_w	M_n			
Pullulan[a,c]	1	471 436 (0.7)	327 751 (0.6)	170 906 (4.2)	259 725 (3.1)	1.9 (4.2)	100
FB2[a,c]	1	1 393 431 (0.4)	1 386 749 (0.3)	1 3794 31 (0.4)	1 419 094 (1.3)	1.1 (8.1)	12
	2	760 705 (1.3)	409 686 (0.9)	94 079 (2.7)	240 675 (1.3)	4.1 (8.1)	57
	3	3327 (3.9)	1395 (3.1)	471 (6.9)	1550 (2.5)	3.0 (7.0)	31
PB2[b,c]	1	795 345 (0.7)	690 557 (1.4)	453 761 (4.3)	898 570 (~0)	1.5 (13)	93
	2	1948 (10.0)	1403 (13.0)	823 (13.9)	1211 (16.4)	1.7 (16.1)	7
PB7[b,d]	1	805 610 (0.7)	717 052 (1.6)	491 132 (9.0)	872 028 (2.8)	1.5 (7.4)	94
	2	1909 (7.7)	1397 (3.0)	1009 (2.0)	1248 (~0)	1.4 (1.0)	6

[a] Values determined using calibration Equation 5.1.

[b] Values determined using calibration Equation 5.2.

[c] Triplicate analyses.

[d] Duplicate analyses.

MP – peak-average molecular weight, PDI – polydispersity index, %RSD – percentage relative standard deviation, M_z – z-average molecular weight, M_w – weight-average molecular weight, M_n – number-average molecular weight

Commercial pullulans are available in a wide range of MWs, even beyond the calibration limits of Column A and B, depending on the fungal strain and fermentation conditions used for its production (Lazaridou *et al.*, 2003b; Shingel, 2004). The pullulan model compound used in this study was not supplied with a certificate of analysis, and the MW data are unknown. Analysis of pullulan on Column A revealed that this model compound had dextran equivalent M_w and M_n values of 327 751 Da (327 kilo Da, kDa) and 170 906 Da (171 kDa), respectively, with a PDI value of 1.9. The PDI value is within the reported literature range of 1.1-4.1 for pullulans (from *A. pullulans*) (Huck *et al.*, 2002; Lazaridou *et al.*, 2002a). Furthermore, pullulan was found to have a high purity as only one peak (unimodal) appeared in the GFC elution profile. Conversely, the crude EPSs revealed bimodal (PB2 and PB7) and trimodal (FB2) GFC profiles. All the EPSs were found to have higher overall MWs than pullulan.

In general, the major EPS fractions in all three preparations had M_z values in the range 761-806 kDa, which was almost double that of pullulan. In PB2 and PB7, the major fraction had a low polydispersity (1.5) that constituted 93% and 94% of each sample, respectively. This indicates that the shake-flask preparations were reproducible and that the EPSs produced were reasonably pure and uniform in size and structure. Furthermore, these EPSs had peak-average molecular weights (PB2 MP = 899 kDa, PB7 MP = 872 kDa) about triple that of pullulan (MP =260 kDa) and the predominant EPS of FB2 (MP = 241 kDa). The low molecular weight fraction in all three EPSs had a M_w of 1.4 kDa. These fractions were most likely to comprise oligosaccharide building blocks of the main EPSs.

The most interesting difference between the preparations of the *P. sacchari* EPSs is the contrast between the trimodal and bimodal distributions. The bimodal EPSs were those prepared in shake-flasks whilst the trimodal EPS was cultured under different conditions in a bioreactor. For FB2, the conditions in the bioreactor appear to have stimulated the organism to produce a small fraction (12%) of very high MW product (> 1 million Da). Unfortunately, samples of EPS product were not taken during the cultivation, so it is not clear whether this fraction was proportionally increasing or decreasing at the time of harvest. A decline in EPS MWs could signal the production and activity of organism-expressed enzymes within the culture medium. *A. pullulans* reportedly produce hydrolytic enzymes under certain cultivation conditions, such as, pullulanase, α-amylase and glucoamylase. During extended cultivations, pullulan yields can be seen to increase together with a concomitant decline in molecular weight if conditions favour enzyme expression and hydrolytic activity (Manitchotpisit *et al.*, 2011). In fact, enzyme activity in FB2 was indicated by the higher polydispersity of the major fraction (4.1) coupled with the much higher proportion of the oligosaccharide fraction (31%), compared to PB2 and PB7. Hence, FB2 was separated into its three distinct fractions, and these were individually analysed. Analysis of the individual fractions would confirm whether the fractions were simply variable chain lengths of the same subunits, or whether the organism produced different EPSs in the bioreactor cultivation. Thus, several batches of FB2 were eluted through the column; the respective fractions were pooled, freeze-dried and stored for further analysis. These purified fractions are referred as FB2 F1 (M_w > 1000 kDa), FB2 F2 (M_w = 410 kDa) and FB2 F3 (M_w = 1.4 kDa). These purified fractionates, the three crude EPSs and pullulan were further explored to establish and compare their carbohydrate make-up.

5.2 Gas chromatography-mass spectrometry

GC-MS was used in this study to determine the composition, absolute configuration and structure (linkage) information of both the crude and purified EPSs produced by *P. sacchari*. The methods carried out were validated against pullulan, and together these results are presented and discussed in this section. First, the work carried out to develop the mass spectral reference libraries required in this study is summarised. This summary provides the reader with some important considerations used when interpreting the data, as well as the definitions for the abbreviations used to describe the various carbohydrate derivatives discussed throughout this section. The proceeding subsections provide the results of the composition, absolute configuration and structure analyses of the EPSs.

5.2.1 Construction of carbohydrate mass spectral libraries

To analyse the composition and structure of the *P. sacchari* EPSs by GC-MS, authentic standards of model carbohydrate compounds had to be similarly prepared and mass spectral reference libraries compiled. Appendix D provides the detailed theory and the experimental steps carried out to prepare these libraries. This subsection provides a summary of this theory, an outline of

some important considerations used when interpreting the GC-MS data and definitions for the various carbohydrate derivatives populating the compiled mass spectral libraries used to assess the composition and structure of the EPSs studied.

EI is required to produce reproducible fragmentation patterns of carbohydrate derivatives in mass spectrometry. Acyclic aldoses and ketoses, acyclic pentoses and hexoses, and cyclic furanoses and pyranoses can each be differentiated based on their predictable EI fragmentation pathways (Kochetkov and Chizhov, 1966). In general, furanosides produce a distinctive 101 *m/z* ion when methylated (OMe) or 217 *m/z* ion when silylated (TMS), whereas, pyranosides provide a predominant 88 *m/z* or 204 *m/z* ion for OMe or TMS derivatives, respectively. As discussed in Section 3.2.2, mutarotation of silylated carbohydrate derivatives give rise to multiple peaks in a GC chromatogram. Each peak corresponds to a different anomer and configuration of a single monomer. Through understanding the possible fragmentation pathways, the mass spectral data for each component can be identified, classified and then stored into a reference library. On analysing similarly prepared samples, the presence of a particular derivative can be confirmed by comparing its RRT and mass spectrum against those stored in the reference library. Identification is also possible if more than one derivative co-elutes. This is done through inspection of the mass spectra. In this study, 18 model compounds were prepared alongside the EPS samples, and their EI spectra saved into respective composition and structure reference libraries. Table 5.2 and Table 5.3 summarise the relevant sugar derivatives defined in the respective reference libraries, used to elucidate the structure of the EPSs produced by *P. sacchari*.

As indicated in Table 5.2 and Table 5.3, there were typical (primary) and atypical (secondary) methanolysate products detected and classified from the model compounds investigated in this study. Secondary products arise due to the presence of moisture in the methanolysis reaction. These by-products do not affect quantitation in composition analyses, but may impact structure analyses. In composition analyses, the presence of moisture increases the quantity of persilylated moieties (the derivatives normally arising from terminal glycosides, T). Since composition analysis sums all moieties (persilylated and methyl glycoside) from the same carbohydrate class together, the overall ratio of the different carbohydrates composing the sample remains unaffected. For structure analysis, the presence of moisture can affect determinations in two ways. First, water prevents complete permethylation of the intact polysaccharide. Second, water prevents preservation of the linkage information during acidic methanolysis. In the first instance, water hinders alkoxide formation, which is necessary for methylation to occur. In the second instance, hydroxide ions (OH^-) compete with the methoxide ions (MeO^-) during glycosidic bond cleavage, preventing the latter from protecting the exposed reducing-end. In both instances, all unprotected sites are silylated during derivatisation, producing by-products with multiple silylation sites that mimic branch points. Whilst every effort was taken to minimise moisture during sample preparations, these by-products were evident in the standards. Hence, the EI spectra of these by-products were included in the structure reference library. Samples presenting these products were cautiously scrutanised. Other secondary derivatives considered in the analyses were moieties arising from incomplete silylations. These derivatives contain mass spectral fragments indicating a hydroxide group instead of a silyl group at any position of the residue.

Table 5.2 Defined derivatives identified from the composition analysis of relevant carbohydrate compounds.

Derivative	Residue name[a]	Residue abbreviation[a]	Other abbreviation[a]
Per-*O*-trimethylsilylated sorbitol[b]	Sorbitol[$]	Sorbitol[$]	IS[$]
Methyl tetrakis-*O*-trimethylsilylated-hexoside[b]	Methyl 2,3,4,6-tetrakis-*O*-TMS-mannopyranoside Methyl 2,3,4,6-tetrakis-*O*-TMS-galactopyranoside Methyl 2,3,4,6-tetrakis-*O*-TMS-glucoopyranoside	Man*p*-1OMe Gal*p*-1OMe Glc*p*-1OMe	ManT[$] GalT[$] GlcT[$]
Per-*O*-trimethylsilylated-hexoside[c]	1,2,3,4,6-pentakis-*O*-TMS-mannopyranoside 1,2,3,4,6-pentakis-*O*-TMS-galactopyranoside 1,2,3,4,6-pentakis-*O*-TMS-galactofuranoside 1,2,3,4,6-pentakis-*O*-TMS-glucospyranoside 1,2,3,4,6-pentakis-*O*-TMS-galactose	Man*p*-1OTMS Gal*p*-1OTMS Gal*f*-1OTMS Glc*p*-1OTMS GalL-1OTMS	Man-TMS Gal-TMS Gal*f*-TMS Glc-TMS GalL-TMS

[a] Includes both the α- and β-anomers of the methyl glycosides.

[b] Expected residue arising from methanolysis and silylation (primary derivative).

[c] Terminal residue (primary derivative) or due to the presence of moisture (secondary derivative, see text).

[$] From composition analysis.

TMS/OTMS – trimethylsilylated, IS – internal standard, T – terminal residue, OMe – methylated, *f* – furanoside, *p* – pyranoside, L – linear/acyclic.

Table 5.3: Defined derivatives identified from the structure analysis of relevant carbohydrate compounds.

Derivative	Residue name[a]	Residue abbreviation[a]	Other abbreviation[a]
Per-*O*-trimethylsilylated sorbitol[b]	Sorbitol	Sorbitol	IS
Per-*O*-methyl-hexoside[b]	Methyl 2,3,4,6-tetrakis-*O*-methyl mannopyranoside	Man*p*-1OMe	ManT
	Methyl 2,3,4,6-tetrakis-*O*-methyl mannofuranoside	Man*f*-1OMe	Man*f*T
	Methyl 2,3,4,6-tetrakis-*O*-methyl galactopyranoside	Gal*p*-1OMe	GalT
	Methyl 2,3,4,6-tetrakis-*O*-methyl galactofuranoside	Gal*f*-1OMe	Gal*f*T
	Methyl 2,3,4,6-tetrakis-*O*-methyl glucopyranoside	Glc*p*-1OMe	GlcT
Tetrakis-*O*-methyl-*O*-trimethylsilylated-hexoside	2,3,4,6-tetrakis-*O*-methyl-1-*O*-TMS galactopyranoside[c]	Gal*p*-1OTMS	Gal-1
	2,3,4,6-tetrakis-*O*-methyl-1-*O*-TMS galactofuranoside[c]	Gal*f*-1OTMS	Gal*f*-1
	1,2,3,6-tetrakis-*O*-methyl-4-*O*-TMS glucopyranoside[b]	Glc*p*-4OTMS	Glc-4
	1,2,3,4-tetrakis-*O*-methyl-6-*O*-TMS glucopyranoside[b]	Glc*p*-6OTMS	Glc-6
	1,2,4,6-tetrakis-*O*-methyl-3-*O*-TMS glucopyranoside[b]	Glc*p*-3OTMS	Glc-3
	1,2,3,4-tetrakis-*O*-methyl-6-*O*-TMS galactopyranoside[b]	Gal*p*-6OTMS	Gal-6
Tris-*O*-methyl-bis-*O*-trimethylsilylated-hexoside	2,3,6-tris-*O*-methyl-1,4-bis-*O*-TMS glucopyranoside[c]	Glc*p*-1,4OTMS Glc*p*-1,6OTMS	Glc-1,4
	2,3,4-tris-*O*-methyl-1,6-bis-*O*-TMS glucopyranoside[c]	GlcL-1,6OTMS	Glc-1,6
	2,3,4-tris-*O*-methyl-1,6-bis-*O*-TMS glucopyranose		GlcL-1,6
Tris-*O*-methyl-1-hydroxy-*O*- trimethylsilylated-hexoside	2,3,4-tris-*O*-methyl-1-hydroxy-6-*O*-methyl glucopyranose[e]	Glc*p*-1,6OTMS*	Glc-1,6*
Bis-*O*-methyl-tris-*O*-trimethylsilylated-hexoside	2,3-bis-*O*-methyl-1,4,6-tris-*O*-TMS glucopyranoside[c,d]	Glc*p*-1,4,6OTMS	Glc-1,4,6

[a] Includes both the α- and β-anomers of the methyl glycosides.
[b] Expected residue arising from the permethylation protocol (primary derivative).
[c] Residue arising due to the interfering presence of moisture (secondary derivative).
[d] Suspected to arise due to incomplete permethylation (secondary derivative).
[e] Suspected to arise due to incomplete silylation (secondary derivative).
TMS/OTMS – trimethylsilylated, IS – internal standard, T – terminal residue, OMe – methylated, *f* – furanoside, *p* – pyranoside, L – linear/acyclic.

The two reference libraries compiled from model compounds are the Carb Comp and Models libraries for the composition and structure analyses, respectively. The results for similarly prepared pullulan and EPS samples were processed against the RRTs and stored EI spectra in the respective reference libraries. The processed chromatograms and data for each analysis are located in Appendix E. The identified peaks for each analysis were broadly classified as: primary or secondary, and major or minor (based on area). Due to the sample peak multiplicity in the GC chromatograms, quantitation was carried out by using internal normalisation with the identified peaks expressed in terms of relative percent area (Anonymous, 2011).

The next subsections provide the GC-MS results for the analysis of pullulan and the *P. sacchari* EPSs.

5.2.2 Composition and absolute configuration analyses

Pullulan and the *P. sacchari* EPSs were subjected to acidic methanolysis and silylation to determine their monosaccharide composition by GC-MS. The samples were analysed in EI mode, scanning from 40-650 *m/z*. The identified components of pullulan and the three FB2 fractionates were confirmed by tandem mass spectrometry (MS/MS) of the 204 *m/z* precursor ion. Furthermore, all the crude EPSs and the purified FB2 F2 sample were subjected to acidic S-(+)-2-butanolysis and silylation to determine the absolute configuration of the component monosaccharides by GC-MS.

Figure 5.4 illustrates the multiple peak profiles for pullulan and the purified FB2 fractionates (FB2 F1, FB2 F2 and FB2 F3). Pullulan was confirmed to contain glucose only, whilst the *P. sacchari* EPSs were found to comprise largely of glucose, and some galactose and mannose. The α- and β-conformations of each of the identified peaks were assigned based on the elution order (α before β) of TMS methyl glucoside, -galactoside and -mannoside anomeric pairs (Bleton *et al.*, 1996). In pullulan, peaks identified included both major primary glucose peaks (α- and βGlc*p*-1OMe) and minor secondary glucose peaks (α- and βGlc*p*-1OTMS). Likewise, all the *P. sacchari* samples contained these primary and secondary glucose peaks (except for αGlc*p*-1OTMS, in some cases). One major primary mannose peak (αMan*p*-1OMe) and two major primary galactose peaks (α- and βGal*p*-1OMe) were also identified in all the EPS samples, albeit in very little abundance. Of the EPSs, the purified FB2 F1 contained the highest relative amount of mannose and galactose. FB2 F1 was also the only EPS to contain αGal*f*-1OTMS as an additional minor, secondary peak.

MS/MS analysis of the 204 *m/z* precursor ion, as illustrated in Figure 5.5, confirmed the identification of mannose, galactose and glucose in the FB2 fractionates. The absolute configurations of these components were also established in all the samples (except FB2 F1 and FB2 F3). Figure 5.6 provides the absolute configuration chromatograms for FB2, PB2 and PB7 against a mixture of D- and L-mannose, -galactose and -glucose standards. Table 5.4 provides a summary of both the composition and absolute configuration data for all the samples analysed.

The summary of results in Table 5.4 confirmed that pullulan was a polyglucan comprising solely of D-(+)-glucose (Jeans, 1977; Sandford, 1979). Table 5.4 also provides that the *P. sacchari* EPSs were largely D-polyglucans, containing some D-galactose and smaller amounts of D-mannose. It is interesting to note that, depending on the cultivation conditions, pullulans prepared from *A. pullulans* can contain contain > 5% galactose and mannose (Zajic and LeDuy, 1973).

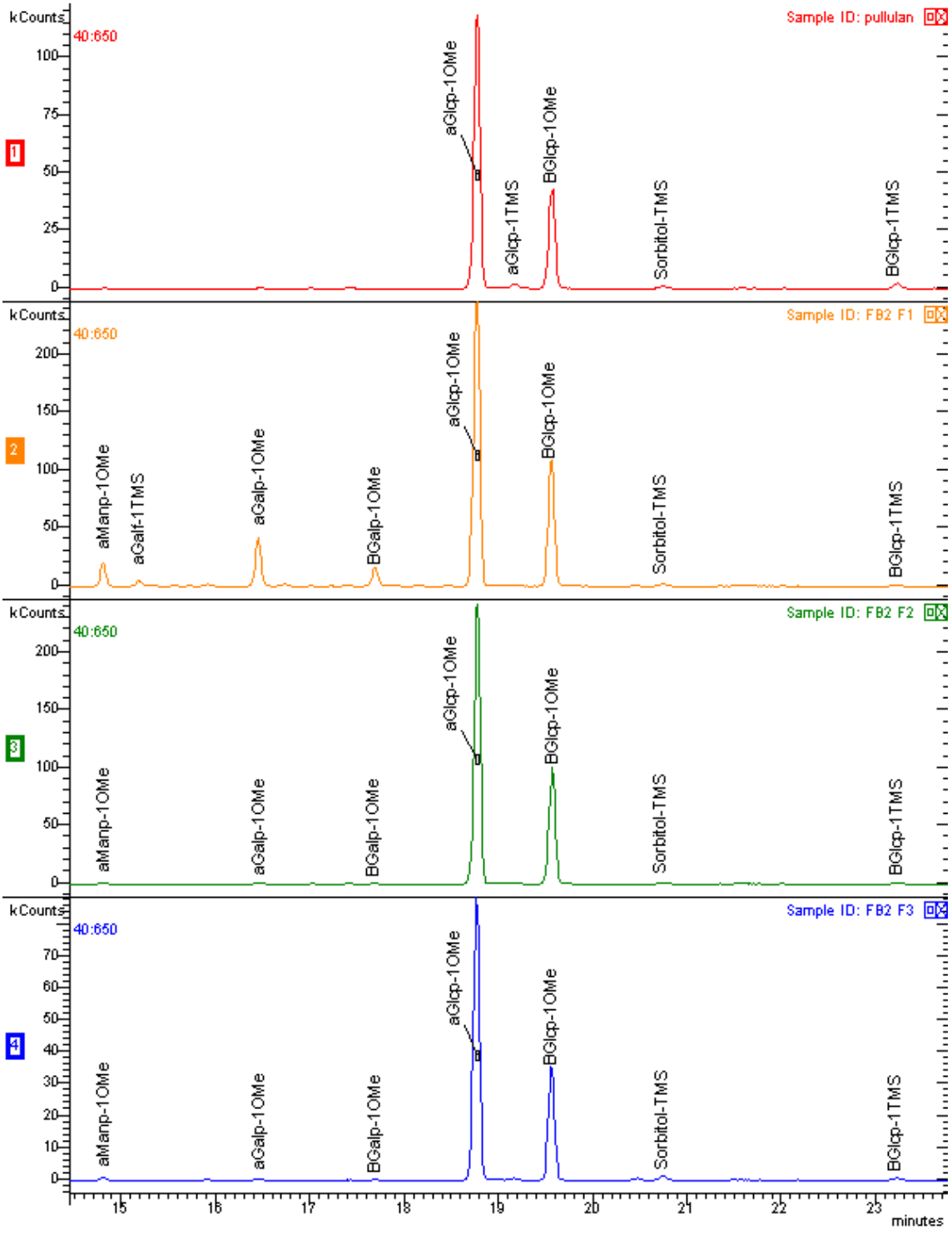

Figure 5.4: GC-MS chromatograms for pullulan, and the three fractionates of the FB2 EPS from *P. sacchari* (FB2 F1, FB2 F2 and FB2 F3). The major and minor primary and secondary peaks identified are labelled. Pullulan is exclusively glucose-based. The FB2 EPSs all are predominantly glucose-based; however, FB2 F1 also contains a fair quantity of galactose and mannose, whilst FB2 F2 and FB2 F1 only have trace amounts of these lesser components.

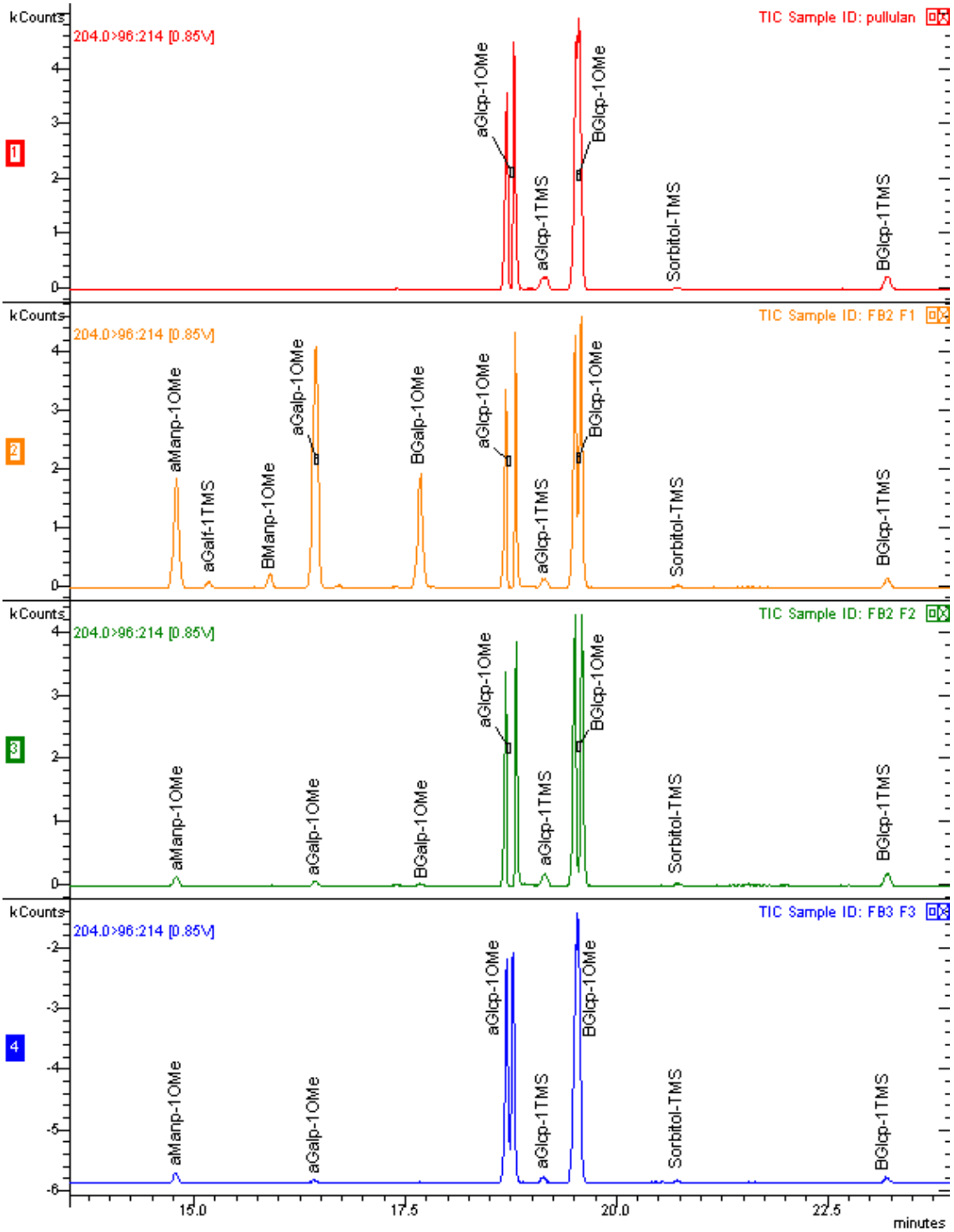

Figure 5.5: The GC-MS/MS chromatograms of the 204 *m/z* precursor ion for pullulan, FB2 F1, FB2 F2 and FB2 F3 confirming the glucose, galactose and mannose components detected in the samples. Pullulan is confirmed to be a polyglucan, whilst the FB2 fractionates are predominantly glucose-based but also contain mannose and galactose. FB2 F1 has a fair quantity of mannose and galactose, whilst FB2 F2 and FB2 F1 contain only trace amounts.

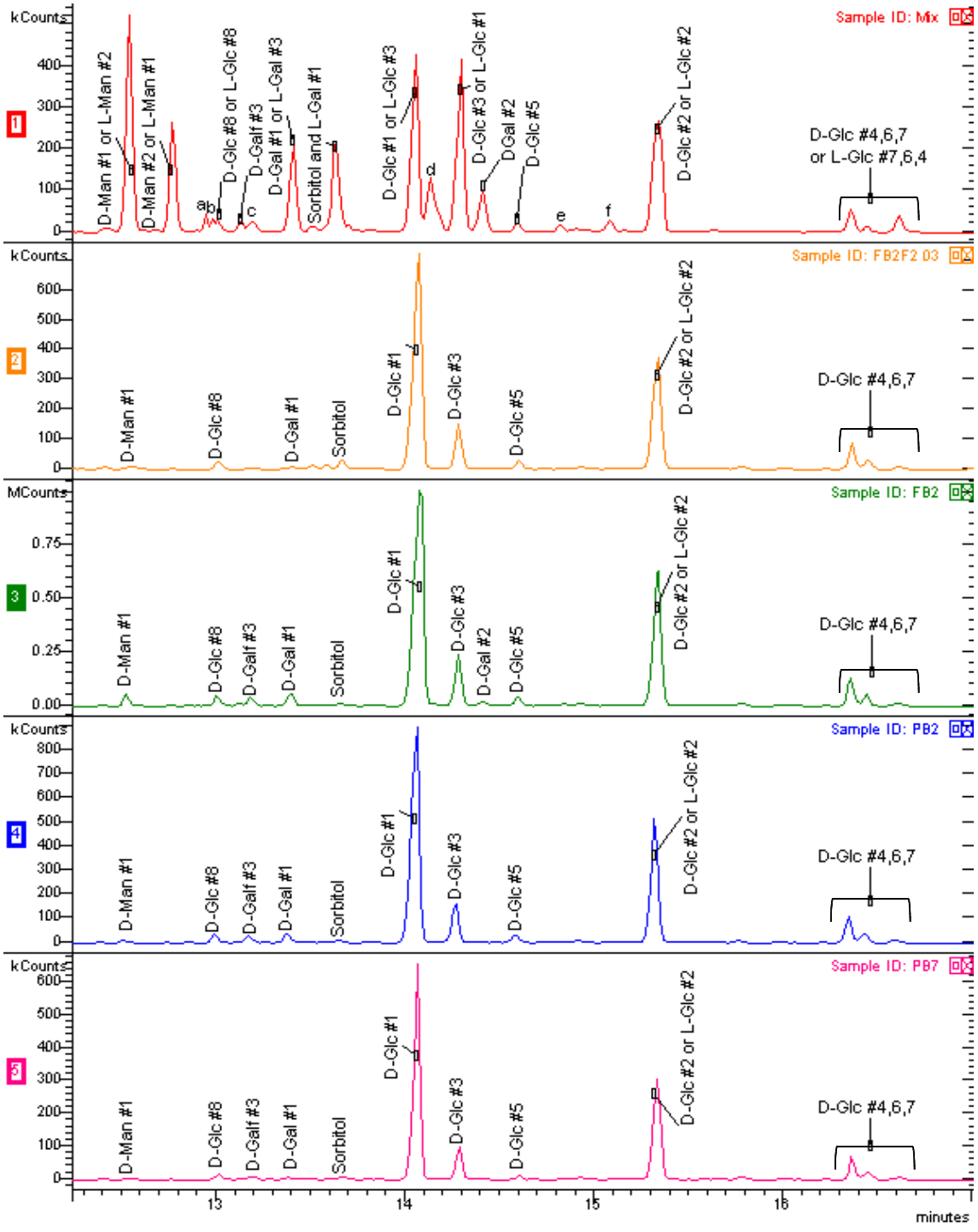

Figure 5.6: Chromatograms illustrating the separation of a mixture of standards containing both D and L enantiomers of galactose, mannose and glucose (Mix), against the enantiomeric peaks identified in the EPS samples. Letters a-f represents the less significant D- or L-galactose/mannose/glucose peaks identified in the standards. The numbers (#1-#7) indicate the relative sizes of the peaks found in the individual enantiomeric standards, with #1 being the largest. The only peaks that cannot be unambiguously determined are those co-eluting for D-Glc #2 and L-Glc #2.

Table 5.4: Relative percent abundance of each of the components identified in pullulan and the *P. sacchari* EPS samples analysed.

Sample	Composition (±SD)/%			Absolute configuration (±SD)/%			Sample
	Man	Gal	Glc	D-Man	D-Gal	D-Glc	
Pullulan[b]	0	0	100.0 (0.0)	0	0	100.0	**Pullulan[a]**
FB2 F1[b]	3.2 (0.3)	13.0 (0.5)	83.8 (0.2)	n.d.	n.d.	n.d.	**FB2 F1**
FB2 F2[d]	0.1 (0.03)	0.1 (0.03)	99.9 (0.1)	0.1	0.1	99.8	**FB2 F2[a]**
FB2 F3[a]	0.2	0.1	99.7	n.d.	n.d.	n.d.	**FB2 F3**
FB2[a]	0.5	1.7	97.8	0.5 (0.1)	1.7 (0.1)	97.9 (0.2)	**FB2[d]**
PB2[a]	0.3	0.5	99.3	0.3 (0.1)	0.3 (0.2)	99.3 (0.3)	**PB2[c]**
PB7[a]	0.5	0.9	98.6	0.4 (0.04)	0.9 (0.2)	98.7 (0.1)	**PB7[c]**

[a] Single analysis
[b] Duplicate analyses
[c] Triplicate analyses
[d] Quadruplicate analyses
SD – standard deviation, n.d. – not determined, Man – mannose, D-Man – D-(+)-mannose, Gal – galactose, D-Gal – D-(+)-galactose, Glc – glucose, D-Glc – D-(+)-glucose

The crude FB2 bioreactor sample is first compared with its purified fractionates (F1, F2 and F3), and then to the two crude shake-flask EPSs (PB2 and PB7). Analysis of the purified fractions from FB2 revealed that there were potentially two different EPSs excreted by *P. sacchari* under the bioreactor fermentation conditions. FB2 F1 was most different as it had higher concentrations of galactose (13.0%) and mannose (3.2%). Whereas, the remaining two fractionates were compositionally similar to each other, as they were largely composed of glucose (≥99.7%). As a whole, the crude FB2 EPS comprised only 12% of the very high MW FB2 F1 (see the results from the GPC analysis in Section 5.1), and so the contribution of galactose and mannose from this fraction was largely diluted. Ultimately, the crude FB2 EPS contained only 0.5% mannose and 1.7% galactose. Compared to the crude shake-flask EPSs (PB2 and PB7), FB2 is richer in galactose. In general, all three EPS were remarkably similar as all comprised mostly D-glucose (97.9-99.3%) and have trace amounts of galactose (0.9-1.7%) and mannose (0.3-0.5%).

These compositional results indicated that the *P. sacchari* EPSs were somewhat different to pullulan, particularly as they all contained mannose and galactose. Further structural detail was required to establish the degree to which these EPSs differed from pullulan, and before comparisons could be made against the available literature on sarkaran.

5.2.3 Structure analysis

The structural linkages within pullulan and the EPS samples were investigated by using the permethylation protocol (Section 4.2.2) followed by silylation and GC-MS analysis. The chromatograms in Figure 5.7 provide the elution profiles for all the structural derivatives of pullulan and the three crude EPS samples. The relative percent area of each structural component is summarised in Table 5.5. The table provides a comparison between total residues determined for galactose, mannose and glucose within each of the samples, as well as the breakdown of the determined glucose structural components.

The results for pullulan are first assessed. The primary glucose structural components confirmed in pullulan included (1,6)-linked glucose (Glc6) and (1,4)-linked glucose (Glc4). Despite all precautionary steps taken, secondary derivative peaks arising due to incomplete permethylations and/or due to the presence of moisture were also determined in pullulan. These secondary residues included Glc-1,4,6TMS, Glc-1,4TMS and Glc-1,6TMS, which amounted to an average of 3.8% (data not shown). The maltotriose repeat sub-structure of pullulan was verified by determining the ratio of Glc4:Glc6. In order for this ratio to be accurately determined, the respective secondary peak areas needed to be added to the primary peak areas. Following this principle, the Glc4:Glc6 ratio for pullulan was found to be 2.0, which corresponds to literature (Forabosco *et al.*, 2006; Lazaridou *et al.*, 2002b; Lee *et al.*, 2001).

The GC-MS structural makeup of the *P. sacchari* EPSs were assessed in a similar fashion to the composition analyses. In general, the distribution of mannose, galactose and glucose determined from the structure analysis concurred with the results obtained by the composition and absolute configuration analyses (Table 5.4). The greatest differences lay in an under-recovery of the mannose component in the structure analyses for most of the EPSs. Permethylated monosaccharides are particularly volatile, and can be underestimated due to evaporative losses during the drying steps of the preparation (Carpita and Shea, 1988; Laine *et al.*, 2002). The elution times for permethylated mannose, galactose and glucose from standards indicated that permethylmannosides were the most volatile. Hence, high evaporative losses of permethylmannosides must account for the deficit between the mannose determined in the composition and structure analyses for FB2 F1, PB2 and PB7.

The results of the permethyl-D-mannosides in the EPSs provided that these sugars exist only at the chain terminus of the samples. This is because no mannofuranoses were detected. Conversely, both pyranoses and furanoses were determined for the permethyl-D-galactosides of the EPSs. In this case, the galactoses arose due to either galactopyranoses substituted at C-4 or galactofuranoses substituted at C-5. Hence, it is indicated that galactose exists within the EPS chains rather than at the chain terminals. However, on inspection of the GC-MS data of similarly prepared authentic galactose monosaccharide standards, a mixture of galactopyranosides and galactofuranosides also arose – the latter derivative being the most thermodynamically stable. Therefore, it is not possible to state whether the galactose constituents exist as terminal, intrachain or branch substitutions within the EPS with the available information.

The bulk of the EPSs were found to contain the same primary and secondary glucan features as determined in pullulan. In contrast, the ratio of Glc4:Glc6 in each of the EPS was found to differ and all were higher than pullulan. This result suggests that the EPS glucans are not arranged exclusively as maltotriose subunits. Furthermore, the glucans within the EPSs also appeared to have variable ratios. For example, the crude FB2 EPS had a Glc4:Glc6 ratio of 3.0. This ratio may indicate a maltotetraose-only arrangement, yet, the purified fractions of FB2 each revealed different ratios. These inconsistencies indicate that the glucans may be arranged as a varying series of malto-oligomers; such as, DP2, DP3, DP4, DP5, DP6, DP7, *etc.*

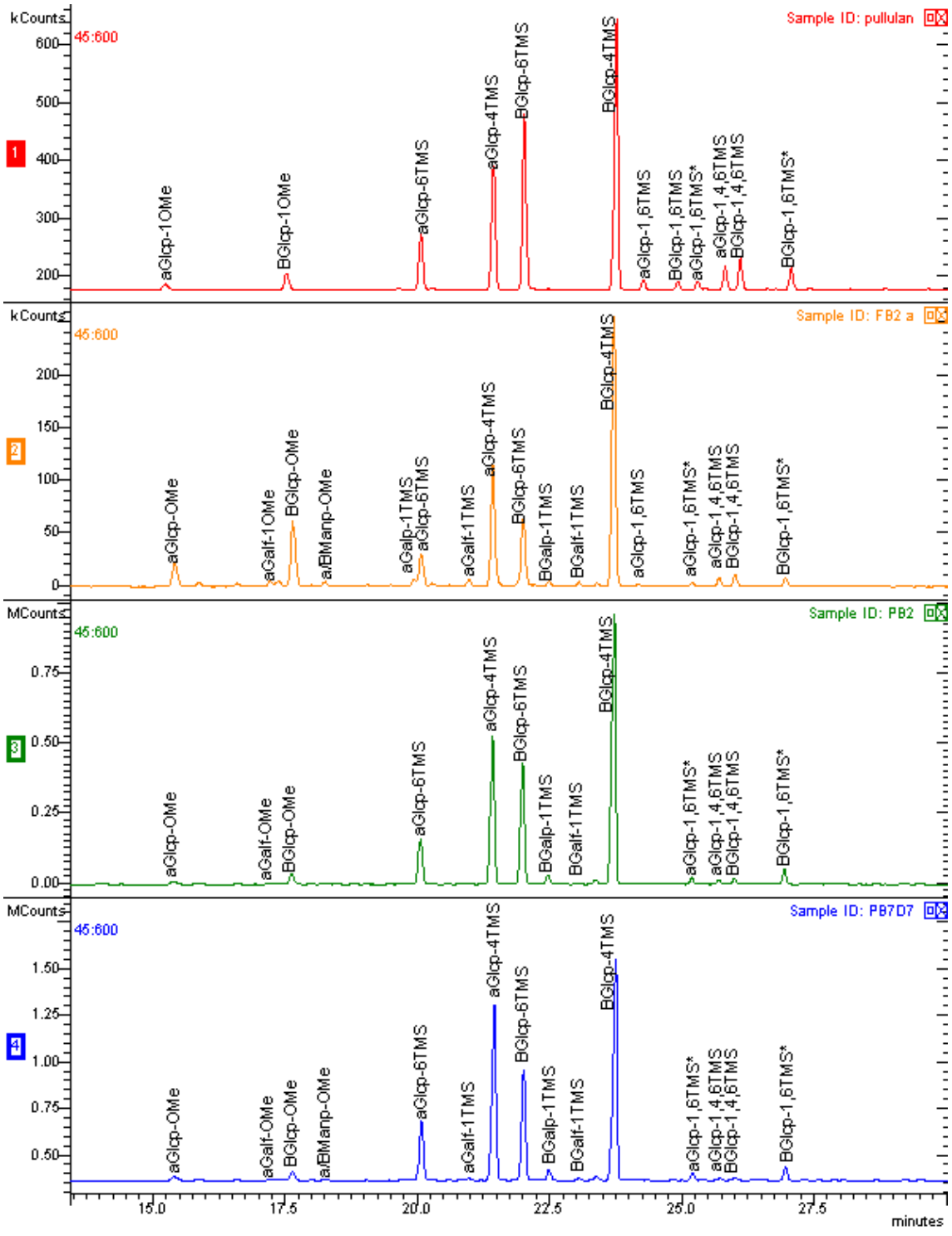

Figure 5.7: GC chromatograms for the structure analysis of pullulan and the three EPS samples (FB2, PB2 and PB7).

Table 5.5 The structural components determined in pullulan and the *P. sacchari* EPSs together with the ratio of the major glucose features determined.

Sample	Relative amount of monosaccharides (± SD)/%			Relative amount of glucose structural components† (± SD)/%			Ratio
	Total Man	Total Gal	Total Glc	GlcT	Glc6	Glc4	Glc4:Glc6
Pullulan[d]	0.0	0.0	100.0	1.5 (1.3)	31.8 (1.1)	62.8 (1.0)	2.0 (0.1)
FB2 F1[c]	0.6 (0.2)	12.9 (0.8)	86.5 (0.9)	2.2 (1.4)	18.7 (0.4)	61.6 (1.6)	3.3 (0.1)
FB2 F2[b]	0.0 (0.0)	0.1 (0.0)	99.8 (0.0)	3.6 (0.5)	22.2 (1.2)	69.2 (1.3)	3.1 (0.2)
FB2 F3[a]	0.1	0.4	99.6	48.7	13.3	34.9	2.6
FB2[b]	0.6 (0.0)	1.8 (0.1)	97.7 (0.1)	14.9 (0.8)	19.5 0.6)	58.7 (1.4)	3.0 (0.2)
PB2[a]	0.1	0.5	99.4	2.0	24.8	66.2	2.7
PB7[a]	0.1	0.8	99.1	2.0	23.7	67.6	2.8

[a] Single analysis [b] Duplicate analyses
[c] Triplicate analyses [d] Quadruplicate analyses
† This is the percentage of only the glucose components; excluded are those glucose residues arising due to the presence of moisture.
SD – standard deviation, Man – mannose, Gal – galactose, Glc – glucose, GlcT – terminal glucose derivatives, Glc6 – the sum of all glucose derivatives with glycosidic linkages indicated at the C-6 position, Glc4 – the sum of all glucose derivatives with glycosidic linkages indicated at the C-4 position.

Further exploration of the EPS structure was required to confirm and compare the malto-oligomer arrangement of the *P. sacchari* samples. To this end, further structural characterisation was carried out with NMR and enzymatic-HPLC analyses. These results are detailed in the sections that follow.

5.3 Nuclear magnetic resonance spectroscopy

1D and 2D NMR spectroscopy was used in this study to further assess the structure of the prepared *P. sacchari* EPSs. Specifically, the NMR experiments were used to determine the anomeric conformation and major repeat sequences of the EPSs. All determinations were verified against pullulan. Samples were analysed in the native form and/or as their peracetate derivatives. All the NMR spectra are available in Appendix F together with details on the impurity peaks that were identified in some of the NMR analyses. Impurities identified included traces of methanol (D_2O δ_H 3.31 ppm, δ_C 48.9 ppm), acetone (D_2O δ_H 2.17 ppm, δ_C 30.9 ppm and 215.5 ppm; $CDCl_3$ δ_H 1.25 ppm, δ_C 30.1 ppm) and water or acetate anomers ($CDCl_3$ δ_H 1.66 ppm) (Fulmer *et al.*, 2010; Pramanik *et al.*, 2005). The impurities did not interfere with the polysaccharides' atom assignments. These results are presented, beginning with the assignment of pullulan.

5.3.1 Analysis of pullulan

Although pullulan is commonly viewed as a polymaltotriosyl glucan, there can exist a minor amount of maltotetraose subunits that are randomly distributed within the polysaccharide (Catley *et al.*, 1966; Leathers, 2003). Figure 5.8 illustrates the difference between the major DP3 repeat subunit ($A + B + C$) and the minor DP4 subunit ($A' + B' + B'' + C'$) in pullulan. A full suite of NMR experiments was carried out on pullulan to assign and confirm the major DP3 repeating units, to determine the contribution of DP4 units to the polysaccharide, and to form a basis against which the *P. sacchari* EPS structures could be analysed and compared.

To begin, the ^{13}C spectrum of pullulan was inspected and 18 carbon resonances were found. This coincides with the number of carbon atoms expected in a maltotriosyl repeat sequence. Next, the anomeric region of the ^{1}H spectrum was reviewed and three α-glucan resonances at δ_H 5.32, 5.36, and 4.91 ppm appeared as seen in Figure 5.9 (Dag, 2005; Perlin and Casu, 1982; Vuorinen and Alen, 1999). The $^{3}J_{1,2}$ splitting patterns of each of these resonances was less than 4 Hz, which is typical for α-glucans (Ferreira *et al.*, 1995; Harding *et al.*, 2005). Then, the contribution of anomeric resonances due to the presence of any DP4 units in the pullulan sample was assessed. From Figure 5.8, it is obvious that any presence of DP4s would increase the abundance of B-type resonances (*i.e.*, $B + B' + B''$) in the ^{1}H spectra of pullulans. In this sample, however, the anomeric signals had equivalent d-splitting patterns and each signal integrated close to a single proton (unity). In fact, the anomeric proton intensities were used to determine that the contribution of DP4 in this pullulan sample was only 1.1%, as calculated by Delben *et al.* (2006) (this data is found in Appendix F).

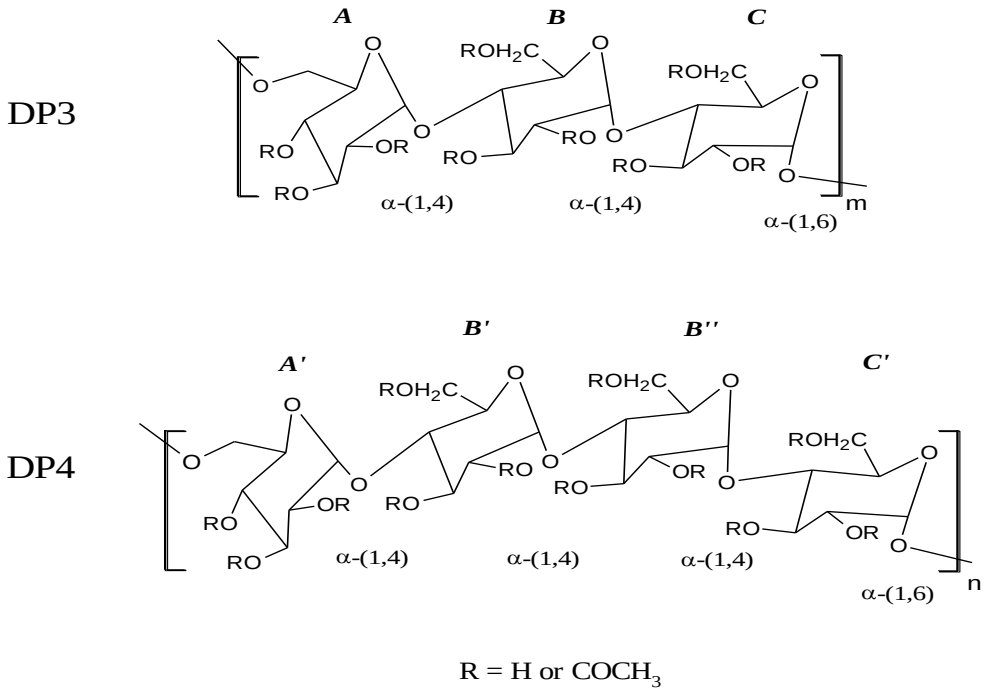

Figure 5.8: Representative structure of pullulan showing the maltotriose (DP3) and potential maltotetraose (DP4) repeat units in either the native (R = H) or peracetylated forms (R = $COCH_3$). The ratio of DP3:DP4 (m:n) in pullulan is usually greater than 93:7 (adapted from Delben *et al.,* 2006).

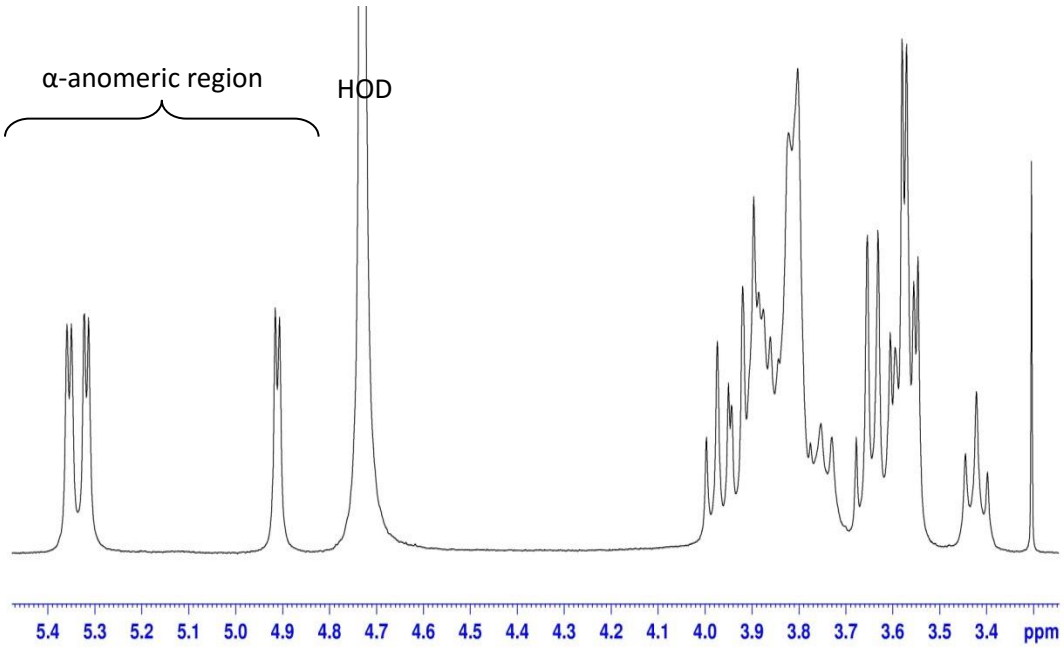

Figure 5.9: ^{1}H NMR spectrum of pullulan reveals three resonances in the α-anomeric region.

Next, the $A-B-C$ sequence of the major DP3 subunit in this pullulan sample had to be confirmed. To do so, the remaining protons (H-2 to H-6) and carbons (C-1 to C-6) of each sugar ring (A, B and C) were assigned.

To begin the ring assignments, the anomeric signals (C-1) were alphabetically labelled from the most downfield anomeric carbon in the ^{13}C spectrum (Delben *et al.*, 2006; Harding *et al.*, 2005). Hence, the resonances at δ_C 100.1, 99.8, and 98.0 ppm were labelled A, B and C, respectively. The A and B anomeric signals were in similar chemical environments, and were anticipated to belong to the two α-(1,4)-linked rings. Hence, the more upfield resonance C was assigned as the α-(1,6)-linked ring. This assignment was later confirmed with the HMBC correlation.

The DEPT135 experiment aided the initial identification of the C-6 resonances. These carbons have a different multiplicity (CH_2) and appeared on the negative axis at δ_C 66.6, 60.7, and 60.6 ppm, as seen in Figure 5.10. The resonance with the greatest difference in chemical shift (66.6 ppm) belongs to the C-6 involved in a glycosidic linkage, and so this signal was assigned as AC-6. The more upfield signals were allocated to CC-6 (60.6 ppm) and BC-6 (60.7 ppm), respectively (Delben *et al.*, 2006). The remaining resonances in the ^{13}C spectrum appear between the anomeric and C-6 regions. There are only two unique resonances here. These appear most downfield toward the anomeric region, and are anticipated to belong to the two α-(1,4)-linked carbons; namely, BC-4 (77.7 ppm) and CC-4 (77.4 ppm). These allocations were confirmed with the HMBC correlations.

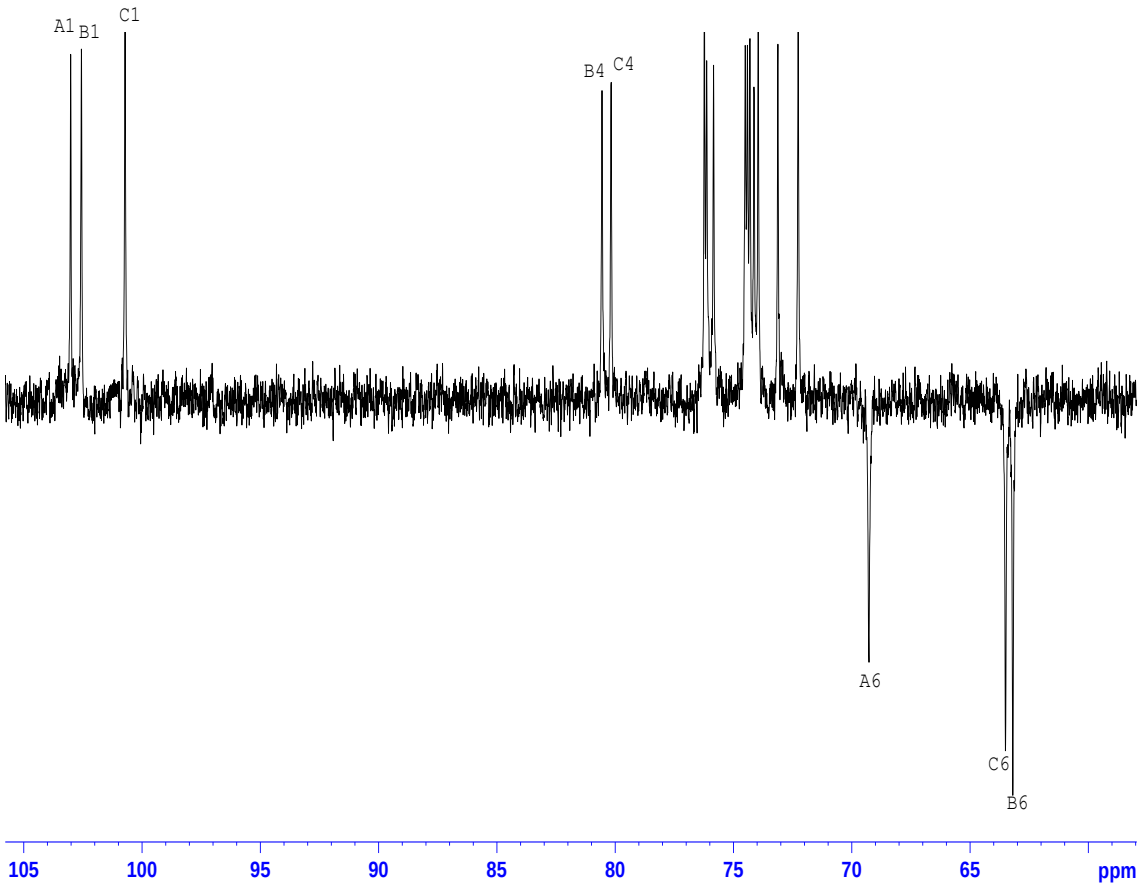

Figure 5.10: The DEPT135 ^{13}C NMR spectrum for pullulan. The distinguishable features are labelled, the assignments of which were confirmed by 2D NMR experiments.

Following the allocation of AC-1, BC-1 and CC-1 from the ^{13}C spectrum, the associated ^{1}H resonances could be ascribed as δ_H 5.32, 5.36, and 4.91 ppm, respectively. These labelled anomeric protons served as starting points in the COSY and HSQC spectra for assignment of the remaining atoms in the DP3 sequence. In the HSQC spectrum (Figure 5.11), the oppositely phased CH_2 groups on each ring, seen as a lighter shade of blue, made for easier assignment of the $A6, B6$ and $C6$ correlations. These agreed with the assignments made from the DEPT135 experiment.

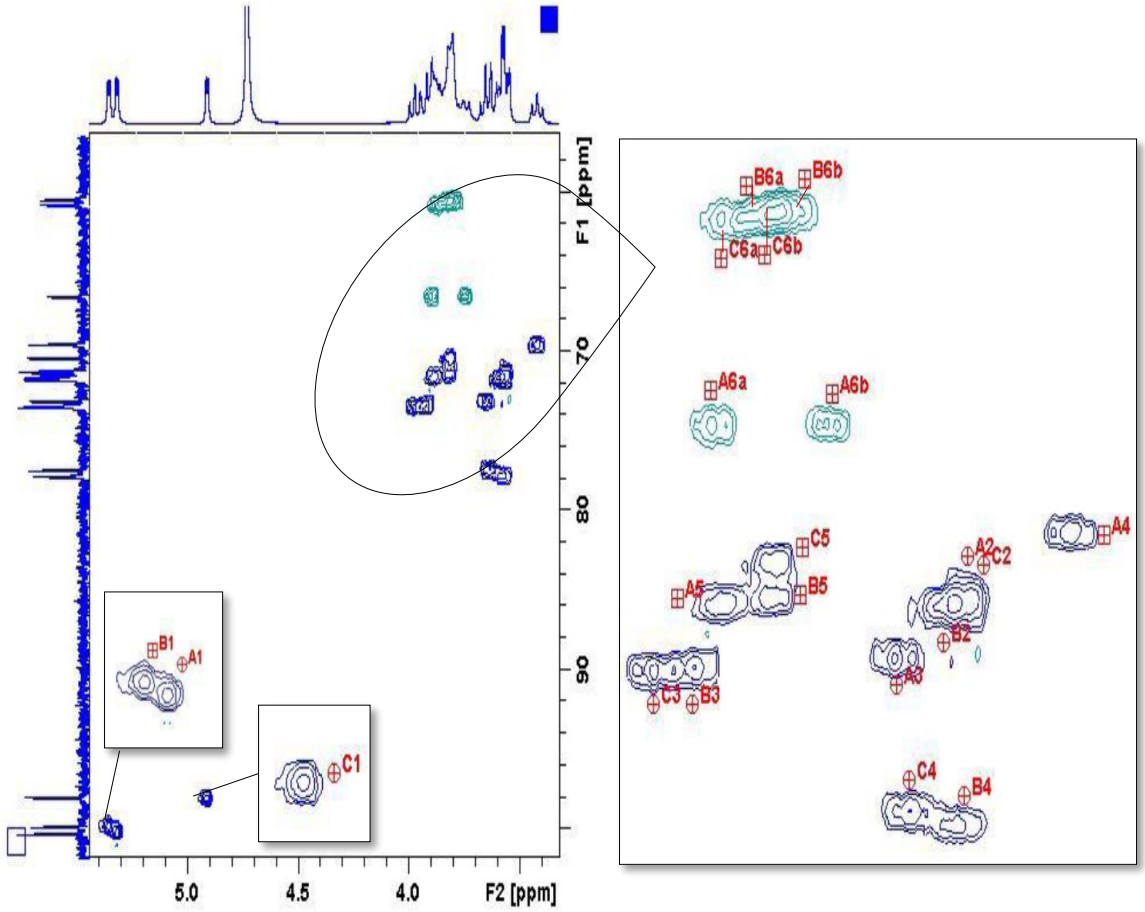

Figure 5.11: Labelled HSQC spectrum for pullulan. The F1 axis shows the projected ^{13}C spectrum and the F2 axis shows the projected ^{1}H spectrum. The labelled anomeric region is shown ($A1$, $B1$ and $C1$). The crowded region is expanded and labelled. For clarity, these labels are offset from the centre of the correlations – the centres are indicated for the B6 and C6 resonances. The correlations for the CH_2 groups are oppositely phased and a lighter shade of blue.

With the the aid of the COSY and HSQC spectra, the peaks in the crowded region between δ_H 3.5-4.0 ppm (known as the carbohydrate skeleton region) were then assigned by tracing the *J*-couplings from either the anomeric or -CH_2 correlations. Figure 5.11 provides the labelled HSQC spectrum and Table 5.6 lists the associated assignments, which were found to correspond with literature (Delben *et al.*, 2006; Singh *et al.*, 2009).

Table 5.6 Assigned proton and carbon chemical shifts for pullulan in D_2O at 25 °C established from COSY and HSQC experiments.

Atom	Shift ($\delta^1H^{a,b}$) /ppm	Shift ($\delta^{13}C^{a,c}$) /ppm
Ring *A*		
1	5.32 (1H, d, $^3J_{1,2}$=3.80 Hz)	100.1
2	3.56	71.5
3	3.65	73.1
4	3.42	69.6
5	3.88	71.6
6a[d]	3.90	66.6
6b[d]	3.73	66.5
Ring *B*		
1	5.36 (1H, d, $^3J_{1,2}$=3.96 Hz)	99.8
2	3.59	71.6
3	3.92	73.4
4	3.58	77.7
5	3.83	71.2
6a[d]	3.84	60.6
6b[d]	3.78	60.6
Ring *C*		
1	4.91 (1H, d, $^3J_{1,2}$=3.48 Hz)	98.0
2	3.55	71.5
3	3.97	73.5
4	3.63	77.4
5	3.80	70.3
6a[d]	3.89	60.7
6b[d]	3.82	60.5

[a] Solvent D_2O.
[b] 400.2 MHz for ^1H.
[c] 100.6 MHz for ^{13}C.
[d] Assignment for diastereotopic protons (*a* and *b*) can be interchanged.
d – doublet

With the aid of the ROESY and HMBC spectra, the $A-B-C$ sequence of the pullulan sample was then confirmed. The HMBC experiment records long range ^1H-^{13}C correlations, whilst the ROESY experiment records inter-residue NOEs that are up to 5 Å apart (Cheng and Neiss, 2012).

The cross-peaks of the anomeric protons and carbons for each ring were examined to determine both their intra- and inter-residue connections. In the ROESY spectrum, AH-1 (δ_H 5.32 ppm) correlations were observed with AH-3 (δ_H 3.65 ppm), BH-3 (δ_H 3.92 ppm), BH-4 (δ_H 3.58 ppm), and BH-5 (δ 3.83). This indicates either an $A1-B3$, $A1-B4$ or $A1-B5$ linkage. The HMBC spectrum provided further clarification. This spectrum revealed AH-1 correlations with AC-3 (δ_C 71.6 ppm), AC-5 (δ_C 73.0 ppm), and BC-4 (δ_C 77.7 ppm). Thus, an α-(1,4)-linkage between rings $A-B$ was confirmed. The ROESY spectrum showed BH-1 (δ_H 5.36 ppm) correlations with BH-2 (δ_H 3.59 ppm) and BH-3 (δ_H 3.92 ppm), as well as CH-3 (δ_H 3.97 ppm), CH-4 (δ_H 3.63 ppm), and CH-6b (δ_H 3.82 ppm). The HMBC spectrum revealed BH-1 correlations with BC-2 (δ_C 71.6 ppm), BC-3 (δ_C 73.4 ppm) and CC-4 (δ_C 77.4 ppm). This information supports that rings $B-C$ are joined by an α-(1,4)-linkage. ROESY correlations were also observed for CH-1 (δ_H 4.92 ppm) with CH-2 (δ_H 3.55 ppm), CH-3 (δ_H 3.97 ppm), AH-6a (δ_H 3.90 ppm) and AH-6b (δ_H 3.73 ppm). The HMBC spectrum also showed correlations between CH-1 and CC-3 (δ_C 73.5 ppm), CC-5 (δ_C 70.3 ppm), and AC-6 (δ_C 66.5 ppm). Hence, this information supports that rings $C-A$ are joined by an α-(1,6)-linkage, and so the full $A-B-C$ repeat sequence could be elucidated for the pullulan sample. All the significant ROESY and HMBC correlations are labelled in Figure 5.12 and 5.13, respectively.

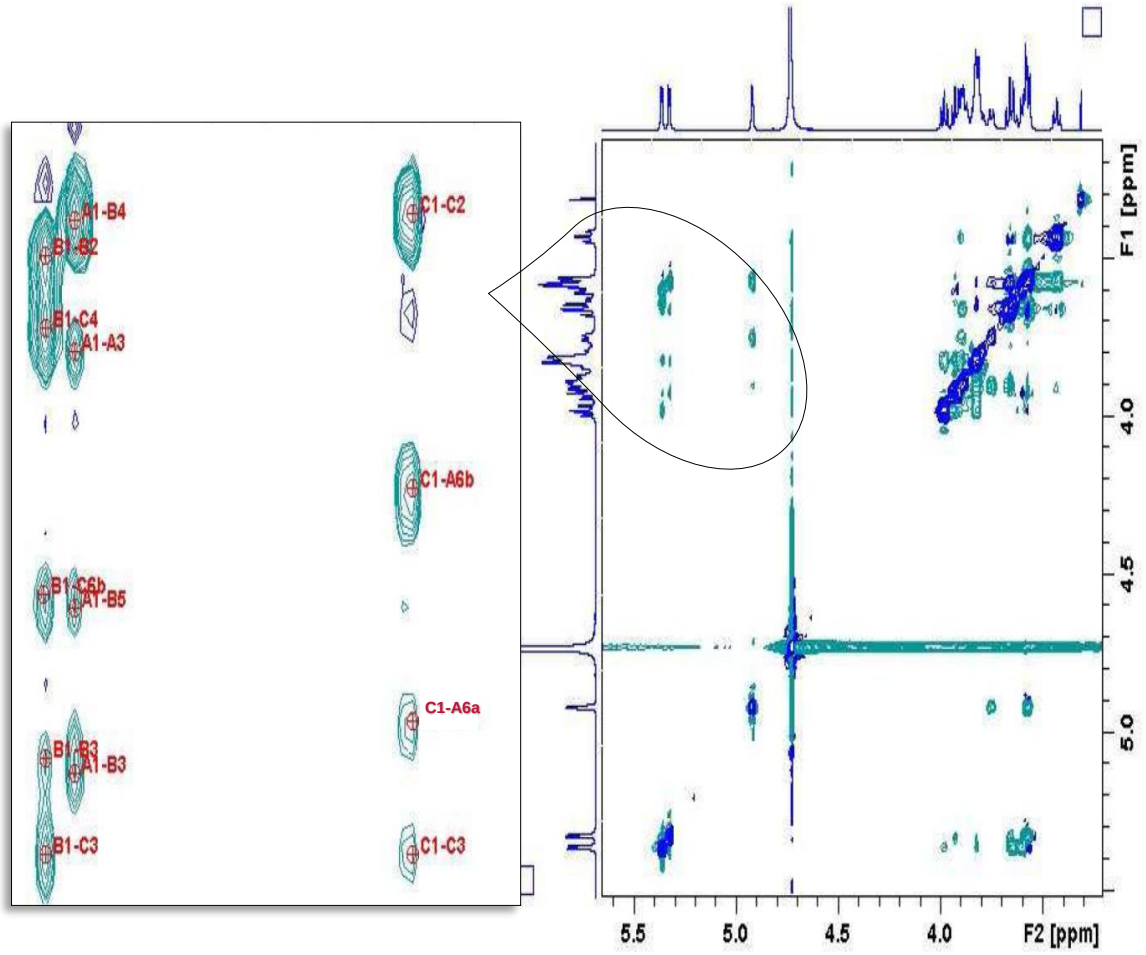

Figure 5.12: ROESY spectrum of pullulan with an expanded insert of the labelled significant correlations.

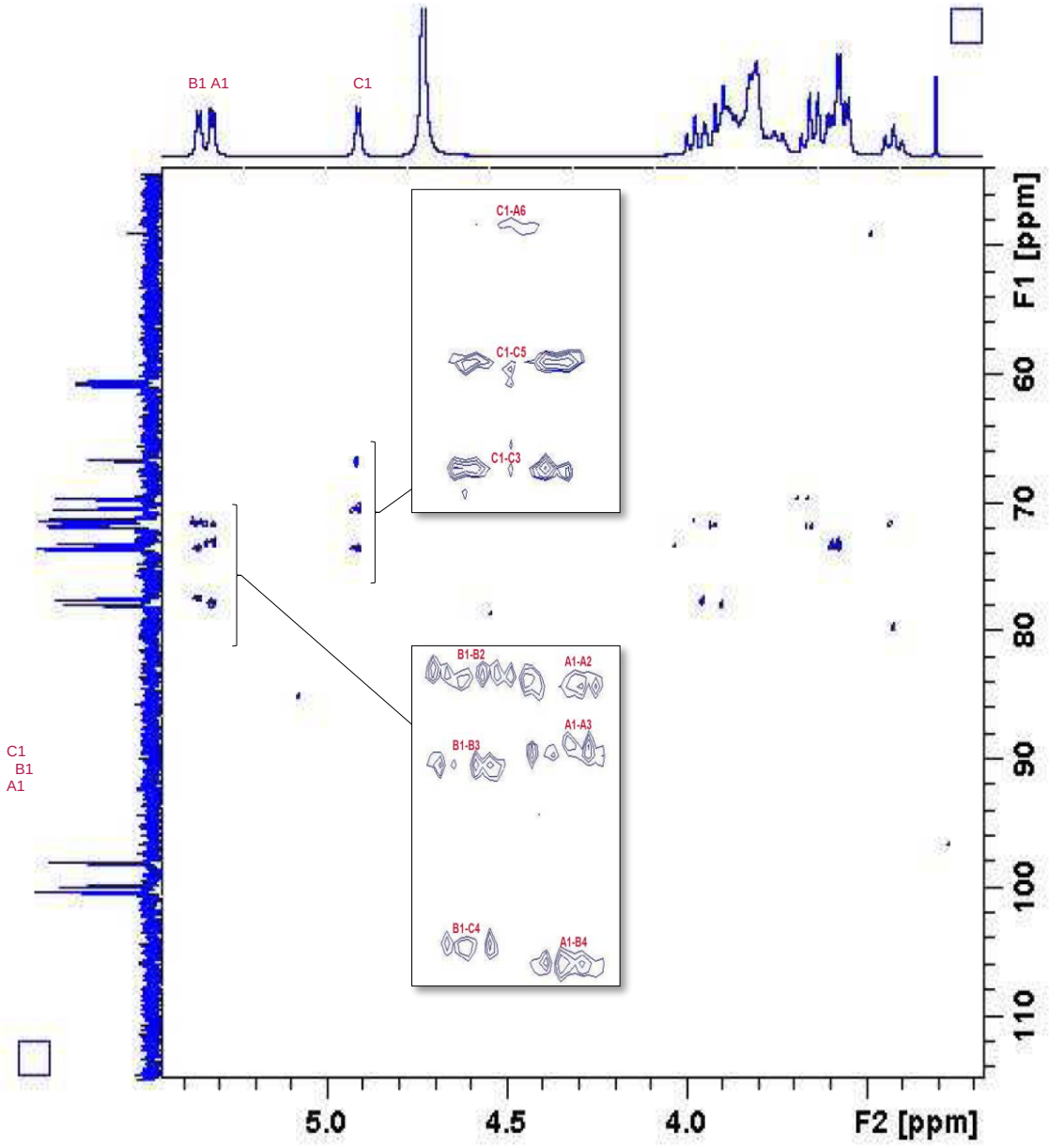

Figure 5.13: HMBC spectrum of pullulan with expanded inserts showing the labelled significant correlations.

Since it was demonstrated that pullulan could be fully assigned with the NMR analyses carried out, the spectra of the *P. sacchari* EPSs were next collected and scrutinised.

5.3.2 Analysis of the *P. Sacchari* polysaccharides

^{1}H-NMR spectra were collected for all the *P. sacchari* EPSs in their native form, but only the purified EPSs (FB2 F1 and FB2 F2) were analysed and (where possible) assigned by 1D and 2D NMR. Figure 5.14 illustrates the similarity between the ^{1}H NMR profiles of the native EPS samples and pullulan. Slight structural dissimilarities between the EPSs and pullulan are indicated by the subtle differences in these spectra. To explore these differences, the purified EPSs were subjected to ^{13}C and various 2D-NMR experiments.

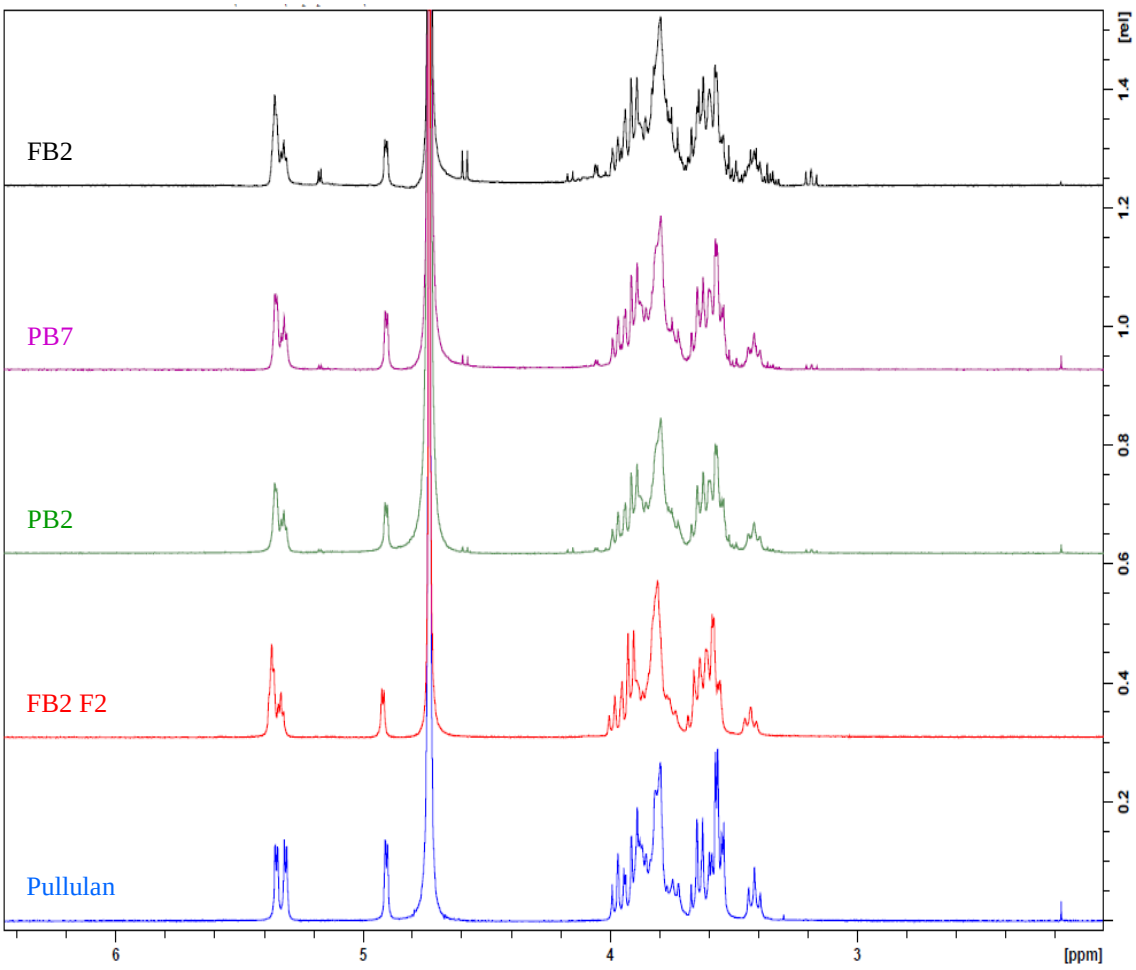

Figure 5.14: 1H-NMR Spectra (δ 2.0-6.2 ppm) for pullulan (blue), purified FB2 F2 (red), crude PB2 (green), crude PB7 (magenta) and crude FB2 (black). Samples were prepared in D_2O and analysed at 600.1 MHz and 25 °C, except for FB2 F2, which was analysed at 400 MHz and room temperature. The chemical shifts are referenced to the HOD solvent peak at δ = 4.73 ppm. The internal acetone peak is visible at δ = 2.1741 ppm for all spectra, except for FB2 F2.

For the repeat sequences in FB2 F1 and FB2 F2 to be determined, the same methodology as outlined in the elucidation of pullulan was followed. From the ^{1}H and ^{13}C spectra, the two purified EPSs appeared to have a predominant polymaltotriose structure that was similar to pullulan (see Figure 5.15 and 5.16, respectively). In particular, the ^{1}H peaks and ^{13}C peaks labelled $A1$, $B1$ and $C1$ in FB2 F1 and FB2 F2 appeared at the same chemical shifts as pullulan. In addition, the ^{1}H $^{3}J_{1,2}$ values for the A and C signals were below 4 Hz. Hence, α-glucopyranoses were indicated in these two purified FB2 fractions of this native EPS.

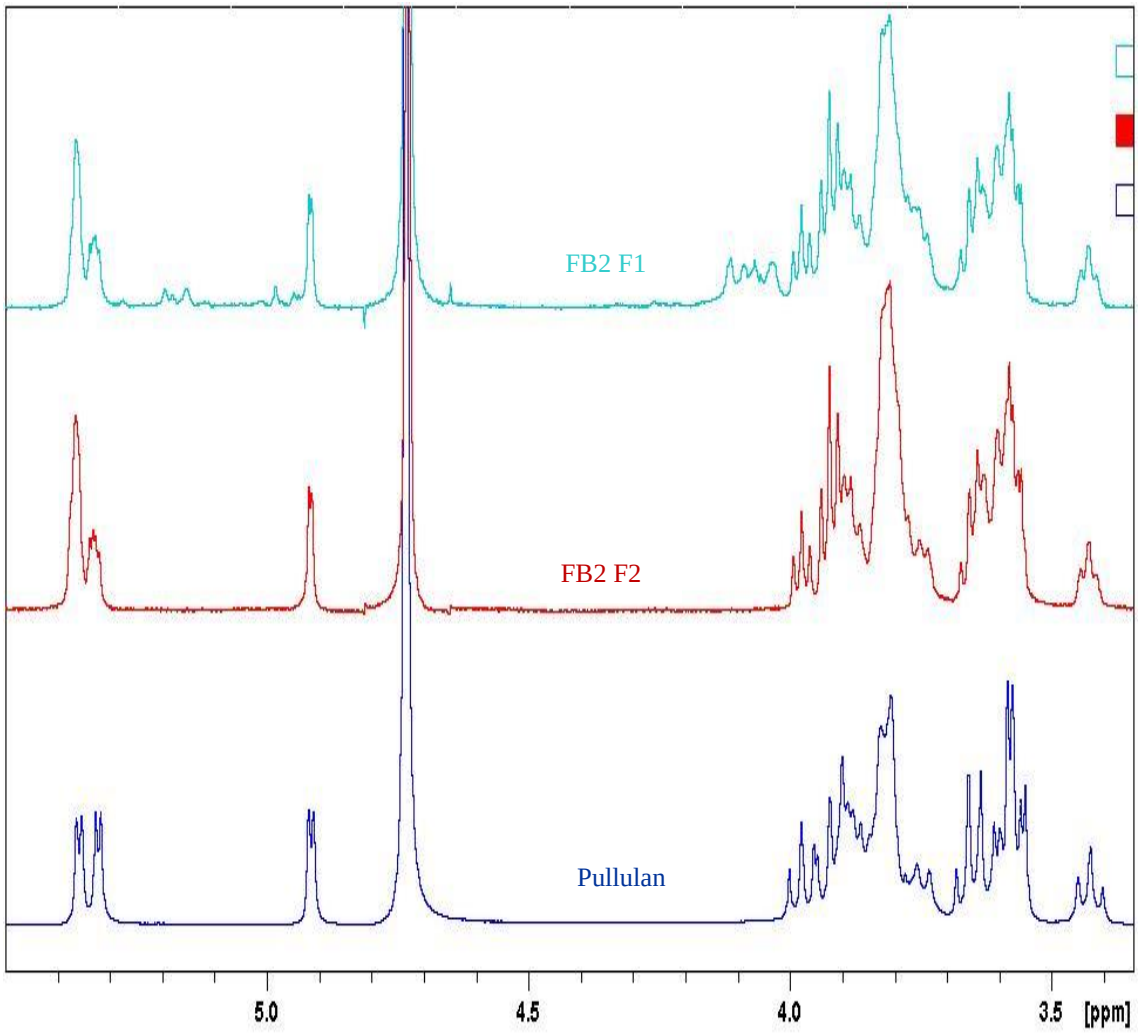

Figure 5.15: ^{1}H-NMR Spectra (δ 3.3-5.5 ppm) for pullulan (bottom), FB2 F2 (middle) and FB2 F1 (top). Samples were prepared in D_2O and analysed at 600.1 MHz and 25 °C. The chemical shifts are referenced to the HOD solvent peak at δ = 4.73 ppm.

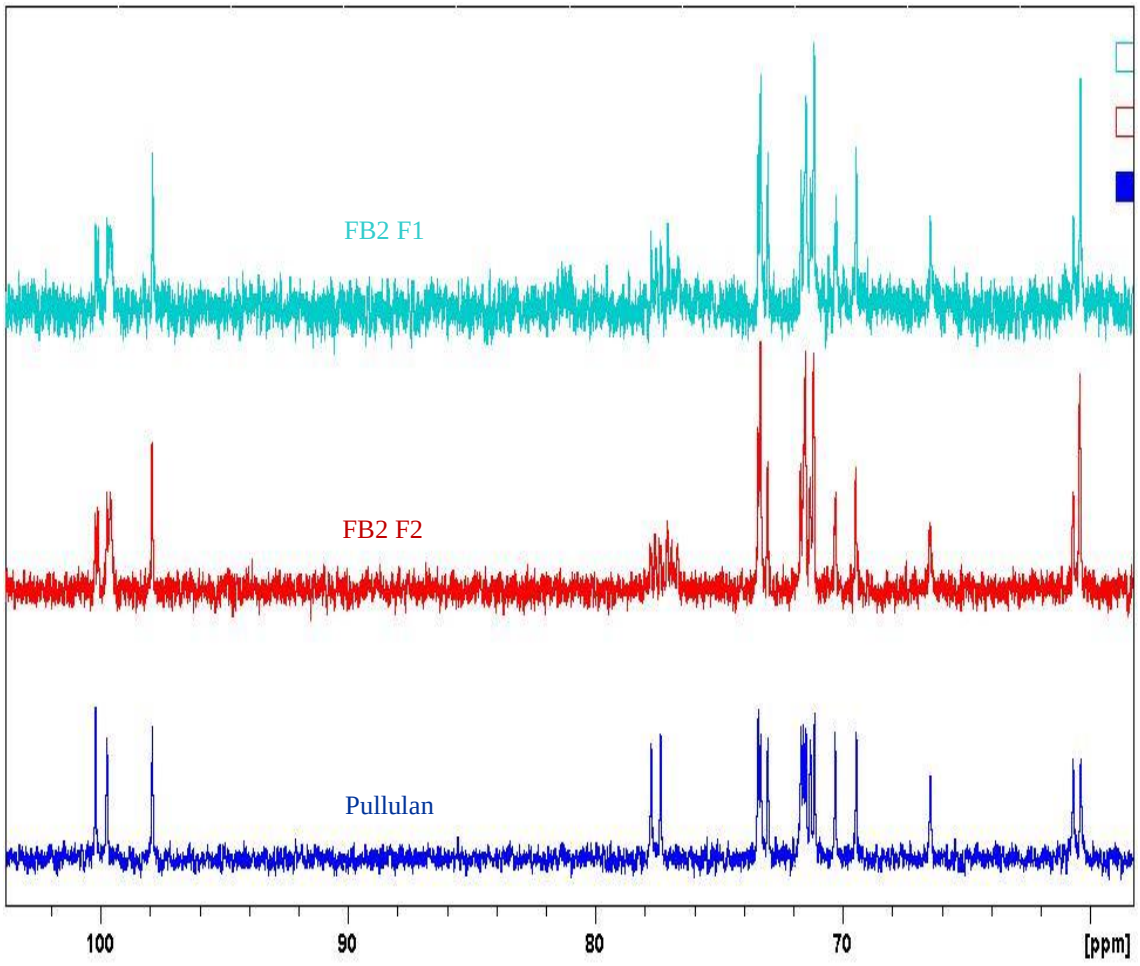

Figure 5.16: ^{13}C Spectra (δ 58.0-104.4 ppm) for pullulan (blue), FB2 F2 (red) and FB2 F1 (pale blue). The samples were prepared in D_2O. Pullulan was analysed ar 101 MHz at room temperature, whilst FB2 F2 and FB2 F1 were analysed at 151 MHz and 25 °C.

The ^{1}H spectrum for FB2 F2 was most similar to pullulan and no additional resonances were noted. Furthermore, the ^{13}C spectrum for the same sample did not contain any resonances between δ_C 93-97 ppm, which would otherwise indicate the presence of oligomers (Delben *et al.*, 2006). Hence, GFC fractionation of FB2 F2 was effective at removing the lower molecular weight components from the crude FB2 sample. The major resonances in the ^{1}H spectrum of FB2 F1 mirrors those of FB2 F2, however, several additional, less intense resonances also appeared in this sample. These resonances appeared in the order of 0.1-0.3 protons and were suspected to be due to the lesser mannose and galactose constituents that were detected in the GC-MS analyses. To confirm these, the resonances in FB2 F1 and FB2 F2 needed to be assigned. As before, the process was initiated by first assessing each samples' respective anomeric regions.

Both EPSs contained anomeric signals that coincided with pullulan, however, the intensities of the $A1$ and $B1$ signals no longer equaled that of $C1$ (unity) in either the ^{1}H or ^{13}C spectra of the EPS samples. This significant difference provided a clue that these pullulan-like samples may have consitituted a large proportion of DP4s. The anomeric region of the ^{1}H spectrum provided the initial pieces of evidence to support this; the A signal displayed additional splitting and the

B signal was more intense but has poorer symmetry. The splitting patterns in the anomeric region of the ^{13}C spectrum provide further evidence (refer to Figure 5.17). First, an additional signal appeared in the AC-1 region (δ_C ~100.1 ppm) and was labelled A'C-1. Second, additional resonances appeared in the BC-1 region (δ_C ~99.8 ppm) and were allocated as B'C-1 and B''C-1. Third, the singlet in the CC-1 region (δ_C ~98.0 ppm) had the highest intensity of the anomeric signals. Since there were additional anomeric resonances for both A and B, an additional C'C-1 resonance was expected. Therefore, the increased intensity at CC-1 indicated that these two resonances overlap. Indeed, the CC-1 resonances are expected to coincide for polysaccharides containing both DP3 and DP4 subunits as the topological situation of both CC-1 atoms are identical in the direction of the reducing-end of either sequence. In both cases, rings C and C' have equivalent sequences up to three linkages away, *i.e.*, they are proceeded by one α-(1,6)-, and two α-(1,4)-linkages. In contrast, the AC-1 atoms for A and A' have only two equivalent α-(1,4)-linkages but the third is either an α-(1,6)- or an α-(1,4)-linkage, respectively, and two separate signals are generated. A similar scenario is anticipated for anomeric resonances for B, B' and B''. Although both B and B'' have an α-(1,4)- followed by an α-(1,6)- and then an α-(1,4)-linkage, B' is proceeded by two α-(1,4)- and one α-(1,6)-linkage instead. Hence, a more intense $B + B''$ signal and a weaker B' signal are expected (Delben *et al.*, 2006). Interestingly, FB2 F1 and FB2 F2, had a minimum of three resonances in the B region (see Figure 5.17), indicating that additional B-type rings may have been present. This is possible if malto-oligomers greater than maltotetraose (> DP4) were present in the repeat sequence of the EPSs. Additional splitting in the A signals would provide further evidence of the presence of higher malto-oligosaccharides but the poor signal-to-noise ratio of these resonances could not substantiate this. Later on, it is demonstrated through enzyme hydrolysis and HPAEC-PAD analysis that higher malto-oligosaccharides were present within the repeat structure of these EPSs (refer to Section 5.4). Continuing, the remainder of the polysaccharide skeleton was further assessed and the atom assignments where made where possible.

In the ^{13}C spectrum of FB2 F1 and FB2 F2, splitting was also present in the region of C-4. For pullulan, two C-4 signals appeared at δ_C 77.7 and 77.4 ppm, and were assigned as BC-4 and CC-4, respectively. In the EPSs, these same resonances were identified, with the additional associated peaks being assigned to the respective B', B'' and C' resonances for the same atom. A total of four signals in this region were expected (Delben *et al.*, 2006), however, at least six were discernable. Hence, the possibility of subunits > DP4 in the repeat sequences was indicated, however, it was impossible to assign these peaks with higher precision.

The C-6 region of FB2 F1 and FB2 F2 was next assessed. The signal intensities for both samples differed from pullulan in this region. First, the more upfield signal was most intense and so it was allocated as $C + C'$. The more downfield signal was the weaker of the three, and the one that was most split. This signal was assigned as the resonances of $A + A'$. The splitting of the A signal occured due to the diastereotopic effect arising from the fixed conformation of the $–CH_2$ group involved in the (1,6)-glycosidic bond (Delben *et al.*, 2006). Conversely, the $–CH_2OH$ groups at C-6 for all the C- and B-rings had more freedom and so their signals should appear as singlets. Hence, the remaining singlet was assigned for $B + B' + B''$.

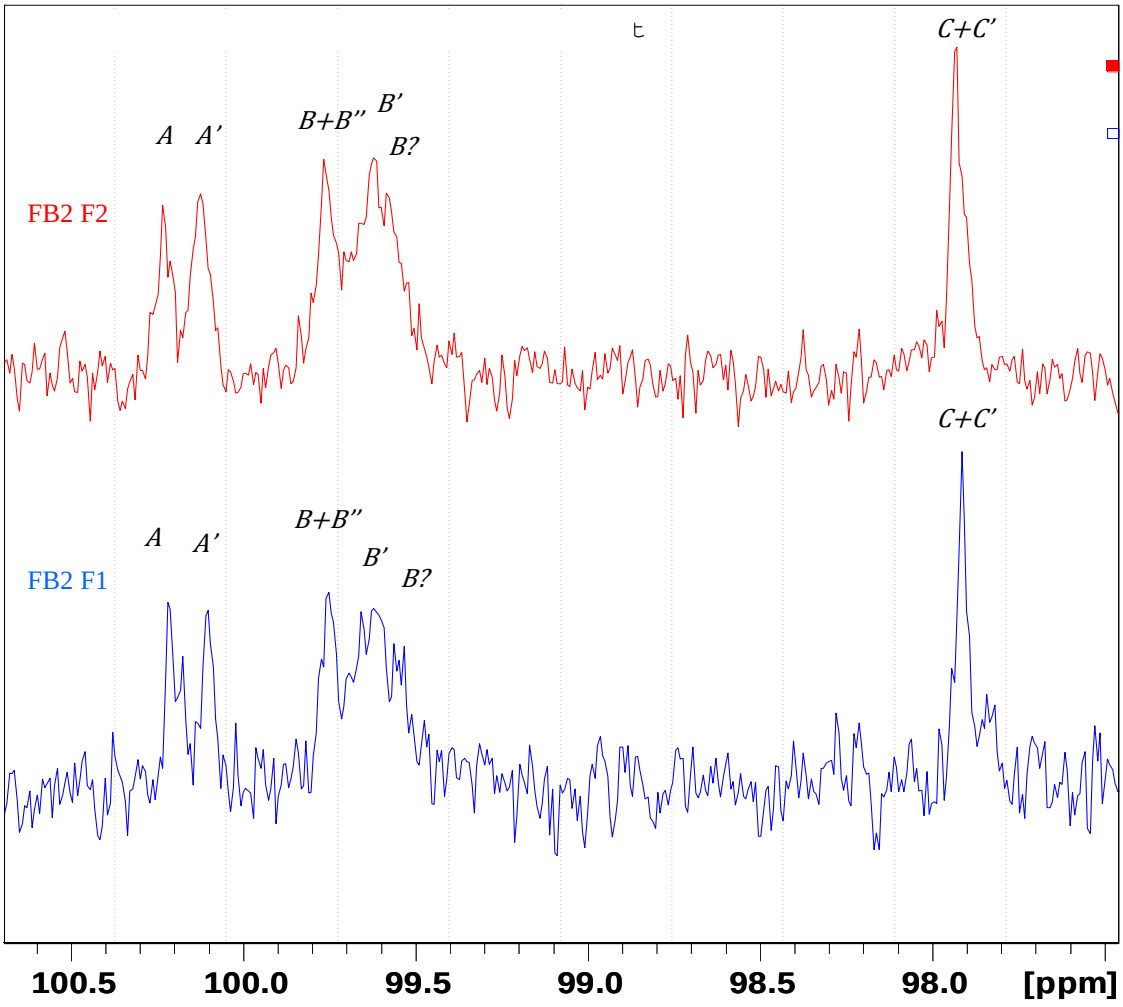

Figure 5.17: Comparison of the ^{13}C A, B and C splitting patterns of FB2 F1 (blue) and FB2 F2 (red).

Proceeding, the remaining assignments listed in Table 5.7 were made through tracing the *J*-coupling network from the anomeric protons in the COSY spectrum, together with the HSQC spectrum, as described for pullulan. Since there was extensive overlap in the COSY spectrum, ^{1}H assignments were made against the most distinctive cross-peaks. Hence, the assigned values for A and A', and B, B' and B'', and C and C' represent an average.

Following the assignment of all the carbons and protons in the EPSs, the possibility of a $A - B - C$ type pattern, synonymous with pullulan, between the malto-oligomer sequences was investigated. As in the case of pullulan, the HMBC and ROESY spectra were consulted. For simplicity, only the anomeric protons were considered in the ROESY, and only C-1, H-1, C-4 and C-6 positions were reviewed for rings A, B and C in the HMBC. This selection was based on the structural analysis results obtained for the EPSs by GC-MS.

Table 5.7 Proton and carbon chemical shifts for the *P. sacchari* EPS FB2 F1 and FB2 F2 in D_2O at 25 °C.

Atom	FB2 F1/ppm		FB2 F2/ppm	
	δ^1H[a,b]	$\delta^{13}C$[a,c]	δ^1H[a,b]	$\delta^{13}C$[a,c]
Ring *A*, *A'*[d]				
1	5.33,5.32 (2.4H,dd,$^3J_{1,2}$=3.90,4.38 Hz)	100.1,100.2	5.33 (2.2H,dd,$^3J_{1,2}$=3.36,3.78 Hz)	100.2,100.3
2	3.57	71.2	3.56	71.6
3	3.66	73.0	3.66	73.1
4	3.43	69.5	3.43	69.5
5	3.89	71.5	3.89	71.6
6a[e]	3.90	66.5	3.90	66.6
6b[e]	3.74	66.5	3.74	66.5
Ring *B*, *B'*, *B''*[f]				
1	5.36	99.8	5.36	99.8
2	3.60	71.7	3.60	71.6
3	3.92	73.3	3.92	73.4
4[g]	3.58	77.1,77.3 77.6,77.8	3.64	76.7,76.9 77.1,77.6,77.8
5	3.82	70.3	3.83	70.4
6a[e]	3.86	60.7	3.84	60.6
6b[e]	3.76	60.7	3.78	60.6
Ring *C*, *C'*[f]				
1	4.92 (2H,d,$^3J_{1,2}$=2.52 Hz)	97.9	4.91 (2H,d,$^3J_{1,2}$=2.52 Hz)	97.9
2	3.57	71.3	3.55	71.3
3	3.98	73.4	3.98	73.6
4[g]	3.63	77.1,77.4	3.64	77.1,77.4
5	3.81	71.7	3.81	71.4
6a[e]	3.83	60.4	3.88	60.6
6b[e]	3.78	60.4	3.82	60.5

[a] Solvent D_2O.
[b] 600.1 MHz for ^1H.
[c] 150.9 MHz for ^{13}C.
[d] The chemical shifts of *A* and *A'* can be interchanged.
[e] Assignment for diastereotopic protons (*a* and *b*) can be interchanged.
[f] The chemical shifts for *B*, *B'*, *B''*, *C* and *C'* can be interchanged.
[g] The chemical shift assignments are based on the spectra of pullulan.
d – doublet, dd – doublet of doublets

In FB2 F1, the ROESY revealed several cross-peaks for CH-1 (δ_H 4.92 ppm), these included: CH-2 (δ_H 3.57 ppm), CH-3 (δ_H 3.98 ppm), AH-6b (δ_H 3.74 ppm), and AH-6a/AH-5 (δ_H 3.90/3.89 ppm). In the HMBC spectrum, a cross-peak between AC-6 (δ_C 66.5 ppm) and CH-1 (δ_H 4.92 ppm) was observed. Together, the ROESY and HMBC measurements indicated that rings $C-A$ were joined by an α-(1,6)-linkage. In the ROESY spectrum, BH-1 (δ_H 5.36 ppm) also had several cross-peaks, these included: BH-2 (δ_H 3.60 ppm), BH-3 (δ_H 3.92 ppm), BH-5 (δ_H 3.82 ppm), CH-3 (δ_H 3.98 ppm), and CH-4 (δ_H 3.63 ppm). A cross-peak in the HMBC spectrum was observed between BC-1 (δ_C 99.5 ppm) and two resonances for CH-4 (δ_H 3.62 and 3.64 ppm). Likewise, there was a cross-peak between the BH-1 (δ_H 5.36 ppm) and CC-4 (δ_C 77.1 ppm) resonances. Together, these sets of correlations were believed to be between $B+B''$ and C+C'. Hence, the HMBC and ROESY correlations indicated that the $B-C$ rings are joined by an α-(1,4)-linkage. The ROESY spectrum showed correlations between AH-1 (δ_H 5.33 ppm) and AH-3 (δ_H 3.66 ppm), BH-3 (δ_H 3.92 ppm), BH-4 (δ_H 3.58 ppm), and BH-5 (δ_H 3.82 ppm). Unfortunately, there were no HMBC cross-peaks to verify the $A1-B4$ linkage. However, by elimination, if two (1,4)-linkages and one (1,6)-linkage are expected, then $A-B$ must display the final (1,4)-configuration. Hence, it was demonstrated that the $A-B-C$ and $A'-B'-B''-C'$ sequence types were present in FB2 F1.

In FB2 F2, the ROESY spectrum revealed three cross-peaks for CH-1 (δ_H 4.91 ppm); these included: CH-2 (δ_H 3.55 ppm), AH-6b (δ_H 3.75 ppm), and AH-6a/AH-5 (δ_H 3.90/3.89 ppm). In the HMBC spectrum a cross-peak between CH-1 (δ_H 4.91 ppm) and AC-6 (δ_C 66.5 ppm) was also observed. As with FB2 F1, together the ROESY and HMBC indicated an α-(1,6)-linkage between rings $C-A$ ($C1\rightarrow6A$). In the ROESY spectrum, BH-1 (δ_H 5.36) had several cross-peaks, including: BH-2 (δ_H 3.60 ppm), CH-3 (δ_H 3.98 ppm), CH-4 (δ_H 3.63 ppm), CH-5 (δ_H 3.81 ppm), and CH-6a (δ_H 3.88 ppm). A cross-peak in the HMBC spectrum was observed between BC-1 (δ_C 99.5 ppm) and CH-4 (δ_H 3.64 ppm). Unlike FB2 F1, FB2 F2 did not have an additional cross-peak in the HMBC spectrum between BH-1 and CC-4. However, the identified HMBC and ROESY correlations provided enough evidence that an α-(1,4)-linkage existed between the $B-C$ rings ($B1\rightarrow4C$). Continuing, the ROESY spectrum showed correlations between AH-1 (δ_H 5.33 ppm) and AH-5 (δ_H 3.89 ppm), BH-4 (δ_H 3.64 ppm), and BH-5 (δ_H 3.83 ppm). As was the case with FB2 F1, there were no HMBC cross-peaks in FB2 F2 to verify the $A1\rightarrow4$B linkage. Again, by elimination, $A-B$ was assumed to have the final α-(1,4)-configuration in the repeat sequence. Hence, the $A-B-C$ and $A'-B'-B''-C'$ sequence types were also found to be present in FB2 F2 and, hence, both fractions isolated from the crude FB2 EPS had the same predominant glucan makeup. In addition to glucose, the GC-MS data revealed that the EPSs also contained mannose and galactose. These components were next assessed.

As described in Section 4.2, the GC-MS analyses established that there were D-galactopyranoses and terminal D-mannopyranoses present in the EPS samples, with FB2 F1 having the highest proportion (~13% galactose and ~3.2% mannose) and FB2 F2 having almost none (< 0.1%) of either. The ^{1}H spectrum for FB2 F1 revealed additional, minor resonances in the regions of δ_H 4.9-5.3 ppm and δ_H 4.0-4.7 ppm (Figure 5.15). These resonances were assessed to determine which belonged to mannose or galactose, and whether they revealed their connectivity within the EPS subunits. Table 5.8 provides the assignments made for the identified resonances in these regions. Galactose was found to belong to either an α-(1,6)-linked interchain residue, or a 6-linked reducing-end residue of the EPS (Pramanik *et al.*, 2005; van Leeuwen *et al.*, 2014). Whereas, mannose was confirmed to exist as a terminal beta residue (Pramanik *et al.*, 2005). Integration of the anomeric protons indicated that galactose and mannose accounted for ~20% and ~10% of FB2 F1, respectively. These values are both greater than those estimated by the GC-MS analyses. This is reasonable since NMR is a non-destructive analysis technique, where the sample is directly analysed. On the other hand, the GC-MS technique involves a number of

preparation steps, one of which provides the potential for evaporative losses of permethylated monosaccharide derivatives. These losses cause the relative contribution of terminal and reducing-end residues to be underestimated.

Following assignment of the mannose and galactose residues, the glucose reducing-ends needed to be assigned. Since both FB2 F1 and FB2 F2 were high molecular weight isolates of the FB2 EPS, the abundance of reducing-end residues in these samples is expected to be very low. So, instead, the crude EPSs were assessed. The ^{1}H spectra of the three crude EPSs (FB2, PB2 and PB7) were compared with those of pullulan and FB2 F2 in order to establish the glucose reducing-end resonances and to establish whether there was any notable difference between the makeup of the shake-flask EPSs compared with the bioreactor sample. Figure 5.14 reveals that all the crude samples havd remarkably similar ^{1}H speactra compared to FB2 F2. Notably, the crude samples displayed a series of less intense signals that were not present in pullulan or the FB2 F2 fractionate. These resonances belonged to the α- and β-anomers of 6-linked D-glucopyranose reducing-ends, as detailed in Table 5.9 (Cheng and Neiss, 2012; Goffin *et al.*, 2009; McIntyre and Vogel, 1991; van Leeuwen *et al.*, 2014; van Leeuwen *et al.*, 2008). The quantity of reducing-ends present in each sample indicated the abundance of lower molecular weight polysaccharides (or oligosaccharides) present in the crude EPSs. The spectra revealed that FB2 had the largest proportion of reducing-ends and PB2 the smallest.

Table 5.8 ^{1}H NMR assignments for mannose and galactose in FB2 F1 together with the possible mode of linkage of each residue in the repeating unit, as indicated by literature.

Shift (δ ^{1}H[a]) /ppm	Assignment	Possible linkage
5.22	αGal*p*H-1 or αGalp_RH-1	→6)-α-D-Gal*p*-(1→ [1] or →6)-D-Gal*p* [2]
5.03	βMan*p*H-1	β-D-Man*p* [1]
4.11	βMan*p*H-6a/b and/or αGal*p*H-6a/b or αGalp_RH-6a	β-D-Man*p* [1] and/or →6)-α-D-Gal*p*-(1→ [1] or →6)-D-Gal*p* [2]
4.09	αGal*p*H-2	→6)-α-D-Gal*p*-(1→ [1]
4.03	βMan*p*H-4 and/or βGalp_RH-4	β-D-Man*p* [1] and/or →6)-D-Gal*p* [2]

[a] The D_2O water peak (HOD) was referenced to δ_H 4.73 ppm at 25 °C.

[1] Assignments are according to Pramanik *et al.* (2005). The authors' reference HOD peak was at δ_H 4.51 ppm (50 °C). Hence, the reflected assignments are ~0.22 ppm more than those reported by the authors.

[2] Assignments are according to van Leeuwen *et al.* (2014). The authors' reference internal acetone was at δ_H 2.225 ppm (25 °C), and their HOD peak was at δ_H 4.78 ppm. Hence, the reflected assignments are ~0.05 ppm less than those reported by the authors.

H – proton, ppm – parts per million, α – alpha anomer, β – beta anomer, R – reducing-end, Gal*p* – galactopyranose, Man*p* – Mannopyranose, → – Indicates an inter-residue glycosidic bond and the number indicates the connectivity onto the associated ring.

Table 5.9 ^{1}H NMR assignments for the minor 6-linked α-D-glucopyranose reducing-ends determined in the crude *P. sacchari* EPS samples.

Shift (δ ^{1}H[a]) /ppm	Polysaccharide			Atom
	PB2	PB7	FB2	
5.17	0.04H, d, 4.02 Hz	0.04H, d, 4.02 Hz	0.19H, d, 4.02 Hz	αA_RH-1
4.59	0.06H, d, 8.03 Hz	0.16H, d, 8.03 Hz	0.33H, d, 8.03 Hz	βA_RH-1
4.16	0.04H, d, 8.52 Hz	n.d.	0.20H, d, 9.01 Hz	βA_RH-6a
4.05	0.07H, d, 3.52 Hz	0.14H, d, 3.51 Hz	0.35H, d, 3.52 Hz	αA_RH-6a
3.18	0.06H, t, 8.52 Hz	0.07H, t, 8.52 Hz	0.27H, t, 8.54 Hz	βA_RH-2

[a] The D_2O water peak (HOD) was referenced to δ_H 4.73 ppm at 25 °C. Assignments are according to van Leeuwen *et al.* (2014). The authors' internal acetone peak was at δ_H 2.225 ppm (25 °C), and their HOD peak was at δ_H 4.78 ppm. Hence, the reflected assignments are ~0.05 ppm less than those reported by the authors.

H – proton, ppm – parts per million, n.d. – not detected, α – alpha anomer, β – beta anomer, R – reducing-end, *A* – ring represented by the 6-linked α-D-Glucopyranoses

To summarise thus far, the NMR data for both the purified FB2 F1 and FB2 F2 provided sufficient evidence that the FB2 EPSs comprised a predominant $A-B-C$ malto-oligosaccharide structure, with additional malto-oligosaccharide sequences of DP4 and greater indicated. Both the poor symmetry and the large peak area of the BH-1 signals indicated the possibility of higher malto-oligosaccharides in these purified samples. The ^{13}C spectra provided further support, as the BC-1 and BC-4 signals contained additional splitting. The mannose and galactose components in FB2 F1 were next determined, confirming that these components existed as 6-linked terminal β-D-mannopyranoses and either 1,6-linked inter-chain or 6-linked reducing-end α-D-galactopyranoses, in a quantity of ~10% and ~20%, respectively. The α-D-glucospyranose reducing-ends of the lower molecular weight components in the crude EPSs were next determined, and all the EPSs were found to have the same predominant DP3 – DP4 – > DP4 make-up. To confirm this finding, the atoms in the crude EPSs were next assigned. To simplify the task, the samples were first acetylated (Heinze *et al.*, 2006; Tezuka, 1998). The results for pullulan peracetate and the EPS peracetates are presented and discussed in the following subsections.

5.3.3 Analysis of pullulan peracetate

Tezuka (1998) has previously demonstrated the power of using the acetyl structure probe to determine the maltotriosyl repeat subunit of pullulan. In general, this derivatisation technique provides acetyl protons and acetyl carbonyl carbon signals that are sensitive to their location on glucosyl rings in ^{1}H and ^{13}C NMR analyses, respectively. Tezuka made use of several 2D NMR techniques to elucidate pullulan peracetate; namely, ^{1}H-^{1}H COSY, ^{1}H-^{1}H NOESY, and HMBC. In this study, the prepared pullulan peracetate was analysed by COSY, HSQC, HMBC and NOESY. The steps followed to elucidate pullulan peracetate are outlined. In Step 1, the maltotriosyl protons were assigned by tracing the J-couplings in the COSY spectrum (Figure 5.18). In Step 2, the HSQC spectrum enabled the maltotriosyl carbons to be assigned according to their correlations with the maltotriosyl protons (Figure 5.19). In Step 3, the HMBC

spectrum facilitated the assignment of the acetyl protons according to their correlations with the maltotriosyl carbons (Figure 5.20). In Step 4, the acetyl protons assigned in Step 3 where then used to assign the more downfield carbonyl carbons in the same spectrum (Figure 5.21). In Step 5, the cross-peaks in the NOESY spectrum were assessed to establish the linkage arrangement of the assigned maltotriosyl rings.

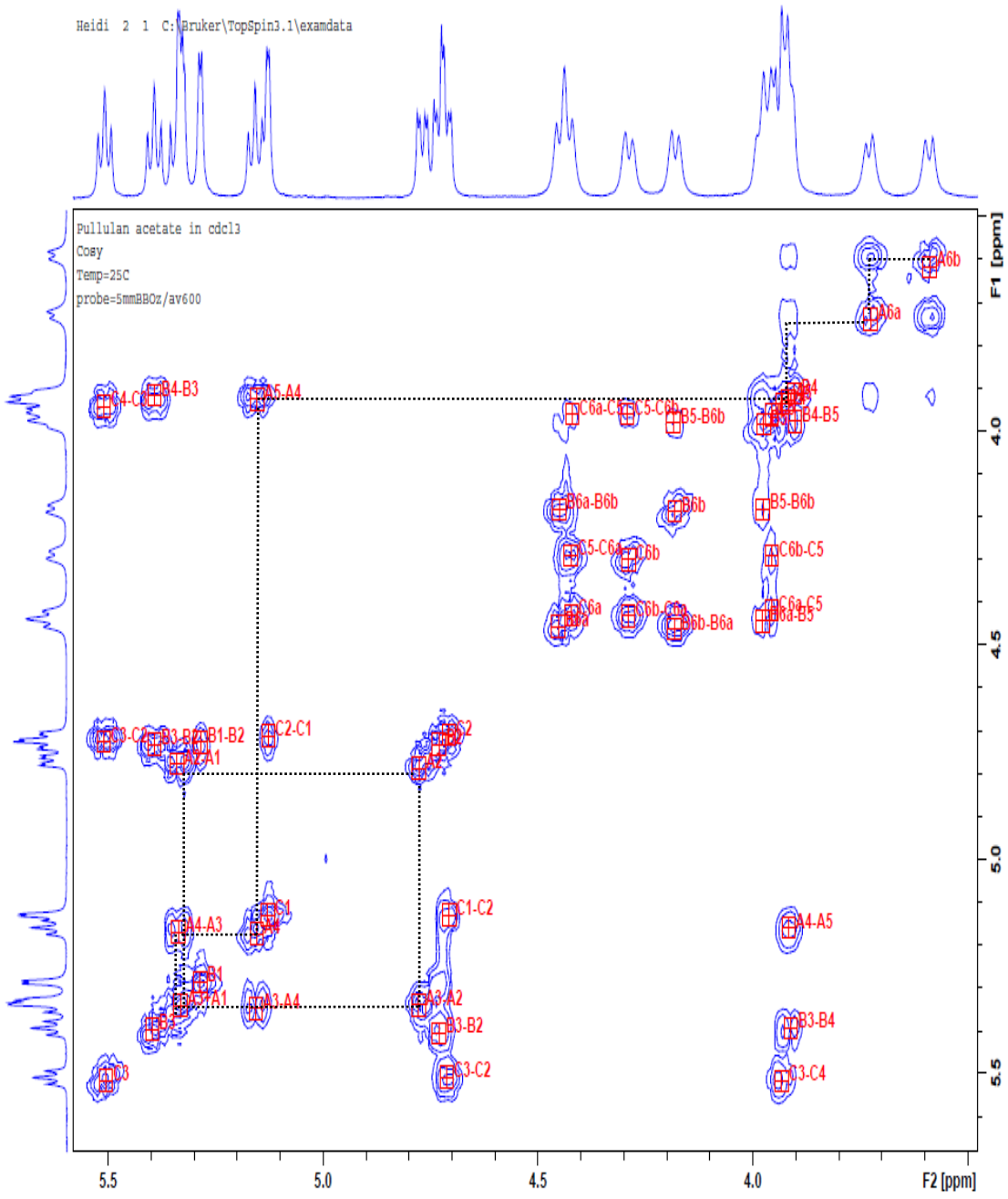

Figure 5.18: Correlations in the COSY spectrum used to assign the maltotriosyl protons for pullulan peracetate. The tracing of the *J*-couplings from the H-6 geminal protons is illustrated for ring *A* ($CDCl_3$, 25 °C, 600 MHz, referenced at δ_H 7.26 ppm).

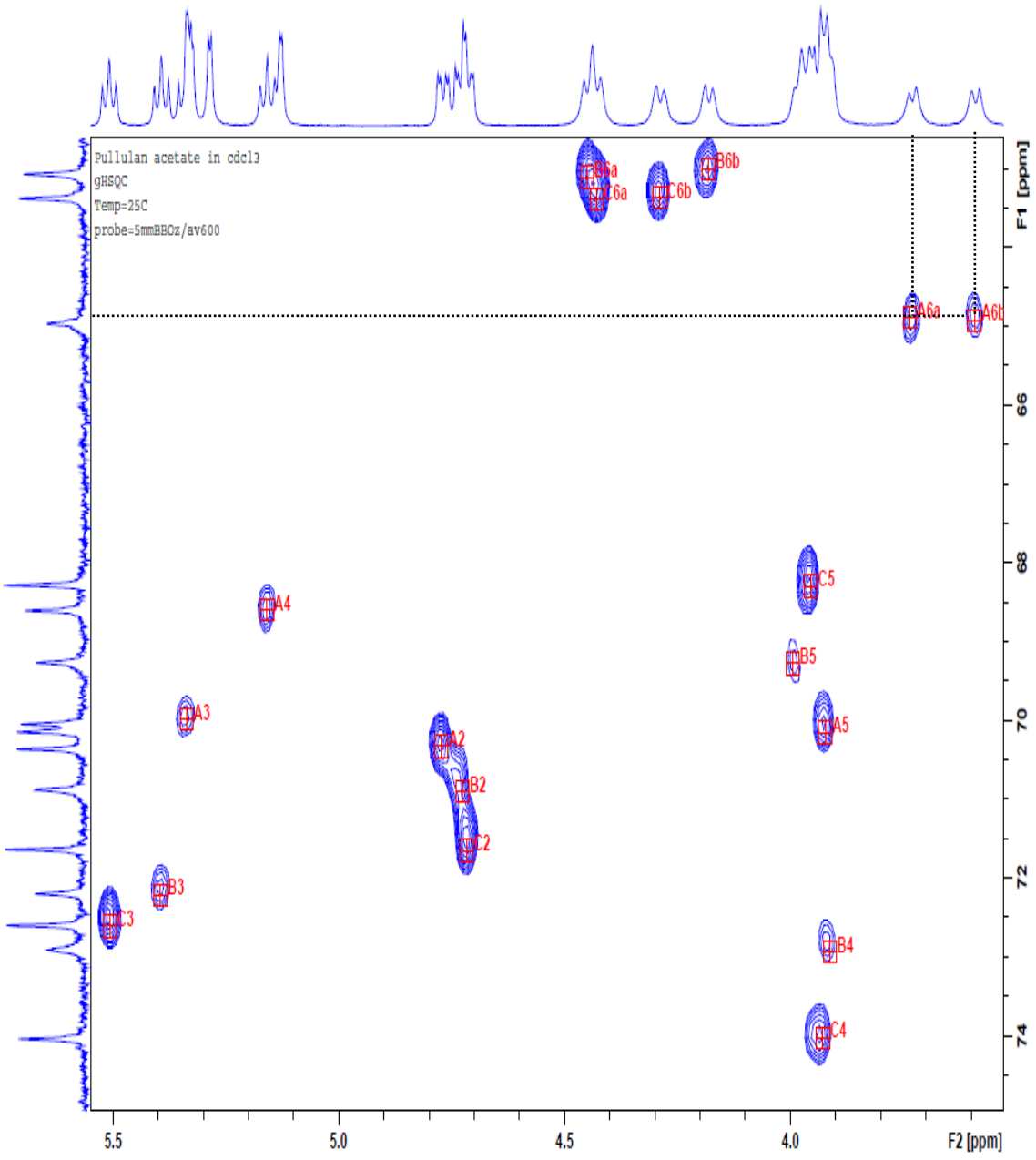

Figure 5.19: Correlations in the HSQC spectrum used to assign the maltotriosyl carbons for pullulan peracetate. The correlations with $A1$, $B1$ and $C1$ are not shown. The tracing of the $A6$ correlation from the geminal maltosyl protons to their associated maltosyl carbon is illustrated ($CDCl_3$, 25 °C, 600 MHz, referenced at δ_H 7.26 ppm, δ_C 77.36 ppm).

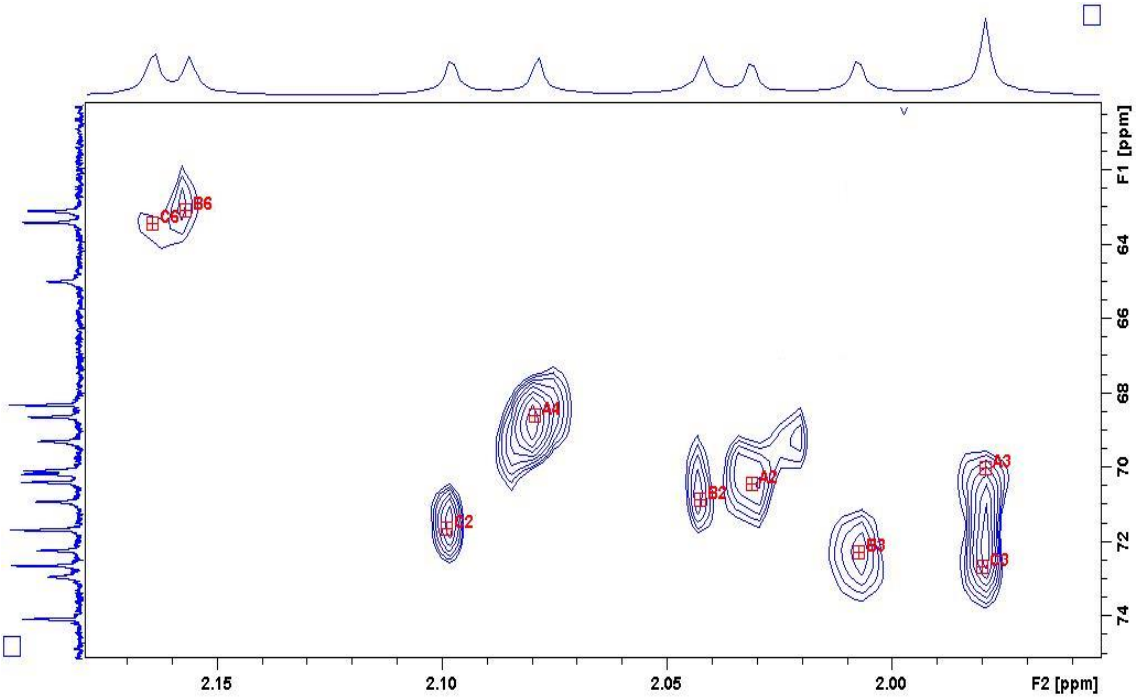

Figure 5.20: Correlations in the HMBC spectrum used to assign the acetyl protons for pullulan peracetate ($CDCl_3$, 25 °C, 600 MHz, referenced at δ_H 7.26 ppm, δ_C 77.36 ppm).

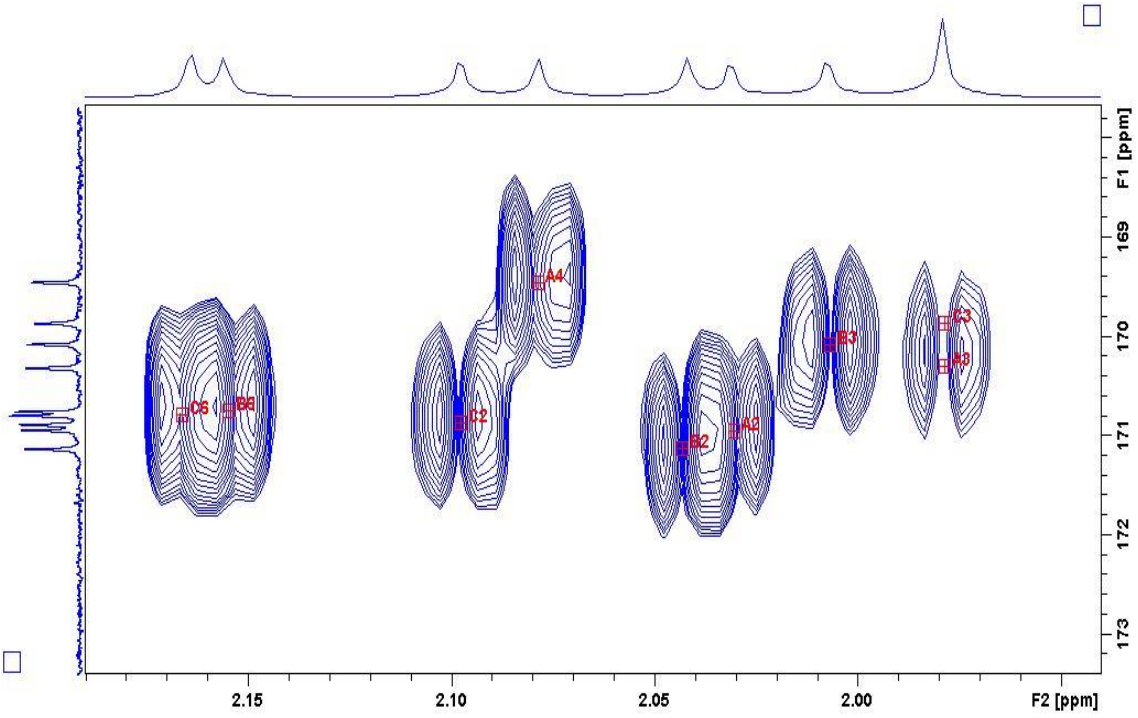

Figure 5.21: Correlations in the HMBC spectrum used to assign the carbonyl carbons for pullulan peracetate ($CDCl_3$, 25 °C, 600 MHz, referenced at δ_H 7.26 ppm, δ_C 77.36 ppm).

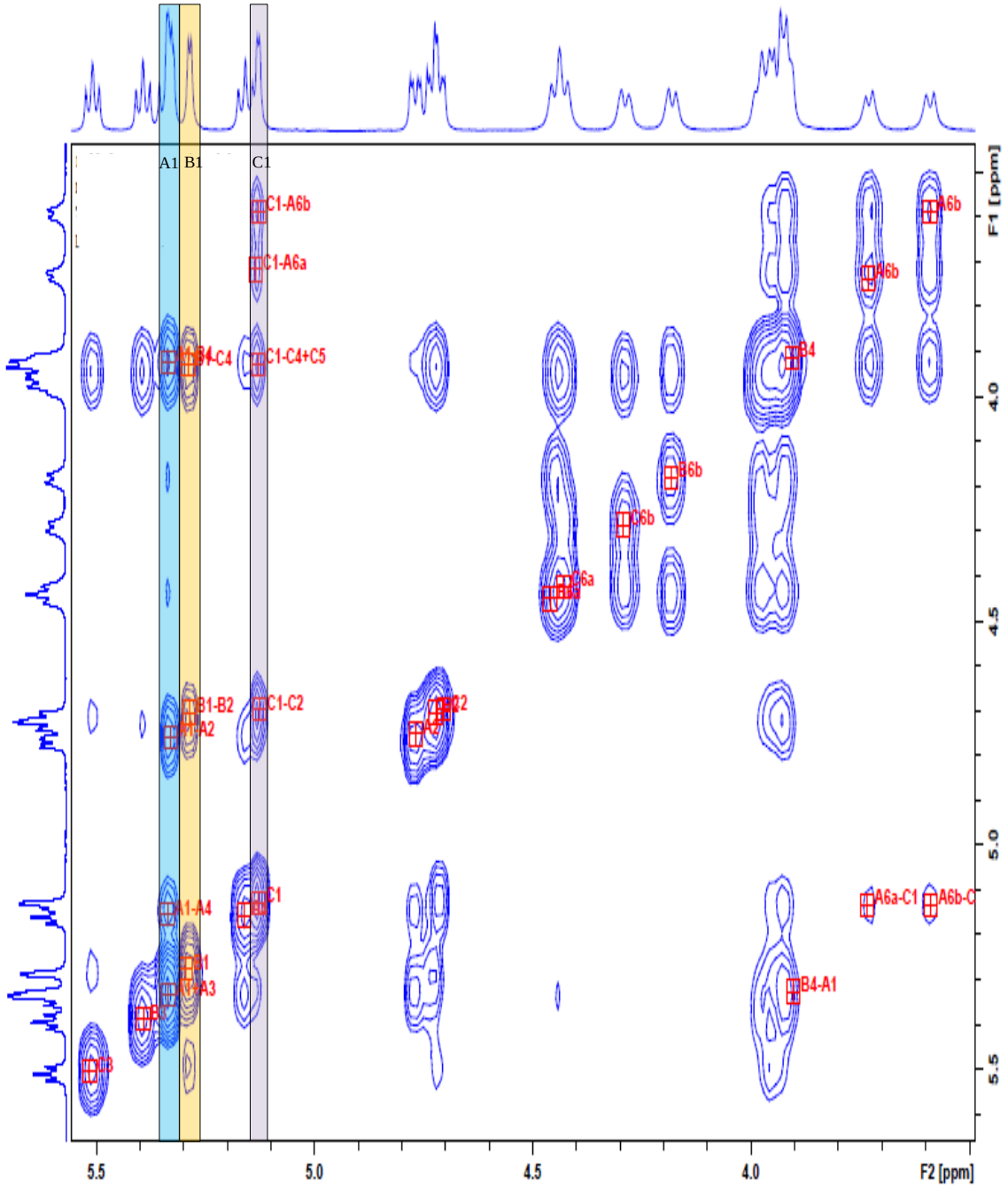

Figure 5.22: The NOESY spectrum of pullulan peracetate. Correlations between the protons of $A1$ with $B4$, $B1$ with $C4$, and $C1$ with both $A6a$ and $A6b$ confirm the $A-B-C$ linkage profile for pullulan. The $A1$ (blue shading), $B1$ (yellow shading) and $C1$ (purple shading) tracks are indicated ($CDCl_3$, 25 °C, 600 MHz, referenced at δ_H 7.26 ppm).

Following these steps, the structure of pullulan peracetate was confirmed. In Step 1, analysis began from the well resolved anomeric doublets for $A6$, and each doublet of doublets (appearing as a triplet) for $B3$ and $C3$. The connectivity between the protons of maltotriosyl rings A, B and C could then be traced, despite the crowding of peaks in the δ_H 4.7-4.8 ppm region. In Step 2, the 18 maltosyl carbons were subsequently assigned with the aid of the HSQC measurements. In Step 3, the long-range, four-bond correlations between the maltotriosyl carbons and the acetyl protons (**C**-O-CO-C-**H**) were observed and all nine acetyl protons were assigned. Following on with Step 4, the two-bond correlation between the acetyl protons and carbonyl carbons (**C**O-C-**H**) were assigned in the HMBC spectrum. Unfortunately, the resonance of the acetyl protons of $A3$ and $C3$ occur at the same shift (δ_H 1.97 ppm), which made assignment of the correlated carbonyl carbons for these resonances challenging. To resolve these assignments, the three-bond heteronuclear connectivity between $A3$ and $C3$ maltotriosyl protons with the carbonyl carbons (**H**-C-O-**C**O) were used to assign these two carbonyl resonances instead. Table 5.10 provides all the pullulan peracetate assignments made as described in Steps 1-4, and which correspond to literature (Tezuka, 1998).

In Step 5, the NOESY measurements were used to confirm the $A-B-C$ linkage profile for pullulan peracetate. The $C1{\rightarrow}6A$ linkage was established by observing the through-space connectivity between the protons of $C1$ with $A6$a and $A6$b. This linkage was further supported by the absence of a correlation between the same geminal protons and $B1$. The $A1{\rightarrow}4B$ linkage was observed through a NOE correlation between the protons of $B4$ and $A1$. Finally, the $B1{\rightarrow}4C$ connection was indicated by the presence of a NOE correlation between the protons of $B1$ and $C4$, and was further supported by the absence of a correlation between the $B1$ and $A4$ protons.

The results demonstrate that peracetylation offers an alternate means of establishing the subunit structure and sequence of pullulan. Derivatisation allowed improved resolution of peaks for both the proton and carbon resonances in the maltotriosyl region, which aided the assignment of the subunit skeleton atoms. Hence, the crude *P. sacchari* EPSs were also peracetylated and the derivatives similarly analysed.

Table 5.10 The NMR proton and carbon assignments of pullulan peracetate from the ^{1}H, ^{13}C, COSY, HSQC and HMBC analyses.

Atom	Maltotriosyl regions/ppm		Acetyl regions/ppm	
	$\delta^{1}H^{a,b}$	$\delta^{13}C^{a,c}$	$\delta^{1}H^{a,b}$	$\delta^{13}C^{a,c}$
Ring *A*				
1	5.33 (1H, d, J=3.8 Hz)	95.89	-	-
2	4.77 (1H, dd, J=4.0, 10.5 Hz)	70.34	2.03	170.94
3	5.34 (1H, t, J=9.8 Hz)	70.04	1.97	170.30
4	5.16 (1H, t, J=9.6 Hz)	68.60	2.08	169.44
5	3.92[d]	70.15	-	-
6a	3.74 (1H, d, J=9.2 Hz)	64.97	-	-
6b	3.59 (1H, d, J=10.1 Hz)	64.97	-	-
Ring *B*				
1	5.29 (1H, d, J=3.8 Hz)	95.94	-	-
2	4.73 (1H, dd, J=3.85, 9.8 Hz)	70.90	2.04	171.14
3	5.39 (1H, t, J=9.4 Hz)	72.21	2.01	170.07
4	3.91[d]	72.91	-	-
5	3.97[d]	69.27	-	-
6a	4.45 (1H, d, J=10.9 Hz)	63.07	2.16	170.75
6b	4.18 (1H, d, J=8.9 Hz)	63.07	-	-
Ring *C*				
1	5.13 (1H, d, J=3.3 Hz)	96.29	-	-
2	4.72 (1H, dd, J=4.7, 10.5 Hz)	71.68	2.10	170.89
3	5.51 (1H, t, J=9.2 Hz)	72.56	1.98	169.86
4	3.93[d]	74.02	-	-
5	3.95[d]	68.29	-	-
6a	4.43 (1H, d, J=11.2 Hz)	63.38	2.17	170.78
6b	4.29 (1H, d, J=10.4 Hz)	63.38	-	-

[a] $CDCl_3$ solvent, referenced at δ_H 7.26 ppm and δ_C 77.36 ppm (25 °C).
[b] 600 MHz for ^{1}H.
[c] 151 MHz for ^{13}C.
[d] Total integration is for five protons, for all the assignments crowded between δ_H 3.9-4.0 ppm.

5.3.4 Analysis of the peracetylated *P. sacchari* polysaccharides

In Section 5.3.2, it was demonstrated that the purified *P. sacchari* EPSs (FB2 F1 and FB2 F2) could be assigned in their native form. However, the extensive overlap in the carbohydrate skeleton region (δ_H 3.5-4.0 ppm) did make assignments for all the atoms difficult. It was anticipated that the NMR analyses of the crude EPSs would present a greater challenge. After demonstrating that the analysis of pullulan peracetate allowed for easier assignment of the polysaccharide's atoms, this procedure was also followed for the analysis of the crude EPS samples. Figure 5.23 and 5.24 provide the ^{1}H spectra for the maltosyl regions and acetyl regions, respectively, of the peracetylated pullulan, -PB2, -PB7 and -FB2 samples. Table 5.11 (PB7 peracetate), Table 5.12 (PB2 peracetate) and Table 5.13 (FB2 peracetate) summarise the assignments made for each sample by following the same steps as outlined for pullulan peracetate.

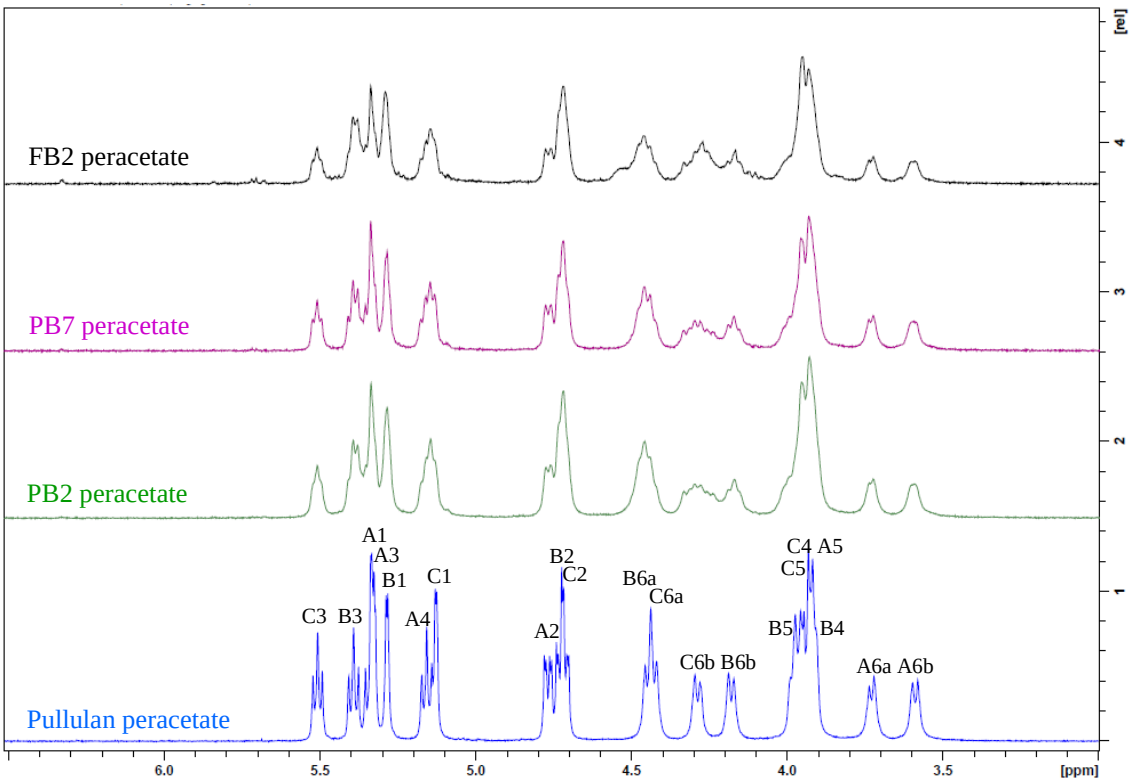

Figure 5.23: ^{1}H NMR spectra (δ_H 3.5-6.5 ppm) comparing the maltosyl regions of acetylated pullulan (blue, scale 1.0), and the acetylated crude EPSs: PB2 (green, scale 1.0), PB7 (magenta, scale 2.0) and FB2 (black, scale 2.0). The maltosyl assignments are provided for acetylated pullulan ($CDCl_3$ referenced at δ_H 7.26 ppm, 600 MHz, 25 °C).

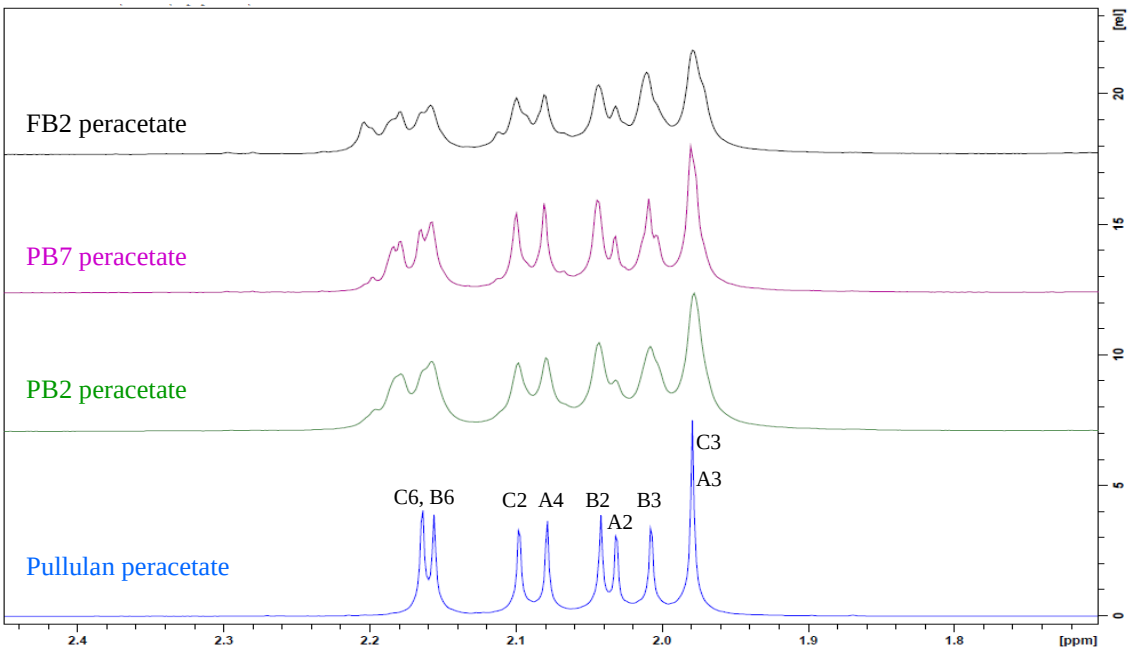

Figure 5.24: ^{1}H NMR spectra (δ_H 1.70-2.45 ppm) comparing the acetyl regions of pullulan peracetate (blue, scale 0.5), PB2 peracetate (green, scale 1.0), PB7 peracetate (magenta, scale 2.0) and FB2 peracetate (black, scale 2.0). The acetyl assignments are provided for pullulan peracetate ($CDCl_3$ referenced at δ_H 7.26 ppm, 600 MHz, 25 °C).

As was evident in the ^{1}H NMR spectra for the native crude EPS samples (Figure 5.14), all three of the acetylated crude EPSs reflected very similar proton profiles compared to pullulan peracetate (Figure 5.23 and 5.24). The noticeable differences included line-broadening of the peaks, changes in relative peak intensities as well as additional proton signals (particularly in the acetyl region). The EPS signals had suffered from some line-broadening compared with the pullulan sample, which could have occurred due to the possible superimposition of nearly equivalent spin-systems (*i.e.*, DP3 + DP4) and/or due to the higher molecular weights of the EPS samples (Laignel *et al.*, 1997). Samples of high molecular weight increase the solution viscosity. In turn, the sample rotational diffusion is slower, causing the spin-spin times of the atoms of interest to be longer, and thus increasing the resonance line-widths (Goux, 1990). Despite this loss in peak resolution, there were differences in some of the relative peak intensities, particularly for the *B*2 (δ_H 2.04 ppm) and *B*3 (δ_H 2.01 ppm) proton resonances in the acetyl region. Furthermore, additional acetyl proton signals appear slightly downfield to those of *B*6 (δ_H 2.16 ppm) and *C*6 (δ_H 2.17 ppm). Together, these observations indicated that all the crude EPSs must contain additional *B*-type rings, as indicated in previous analyses of FB2 F1 and FB2 F2 (Section 5.3.2).

Table 5.11 The NMR proton and carbon assignments of PB7 peracetate from the ^{1}H, ^{13}C, COSY, HSQC and HMBC analyses.

Atom	Maltosyl regions/ppm		Acetyl regions/ppm	
	$\delta^{1}H^{a,b}$	$\delta^{13}C^{a,c}$	$\delta^{1}H^{a,b}$	$\delta^{13}C^{a,c}$
Ring A, A'				
1	5.33 (1H, d, J=8.6 Hz)	95.87	-	-
2	4.77 (1H, d, J=9.8 Hz)	70.34	2.03	170.96
3	5.34 (1H, t, J=9.4 Hz)	70.05	1.98	170.32
4	5.16 (1H, t, J=8.9 Hz)	68.54	2.08	169.45
5	3.93[f]	70.19	-	-
6a	3.73 (1H, d, J=8.6 Hz)	64.80	-	-
6b	3.59 (1H, d, J=8.0 Hz)	64.80	-	-
Ring B, B', B''				
1	5.28 (1.57H)	96.07	-	-
2	4.73 (2.5H)[d]	70.82	2.04	171.13
3	5.38 (1.56H, dd, J=7.5, 18.1 Hz)	71.97	2.01	168.98
4	3.93[f]	72.72	-	-
5	3.96[f]	69.29	-	-
6a	4.47 (2.5H)[e]	63.00	2.16	170.76
6b	4.17 (1.1H, t, J=11.2 Hz)	63.00	-	-
Ring C, C'				
1	5.14 (1H, d, J=7.4)	96.30	-	-
2	4.71 (2.5H)[d]	71.68	2.10	170.89
3	5.51 (1H, t, J=8.4)	72.58	1.98	169.89
4	3.96[f]	73.90	-	-
5	3.96[f]	68.26	-	-
6a	4.43 (2.5H)[e]	63.36	2.17	170.80
6b	4.29 (1.8H, m)	63.36	-	-

[a] $CDCl_3$ solvent, referenced at δ_H 7.26 ppm and δ_C 77.36 ppm (25 °C).
[b] 600 MHz for ^{1}H.
[c] 151 MHz for ^{13}C.
[d,e] Total integration is shared between overlapping resonances.
[f] Broad peak prevents integration of the individual resonances, assignment is made from the COSY and HSQC spectra together with reference to pullulan peracetate.
d – doublet, dd – doublet of doublets, t – triplet, m – multiplet

Table 5.12 The NMR proton and carbon assignments of PB2 peracetate from the ^{1}H, ^{13}C, COSY, HSQC and HMBC analyses.

Atom	Maltosyl regions/ppm		Acetyl regions/ppm	
	$\delta^{1}H^{a,b}$	$\delta^{13}C^{a,c}$	$\delta^{1}H^{a,b,g}$	$\delta^{13}C^{a,c}$
Ring A, A'				
1	5.33 (1H, d,J=9.0 Hz)	95.87	-	-
2	4.77 (1H, d, J=8.3 Hz)	70.35	2.03	170.98
3	5.34 (1H, t, J=9.9 Hz)	70.03	1.98	170.31
4	5.16 (1H, t, J=8.7 Hz)	68.54	2.08	169.43
5	3.93[f]	70.20	-	-
6a	3.73 (1H, d, J=7.5 Hz)	64.85	-	-
6b	3.60 (1H, d, J=8.4 Hz)	64.85	-	-
Ring B, B', B''				
1	5.29 (1.80H)	96.07	-	-
2	4.73 (2.8H)[d]	70.74	2.04	171.14
3	5.39 (1.79H, dd, J=7.5, 15.8 Hz)	72.00	2.01	169.99
4	3.93[f]	72.72	-	-
5	3.99 (1H, t, J=11.1 Hz)	69.31	-	-
6a	4.48 (2.7H)[e]	62.93	2.17	170.75
6b	4.17 (1.2H, t, J=10.9 Hz)	62.93	-	-
Ring C, C'				
1	5.14 (1H, d, J=8.4 Hz)	96.30	-	-
2	4.72 (2.8H)[d]	71.68	2.10	170.88
3	5.51 (1H, t, J=7.7 Hz)	72.59	1.97	169.84
4	3.95[f]	73.86	-	-
5	3.95[f]	68.27	-	-
6a	4.44 (2.7H)[e]	63.38	-	-
6b	4.29 (1.8H, m)	63.38	-	-

[a] $CDCl_3$ solvent, referenced at δ_H 7.26 ppm and δ_C 77.36 ppm (25 °C).
[b] 600 MHz for ^{1}H.
[c] 151 MHz for ^{13}C.
[d,e] Total integration is shared between overlapping resonances.
[f] Broad peak prevents integration of the individual resonances, assignment is made from the COSY and HSQC spectra together with reference to pullulan peracetate.
[g] Acetyl proton three-bond correlations were not visible in the HMBC, assignments were made on the basis of the acetylated PB7 assignments and were referenced against the peracetylated pullulan assignments.
d – doublet, dd – doublet of doublets, t – triplet, m – multiplet

Table 5.13 The NMR proton and carbon assignments of FB2 peracetate from the ^{1}H, ^{13}C, COSY, HSQC and HMBC analyses.

Atom	Maltosyl regions/ppm		Acetyl regions/ppm	
	$\delta^{1}H^{a,b}$	$\delta^{13}C^{a,c}$	$\delta^{1}H^{a,b,g}$	$\delta^{13}C^{a,c,g}$
Ring *A*, *A′*				
1	5.34 (1.1H, d,J=9.0 Hz)	95.87	-	-
2	4.77 (1H, d, J=10.5 Hz)	70.34	n.d.	n.d.
3	5.33 (1.1H, d, J=9.2 Hz)	70.06	n.d.	n.d.
4	5.16 (1.1H, t, J=9.1 Hz)	68.58	n.d.	n.d.
5	3.92[f]	70.21	-	-
6a	3.73 (1H, d, J=8.3 Hz)	64.87	-	-
6b	3.60 (1H, d, J=7.1 Hz)	64.87	-	-
Ring *B*, *B′*, *B″*				
1	5.29 (2.4H)	96.00	-	-
2	4.73 (3.25H)	70.81	n.d.	n.d.
3	5.39 (2.25H, dd, J=7.5, 14.3 Hz)	72.05	n.d.	n.d.
4	3.93[f]	72.69	-	-
5	3.97[f]	69.31	-	-
6a	4.46 (m)[e]	62.95	n.d.	n.d.
6b	4.17 (m)[e]	62.95	-	-
Ring *C*, *C′*				
1	5.14 (1.1H, d, J=8.3 Hz)	96.29	-	-
2	4.71 (3.25H)	71.64	n.d.	n.d.
3	5.51 (1H, t, J=8.4 Hz)	72.60	n.d.	n.d.
4	3.94[f]	73.92	-	-
5	3.96[f]	68.27	-	-
6a	4.42 (m)[e]	63.37	-	-
6b	4.31 (m)[e]	63.37	-	-

[a] $CDCl_3$ solvent, referenced at δ_H 7.26 ppm and δ_C 77.36 ppm (25 °C).
[b] 600 MHz for ^{1}H.
[c] 151 MHz for ^{13}C.
[d] Total integration is shared between overlapping resonances.
[e,f] Cluster peaks prevent integration of the individual resonances, assignment is made from the COSY and HSQC spectra together with reference to pullulan peracetate.
[g] The HMBC correlations in the acetyl regions were not visible and these assignments could not be made.
d – doublet, dd – doublet of doublets, t – triplet, m – multiplet, n.d. – not detected.

Integration of all the *B*-type resonances in the maltosyl regions of the ^{1}H NMR spectra reveal that the peracetates of PB7, PB2 and FB2 had about 55%, 78% and 133% more *B*-type resonances than pullulan peracetate, respectively. Further evidence of the presence of these additional *B*-type rings arises due to the notably more complex multiplets for the *B*6b and *C*6b geminal protons in the EPS samples. In fact, Laignel *et al.* (1997) had demonstrated exactly this phenomenon. The authors assessed the impact that an increase in the number of *B*-type rings had on the chemical shifts of maltotriose-, maltotetraose- and maltoheptaose peracetates. They found that superimposition of each additional spin system had less impact on the H-1, H-2, H-3 and only one of the H-6 protons, whilst affecting the broadening of the H-4, H-5 and the other H-6 protons' chemical shifts. In addition, superimposition of the anomeric terminal and reducing-end spin-systems of the lower molecular weight fractions or oligomers present in the crude EPS peracetates, contribute to the broadening of the H-5 and H-6 resonances. Where possible, these trace signals were assigned, as detailed in Table 5.14. The traces of acetylated mannose and galactose resonances were also sought.

In the GC-MS analyses, galactose and mannose were found to be present in all the EPS samples. Whilst the contribution of these constituents was found to be significant in the purified FB2 F1 sample (galactose 13.0%, mannose 3.2%), they were much less prevalent in the crude EPSs (galactose: FB2 1.7%, PB7 0.9%, PB2 0.5%; mannose: FB2 0.5%, PB7 0.4%, PB2 0.3%). When the native FB2 F1 sample was analysed by NMR, these minor constituents were detected. From these NMR analyses, it was established that mannose existed as a β-D-mannopyranose terminal residue on the polyglucan chains. However, it was not clear whether galactose existed as inter-chain α-D-galactopyranoses or reducing-end α/β-D-galactopyranoses. In the NMR analyses of the crude EPSs, resonances for the mannose components evaded detection and galactose was detected in only the FB2 and PB7 peracetates. These resonances were found through the increased intensity in the same regions where the beta reducing-ends of glucose were established (βA_{R}H/C-1:δ_{H} 5.68-5.71 ppm, δ_{C} 92.0 ppm) compared to the corresponding alpha reducing-ends of glucose (Farkas *et al.*, 1997; Giordano and Trincone, 2002). These coinciding resonances were found to correspond to the anomeric signals of beta-D-galactopyranose pentacetate in both the ^{1}H (βGal_{R}H-1) and ^{13}C (βGal_{R}C-1) spectra, and are detailed in Table 5.14 (Anonymous, 2016b).

Table 5.14 Minor resonances in the ^{1}H and ^{13}C NMR spectra identified for the alpha and beta terminal and reducing-ends of glucose and galactose in the peracetate samples analysed.

Shift		Polysaccharide peracetate				Atom
$\delta^{1}H^{a,b}$ /ppm	$\delta^{13}C^{a,b}$ /ppm	Pullulan	PB2	PB7	FB2	
6.28-33	89.4[d]	<0.01H	0.01H	0.01H	0.06H	αA_RH/C-1 [1-5]
5.68-71	92.0[d]	n.d.	n.d.	0.02H	0.13H	βGal_RH/C-1 [6] and/or βA_RH/C-1 [2][5]
5.47[b]	n.d.	n.d.	n.d.	n.d.	detected	Gal_RH-x [6] and/or A_RH-3 [3][4]
5.09-13[e]	n.d.	n.d.	n.d.	detected	detected	A_RH-2 [1][3] and A_RH-4 [3]
4.11[e]	n.d.	n.d.	n.d.	n.d.	detected	A_RH-5 [1] [3]
4.26[e,m],4.19[e,m]	61.8[a]	n.d.	n.d.	n.d.	detected	A_RH-6a,b [1] [3]
4.53[e,m], 4.26[e,m]	62.7[a,m]	n.d.	n.d.	n.d.	detected	A_TH-6a,b [1]

[a] $CDCl_3$ solvent, referenced at δ_H 7.26 ppm and δ_C 77.36 ppm (25 °C).
[b] 600 MHz for ^{1}H.
[c] 151 MHz for ^{13}C.
[d] Assigned from the HSQC correlations
[e] Assigned through the COSY correlations
[1] Laignel *et al.*, 1997. [2] Giordano and Trincone, 2002.
[3] Pretsch *et al.*, 2002.
[4] Lammerts van Bueren *et al.*, 2011.
[5] Farkas *et al.*, 1997.
[6] Anonymous, 2016.
n.d. – not detected, m – mean value of broad peak, R – reducing-end, T – terminal end, Gal – galactopyranose, A – ring represented by the 6-linked α-D-Glucopyranoses, x – ring position 2/3/4/5/6

In summary, NMR analyses of the crude EPS peracetates confirmed that all three crude EPSs had a similar DP3 – DP4 – >DP4 makeup of subunits, as was determined from the NMR analyses of the purified fractions of FB2 F1 and FB2 F2. Since all indications were that FB2, PB2 and PB7 shared s similar glucan make-up and since GC-MS analysis provided that they all contained mannose and galactose, it is inferred that these latter components share the same arrangements in the polyglucan chains. NMR analysis of the native FB2 F1 sample established that mannose resided as a β-D-mannopyranose terminal residue whilst analysis of the FB2 and PB7 peracetates provided that galactose existed as 6-linked reducing-end β-D-galactopyranoses in the EPS subunits. What remains unknown at this point, however, is how the malto-oligomers within each of the EPS samples are distributed. The distribution and ratio of these components were explored following pullulanase enzyme hydrolysis and HPLC analysis of each of the EPSs. These results are presented in the next section.

5.4 Enzymatic hydrolysis and high performance liquid chromatography

Enzymatic hydrolysis was selected as a complementary tool to NMR to elucidate the repeat subunits in the *P. sacchari* EPSs. Hence, this method was used to confirm and quantify the proportion of DP3 and DP4 in the subunits, and to identify and quantify (where possible) the presence of higher malto-oligosaccharides in the pullulan and EPS samples. Malto-oligomers standards, ranging from DP2-DP7, were used to quantify the hydrolysate peaks arising from the pullulanase treated samples with their respective response factor (RF) as follows:

$$RF = \frac{Height}{Amount} \tag{5.3}$$

The following sections present and discuss the results from two sets of enzyme experiments, *viz.* E1 and E2.

5.4.1 Results from enzyme treatment E1

According to Singh and co-workers (2006), pullulanase from *B. acidopullulyticus* is optimised under the conditions used in E1. To ensure complete hydrolysis of the samples analysed, both an excess of catalytic enzyme and an increased incubation time were employed. An aliquot was measured after the optimum incubation time of six hours was reached, and compared to the results from the same samples incubated overnight for a total of 19 hours. No discernable difference between the chromatographic peak heights was noted, and it was accepted that maximum hydrolysis had been achieved.

Figure 5.25 shows the elution profiles for an E1 pullulanase blank, one of the pullulan samples and two EPS samples each hydrolysed with E1. Successful hydrolysis of the pullulan samples resulted in a primary DP3 peak with a recovery of 101.9 ± 1.7% (refer to Section G.1.2 of Appendix G). Although tiny DP4 peaks (< 7 mV) were detected for pullulan, they could not be accurately quantified as their response was considerably smaller than that of the lowest calibration standard (108.7 mV, 50 ppm). However, when the RF of the lowest DP4 calibration standard was used, it was estimated that ~1.2% DP4 was present (data not shown). This value approximates the 1.1% DP4 result as determined by NMR (refer to Section 5.3.1).

The results for the enzyme-treated EPSs were then assessed. Efficient hydrolysis of the samples will provide hydrolysate products representative of the repeat sequences in the polysaccharides. The E1 pullulanase was able to hydrolyse the FB2 F1 and FB2 F2 samples to produce several peaks in their chromatograms (Figure 5.25). In fact, the samples had very similar elution profiles, with successive peaks appearing at regular intervals. The retentions times of the successive peaks increased linearly, thus representing sequentially higher malto-oligosaccharides (Duedahl-Olesen *et al.*, 2000). These malto-oligosaccharides eluted in the following order: DP2, DP3, DP4, DP5, DP6, DP7, maltooctaose (DP8), maltononaose (DP9), maltodecaose (DP10), *etc*. Since there were no homologous standards available for DP5-DP10 at the time of analysis, their respective RFs could not be determined and the recovery of the samples could not be accurately calculated. However, the relative quantities of these malto-oligomers were estimated in terms of the RF of the highest standard available (DP4). This rationale comes from the methodology employed by Morel du Boil (2000), where the author quantified the DP4 of sarkaran digests in terms of DP3

calibrations, arising from similarly treated pullulan standards. Likewise, DP2 was estimated in terms of the lowest available standard (DP3).

Galactose and mannose are constituents that were detected in the GC-MS and NMR analyses of FB2 F1. More specifically, these were determined to be terminal β-D-mannopyranoses and 6-linked reducing-end β-D-galactopyranoses. If the pullulanase enzyme was able to cleave the glycosidic linkage between these residues and the polyglucan chains, then galactose and mannose should have appeared in the hydrolysates. Quantitation of these monosaccharides, however, proved challenging as analogous standards were found to elute in the region of the enzyme matrix. The difference in the respective peak heights of the blank and sample enzyme matrix region was, therefore, used to estimate the liberated galactose and mannose from the FB2 F1 polysaccharide (see Section G.1.3 for more detail).

Table 5.15 provides the estimated quantities of galactose, mannose and malto-oligosaccharides DP2-DP10 determined in the hydrolysed samples. The results provide that FB2 F1 contained 19.9% galactose and 1.8% mannose. The result for galactose is in fair agreement with the NMR result of ~20% (refer to Section 5.3.4). Conversely, mannose was underestimated, as the NMR analysis provided a value of ~10% in this sample. To accurately determine these lesser constituents in the enzyme digest, a clean-up step would need to precede HPAEC-PAD analysis. For example, microdialysis could be employed to remove the enzyme matrix (Nilsson *et al.*, 2001; Torto *et al.*, 2000). Nonetheless, addition of the accounted for mannose and galactose provided that the pullulanase was 86.2% effective at hydrolysing FB2 F1 and 79.9% for FB2 F2. It is anticipated that these values are still an underestimation of the true efficiency of pullulanase on these samples. This is because the response of each malto-oligomer above DP4 (> DP4) is expected to progressively decrease with the increasing molecular size. A decrease in response will provide a smaller RF. Dividing the same hydrolysate responses of FB2 F1 and FB2 F2 by sequentially smaller RF values (than that of DP4), would result in greater relative quantities for each > DP4 component determined. Hence, use of analogous standards will reflect improved efficiency estimates for the hydrolysis of the EPSs with pullulanase enzymes.

Whilst the results of E1 provided additional insight into the make-up of the repeating units in the EPS fractionates, a subsequent and improved enzymatic study was carried out. The next section details the further enzyme work conducted that incorporates additional authentic standards; including, DP2, DP5, DP6 and DP7. Pullulan and one fractionate (FB2 F2) were re-analysed alongside the three crude EPS samples (FB2, PB2 and PB7).

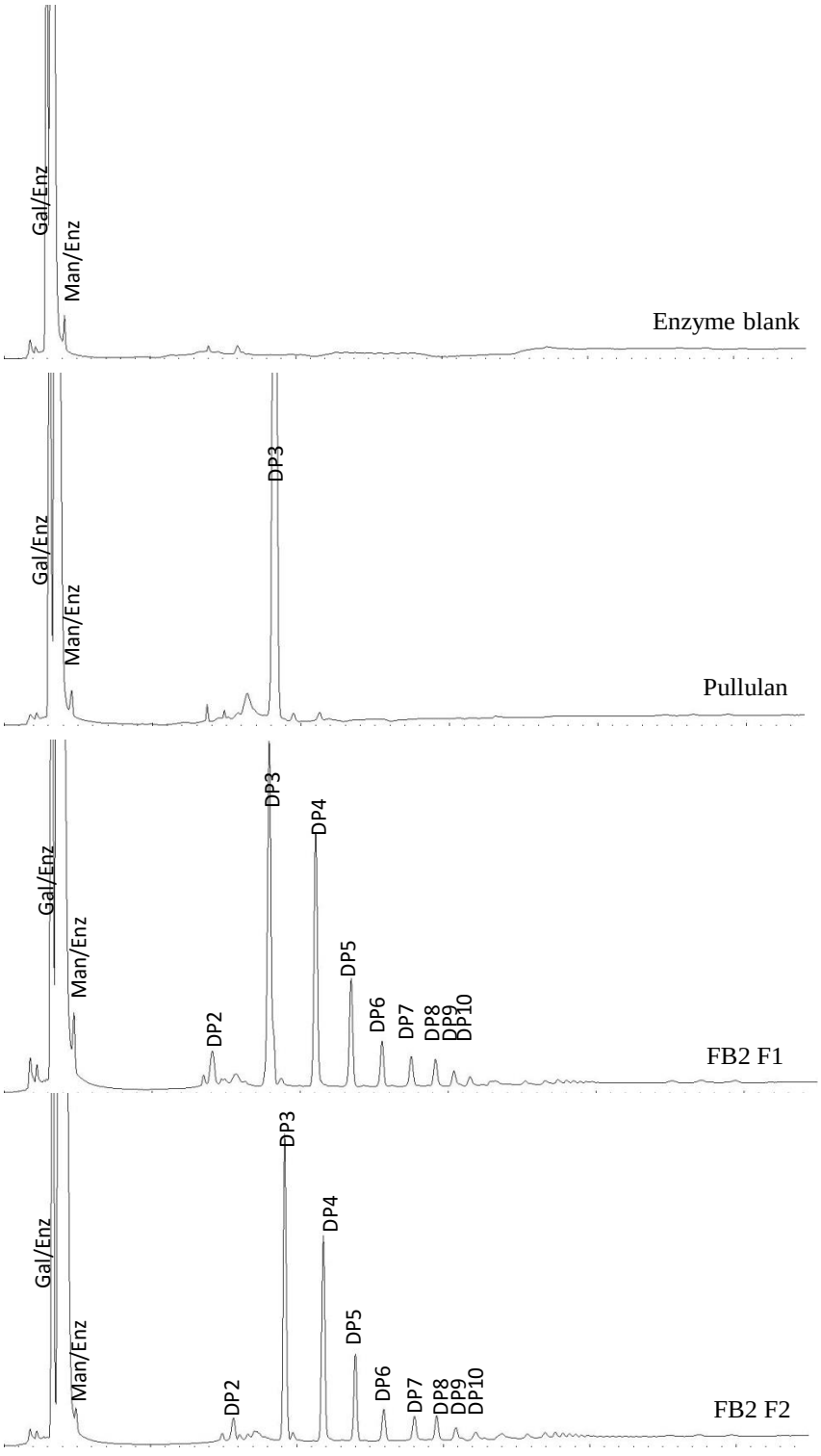

Figure 5.25: HPAEC chromatograms of the enzyme blank, pullulan, FB2 F1 and FB2 F2 treated with E1 pullulanase. The malto-oligosaccharides DP2-DP10 are labelled on each chromatogram. Peaks identified in the enzyme matrix (Enz) that coincides with galactose (Gal) and mannose (Man) are indicated. The chromatogram area shown for each sample is 0-55 min and 80-400 mV.

Table 5.15 HPAEC-PAD estimated recovery and relative amounts for hydrolysates derived from treatment of FB2 F1 and FB2 F2 fractionates with E1 pullulanase.

Sample	Total Hydrolysed /%	Relative amount/%										
		Gal[a]	Man[a]	DP2[b]	DP3	DP4	DP5[c]	DP6[c]	DP7[c]	DP8[c]	DP9[c]	DP10[c]
FB2 F1	86.2	19.9	1.8	2.7	27.6	25.1	10.6	4.5	2.9	2.6	1.2	0.9
FB2 F2	79.9	n.d.	n.d.	2.7	37.7	31.3	13.1	4.9	3.6	3.7	2.0	1.1

[a] The component co-elutes with the enzyme matrix, so the difference in corresponding peak height between the sample and pullulan/blank together with the RF is used to estimate the quantity.

[b] Since no standard was run for this malto-oligomer, the relative amount was estimated based on the average RF of DP3 (2.703 mV ppm^{-1}).

[c] Since no standards were available for these malto-oligomers at the time of analysis, the relative amounts were estimated based on the average RF of DP4 (2.174 mV ppm^{-1}).

RF – response factor, Gal – galactose, Man – mannose, DP2 – maltose, DP3 – maltotriose, DP4 – maltotetraose, DP5 – maltopentaose, DP6 – maltohexaose, DP7 – maltoheptaose, DP8 – maltooctaose, DP9 – maltononaose, DP10 – maltodecaose, n.d. – not detected

5.4.2 Results from enzyme treatment E2

A second series of enzyme experiments was carried out. In these tests, the E2 pullulanase from Sigma was used. Furthermore, a larger array of standards (including galactose, mannose and malto-oligomers from DP2-DP7) were utilised for quantitation. The activity of the E2 pullulanase was determined to be 1845 U mL^{-1} (refer to Appendix G, Section G.2.1). To ensure maximum hydrolysis, each sample was treated with an excess of 15 U pullulanase for 24 hours.

The hydrolysed, filtered samples were injected and analysed on the equilibrated HPAEC column. Various calibration standards were included alongside each run. Refer to Appendix G (Section G.2.2) for the calibration data corresponding to each set of analyses.

Figure 5.26 provides a chromatogram of a hydrolysed pullulan sample along with each of the four EPS samples analysed. For pullulan, DP3 was the only hydrolysate product detected. The peak heights for DP4 fell below the lowest concentration standard of 2.4 ppm (~2.4%), and could not be quantified. Table 5.16 provides that the recovery of pullulan is 98.8% with respect to DP3. With this recovery, the E2 enzyme was confirmed to be effective at hydrolysing pullulan under the experimental conditions. Second, it is inferred that DP4 comprised the difference in the average recovery determined, equivalent to ~1.2%. This estimation reflects a similar result as obtained with E1 (~1.2%), and as calculated from the NMR data (1.1%). In addition to the pullulan results, Figure 5.26 and Table 5.16 provide the elution profiles and quantities of malto-oligosaccharides determined in the E2 treated samples, respectively.

First, the results of FB2 F2 between the two enzyme treatments are compared. In this comparison, comments will be made concerning the applicability of using the RF values for either DP3 or DP4 to estimate other malto-oligosaccharides, in the absence of an authentic standard. For both enzyme treatments, the digest of FB2 F2 provided that the fractionated EPS was quite complex in structure with several peaks eluting in the chromatograms beyond DP4 (Figure 5.25 and 5.26). In order to compare the two results, the quantities of the various malto-oligomer products had to be determined. In E1, DP2 was estimated in terms of DP3, and DP5-DP10 estimated in terms of DP4, in the absence of appropriate standards. In E2, only the > DP7 components needed estimation, and this was done in terms of the RF for DP7. The determined values for DP2-DP10

in FB2 F2 from E1 and E2 are provided in Table 5.15 and 5.16, respectively, which were found to be in fair agreement between the two enzyme treatments. In E1, DP2 was estimated in terms of DP3. Doing so overestimated the amount of DP2 present compared to that determined in E2 (2.7% versus 2.2%). This is due to the smaller response of DP3 compared to DP2 (refer to Appendix G, Table G.2.9). Conversely, making use of the RF of DP4 to estimate > DP4 resulted in slight underestimations in E1 compared to E2, *i.e.*, DP5 was 13.1% versus 13.3%, DP6 was 4.9% versus 6.5% and DP7 was 3.6% versus 6.4%, respectively. Nonetheless, these results show that making use of the RF of DP4, in the absence of the higher malto-oligomer standards, provides a reasonable estimate of these residual components in the samples. Furthermore, the close agreement of the results lends support that the FB2 F2 substrate is homogenous, and that the E1 and E2 enzymes are equally effective at hydrolysing this substrate.

Second, the malto-oligomer make-up of the crude FB2 sample could be compared to that of the fractionated FB2 F2 sample. Table 5.16 shows that the distribution of malto-oligomers in both EPSs was remarkably similar, with the only major differences in the DP2 and DP8 components. FB2 F2 comprises 57% of the unfractionated FB2 sample (refer to Section 5.1). Differences in the DP2 and DP8 components were attributable to the contribution of fractions FB2 F1 and FB2 F3 making up the remainder of the sample. Since FB2 F1 and FB2 F2 provided equivalent responses for DP2 in their hydrolysates (Table 5.15 in E1), the increase in the DP2 component in FB2 must have been due to the FB2 F3 fraction (not analysed), which comprised 31% of the EPS. Another striking difference between the results for FB2 and FB2 F2, was the discrepancy in the hydrolysis efficiencies – as determined by the sum of the malto-oligomers accounted for. Seemingly, with an average of 95.8% versus 79.6%, the pullulanase was more successful at hydrolysing the fractionated FB2 F2 sample than the unfractionated FB2 sample. In the GFC results, FB2 was found to comprise 12% of FB2 F1. In the NMR analyses, FB2 F1 was found to contain ~20% galactose and ~10% mannose. Likewise, in E1, FB2 F1 was estimated to contain 19.9% galactose and 1.8% mannose. However, in E2, these components were not accounted for. Unfortunately, deterioration of the column and PAD cell resulted in poorer resolution in the region where galactose and mannose eluted together with the enzyme matrix. Consequently, although these components were expected to compose about 3.6% of the digest, they could not be accounted for in the recovery of FB2. Hence, the pullulanase efficiency on this substrate has been underestimated.

Third, the three crude EPS samples could be compared. From Figure 5.26, it is clear that the bioreactor prepared sample (FB2) is more complex in structure than the two shake-flask samples (PB2 and PB7). FB2 eluted successive peaks beyond DP7, whilst PB2 and PB7 only have peaks detectable up to DP7. The recoveries for PB2 and PB7 in Table 5.16, confirm that the E2 enzyme effectively hydrolyses them – despite their relatively large M_ws of 691 kDa and 717 kDa, respectively (see Section 5.1). Contributions due to galactose and mannose were not detected and, if present, were expected to be in very low amounts due to the EPS recoveries being so close to unity. Indeed, the results from the GC-MS analyses revealed that PB2 and PB7 contained only up to 0.8% and 1.4% of galactose and mannose combined, respectively. The hydrolysis efficiency also affirmed that the low M_w fractions (1.4 kDa) composing 6-7% of these EPSs were malto-oligomer building blocks of the primary EPS.

Ultimately, the pullulanase analysis of the three *P. sacchari* EPSs provided that each of the EPSs were predominated by DP3 subunits (34-45%), closely followed by DP4 subunits (28-38%), together with an array of DP2, DP5-DP10 subunits (varying from 0-17%). Furthermore, the results show that, although the bioreactor prepared EPS (FB2) had a higher degree of subunit arrangement from those prepared in shake-flasks (PB2 and PB7), all three EPSs produced by *P. sacchari* are predominantly malto-glucans that are fully hydrolysable by pullulanase under the tested conditions.

Figure 5.26: HPAEC chromatograms of pullulan, FB2 F2, FB2, PB2 and PB7 with malto-oligosaccharides DP2-DP10 labelled on each chromatogram. The areas of the chromatograms shown are 0-55 min and 30-400 mV.

Table 5.16 HPAEC results of the malto-oligomers determined from the E2 pullulanase treatment of pullulan and the EPS samples.

Sample	Total Hydrolysed (±SD)/%	Relative Amount (±SD)/%								
		DP2	DP3	DP4	DP5	DP6	DP7	DP8[d]	DP9[d]	DP10[d]
Pullulan[#]	98.8 (4.2)	n.d.	98.8 (4.2)	n.d.	n.d.	n.d.	n.d.	n.d.	n.d.	n.d.
FB2 F2[#]	95.8 (4.0)	2.2 (0.1)	32.3 (0.4)	28.0 (1.0)	13.3 (0.6)	6.5 (0.1)	6.4 (0.2)	6.0 (0.6)	3.3 (0.3)	1.9 (1.0)
FB2[&]	79.6 (13.9)	6.1 (0.3)	33.5 (1.3)	28.2 (1.1)	13.9 (0.6)	6.2 (0.4)	5.5 (0.2)	3.9 (0.7)	2.2 (1.2)	1.3 (0.6)
PB2[&]	101.6 (8.1)	2.6 (0.1)	37.2 (1.2)	37.9 (0.5)	16.8 (0.8)	4.0 (0.2)	1.6 (0.1)	n.d.	n.d.	n.d.
PB7[$]	101.9 (10.5)	2.4 (0.2)	45.0 (1.5)	36.9 (0.9)	12.2 (0.5)	2.7 (0.0)	0.9 (0.1)	n.d.	n.d.	n.d.

[$] Triplicate analyses

[#] Quadruplicate analyses

[&] Quintuplicate analyses

[d] Since no standards were available for these malto-oligomers, the relative amounts were estimated based on the response factors of DP7.

SD – standard deviation, n.d. – not detected, DP2 – maltose, DP3 – maltotriose, DP4 – maltotetraose, DP5 – maltopentaose, DP6 – maltohexaose, DP7 – maltoheptaose, DP8 – maltooctaose, DP9 – maltononaose, DP10 – maltodecaose.

5.5 Physical properties

The rheological and film-forming properties of the *P. sacchari* EPSs were examined and compared to pullulan. This section provides these results.

5.5.1 Rheological properties

The solution rheology for pullulan and the crude *P. sacchari* EPSs were examined in the concentration range of 1.0-4.0% (m/m). The steady-shear flow behaviour of each of the solutions was determined through assessing the dependence of shear stress (τ) on the shear rate ($\dot{\gamma}$), as illustrated in Figure 5.27. Newtonian behaviour is indicated when the shear stress response is directly proportional to the applied shear rate. Pullulan solutions exhibit Newtonian behaviour over a range of concentrations and shear rates (Lazaridou *et al.*, 2002b). Whilst the steady-shear flow curves for pullulan appeared largely linear for all concentrations up to 400 s^{-1}, the curves did begin to concave downward above these shear rates. This type of curvature indicates shear-thinning behaviour, and the more concave downward the slope is, the more shear-thinning the fluid. The curvature of the 4.0% solutions of PB2 and PB7 were most notably concaved, whilst

all the curves for the EPS samples showed regions that deviated from linearity. Further analysis of the data was required to describe and quantify the flow behaviour of the various samples. First, possible yield point (τ_0) values were determined by extrapolation of the shear stress versus shear rate curves. Then, the power law function was applied to determine the flow behaviour indices and the flow consistency coefficients of each of the solutions. Figure 5.28 illustrates the bilogarithmic plots of shear stress against shear rate fitted with the power law function, whereby the flow indices were determined from the power law exponent (n) and the consistency indices were determined from the power law constant (K) per Equation 3.6 (Section 3.5.1). Finally, the steady-shear viscosity (apparent viscosity, η) of each sample was plotted against the shear rate range as seen in the flow curves found in Figure 5.29. These curves were used to examine and compare the flow properties of each of the solutions. Furthermore, the apparent viscosities of each solution could be compared at a common shear of 10 s^{-1}. All the results obtained from Figure 5.27 to 5.29 are summarised in Table 5.17, together with the M_w molecular weights, the (1,6)-D-glucopyranose concentrations and relative quantities of DP3 and DP4 for comparison purposes.

The steady-shear flow behaviour results provide that the 1.0% and 1.9% pullulan solutions were the least viscous of all the solutions tested, with apparent viscosities of 3.5 mPa s and 3.8 mPa s, respectively. These values are in fair agreement with literature, which provides that a 1% pullulan solution has a viscosity of 2 mPa s when measured at 30 °C (Tsujisaka and Mitsuhashi, 1993). The relatively low viscosity of pullulan solutions is due to the nature of the α-(1,6)-D-glucopyranose linkages present. These linkages afford the pullulan hydrocolloids their random coil molecular conformation in solution, and provide the polymeric chains with increased rotational freedom (Singh *et al.*, 2008). The increase in rotational freedom enables the polymeric chains to readily align with an applied shear, thus exhibiting lower viscosities compared to conformations that are more rigid. A Newtonian response is exhibited if the rate of detanglement and subsequent re-entanglement results in a zero net change. All three pullulan concentrations displayed an extended Newtonian plateau between 1-400 s^{-1}. Above 400 s^{-1}, the pullulan solutions exhibited shear-thinning behaviour (Figure 5.29). The tendency for slight shear-thinning in pullulan solutions has been previously reported (Lazaridou *et al*., 2002b). Fitting of the power law function to the pullulan data confirmed the predominant Newtonian nature of these polysaccharide solutions, with flow indices approaching unity and consistency indices approaching zero, particularly as the solutions became more dilute (Table 5.17). In general, shear-thinning behaviour occurs when a solution is subjected to increasing shear and the rate of polymeric detanglements occur more rapidly than the formation of new entanglements, resulting in a reduction in viscosity (Miyoshi and Nishinari, 1999). Since a higher concentration of overlapping chains hinders realignment, the onset of shear-thinning generally occurs at lower shears and extends for a broader range of shear rates in more concentrated solutions (Lapasin and Pricl, 1995).

The sample that most closely resembled the flow behaviour of pullulan was the 2.0% FB2 solution, both graphically (from 1-400 s^{-1}) and according to the calculated power law parameters (Table 5.17). The 2.0% FB2 solution also had a low relative viscosity (5.8 mPa s), an extended Newtonian plateau (0.2-400 s^{-1}), a near-zero yield point (0.0010 Pa), a near-zero consistency coefficient (0.0077 Pa s^n) yet it was more shear-thinning ($n = 0.9281$). The remaining EPS solutions appeared to be increasingly more different from pullulan. Most significantly, the remaining EPS solutions displayed higher apparent viscosities and markedly different flow curves (Figure 5.29).

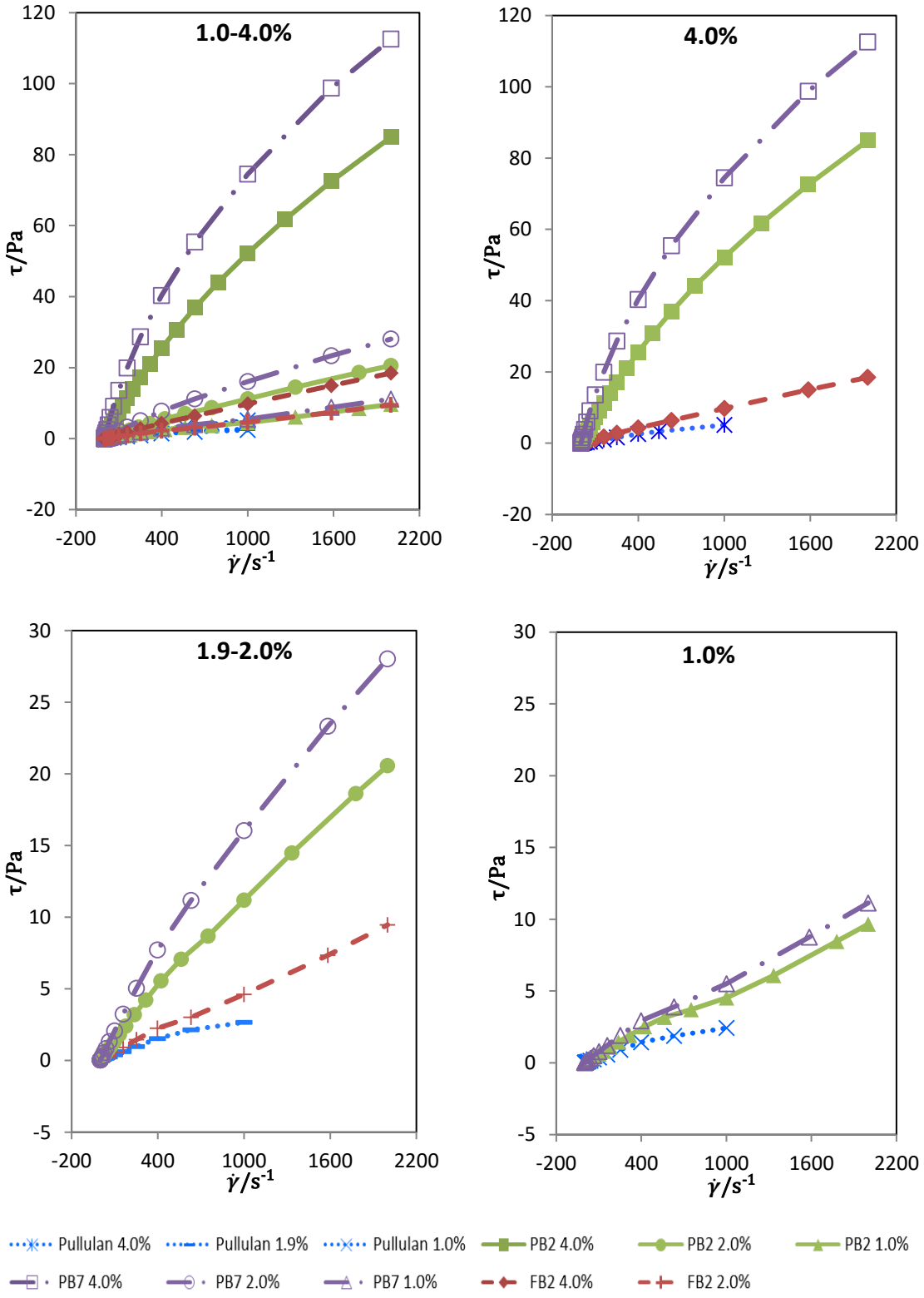

Figure 5.27: Steady-shear flow behaviour of the 1.0-4.0% (m/m) solutions of pullulan and the three *P. sacchari* EPSs showing the dependence of shear stress (τ, Pa) on the shear rate ($\dot{\gamma}$, s^{-1}).

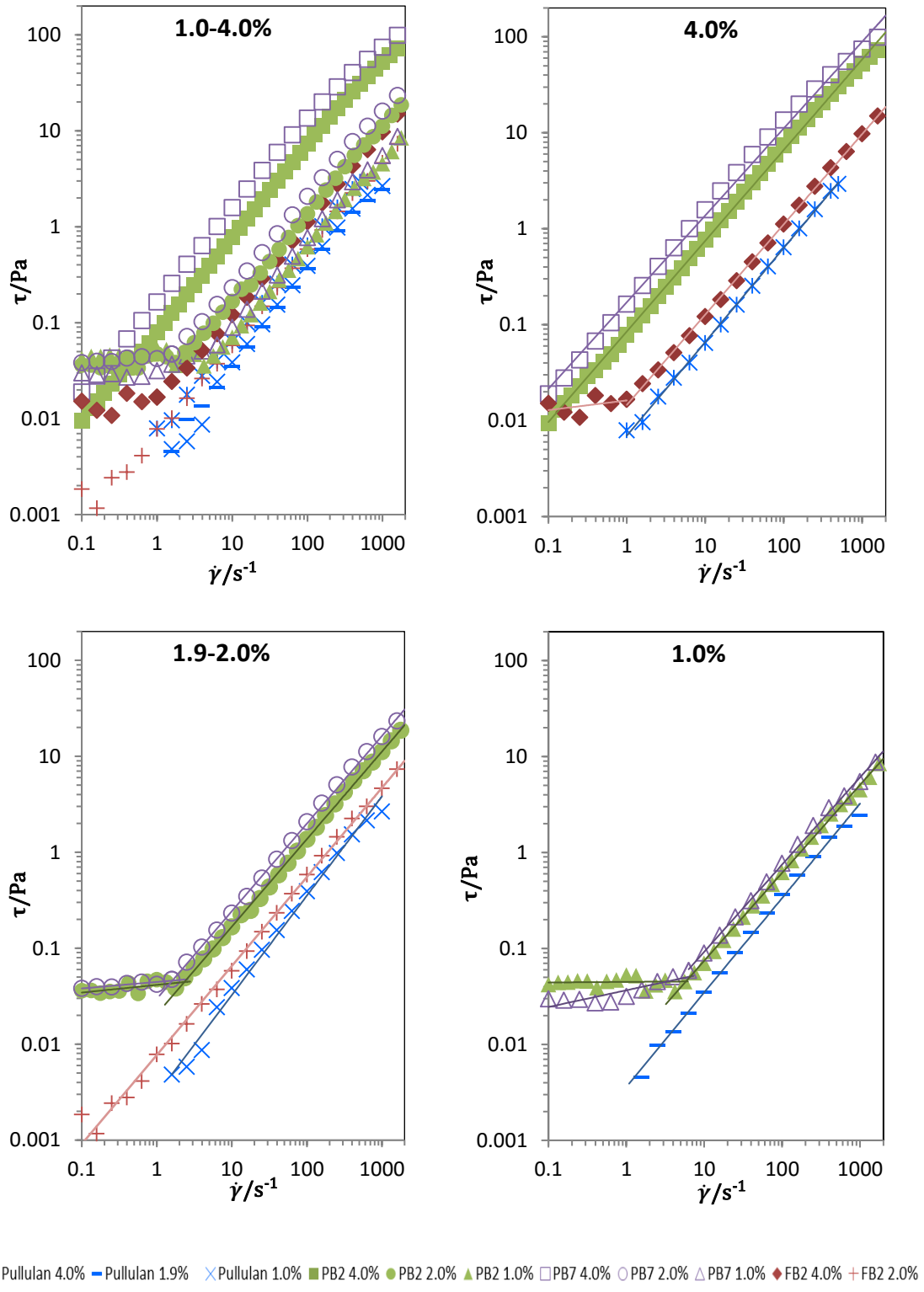

Figure 5.28: Bilogarithmic plots of shear stress (τ, Pa) and shear rate ($\dot{\gamma}$, s^{-1}) to illustrate the steady-shear flow behaviour for the 1.0-4.0% (m/m) solutions of pullulan and the three *P. sacchari* EPSs. The data were fitted with the power law equation.

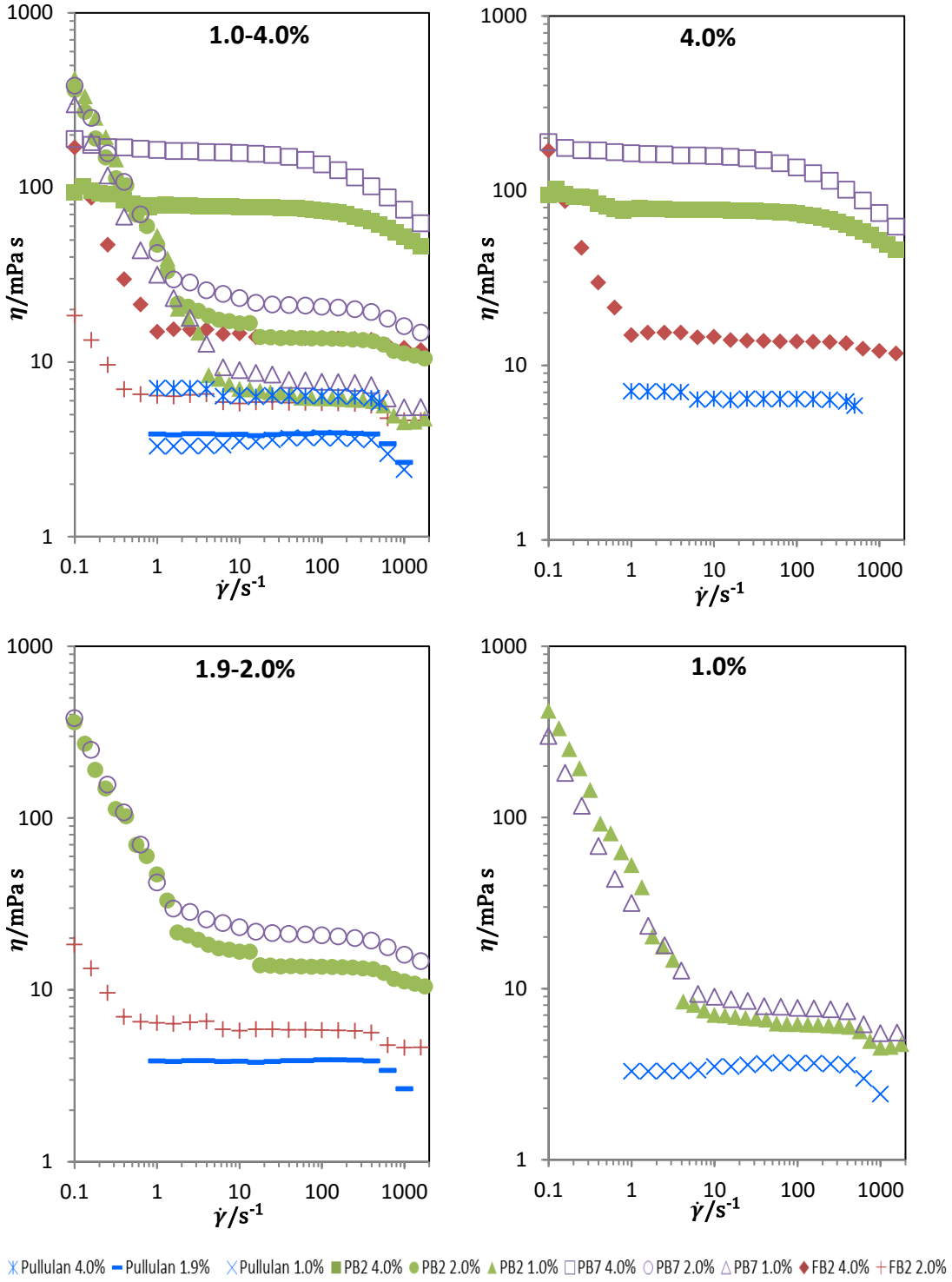

Figure 5.29: Flow curves for the 1.0-4.0% (m/m) solutions of pullulan and the three *P. sacchari* EPSs illustrating the dependence of steady-shear viscosity (η, mPa s) on the shear rate ($\dot{\gamma}$, s^{-1}).

Table 5.17 Summary of apparent viscosity, yield stress, flow behaviour index and consistency values determined from the steady-shear flow data of pullulan and the three *P. sacchari* EPSs at different concentrations (at 20 °C). Also provided is a summary of the M_w molecular weights, (1,6)-D-glucopyranose, maltotriose and maltotetraose concentrations of each sample for comparison.

Sample	Concentration (m/m)/%	Apparent viscosity at 10 s^{-1} (±SD), η /mPa s	Yield stress[g], τ_0/Pa	Flow behaviour index, n	Consistency coefficient, K/Pa s^n	M_w /kDa	Glc6 /%	DP3:DP4
Pullulan	4.0[d]	6.8 (0.6)	0.0004	0.9776	0.0070	328	31.8	99:1
	1.9[a]	3.8 -	0.0002	0.9758	0.0041			
	1.0[a]	3.5 -	0.0000	0.9864	0.0036			
FB2	4.0[d]	14.6 (2.4)	0.0174	0.1009[α] 0.9408[β]	0.0162[α] 0.0146[β]	±410	19.5	34:28
	2.0[a]	5.8 -	0.0010	0.9281	0.0077			
PB2	4.0[b]	77.4 (2.7)	n.d.	0.9448	0.0851	691	24.8	37:38
	2.0[a]	16.7 -	0.0368	0.0800[γ] 0.9168[δ]	0.0448[γ] 0.0206[δ]			
	1.0[b]	7.0 (0.8)	0.0401	0.0063[ε] 0.9121[ζ]	0.0415[ε] 0.0090[ζ]			
PB7	4.0[f]	157.8 (3.8)	n.d.	0.9045	0.1721	717	23.7	45:37
	2.0[c]	23.2 (2.7)	0.0379	0.0673[η] 0.9133[θ]	0.0445[η] 0.0297[θ]			
	1.0[b]	9.0 (0.1)	0.0298	0.1740[κ] 0.9092[λ]	0.0367[κ] 0.0114[λ]			

[a] Single analysis
[b] Duplicate analyses
[c] Triplicate analyses
[d] Quadruplicate analyses
[e] Quintuplicate analyses
[f] Sextuplicate analyses
[g] Extrapolated from 0.25 s^{-1}

[α] n determined from 0.1-1.0 s^{-1}
[β] n determined from 1.0-2000 s^{-1}
[γ] n determined from 0.1-1.8 s^{-1}
[δ] n determined from 1.8-2000 s^{-1}
[ε] n determined from 0.1-3.2 s^{-1}
[ζ] n determined from 3.2-2000 s^{-1}
[η] n determined from 0.1-1.6 s^{-1}
[θ] n determined from 1.6-2000 s^{-1}
[κ] n determined from 0.1-6.3 s^{-1}
[λ] n determined from 6.3-2000 s^{-1}

n.d. – not determined, kDa – kilo daltons, SD – standard deviation, mPa s – millipascal seconds, s^{-1} – per second, M_w – weight-average molecular weight, m/m – mass on mass, Glc6 – (1,6)-linked D-glucopyranose, DP3 – maltotriose, DP4 – maltotetraose

Rheological properties of polymeric solutions are affected by parameters including the concentration, molecular weight, molecular weight distribution and molecular structure (Lapasin *et al.*, 1991). Table 5.17 reflects how the apparent viscosities of each solution increased with an associated increase in concentration. Furthermore, when the different polysaccharide solutions were compared at the same concentration level, the apparent viscosity increased according to their increasing M_ws, *i.e.*, pullulan < FB2 < PB2 < PB7. More interesting, however, are the differences between the flow curve shapes (Figure 5.29) and the power law parameters (Table 5.17) of the

P. sacchari EPS solutions to those of pullulan. These differences are most likely due to the variation in the molecular make-up of each of the EPSs.

Other than pullulan, the flow curves in Figure 5.29 represent the high viscosity shear-thinning profiles of the 4.0% PB2 and PB7 solutions, or the multi-region shear-thinning profiles of the remaining solutions. The flow curves for the 4.0% PB7 and PB2 solutions were predominated by a relatively broad Newtonian-like plateau from 0.1 s^{-1}, followed by a gradual decline into a more shear-thinning region as shear rates increase above ~100 s^{-1} and ~200 s^{-1}, respectively. Not only was the 4.0% PB7 solution the most viscous of all the solutions (η_{10} = 157.8 mPa s), but the power law parameters also reveal that this solution had the highest consistency index (K = 0.1721 Pa s^n). The same parameters for the 4.0% PB2 solution had somewhat smaller values, and this is most likely due to the subtle differences in molecular weights and arrangements of DP3:DP4 subunits in the two shake-flask preparations of the EPSs. However, as the PB2 and PB7 solutions become more dilute, their flow behaviours became more interesting; displaying multi-region viscosity profiles with steeply shear-thinning regions at lower shear rates. These fascinating flow properties were also present in the 4.0% and 2.0% solutions of the bioreactor EPS (FB2).

The solutions with multi-region viscosity profiles in Figure 5.29 exhibited a steep shear-thinning region under low shear rates. For the shake-flask EPSs, this initial shear-thinning region extended to higher shear rates (*i.e.*, from ~2 s^{-1} to ~6 s^{-1}) as the solutions became more dilute. This suggests that the higher concentrations of these respective solutions may have also had an initial steeply shear-thinning region, but which occurred at lower shears than 0.1 s^{-1}. Indeed, the critical points at which the flow is expected to change between shear-thinning and Newtonian regimes occurs at lower shear rates for increasing concentrations of power law fluids (Timilsena *et al.*, 2015). Likewise, the Newtonian-like plateau transitions to the next shear-thinning region at progressively lower relative shear rates at lower concentrations. It also appears that the lowest concentration of all three solutions had a second Newtonian-like region, appearing at shear rates beyond 400 s^{-1} (2.0% FB2) or 1000 s^{-1} (1.0% PB2 and PB7). Extrapolation of the multi-region flow curves from ~0.25 s^{-1} revealed that these solutions had yield points – with 2.0% PB2 and PB7 requiring the highest stresses (≥0.030 Pa) to initiate flow. The power law relationship provided that the EPS solutions were increasingly shear-thinning at lower concentrations, whilst their corresponding consistency coefficients and apparent viscosities diminished (Table 5.17). In general, the multi-distinct regions appearing in the EPS solutions reflect a complex rheological behaviour. Similar flow profiles have been observed in novel nanocomposite solutions of polyurethane and silk fibroin dispersions in which weak gel networks appeared (Timilsena *et al.*, 2015). The complex flow behaviour of the *P. sacchari* EPSs may indicate similar network interactions due to the complex malto-oligomer arrangements of these biopolymers.

Characterisation studies in the preceding sections established that each of the EPSs contained a variety of malto-oligomer segments, predominated by DP3 and DP4. Furthermore, as the concentration of DP3 decreased, the propensity of α-(1,6)-linkages diminished. These linkages are responsible for the chain flexibility, low viscosities and Newtonian characteristic in pullulan solutions. Conversely, the EPSs each had fewer α-(1,6)-linkages, had higher molecular weights and were more polydisperse than pullulan (Table 5.17). These factors had a number of effects on their solution viscosities and flow behaviours. First, a minimum shear rate was required before flow could be initiated. Yield points generally occur when a high degree of chain entanglement causes stability within the chain network, and a subsequent resistance to initiate flow under an applied stress. This behaviour can occur in entanglement solutions where the macromolecule is stiff, and becomes rod-like. For instance, scleroglucan, schizopyllan and xanthan all display such behaviour (Picout and Ross-Murphy, 2003). Second, after yielding, shear-thinning is generally observed as chain detanglements occur more rapidly than re-alignments – even at low shear rates. This response indicates that the bonds within the network are of limited strength (Clark, 2000).

Considering these factors, the flow behaviours of the EPS solutions are considered in terms of the molecular make-up. It is possible that the non-regular arrangement of malto-oligomer subunits caused a stable entanglement at rest, which resists disruption to initial stresses. Then, as the entanglements begin to be affected by the shear, the more rigid α-(1,4)-D-glucopyranose segments, corresponding to the malto-oligosaccharides with higher DPs, are also disturbed. However, the inflexibility of these rigid regions prevents their simultaneous realignment, and so marked shear-thinning is observed. Then, as the shear increases and both the long- and short-chained malto-oligomer segments begin to unravel, the shorter, more flexible segments facilitate more rapid realignments within the network. Hence, shear-thinning becomes less pronounced and the viscosity of the solution becomes more stable. At increasingly higher shears, chain stretching occurs and the re-entanglements can no longer keep up with the deforming shear. Hence, the solution viscosity declines as the degree of shear-thinning increases again.

In general, PB2 and PB7 were most similar in respect of their malto-oligosaccharide arrangements, molecular weights and molecular weight distributions and displayed very similar steady-shear flow properties. Although FB2 had similar flow properties to its shake-flask EPS counterparts, its lower molecular weight resulted in overall lower viscosities and less pronounced flow behaviours at comparable concentrations. To gain a better understanding of the possible network structures and behaviour of the EPSs in solution, the viscoelastic properties of these solutions were also examined.

The dynamic rheological behaviour of pullulan and the three EPS solutions was determined by examining the dynamic shear moduli dependence on the angular frequency of oscillations. Figure 5.30 to 5.32 demonstrate the change in both storage (G') and loss (G'') moduli over the angular frequency (ω) range of 0.1-100 rad s^{-1} for each of the solutions at 20 °C. In each of the Figures (Figures 5.30-5.32), the dependence of the absolute value of the complex viscosity (η^*) on the angular frequency is provided together with the superimposed shear-rate ($\dot{\gamma}$) dependence of the apparent viscosity (η).

Figure 5.30 illustrates the viscous nature of the 4.0% pullulan solution, with the loss modulus predominating over the storage modulus for the majority of the frequency range. There are two cross-over points where G' and G'' overlap, one at low frequency (~0.15 rad s^{-1}) and one at high frequency (~70 rad s^{-1}). The pullulan solution becomes liquid-like between these cross-over frequencies but solid-like beyond these (Haddarah *et al.*, 2014; Xiao *et al.*, 2012). At very low and high angular frequencies, pullulan behaves more like an elastic solid due to entanglement junctions acting like anchors. These anchors physically fix the network of chains by sterically hindering their flow (Xiao *et al.*, 2012).

The complex viscosity of pullulan is also depicted in Figure 5.30. The complex viscosity indicates a hint of shear-thinning behaviour that coincides up to the first cross-over frequency. Thereafter, the complex viscosity remains independent of the frequency. This Newtonian property was also observed in the steady-shear analysis of the solution. In fact, for equal values of angular frequency and shear rate, the complex and steady-shear viscosities are generally equivalent in dilute polymeric solutions. This is known as the empirical Cox-Merz rule, as described in Equation 5.1 (Wen *et al.*, 2004).

$$\eta(\omega) = |\eta^*(\omega)|_{\omega=\dot{\gamma}} = \sqrt{\left[\left(\frac{G'}{\omega}\right)^2 + \left(\frac{G''}{\omega}\right)^2\right]_{\omega=\dot{\gamma}}} \tag{5.1}$$

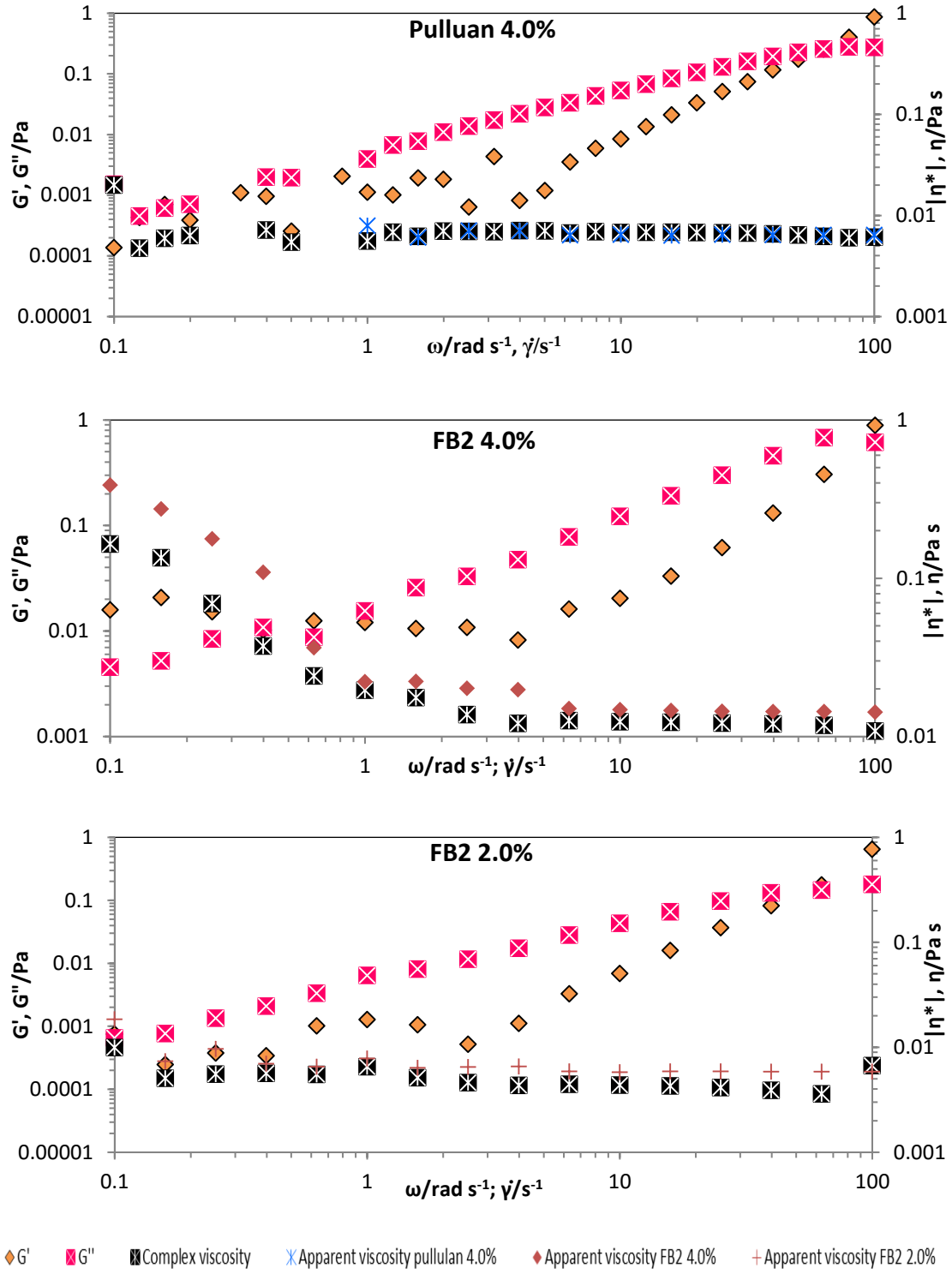

Figure 5.30: Angular frequency (ω) dependence of the absolute complex viscosity (η^*), storage (G') and loss (G'') moduli as well as shear rate ($\dot{\gamma}$) dependence of apparent viscosity (η) for the 4.0% pullulan solution compared with the 4.0% and 2.0% FB2 solutions at 20 °C.

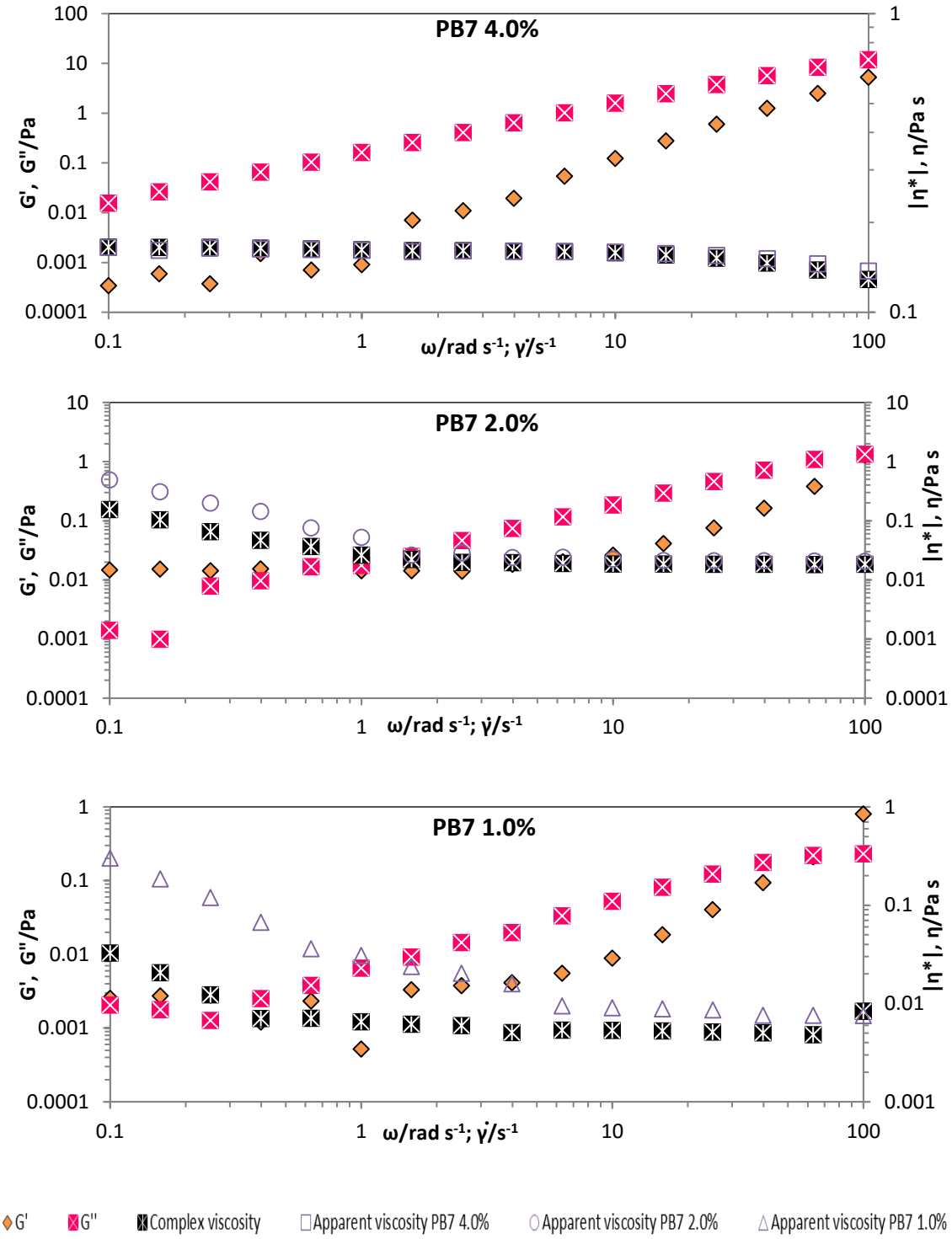

Figure 5.31: Angular frequency (ω) dependence of the absolute complex viscosity (η^*), storage (G') and loss (G'') moduli as well as shear rate ($\dot{\gamma}$) dependence of apparent viscosity (η) for the 4.0%, 2.0% and 1.0% PB7 solutions at 20 °C.

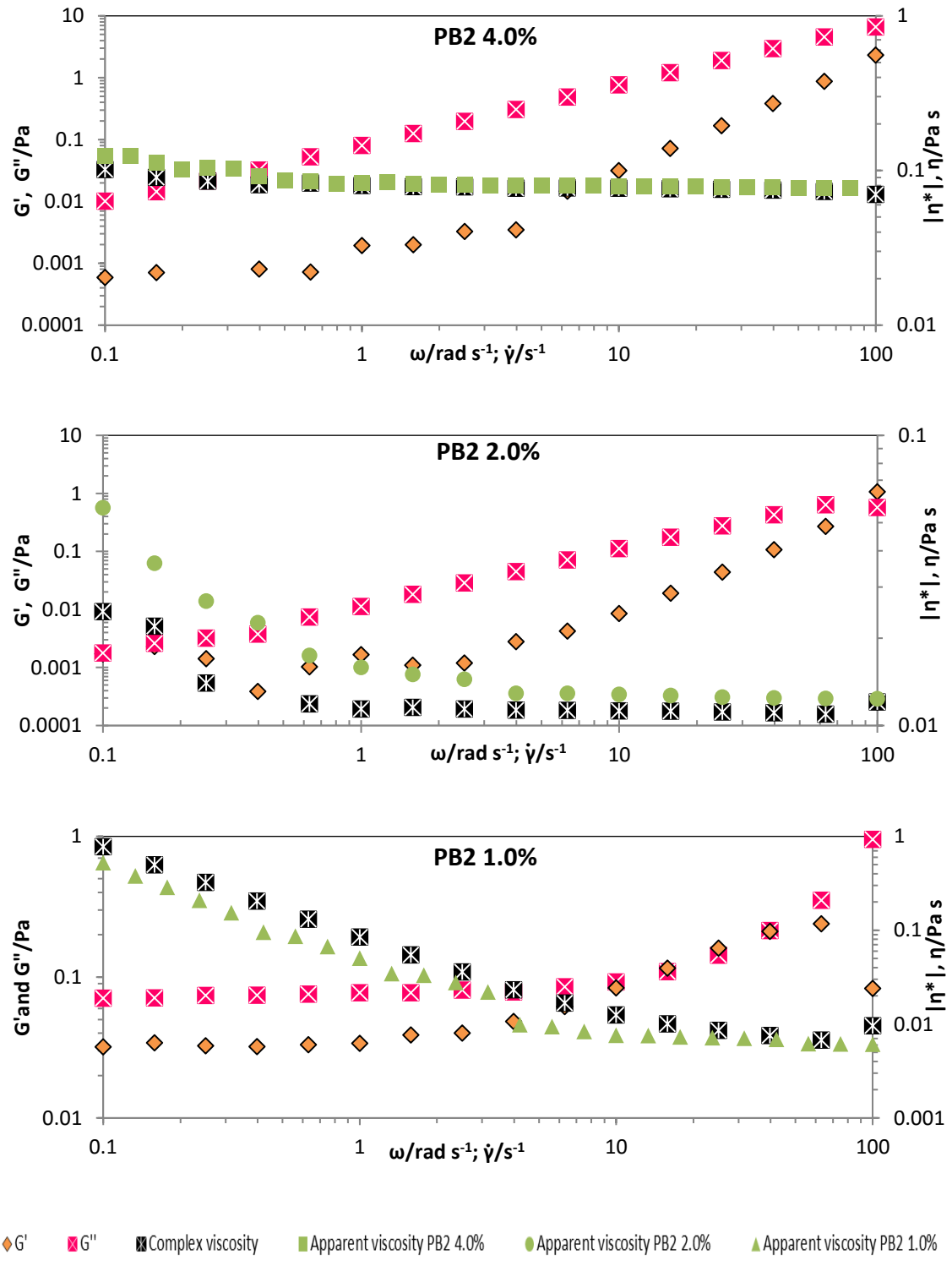

Figure 5.32: Angular frequency (ω) dependence of the absolute complex viscosity (η^*), storage (G') and loss (G'') moduli as well as shear rate ($\dot{\gamma}$) dependence of apparent viscosity (η) for the 4.0%, 2.0% and 1.0% PB2 solutions at 20 °C.

Dilute polymer solutions, including pullulans, generally obey the Cox-Merz rule (Chronakis and Ramzi, 2002). The 4.0% pullulan solution in Figure 5.30 was shown to obey this rule as the apparent and dynamic viscosities superimposed. Other polymeric solutions known to obey the Cox-Merz rule include entanglement systems for xanthan gum, galactomannan and gellan gum (Miyoshi and Nishinari, 1999). The remaining EPS solutions were next compared to pullulan, with respect to their viscoelastic properties and their deviation from the Cox-Merz rule.

Of all the solutions, 4.0% PB7 (Figure 5.31) and 4.0% PB2 (Figure 5.32) were the only systems with viscous properties dominating throughout (*i.e.*, $G''>G'$), where no cross-over between the storage and loss moduli occurred, and both moduli were frequency-dependent. Furthermore, these solutions were satisfactory in obeying the Cox-Merz rule. These factors reflect the typical behaviour of an entangled polymer solution, as was first indicated in the steady-shear experiments (see Figure 5.29).

The 2.0% FB2 solution was somewhat different from the 4.0% PB2 and PB7 solutions, whilst revealing some similarities to the 4.0% pullulan solution. The 2.0% FB2 solution was also largely viscous in nature and also displayed two cross-over points to elastic behaviour, albeit at lower relative frequencies compared with pullulan. The first transition from elastic to viscous behaviour occurred at the lowest recorded frequency (0.1 rad s^{-1}), whilst the second transition from viscous to elastic behaviour occurred at ~60 rad s^{-1}. Interestingly, the elastic component was independent of the angular frequency up to 3 rad s^{-1}. Thereafter, this modulus became largely dependent on the change in frequency – even beyond mergence with the frequency-dependent viscous modulus. Additionally, there was slight deviation from the Cox-Merz rule, as the apparent viscosity appeared to shift slightly above the complex viscosity up to the second cross-over point. Conversely, the 4.0% FB2 solution (Figure 5.30) disobeyed the Cox-Merz rule, with $\eta > |\eta^*|$, particularly up to 1 s^{-1} and 1 rad s^{-1}, respectively. Although the complex viscosity fell below the apparent viscosity, both measures indicated steep shear-thinning behaviour before almost merging along their respective Newtonian-like plateaus. Furthermore, this 4.0% FB2 solution reflected a slightly longer region of frequency-independent elastic behaviour, of which a larger portion dominated over the viscous properties of this solution. These interesting elasticity and Cox-Merz deviations were also exhibited in the PB7 solutions (2.0% and 1.0%, Figure 5.31) and the 2.0% PB2 solution (Figure 5.32). The exception was the 1.0% PB2 solution, which was the only solution that violated the Cox-Merz rule with $|\eta^*| > \eta$. Interestingly, most polymeric solutions that disobey the Cox-Merz rule do so with the complex viscosity falling above the apparent viscosity, as observed in the 1.0% PB2 solution. Systems that disobey the rule, and which display power-law regions in their log-log viscosity versus shear rate curves, are those that have long-range ordering and structure. For instance, polymeric systems that form weak gels (Miyoshi and Nishinari, 1999; Tao *et al.*, 2016) have ordered and rigid conformations (Timilsena *et al.*, 2015) and/or have stable chain entanglement networks (Xiao *et al.*, 2012) that can stretch (Wen *et al.*, 2004) can all violate the Cox-Merz rule. However, it is rare for power-law polymeric solutions to violate the rule having $\eta > |\eta^*|$, as was observed in most of the *P. sacchari* EPS solutions (Lopes da Silva and Rao, 2006). Literature has shown that a number of hydrophobically modified polymers and micellar gels behave similarly (Djabourov *et al.*, 2013), as do solutions with water soluble galactomannan derivatives (Lapasin *et al.*, 1991), semi-dilute xanthan gum saline solutions (Rochefort and Middleman, 1987) and pectin dispersions (due to aggregation) (Davis *et al.*, 1980).

Whilst the rheological profiles for all the EPSs were largely similar, subtle differences arose due to differences in molecular weights, molecular weight profiles and complexities of the malto-oligomer arrangements. In general, the shake-flask preparations of the EPSs were rheologically most similar. The 4.0% solutions behaved as concentrated, slightly shear-thinning polymer solutions that were viscous in nature and conformed to the Cox-Merz rule. The 2.0% solutions of the shake-flask preparations had slightly more interesting rheological properties than their more

concentrated counterparts. The 2.0% solutions were more shear-thinning and revealed two cross-over points in their viscoelastic profiles. These profiles closely resembled that of the 4.0% FB2 solution – the EPS that was prepared in the bioreactor. In all three cases, elastic properties were evident at the very low and very high angular frequencies. Furthermore, all three of these solutions disobeyed the Cox-Merz rule by displaying the rare deviation of $\eta > |\eta^*|$. This behaviour was also true for the more dilute FB2 solution. The most different of the EPS solutions was the 1.0% PB2 sample, where $|\eta^*| > \eta$.

The fact that the Cox-Merz rule was violated for most of the EPS solutions confirms that some sort of order or rigidity existed in their structures, which induced intermolecular associations within their entanglement networks. Structured fluids (also known as weak gels) occur when ordered molecules have intermolecular associations that are strong enough to form a network in solution. Such solutions do exhibit significant shear-thinning behaviour, with conformational changes occurring during applied stresses that result in flow or viscoelastic behaviour changes (Lazaridou *et al.*, 2003a). Networks arising due to ordering and aggregation have been observed in other neutral glucans. For example, glucans containing *"cellulose-like sequences of more than three contiguous β-(1→4)-linked glucose units"* have formed weak gels. Also, polydispersed glucan samples where low molecular weight chains aggregated via lateral associations to form *"physical cross-links for a tenuous network"* have also been observed (Lazaridou *et al.*, 2003a). The networks established in weak gels remain intact during small-amplitude oscillations but become disrupted during continuous shear (Miyoshi and Nishinari, 1999). All the EPS samples examined were crude isolates that were polydisperse and contained oligosaccharides. In particular, the FB2 sample had the highest variation in molecular weights and contained the highest concentration of oligosaccharides (see the GFC results in Section 5.1). It is likely that the oligomer segments in the samples were potentially more mobile, more able to diffuse through the high molecular weight entanglements and may potentially have clustered together. These clusters then would have acted as slippage barriers for the longer polymeric chains, hence establishing the more elastic system observed under low-amplitude deformations. Conversely, elasticity at higher rates of oscillation are likely to have resulted when the long polymeric chains were unable to detangle, and these entanglement junctions enabled temporary cross-linking to occur (Lazaridou *et al.*, 2003a). These processes also explain why the elastic zones in the structured EPS solutions were observed to shift toward lower frequencies as the relative concentrations and molecular weights diminished, *i.e.*, FB2 4.0% > PB7 2.0% > PB2 2.0% > FB2 2.0% > PB7 1.0% > PB2 1.0%.

What these initial rheological assessments of the *P. sacchari* EPSs provide is a glimpse of the possibilities for such biopolymer solutions. In particular, the cultivation conditions of the EPSs can be optimised to produce polysaccharides that can be tailored to exhibit desired rheological properties, depending on specific end-user requirements. These properties can be varied in terms of viscosity, shear-thinning and viscoelastic behaviours; each of which can be adjusted based on concentration, molecular weight, polydispersity, malto-oligomer arrangement, *etc.* Hence, these primary rheological studies that, *hitherto*, have never been performed on *P. sacchari* EPSs before, offer a foundation for future investigations into possible niche applications of these fascinating biopolymers as viscosity modifiers. The next section looks at the potential application of *P. sacchari* EPSs for biopolymer films, through assessing differences between the mechanical properties of their native and plasticised films.

5.5.2 Film formation and mechanical properties

Pullulan is said to have excellent film-forming properties. These films are transparent, oil resistant, have low oxygen permeability, a low calorific value, are tasteless, and have good mechanical strength. The mechanical and gas barrier properties of pullulan are also said to be tunable when mixed with other biopolymers or plasticisers. All these properties make pullulan a

versatile biopolymer that can be used as edible coatings or packaging materials (Diab *et al.*, 2001; Roukas and Liakopoulou-Kyriakides, 1999). All of the native (unplasticised) and sorbitol-plasticised pullulan and EPSs formed clear, colourless and transparent films as shown Figure 5.33 for the PB7 film.

Figure 5.33: An aqueous cast *P. sacchari* EPS (PB7) film.

To determine the potential usefulness of the various films prepared, their mechanical properties were determined. Mechanical testing was carried out on the films following conditioning at 25 °C and 18.7% relative humidity for a minimum of 48 hours. Figure 5.34 illustrates the stress-strain tensile curves for each of the films, including the native and sorbitol-plasticised samples. The mean values calculated for each of the tensile parameters determined from the stress-strain curves are provided in Table 5.18, together with the moisture contents of each of these conditioned films. The mechanical property mean values are illustrated in the bar graphs of Figure 5.35, allowing these differences between the films to be more readily discerned. The shapes of the stress-strain curves (Figure 5.34) and the determined tensile properties (Table 5.18) are discussed and compared below.

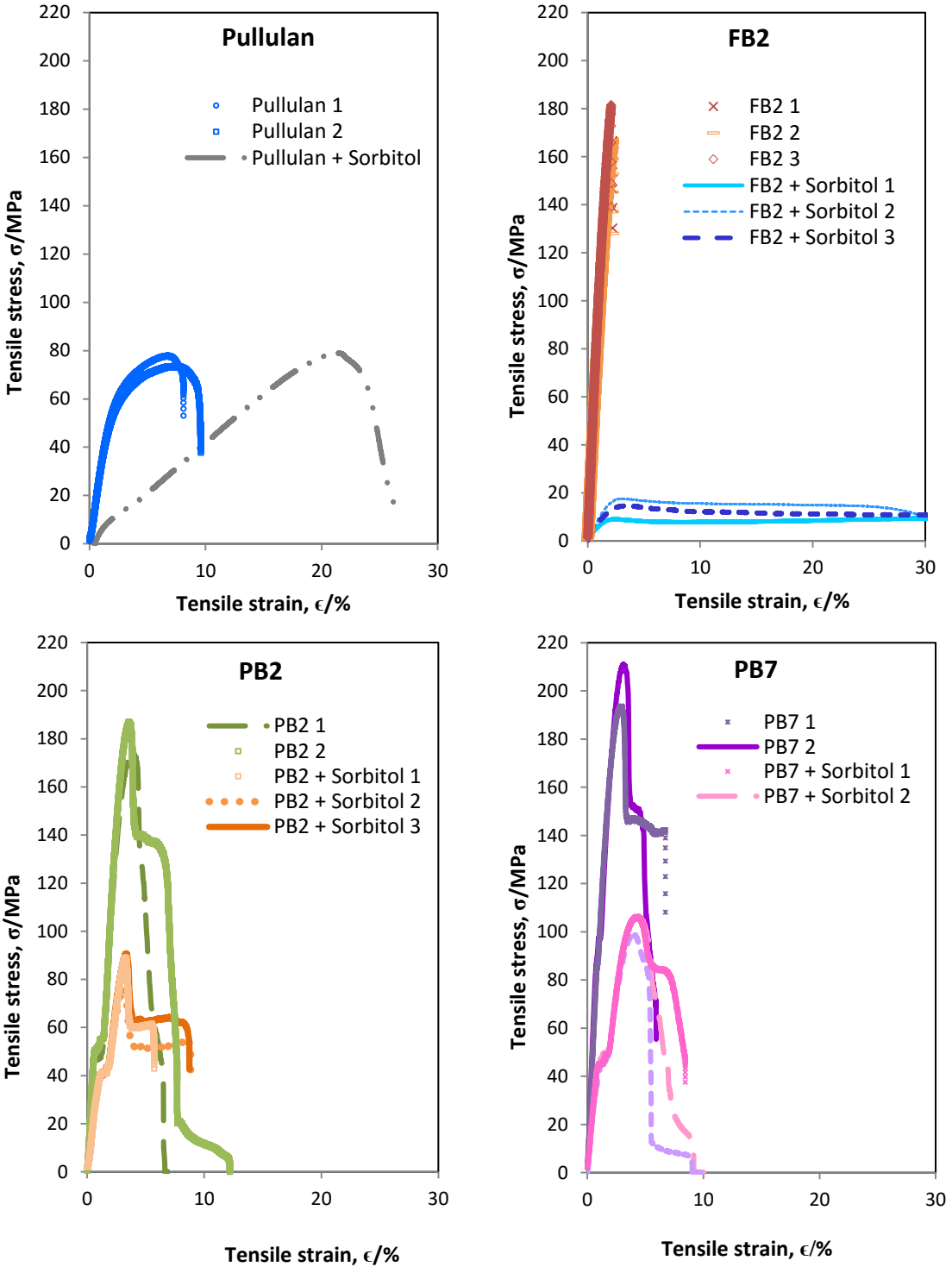

Figure 5.34: Mechanical property stress-strain curves for the native and 10.0% (m/m dry basis) sorbitol plasticised pullulan and *P. sacchari* films conditioned at 25 °C and 18.7% relative humidity.

Table 5.18 Mean values determined for the mechanical properties of the native and sorbitol plasticised films of pullulan and the *P. sacchari* EPSs conditioned at 25 °C and 18.7% relative humidity.

Film	Sample	Moisture /%	Young's Modulus, E (±SD) /GPa	Max. tensile stress, σ_M (±SD) /MPa	Tensile strain at max. tensile stress (±SD) /%	Tensile strain at break (±SD) /%
Native	Pullulan[b]	11.5[a]	3.0 (0.1)	75.5 (3.1)	7.3 (0.4)	10.6 (0.9)
	FB2[c]	6.9 [a]	10.4 (1.0)	171.7 (8.5)	2.2 (0.1)	2.2 (0.1)
	PB2[b]	11.9 [a]	7.3 (1.0)	180.5 (9.1)	3.7 (0.2)	7.1 (0.8)
	PB7[b]	11.7 [a]	8.7 (0.7)	202.3 (12.4)	3.0 (0.1)	6.3 (0.6)
Plasticised[S]	Pullulan[a]	13.8 [a]	0.4	79.0	21.5	27.0
	FB2[c]	9.0 [a]	0.9 (0.1)	14.3 (3.5)	26.1 (29.8)	55.2 (28.3)
	PB2[c]	9.3[a]	4.5 (0.3)	85.3 (7.9)	3.3 (0.1)	7.7 (1.8)
	PB7[c]	9.0[a]	5.3 (0.2)	103.9 (4.2)	4.2 (0.2)	8.7 (0.3)

[a] Single analysis
[b] Duplicate analyses
[c] Triplicate analyses
[S] Plasticised with 10.0% sorbitol on dry mass basis
MPa – mega Pascals, max. – maximum

The shape of stress-strain curves provides insight into the mechanical behaviour of materials under strain and allows differences in strength and ductility to be observed between each of the different polysaccharides. Changes in mechanical behaviour affected by the addition of sorbitol plasticiser are also immediately obvious. On first inspection of Figure 5.34, it is clear that pullulan behaves differently to each of the three EPSs under tensile strain, and that sorbitol has a marked effect on the mechanical properties of pullulan films. The stress-strain curves of the native pullulan films reflect the behaviour of a ductile material, which becomes increasingly more elastic with the addition of sorbitol. Table 5.18 provides that the conditioned pullulan film had 11.5% moisture and that it was the most ductile of all the native films, with a tensile strain at break (percentage elongation) value of 10.6%. Pullulan had the lowest Young's elastic modulus of 3.0 GPa and the lowest maximum tensile strength of 75.5 MPa, which are comparable to the values for nylon (2-4 GPa and 75 MPa, respectively) and acrylic (3.2 GPa and 70 MPa, respectively) (Anonymous, 2013; Callister, 2001). The Young's elastic modulus provides an indication of the stiffness of the sample. In this case, pullulan was almost three times stiffer yet of equivalent maximum tensile strength compared to the pullulan films prepared by Diab and

co-workers (2001). The pullulan films prepared by these authors were of comparable moisture (11%), but recorded a Young's modulus of ~1200 MPa and a maximum tensile strength of ~80 MPa at 25 °C (Diab *et al.*, 2001). Differences between the pullulans that may account for the differences in elastic moduli include differences in the pullulan molecular weights used (unreported by the authors) and the film preparations (the authors prepared thick specimens of 1.0-1.5 mm from hot compressed hydrated pullulan powders) (Diab *et al.*, 2001). In both studies, the addition of sorbitol had a marked effect on the pullulan film tensile properties (Diab *et al.*, 2001). In this study, the Young's elastic modulus dropped almost tenfold to 412 MPa, and the maximum tensile strength improved almost three fold, rising to 21.5 MPa – both values were remarkably similar to those reported by Diab and co-workers for films prepared with 15% (m/m) sorbitol and containing 11% moisture (Diab *et al.*, 2001). The degree to which sorbitol changes the mechanical properties of pullulan are notable in the bar graph shown in Figure 5.35.

The stress-strain curves for the *P. sacchari* EPSs in Figure 5.34 were markedly different to those for pullulan. Furthermore, the curves for the bioreactor preparation (FB2) were substantially different from those of the two shake-flask preparations (PB2 and PB7). In turn, these latter two films had the most similar mechanical properties to each other. The native FB2 film reflects a stress-strain curve of a very stiff and brittle polymer. Indeed, these conditioned films were most unforgiving and readily shattered when preparing the strips required for mechanical testing. Table 5.18 summarises that the FB2 films had the lowest affinity to water (6.9%), the highest Young's elastic modulus (10.4 GPa) and were the least ductile, with only 2.2% elongation on fracturing. All three of the EPS films proved to be more than twice as strong as pullulan, with FB2 having a maximum tensile strength of 171.7 MPa and the tensile properties similar to reinforced polyesters, although it was somewhat weaker than the PB2 and PB7 films (Kalpakjian and Schmidt, 2008). On addition of sorbitol, the FB2 films were converted from the most brittle to the most elastic, with tensile elasticities and strengths more similar to high density polyethylene (Anonymous, 2016a).

Plasticisers are added to films to reduce their brittleness. Brittleness arises from extensive intermolecular forces in the material that plasticisers are able to disrupt, thereby inducing greater chain mobility and producing more flexible and extendable films (Banker, 1966). The noticeably brittle nature of the unplasticised FB2 films indicated that there was a high degree of crystallinity within these samples. This crystallinity must be due to extensive intermolecular forces between linear malto-oligomer regions within the polysaccharide, of which FB2 had the highest propensity (particularly of DP7 and above). This high crystallinity would also affect the affinity of FB2 films to moisture. Despite the high crystallinity and resultant intermolecular forces of FB2, this EPS formed slightly weaker films than PB2 and PB7. It is likely that the overall lower molecular weight and higher polydispersity of the FB2 sample caused these films to be marginally weaker. Conversely, the PB2 and PB7 films were somewhat stronger (180.5 MPa and 202.3 MPa), more ductile (7.1% and 6.3%), and more elastic (7.3 GPa and 8.7 GPa) than the FB2 films, respectively. These films also had higher affinities for moisture (11.9% and 11.7%, respectively). Interestingly, the plasticising effect was less noticeable and the moisture affinity was reduced on the addition of sorbitol to PB2- and PB7-, compared to FB2. The less subtle changes to the elasticity and ductility of the former two films are illustrated in Figure 5.35. More interesting, is the fact that the addition of sorbitol did not change the overall shape of the stress-strain curves for these samples (Figure 5.34).

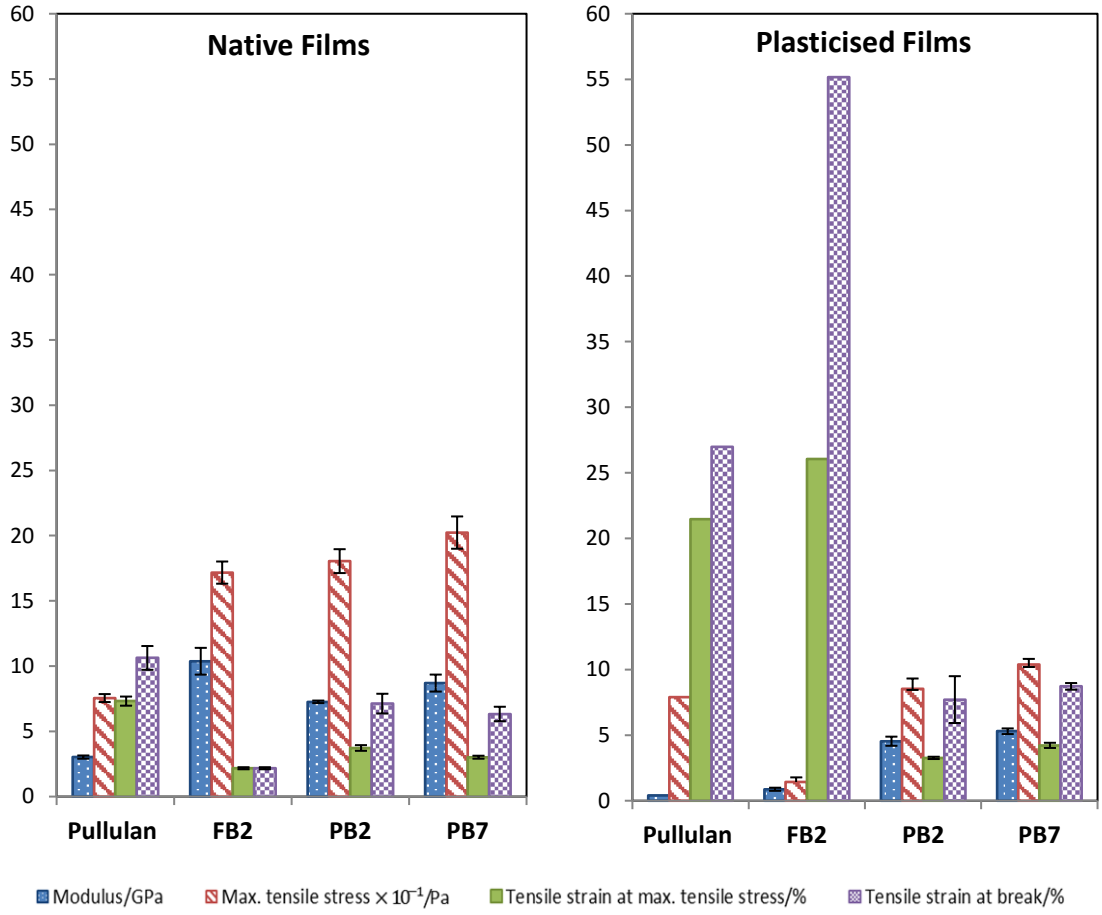

Figure 5.35: Mean values determined for the mechanical properties of the native and plasticised pullulan and *P. sacchari* EPS films conditioned at 25 °C and 18.7% relative humidity.

The stress-strain curves for PB2 and PB7 revealed that these EPSs behaved as semi-crystalline polymers, as there was more than one yield point present in their mechanical property profiles (Callister, 2001). Semi-crystalline polymers represent composite materials containing both crystalline and amorphous regions within their polymeric networks, as illustrated in Figure 5.36.

Deformation in semi-crystalline polymers is a complex, multi-step process. During the initial elastic deformation, the molecular chains in the network begin to elongate in the direction of the tensile strain. As the strain increases beyond the elastic region, the sample yields and plastic deformation begins. This first yield is observed as a constriction (neck) in the sample. During plastic deformation, the amorphous regions elongate in the direction of the applied strain at faster rates, whilst the lamellar crystalline segments are brought into alignment with the tensile axis by the connected amorphous tie chains. This alignment increases the strength in the neck region, whilst elongation and stress continue to increase with the applied strain. Semi-crystalline polymers differ from metal polymers, in that deformation is not confined to only the neck region of the former material (Zhigilei, 2010). When strain increases enough, the sample yields once again and the crystalline segments begin to separate. Elongation then occurs between both the crystallite and amorphous lamellae until the sample fractures (Callister, 2001). The multi-stage

stress-strain profiles of the PB2 and PB7 films reveal that these polymers have semi-crystalline molecular networks. Indeed, during tensile strain testing, deformation was observed as stretching along both the constriction zone and along the entire length of the specimens and the moment of rupture was far less abrupt, compared to FB2. During the advanced stages of deformation, the samples were seen to tear along the fracture zone rather than simply snapping. This tearing must have been the visualisation of the amorphous ties between the crystalline segments failing in groups, until final rupture of the sample occurred. Like FB2, the crystalline regions would have consisted of linear malto-oligomer segments. These crystalline segments were less extensive than those in FB2, as neither PB2 nor PB7 had malto-oligomers beyond DP7. Furthermore, PB2 and PB7 had a higher concentration of higher molecular weight chains and Glc6 kinks within these chains. These kinks would have been more concentrated in the chain regions of lower malto-oligosaccharide subunits. Since these kinks hinder intermolecular interactions, these regions would have occupied a greater volume and would have formed the amorphous zones within the polymeric network. These amorphous zones provided the polysaccharides with their higher affinity to moisture, and were the regions that were least likely to be affected by the addition of sorbitol. In general, PB2 and PB7 shared similar tensile properties to nylon 6/6 reinforced with glass fibre, a composite polymer, and the addition of 10.0% sorbitol was far less effective as a plasticising agent on these EPSs compared with FB2 and pullulan (Anonymous, 2012).

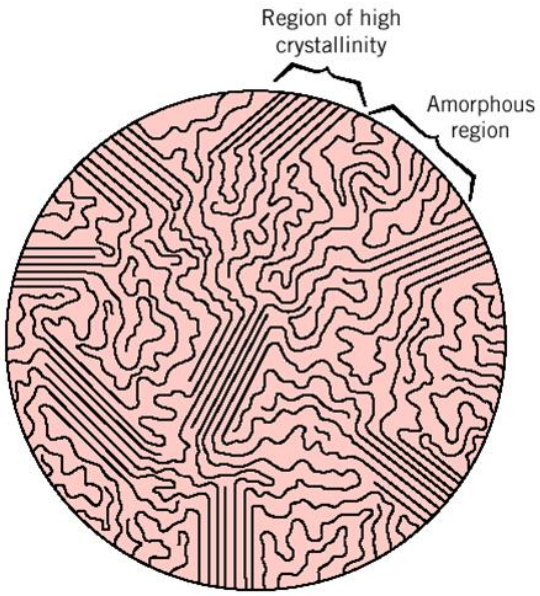

Figure 5.36: Spherulitic arrangement of polymeric chains in a semi-crystalline lattice, comprising lamellae in the crystalline regions, separated by amorphous regions connected by tie chains (Callister, 2001; Zhigilei, 2010).

The effects of molecular weight, molecular weight distribution, and molecular structure all have a significant effect on film tensile properties. Whilst the overall molecular make-up of the EPSs was similar, variations in the culture conditions led to some differences in the molecular weight properties of the EPSs – which had a significant effect on the tensile properties of their films. Furthermore, the addition of plasticiser was shown to have different degrees of effect on the different EPSs. Hence, the tensile properties of *P. sacchari* EPS films can be altered by changes

in molecular arrangements and size or through varying the addition of plasticisers such as water and sorbitol. Furthermore, the differences between these shake-flask and bioreactor products have demonstrated that the molecular weight distributions and malto-oligomer arrangements of the EPSs can potentially be altered through tuning the culture conditions of the producer organism. Ultimately, this represents the first ever study of the tensile properties of films prepared from *P. sacchari* EPSs and forms a foundation from which biofilm products from this organism having desired mechanical properties for specific end-user applications can be explored.

5.6 Summary and discussion of findings

The results from the characterisation of pullulan and the *P. sacchari* EPS samples are summarised and then their determined structures are compared to pullulan and the literature on sarkaran. For ease of reference, Table 5.19 provides a comparative summary of the more pertinent data collected on pullulan and the various *P. sacchari* EPSs and which is referred to in the text that follows.

Table 5.19 Summary of molecular weight and structural characterisation data of pullulan and the *P. sacchari* EPSs (fractionated and crude).

Sample	M_w[a] /kDa	PDI[a]	Glc /%	Gal /%	Man /%	Glc4:Glc6[c]	DP Range	DP3:DP4 /%
Pullulan	328	1.9	100[b]	0	0	2.0	DP3[f]	99:1[f]
FB2 F1	>1000	1.1	70[d]	20[d]	10[d]	3.3	DP2-DP10[e]	28:25[e]
FB2 F2	410	4.1	99.9[b]	0.1[b]	0.1[b]	3.1	DP2-DP10[f]	32:28[f]
FB2	n/a	n/a	97.8[b]	1.7[b]	0.5[b]	3.0	DP2-DP10[f]	34:28[f]
PB2	691	1.5	99.3[b]	0.5[b]	0.3[b]	2.7	DP2-DP7[f]	37:38[f]
PB7	717	1.5	98.6[b]	0.9[b]	0.5[b]	2.8	DP2-DP7[f]	45:37[f]

[a] Determined by GFC. [b] Determined by GC-MS compositional analysis. [c] Determined by GC-MS permethylation analysis. [d] Determined by NMR analysis of the native sample. [e] Determined by pullulanase digestion with enzyme E1 and HPAEC-PAD analysis against DP3 and DP4 standards. [f] Determined by pullulanase digestion with enzyme E2 and HPAEC-PAD analysis against DP2-DP7 standards. M_w – weight-average molecular weight, kDa – kilo daltons, PDI – polydispersity index, Glc – glucose, Gal – galactose, Man – mannose, Glc4 – (1,4)-linked D-glucopyranose, Glc6 – (1,6)-linked D-glucopyranose, DP – degree of polymerisation for malto-oligomers, DP2 – maltose, DP3 – maltotriose, DP4 – maltotetraose, DP5 – maltopentaose, DP6 – maltohexaose, DP7 – maltoheptaose, DP8 – maltooctaose, DP9 – maltononaose, DP10 – maltodecaose, n/a – not applicable.

5.6.1 Summary of the pullulan results

Sarkaran is believed to belong to a class of polysaccharides called pullulans (Morel du Boil, 2000a). Hence, pullulan was used as a model compound throughout this study. GFC analysis established that the pullulan sample had a dextran equivalent M_w of 328 kDa and a PDI of 1.9 (Table 5.19). The various GC-MS techniques carried out confirmed that pullulan comprised (1,4)-linked and (1,6)-linked D-glucose in a ratio of 2.0, the expected ratio for a polymaltotriose compound (Table 5.19). The NMR analyses verified the conformation and sequence information

of pullulan. 1D NMR showed the three distinct maltotriose anomeric protons, specifically, the two α-(1,4)-linked D-glucopyranoses of rings B and C, and the one α-(1,6)-glucopyranose of ring A. Together with the COSY, HSQC, and HMBC spectra, these three rings were fully assigned. The ROESY measurements also confirmed the DP3 sequence of the rings ($A-B-C$). Furthermore, integration of the anomeric protons enabled the increase in B-type resonances arising from any DP4 subunits present in the pullulan sample to be determined. The contribution of these was 1.1%. Pullulanase hydrolysis and analysis by HPAEC-PAD confirmed that pullulan had a composition of 99% DP3 and 1% DP4 (Table 5.19).

Since all the analytical techniques were successful in verifying the structural makeup of the model pullulan sample, the *P. sacchari* EPSs were similarly analysed.

5.6.2 Summary of the *P. sacchari* FB2 (crude and purified fractions) results

FB2 is an EPS cultivated from *P. sacchari* in a bioreactor. The crude FB2 sample was purified by GFC into three distinct fractions. Some of the data for the crude FB2 EPS and fractionates FB2 F1 and FB2 F2 are summarised in Table 5.19. The crude FB2 sample was found to comprise 12% of M_w > 1000 kDa (FB2 F1), 57% of M_w 410 kDa (FB2 F2), and 31% of M_w 1.4 kDa (FB2 F3). The crude and the purified fractions were subjected to some/all of the remaining analyses. GC-MS analyses established that all the samples comprised primarily (1,4)- and (1,6)-linked D-glucose, together with lesser amounts of D-galactose and D-mannose. The ratio of Glc4:Glc6 varied amongst the FB2 fractionates (from 2.6-3.3), whilst the crude FB2 sample had a ratio of 3.0. NMR analyses were carried out on native and acetylated samples. In all cases, the fractionated and crude FB2 samples shared many NMR features with pullulan, although they certainly were not the same. NMR analysis of pullulan provided it was primarily a DP3 polyglucan, whilst the various NMR analyses confirmed that FB2 comprised DP3 – DP4 – >DP4 subunits, as indicated by the splitting patterns and integration values of the anomeric signals. Furthermore, NMR analyses of the native FB2 F1 sample established that galactose and mannose reside as terminal β-D-mannopyranoses and reducing-end β-D-galactopyranoses on the repeating glucan chains of the EPS. Whilst GC-MS analysis provided that FB2 was primarily a glucan (97.8%), the pullulanase hydrolysis and HPAEC-PAD analyses revealed that the polyglucan component comprised a variety of malto-oligomer subunits ranging from DP2-DP10, with DP3 (34%) and DP4 (28%) predominating. This high complexity of malto-oligomer arrangement in the repeating units precludes the EPS from being classified as a pullulan.

5.6.3 Summary of the *P. sacchari* PB2 and PB7 results

PB2 and PB7 are EPSs that were prepared from two separate shake-flask preparations of *P. sacchari.* Some of the data for these EPSs are summarised in Table 5.19. GFC analysis established two distinct fractions in both these crude EPSs. In PB2, 93% comprised M_w 691 kDa with a PDI of 1.5. In PB7, 94% comprised M_w 717 kDa, also with a PDI of 1.5. The lesser fraction in both EPSs was due to oligosaccharides of M_w 1.4 kDa. GC-MS analyses revealed that the subunits of PB2 and PB7 were very similar to FB2, but with higher glucose concentrations of 99.3% (PB2) and 98.6% (PB7) and smaller Glc4:Glc6 ratios of 2.7 (PB2) and 2.8 (PB7). NMR analyses of the peracetate derivatives confirmed that both EPSs had the same glucan subunit elements compared to FB2, however, the low levels of mannose and galactose in these EPSs were not detected in these spectra. Pullulanase hydrolysis and HPAEC-PAD analysis provided that, like FB2, PB2 and PB7 were both polyglucans (>99%) with DP3 (37-45%) and DP4 (37-38%) predominating their structures, but containing a slightly less complex assembly of malto-oligomers ranging from DP2-DP7. Similar to FB2, the complexity

of malto-oligomer arrangement beyond DP4 in the repeating units precludes these EPSs from being classified as pullulans.

5.6.4 Summary of the *P. sacchari* physical properties

The solution rheology and film mechanical properties of the *P. sacchari* EPSs were investigated and compared against pullulan. Pullulan solutions were found to be largely Newtonian, whilst the EPS solutions became increasingly shear-thinning as their concentrations dropped, with most solutions displaying multi-region viscosity profiles. All the EPS solutions had higher apparent viscosities compared with pullulan, and the difference in overall molecular weight resulted in PB2 and PB7 having the highest apparent viscosities, whilst the similar molecular weight and malto-oligomer distributions caused the two EPS solutions to behave most similarly and somewhat differently from the FB2 solutions of comparable concentration. Likewise, the dynamic rheological behaviour of the two shake-flask EPS solutions was most similar compared with the bioreactor samples. The higher concentrations of the shake-flask samples behaved like typical entangled polymer solutions. All the other EPS solutions exhibited both viscous and elastic behaviour across the angular frequencies investigated, and these solutions all disobeyed the Cox-Merz rule. These factors indicated that there existed intermolecular associations within the EPS entanglement networks of the solution. Elastic properties were postulated to arise from ordering between lateral malto-oligosaccharide segments within the polymeric chains, from temporary cross-linking owed to long chain entanglement junctions and/or from chain slippage barriers due to short-chained oligomer clustering within the crude samples (particularly in the FB2 solutions). The differences in the molecular weights, molecular weight distributions and the malto-oligomer arrangements between the EPS samples also had an effect on the product film tensile properties. All the clear and transparent EPS films prepared were found to be stiffer and stronger than pullulan films. All these EPS films, besides plasticised FB2, were also found to be less ductile than the pullulan films. The same intermolecular forces between the linear malto-oligomer segments (particularly for segments >DP7) that imparted FB2 solutions with their elastic tendencies at low and high angular frequencies, provided very stiff and brittle films. The addition of plasticiser had the greatest effect on disrupting the intermolecular networks within these films, providing the most elastic of all the films prepared. Conversely, the PB2 and PB7 films displayed mechanical properties of semi-crystalline polymers, whereby the higher propensity of Glc6 kinks in the shorter malto-oligomer segments of these polymers established amorphous zones amongst the crystalline networks of longer malto-oligomer segments. These amorphous zones afforded the samples with several yield points under continued tensile strain, the overall properties of which were far less affected by the addition of sorbitol. In general, both the rheological and film tensile property investigations revealed that the differences in cultivation conditions afforded the EPS samples with subtle variations in malto-oligomer arrangements and molecular weight profiles which imparted changing properties on their product solutions and films – all of which were all markedly different to the tested pullulan samples.

5.6.5 Discussion comparing the results of pullulan and the *P. sacchari* polysaccharides

Whilst PB2 and PB7 were prepared from *P. sacchari* under similar cultivation conditions in shake-flasks, FB2 was cultivated from the same organism under a different set of conditions in a bioreactor. The different cultivation conditions caused FB2 to display some differences from PB2 and PB7. In general, FB2 had a wider molecular weight distribution, a higher trace of galactose and mannose and a more complex arrangement of malto-oligomers. The first difference between the samples was detected in the GFC analyses. The appearance of a small peak near the exclusion volume of the column (>1000 kDa) suggests that the bioreactor conditions stimulated the organism to produce a small amount of a particularly high molecular weight EPS, compared to

the shake-flask preparations of PB2 and PB7. Also, whilst the bulk of all three EPSs were largely in the same molecular weight region (M_w 410-717 kDa), the polydispersity index for FB2 was far greater (4.1 versus 1.5). Furthermore, FB2 had a higher quantity (31%) of components eluting near the totally included volume, indicating a higher proportion of oligosaccharides in FB2 compared to PB2 and PB7. The conditions in the bioreactor may have favoured the production of hydrolytic enzymes. These enzymes may have degraded some of the FB2 product, thereby increasing the polydispersity and quantity of oligosaccharides. Despite this, the GC-MS analyses provided that pullulan and all three of the EPSs shared the same predominant glucan structural features (*i.e.*, Glc4 and Glc6), except that the EPS also contained traces of mannose and galactose. Furthermore, FB2 F1 was found to be most different as it contained the highest amounts of both these lesser components. The NMR analyses reflected that the three EPSs and pullulan share many similarities; however, there were three standout features. First, in comparison to pullulan, the EPSs all displayed increased integrations and splitting patterns in the anomeric regions. This provided the initial evidence that all the EPSs comprised high levels (*i.e.*, >7%) of other malto-oligomers, besides DP3 and DP4. Second, comparing FB2 to the other EPSs, the higher amount of oligosaccharides (as determined in the GFC analysis) caused additional, less intense spin-systems to appear in the NMR spectra. These were assigned to the reducing-ends of shorter-chained α-D-glucopyranose oligomers. Third, the additional spin-systems for the mannose (~10%) and galactose (~20%) residues in the FB2 F1 fractionate were visible, and these were assigned to terminal β-D-mannopyranoses and reducing-end β-D-galactopyranoses on the very high molecular weight glucan chains. Besides these differences, the glucan components of the samples were all largely the same. The similarities in the glucan makeup of the EPSs were further explored by pullulanase treatment followed by HPAEC-PAD analysis. These data revealed that the EPSs mostly comprised malto-oligomers ranging from DP2-DP7, with DP3 and DP4 predominating. Since the EPSs contained malto-oligomers >DP4, they had to be precluded from being classed as pullulans, as previously suggested by Morel du Boil (2000). The enzyme-HPLC analyses also revealed subtle differences between FB2 and the shake-flask EPSs. Compared to PB2 and PB7, FB2 displayed a more complex arrangement of malto-oligomers that extended beyond DP7, albeit in diminishing quantities. Ultimately, the complete set of data provided sufficient evidence that all the EPSs produced *in vitro* by *P. sacchari* were fundamentally the same. The subtleties between the EPS samples highlighted that the molecular weight, molecular weight distribution, malto-oligosaccharide complexity, malto-oligosaccharide ratios and amounts of mannose and galactose are potentially tunable through optimising the fungal fermentation conditions. Nevertheless, the question remains as to whether the EPS prepared from *P. sacchari* are sarkaran, or not. To determine this, the literature detailing the history and structure of sarkaran is first presented.

5.6.6 The story of sarkaran

In 1959, Nicholson and Lilienthal identified an "*unusual dextran*" isolated from standover[11] sugarcane in Australia and Fiji. The polysaccharide was found to have 1,6-linked glucose (29%) and 1,4-linked glucose (60%), which was different from the classic 1,6-linked dextran produced from the *Leuconostoc* associated with it (Nicholson and Lilienthal, 1959a). In 1960, Sutherland further investigated Nicholson and Lilienthal's "*abnormal dextran*". Sutherland isolated the crude polysaccharide from viscous sugar syrups and established that two polysaccharides were present: a hemicellulose-like heteroglycan (comprising glucose, galactose, arabinose, xylose and rhamnose) and the polyglucan described by Nicholson and Lilienthal (Sutherland, 1960).

In 1966, Bruijn investigated a polysaccharide that was isolated from the juice of deteriorating sugarcane in South Africa and compared it to dextran (Bruijn, 1966a; Bruijn, 1966b). Bruijn

[11] Standover cane is that which is harvested in the second season of its growth (Morel du Boil, 2000).

investigated the polysaccharide by acid hydrolysis, paper chromatography, molecular weight (by various measures), periodate oxidations, methylation with GC analysis, and pullulanse digestion detected with paper chromatography. Bruijn found that the polysaccharide had M_ws between 30-260 kDa (with a PDI of ~5), was a straight-chain α-glucan with (1-4)-glucose (~70%) and (1-6)-glucose (~30%) linkages, and comprised DP3 (~50%), DP4 (~37%) and other malto-oligomers (DP2+DP5+DP6≈13%) (Bruijn, 1973; Bruijn, 1966a; Bruijn, 1966b; Bruijn, 1970). Bruijn concluded that the polysaccharide isolated from deteriorated post-harvest cane was a new α-glucan – although it was possibly the same polysaccharide first identified by Nicholson and Lilienthal (Morel du Boil *et al.*, 2005). Bruijn suggested the polysaccharide be named "*sarkaran*" – which is derived from the Sanskrit word for sugar, "*sarkara*" (Bruijn, 1973). Unfortunately, Bruijn was unable to establish the cause of sarkaran in his investigations.

In 1976, Fulcher and Inkelman suggested that the problems associated with processing standover cane (such as high syrup viscosities and longer boiling times) were possibly exacerbated by the presence of the polysaccharide identified by Bruijn (sarkaran) (Fulcher and Inkerman, 1976). Then, in 1984, Blake and Littlemore isolated and characterised a polysaccharide from the juice and molasses of standover cane that was linked to processing difficulties in Australian mills (Blake and Littlemore, 1984a; Blake and Littlemore, 1984b). The authors compared these isolates to a donated sample of sarkaran; one that Bruijn had previously isolated from deteriorated post-harvest cane.

The crude sarkaran isolated from the expressed juice of the standover came was found to contain glucose (88%), galactose (4%) and mannose (4%), along with lesser amounts of arabinose, xylose and rhamnose. The crude molasses isolate also contained glucose (65%), galactose (11%) and mannose (5%), together with arabinose, xylose and rhamnose. Like Sutherland, Blake and Littlemore presumed that the non-glucan components were due to a co-precipitated hemicellulose – such as indigenous sugarcane polysaccharide (an arabinogalactan). Both the juice and molasses isolates were hydrolysable by pullulanse, revealing four oligosaccharides (DP2-DP5). The purified polysaccharides were also analysed by ^{1}H (100 MHz) and ^{13}C NMR (14.9 MHz) spectroscopy. Although these spectra were of low resolution, the anomeric signals corresponding to α-(1,4)-linked and α-(1,6)-linked glucose were detected at a ratio of 74.5:25.5 (juice sample), 73.5:26.5 (molasses sample) and 75.0:25.0 (Bruijn's sarkaran). Following the NMR, enzyme, periodate oxidation, and methylation with GC-MS analyses, the authors concluded that the isolated polysaccharides from both the standover cane juice and molasses were "*essentially the same*" as Bruijn's sarkaran (Blake and Littlemore, 1984a; Blake and Littlemore, 1984b). Unfortunately, the "*arabinogalactan*" components were not further elucidated or verified.

Again in 1984, Blake and Clarke carried out two subsequent studies on (what they had now established was) sarkaran isolated from Australian cane samples. The authors set out to characterise these samples in terms of molecular weight and impact on pol (sucrose) measurements (Blake and Littlemore, 1984b). They also aimed to establish a pullulanase HPLC-RI assay for the specific determination of sarkaran in polysaccharides isolated from sugar processing streams (Blake and Littlemore, 1984a). In the process of these investigations, they tried to establish the origin of sarkaran (Blake and Clarke, 1984b).

In one part of these investigations, Blake and Clarke isolated sarkaran from the juice of 30 kg poor-quality, standover cane. The isolates were purified on a diethylaminoethyl cellulose column, followed by a Sephacryl S-200 superfine column, and established the sample to be "*pure enough for examination of some bulk properties*", despite containing "*trace of arabinogalactan*". The molecular weights were determined by gel filtration against dextran standards. The bulk polysaccharide returned figures of 185-200 kDa, whilst the authors speculated that a small peak appearing in the order of 410 kDa was due to the "*arabinogalactan impurity*" (Blake and Clarke, 1984b).

In the other part of these investigations, Blake and Clarke established a pullulanase HPLC-RI analysis assay for the direct determination of sarkaran in isolates. The assay was used to identify sarkaran-containing standover cane samples. Positively identified whole stalk samples were then billeted and incubated in several batches for 36 days (30 °C) or 57 days (ambient temperature). The authors expressed the juice from the incubated stalks, then deproteinated the juice before precipitating the sarkaran with alcohol. The sarkaran samples where digested with pullulanse (from *Aerobacter aerogenes*), and these digests were analysed by HPLC-RI. In the absence of authentic standards, the authors normalised the areas of the eluting oligomers and reported their relative concentrations. Oligomers ranging from DP2-DP6 were detected, with either DP3 or DP4 predominating. The authors commented that the different incubation conditions affected both the type and amount of the oligomer subunits in each of the sarkaran products. The authors then attempted to identify the causative agent of sarkaran. They isolated four fungi from the 30 °C incubated billets and separately inoculated synthetic cane juice media. The resultant polysaccharides were precipitated, their alditol acetates were prepared and analysed by GC, and they were found to contain mannose (74-88%), glucose (10-21%), and galactose (2-12%). From these results, the authors concluded that none of the fungi had produced sarkaran. However, they did comment that "*the possibility still exists that conditions necessary for biosynthesis of sarkaran from these organisms were not established*" (Blake and Littlemore, 1984b).

In 2000, Morel du Boil investigated an HPAEC-PAD method for the analysis of sarkaran in a variety of sugarcane products (mixed juice, raw sugar, very high pol sugar and refined sugar) (Morel du Boil, 2000a). Sarkaran was obtained from the various samples by acidic ethanol precipitation, the isolates were subsequently hydrolysed with pullulanase (*Bacillus acidopullulyticus*) and the digests analysed by the developed HPAEC-PAD assay. Sarkaran was identified based on DP3 and DP4 appearing in characteristic ratios. Quantitation of these malto-oligomers was based on the response of a DP3 "*marker*" generated from concurrently hydrolysed pullulan standards. The author used this technique to monitor the seasonal and geographic differences in the incidence of sarkaran in the South African sugar industry during 1999-2000. From these findings, Morel du Boil (2000a) established that sarkaran occurred more prevalently and widespread than was previously realised.

It was only in 2005, that Morel du Boil and co-workers suggested a likely causal agent of sarkaran (Morel du Boil *et al.*, 2005). The authors had collected poor-quality cane from the South African Midlands region, which was affected by frost or drought. From this cane, the authors isolated and identified several fungi. The South African Sugar Research Institute and the Centre for Applied Mycological Studies positively identified one of these fungi, which had infected several different cane samples, as the stalk pathogen *Phaeocytostroma sacchari*. The authors inoculated sucrose broth and mixed juice samples with the mycelia of cultured *P. sacchari*, producing maximum yields of EPSs after seven days, at ambient temperature, in flask experiments. The isolated EPSs were treated with pullulanase, and the enzyme digests were analysed by the HPAEC-PAD assay that Morel du Boil had previously developed (Morel du Boil, 2000a). The authors established that the crude EPSs comprised the characteristic DP3 and DP4 oligomers of sarkaran, in similar ratios to those reported by Bruijn (Bruijn, 1966b) and by Blake and Clarke (Blake and Littlemore, 1984a; Blake and Littlemore, 1984b). In the same study, Morel du Boil and co-workers provided extensive detail on the isolation, plate culturing, flask culturing and identification of *P. sacchari* and concluded they believed their work to be the first published observation linking the fungal pathogen of sugarcane to the production of sarkaran (Morel du Boil *et al.*, 2005). The authors based this observation on the ratio of DP3 and DP4 determined by the pullulanase-HPLC assay in the *P. sacchari* EPSs. Thus, this current study continued from the work of Morel du Boil and her colleagues, where the EPSs prepared from several cultivations of *P. sacchari*, under varying conditions, were structurally elucidated to establish a more definitive link with sarkaran.

5.6.7 Evidence that *P. sacchari* produces sarkaran

Reviewing the literature, sarkaran isolated by alcohol precipitation from various sources has primarily been identified according to its ratio of DP3 and DP4 in its pullulanase digests (Blake and Littlemore, 1984a; Bruijn, 1973; Morel du Boil, 2000a; Morel du Boil, 2006; Morel du Boil *et al.*, 2005). More specifically, sarkaran was shown to have a malto-oligosaccharide composition that varies between DP2-DP6, which is predominated by either DP3 or DP4 subunits. In general, quantitation of the sarkaran malto-oligomers was carried out without authentic standards.

In the current study, the prepared *P. sacchari* EPSs were effectively hydrolysed by pullulan. The EPSs revealed similar malto-oligosaccharide arrangements to sarkaran, which were predominated by either DP3 or DP4. However, the EPS malto-oligomer arrangements appeared more complex compared to sarkaran. For instance, PB2 and PB7 contained DP2-DP7, whereas, FB2 contained DP2-DP10 – which where quantified against authentic standards up to DP7, where possible. There are three possible explanations for the differences observed in the malto-oligomer arrangement of the *P. sacchari* EPSs compared with the literature on sarkaran. First, sarkaran digests were detected with paper chromatography (Bruijn, 1970) and HPLC-RI (Blake and Littlemore, 1984a), where lower quantities and/or responses of higher malto-oligosaccharide subunits could not be detected. Second, the responses for higher malto-oligosaccharides from sarkaran may have been masked by the presence of non-sarkaran hydrolysates. For instance, Morel du Boil (2006) analysed sarkaran isolated from cane juice samples containing starch present. Hence, the progressive peaks appearing in the chromatograms were attributed to limit dextrins arising from the pullulanase activity on the starch (Morel du Boil, 2000a). Third, it is possible that the different cultivation conditions caused sarkaran to have different malto-oligosaccharide arrangements. Indeed, Blake and Clarke (1984b) recognised that the different incubation conditions (time and temperature) tested on their billets of cane caused the malto-oligomer distributions and ratios to vary, and which influenced whether DP3 or DP4 predominated in the sarkaran samples (Blake and Littlemore, 1984a). Morel du Boil and co-workers (2005) echoed this finding, commenting that the HPAEC-PAD analysis of sarkaran in 740 mixed juice pullulanase digests revealed a DP3:DP4 ratio that varied from 1.6-2.5, with an average of 1.8 ± 0.3.

The literature also suggests that cultivation conditions affect the molecular weights of sarkaran. Bruijn established that sarkaran from deteriorated, post-harvest cane had M_ws between 30-260 kDa (by various measures) (Bruijn, 1973). Blake and Clarke (1984a) isolated sarkaran from poor-quality, standover cane that had average M_ws between 185-200 kDa. The samples also contained a small amount of a higher molecular weight fraction (410 kDa) that was considered a hemicellulose impurity (Blake and Clarke, 1984b). All the molecular weight data gathered on sarkaran to date is derived from samples isolated from natural sources. In general, these all had lower molecular weights than those determined for the *P. sacchari* EPSs prepared in this study. For the shake-flask EPS, the bulk M_ws were about triple (~700 kDa) than those reported for sarkaran. For the fed-batch EPS, the bulk M_ws was about double (410 kDa) that of sarkaran, but also displayed a small quantity of a very high M_w (> 1 million Da) EPS. Similar to sarkaran, it appears that the EPSs prepared from *P. sacchari* can vary in molecular weight, depending on the cultivation conditions. In general, all the EPSs had average molecular weights higher than the model pullulan compound (M_w = 328 kDa) and higher than the values reported for sarkaran. However, it is also important to note that molecular weights determined by relative techniques are difficult to compare unless all parameters are identical. In each study discussed, the molecular weights were determined by different techniques and by using different standards.

The greatest difference between the identified structures of the *P. sacchari* EPSs and that surrounding the literature on sarkaran, lies in the minor mannose and galactose components

confirmed in the former. The literature was critically reviewed, and several possibilities were explored to explain why the mannose and galactose components identified together with sarkaran were not identified as part of its structure. It is again important to note that all sarkaran samples analysed prior to 2005 were isolated from sugarcane or sugar processing streams (*i.e.*, expressed cane juice, syrup and molasses). These sources provided complex and varied matrices from which all alcohol-insoluble products would have co-precipitated, together with sarkaran. Sutherland (1960), Blake and Littlemore (1984a and b), and Blake and Clarke (1984a and b) acknowledged this, and assumed that all the non-glucans isolated together with sarkaran were due to co-precipitated hemicelluloses, such as arabinogalactan. In all these reported studies, the crude sarkaran isolates contained significant levels of galactose and mannose, which were largely removed by several fractionation and/or purification steps. In the present study, the crude *P. sacchari* EPSs comprised largely α-D-glucopyranoses, *i.e.*, 97.8% (FB2), 99.3% (PB2) and 98.6% (PB7). The balance comprised trace amounts of galactose and mannose, as detected by GC-MS/MS in all three of the crude EPSs and purified fractions of FB2. For the three EPSs, the quantity of mannose and galactose varied depending on the cultivation conditions. The concentration of these minor components also varied between the fractions of FB2. Overall, the very high molecular weight fraction (FB2 F1), comprising 12% of the crude FB2 sample, was richest in galactose (~20%) and mannose (~10%). Despite these seemingly high levels, their contribution was largely diluted by the glucan component (97.8%) of FB2. The bulk fraction of the same EPS (FB2 F2) contained trace amounts of galactose and mannose (<0.1%), and these were almost undetectable by GC-MS and GC-MS/MS analyses, and undetectable by NMR and HPAEC-PAD analyses. Similarly, detection and confirmation of galactose and mannose in the crude EPSs was only possible with GC-MS and GC-MS/MS analyses.

If the various sarkaran samples analysed in literature were likely to contain mannose and galactose in their structure, these may have been overlooked for a number of reasons. Primarily, since these components were assumed to belong to co-precipitated hemicellulose impurities, several steps were taken to remove these when they were detected in significant concentrations. Secondly, these components were ignored when they were detected in trace amounts. In all the cases where these so-called impurity fractions were detected, however, none were analysed to confirm their nature. In one study, Blake and Littlemore (1984b) isolated crude sarkaran samples containing significant amounts of galactose, mannose and other components from molasses samples. The crude sample had to undergo several chromatographic separations, followed by digestion with both β-amylase and dextranase, to remove the perceived impurity-containing components from the target sarkaran glucan. It is possible that the chromatographic steps incorporated caused any minor fractions of sarkaran that may have contained appreciable amounts of mannose and galactose (analogous to FB2 F1) to be excluded. Then, it is possible that the bulk glucan remaining from the chromatographic separations may, or may not, have still contained smaller amounts of galactose and mannose (analogous to FB2 F2). Then the subsequent enzyme treatments could have cleaved any terminal mannose or reducing-end galactoses remaining on the glucan structure before the final product was analysed. The glucan component surviving all the purification steps was analysed by low resolution NMR, periodate oxidation and pullulanase degradation and was described as "*essentially sarkaran*", without quoting the final purity (Blake and Littlemore, 1984b). Further evidence to support that mannose and galactose were part of the sarkaran structure in early studies is found in the investigation conducted by Blake and Clarke (1984b). In this study, crude samples were isolated from the juice of cane that was established as having high concentrations of sarkaran by pullulanase digestion and HPLC-RI analyses. These isolates were purified by two different chromatographic separations, but an "*arabinogalactan impurity*" persisted in the final product. The authors did not quantify or verify the impurity, but rather chose to ignore it as they believed it would not interfere with their examination of the bulk properties of sarkaran (Blake and Clarke, 1984b).

Since the literature has shown that cultivation conditions affect the molecular weights as well as the malto-oligomer arrangements and ratios of the glucan component of sarkaran, it is also conceivable that similar variations in the quantity and distribution of galactose and mannose can occur. This variation would explain why some sarkaran isolates in the literature required many more separation and conversion steps to obtain a pure, or near pure, glucan product. In addition, various reports on pullulan-producers suggest that differences in fungal strains and/or culture conditions affect the composition of pullulan products. Accepted anomalies in pullulan include possible branches and, more recently, DP4 subunits in excess of 7%. Due to these variations, similar EPSs are now classed into a family called "*pullulans*" (Forabosco *et al.*, 2006). Furthermore, pullulan production with *A. pullulans* and *C. parasitica* has produced both classic pullulan and pullulans containing trace amounts (<5%) of galactose and mannose (Forabosco *et al.*, 2006; Zajic and LeDuy, 1973).

The last point worth noting looks to the work carried out by Blake and Clarke (1984a) in their attempt to identify the causative organism for sarkaran. The authors had isolated four fungi from sarkaran-laden cane and cultivated these on synthetic cane juice. The arising EPSs contained high levels of mannose, glucose and galactose. Unfortunately, the authors did not characterise the EPSs further. They concluded that the isolated organisms were not sarkaran producers, despite acknowledging that the conditions they were tested under may not have been conducive for sarkaran biosynthesis (Blake and Clarke, 1984b). It would certainly have been telling if the glucan components of these EPSs were found to comprise malto-oligomers. It would also certainly have been telling if any of these fungi were found to be *P. sacchari*.

Similar to the early suspicions by Catley and co-workers (1966) regarding pullulan, analysis of the literature also suggests that there may be "*no unique structure*" for sarkaran (Catley *et al.*, 1966b). Certainly, the EPSs prepared from *P. sacchari* contained 97.8-99.3% of a glucan component sharing similar malto-oligosaccharide structures as described for sarkaran in the literature. Consequently, this study provides a more definitive link between *P. sacchari* and sarkaran. By adopting a similar view of sarkaran as Forabosco and co-workers (2006) did of pullulan, glucans named "*sarkaran*" can be considered as belonging to a class of EPSs called *sarkarans*, of which *P. sacchari* is a confirmed producer. Hence, the sarkarans prepared in this study had M_ws ranging from 410 kDa to over 1 million kDa and comprised a variety of α-D-glucopyranose malto-oligosaccharides from DP2-DP7 (and above), predominated by DP3 and DP4, and sometimes capped by terminal β-D-mannopyranoses and reducing-end β-D-galactopyranoses. This novel and comprehensive body of work demonstrates that sarkarans prepared *in vitro* from *P. sacchari* are complex, linear heteropolysaccharides, consisting largely of α-malto-oligosaccharides.

Through understanding both the cause and nature of sarkarans, the sugar industry could look to targeted approaches to reducing the impact of sarkaran. From an agricultural stance, the occurrence of *P. sacchari* could be minimised through application of appropriate fungicides. If *P. sacchari* infection is unavoidable, sarkaran production can be minimised through shortening delays between harvesting and crushing. From a milling perspective, the deleterious effect of sarkaran on processing streams can be minimised by investigating the application of pullulanse or other appropriate hydrolytic enzymes when processing cane with high levels of sarkaran. On the other hand, various fermentation strategies for *P. sacchari* can be explored to produce sarkaran products with desired characteristics specific to end-user requirements. In this study, the three sarkaran products prepared from *P. sacchari* were demonstrated to be effective viscosity modifying agents. These sarkarans were able to form clear native, peracetate and sorbitol-plasticised films. The native and plasticised films revealed that differences in MW and MW distribution play a primary role in the film mechanical properties.

Chapter 6
Conclusions

Sarkaran is described as a polyglucan believed to be a class of pullulans (Morel du Boil, 2000a) and has been implicated in processing difficulties of standover cane (Fulcher and Inkerman, 1976). *P. sacchari* is a fungal pathogen that affects sugarcane damaged by either frost or drought; it causes rind disease and sour rot and is particularly prevalent in the Midlands region, in South Africa (McFarlane and Bailey, 2001; Morel du Boil *et al.*, 2005). Morel du Boil and co-workers at the SMRI had previously isolated and positively identified this fungal organism from infected cane. After establishing that this fungus produces EPSs with molar equivalents of DP3 and DP4, the authors suggested that *P. sacchari* is the causal agent of sarkaran (Morel du Boil, *et al.*, 2005). Since then, the SMRI has been preparing EPS material from the same *P. sacchari* isolate under various fermentations conditions. These EPSs required extensive characterisation in order to confirm that *P. sacchari* produces sarkaran. Hence, the main objective of this investigation was to elucidate the primary structure of several cultivations of *P. sacchari* EPSs and to confirm whether these are sarkaran. An extension of this study was to determine some physical characteristics of these EPSs, including their molecular weight properties, solution behaviour and film mechanical properties. Pullulan was used as a model compound throughout this study to validate the methods employed and to compare the *P. sacchari* EPSs, as no standard for sarkaran exists.

Two of the *P. sacchari* EPSs studied were cultured in shake-flasks (PB2 and PB7) whilst one other was cultured in a bioreactor (FB2) under a different set of culture conditions. These EPSs required characterisation and were provided as crude isolates from their fermentation broths by the SMRI laboratory. Analysis commenced with the molecular weight and molecular weight distribution assessments of pullulan and the three EPSs as well as the subsequent purification of FB2 by GFC. The three FB2 fractionates, the three crude EPSs and pullulan were further characterised. The monosaccharide composition, absolute configuration and linkage information were established through analysis by GC-MS. The conformation and oligosaccharide repeat units of the biopolymer chains were established by means of ID and 2D NMR spectroscopy, as well as with pullulanase hydrolysis and HPAEC-PAD analysis against authentic standards up to DP7. These results allowed comparisons between pullulan, the purified EPS fractionates and the three crude EPSs to be made, and then the EPSs were compared to the literature on sarkaran.

The literature suggests that sarkaran isolated from sugarcane sources is a linear, polyglucan of molecular weights between 30-260 kDa and comprises malto-oligosaccharides between DP2-DP6, predominated by either DP3 or DP4 subunits. Comprehensive analysis of the *P. sacchari* EPSs revealed structures that very closely resembled those reported for sarkaran. The crude EPSs comprised largely α-D-glucopyranoses (≥97.8%) arranged in a series of malto-oligomers, including DP2-DP6 also with either DP3 or DP4 predominating. The differences between the EPSs and the reported structures for sarkaran included a greater complexity in malto-oligomer arrangements, higher overall molecular weights and the presence of trace amounts of mannose and galactose (≤2.2%). Review of the literature on sarkaran provided evidence that the structure and molecular weights of sarkaran are variable, and that these variations depend on several factors. These factors include: differences in the source and/or culture conditions, differences in isolation and purification steps followed to remove co-precipitating matrix impurities, differences in analysis techniques, limitations due to the resolution capability or sensitivity of the analyses used, and differences in the degree of detail to which the sarkaran (or

impurities) was studied and reported. Since the literature could not provide a definitive structure for sarkaran, this polysaccharide must be viewed as belonging to a class of EPSs called *sarkarans*.

A major consideration is that naturally occurring sarkarans were produced under various conditions and were isolated from different and complex matrices together with co-precipitating compounds. On the other hand, the EPSs investigated in this study were cultured from a pure isolate of the fungal pathogen under a defined set of conditions. Even so, the *P. sacchari* EPSs also showed a degree of variability, depending on whether they were cultured in shake-flasks or a bioreactor. Variations were evident in their molecular weight distributions, complexities and arrangements of malto-oligomer subunits and concentrations of trace components. Despite these differences, FB2, PB2 and PB7 were essentially the same polysaccharide and essentially the same as sarkaran. Hence, the sarkarans prepared from *P. sacchari* in this study had M_ws ranging from 410 kDa to over 1000 kDa. These sarkarans comprised a variety of α-D-glucopyranose malto-oligosaccharides ranging between DP2 and DP10, which were predominated by DP3 and DP4, and sometimes capped by terminal β-D-mannopyranoses and reducing-end β-D-galacto-pyranoses. Optimisation of the fermentation conditions results in sarkarans with variable physical properties that have the potential of being adapted for niche biopolymer applications. An investigation of the rheological and film-forming properties of isolated sarkarans or sarkarans produced from *P. sacchari* has, *hitherto*, never been reported. The findings from this study suggest that *P. sacchari* sarkarans are capable of forming structured, shear-thinning solutions that are more viscous than similarly prepared pullulan solutions. Furthermore, *P. sacchari* sarkarans are also able to form clear and transparent biofilms that can potentially be tuned to satisfy end-user applications based on different cultivation conditions and the addition of plasticisers such as sorbitol.

This comprehensive and novel body of work demonstrates that sarkarans prepared *in vitro* from *P. sacchari* are complex, linear heteropolysaccharides, consisting largely of α-malto-oligosaccharides, with potentially tunable characteristics. Through having a definitive understanding of both the origin and structure of sarkarans, the sugar industry can now look toward targeted approaches to reducing the deleterious effects of these polysaccharides in the industry. These approaches may include looking to appropriate fungicides for prevention of *P. sacchari* infestations or investigating cost-effective hydrolytic enzymes for sarkaran eradication. On the other hand, exploration of various fermentation strategies for *P. sacchari* may lead to the production of sarkaran products with desired characteristics specific to end-user requirements. In this way, the sugar industry can rather stand to benefit from a polysaccharide that otherwise has plagued the industry from time to time.

References

Abdel-Akher M, Hamilton JK, Montgomery R and Smith F (1952). A new procedure for the determination of the fine structure of polysaccharides. *Journal of the American Chemical Society*. **74** (19):4970-4971.

Abdel-Akher M, Hamilton JK and Smith F (1951). The reduction of sugars with sodium borohydride. *Journal of American Chemical Society*. **73** 4691-4692.

An L (2014). Inferential tools for multiple regression. 98-106. 14 June 2016, <ag.arizona.edu/classes/rnr613/Notes10.pdf>

Anonymous (n.a.) GPC/SEC Theory: Conventional Calibration Malvern Instruments Ltd, 06 May 2009, <http://www.malvern.com/LabEng/technology/gel_permeation_chromatography_theory/conventional_calibration_gpc_theory.htm>

Anonymous (2008) Size exclusion chromatography. The physical properties of the base beads for all Toyopearl Products. Tosoh Bioscience, 16 September 2009, <http://www.separations.eu.tosohbioscience.com/NR/rdonlyres/3C7695EF-000D-4311-9ADB-CF4BA8BE82E5/0/C08P04A1_SEC_Chapter_ProcessCatalog.pdf>

Anonymous (2004) Toyopearl® and TSK-GEL 5PW Instruction Manual. Tosoh Biosciences, <http://www.separations.asia.tosohbioscience.com/NR/rdonlyres/50AEB751-2189-48FC-8B9A-F994CFECA891/0/IM02_PackingGuide.pdf>

Anonymous (1996) Enzymatic Assay of Pullulanase. Sigma-Aldrich, 14 October 2014, <https://www.sigmaaldrich.com/content/dam/sigma-aldrich/docs/Sigma/Enzyme_Assay/pullulanase.pdf>

Anonymous (2016a) Mechanical properties of plastic materials. Professional Plastics, <http://www.professionalplastics.com/>

Anonymous (2011). Guidelines for the quantitative gas chromatography of volatile flavouring substances, from the Working Group on Methods of Analysis of the International Organization of the Flavor Industry (IOFI). *Flavour and Fragrance Journal*. **26** 297-299.

Anonymous (2016b) Product 134031 B-D-galactose pentaacetate FT-NMR spectrum. Sigma-Aldrich, 09 June 2016, <www.sigmaaldrich.com/catalog/product/aldrich/134031>

Anonymous (2015). Product Specification P5420. 1.

Anonymous (2013) Elastic properties and Young's modulus for some materials. The Engineering Toolbox, 6 February 2013, <www.engineeringtoolbox.com/youngs-modulus-d_417.html>

Anonymous (2012) Nylon 6/6 glass fibre reinforced (PA66-GF). <http://www.grantadesign.com/products/data/materialuniverse.htm>

Anonymous (2006). Material safety and data sheet: Extran(R) MA02. 1-6.

Aspinall GO (1982a). Chemical characterization and structure determination of polysaccharides. pp. 35-124. In: GO Aspinall (Ed). *The Polysaccharides*. **1**. Academic Press, Inc., New York.

Aspinall GO (1982b). Isolation and fractionation of polysaccharides. pp. 19-35. In: GO Aspinall (Ed). *The Polysaccharides*. **1**. Academic Press, Inc., New York.

Azwar E and Hakkarainen M (2012). Tuning mechanical properties of tapioca starch by plasticizers, inorganic fillers and agrowaste-based fillers. *ISRN Polymer Science*. **2012** 1-7.

Baba Hamed S and Belhadri M (2009). Rheological properties of biopolymers drilling fluids. *Journal of Petroleum Science and Engineering*. **67** (3-4):84-90.

Barnes HA (2000). A Handbook of Elementary Rheology. The University of Wales Institute of Non-Newtonian Fluid Mechanics, Aberystwyth. pp 1-210.

Barth HG (2003). High-performance SEC column technology. *LC GC Europe: Recent developments in LC column technology*. 2-6. 29 September 2010, <http://www.lcgceurope.com/lcgceurope/data/articlestandard/lcgceurope/232003/59049/article.pdf>

Berg JM, Tymoczko JL and Stryder L (2002) Biochemistry. 5th Edition. W.H.Freeman and Company, New York, 23 May 2009, <http://www.ncbi.nlm.nih.gov/bookshelf/br.fcgi?book=stryer&part=A438>

Bhat SA, Nagasampagi BA and Sivakumar M (2005). Chemistry of natural products. Springer, Berlin. pp 475.

Bixler GH, Hines GE, McGhee RM and Shurter RA (1953). Dextran. *Industrial & Engineering Chemistry*. **45** (4):692-705.

Blake JD and Clarke ML (1984a). A water-soluble plysaccharide from stand-over cane. Part III. Studies on the measurement of sarkaran. *International Sugar Journal*. **86** 255-259.

Blake JD and Clarke ML (1984b). A water-soluble polysaccharide from stand-over cane. Part IV. Studies of the physical properties and origin of sarkaran. *International Sugar Journal*. **86** 276-279.

Blake JD and Littlemore J (1984a). A water-soluble polysaccharide from standover cane. Part I. Isolation and structural characterisation from the field. *International Sugar Journal*. **86** 222-226.

Blake JD and Littlemore J (1984b). A water-soluble polysaccharide from stand-over cane. Part II. Isolation and structure characterisation from molasses. *International Sugar Journal*. **86** 235-239.

Bleton J, Mejanelle P, Sansoulet J, Goursaud S and Tchapla A (1996). Characterization of neutral sugars and uronic acids after methanolysis and trimethylsilylation for recognition of plant gums. *Journal of Chromatography A*. **720** (1-2):27-49.

Bochkov AF, Zaikov GE and Afanasiev VA (1991). Carbohydrates. VSP, Den Haag. pp 63-64.

Bock K and Pedersen C (1974). A study of ^{13}CH coupling constants in hexopyranoses. *Perkin Transactions 2*. (3):293-297.

Bourdichon F, Casaregola S, Farrokh C, Frisvad JC, Gerds ML, Hammes WP, Harnett J, Huys G, Laulund S, Ouwehand A, Powell IB, Prajapati JB, Seto Y, Ter Schure E, Van Boven A, Vankerckhoven V, Zgoda A, Tuijtelaars S and Hansen EB (2012). Food fermentations: Microorganisms with technological beneficial use. *International Journal of Food Microbiology*. **154** (3):87-97.

Bourne M (2002). Food Texture and Viscosity: Concept and Measurement. 2nd Edition. Academic Press, London. pp 59-90.

Bruice PY (2004). Organic chemistry. 4th. Pearson Prentice Hall, New Jearsey. pp 526-530.

Bruijn J (1973). Changes in the chemical composition of sugar cane (*Saccharum officinarum*) during storage. University of Natal, Durban.

Bruijn J (1966a). Deterioration of sugar cane after harvesting. Part I. Changes in juice composition. *International Sugar Journal*. **68** 331-334.

Bruijn J (1966b). Deterioration of sugar cane after harvesting. Part II. Investigation of the polysaccharide formed. *International Sugar Journal*. **68** 356-358.

Bruijn J (1970). Deterioration of sugar cane after harvesting. Part III. Enzymatic hydrolysis of the polysaccharide formed. *International Sugar Journal*. **72** 195-198.

Buchanan CM, Hyatt JA and Lowman DW (1987). Two-Dimensional NMR of polysaccharides: Spectral assignments of cellulose triesters. *Macromolecules*. **20** (11):2750-2754.

Bui B, Saasen A, Maxey J, Ozbayoglu ME, Miska SZ, Yu M and Takach NE (2012). Viscoelastic properties of oil-based drilling fluids. *Annual Transactions of the Nordic Rheology Society*. **20** 33-47.

Busuioc M, Mackiewicz K, Buttaro BA and Piggot PJ (2009). Role of intracellular polysaccharide in persistence of *Streptococcus mutans*. *Journal of Bacteriology*. **191** (23):7315-7322.

Callister WD (2001). Fundamentals of material science and engineering. An interactive eText. Fifth Edition. John Wiley & Sons, Inc., New York. pp 148-229.

Carpita NC and Shea EM (1988). Linkage structure of carbohydrates by gas chromatography-mass spectrometry (GC-MS) of partially methylated alditol acetates. pp. 292. In: CJ Biermann and GD McGinnis (Ed). *Analysis of carbohydrates by GLC and MS*. CRC Press, New York.

Cataldi TRI, Campa C and Benedetto GED (2000). Carbohydrate analysis by high-performance anion-exchange chromatography with pulsed amperometric detection: The potential is still growing. *Fresenius Journal of Analytical Chemistry*. **368** 739-758.

Catley BJ, Ramsay A and Servis C (1986). Observations of the structure of the fungal extracellular polysaccharide, pullulan. *Carbohydrate Research*. **153** (1):79-86.

Catley BJ, Robyt JF and Whelan WJ (1966). Minor structural feature of pullulan. *Biochemical Journal*. (100):5-8.

Cheng HN and Neiss TG (2012). Solution NMR spectroscopy of food polysaccharides. *Polymer Reviews*. **52** 81-114.

Cheng K-C, Demirci A and Catchmark JM (2011). Pullulan: biosynthesis, production, and applications. *Applied Microbiology and Biotechnology*. **92** (1):29-44.

Chronakis IS and Ramzi M (2002). Isotropic-nematic phase equilibrium and phase separation of K–carrageenan in aqueous salt solution: experimental and theoretical approaches. *Biomacromolecules*. **3** 793-804.

Churms SC (1996). Recent progress in carbohydrate separation by high-performance liquid chromatography based on size exclusion. *Journal of Chromatography A*. **720** (1-2):151-166.

Ciucanu I and Caprita R (2007). Per-*O*-methylation of neutral carbohydrates directly from aqueous samples for gas chromatography and mass spectrometry analysis. *Analytica Chimica Acta*. **585** 81-85.

Claridge TDW (1999). High-resolution NMR techniques in organic chemistry. **19**. Elsivier, Oxford. pp 221-258.

Clark AH (2000). Polysaccharide gelatin. pp. 89-165. In: PA Williams and GO Phillips (Ed). *Gums and stabilisers for the food industry*. **10**. The Royal Society of Chemistry, Cambridge.

Courtin CM, Van den Broeck H and Delcour JA (2000). Determination of reducing end sugar residues in oligo- and polysaccharides by gas-liquid chromatography. *Journal of Chromatography A*. **866** (1):97-104.

Cuddihy Jr JA, Porro ME and Raiih JS (2001). The presence of total polysaccharides in sugar production and methods for reducing their negative effects. *J. Am. Soc. Sugar Cane Technol.* **21** 73-91.

Cui SW (2005). Structural analysis of polysaccharides. pp. 105-157. In: SW Cui (Ed). *Food Carbohydrates: Chemistry, Physical Properties, and Applications*. Taylor & Francis,

Cui SW (2002). Application of two Dimensional (2D) NMR spectroscopy in the structural analysis of selected polysaccharides. pp. In: PA Williams and GO Phillips (Ed). *Gums and Stabilisers for the Food Industry 11*. Royal Society of Chemistry, Cambridge.

Cui SW and Wang Q (2006). Functional properties of carbohydrates. pp. 1-15. In: YH Hui (Ed). *Handbook of food science, technology, and engineering*. **1**. CRC Press, New York.

Cummins C and Sutton K (2005). The production of microbial polysaccharides. University of Dublin, Dublin. pp 1-10

Dag S (2005). Structural studies of some bacterial lipopolysaccharides using NMR spectroscopy and mass spectroscopy. *Dissertation*. Swedish University of Agricultural Sciences, Uppsala.

Davis JR (2004). Tensile Testing. 2nd Edition. ASM International, Ohio. pp 1-14.

Davis MAF, Gidley MJ, Morris ER, Powell DA and Rees DA (1980). Intermolecular association in pectin solutions. *International Journal of Biological Macromolecules*. **2** 330.

Dea ICM (1993). Conformational Origins of Polysaccharide Solution and Gel Properties. pp. 21-55. In: JN BeMiller and RL Whistler (Ed). *Industrial Gums: Polysaccharides and Their Derivatives.* Academic Press, Inc., London.

Delben F, Forabosco A, Guerrini M, Liut G and Torri G (2006). Pullulans produced by strains of *Cryphonectria parasitica*-II. Nuclear magnetic resonance evidence. *Carbohydrate Polymers*. **63** 545-554.

Determann H (1969). Gel chromatography. Second. Springer-Verlang, Berlin. pp 1-52, 64-129.

Diab T, Biliaderis CG, Gerasopoulos D and Sfakiotakis E (2001). Physicochemical properties and application of pullulan edible films and coatings in fruit preservation. *Journal of the Science of Food and Agriculture*. **81** 988-1000.

Dixon MB, Abbott PJ, Verger P, Pascal G and DiNovi M (2006). Pullulan. pp. In: (Ed). *Safety evaluation of certain food additives*. World Health Organisation, Geneva.

Djabourov M, Nishinari K and Ross-Murphy SB (2013). Physical gels from biological and synthetic polymers. Cambridge University Press, New York. pp 48-170.

Dobruchowska JM, Gerwig GJ, Babuchowski A and Kamerling JP (2008). Structural studies on exopolysaccharides produced by three different propionibacteria strains. *Carbohydrate Research*. **343** (4):726-745.

Dubois M, Gilies KA, Hamilton JK, Rebers PA and Smith F (1956). Colorimetric methods of determination of sugar and related substances. *Analytical Chemistry*. **28** 350-356.

Duedahl-Olesen L, Matthias Kragh K and Zimmermann W (2000). Purification and characterisation of a malto-oligosaccharide-forming amylase active at high pH from *Bacillus clausii* BT-21. *Carbohydrate Research*. **329** (1):97-107.

Farkas E, Janossy L, Harangi J, Kandra L and Liptak A (1997). Synthesis of chromogenic substrates of a-amylases on a cyclodextrin basis *Carbohydrate Research*. **303** 407-415.

Ferreira F, Andersson M, Kenne L, Cotta MA and Stack RJ (1995). Structural studies of the extracellular polysaccharide from *Butyrivibrio fibrisolvens* strain 49. *Carbohydrate Research*. **278** (1):143-153.

Forabosco A, Bruno G, Sparapano L, Liut G, Marino D and Delben F (2006). Pullulans produced by strains of Cryphonectria parasitica--I. Production and characterisation of the exopolysaccharides. *Carbohydrate Polymers*. **63** (4):535-544.

Fulcher RP and Inkerman PA (1976). Dextranase. I. Characterization of the enzyme for use in sugar mills. *Proceedings of the Queensland Society of Sugar Cane Technologists*. **43** 295-305.

Fulmer GR, Miller AJM, Sherden NH, Gottlieb HE, Nudelman A, Stoltz BM, Bercaw JE and Goldberg KI (2010). NMR Chemical shifts of trace impurities: Common laboratory solvents, organics, and gases in deuterated solvents relevant to the organometallic chemist. *Organometallics*. **29** (9):2176-2179.

Gavilan (2002) GFC from PeakSimple data aquisition. SRI Instruments, 06 June 2010, <www.srigc.com/gpc.pdf >

Ge Y, Duan Y, Fang G, Zhang Y and Wang S (2009). Polysaccharides from fruit calyx of *Physalis alkekengi* var. francheti: Isolation, purification, structural features and antioxidant activities. *Carbohydrate Polymers*. **77** (2):188-193.

Gelders GG, Bijnens L, Loosveld A-M, Vidts A and Delcour JA (2003). Fractionation of starch hydrolysates into dextrins with narrow molecular mass distribution and their detection by high-performance anion-exchange chromatography with pulsed amperometric detection. *Journal of Chromatography A*. **992** (1-2):75-83.

Gerwig GJ, Kamerling JP and Vliegenthart FG (1978). Determination of the D and L configuration of neutral monosaccharides by high-resolution capillary G.L.C. *Carbohydrate Research*. **62** 349-357.

Giordano A and Trincone A (2002). Freeing anomeric hydroxyl groups of peracetylated oligosaccharides by *Aspergillus niger* lipase. *Tetrahedron Letters*. **43** 4939-4942.

Girard JE (2010). Principles' of environmental chemistry. 2nd Edition. Jones and Bartlett Publishers, Sudbury. pp 430.

Goffin D, Bystricky P, Shashkov AS, Lynch M, Hanon E, Paquot M and Savage AV (2009). A systematic NMR determination of α-D-glucooligosaccharides, effect of linkage type, anomeric configuration and combination of different linkages type on ^{13}C chemical shifts for the determination of unknown maltooligosaccharides. *Bulletin of the Korean Chemical Society*. **30** (11):2535-2541.

Gottlieb HE, Kotlyar V and Nudelman A (1997). NMR Chemical shifts of common laboratory solvents as trace impurities. *Journal of Organic Chemistry*. **62** 7512-7515.

Goux WJ (1990). Determination of complex carbohydrate structure using carbonyl carbon resonances of peracetylated derivatives. pp. 47-52. In: JW Finley, SJ Schmidt and AS Serianni (Ed). *NMR Applications in Biopolymers*. Plenum Press, New York.

Graham LD (2008). Biological Adhesives from Nature. pp. 236-245. In: GE Wnek and GL Bowlin (Ed). *Encyclopedia of Biomaterials and Biomedical Engineering*. Informa Healthcare, USA.

Guillouet S, Choi HJ, Rha KC and Sinskey JA (1999). Effects of yeast extract on the production and the quality of the exopolysaccharide, zooglan, produced by *Zoogloea ramigera* 115SLR. *Applied Microbiology and Biotechnology*. **51** (2):235-240.

Gusakov AV, Kondratyeva EG and Sinitsyn AP (2011). Comparison of Two Methods for Assaying Reducing Sugars in the Determination of Carbohydrase Activities. *International Journal of Analytical Chemistry*. **2011** 4.

Haddarah A, Bassal A, Ismail A, Gaiani C, Ioannou I, Charbonnel C, Hamieh T and Ghoul M (2014). The structural characteristics and rheological properties of Lebanese locust bean gum. *Journal of Food Engineering*. **120** 204-214.

Hagel L (1998). Gel-filtration chromatography. *Current Protocols in Protein Science*. **8.3.1-8.2.30.** 14:1-30. 03 June 2009, <http://www.nshtvn.org/ebook/molbio/Current%20Protocols/CPPS/ps0803.pdf>

Hakomori S-I (1965). A rapid permethylation of glycolipid, and polysaccharide catalyzed by methylsulfinyl carbanion in dimethyl sulfoxide *Journal of Biochemistry*. **55** 205-208.

Harding LP, Marshall VM, Hernandez Y, Gu Y, Maqsood M, McLay N and Laws AP (2005). Structural characterisation of a highly branched exopolysaccharide produced by *Lactobacillus delbrueckii* subsp. *bulgaricus* NCFB2074. *Carbohydrate Research*. **340** (6):1107-1111.

Heinze T, Liebert T and Koschella A (2006). Esterification of polysaccharides. Springer-Verlag, Berlin. pp 151-156.

Hepper C (1972). Composition of extracellular polysaccharides of *Rhizobium trifolii*. *Antonie van Leeuwenhoek*. **38** (1):437-445.

Hites RA (1997). Gas chromatography mass spectrometry. pp. 609-625. In: F Settle (Ed). *Handbook of instrumental techniques for analytical chemistry*. Prentice-Hall, Inc., New Jersey.

Huber CG and Bonn GK (1995). HPLC of carbohydrates with cation- and anion-exchange silica and resin-based stationary phases. pp. 147-180. In: ZE Rassi (Ed). *Carbohydrate analysis: high performance liquid chromatography and capillary electrophoresis*. **58**. Elsevier Sciences B.V, Amsterdam.

Huck CW, Huber CG and Bonn GK (2002). HPLC of carbohydrates with cation- and anion-exchange silica and resin-based stationary phases. pp. In: Z El-Rassi (Ed). *Carbohydrate analysis by modern chromatography and electrophoresis*. **86**. Elsevier, Amsterdam.

Imrie FKE and Tilbury RH (1972). Polysaccharides in sugar cane and its products. *Sugar Technology Reviews*. **1** 291-361.

Ismail B and Nielsen SS (2010). Basic principles of chromatography. pp. 476. In: (Ed). *Food Analysis*. Springer, London.

Jamshidian M, Jennrich RI and Liu W (2007). A study of partial F tests for multiple linear regression models. *Computational Statistics & Data Analysis*. **51** (12):6269-6284.

Janca J (1984). Field-flow fractionation. pp. 526. In: Z Deyl (Ed). *Separation Methods*. **8**. Elsevier, Amsterdam.

Jeans A (1977). Dextrans and Pullulans: Industrially significant a-D-glucans. pp. 284-298. In: PA Sandfor and A Laskin (Ed). *Extracellular microbial polysaccharides*. American Chemical Society,

Kajiwara K and Miyamoto T (2004). Progress in structural characterization of functional polysaccharides. pp. 1-11. In: S Dumitriu (Ed). *Polysaccharides: structural diversity and functional versatility*. CRC Press, New York.

Kalpakjian S and Schmidt SR (2008). Manufacturing processes for engineering materials. 5th Edition. Pearson Education, Illinois. pp 1-55.

Keeler J (2005). Understanding NMR spectroscopy. John Wiley & Sons Ltd, Chichester. pp 187-245.

Kim HM, Kim SW, Hwang HJ, Park MK, Mahmoud Y-G, Choi JW and Yun J (2006a). Influence of agitation intensity and aeration rate on the production of antioxidative exoplysaccharides from submerged mycelial culture of *Ganoderma resinaceum*. *Journal of Microbiology and Biotechnology*. **16** 1240-1247.

Kim HM, Paik S-Y, Ra KS, Koo KB, Yun J and Choi JW (2006b). Enhanced production of exopolysaccharides by fed-batch culture of *Ganderma resinaceum* DG-6556. *Journal of Microbology*. **44** 233-242.

Kitchen RA (1988). Polysaccharides of sugarcane and their effects on sugar manufacture. pp. 208-235. In: C MA and G MA (Ed). *Chemistry and processing of sugarbeet and sugarcane*. Elsevier, Amsterdam.

Kochetkov NK and Chizhov OS (1966). Mass spectrometry of carbohydrate derivatives. *Advances in Carbohydrate Chemistry*. **21** 39-93.

Kost J and Shefer S (1990). Chemically-modified polysaccharides for enzymatically-controlled oral drug delivery. *Biomaterials*. **11** (9):695-698.

Kroon G, Gortz CM and Lusvardi KM (2008) Patent title: Mixed hydrophobe polysaccharide as polymeric emulsifier and stabilizer. AA61K4738FI

Laignel B, Bliard C, Massiot G and Nuzillard JM (1997). Proton NMR spectroscopy assignment of D-glucose residues in highly acetylated starch. *Carbohydrate Research.* **298** 251-260.

Laine C, Tamminen T, Vikkula A and Vuorinen T (2002). Methylation analysis as a tool for structural analysis of wood polysaccharides. *Holzforschung*. **56** (6):607-614.

Lammerts van Bueren A, Ficko-Blean E, Pluvinage B, Hehemann J-H, Higgins MA, Deng L, Ogunniyi D, Stroeher UH, El Warry N, Burke RD, Czjzek M, Paton JC, Vocadlo DJ and Boraston AB (2011). The conformation and function of a multimodular glycogen-degrading pneumococcal virulence factor. *Structure*. **19** (5):640–651.

Lapasin R and Pricl S (1995). Rheology of Industrial Polysaccharides: Theory and Applications. First. Chapman & Hall, Glasgow. pp 1-46, 134-150, 163-214, 267-277, 507-522.

Lapasin R, Pricl S and Tracanelli P (1991). Rheology of hydroxyethyl guar gum derivatives. *Carbohydrate Polymers*. **14** (4):411-427.

Lazaridou A, Biliaderis CG and Izydorczyk MS (2003a). Molecular size effects on rheological properties of oat β-glucans in solution and gels. *Food Hydrocolloids*. **17** (5):693-712.

Lazaridou A, Biliaderis CG and Kontogiorgos V (2003b). Molecular weight effects on solution rheology of pullulan and mechanical properties of its films. *Carbohydrate Polymers*. **52** 151-166.

Lazaridou A, Biliaderis CG, Roukas T and Izydorczyk M (2002a). Production and characterization of pullulan from beet molasses using a nonpigmented strain of Aureobasidium pullulans in batch culture. *Appl Biochem Biotechnol*. **97** (1):1-22.

Lazaridou A, Roukas T, Biliaderis CG and Vaikousi H (2002b). Characterization of pullulan produced from beet molasses by *Aureobasidium pullulans* in a stirred tank reactor under varying agitation. *Enzyme and Microbial Technology*. **31** (1-2):122-132.

Leathers TD (2003). Biotechnological production and applications of pullulan. *Applied Microbiology and Biotechnology*. **62** 468-473.

Lee J, Kim J, Zhu I, Zhan X, Lee J, Shin D and Kim S (2001). Optimization of conditions for the production of pullulan and high molecular weight pullulan by *Aureobasidium pullulans*. *Biotechnology Letters*. **23** 817-820.

Levin S (2002) GPC for students. BioForum Applied Knowledge Centre, 25 August 2010, <www.forumsci.co.il/HPLC/gpc_handouts.pdf >

Lindhorst TK (2000). Essentials of carbohydrate chemistry and biochemistry. Wiley-VCH, Weinheim. pp 3-31, 195-208.

Lopes da Silva JA and Rao MA (2006). Pectins: Structure, functionality, and uses. pp. 354-405. In: AM Stephen, GO Phillips and PA Williams (Ed). *Food polysaccharides and their applications*. Taylor & Francis Group, Boca Raton.

Lopez EC, Champion D, Blond G and Le Meste M (2005). Influence of dextran, pullulan and gum arabic on the physical properties of frozen sucrose solutions. *Carbohydrate Polymers*. **59** (1):83-91.

Manitchotpisit P, Skory CD, Leathers TD, Lotrakul P, Eveleigh DE, Prasongsuk S and Punnapayak H (2011). α-Amylase activity during pullulan production and α-amylase gene analyses of *Aureobasidium pullulans*. *Journal of Industrial Microbiology*. **38** 1211–1218.

Manivasagan P, Venkatesan J, Senthilkumar K, Sivakumar K and Kim S-K (2013). Isolation and characterization of biologically active melanin from Actinoalloteichus sp. MA-32. *International Journal of Biological Macromolecules*. **58** 263-274.

Marshall JJ (1974). Polysaccharide analysis by enzymatic methods. *Advances in Carbohydrate Chemistry and Biochemistry*. **30** 257-370.

Matheson NK and McCleary BV (1985). Enzymes metabolizing polysaccharides and their application to the analysis of structure and function of glycans. pp. 1-105. In: GO Aspinall (Ed). *The Polysaccharides*. **3**. Academic Press, Inc., Orlando.

Mathur V and Mathur NK (2006). Microbial polysaccharides based food hydrocolloid additives. pp 1-10.

McCleary BV and Matheson NK (1986). Enzymatic analysis of polysaccharide structure. *advances in Carbohydrate Chemistry and Biochemistry*. **44** 147-276.

McFarlane SA and Bailey RA (2001). A stalk rot caused by *Phaeocytostroma sacchari* in the KwaZulu-Natal Midlands regio of South Africa. *Proceedings of the International Society of Sugar Cane Technologists*. **24** 456-458.

McIntyre DD and Vogel HJ (1991). NMR studies of homopolysaccharides related to starch. *Starch*. **43** 69-76.

Mekonnen T, Mussone P, Khalil H and Bressler D (2013). Progress in bio-based plastics and plasticizing modifications. *Journal of Materials Chemistry A*. **1** 13379-13398.

Meunier DM (1997). Molecular weight determinations. pp. 853-866. In: F Settle (Ed). *Handbook of instrumental techniques for analytical chemistry*. Prentice-Halll, Inc., New Jersey.

Mezger TG (2006). The Rheology Handbook: For Users of Rotational and Oscillatory Rheometers. 2nd Edition. Vincentz Network GmbH & Co., Hannover. pp 16-74.

Miller JN (1991). Basic statistical methods for analytical chemistry. Part 2. Calibration and regression methods. *Analyst*. **116** 3-14.

Mitchell JR (1979). Rheology of polysaccharide solutions and gels. pp. 62. In: JMV Blanshard and JR Mitchell (Ed). *Polysaccharides in Food.* Butterworths, London.

Miyoshi E and Nishinari K (1999). Non-Newtonian flow behaviour of gellan gum aqueous solutions. *Colloid Polymer Science*. **277** 727-734.

Mohsen MSA, Manal GM and Ghada SI (2007). Structural characterization and biological activity of acidic polysaccharide fractions Isolated from *Bacillus polymyxa* NRC-A. *Journal of Applied Sciences Research*. **3** (10):1170-1177.

Morel du Boil P (2000a). An enzymatic-HPAEC protocol for the analysis of polysaccharides in sugarcane products - dextran and sarkaran. *Proceedings of the South African Sugar Technologists' Association*. **74** 317-327.

Morel du Boil PG (2006). The occurence of sarkaran in the South African cane industry. TR1974. Sugar Milling Research Institute NPC, Durban. pp 1-33

Morel du Boil PG (2000b). An overview of the impact of poly- and oligosaccharides on sugar quality. 1-6.

Morel du Boil PG (2001). The analysis of dextran and sarkaran in cane products using enzymatic hydrolysis and HPAEC. *Proc. Int. Soc. Sug. Cane Technol.* **24** 53-58.

Morel du Boil PG and Wienese S (2002). Enzymatic reduction of dextran in process - laboratory evaluation of dextranases. *Proc. S. Afr. Sug. Technol Ass.* **76** 435-443.

Morel du Boil PG, Wienese S and Schooneed BM (2005). The cause of sarkaran in sugarcane. *Proceedings of the South African Sugar Technologists' Association*. **79** 48-62.

Mori S and Barth HG (1999). Size exclusion chromatography. Springer Laboratory, Berlin. pp 1-7, 77-89.

Müller CMO, Yamashita F and Laurindo JB (2008). Evaluation of the effects of glycerol and sorbitol concentration and water activity on the water barrier properties of cassava starch films through a solubility approach. *Carbohydrate Polymers*. **72** (1):82-87.

Nagamine T and Komae K (1996). Improvement of a method for chain-length distribution analysis of wheat amylopectin. *Journal of Chromatography A*. **732** 255-259.

Neeser J and Schweizer TF (1988). Analysis of carbohydrates as *O*-alkyloxime derivatives by gas-liquid chromatography (GLC). pp. 292. In: CJ Biermann and GD McGinnis (Ed). *Analysis of Carbohydrates by GLC and MS*. CRC Press, New York.

Nelson N (1944). A photometric adaptation of the Somogyi method for the determination of glucose. *The Journal of Biological Chemistry*. **153** 375-380.

Nicholson R and Lilienthal B (1959a). Formation of a Polysaccharide in Sugar-Cane. *Australian Journal of Biological Sciences*. **12** (2):192-203.

Nicholson RI and Lilienthal B (1959b). Formation of a Polysaccharide in Sugar-Cane. *Australian Journal of Biological Sciences*. **12** (2):192-203.

Nilsson GS, Richardson S, Huber A, Torto N, Laurell T and Gorton L (2001). Microdialysis clean-up and sampling in enzyme-based methods for the characterisation of starch. *Carbohydrate Polymers*. **46** (1):59-68.

Orlov ML (1996). Multiple linear regression analysis using Microsoft Excel. 1-19. 15 June 2016, <chemistry.oregonstate.edu/courses/ch361-464/ch464/RegrssnFnl.pdf>

Papagianni M (2004). Fungal morphology and metabolite production in submerged mycelial processes. *Biotechnology Advances*. **22** 189-259.

Patamaporn Sukplang BS (2000). Production and characterization of a novel extracellular polysaccharide produced by *Paenibacillus valaei*, sp. Nov. *Dissertation*. University of North Texas, Denton.

Perlin AS and Casu B (1982). Spectroscopic methods. pp. 133-195. In: GO Aspinall (Ed). *The Polysaccharides*. **1**. Academic Press, Inc., New York.

Persin Z, Stana-Kleinschek K, Foster TJ, van Dam JEG, Boeriu CG and Navard P (2011). Challenges and opportunities in polysaccharide research and technology: The EPNOE views for the next decade in areas of materials, food and health care. *Carbohydrate Polymers*. **84** (1):23-32.

Picout DR and Ross-Murphy SB (2003). Rheology of biopolymer solutions and gels. *The Scientific World Journal*. **3** 105-121.

Prajapati VD, Jani GK and S.M. K (2013). Pullulan: An exopolysaccharide and its various applications. *Carbohydrate Polymers*. **95** 540-549.

Pramanik M, Mondal S, Chakraborty I, Rout D and Islam SS (2005). Structural investigation of a polysaccharide (Fr. II) isolated from the aqueous extract of an edible mushroom, Pleurotus sajor-caju. *Carbohydrate Research*. **340** (4):629-636.

Pretsch E, Toth G, Munk ME and Badertscher M (2002). Computer-aided structure elucidation. Wiley-VCH, Weinheim. pp 279.

Pryde A and Gilbert MT (1979). Applications of high performance liquid chromatography. Chapman and Hall, New York. pp 50-52.

Qian MC, Peterson DG and Reineccius GA (2010). Gas chromatography. pp. 515-535. In: (Ed). *Food Analysis*. Springer, London.

Reece N, Campbell L and Roman S (2008). A comparative study of polysaccharides within the Jamaican sugarcane industry. *Proceedings of the West Indies Sugar Technologists' XXIX Conference*. 1-12.

Rees DA, Morris ER, Thom D and Madden JK (1982). Shapes and interactions of carbohydrate chains. pp. 195-290. In: GO Aspinall (Ed). *The Polysaccharides*. **1**. Academic Press, New York.

Robyt JF (2012). Essentials in carbohydrate chemistry. Springer, New York. pp 1-18.

Robyt JF (1998). Essentials of carbohydrate chemistry. Springer-Verlag, Iowa. pp 22-39, 48, 157-202, 345-359

Rochefort WE and Middleman S (1987). Rheology of xanthan gum: salt, temperature, and strain effects in oscillatory and steady shear experiments. *Journal of Rheology*. **31** 337.

Rodríguez M, Osés J, Ziani K and Maté JI (2006). Combined effect of plasticizers and surfactants on the physical properties of starch based edible films. *Food Research International*. **39** (8):840-846.

Roukas T and Liakopoulou-Kyriakides M (1999). Production of pullulan from beet molasses by *Aureobasidium pullulans* in a stirred tank fermentor. *Journal of Food Engineering*. **40** 89-94.

Ruas-Madiedo P and de los Reyes-Gavilan CG (2005). Invited Review: Methods for the screening, isolation, and characterization of exopolysaccharides produced by lactic acid bacteria. *J. Dairy Sci.* **88** (3):843-856.

Rumpel C and Dignac M-F (2006). Gas chromatographic analysis of monosaccharides in a forest soil profile: Analysis by gas chromatography after trifluoroacetic acid hydrolysis and reduction-acetylation. *Soil Biology and Biochemistry*. **38** (6):1478-1481.

Sahadeo P (1999). Further work on the effect of selected impurities on molasses exhaustion. Sugar Milling Research Institute, Technical Report No. 1802:, pp 1-9

Sahadeo P (1998). The effect of some impurities on molasses exhaustion. *Proc. S. Afr. Sug. Technol. Ass.* **72** 285-289.

Sahadeo P and Lionnet GRE (1999). An analytical survey of final molasses from fifteen cane producing countries. *Sugar Technol. Assoc. India*. 92-103.

Sandford PA (1979). Exocellular, microbial polysaccharides. pp. 265-313. In: R.S. Tipson and D Horton (Ed). *Advances in Carbohydrate Chemistry and Biochemistry*. **36**. Academic Press, New York.

Sani AM, Hedayati G and Arianfar A (2014). Effect of temperature and concentration on density and rheological properties of melon (*Cucumis melo* L. var. *Inodorus*) juice. *Nutrition and Food Science*. **44** (2):168-178.

Sanz ML and Martínez-Castro I (2007). Recent developments in sample preparation for chromatographic analysis of carbohydrates. *Journal of Chromatography A*. **1153** (1-2):74-89.

Schoonees BM (2004). Starch hydrolysis using α-amylase: a laboratory evaluation using response surface methodology. *Proc. S. Afr. Sug. Technol. Ass.* **78** 427-440.

Schoonees BM (2003). Use of enzymes for the reduction of starch in a sugar factory. SMRI Technical Bulletin 01/03. Sugar Milling Research Institute, Durban. pp 1-9

Shaffler KJ and Morel du Boil PG (1984). A review of gas chromatography in the South African sugar industry. Development and application of accurate methods for sugar analysis. *Sugar Technology Reviews*. **11** 95-185.

Shingel KI (2004). Current knowledge on biosynthesis, biological activity, and chemical modification of the exopolysaccharide, pullulan. *Carbohydrate Research*. **339** (3): 447-460.

Simas FF, Gorin PAJ, Wagner R, Sassaki GL, Bonkerner A and Iacomini M (2008). Comparison of structure of gum exudate polysaccharides from the trunk and fruit of the peach tree (*Prunus persica*). *Carbohydrate Polymers*. **71** (2):218-228.

Singh RS, Saini GK and Kennedy JF (2010). Maltotriose syrup preparation from pullulan using pullulanase. *Carbohydrate Polymers*. **80** (2):401-407.

Singh RS, Saini GK and Kennedy JF (2009). Downstream processing and characterization of pullulan from a novel colour variant strain of *Aureobasidium pullulans* FB-1. *Carbohydrate Polymers*. **78** (1):89-94.

Singh RS, Saini GK and Kennedy JF (2008). Pullulan: Microbial sources, production and applications. *Carbohydrate Polymers*. **73** (4):515-531.

Skoog DA, West DM, Holler FJ and Crouch SR (2004). Fundamentals of analytical chemistry. 8. Thomson Brooks/Cole, Belmont. pp 775-781, 811-817, 988-989.

Smith EEB, Mills GT, Harper EM and Galloway B (1957). The cellular polysaccharide of a type-II non-capsulated pneumococcus. *Journal of General Microbiology*. **17** 437-444.

Somogyi M (1945). A new reagent for the determination of sugars. *Journal of Biological Chemistry*. **160** 61-68.

Steffe JF (1996). Rheological Methods in Food Process Engineering. 2nd Edition. Freeman Press, Michigan. pp

Stephen AM and Churms SC (2006). Introduction. pp. 1-25. In: AM Stephen and GO Phillips (Ed). *Food Polysaccharides and Their Applications*. Taylor and Francis Group, USA.

Stroop CJM, Bush CA, Marple RL and LaCourse WR (2002). Carbohydrate analysis of bacterial polysaccharides by high-pH anion-exchange chromatography and online polarimetric determination of absolute configuration. *Analytical Biochemistry*. **303** 176-185.

Stulík K, Pacáková V and Tichá M (2003). Some potentialities and drawbacks of contemporary size-exclusion chromatography. *Journal of Biochemical and Biophysical Methods*. **56** (1-3):1-13.

Sutherland G (1960). An Investigation of the Polysaccharides Present in Sugar Mill Syrups. *Australian Journal of Biological Sciences*. **13** (3):300-306.

Sutherland IW (1996). Microbial biopolymers from agrivultural products: production and potential. *International Biodeterioration and Degradation*. **38** 34-261.

Svensson S, Lindberg B and Lonngren J (1975). Specific Degradation of Polysaccharides. pp. 185-240. In: RS Tipson and D Horton (Ed). *Advances in Carbohydrate Chemistry and Biochemistry*. **31**. Academic Press, New York.

Tao Y, Hasan H, Deeb G, Hu C and Han H (2016). Rheological and mechanical behviour of silk fibroin reinforced waterbourne polyurethane. *Polymers*. **8** (94):1-18.

Tezuka Y (1998). Pullulan nonaacetate: Assignement of chemical shifts of the acetyl protons and acetyl carbonyl carbons by 2D-NMR spectroscopy. *Carbohydrate Research*. **305** 155-161.

Timilsena YP, Adhikari R, Kasapis S and Adhikari B (2015). Rheological and microstructural properties of the chia seed polysaccharide. *International Journal of Biological Macromolecules*. **81** 991-999.

Torto N, Lobelo B and Gorton L (2000). Determination of saccharides in wastewater from the beverage industry by microdialysis sampling, microbore high performance anion exchange chromatography and integrated pulsed electrochemical detection. *Analyst*. **125** (8):1379-1381.

Toskoy Öner E (2013). Microbial production of extracellular polysaccharides from biomass. pp. 35-56. In: A Fang (Ed). *Pretreatment techniques for biofuels and biorefineries*. Springer-Verlang, Berlin.

Tsai CS (2007). Biomacromolecules: Introduction to structure, function, and informatics. John Wiley & Sons, New Jersey. pp 155-156.

Tsujisaka Y and Mitsuhashi M (1993). Pullulan pp. 447-460. In: R Whistler and JN BeMiller (Ed). *Industrial gums: Polysaccharides and their derivatives* Academic Press, Inc. , San Diego

Van Geel-Schutten GH, Faber EJ, Smit E, Bonting K, Smith MR, Ten Brink B, Kamerling JP, Vliegenthart JFG and Dijkhuizen L (1999). Biochemical and structural characterization of the glucan and fructan exopolysaccharides synthesized by the Lactobacillus reuteri wild-type strain and by mutant strains. *Applied and Environmental Microbiology*. **65** (7):3008-3014.

van Leeuwen SS, Kuipers BJH, Dijkhuizen L and Kamerling JP (2014). Development of a ^{1}H NMR structural-reporter-group concept for the analysis of prebiotic galacto-oligosaccharides of the [β-D-Gal*p*-(1–*x*]$_{n}$-D-Glc*p* type. *Carbohydrate Research*. **400** 54-58.

van Leeuwen SS, Leeflang BR, Gerwig GJ and Kamerling JP (2008). Development of ^{1}H NMR structure-reporter-group concept for the primary structural characterisation of α-D-glucans. *Carbohydrate Research*. **343** 1114-1119.

Vaningelgem F, Zamfir M, Mozzi F, Adriany T, Vancanneyt M, Swings J and De Vuyst L (2004). Biodiversity of exopolysaccharides produced by Streptococcus thermophilus strains is reflected in their production and their molecular and functional characteristics. *Applied and Environmental Microbiology*. **70** (2):900-912.

Vieira MGA, da Silva MA, dos Santos LO and Beppu MM (2011). Natural-based plasticizers and biopolymer films: A review. *European Polymer Journal*. **47** (3):254-263.

Viswanath DS, Ghosh TK, Prasad DHL, Dutt NVK and Rani KY (2007). Viscosity of Liquids: Theory, Estimation, Experiment, and Data. Springer, Dordrecht. pp 1-8.

Vliegenthart JFG (2006). Introduction to NMR spectroscopy of carbohydrates. pp. 1-19. In: JFG Vliegenthart and RJ Woods (Ed). *NMR spectroscopy and the modeling of carbohydrates. Recent advances*. American Chemical Society,

Vliegenthart JFG, van Halbeek H and Dorland L (1981). The applicability of 500-MHz high-resolution 1H-NMR spectroscopy for the structure determination of carbohydrates derived from glycoproteins. *Pure and Applied Chemistry*. **53** 45-77.

Vuorinen T and Alen R (1999). Carbohydrates. pp. 46-72. In: E Sjöström and R Alén (Ed). *Analytical Methods in Wood Chemistry, Pulping and Papermaking*. Springer, USA.

Wang Q and Wood PJ (2005). Carbohydrates: Physical properties. pp. 9-11. In: YH Hui (Ed). *Handbook of Food Science, Technology and Engineering*. **1**. Taylor & Francis Group, Florida.

Wen YH, Lin HC, Li CH and Hua CC (2004). An experimental appraisal of the Cox-Merz rule and Laun's rule based on bidispersed entangled polystyrene solutions. *Polymer*. **45** 8551-8559.

Willför S, Pranovich A, Tamminen T, Puls J, Laine C, Suurnäkki A, Saake B, Uotila K, Simolin H, Hemming J and Holmbom B (2009). Carbohydrate analysis of plant materials with uronic acid-containing polysaccharides-A comparison between different hydrolysis and subsequent chromatographic analytical techniques. *Industrial Crops and Products*. **29** (2-3):571-580.

Williams DH and Fleming I (1987). Spectroscopic methods in organic chemistry. 4th. McGraw-Jill Book Company (UK) Limited, London. pp 63-149.

Wolf C (2008). Dynamic stereochemistry of chiral compounds: principles and applications. The Royal Society of Chemistry, Cambridge. pp 40-41.

Wurzburg OB (2006). Modified starches. pp. 87-118. In: AM Stephen, GO Phillips and PA Williams (Ed). *Food polysaccharides and their applications*. Taylor & Francis, Florida.

Xiang Q, Lee YY, Petterson PO and Torget RW (2003). Heterogeneous aspects of acid hydrolysis of a-cellulose. pp. 505-514. In: DW Walt, BH Davison, JW Lee, JD McMillan and M Finkelstein (Ed). *Applied Biochemistry and Biotechnology. Biotechnology for fuels and chemicals: The twenty-fourth symposium*. **107**. Hermana Press Inc,

Xiao Q, Tong Q and Lim L-T (2012). Pullulan-sodium alginate based edible films: Rheological properties of film forming solutions. *Carbohydrate Polymers*. **87** 1689-1695.

Yang L and Zhang L-M (2009). Chemical structural and chain conformational characterization of some bioactive polysaccharides isolated from natural sources. *Carbohydrate Polymers*. **76** (3):349-361.

Yau WW, Striegel A, Kirkland JJ and Bly DD (2009). Modern size-exclusion liquid chromatography: Practice of gel permeation filtration chromatography. 2nd. John Wiley & Sons, Berlin. pp 200-203.

Youssef F, Roukas T and Biliaderis CG (1999). Pullulan production by a non-pigmented strain of *Aureobasidium pullulans* using batch and fed-batch cultures. *Process Biochemistry*. **34** 355-366.

Zajic JE and LeDuy A (1973). Flocculant and chemical properties of a polysaccharide from *Pullularia pullulans*. *Applied Microbiology*. **25** (4):628-635.

Zhigilei LV (2010). Introduction to material science. University of Virginia, Department of Material Science and Engineering, Virginia. pp 1-55.

Appendix A
Column packing and evaluation for gel filtration chromatography

As outlined in Chapter 3 and Chapter 4, GFC was the method selected to fractionate the crude FB2 *P. sacchari* EPS into its purified polysaccharide components, as well as to determine the MW, MWD and MW statistical averages of pullulan and all the *P. sacchari* EPSs (FB2, PB2 and PB7). This appendix provides further background to the experimental technique outlined in Section 4.1. Outlines for Toyopearl® resin preparation, column packing and packed column evaluation are provided herein.

A.1 Resin preparation and column packing parameters

This section explains the procedures for preparing the resin before packing the column, as well as the column packing procedure. These steps involve a resin de-fining step, a resin-solvent equilibrating step, the resin slurry preparing step, and then the column packing procedure.

A.1.1 Resin de-fining

Resin fines arise from broken beads and dirt. These fines eventually block the screens, frits or filters of the column – resulting in an undesirable increased pressure drop across the column. To de-fine the supplied resin, it must be washed with water or packing solvent until the supernatant solution above the settled resin is clear. This is achieved by stirring the resin in four volumes of solvent, settling the resin, then carefully decanting the liquid, and repeating the process. Care is needed in the stirring step; the sides of the vessel should be avoided as grinding the resin against the walls causes more fines.

A.1.2 Resin-solvent equilibrating

As mentioned in the previous paragraph, the resin can be de-fined in water or packing solvent. If the de-fining and packing solvents differ, then the resin is equilibrated against the packing solvent for several hours before packing can begin. There is a variety of packing solvent options available for Toyopearl® resins. Although a high ionic strength solvent is recommended, water can be used. When choosing an ionic strength buffer, care should be taken to pack with the highest ionic strength that will be used in separations. Ionic solvents for SEC include 0.1 M sodium sulfate/sodium nitrate/sodium chloride in 50 mM phosphate or Tris buffer (*i.e.*, tris(hydroxymethyl)aminomethane). Toyopearl® columns packed in ionic solvents exhibit higher theoretical plate counts and tend to have asymmetry values that approach unity (refer to Section A.3).

A.1.3 Resin slurry preparing

Following the de-fining and equilibrating steps for the resin preparation, a slurry is required to allow the resin to pour correctly into the column. The slurry concentration is calculated as the percentage settled resin of the total slurry volume. There are two methods of slurry preparation, volumetric or gravimetric. To prepare the resin slurry volumetrically, the resin is first left to settle in a graduated cylinder for more than 12 hours. Once settled and measured, enough packing buffer is added to make a final slurry concentration of 30-50%. It is also important to note that

the unpacked settled resin volume is approximately 1.1 times greater than the packed column volume – an important consideration if columns of fixed length are used. To determine the slurry concentration gravimetrically, the de-fined resin is filtered under suction and the appropriate amount of dried resin cake is weighed out (1 g cake = 1 cm^3 gravity settled resin) before being made to the final concentration with packing solvent.

A.2 Column packing

When packing HW resin columns the method of packing will depend on the available equipment. These columns can be packed by a constant velocity method, a semi-constant pressure method or by assisted gravitational settling. Generally, the equipment required includes a pump, a pressure gauge, a column (glass, acrylic, metal, *etc.*), a level and a reservoir. Regardless of the method chosen, the packing velocity for HW-65 columns is 40-150 cm hr^{-1}. In the semi-constant pressure method, optimal packing is achieved at 300 kPa. Assisted gravity was the method chosen to pack the two columns used in this investigation. For details regarding this method, refer to Section 4.1.1

A.3 Column evaluation

Once a SEC column has been packed, the efficacy of the packing procedure must be evaluated. This is achieved through determination of the theoretical number of plates (N) and the asymmetry at 10% of the peak height (A_s). These parameters are calculated per Equations A.1 and A.2, respectively.

$$N = 5.54\left(\frac{V_e}{W_{1/2}}\right)^2 \tag{A.1}$$

N is calculated according to Equation A.1, where V_e is the elution volume of the column and $W_{1/2}$ is the width of the peak at half height, as shown in Figure A.3.1. V_e is determined by eluting a low MW compound that will be retained by the resin through the column. This probe molecule can be acetone or sodium chloride (NaCl) (Hagel, 1998).

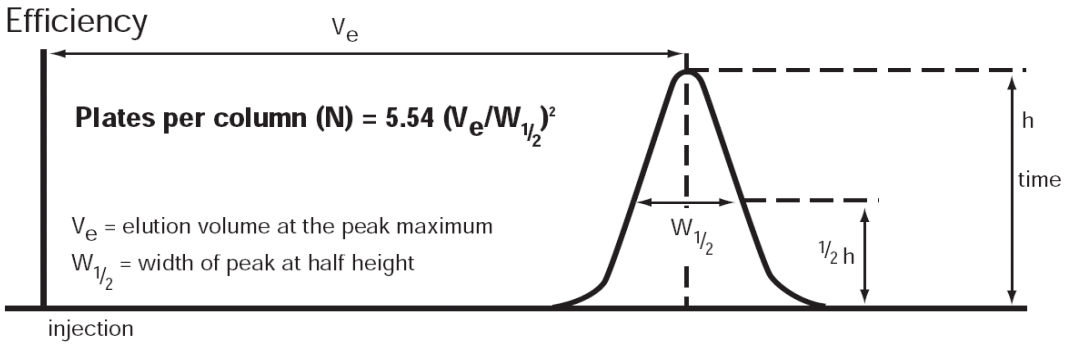

Figure A.3.1: Calculation of column efficiency by determination of the number of theoretical plates present (Anonymous, 2004).

$$A_s = {}^{b}/_{a} \qquad \text{(A.2)}$$

Equation A.2 calculates the A_s value, where b is the peak width to the right of the vertical from the peak vertex, and a is the peak width to the left of the vertical from the peak vertex, both measured at the 10 % peak height as shown in Figure A.3.2.

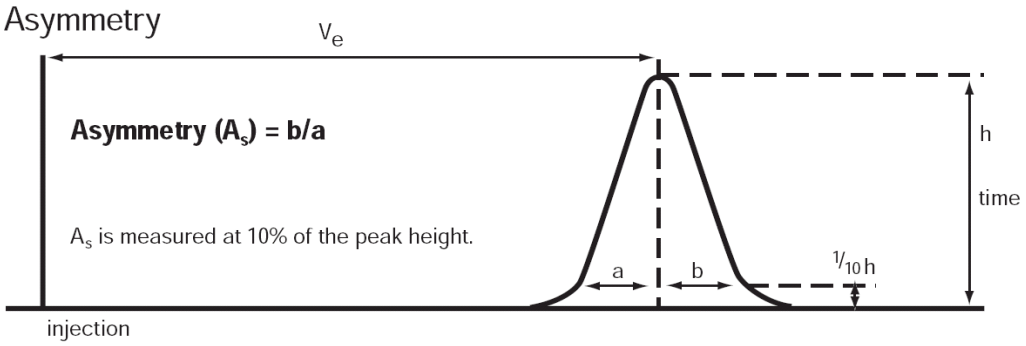

Figure A.3.2: Calculation of column efficiency by determination of the peak asymmetry (Anonymous, 2004).

For HW-65F SEC columns, it is recommended that there should be 3500 plates per meter (m^{-1}) for columns with a diameter (ø) of 2.2 cm, and 3300 m^{-1} for ø =5.5 cm. The A_s value for Toyopearl® columns should be between 0.8 and 1.4. Table A.3.1 is useful in troubleshooting non-ideal A_s and N values.

Table A.3.1 Non-ideal asymmetry and plate count troubleshooting (Anonymous, 2004).

A_s < 0.8	A_s > 1.4
Overpacking the column. Packing at too high a pressure. Column bed cracking.	Column not packed "tight" enough. Clogged screens or frits at the top or bottom of the column. Small void at top of column. Air pockets in column hardware void spaces. Poor injection technique.
Low *N* or High HETP	**High *N* or Low HETP**
Sample injector or detector is too far from the column. Injection volume is too high. The column is not packed efficiently.	The probe molecule is retained on the column due to interaction with the column packing functional groups or backbone.

A_s – asymmetry at 10% peak height, N – theoretical plate, HETP – height equivalent to a theoretical plate

A.4 References

Anonymous (2004) Toyopearl® and TSK-GEL 5PW Instruction Manual. Tosoh Biosciences, http://www.separations.asia.tosohbioscience.com/NR/rdonlyres/50AEB751-2189-48FC-8B9A-F994CFECA891/0/IM02_PackingGuide.pdf

Hagel L (1998). Gel-filtration chromatography. Current Protocols in Protein Science**. 8.3.1-8.2.30**. 14:1-30. 03 June 2009, http://www.nshtvn.org/ebook/molbio/Current%20Protocols/CPPS/ps0803.pdf

Appendix B
Gel filtration chromatography column calibration

This chapter provides the results of the packed Toyopearl® resin columns (A and B) efficiency tests and calibration determinations, as described in Section 4.1.

B.1 Column evaluation

The packed GFC column efficiencies were evaluated prior to calibration. This was carried out as described in Section 4.1.2, with NaCl used as the probe molecule. Table B.1.1 lists the results with respect to N and A_s for column A and B. For A, the average N value was 3738 m^{-1}, which indicates an efficiently packed column. With an average value of 1.25, the A_s value is in the upper limit of the acceptable range, indicating that the column could be packed more tightly. Hence, Column B was packed with a higher flow rate. As a result, Column B had greater efficiency values with N tripling to 11 716 m^{-1} and A_s improving to 0.92. Both columns were suitable for their intended used.

Table B.1.1 Efficiency values from 0.200 µL injections of 2 M NaCl for GFC columns A and B.

Column	T_0 (±SD)/min or V_0 (±SD)/mL	N/m^{-1}	A_s
A[a]	66.247 (0.082)	3738 (292)	1.25 (0.09)
B[b]	45.820 (0.019)	11 716 (1680)	0.92 (0.03)

[a] Triplicate analyses
[b] Quintuplicate analyses

B.2 Calibration for molecular weight determination

Column A and B were separately calibrated as described in Section 4.1.3. A calibration curve was constructed from the elution data of the dextran GPC grade standards against the $\log_{10}$ values of their respective peak-average molecular weights, as supplied by the manufacturer (Sigma). The 1 million Da upper calibration limit were set by the elution times of the totally excluded T5000 dextran standard. The 1000 Da lower calibration limit was set by the elution times of the totally included compound (NaCl). Both columns produced non-linear curves and regression analysis and the partial F-test were used to determine the best-fit polynomial model for each.

B.2.1 Partial F-test for multilinear regression analysis

The x-residual scatter plots for the calibration data of both column A and B did not show a random distribution. Hence, a multilinear relationship between the variables needed to be explored (Miller, 1991). In general, regression analyses look to establish the relationship between the dependent variable (y) and a set of several independent variables (x_i) and other unknown parameters (β_i). When all the parameters are linear, then the model is linear, whereas, linear regression models with more than one independent variable are called multilinear regression models. Equation B.1, Equation B.2 and Equation B.3 describe a simple linear model, a general multilinear model and a polynomial form of a multilinear model, respectively (Orlov, 1996).

$$y = \beta_0 + \beta_1 x_1 \tag{B.1}$$

$$y = \beta_0 + \beta_1 x_1 + \beta_2 x_2 + \ldots \beta_p x_p \tag{B.2}$$

$$y = \beta_0 + \beta_1 x^1 + \beta_2 x^2 + \ldots \beta_p x^p \tag{B.3}$$

where x_i $(i = 1, 2, 3 \ldots p)$ and $b_i (i = 1,2,3 \ldots p)$ are the ith terms and coefficients, respectively, in a set of p independent variables.

When successive terms are added to polynomial expressions, the coefficient of determination is generally high ($R^2 >> 0.9$). Hence, the influence of each additional variable is assessed to determine whether this contribution is significant in explaining the variance in the response variable (An, 2014). Partial F-tests, also called extra-sum-of-squares F-tests, are central in the determination of best-fit models for multilinear regressions (An, 2014; Jamshidian *et al.*, 2007). In a partial F-tests, the calculated result (F_{calc}) looks at the sum-of-squares error (SSE) between the complete model (C) and the reduced model (R) and is compared against the critical F-value (F_{crit}) from tables. Equation B.4 provides the partial F-test.

$$F_{calc} = \frac{\frac{SSE_R - SSE_C}{k_C^*}}{\frac{SSE_C}{n - k_C}} \tag{B.4}$$

where k_C^* is the number of additional b parameters in the complete model, k_C is the number of β parameters in the complete model (*i.e.*, a cubic function has $\beta = 4$ parameters), and n is the sample size. The null hypothesis (H_0) and alternate hypothesis (H_a) are described according to Equation B.5 and Equation B.6, respectively.

$$H_0: \beta_i = 0 \tag{B.5}$$

$$H_a: \beta_i \neq 0 \quad \text{(B.6)}$$

Regression analyses of both calibrations were carried out. Table B.2.1 and Table B.2.2 provide the summary for the partial F-test results of Column A and Column B, respectively.

Table B.2.1 Results for the partial F-test performed on the regression analysis data for determination of the polynomial function to describe the calibration curve for Column A.

Model Parameter	Linear	Quadratic	Cubic
k_C	2	3	4
Residual df	19	18	17
R^2	0.760688	0.998610	0.998611
Residual SSE	5.149582	0.029912	0.029898
$SSE_R - SSE_C$	-	5.11967	1.40874×10^{-5}
$n - k_C$	-	18	17
k_C^*	-	1	1
F_{calc}	-	3081	0.008010
F_{crit}[a]	-	4.413	4.451
p-value	-	1.40×10^{-21}	0.929731551
Result	-	Reject H_0	Accept H_0

[a] At α = 0.05 for a confidence level of 95%.
df – degrees of freedom, SSE – sum-of-squares error, C – complete model, R – reduced model, k_C – are the number of β parameters in the complete model, k_C^* – is the number of additional β parameters in the complete model, n – is the sample size, F_{calc} – the calculated partial F-test result, F_{crit} – the critical F-test value, H_0 – null hypothesis

Since the model that includes the additional term to satisfy a cubic relationship yielded a $F_{calc} < F_{crit}$ result, which is not statistically significant (p > 0.05) at the 95% confidence level, the null hypothesis is accepted. Conversely, the additional term used to satisfy the quadratic function yielded a $F_{calc} > F_{crit}$ result, that is highly statistically significant (p ~ 0) at the 95% confidence level, and the null hypothesis is rejected. Hence, addition of an extra term from the linear model to a quadratic model statistically reduced the unexplained variance in the calibration model for Column A. The calibration equation for Column A is provided in Equation B.7, and the Calibration curve is provided in Figure B.2.1.

$$y = -3.980\times10^{-3}\, x^2 \; + \; 3.127\times10^{-1}\, x \; + \; 0.02663 \quad \text{(B.7)}$$

Table B.2.2 Results for the partial F-test performed on the regression analysis data for determination of the polynomial function to describe the calibration curve for Column B.

Model Parameter	Linear	Quadratic	Cubic	Quartic
k_C	2	3	4	5
Residual df	19	18	17	16
$\mathbf{R^2}$	0.85874	0.998690	0.999415	0.999532
Residual SS	3.039741	0.028187	0.012578	0.010077
$SSE_R - SSE_C$	-	3.01155	0.01561	0.002501
$n - k_C$	-	18	17	16
k_C^*	-	1	1	1
F_{calc}	-	1923	21	4.0
F_{crit}[a]	-	4.413	4.451	4.494
p-value	-	9.44×10^{-20}	0.000259	0.0636
Result		Reject H_0	Reject H_0	Accept H_0

[a] At α = 0.05 for a confidence level of 95%.
df – degrees of freedom, SSE – sum-of-squares error, C – complete model, R – reduced model, k_C – are the number of β parameters in the complete model, k_C^* – is the number of additional β parameters in the complete model, n – is the sample size, F_{calc} – the calculated partial F-test result, F_{crit} – the critical F-test value, H_0 – null hypothesis

Since the model that includes the additional term to satisfy a quartic relationship yielded a $F_{calc} < F_{crit}$ result, which is not statistically significant (p > 0.05) at the 95% confidence level, the null hypothesis is accepted. Conversely, the additional term used to satisfy the cubic function yielded a $F_{calc} > F_{crit}$ result, that is statistically significant (p < 0.05) at the 95% confidence level, and the null hypothesis is rejected. The same result is true for the quadratic model over the linear model. Hence, the addition of an extra two terms from the linear model to the cubic model significantly reduced the unexplained variance in the calibration model for Column B. The calibration equation for Column B is provided in Equation B.8, and the Calibration curve is provided in Figure B.2.2. Refer to Appendix C for the raw data and summary of the regression analyses.

$$y = -1.141\times10^{-4}\,x^3 + 4.905\times10^{-3}\,x^2 - 4.891\times10^{-2}\,x + 5.917 \qquad \text{(B.8)}$$

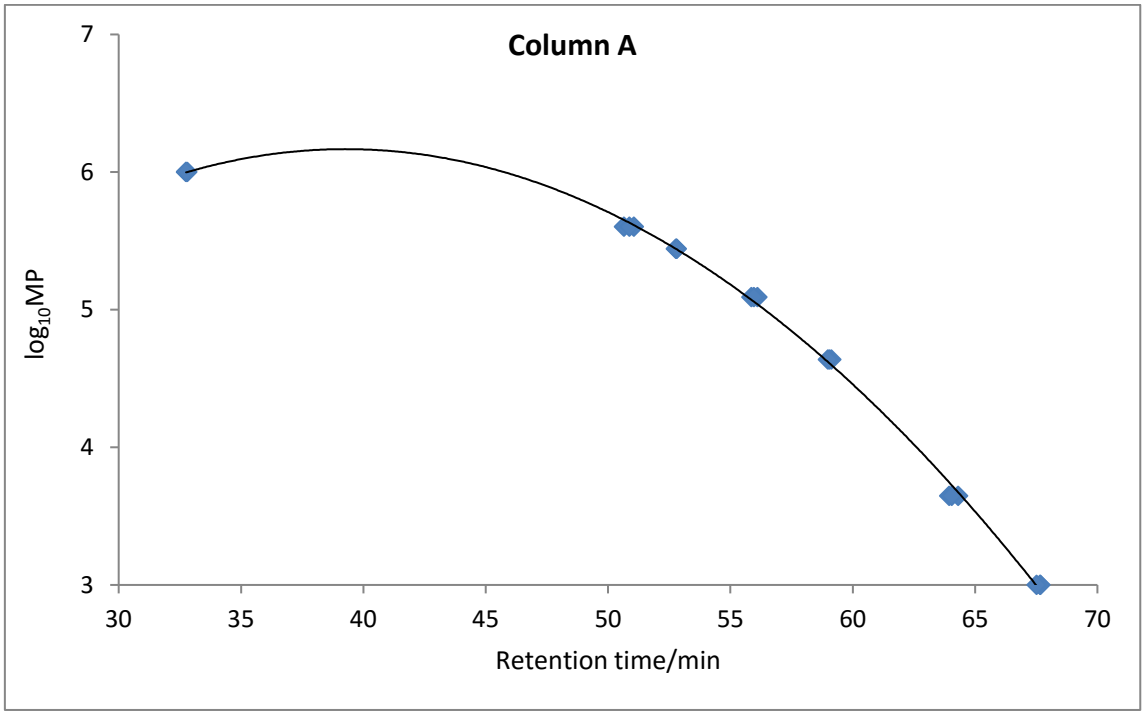

Figure B.2.1: The quadratic calibration curve for the GPC dextran standards eluted from Column A.

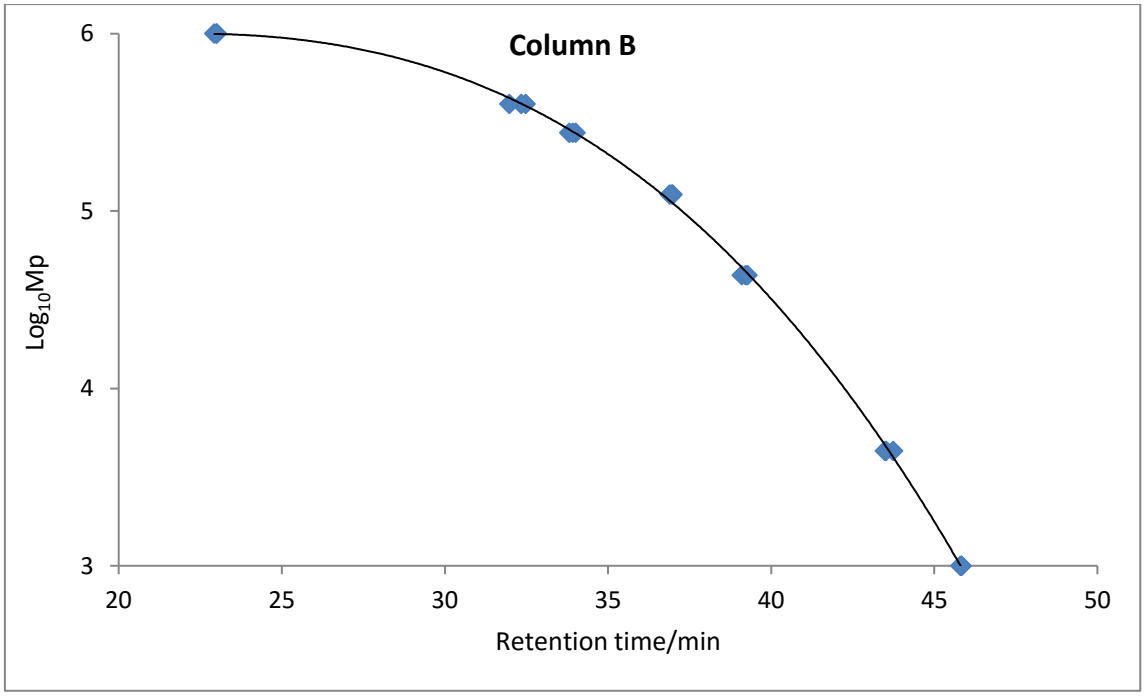

Figure B.2.2: The cubic calibration curve for the GPC dextran standards eluted from Column B.

B.3 Conclusions

The column evaluations revealed that the methods chosen to pack the Toyopearl® GFC columns were satisfactory to provide efficient separations. Calibration of the columns was possible with the GFC grade dextran standards in the range of 5000 Da to 670 000 Da. The calibration set was completed by including a T5000 (>5 million Da) dextran standard and NaCl to establish the V_o and V_t calibration limits, respectively. The calibration curves were constructed with the elution data and supplier provided MP data, and were found to be multilinear by regression analysis. Application of the partial F-test established that the calibrations for Column A and Column B are satisfied by a quadratic and cubic polynomial fit, respectively. These equations were used to determine the MW and MWD statistical averages for pullulan and the *P. sacchari* EPSs, which are discussed in Chapter 5.

B.4 References

An L (2014). Inferential tools for multiple regression. 98-106. 14 June 2016, <ag.arizona.edu/classes/rnr613/Notes10.pdf>

Jamshidian M, Jennrich RI and Liu W (2007). A study of partial F tests for multiple linear regression models. *Computational Statistics & Data Analysis*. **51** (12):6269-6284.

Miller JN (1991). Basic statistical methods for analytical chemistry. Part 2. Calibration and regression methods. *Analyst*. **116** 3-14.

Orlov ML (1996). Multiple linear regression analysis using Microsoft Excel. 1-19. 15 June 2016, <chemistry.oregonstate.edu/courses/ch361-464/ch464/RegrssnFnl.pdf>

Appendix C
Gel filtration chromatography raw data

C.1 Calibration data

This appendix provides the raw calibration data for the GFC columns. These data were used to determine the best-fit calibration models using the partial F-test. The Microsoft Excel® outputs of the regression analyses for the best-fit quadratic model and cubic model are provided for Column A and Column B, respectively.

Table C.1.1 Raw data for the calibration and regression analysis of GFC Column A.

Standard	MP/Da	log_{10}MP	Elution time (x)/min	x^2/min^2	x^3/min^3
NaCl	1000[a]	3.000	67.670	4579	309 876
		3.000	67.663	4578	309 780
		3.000	67.513	4558	307 725
5K	4440[c]	3.647	62.946	4089	261 481
		3.647	63.006	4135	265 922
		3.647	63.046	4102	262 710
50K	43 500[c]	4.638	59.130	3496	206 740
		4.638	59.046	3486	205 860
		4.638	58.986	3479	205 233
150K	123 600[c]	5.092	55.860	3120	174 302
		5.092	56.113	3149	176 681
		5.092	55.963	3132	175 268
410K	276 500[c]	5.442	52.813	2789	147 307
		5.442	52.773	2785	146 972
		5.442	52.793	2787	147 139
670K	401 300[c]	5.603	50.653	2566	129 962
		5.603	51.053	2606	133 065
		5.603	50.870	2588	131 639
T5000K	1 000 000[b]	6.000	32.753	1073	35 136
		6.000	32.807	1076	35 310
		6.000	32.760	1073	35 159

K = 1000 Da, MP – peak average molecular weight.
[a] The molecular weight for NaCl (58.44 g mol^{-1}) was set to 1000 Da due to the minimum possible separable molecular weight for totally included particles on Toyopearl® HW-65 resin columns.
[b] The molecular weight for the T5000K (~5 000 000 Da) standard was set to 1 000 000 Da due to the maximum possible separable molecular weight for totally excluded particles on Toyopearl® HW-65 resin columns.
[c] Peak average molecular weight values were provided by the dextran certificates of analysis from the supplier (Sigma).

Table C.1.2 Raw data for the calibration and regression analysis of GFC Column B.

Standard	MP/Da	log_{10}MP	Elution time (x)/min	x^2/min^2	x^3/min^3	x^4/min^4
NaCl	1000[a]	3.0000	45.800	2098	96 072	4 400 094
		3.0000	45.833	2101	96 280	4 412 789
		3.0000	45.841	2101	96 330	4 415 871
5K	4440[c]	3.6474	43.741	1913	83 689	3 660 622
		3.6474	43.525	1894	82 455	3 588 848
		3.6474	43.483	1891	82 216	3 575 016
50K	43 500[c]	4.6385	39.100	1529	59 776	2 337 260
		4.6385	39.216	1538	60 310	2 365 120
		4.6385	39.275	1543	60 583	2 379 385
150K	123 600[c]	5.0920	36.983	1368	50 583	1 870 719
		5.0920	36.958	1366	50 481	1 865 666
		5.0920	36.891	1361	50 207	1 852 174
410K	276 500[c]	5.4417	33.808	1143	38 642	1 306 405
		5.4417	34.008	1157	39 332	1 337 594
		5.4417	33.916	1150	39 013	1 323 179
670K	401 300[c]	5.6035	32.475	1055	34 249	1 112 235
		5.6035	32.341	1046	33 827	1 093 991
		5.6035	31.975	1022	32 691	1 045 303
T5000K	1 000 000[b]	6.0000	22.933	526	12 061	276 594
		6.0000	23.008	529	12 180	280 231
		6.0000	23.001	529	12 169	279 890

K = 1000 Da, MP – peak average molecular weight.
[a] The molecular weight for NaCl (58.44 g mol^{-1}) was set to 1000 Da due to the minimum possible separable molecular weight for totally included particles on Toyopearl® HW-65 resin columns.
[b] The molecular weight for the T5000K (~5 000 000 Da) standard was set to 1 000 000 Da due to the maximum possible separable molecular weight for totally excluded particles on Toyopearl® HW-65 resin columns.
[c] Peak average molecular weight values were provided by the dextran calibration certificates of analysis from the supplier (Sigma).

Table C.1.3 Quadratic model regression analysis output including the residuals plot for Column A

SUMMARY OUTPUT

Regression Statistics	
Multiple R	0.999304711
R Square	0.998609905
Adjusted R Square	0.99845545
Standard Error	0.040765183
Observations	21

ANOVA

	df	*SS*	*MS*	*F*	*Significance F*
Regression	2	21.48833481	10.74416741	6465.378755	1.9382E-26
Residual	18	0.029912403	0.0016618		
Total	20	21.51824722			

	Coefficients	*Standard Error*	*t Stat*	*P-value*	*Lower 95%*	*Upper 95%*	*Lower 95.0%*	*Upper 95.0%*
Intercept	0.026634175	0.174766848	0.152398325	0.880568038	-0.340537348	0.393805698	-0.340537348	0.393805698
x	0.312652918	0.007194449	43.45751833	1.11003E-19	0.29753794	0.327767895	0.29753794	0.327767895
x^2	-0.003980031	7.17059E-05	-55.50493219	1.4E-21	-0.00413068	-0.003829383	-0.00413068	-0.003829383

Table C.1.3 continued

RESIDUAL OUTPUT

Observation	Predicted log10MP	Residuals
1	2.95838299	0.04161700
2	2.95996483	0.04003517
3	2.99376759	0.00623240
4	3.74482802	-0.097445051
5	3.67362216	-0.026239193
6	3.72515209	-0.077769127
7	4.59819147	0.04029778
8	4.61143754	0.02705171
9	4.62086463	0.01762462
10	5.07237704	0.01964143
11	5.03872725	0.05329122
12	5.05873921	0.03327926
13	5.43761793	0.00407719
14	5.44192124	-0.0002261
15	5.43977118	0.00192395
16	5.65177113	-0.0483019
17	5.61491507	-0.01144591
18	5.63193477	-0.02846561
19	5.99734081	0.00265919
20	6.00013380	-0.00013380
21	5.99770417	0.00229582

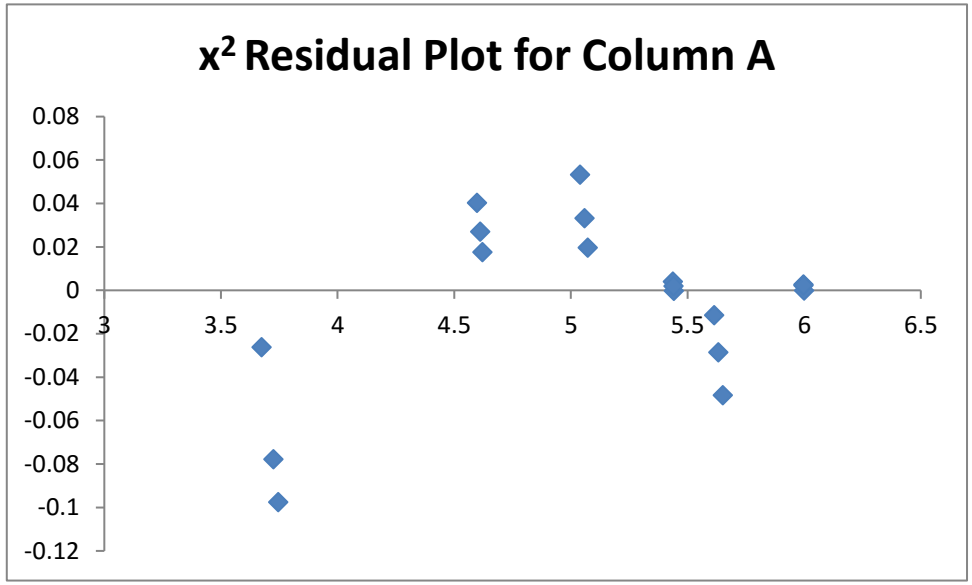

Table C.1.4 Cubic model regression analysis output including the residuals plot for Column B.

SUMMARY OUTPUT

Regression Statistics	
Multiple R	0.999708
R Square	0.999415
Adjusted R Square	0.999312
Standard Error	0.027201
Observations	21

ANOVA

	df	*SS*	*MS*	*F*	*Significance F*
Regression	3	21.50567	7.168556	9688.708	1.13E-27
Residual	17	0.012578	0.00074		
Total	20	21.51825			

	Coefficients	*Standard Error*	*t Stat*	*P-value*	*Lower 95%*	*Upper 95%*	*Lower 95.0%*	*Upper 95.0%*
Intercept	5.917165	0.926397	6.387286	6.75E-06	3.962637	7.871693	3.962637	7.871693
x	-0.04891	0.08606	-0.56828	0.577276	-0.23048	0.132665	-0.23048	0.132665
x^2	0.004905	0.002572	1.907588	0.073484	-0.00052	0.010331	-0.00052	0.010331
x^3	-0.00011	2.48E-05	-4.59311	0.000259	-0.00017	-6.2E-05	-0.00017	-6.2E-05

Table C.1.4 continued

RESIDUAL OUTPUT

Observation	Predicted log10 MP	Residuals
1	3.002095	-0.0021
2	2.991596	0.008404
3	2.989047	0.010953
4	3.611759	0.035624
5	3.670663	-0.02328
6	3.682008	-0.03463
7	4.681935	-0.04345
8	4.659924	-0.02143
9	4.648641	-0.01015
10	5.044621	0.047398
11	5.048476	0.043543
12	5.058759	0.03326
13	5.460248	-0.01855
14	5.438265	0.00343
15	5.448444	-0.00675
16	5.593399	0.01007
17	5.605536	-0.00207
18	5.637561	-0.03409
19	5.998929	0.001071
20	5.998613	0.001387
21	5.998644	0.001356

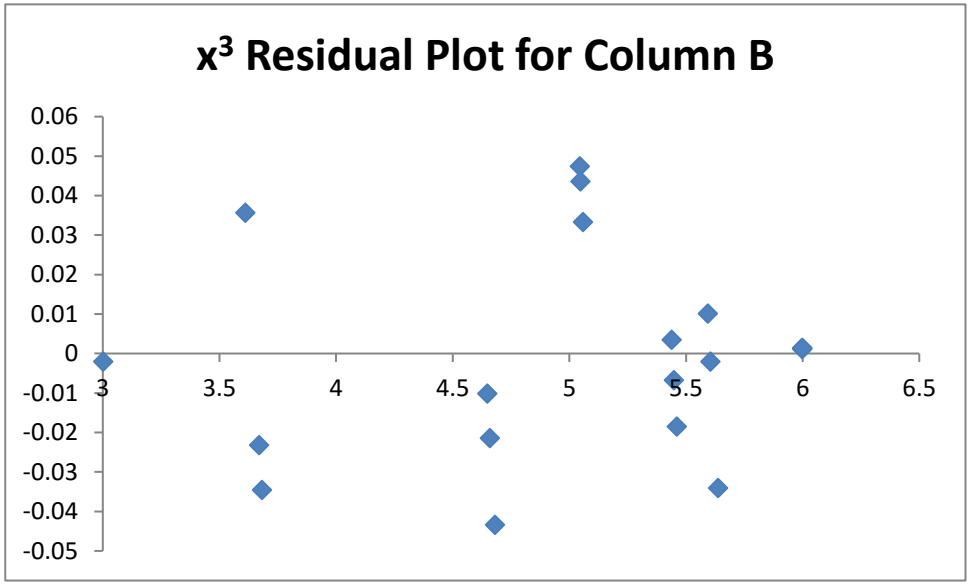

Appendix D
Construction of gas chromatography-mass spectral libraries

This section describes the use of mass spectrometry in the structure elucidation of polysaccharides, with particular focus on the construction of reference libraries from the mass spectra of model compounds. The section first provides some background of the use of mass spectrometry for the elucidation of carbohydrate structures together with detail on the typical fragmentation patterns and expected mass spectra for this class of compounds. Thereafter, detail regarding the use of mass spectra from model carbohydrates to compile spectral lists for the compilation of reference libraries is provided. Two carbohydrate reference libraries were compiled for this study; a carbohydrate composition library (Carb Comp) and a carbohydrate structure library (Models). In creating these libraries, particular consideration was given for the possible sugar derivatives arising from the interference of moisture during preparation, from incomplete permethylations and from incomplete silylations. This section continues by demonstrating how unknown carbohydrate samples are analysed with such reference libraries. In this study, the composition and structure of pullulan and the *P. sacchari* EPSs were determined using the Carb Comp and Models libraries, respectively. This was achieved through processing the samples' mass spectra against the reference spectra stored in the respective libraries according to a set of specified processing parameters. The details regarding these processing parameters are also presented. Finally, this section provides a handy GC-MS structure analysis reference guide. This guide is compiled from the carbohydrates assessed in this study, and that may be of use to select appropriate standards in future carbohydrate structure analyses.

D.1 Introduction

Mass spectrometry has become a fundamental tool in the structural determination of carbohydrate samples (Aspinall, 1982a). Whilst this technique allows the monosaccharide composition of treated polysaccharides to be known, mass spectrometry is mainly used in the determination of the glycosidic linkages within these samples. To obtain information regarding the structure of higher saccharides, EI ionisation is the mode of choice. The fragmentation patterns of the EI mass spectra allow the determination between acyclic and cyclic sugars, between aldose and ketose acyclic sugars, between acyclic pentoses and hexoses, and between cyclic furanoses and pyranoses (Kochetkov and Chizhov, 1966). It is important that EI mass spectra allow these determinations, since each component within a polysaccharide can give rise to several derivatives once treated (refer to Section 3.2.1). Furthermore, EI-MS allows differentiation between overlapping GC peaks of various sugar residues. In order to perform these determinations, knowledge of the fragmentation pathways of sugar derivatives is required.

Kochetkov and Chizhov (1966) developed a nomenclature scheme for the different fragmentation pathways of monosaccharides. These pathways begin when the molecular ion (M^+) undergoes cleavage, and loses a neutral fragment (Aspinall, 1982a). The different fragmentation pathways of the M^+ are denoted by capital letters A-K, with the numeric subscript denoting the number of steps required by M^+ to form the fragment. A letter subscript denotes the ordinal of which the fragment is in a set of isomers. For example, C_{2a} indicates that the M^+ was transformed along fragmentation pathway C in two steps, and that the arising ion is the first in a set of possible isomers (Bleton *et al.*, 1996; Kochetkov and Chizhov, 1966). The assignment of the

fragmentation pathway letter (*i.e.*, A-K) depends on the point of cleavage within the ring when it fragments after ionisation. The major assumption with EI is that ionisation proceeds from the oxygen atom at C-1 in carbohydrate derivatives. This is because the ring-oxygen atom (or the glycosidic linkage oxygen in oligo- and polysaccharides) has the lowest ionisation potential, and is subject to loss of an electron during ionisation. This triggers the fragmentation. Based on this assumption, cleavage in pyranoses proceeds along the bond β to the ring-oxygen, and initiates degradation of the ion. Cleavage between C-1 and C-2 gives rise to the C, F, H and K series, whilst cleavage between C-4 and C-5 gives rise to the B, H, and J series of fragments. The D series of fragments arises from cleavage between either carbon pair (Kochetkov and Chizhov, 1966). Some of these fragmentation pathways are illustrated in Figure D.1.1.

Although anomers of sugar derivatives cannot be distinguished in EI mass spectra, sugars of different sizes and shapes can be. There are several key features in the fragmentation patterns that allow furanose and pyranose sugar derivatives to be differentiated. In general, the F and H series are useful for this purpose. Sugar furanoses will reveal a predominant F_1 ion (*m/z* = 101 if methylated, or *m/z* = 217 if silylated), whilst similar pyranoses contain a distinctive H series ion (*m/z* = 88 if methylated, and *m/z* = 204 if silylated) (Kochetkov and Chizhov, 1966). These features are illustrated in Figure D.1.2.

EI-MS provides reproducible mass spectra of carbohydrate compounds. Hence, EI-MS mass spectra derived from authentic standards are useful for compiling reference libraries for the assessment of unknown carbohydrate samples. Although NIST offers a comprehensive compound database, this database is not complete. It is, therefore, possible to compile specific libraries in the MS Workstation software (Varian) from the identified fragments of authentic standards. In order to identify these fragments, a detailed understanding of the fragmentation pathways and possible mass spectra for the standards is required. The construction of such libraries enables the rapid identification of fragments that arise from similarly prepared samples. In this study, several mono-, oligo-, and polysaccharide model compounds were investigated, and their individual mass spectra were stored in either a composition or structure library. It is through matching both the RRT and the mass spectra (facilitated by the libraries) that the residues of similarly prepared polysaccharide samples can be identified and quantified. This information enabled the composition and linkage information of the *P. sacchari* EPSs to be determined. The next section details the procedures followed to compile the reference libraries from the model compounds. Thereafter, details for how the libraries were used to assess the EPSs studied are provided. Figure D.1.3 provides a flow diagram summarising the steps followed.

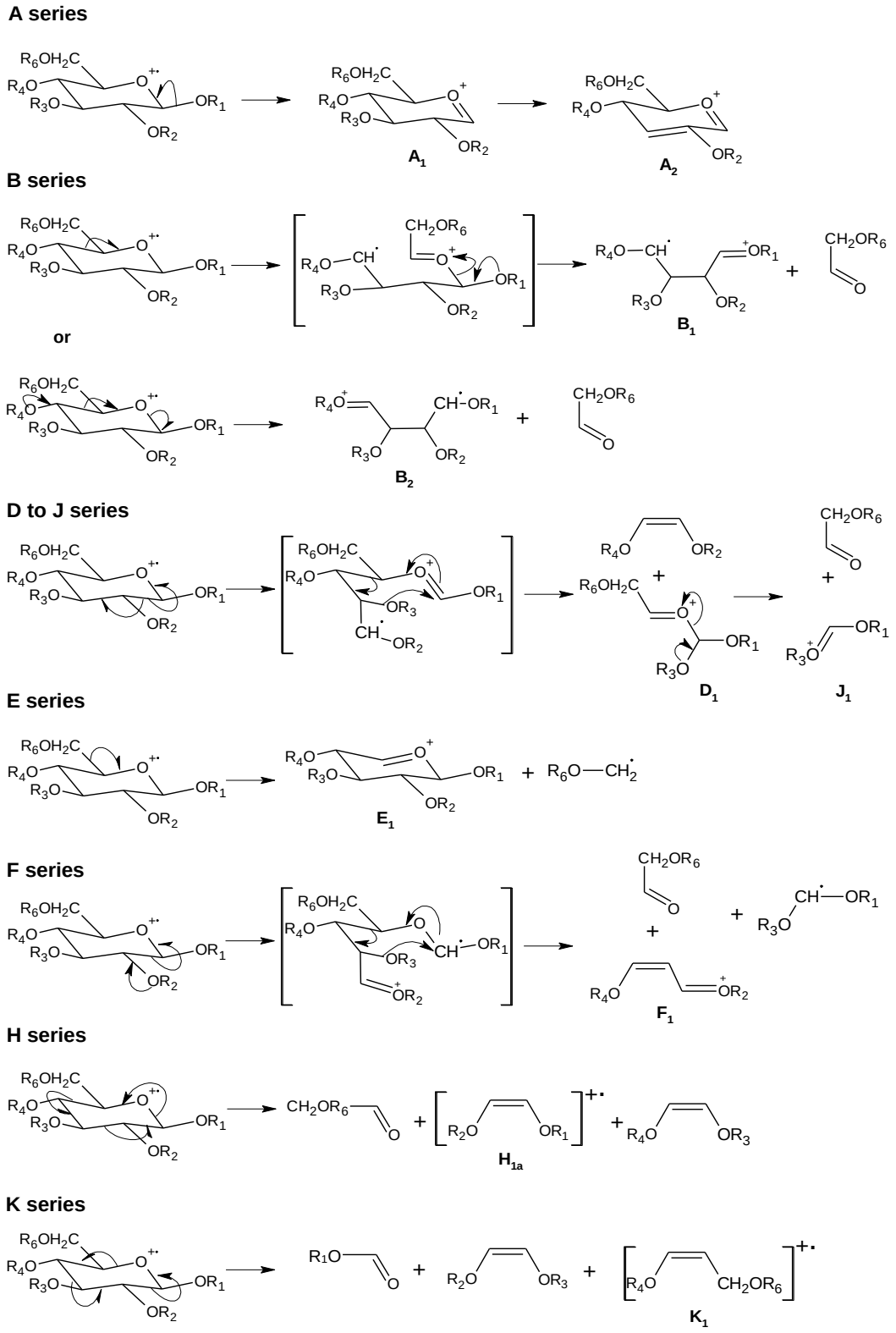

Figure D.1.1: Some mass spectral fragmentation pathways for typical glycopyranosides (R = Me/TMS). Adapted from Aspinall (1982b) and Kochetkov and Chizhov (1966).

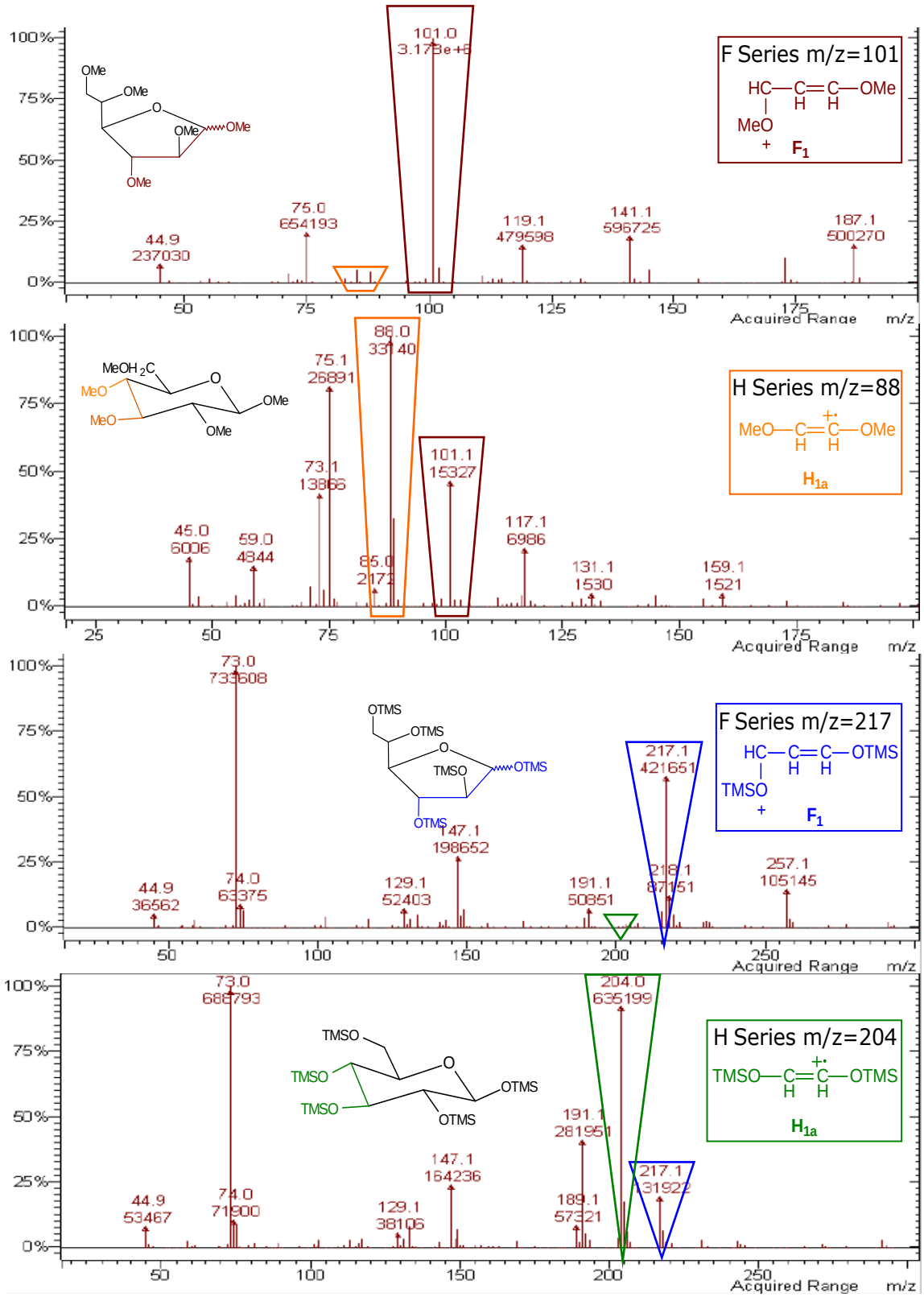

Figure D.1.2: The mass spectra illustrate how fragmentation patterns between pyranoside and furanoside structures of both methylated and silylated sugars can be differentiated according to the F and H series, as defined by Kotchetkov and Chizhov (1966).

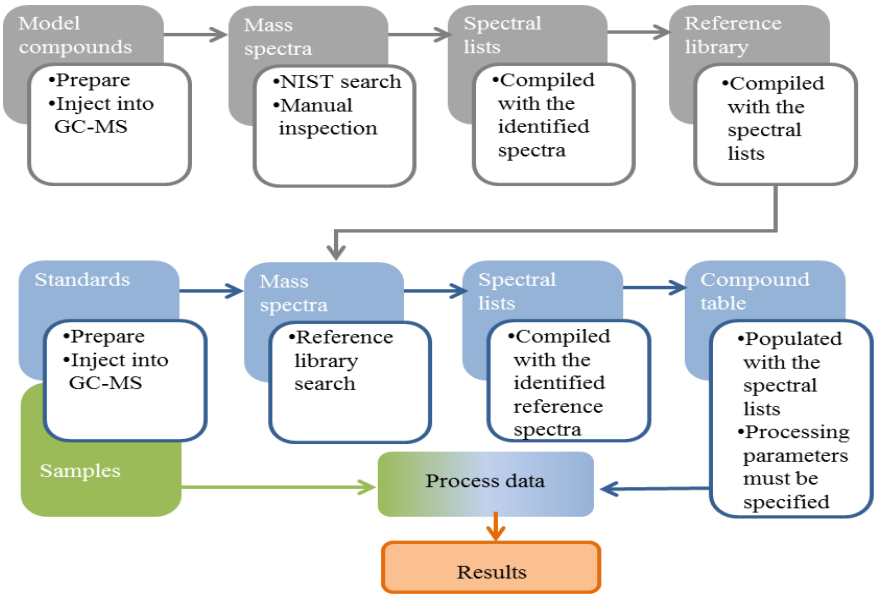

Figure D.1.3: Flow chart to illustrate the process followed to compile reference libraries from model compounds and how these were used to define the processing conditions to analyse samples.

D.2 Carbohydrate model compounds

Eighteen carbohydrate standards were used as model compounds. Sorbitol was included as the internal standard. The model compounds were selected for either their specific composition and/or specific linkages. Certain compounds were included to compare differences between derivatives arising from the preparation of oligosaccharides versus similar higher saccharides. For example, to determine any difference in residues arising for the preparation of maltotriose versus pullulan (a maltotriose polymer linked by α-(1,6)-linkages) was of interest.

All the mono-, oligo-, and polysaccharide standards underwent either methanolysis (composition) or the permethylation protocol (structure) followed by silylation (for these details, refer to Section 4.2). Table D.2.1 details the information from the carbohydrate standards used in this study, together with the composition and linkage types present in each and for which library their information was used. The composition identification library is called Carb Comp, and the structure identification library is called Models.

Table D.2.1 Model compounds prepared and analysed by GC-MS to compile both compositional (Carb Comp) and structural (Models) libraries.

Model compound	Type of saccharide	Composition	Linkage type	Library	Supplier (lot no.)
Amylose from potato starch	Polysaccharide containing glucose (Glc)	Glc	GlcT, Glc-4	Models	Sigma (1593420)
Amylopectin from potato starch	Polysaccharide containing Glc	Glc	GlcT, Glc-4, Glc-6 branches	Models	Sigma (83H3853)
Arabino-galactan from Larch Wood	Polysaccharide containing Arabinose (Ara) and Galactose (Gal)	Ara, Gal	AraT, Ara-3, Gal-3, Gal-1,6 branches, Gal-6	Both	Sigma (90K8806)
Cellobiose	Disaccharide	Glc	GlcT, Glc-4	Models	Sigma (79C-0081)
Dextran from *Leuconostoc mesenteroides*	Polysaccharide containing Glc	Glc	GlcT, Glc-6 (with Glc-4/ Glc-3/Glc-2 branches)	Both	Sigma (101H0297)
D-(+)-Galactose	Monosaccharide	Gal	GalT	Both	Merck (7517506)
D-(+)-Glucose	Monosaccharide	Glc	GlcT	Both	Sigma (129K0051)
Lactose	Disaccharide	Glc, Gal	Glc-4, GalT	Models	Saarchem
Lichenan from *Cetraria islandica*	Polysaccharide containing Glc	Glc	GlcT, Glc-3, Glc-4	Models	Sigma (87H0276)
Locust Bean Gum from *Ceratonia siliqua* seeds	Polysaccharide containing mannose (Man) and Gal	Man, Gal	ManT, Man-4, Gal-6	Both	Sigma (098K0123)
Maltotriose	Trisaccharide	Glc	GlcT, Glc-4	Models	Sigma (104F-0769)
Mannose	Monosaccharide	Man	ManT	Both	BDH (6085740)
Melibiose	Disaccharide	Gal, Glc	GalT, Gal-6	Models	BDH (1162720)
Panose	Trisaccharide	Glc	GlcT, Glc-4, Glc-6	Models	Sigma (25H0395)

Model compound	Type of saccharide	Composition	Linkage type	Library	Supplier (lot no.)
Pullulan P-4516 from *Aureobasidium pullulans*	Polysaccharide containing Glc	Glc	GlcT, Glc-4, Glc-6	Both	Sigma (40K1170)
Stachyose	Tetrasaccharide containing Glc, Gal and fructose (Fru)	Glc Gal Fru	GlcT, Glc-6 Gal-6 Fru-2	Both	Sigma (89F3874)
Sorbitol/ Glucitol	Glucose alcohol (OH)	Glc-OH	None – Internal Standard	Both	Merck (L214259)
D-(+)-Xylose (Xyl)	Monosaccharide	Xyl	XylT	Both	Sigma (022K12527)

T – terminal residue

D.3 Construction of mass spectral libraries from model compounds

Following the respective depolymerisation method used, the silylated derivatives from each of the model compound samples were injected into the GC. The GC chromatograms and individual EI mass spectral data were manually scrutanised and processed against the existing NIST library. In most cases, the NIST library was not sufficient to identify each residue. Consequently, the residues were identified, where possible, through both the knowledge of the parent compound and an understanding of the possible fragmentation pathways of each component sugar derivative. These identified sugar derivatives were then stored in spectral lists in the MS Workstation software. With the aid of the Library Manager function on MS Workstation, the respective spectral lists were imported and saved into two separate libraries that were created. The composition identification library created was called "Carb Comp", and the structure identification library created was called "Models".

D.3.1 Mass spectra from model compounds

The Carb Comp and Models libraries were created in the MS Workstation Library Manager with the mass spectra arising from the preparation of the model compounds described in Table D.2.1. As outlined in Section 5.2.1, different sugar derivatives arise from the preparation of the model compounds that are both expected (primary) and that arise due to incomplete permethylations, due to the interference of moisture and/or due to incomplete silylations (secondary). In Section 5.2.1, Table 5.2 and Table 5.3 summarised both the primary and secondary sugar derivatives that were included in the respective libraries. This section provides more background explaining the occurrence of secondary residues from the presence of moisture during the reaction.

Mass spectra of secondary residues due to moisture

As shown in Section 3.2.2, hydrolysis for both composition and structure analysis is carried out in the same way. The only difference lies in the compound being hydrolysed. In composition analyses, the OH groups on the sugar rings are maintained. However, for structure analyses, all these OH groups are first methylated. In either case, on cleavage of the glycosidic linkages with

acidic methanol, the reducing-end of the residue becomes methylated (OMe) whilst the non-reducing-end is hydroxideated (OH). Figure D.3.1 illustrates the dominant mechanistic steps of this process on a dextran-like oligosaccharide. The reaction comes about when the acidic proton (H^+) interacts with the glycosidic linkage to form a conjugate acid. This conjugate acid breaks down, resulting in cleavage of the C-O bond. The cyclic carbonium ion which arises is in a half-chair conformation (Xiang *et al.*, 2003). This reactive ion then attacks the methoxide ions (MeO^-) in the solution. In the presence of moisture, the hydroxide ions (OH^-) compete.

Moisture in the reaction mechanism gives rise to different sugar derivatives. The consequence of this in the composition analysis (where R = OH in Figure D.3.1) of polysaccharides is not too serious. The only other derivatives that arise are per-*O*-TMS-hexosides (persilylated moieties). These are the same as the derivatives arising from the hydrolysed reducing-end terminal groups. Regardless of these additional residues, the composition of the hydrolysed polysaccharide can still be determined. However, the presence of moisture in the structure analysis (where R = Me in Figure D.3.1) of polysaccharides complicates linkage determinations. The experimental procedure is designed to protect the reducing-end of glycosidic linkages with a methoxide group. Subsequently, the non-reducing-ends can be discriminated once silylated. These linkage positions are then determined by comparing the mass spectra against authentic standards and/or reference libraries. Moisture present during the permethylation protocol prevents the glycosidic reducing-end involved to remain unprotected following cleavage. Consequently, both the reducing and non-reducing-ends are silylated. A carbohydrate derivative with more than one unprotected site indicates a branched residue, hence, the presence of moisture leads to the incorrect classification of branch points in a polysaccharide. For the purpose of clarity, residues that are expected from model compounds are referred to as primary residues, whilst those that are unexpected are referred to as secondary residues. Residues suspected to arise due to the interference of moisture fall into the category of secondary residues. These residues are important to identify, as they are still useful for quantitation purposes.

Table D.3.1 details the expected masses for some primary fragments that arise in both the composition analysis and structure analysis of polysaccharides. An additional column is included to indicate the expected change in the fragment masses when water interferes to produce secondary residues.

Other erroneous branch point classifications can arise due to incomplete permethylations. As discussed in Section 3.2.2, although NaOH is added in excess in the permethylation protocol, the presence of moisture can lead to incomplete alkoxide formation, thus incomplete permethylations (Aspinall, 1982b; Ciucanu and Caprita, 2007). This fact, coupled with the influence of moisture in the methanolysis step, can lead to derivatives that appear to have more than one glycosidic linkage, *i.e.*, Glc-1,4,6TMS. The identification and treatment of such residues is discussed in the compilation of the structural reference library below. Refer to Section 5.2 for the carbohydrate derivative nomenclature for abbreviations used.

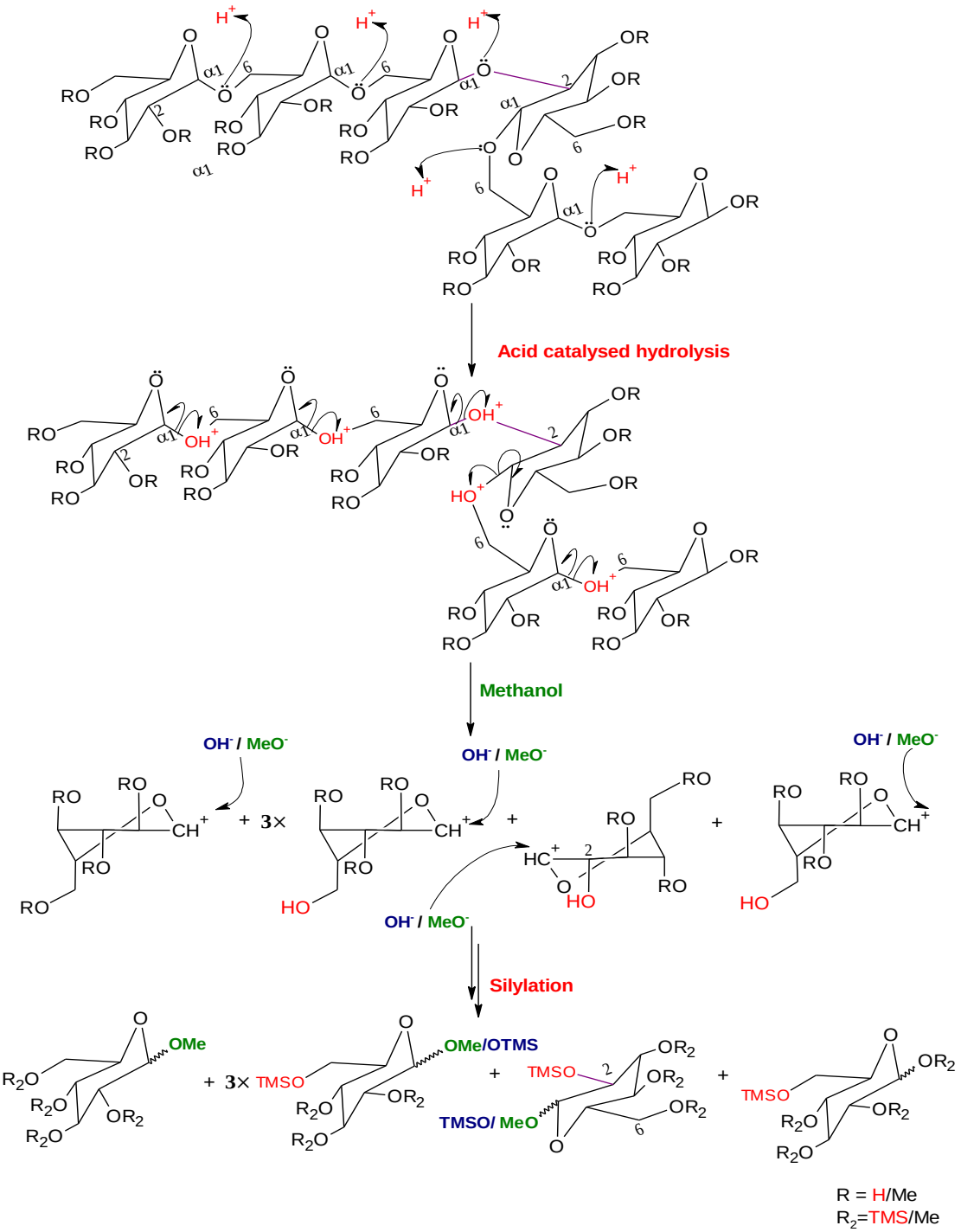

Figure D.3.1: Dominant mechanistic pathway of acidic methanolysis and the competition of hydroxide ions (OH^-) against the methoxide ions (MeO^-) for the reactive cyclic carbonium ion sites following glycosidic cleavage.

Table D.3.1 Typical values for the mass-to-charge ratio (*m/z*) of specific fragments arising from the anomeric end of monosaccharides derived from the composition and structure analysis of carbohydrate samples. The values reflect the difference both in the absence and presence of moisture (refer to Figure D.3.1).

MS Fragment	Composition *m/z*		Structure *m/z*	
	R_2 = OTMS, C-1: R_2 = OMe[1]	R_2 = OTMS[2]	R_2 = OMe[3]	R_2 = OMe, C-1: R_2 = OTMS[4]
A_1	452	452	175	175
A_2	363	363	143	143
A_3	273	273	111	111
B_1	353	410	176	235
B_{2a}	306	306	131	131
B_{2b}	306	364	131	190
D_1	324	265	105	163
E_{3a}	259	259	143	143
F_1	217	217	101	101
H_{1a}	147	204	88	146
H_{1b}	147	147	88	88
H_{2a}	73	73	73	73
H_{2b}	73	131	73	131
J_{1a}	75	75	75	75
J_{1b}	133	191	75	133
K_1	217	217	102	102

[1] Methylation at C-1 where all other positions are silylated (primary).

[2] Persilylated due to moisture/non-methylation of C-1 of a reducing monosaccharide (secondary).

[3] Permethylated derivative (primary).

[4] Moisture prevents C-1 from being methylated (secondary).

D.3.2 Construction of the Carb Comp library for composition analysis

Various model compounds were used to prepare composition sugar derivatives for inclusion in the Carb Comp reference library created (refer to Table D.2.1). Compounds chosen include monosaccharides (mannose, galactose and glucose) and higher saccharides (stachyose, dextran, *etc*.) all containing Glc, Man and/or Gal sugars. In general, only pyranoside derivatives were detectable for Glc and Man, whilst pyranose and furanose derivatives were detected for Gal. All these primary derivatives are methyl tetrakis-*O*-TMS-hexosides, and each was found to exist as an anomeric pair. For the three pairs, the α-derivative was assigned to the first eluting peak, and the β-derivative to the second (Bleton *et al.*, 1996). In all three cases, the α-derivative is more thermodynamically stable, having a higher total ion current (TIC). Each of these manno-, galacto- and gluco-derivatives gave rise to similar mass spectra (Figure D.3.2). Generally, each has an H_{1b} fragment of *m/z* = 147.2, and J_{1b} fragment of *m/z* = 133.1, both arising from an OMe group at C-1. Since all other positions on the rings are OTMS groups, the H_{1a} and K_1 fragments also feature at *m/z* = 204.2 and 217.1, respectively. Pyranoses are distinguished from furanoses as the *m/z* = 204.2 predominates in the former whilst *m/z* = 217.1 predominates in the latter. The base ion in all cases is *m/z* = 73.1 (Kochetkov and Chizhov, 1966).

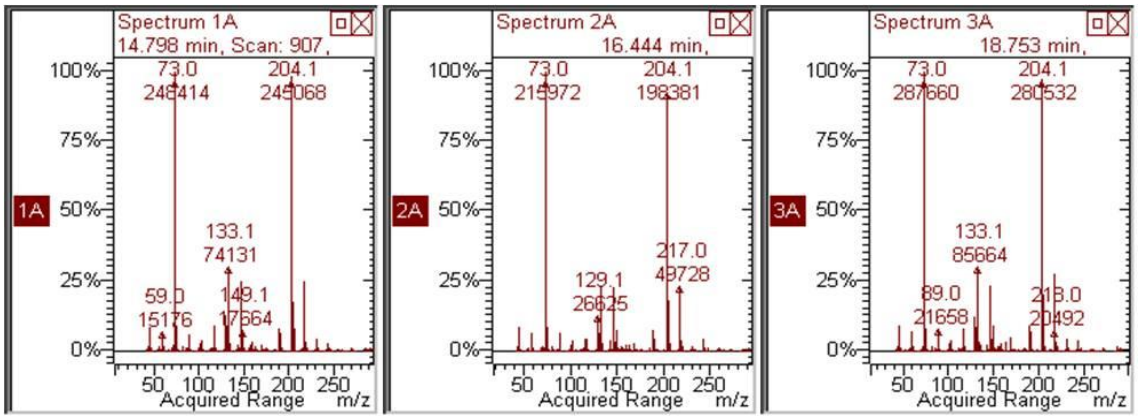

Figure D.3.2: The mass spectra of αManT (1A), αGalT (2A), and αGlcT (3A) are shown. Since their mass spectra are almost identical, they are differentiated with respect to their (relative) retention times.

Moisture present during the preparation of model compounds for composition analysis gave rise to secondary peaks. Moisture causes the C-1 position involved in glycosidic linkages to become silylated to produce per-*O*-TMS hexoside derivatives. These derivatives have similar mass spectra compared to their permethylated counterparts, except there is no longer a J_{1b} fragment of *m/z* = 133.1; instead there is a prominent peak (> 25%) of *m/z* = 191.2. This J_{1b} fragment is possible only if C-1 is silylated. Comparing the secondary derivatives from the different target compounds, Gal was found to give rise to more secondary peaks than Man and Glc. As in the case of the persilylated derivatives, Gal*f*-TMS was distinguished from Gal*p*-TMS with its predominant *m/z* = 217 for F_1 (Figure D.3.3) (Kochetkov and Chizhov, 1966). An additional pair of peaks in the Gal-containing chromatograms was detected at a RRT = 0.859/0.944 (α/β). These peaks had the same mass spectra as the pair of Gal-TMS pyranoses; therefore, these derivatives could not be distinguished as any other type of residue other than those arising from a linear form of the Gal-TMS derivatives. Generally, the secondary peaks were found to contribute about 1.6-2.5% of the total area of residues from higher saccharides. However, the Gal monosaccharide produced a massive 20.6% of these peaks. Hence, these secondary Gal peaks cannot all be caused due to moisture. A possible explanation is that the Gal reducing sugars do not form a reactive carbonium ion and, hence, are less reactive toward the methoxide ions.

All the detected sugar derivatives were named and the spectra saved in the spectral lists for each model compound analysed. These spectral lists were then imported into the new library created in the Library manager, called Carb Comp. Following the successful compilation of this library, the individual peaks arising in the GC chromatograms for pullulan and the *P. sacchari* EPS samples could be analysed.

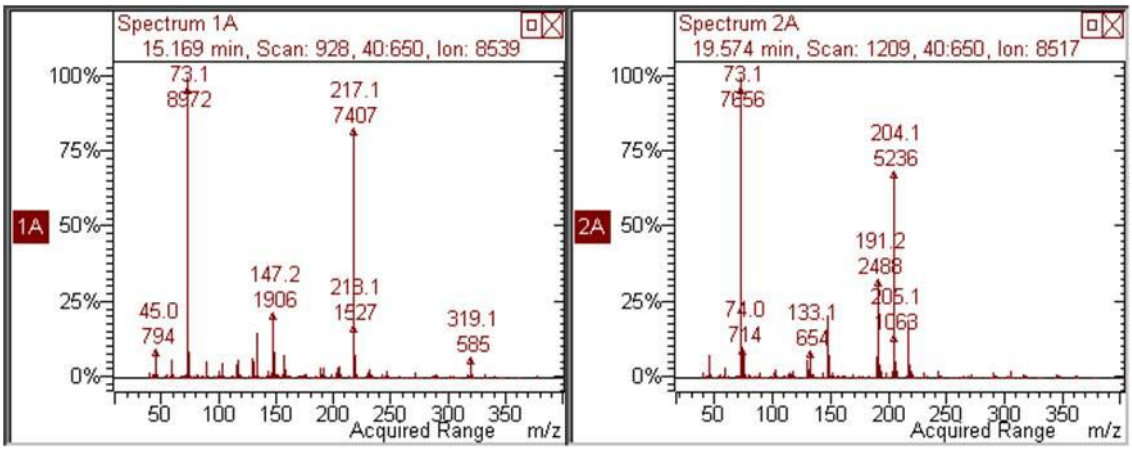

Figure D.3.3: Mass spectra of αGalf-TMS (1A) and αGalp-TMS (2A). 1A has an abundant *m/z* = 217.1, whilst 2A has an abundant *m/z* = 204.1 allowing the furanose and pyranose isomers to be differentiated. Also note the *m/z* = 191.2 ion in 2A, which arises because of the silylation of C-1 in pyranoses.

D.3.3 Construction of the Models library for structure analysis

Various model compounds were used in the determination of the structure of sugar derivatives to include in the Models library (refer to Table D.2.1). As before, monosaccharides (galactose, glucose, *etc.*) were studied in conjunction with higher saccharides (stachyose, dextran, *etc.*). The higher saccharides contained some or all of the derivatives described in Table 5.3. These are the primary derivatives identified, and include both anomers of per-*O*-methyl-hexosides and tetrakis-*O*-methyl-*O*-TMS-hexosides, as described (except for Gal-1 and Gal*f*-1). In all instances, Glc did not give rise to detectable furanose isomers, whereas the permethylated derivatives of Man and Gal did. The Man and Gal furanoses were distinguished from their pyranose counterparts by identification of a prominent F_1 = 101 *m/z* and H_1 = 88 *m/z*, respectively. The primary permethylated derivatives were distinguished from their TMS counterparts firstly by RRTs and by distinction of a few select ions. For instance, Glc-4 (refer to Table 5.3 for the nomenclature) has a predominant *m/z* = 159.0 ion which is not present in the GlcT spectrum. The *m/z* = 159.0 ion for Glc-4 arises from the silyl group on C-4 producing a K_1 fragment with this value. Note that the *m/z* = 159.0 ion is not shown inTable 5.3, as this table only gives the values for differences at the C-1 position. In the case of Glc-3, *m/z* = 131.2 and *m/z* = 146.0 feature. In this instance, the former ion arises from the J_1 fragment that is silylated at C-3, and the latter ion arises due to the C-3 position being silylated in H_{1b} (not represented in Table 5.3, as these changes do not occur at C-1). These differences are shown in Figure D.3.4.

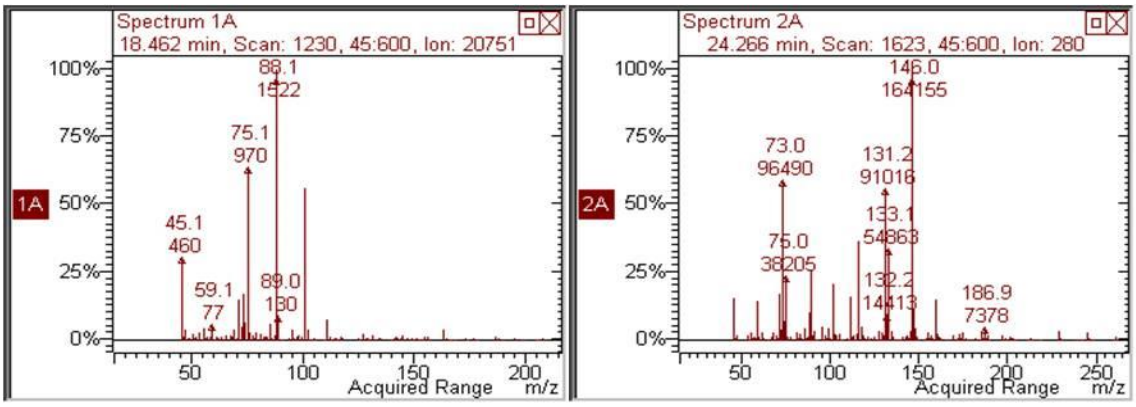

Figure D.3.4: Comparison between GlcT (1A) and Glc-3 (2A). 1A has a predominant H1a/1b of *m/z* = 88, confirming that it is a permethylated pyranose derivative. 2A no longer has this ion, instead it has predominant *m/z* = 146 and *m/z* = 131.2 ions, indicating that the C-3 position is now silylated on the H1b and J1 fragments, respectively. Note that these ions are not represented in Table 5.3, as these differences do not occur at C-1.

With respect to assignment of the anomeric pairs, the α-derivative was assigned to the first eluting peak and the β-derivative to the second (Bleton *et al.*, 1996). In contrast to the derivatives from composition analyses, the majority of pyranose derivatives have more thermodynamically stable β-derivatives, whilst Gal*f*-T, and Man*f*-T derivatives have more thermodynamically stable α-derivatives.

Distinguishing the primary residues arising from the permethylation analysis of the model compounds was relatively straightforward. To do so, the RRTs of several different compounds containing the same derivatives (*i.e.*, amylose and cellobiose, amylose and amylopectin, amylopectin and dextran, *etc.*) were compared as well as their mass spectral data. The challenge, however, lay in differentiating between the various secondary derivatives possible from each of the model compounds. As discussed before, secondary peaks arise either due to the presence of moisture or due to incomplete permethylations. Some of the secondary peaks differentiated are the anomers of Glc-1,4TMS, Glc-1,6TMS, GlcL-1,6TMS and Glc-1,4,6TMS, as illustrated in Figure D.3.5.

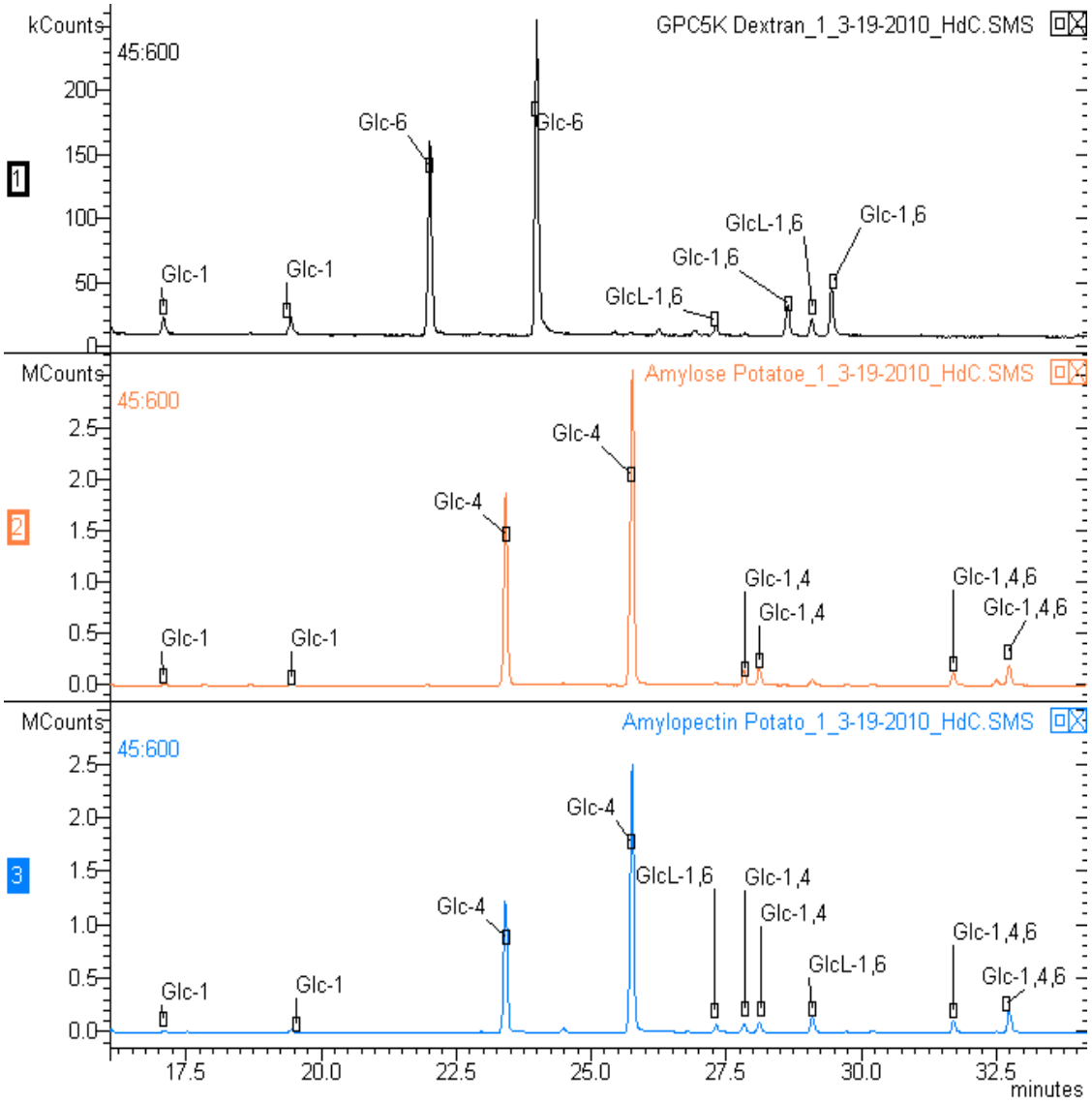

Figure D.3.5: The structural analysis of three standards, namely, dextran (1), amylose (2), and amylopectin (3), show the structural residues that are common and which contrast.

To identify each of the residues, various model compounds containing similar residues were compared. In addition to these derivative RRTs, their individual mass spectra were also examined. Whilst many of the fragments in each mass spectrum were similar, the few distinguishing fragments were analysed to try to classify them further. The GC peaks with identical mass spectra at RRT = 0.677/0.696 (1A and 2A, Figure D.3.6) were assigned to the anomers of Glc-1,6TMS due to the presence of *m/z* = 159. This ion potentially belongs to a K_1 fragment with C-6 being silylated. The presence of *m/z* = 131.3, 133.2 and 146.3 represent the B_{2a}, J_{1b} and H_{1a} derivatives that are silylated at C-1, respectively. These peaks presented in dextran, panose, stachyose and amylopectin – all of which contain Glc (1,6)-linkages.

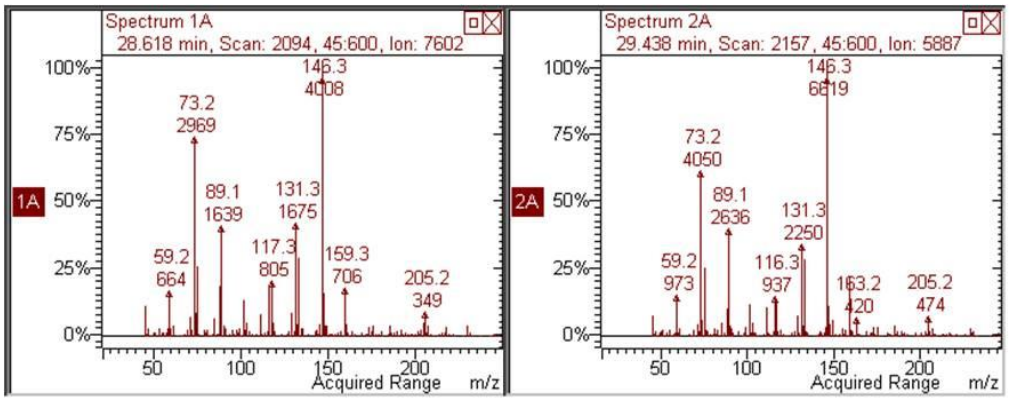

Figure D.3.6: Mass spectra of the peaks assigned as belonging to the anomers of Glc-1,6TMS.

Similarly, there were also peaks with similar mass spectra at RRT = 0.648/0.688 (1A and 2A, Figure D.3.7). Since these peaks were less prominent/non-existent in some of the Glc-1,6 model compounds, they were presumed to be the less abundant linear isomers of the Glc-1,6TMS derivatives. In addition to the ions mentioned for Glc-1,6TMS, these derivatives also have an ion of *m/z* = 185.3, which arises from the C_3 fragment when C-6 is silylated (note that the C fragments do not contain C-1 and, therefore, are not represented in Table D.3.1).

The peaks with identical mass spectra at RRT = 0.660/0.667 (1A and 2A, Figure D.3.8) were assigned to the anomers of Glc-1,4TMS. Unfortunately, the ions in the mass spectra do not allow conclusive assignment of this residue. This is because the *m/z* = 159.2 ion arises from the K_1 fragment, which occurs regardless if the C-4 or C-6 position is silylated. Nonetheless, the J_{1b} ion of *m/z* = 133.2 confirms that the C-1 position is silylated. However, these peaks were labelled as Glc-1,4 as these were found in standards that contain only Glc (1,4)-linkages (and no Glc (1,6)-linkages); namely, maltotriose, lactose, cellobiose, amylose and lichenan.

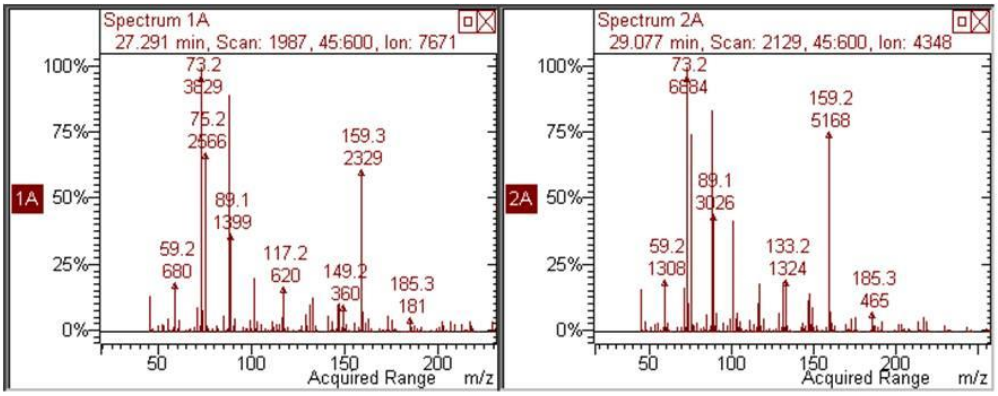

Figure D.3.7: Mass spectra of the peaks assigned as belonging to the anomers of GlcL-1,6TMS.

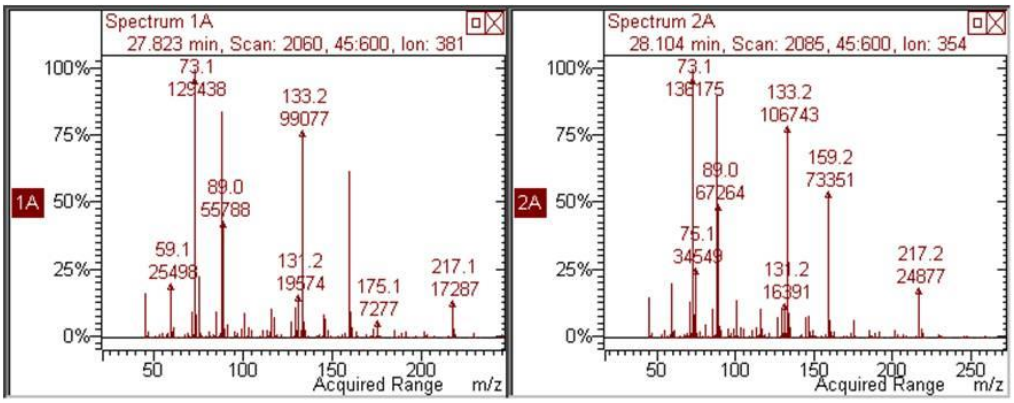

Figure D.3.8: Mass spectra of the peaks assigned as belonging to the anomers of Glc-1,4TMS.

The last important set of GC peaks discussed were evident in almost every chromatogram containing Glc (1,4)- and/or Glc (1,6)-linkages. These occur at RRT = 0.751/0.776 (1A and 2A, Figure D.3.9). Whilst these mass spectra are very similar to those of Glc-1,6TMS, there is a *m/z* = 245.2 ion present. This ion indicates a B_2 fragment that is silylated in both the C-2 and C-4 positions. Together with the ions that represent both C-1, C-4 and C-6 silylations, it is possible that some or all of these positions remain unprotected. Since these fragments occur in the standards, and since only Glc-4TMS and/or Glc-6TMS are expected for the primary derivatives, it is assumed that these peaks (labeled Glc-1,4,6TMS) arise due to incomplete permethylations and moisture. Incomplete permethylations would cause silylation to occur at positions C-2/C-6/C-4, whereas, interference of moisture can cause silylation to occur at position C-1.

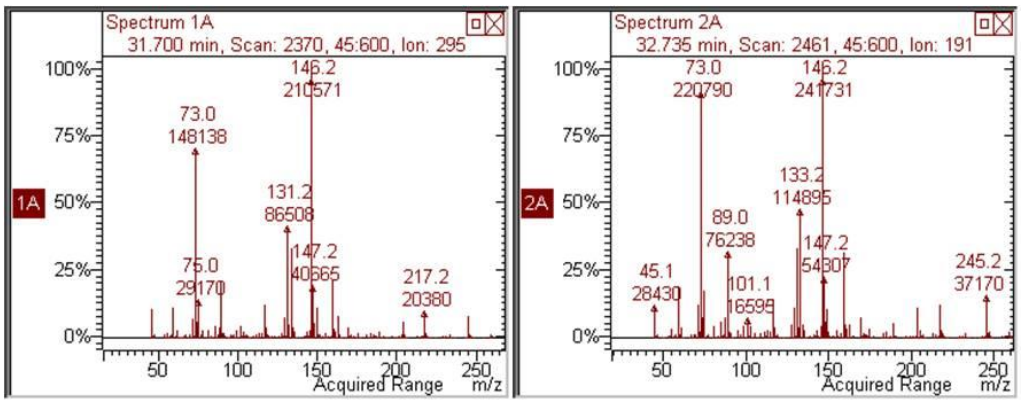

Figure D.3.9 Mass spectra of the peaks assigned as belonging to the anomers of Glc-1,4,6TMS.

Once all the primary derivatives were accounted for, and once all the secondary derivatives were suitably identified, the spectral lists for the individual model compounds were imported into the Models library. The prepared samples were then analysed against the Carb Comp or Models libraries, together with the NIST library, for identification. Compound tables compiled from the mass spectral data of the standards were used to process the sample data and to quantify their composition and structure components. The following subsection provides further detail on these procedures.

D.4 Using the gas chromatography mass spectral libraries: Compound tables and processing parameters for sample analysis

Following the compilation of spectral lists for each standard from the Carb Comp, Models and NIST matches, the compound tables in each analysis method were constructed. Following importation of the spectral lists into the compound tables, parameters for each residue were set. The general identification and integration parameters had to be prescribed, and are discussed with respect to each method below.

D.4.1 Composition analysis

The spectral lists containing the relevant sugar derivatives from the model compounds were imported into the compound table used to process the data from composition analysis. Here the identification and integration parameters were defined as outlined in Table D.4.1.

Table D.4.1 Quantification and qualification parameters set in the compound tables for the relevant reference residues to process the sample data for composition analysis.

Residue	RRT[a]	Quan ion	Qual ion(s) (% ratio)	Integration		Time Events /min	Search window /± min
				Window /± min	Slope sensitivity		
αMan*p*-1OMe	0.706	204.1	133.1 (30.4)	0.250	20	-	0.200
αGal*f*-1OTMS	0.725	73.1	217.1 (86.8)	0.250	20	-	0.200
αMan*p*-1OTMS	0.751	73.0	191.2 (86.8)	0.200	20	II 15.800-15.805	0.180
βMan*p*-1OMe	0.760	73.0	204.1 (71.5)	0.200	10	II 15.690-15.790	0.180
αGal*p*-1OMe	0.786	73.0	204.1 (84.2) 217.0 (22.9)	0.250	20	-	0.200

Table D.4.1 continued

Residue	RRT[a]	Quan ion	Qual ion(s) (% ratio)	Integration		Time Events /min	Search window /± min
				Window /± min	Slope sensitivity		
βGal*f*-1OTMS	0.801	73.1	217.1 (85.5)	0.190	20	-	0.180
βGal*p*-1OMe	0.848	73.0	204.1 (77.9) 217.0 (19.1)	0.180	20	II 17.770-17.860	0.180
αGalL-1OTMS[b]	0.859	73.2	191.2 (28.4) 204.2 (74.6)	0.150	10	II 17.660-17.780	0.150
αGlc*p*-1OMe	0.901	73.0	204.1 (87.5) 133.1 (27.9)	0.250	20	-	0.200
αGlc*p*-1OTMS	0.921	73.1	204.1 (71.8) 191.2 (30.8)	0.250	20	-	0.200
βMan*p*-1OTMS	0.940	73.1	204.2 (71.4) 191.2 (35.8)	0.180	20	-	0.150
βGlc*p*-1OMe	0.941	204.1	147.1 (27.0) 133.1 (29.6)	0.250	20	-	0.200
βGalL-1OTMS	0.942	73.2	191.2 (28.1) 133.1 (9.0)	0.160	10	-	0.150
βGlc*p*-1OTMS	1.124	73.1	204.1 (70.5) 191.2 (33.6)	0.250	20	-	0.200

[a] Relative retention time is reported instead of retention time due to variability of GC conditions.
Quan – quantitation, Qual – qualifier, II – integration inhibit, L – linear

As mentioned before (Section 3.2), heterogeneous polysaccharides give rise to several peaks in their GC chromatograms. In some cases, these peaks may co-elute. Through stipulating certain parameters in the compound table against which their data is processed, closely eluting or co-eluting derivatives may be differentiated. A further complication in carbohydrate determinations is that many arising sugar derivatives produce similar EI fragmentation patterns. When two derivatives are very similar, processing the data may result in all of, some of, or none of the possible sugar derivatives of one peak to be assigned. In this instance, stipulation of the quantitation (quan) and qualifier (qual) ions is necessary. Finally, manual inspection may be required to assign a residue. If the parameters set in the compound table fails, a peak that coincides with more than one derivative can still be identified. This is possible if the chromatogram is manually inspected to establish whether the questionable peak completes a pair of another peak identified in the chromatogram. This is explained in the example that follows. The derivatives from model compounds used to compile the compound tables to process the pullulan and the *P. sacchari* EPS data were selected following a preliminary composition analysis of the samples. Mannose, galactose and glucose were the selected target derivatives required for identification and quantitation of the samples. Furthermore, standards of mannose, galactose and dextran (a glucose-only polysaccharide) were included alongside each preparation of the samples. $ManT^{\$}$, $GalT^{\$}$ and $\alpha GlcT^{\$}$ (refer to Table 5.2 for definitions) were easily identified and quantified in the samples, according to the parameters as set in Table D.4.1. The peak corresponding to $\beta GlcT^{\$}$ posed a greater challenge, as it co-elutes with two other peaks in the GC chromatogram at ~18.7 min, as indicated in Figure D.4.1.

From the RRTs and compound table information, it was established that βGlcp-1OMe, βManp-1OTMS and βGalL-1OTMS co-elute so their quan and qual ions were next considered. Figure D.4.2 shows the mass spectra for these three co-eluting derivatives. βMan-TMS and βGalL-TMS (RRT = 0.940 and 0.942, respectively) are secondary derivatives whilst $\beta GlcT^{\$}$ (RRT = 0.941) is a primary derivative. Both the Man and Gal derivatives contain the J_{1b} = 191.2 *m/z* ion, arising due to the interference of water during their formation. Conversely, fragmentation of $\beta Glc\text{-}T^{\$}$ will not result in a J_{1b} ion. Hence, Man or Gal can be differentiated from $\beta Glc\text{-}T^{\$}$ by addition of the 191.2 *m/z* qual ion in the compound tables. Man or the Gal residues are only successfully identified if this qual ion is present within the specified search window and in the correct relative ratio (35.8% and 29.6%, respectively) to its quan ions (*m/z* 73.1 and 73.2, respectively). If Man and Gal are confirmed, their differentiation depends on manually inspecting the results for the presence of their α-counterparts or evidence of other Man or Gal primary peaks from the sample.

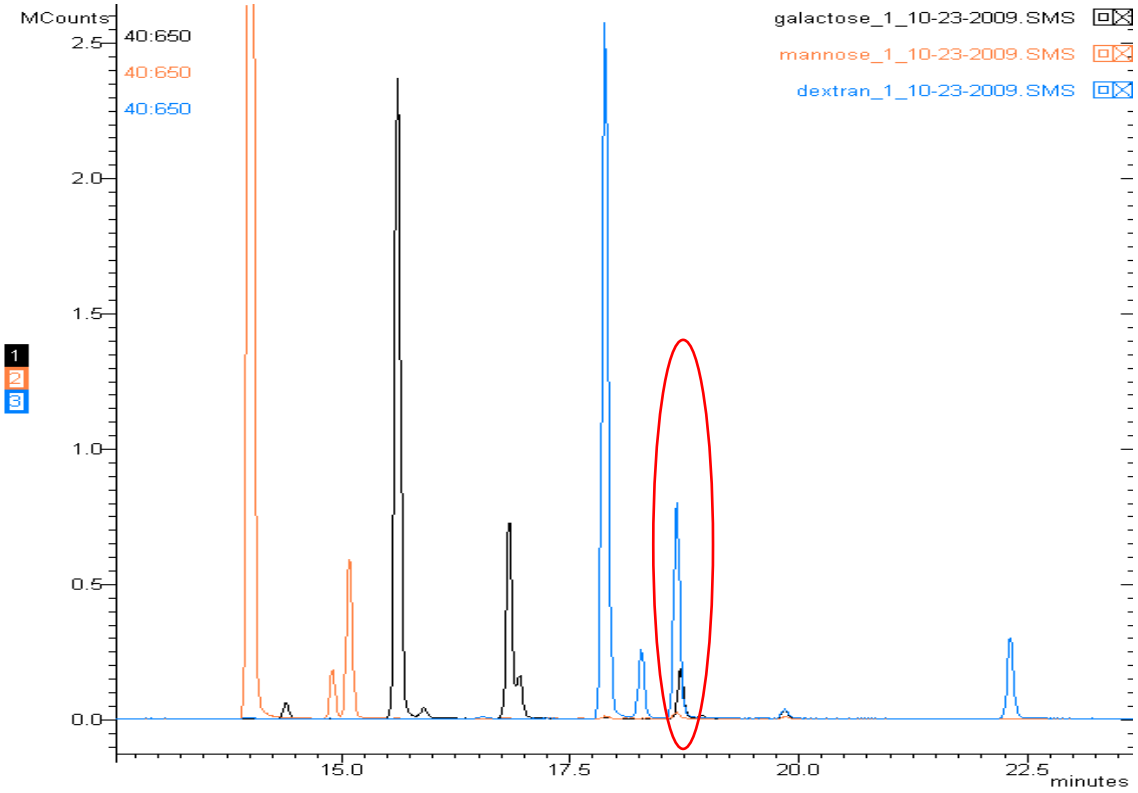

Figure D.4.1 Compositional analysis of mannose, galactose and dextran (glucose-only) reveal that all these compounds have a co-eluting sugar derivative at 18.7 min (circled in red). This peak corresponds to βManp-1OTMS, βGalL-1OTMS and βGlcp-1OMe.

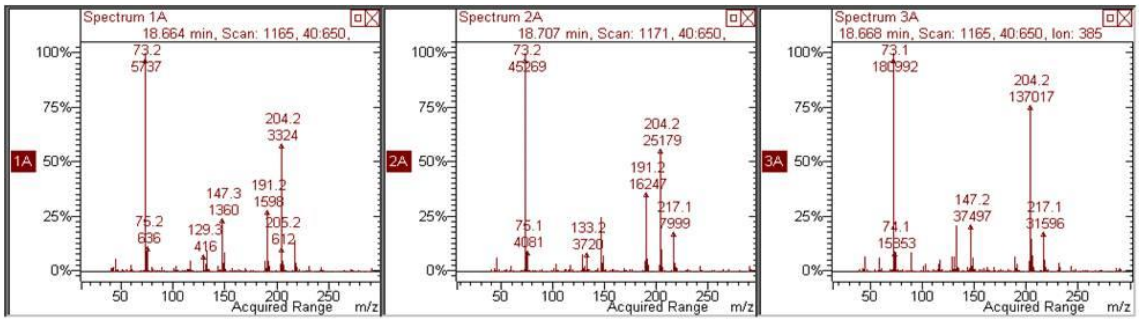

Figure D.4.2 Mass spectra for βManp-1OTMS (1A), βGalL-1OTMS (2A) and βGlcp-1OMe (3A) all eluting at 18.7 min. 1A and 2A have a *m/z* = 191.2, whilst 3A has a higher abundance of *m/z* = 133.2. While there is no difference between 1A and 2A, 3A can be excluded based on the absence of the former ion, and identified based on the ratio of the latter ion to the base peak (*m/z* = 73.1).

The processed spectra of all the standards investigated for composition analysis are found in Appendix E. For the results of the processed composition analysis data of pullulan and the *P. sacchari* EPSs, refer to Section 5.2.

D.4.2 Structure analysis

Structure analysis follows the same methodology as outlined for composition analysis. Following the permethylation protocol, both standards and samples were eluted through the GC and analysed by the MS. The data from each peak was processed against the Models and NIST libraries. Spectral lists were compiled from any matches of the structural derivatives identified in the standards. Thereafter, compound tables were populated from these structural spectral lists and the method processing parameters were defined.

Since the preliminary composition studies on pullulan and the *P. sacchari* EPS samples revealed Man, Gal and Glc components, all standards containing different linkages of these residues were included for processing the structure data. As discussed before (Section 3.2), up to four peaks are expected for each monosaccharide; namely, two anomers and two ring sizes each for per-*O*-methylated hexosides and for tetrakis-*O*-methyl-*O*-TMS hexosides. In addition, any moisture present under the reaction conditions allows both tris-di-*O*-methyl-bis-*O*-TMS hexoside and bis *O*-methyl-tris-*O*-TMS-hexoside residues to arise too. Again, these will each give rise to up to four peaks.

Table D.4.2 lists all the identified residues added to the structure analysis compound table together with the defined processing parameters. The first parameters addressed were the search and integration windows. Since many of the target structure derivatives elute within 0.200 min of each other, tighter search parameters were used and the search windows were reduced from ±0.250 min (default) to ±0.200 min or less. For example, in the first instance αMan*f*-1OMe (18.722 min) is identified from βMan*p*-1OMe (18.889 min) based on search window of ±0.100 min. The two mannose derivatives were further distinguished by specifying their respective quan ions. The furanoside was identified from its quan ion of *m/z* = 101.0 (F_1) compared to a quan of *m/z* = 88.0 (H_1) for the pyranoside. It was not necessary to specify qual ions to distinguish between these two isomers. Finally, the integration parameters were addressed. To accommodate for deviations in retention time, the integration window was made wider than the search window (±0.150 min). Due to the close proximity of the next peak, integration inhibition parameters needed to be outlined. All the remaining residues in the compound tables were similarly treated. Where possible, the search window parameters and quan and qual ions were used as discriminators – especially regarding the secondary residues for Glc.

Table D.4.2 Quantification and qualification parameters set in the compound tables for the relevant reference residues to process the sample data for structure analysis.

Residue	RRT[a]	Quan ion	Qual ion(s) (% ratio)	Integration		Time Events /min	Search window /± min
				Window /± min	Slope sensitivity		
αGlc*p*-1OMe	0.404	88.0	-	0.200	5	-	0.180
αMan*p*-1OMe	0.452	88.0	100.9 (47.8)	0.200	5	-	0.210
αGal*f*-1OMe	0.453	100.9	88.0 (2.6)	0.150	5	-	0.050
βGlc*p*-1OMe	0.459	88.0	-	0.200	10	-	0.010
αGal*p*-1OMe	0.465	88.0	101.0 (48.2)	0.150	10	-	0.050
αMan*f*-1OMe	0.467	101.0	-	0.150	10	II 19.635-17.747	0.100
βMan*p*-1OMe	0.471	88.0	-	0.150	10	II 19.499-19.598	0.100
βGal*p*-1OMe	0.482	88.0	101.0 (45.3)	0.250	10	II 20.278-20.411	0.200
βGal*f*-1OMe	0.486	101.0	-	0.150	10	II 20.010-20.256	0.100
αGlc*p*-6OTMS	0.521	88.0	101.0 (42.5)	0.150	20	-	0.150
αGal*f*-1OTMS	0.541	101.0	132.1 (30.5)	0.100	10	-	0.100
αGlc*p*-4OTMS	0.554	87.9	-	0.250	20	-	0.200
αGlc*p*-3OTMS	0.561	146.1	133.1 (27.7)	0.100	20	-	0.050
αGal*p*-1OTMS	0.565	88.0		0.080	10	-	0.100
βGlc*p*-6OTMS	0.568	87.9	101 (46.1)	0.150	20	-	0.150
βGal*f*-1OTMS	0.591	101.0	-	0.150	20	-	0.150

Table D.4.2 continued

Residue	RRT[a]	Quan ion	Qual ion(s) (% ratio)	Integration		Time Events /min	Search window /± min
				Window /± min	Slope sensitivity		
βGlc*p*-3OTMS	0.593	146.1	131.2 (58.6)	0.130	20	-	0.100
βGlc*p*-4OTMS	0.610	88.0	-	0.250	20	-	0.200
αGal*p*-6OTMS	0.614	88.0	-	0.150	20	-	0.150
βGal*p*-6OTMS	0.624	88.0	-	0.150	20	-	0.150
αGlcL-1,6OTMS	0.648	73.1	159.2 (68.4)	0.150	10		0.100
αGlc*p*-1,4OTMS	0.660	73.1	133.2 (77.0)	0.250	20		0.200
αGlc*p*-1,6OTMS	0.677	146.1	-	0.250	20	-	0.200
βGlc*p*-1,4OTMS	0.667	73.1	133.2 (70.7)	0.250	20		0.200
βGlcL-1,6OTMS	0.688	159.2	-	0.150	10		0.100
βGlc*p*-1,6OTMS	0.696	146.1	-	0.150	20	-	0.150
αGlc*p*-1,4,6OTMS	0.751	146.1	133.1 (31.9)	0.150	20	-	0.100
βGlc*p*-1,4,6OTMS	0.776	146.1	133.1 (44.7)	0.150	20	-	0.100

[a] Relative retention time is reported instead of retention time due to variability of GC conditions.
Quan – quantification, Qual – qualification, II – integration inhibit, L – linear

The processed structure spectra for the standards and samples investigated are found in Appendix E. For the results of the processed structural analysis data of pullulan and the *P. sacchari* EPSs, refer to Section 5.2.

D.5 Structure derivative reference guide from model compounds

Through the information derived from the primary derivatives of all the Glc, Gal and Man model compounds used in this study, a handy reference table was compiled. Table D.5.1 provides the RRTs and variation in anomeric peak percentage areas for the residues derived from several model compounds. This table allows comparisons between derivatives arising from different chain-length model compounds to be made. This table is useful to select appropriate standards in structure investigations. Although the RRTs of each derivative do not differ from one model compound to another (*e.g.*, GlcT from dextran or panose), the anomeric percent ratios for α/β do (*e.g.*, 23/77 for dextran and 50/50 for panose). Hence, it is advisable that a standard more closely resembling the molecular weight of the sample be used.

Other information that is summarised from this study, which is reflected in the table, includes that pyranoses of GlcT, Glc-3, Glc-4 (except lactose), Glc-1,6, GalT and Gal-6 have thermodynamically more stable β-anomers in acidic methanol. This agrees with the findings of Bleton and co-workers (1996). The authors explain that the C-1 methyl constituent adopts the axial position in the ring when in the $^4C_1$ chair conformation (refer to Section 2.1), whereas the opposite trend is seen for pyranoses of Glc-1,4, ManT, as well as all the furanoses. This is due to these residues favouring the $^1C_4$ conformation.

In general, this table provides a quick guide for choosing appropriate standards to identify specific structure residues in future investigations of unknown polysaccharide samples.

D.6 Conclusions

A composition and structure library was successfully compiled from 18 model carbohydrates. Compilation of the respective libraries required an understanding of the possible EI-MS fragmentation pathways possible for each of the compounds' derivatives. The mass spectra of the model compounds were used to compile spectral lists of the various Glc, Gal and Man derivatives possible. In turn, these spectral lists were compiled into compound tables where the integration and quantification parameters were adjusted. Where necessary, these adjustments included that the search and integration windows, as well as the quan ion and qual ions of the reference spectra be specified. These compound tables were used to process the spectra of the similarly prepared pullulan and *P. sacchari* EPS samples, to determine their composition and structure. Finally, together with all the data processed from the 18 model compounds, a reference guide for the structure analysis of polysaccharides was compiled. This reference guide aids in the identification of suitable standards to be used for future structural studies.

Table D.6.1 A structural reference guide for retention time indices and anomer peak area percentages of carbohydrate residues derived for various carbohydrate standards treated by the permethylation protocol in this study.

Anomer	Linkage	Ring Size	Me positions	TMS positions	Carbohydrate Standard (model compound)	Average RRT α/β	Anomer peak area /%
α/β	GlcT	*p*	2,3,4,6	none	Pullulan/ Amylose/ Dextran/ Cellobiose/ Maltotriose/ Panose/ Stachyose	0.404/0.459	30/70 43/57 23/77 19/81 34/66 50/50 n.d.
α/β	Glc-3	*p*	2,4,6	3	Lichenan	0.561/0.593	24/76
α/β	Glc-4	*p*	2,3,6	4	Pullulan/ Amylose/ Amylopectin/ Cellobiose/ Maltotriose/ Panose/ Lichenan/ Lactose	0.554/0.610	39/61 41/59 41/59 39/61 37/63 39/61 23/77 55/45
α/β	Glc-6	*p*	2,3,4	6	Pullulan/ Dextran/ Melibiose/ Stachyose	0.521/0.568	32/68 34/66 32/68 30/70
α/β	Glc-1,4	*p*	2,3,6	1,4	Amylose/ Amylopectin/ Cellobiose/ Pullulan	0.660/0.667	46/54 43/57 38/62 51/49
α/β	Glc-1,6	*p*	2,3,4	1,6	Pullulan/ Dextran/ Amylopectin	0.677/0.696	38/62 44/56 20/80
α/β	Glc-1,4,6	*p*	2,3	1,4,6	Pullulan/ Amylopectin	0.751/0.776	49/51 40/60
α/β	GalT	*p*	2,3,4,6	none	Galactose/ Melibiose/ Stachyose/ Lactose	0.465/0.482	29/71 31/69 31/69 22/78
α/β	GalT	*f*	2,3,5,6	none	Galactose/ Lactose	0.453/0.486	82/18 100/0
α/β	Gal-6	*p*	2,3,4	6	Stachyose	0.614/0.624	31/69
α/β	ManT	*p*	2,3,4,6	none	Mannose/ Melibiose/	0.452/0.471	97/3 100/0
α/β	ManT	*f*	2,3,5,6	none	Mannose/	0.467/n.a.	100/0

f – furanoside, *p* – pyranoside, n.d. – not determined, n.a. – not applicable

D.7 References

Aspinall GO (1982a). Chemical characterization and structure determination of polysaccharides. pp. 35-124. In: GO Aspinall (Ed). *The Polysaccharides*. **1**. Academic Press, Inc., New York.

Aspinall GO (1982b). Isolation and fractionation of polysaccharides. pp. 19-35. In: GO Aspinall (Ed). *The Polysaccharides*. **1**. Academic Press, Inc., New York.

Bleton J, Mejanelle P, Sansoulet J, Goursaud S and Tchapla A (1996). Characterization of neutral sugars and uronic acids after methanolysis and trimethylsilylation for recognition of plant gums. *Journal of Chromatography A*. **720** (1-2):27-49.

Ciucanu I and Caprita R (2007). Per-*O*-methylation of neutral carbohydrates directly from aqueous samples for gas chromatography and mass spectrometry analysis. *Analytica Chimica Acta*. **585** 81-85.

Kochetkov NK and Chizhov OS (1966). Mass spectrometry of carbohydrate derivatives. *Advances in Carbohydrate Chemistry*. **21** 39-93.

Xiao Q, Tong Q and Lim L-T (2012). Pullulan-sodium alginate based edible films: Rheological properties of film forming solutions. *Carbohydrate Polymers*. **87** 1689-1695.

Appendix E
Gas chromatography-mass spectra

This section provides the processed data from the composition, absolute configuration and structure analyses of the various model compounds and pullulan, the fractionated (FB2 F1, FB2 F2 and FB2 F3) and unfractionated (FB2, PB2 and PB7) EPS samples.

The status of each of the identified peaks according to the processing parameters are indicated in each chromatogram as X (error), S (internal standard peak), T (relative retention time peak) and g (peak size reported without calibration data).

E.1 Composition analysis (including GC-MS/MS)

Sample ID:	Blank	Operator:	HdC
Instrument ID:	Varian CP-3800	Last Calibration:	None
Acquisition Date:	3/8/2010 2:02 PM	Data File:	...k_2_3-8-2010_hdc.sms
Calculation Date:	3/19/2016 10:39 AM	Method:	... f2_13032016 v1_.mth
Inj. Sample Notes:	Blank methylated and silylated		

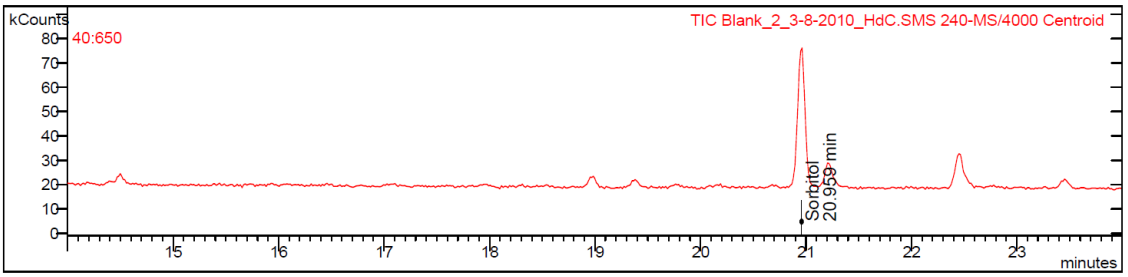

Target Compounds

RT (min)	Peak Name	RRT (min)	Area	Status	Quan Ions	Result Type
20.959	Sorbitol	1.000	62675	X STg	73.2	Identified

Figure E.1.1: Processed GC-MS data for a blank sample.

Sample ID:	Pullulan	Operator:	HdC
Instrument ID:	Varian CP-3800	Last Calibration:	None
Acquisition Date:	3/8/2010 3:46 PM	Data File:	...n_1_3-8-2010_hdc.sms
Calculation Date:	3/19/2016 10:45 AM	Method:	... f2_13032016 v1_.mth
Inj. Sample Notes:	Pullulan methylated and silylated with sorbitol.		

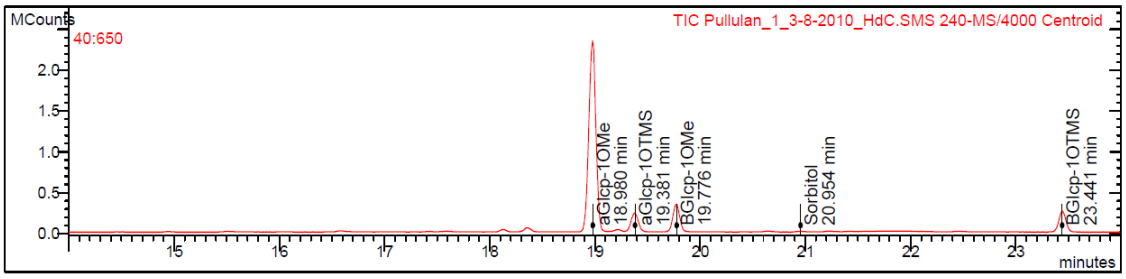

Target Compounds

RT (min)	RRT (min)	Peak Name	Area	Status	Quan Ions	Result Type
20.954		Sorbitol			73.2	Identified
	1.000		9017	X STg		
16.584		aGalp-1OMe			73.2	Failed
	0.791		21656	X Zg		
18.980		aGlcp-1OMe			73.1	Identified
	0.906		2170813	X g		
19.381		aGlcp-1OTMS			73.1	Identified
	0.925		254696	X g		
19.776		BGlcp-1OMe			73.1	Identified
	0.944		322926	X g		
23.441		BGlcp-1OTMS			73.1	Identified
	1.119		286017	X g		

Figure E.1.2: Processed GC-MS data for pullulan.

Sample ID:	pullulan	Operator:	ER
Instrument ID:	Varian CP-3800	Last Calibration:	None
Acquisition Date:	5/22/2010 3:45 AM	Data File:	...n_1_5-22-2010_er.sms
Calculation Date:	3/25/2016 3:22 PM	Method:	...cpd tbl pullulan.mth
Inj. Sample Notes:	Sigma new pullulan. Methanolysis and silylation. 10 uL sorbitol added after 20 hour cook.		

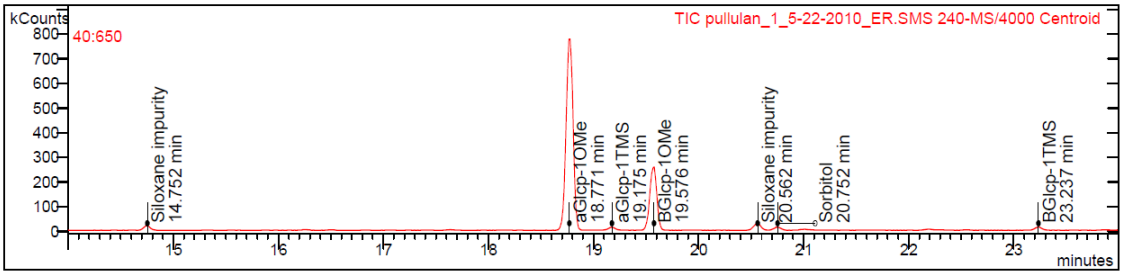

Target Compounds

RT (min)	RRT (min)	Peak Name	Area	Status	Quan Ions	Result Type
20.752		Sorbitol			73.2	Identified
	1.000		11042	X STg		
14.752		Siloxane impurity			73.0	Identified
	0.711		16026	X g		
18.771		aGlcp-1OMe			73.1	Identified
	0.905		769701	X g		
19.175		aGlcp-1TMS			73.2	Identified
	0.924		12108	X g		
19.576		BManp-1TMS			73.2	Failed
	0.943		273947	X Zg		
19.576		BGlcp-1OMe			73.1	Identified
	0.943		274483	X g		
19.576		BGalL-1TMS			73.2	Failed
	0.943		273375	X Zg		
20.562		Siloxane impurity			73.2	Identified
	0.991		23837	X g		
23.237		BGlcp-1TMS			73.2	Identified
	1.120		13038	X g		

Figure E.1.3: Processed GC-MS data for pullulan.

Sample ID:	FB2 F1	Operator:	ER
Instrument ID:	Varian CP-3800	Last Calibration:	None
Acquisition Date:	6/16/2010 9:42 AM	Data File:	...1_1_6-16-2010_er.sms
Calculation Date:	3/13/2016 12:18 PM	Method:	...10 _ 13032016 v1.mth
Inj. Sample Notes:	FB2 F1 140510 methanolysis silylation. solvents freshly dri		
	ed. 5uL of 0.3 mg/mL sorbitol added before cook.		

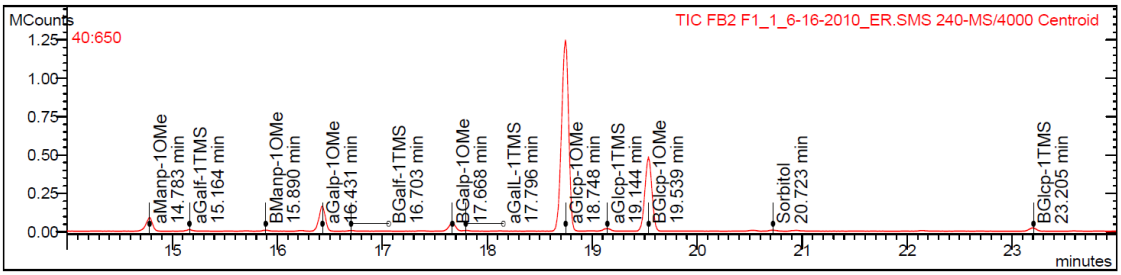

Target Compounds

RT (min)	Peak Name	RRT (min)	Area	Status	Quan Ions	Result Type
20.723	Sorbitol				73.2	Identified
		1.000	7143	X STg		
14.783	aManp-1OMe				204.1	Identified
		0.713	56034	X g		
15.164	aGalf-1TMS				73.1	Identified
		0.732	9549	X g		
15.890	BManp-1OMe				73.1	Identified
		0.767	5908	X g		
16.431	aGalp-1OMe				73.1	Identified
		0.793	162020	X g		
16.703	BGalf-1TMS				73.1	Identified
		0.806	3553	X g		
17.668	BGalp-1OMe				73.1	Identified
		0.853	51623	X g		
17.796	aGalL-1TMS				73.2	Identified
		0.859	2019	X g		
18.748	aGlcp-1OMe				204.1	Identified
		0.905	970622	X g		
19.144	aGlcp-1TMS				73.2	Identified
		0.924	19844	X g		
19.539	BManp-1TMS				73.2	Failed
		0.943	501303	X Zg		
19.539	BGlcp-1OMe				73.1	Identified
		0.943	501303	X g		
19.539	BGalL-1TMS				73.2	Failed
		0.943	489564	X Zg		
23.205	BGlcp-1TMS				73.2	Identified
		1.120	25396	X g		

Figure E.1.4: Processed GC-MS data for FB2 F1.

Sample ID:	FB2 F2	Operator:	ER
Instrument ID:	Varian CP-3800	Last Calibration:	None
Acquisition Date:	5/22/2010 11:36 AM	Data File:	...2_1_5-22-2010_er.sms
Calculation Date:	3/25/2016 2:45 PM	Method:	...d tbl 4_25032016.mth
Inj. Sample Notes:	Fed batch 2 wo celite. Fraction 2 from GPC column. Methanoly sis and silylation. 10 uL sorbitol added after 20 hour cook.		

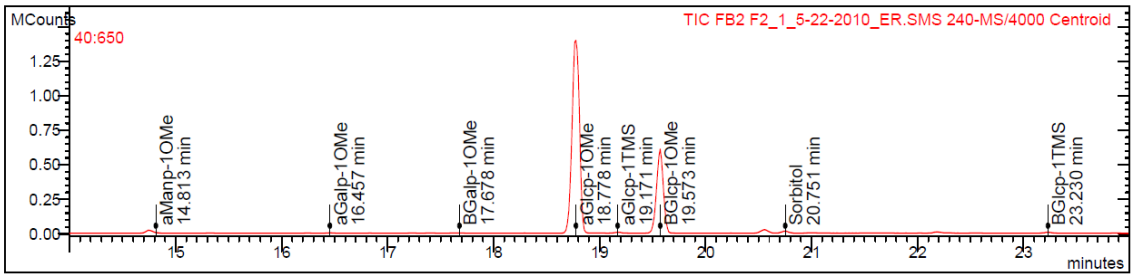

Target Compounds

RT (min)	RRT (min)	Peak Name	Area	Status	Quan Ions	Result Type
20.751	1.000	Sorbitol	14412	X STg	73.2	Identified
14.813	0.714	aManp-1OMe	2849	X g	204.0	Identified
16.457	0.793	aGalp-1OMe	1596	X g	73.1	Identified
17.678	0.852	BGalp-1OMe	440	X g	73.1	Identified
18.778	0.905	aGlcp-1OMe	1368912	X g	73.0	Identified
19.171	0.924	aGlcp-1TMS	7135	X g	73.2	Identified
19.573	0.943	BManp-1TMS	610107	X Zg	73.2	Failed
19.573	0.943	BGlcp-1OMe	610308	X g	73.1	Identified
19.573	0.943	BGalL-1TMS	609669	X Zg	73.2	Failed
23.230	1.119	BGlcp-1TMS	7932	X g	73.2	Identified

Figure E.1.5: Processed GC-MS data for FB2 F2.

Sample ID:	FB2 F3	Operator:	ER
Instrument ID:	Varian CP-3800	Last Calibration:	None
Acquisition Date:	5/22/2010 12:28 PM	Data File:	...3_1_5-22-2010_er.sms
Calculation Date:	3/25/2016 3:06 PM	Method:	...d tbl 5_25032016.mth
Inj. Sample Notes:	Fed batch 2 wo celite. Fraction 3 from GPC column. Methanoly sis and silylation. 10 uL sorbitol added after 20 hour cook.		

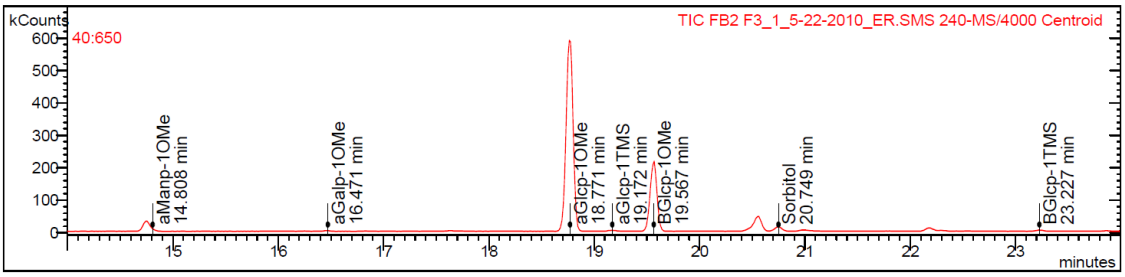

Target Compounds

RT (min)	RRT (min)	Peak Name	Area	Status	Quan Ions	Result Type
20.749		Sorbitol			73.2	Identified
	1.000		11459	X STg		
14.808		aManp-1OMe			204.0	Identified
	0.714		1415	X g		
16.471		aGalp-1OMe			73.1	Identified
	0.794		1028	X g		
18.771		aGlcp-1OMe			73.1	Identified
	0.905		597986	X g		
19.172		aGlcp-1TMS			73.2	Identified
	0.924		3337	X g		
19.567		BManp-1TMS			73.2	Failed
	0.943		224221	X Zg		
19.567		BGlcp-1OMe			73.1	Identified
	0.943		224221	X g		
19.567		BGalL-1TMS			73.2	Failed
	0.943		224021	X Zg		
23.227		BGlcp-1TMS			73.2	Identified
	1.119		4079	X g		

Figure E.1.6: Processed GC-MS data for FB2 F3.

Sample ID:	FB2 B1 Fr2	Operator:	HdC
Instrument ID:	Varian CP-3800	Last Calibration:	None
Acquisition Date:	3/8/2010 5:31 PM	Data File:	...2_1_3-8-2010_hdc.sms
Calculation Date:	3/25/2016 4:20 PM	Method:	... f2_13032016 v2_.mth
Inj. Sample Notes:	FB2 batch 1 fraction 2 methylated and silylated with sorbito l.		

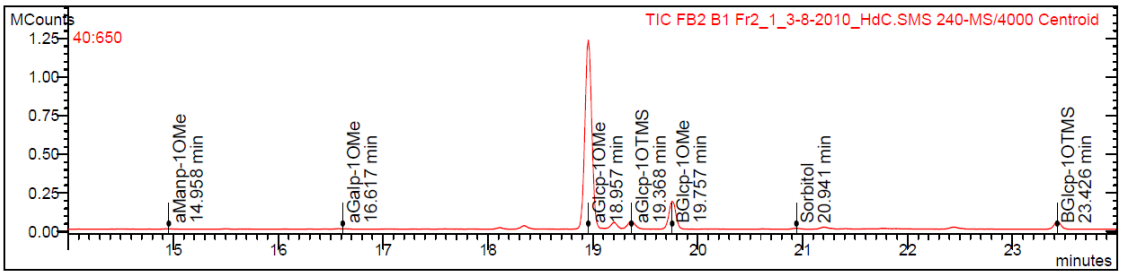

Target Compounds

RT (min)	Peak Name	RRT (min)	Area	Status	Quan Ions	Result Type
20.941	Sorbitol	1.000	5402	X STg	73.2	Identified
14.958	aManp-1OMe	0.714	945	X g	73.0	Identified
16.617	aGalp-1OMe	0.793	239	X g	73.2	Identified
18.957	aGlcp-1OMe	0.905	1155594	X g	73.1	Identified
19.368	aGlcp-1OTMS	0.925	57136	X g	73.1	Identified
19.757	BGlcp-1OMe	0.943	181265	X g	73.1	Identified
23.426	BGlcp-1OTMS	1.119	54894	X g	73.1	Identified

Figure E.1.7: Processed GC-MS data for FB2 F2.

Sample ID:	FB2 Batch2 Fr2	Operator:	HdC
Instrument ID:	Varian CP-3800	Last Calibration:	None
Acquisition Date:	3/8/2010 7:16 PM	Data File:	...2_1_3-8-2010_hdc.sms
Calculation Date:	3/25/2016 4:40 PM	Method:	... f2_13032016 v3_.mth
Inj. Sample Notes:	FB2 Batch 2 fraction 2methylated and silylated with sorbitol		

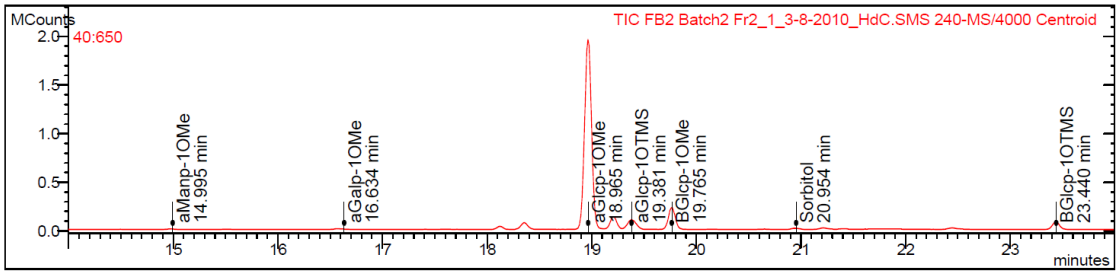

Target Compounds

RT (min)	Peak Name	RRT (min)	Area	Status	Quan Ions	Result Type
20.954	Sorbitol				73.2	Identified
	1.000		14438	X STg		
14.995	aManp-1OMe				73.0	Identified
	0.716		1696	X g		
16.634	aGalp-1OMe				204.3	Identified
	0.794		1118	X g		
18.965	aGlcp-1OMe				73.1	Identified
	0.905		1818546	X g		
19.381	aGlcp-1OTMS				73.1	Identified
	0.925		123897	X g		
19.765	BGlcp-1OMe				73.1	Identified
	0.943		218960	X g		
23.440	BGlcp-1OTMS				73.1	Identified
	1.119		89880	X g		

Figure E.1.8: Processed GC-MS data for FB2 F2.

Sample ID:	FB2 F1	Operator:	ER
Instrument ID:	Varian CP-3800	Last Calibration:	None
Acquisition Date:	6/16/2010 9:42 AM	Data File:	...1_1_6-16-2010_er.sms
Calculation Date:	3/13/2016 12:18 PM	Method:	...10 _ 13032016 v1.mth
Inj. Sample Notes:	FB2 F1 140510 methanolysis silylation. solvents freshly dri ed. 5uL of 0.3 mg/mL sorbitol added before cook.		

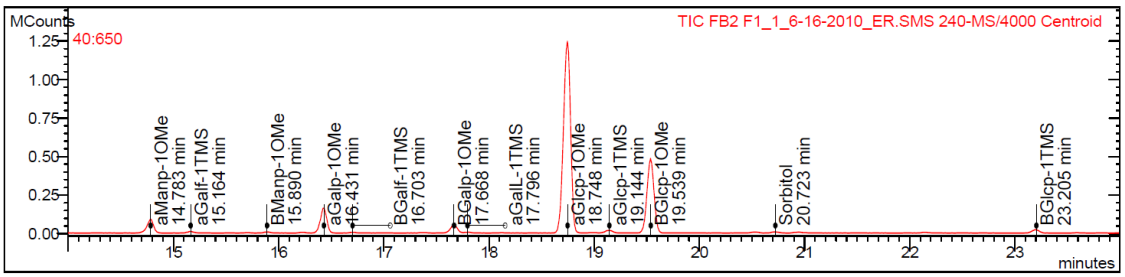

Target Compounds

RT (min)	RRT (min)	Peak Name	Area	Status	Quan Ions	Result Type
20.723		Sorbitol			73.2	Identified
	1.000		7143	X STg		
14.783		aManp-1OMe			204.1	Identified
	0.713		56034	X g		
15.164		aGalf-1TMS			73.1	Identified
	0.732		9549	X g		
15.890		BManp-1OMe			73.1	Identified
	0.767		5908	X g		
16.431		aGalp-1OMe			73.1	Identified
	0.793		162020	X g		
16.703		BGalf-1TMS			73.1	Identified
	0.806		3553	X g		
17.668		BGalp-1OMe			73.1	Identified
	0.853		51623	X g		
17.796		aGalL-1TMS			73.2	Identified
	0.859		2019	X g		
18.748		aGlcp-1OMe			204.1	Identified
	0.905		970622	X g		
19.144		aGlcp-1TMS			73.2	Identified
	0.924		19844	X g		
19.539		BManp-1TMS			73.2	Failed
	0.943		501303	X Zg		
19.539		BGlcp-1OMe			73.1	Identified
	0.943		501303	X g		
19.539		BGalL-1TMS			73.2	Failed
	0.943		489564	X Zg		
23.205		BGlcp-1TMS			73.2	Identified
	1.120		25396	X g		

Figure E.1.9: Processed GC-MS data for FB2 F1.

Sample ID:	FB2 F2	Operator:	ER
Instrument ID:	Varian CP-3800	Last Calibration:	None
Acquisition Date:	6/16/2010 10:34 AM	Data File:	...2_1_6-16-2010_er.sms
Calculation Date:	3/25/2016 4:07 PM	Method:	...10 _ 13032016 v2.mth
Inj. Sample Notes:	FB2 F2 030310 methanolysis silylation. solvents freshly dri ed. 5uL of 0.3 mg/mL sorbitol added before cook.		

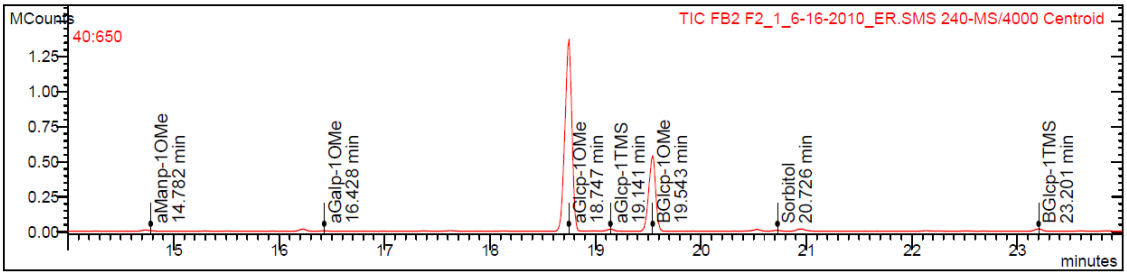

Target Compounds

RT (min)	RRT (min)	Peak Name	Area	Status	Quan Ions	Result Type
20.726		Sorbitol			73.2	Identified
	1.000		7112	X STg		
14.782		aManp-1OMe			204.1	Identified
	0.713		1356	X g		
16.428		aGalp-1OMe			73.1	Identified
	0.793		635	X g		
18.747		aGlcp-1OMe			204.1	Identified
	0.905		1037026	X g		
19.141		aGlcp-1TMS			73.2	Identified
	0.924		16212	X g		
19.543		BManp-1TMS			73.2	Failed
	0.943		553938	X Zg		
19.543		BGlcp-1OMe			73.1	Identified
	0.943		554297	X g		
19.543		BGalL-1TMS			73.2	Failed
	0.943		547873	X Zg		
23.201		BGlcp-1TMS			73.2	Identified
	1.119		20983	X g		

Figure E.1.10: Processed GC-MS data for FB2 F2.

Sample ID:	Fed Batch 2	Operator:	ER
Instrument ID:	I	Last Calibration:	None
Acquisition Date:	12/12/2008 9:34 PM	Data File:	...h 2_1_12-12-2008.sms
Calculation Date:	3/31/2016 11:54 AM	Method:	...compositional v2.mth
Inj. Sample Notes:	Img methanolysis,dried and sily		

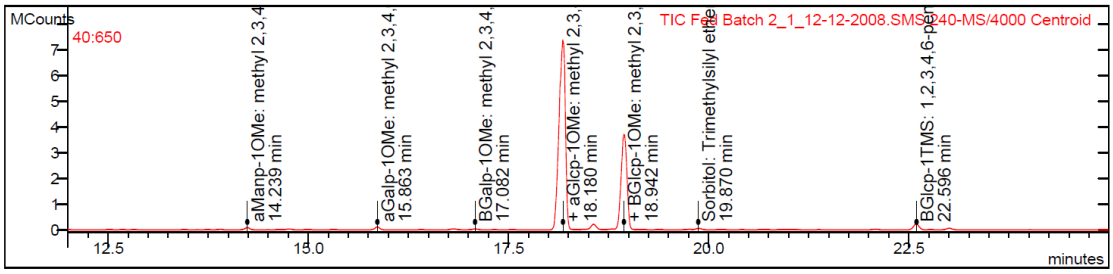

Target Compounds

RT (min)	RRT (min)	Peak Name / Area	Status	Quan Ions	Result Type
19.870		Sorbitol: Trimethylsilyl ether of glucit		73.1	Identified
	1.000	50616	X STg		
14.239		aManp-1OMe: methyl 2,3,4,6-tetrakis-O-(t		204.2	Identified
	0.717	50924	X g		
15.863		aGalp-1OMe: methyl 2,3,4,6-tetrakis-O-(t		73.1	Identified
	0.798	121536	X g		
17.082		BGalp-1OMe: methyl 2,3,4,6-tetrakis-O-(t		73.1	Identified
	0.860	35597	X g		
18.180		aGlcp-1OMe: methyl 2,3,4,6-tetrakis-O-(t		204.2	Identified
	0.915	5219162	X g		
18.567		aGlcp-1TMS: 1,2,3,4,6-pentakis-O-(trimet		73.1	Identified
	0.934	233323	X g		
18.942		BGlcp-1OMe: methyl 2,3,4,6-tetrakis-O-(t		204.2	Identified
	0.953	3438325	X g		
18.942		BGalL-1TMS: 2,3,4,5,6-pentakis-O-(trimet		204.2	Identified
	0.953	3438325	X g		
18.942		BManp-1TMS: 1,2,3,4,6-pentakis-O-(trimet		204.2	Identified
	0.953	3438325	X g		
22.596		BGlcp-1TMS: 1,2,3,4,6-pentakis-O-(trimet		73.1	Identified
	1.137	278477	X g		

Figure E.1.11: Processed GC-MS data for FB2.

Sample ID:	PB2	Operator:	HdC
Instrument ID:	Varian CP-3800	Last Calibration:	None
Acquisition Date:	9/20/2012 12:22 AM	Data File:	..._1_9-20-2012_hdc.sms
Calculation Date:	4/10/2016 11:11 AM	Method:	...ional mar2016_v2.mth
Inj. Sample Notes:	SACPOL Batch2. IS=0.1886g/25ml. Compositional.		

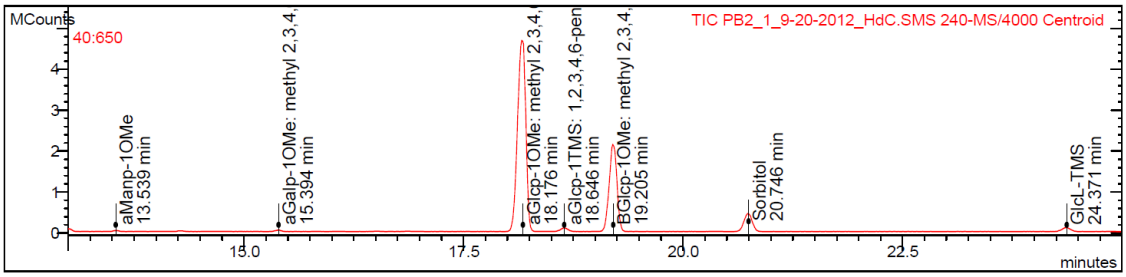

Target Compounds

RT (min)	RRT (min)	Peak Name	Area	Status	Quan Ions	Result Type
20.746		Sorbitol			73.2	Identified
	1.000		681111	X RSTg		
13.539		aManp-1OMe			73.1	Identified
	0.653		25975	X g		
15.394		aGalp-1OMe: methyl 2,3,4,6-tetrakis-O-(t			73.2	Identified
	0.742		41821	X g		
15.394		BManp-1OMe			73.1	Failed
	0.742		37137	X Zg		
15.394		BGalf-1TMS: 1,2,3,5,6-pentakis-O-(trimet			73.2	Failed
	0.742		40903	X bg		
18.176		aGlcp-1OMe: methyl 2,3,4,6-tetrakis-O-(t			73.2	Identified
	0.876		5850761	X g		
18.646		aGlcp-1TMS: 1,2,3,4,6-pentakis-O-(trimet			73.2	Identified
	0.899		137206	X g		
19.205		BGlcp-1OMe: methyl 2,3,4,6-tetrakis-O-(t			73.2	Identified
	0.926		2804891	X g		
24.371		GlcL-TMS			73.3	Identified
	1.175		182299	X g		

Figure E.1.12: Processed GC-MS data for PB2.

Sample ID:	PB7D7	Operator:	HdC
Instrument ID:	Varian CP-3800	Last Calibration:	None
Acquisition Date:	9/20/2012 8:34 AM	Data File:	..._1_9-20-2012_hdc.sms
Calculation Date:	4/10/2016 11:12 AM	Method:	...ional mar2016_v2.mth
Inj. Sample Notes:	SACPOL Batch7 Day7. IS=0.1886g/25ml. Compositional.		

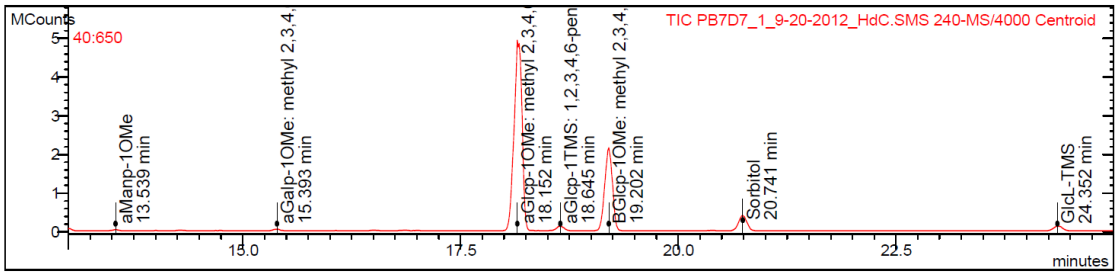

Target Compounds

RT (min)	RRT (min)	Peak Name / Area	Status	Quan Ions	Result Type
20.741		Sorbitol		73.2	Identified
	1.000	612849	X RSTg		
13.539		aManp-1OMe		73.1	Identified
	0.653	29202	X g		
15.393		aGalp-1OMe: methyl 2,3,4,6-tetrakis-O-(t		73.2	Identified
	0.742	55564	X g		
15.393		BManp-1OMe		73.1	Failed
	0.742	45325	X Zg		
15.393		BGalf-1TMS: 1,2,3,5,6-pentakis-O-(trimet		73.2	Failed
	0.742	53660	X bg		
18.152		aGlcp-1OMe: methyl 2,3,4,6-tetrakis-O-(t		73.2	Identified
	0.875	3007625	X g		
18.645		aGlcp-1TMS: 1,2,3,4,6-pentakis-O-(trimet		73.2	Identified
	0.899	186134	X g		
19.202		BGlcp-1OMe: methyl 2,3,4,6-tetrakis-O-(t		73.2	Identified
	0.926	2775410	X g		
24.352		GlcL-TMS		73.3	Identified
	1.174	107919	X g		

Figure E.1.13: Processed GC-MS data for PB7.

Sample ID:	Dextran	Operator:	HdC
Instrument ID:	Varian CP-3800	Last Calibration:	None
Acquisition Date:	3/8/2010 2:54 PM	Data File:	...n_1_3-8-2010_hdc.sms
Calculation Date:	3/19/2016 10:51 AM	Method:	... f2_13032016 v1_.mth
Inj. Sample Notes:	Dextran methylated and silylated with sorbitol.		

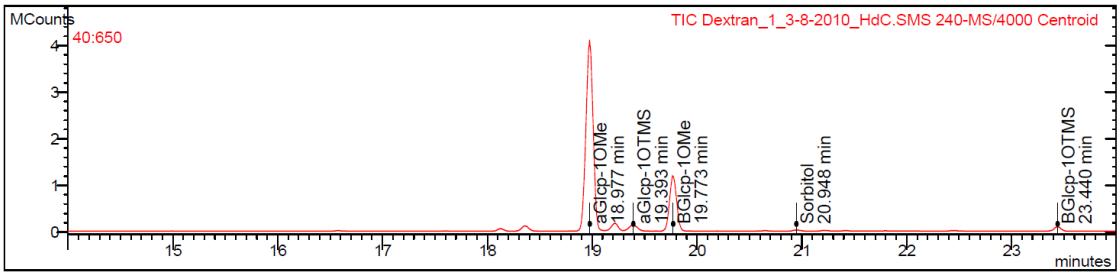

Target Compounds

RT (min)	RRT (min)	Peak Name	Area	Status	Quan Ions	Result Type
20.948		Sorbitol			73.2	Identified
	1.000		27078	X STg		
14.999		aManp-1OMe			204.1	Failed
	0.716		1906	X Zg		
18.977		aGlcp-1OMe			73.1	Identified
	0.906		3685665	X g		
19.393		aGlcp-1OTMS			73.1	Identified
	0.926		157384	X g		
19.773		BGlcp-1OMe			73.1	Identified
	0.944		1160832	X g		
23.440		BGlcp-1OTMS			73.1	Identified
	1.119		106778	X g		

Figure E.1.14: Processed GC-MS data for dextran.

Sample ID:	galactose	Operator:	ER
Instrument ID:	Varian CP-3800	Last Calibration:	None
Acquisition Date:	5/22/2010 5:30 AM	Data File:	...e_1_5-22-2010_er.sms
Calculation Date:	3/13/2016 11:40 AM	Method:	...d tbl 3_13032016.mth
Inj. Sample Notes:	D-(+)-galactose. Methanolysis and silylation. 10 uL sorbitol added after 20 hour cook.		

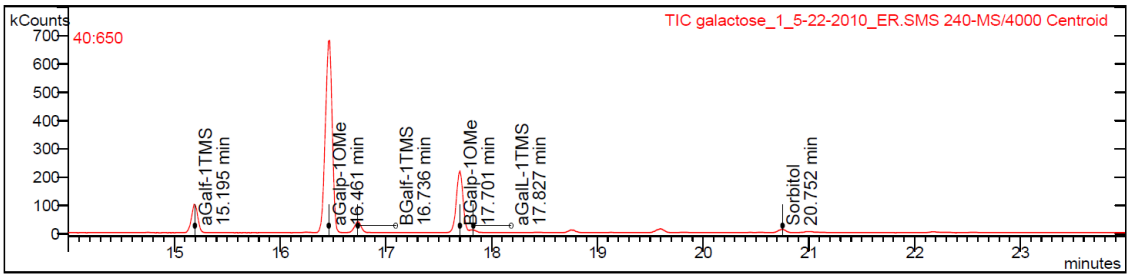

Target Compounds

RT (min)	RRT (min)	Peak Name	Area	Status	Quan Ions	Result Type
20.752		Sorbitol			73.2	Identified
	1.000		11697	X STg		
15.195		aGalf-1TMS			73.1	Identified
	0.732		92784	X g		
16.461		aGalp-1OMe			73.1	Identified
	0.793		680494	X g		
16.736		BGalf-1TMS			73.1	Identified
	0.806		35392	X g		
17.701		BGalp-1OMe			73.1	Identified
	0.853		210974	X g		
17.827		aGalL-1TMS			73.2	Identified
	0.859		3400	X g		
18.757		aGlcp-1OMe			73.0	Failed
	0.904		8720	X Zg		
19.597		BManp-1TMS			73.2	Failed
	0.944		15342	X Zg		
19.597		BGlcp-1OMe			73.1	Failed
	0.944		15342	X Zg		
19.597		BGalL-1TMS			73.2	Failed
	0.944		15342	X Zg		

Figure E.1.15: Processed GC-MS data for galactose.

Sample ID:	mannose	Operator:	ER
Instrument ID:	Varian CP-3800	Last Calibration:	None
Acquisition Date:	5/22/2010 6:22 AM	Data File:	...e_1_5-22-2010_er.sms
Calculation Date:	3/13/2016 11:44 AM	Method:	...bl 3_13032016 v2.mth
Inj. Sample Notes:	D-(+)-mannose. Methanolysis and silylation. 10 uL sorbitol added after 20 hour cook.		

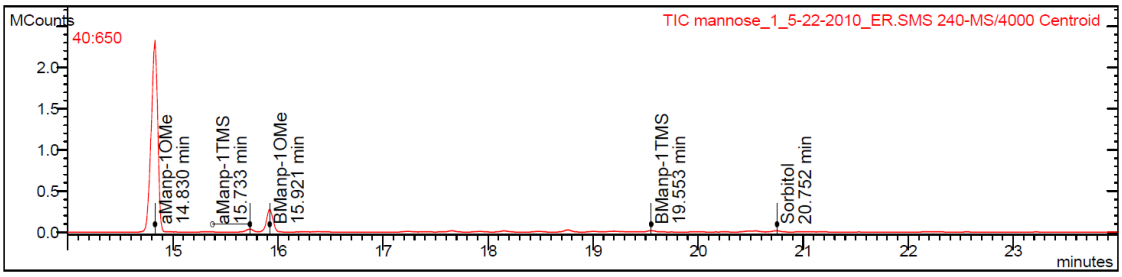

Target Compounds

RT (min)	Peak Name	RRT (min)	Area	Status	Quan Ions	Result Type
20.752	Sorbitol				73.2	Identified
	1.000		16251	X STg		
14.830	aManp-1OMe				204.1	Identified
	0.715		1788826	X g		
15.733	aManp-1TMS				73.1	Identified
	0.758		34465	X g		
15.921	BManp-1OMe				73.1	Identified
	0.767		264835	X g		
17.918	aGalL-1TMS				73.2	Failed
	0.863		2855	X bg		
19.553	BManp-1TMS				73.2	Identified
	0.942		17547	X g		
19.553	BGlcp-1OMe				73.1	Failed
	0.942		17547	X Zg		
19.553	BGalL-1TMS				73.2	Failed
	0.942		17547	X Zg		

Figure E.1.16: Processed GC-MS data for mannose.

Sample ID:	dextran	Operator:	ER
Instrument ID:	Varian CP-3800	Last Calibration:	None
Acquisition Date:	5/22/2010 4:37 AM	Data File:	...n_1_5-22-2010_er.sms
Calculation Date:	9/15/2010 3:16 PM	Method:	...cpd tbl 3_151009.mth
Inj. Sample Notes:	GPC 50 000 Da dextran. Methanolysis and silylation. 10 uL so rbitol added after 20 hour cook.		

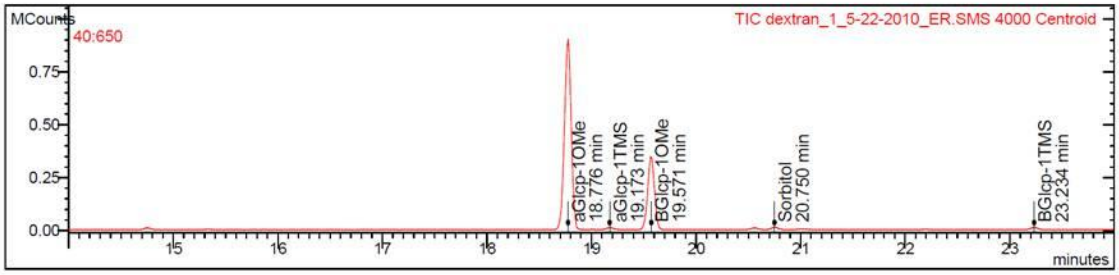

Target Compounds

RT (min)	Peak Name	RRT (min)	Area	Status	Quan Ions	Result Type
20.750	Sorbitol	1.000	11082	X STg	73.2	Identified
18.776	aGlcp-1OMe	0.905	865430	X g	73.0	Identified
19.173	aGlcp-1TMS	0.924	9721	X g	73.2	Identified
19.571	BManp-1TMS	0.943	356905	X Zg	73.2	Failed
19.571	BGlcp-1OMe	0.943	357009	X g	73.1	Identified
19.571	BGalL-1TMS	0.943	357009	X Zg	73.2	Failed
23.234	BGlcp-1TMS	1.120	10357	X g	73.2	Identified

Figure E.1.17: Processed GC-MS data for dextran.

Sample ID:	cellobiose	Operator:	HdC
Instrument ID:	Varian CP-3800	Last Calibration:	None
Acquisition Date:	10/23/2009 12:56 PM	Data File:	...ose_1_10-23-2009.sms
Calculation Date:	11/10/2010 9:39 AM	Method:	...e and cellobiose.mth
Inj. Sample Notes:	cellobiose methanolysis and silylation with 10uL sorbitol st d added after the 20 hour cook		

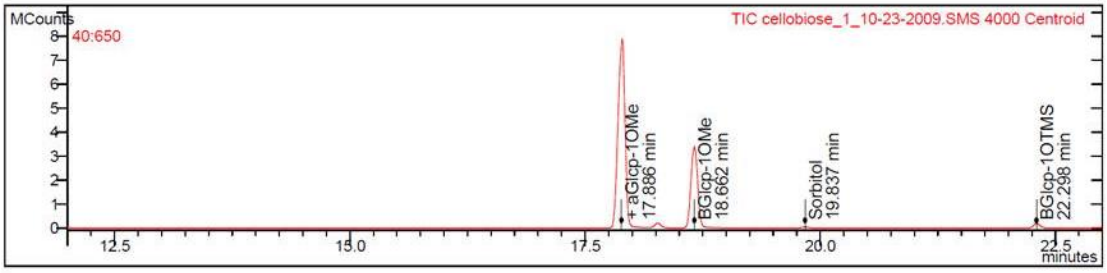

Target Compounds

RT (min)	Peak Name	RRT (min)	Area	Status	Quan Ions	Result Type
19.837	Sorbitol	1.000	43128	X STg	73.1	Identified
17.886	aGlcp-1OMe	0.902	3424952	X g	73.0	Identified
18.273	aGlcp-1TMS	0.921	215186	X g	73.1	Identified
18.665	BManp-1OTMS	0.941	3504694	X Zg	73.1	Failed
18.662	BGlcp-1OMe	0.941	3056624	X g	204.1	Identified
18.665	BGalL-1OTMS	0.941	3503394	X Zg	73.2	Failed
22.298	BGlcp-1OTMS	1.124	232875	X g	73.1	Identified

Figure E.1.18: Processed GC-MS data for cellobiose.

Sample ID:	galactose	Operator:	HdC
Instrument ID:	Varian CP-3800	Last Calibration:	None
Acquisition Date:	10/23/2009 3:33 PM	Data File:	...ose_1_10-23-2009.sms
Calculation Date:	11/10/2010 9:33 AM	Method:	... 150610_6_101110.mth
Inj. Sample Notes:	galactose methanolysis and silylation with 10uL sorbitol std added after the 20 hour cook		

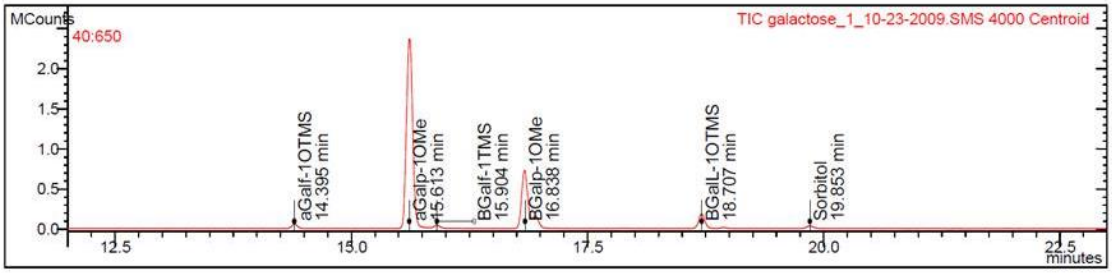

Target Compounds

RT (min)	Peak Name	RRT (min)	Area	Status	Quan Ions	Result Type
19.853	Sorbitol	1.000	37853	X STg	73.1	Identified
14.395	aGalf-1OTMS	0.725	58735	X g	73.1	Identified
15.613	aGalp-1OMe	0.786	2338322	X g	73.0	Identified
15.904	BGalf-1TMS	0.801	35110	X g	73.1	Identified
16.838	BGalp-1OMe	0.848	688620	X g	73.0	Identified
18.707	BManp-1OTMS	0.942	209060	X Zg	73.1	Failed
18.708	BGlcp-1OMe	0.942	118564	X Zg	204.1	Failed
18.707	BGalL-1OTMS	0.942	209629	X g	73.2	Identified

Figure E.1.19: Processed GC-MS data for galactose.

Sample ID:	glucose	Operator:	HdC
Instrument ID:	Varian CP-3800	Last Calibration:	11/10/2010 10:05 AM
Acquisition Date:	10/28/2009 3:21 AM	Data File:	...ose_1_10-28-2009.sms
Calculation Date:	11/10/2010 10:05 AM	Method:	...1110 for glucose.mth
Inj. Sample Notes:	glucose methanolysis silylation with 10 uL of the sorbitol s olution added BEFORE the 20hr cook		

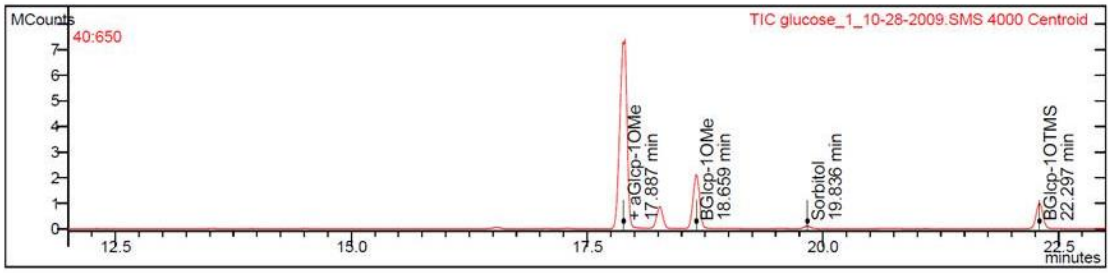

Target Compounds

RT (min)	Peak Name	RRT (min)	Area	Status	Quan Ions	Result Type
19.836	Sorbitol	1.000	115771	ST	73.1	Identified
17.887	aGlcp-1OMe	0.902	6678404		73.0	Identified
18.270	aGlcp-1TMS	0.921	965170		73.1	Identified
18.657	BManp-1OTMS	0.941	2148405	X Z	73.1	Failed
18.659	BGlcp-1OMe	0.941	1787497		204.1	Identified
18.657	BGalL-1OTMS	0.941	2144642	X Z	73.2	Failed
22.297	BGlcp-1OTMS	1.124	1222616		73.1	Identified

Figure E.1.20: Processed GC-MS data for glucose.

Sample ID:	maltotriose	Operator:	HdC
Instrument ID:	Varian CP-3800	Last Calibration:	None
Acquisition Date:	10/23/2009 4:25 PM	Data File:	...ose_1_10-23-2009.sms
Calculation Date:	11/10/2010 9:38 AM	Method:	...e and cellobiose.mth
Inj. Sample Notes:	maltotriose methanolysis and silylation with 10uL sorbitol s td added after the 20 hour cook		

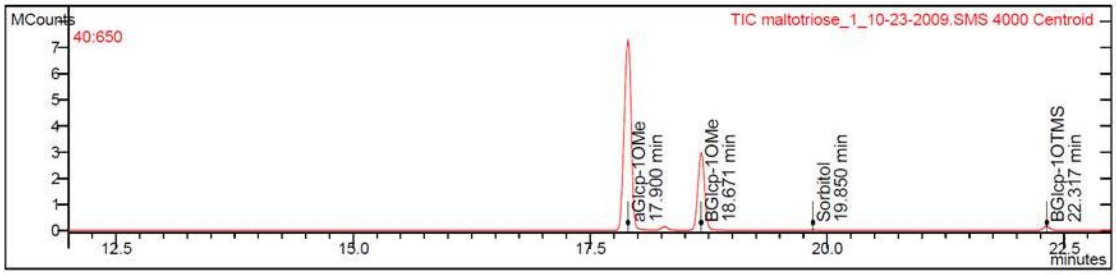

Target Compounds

RT (min)	Peak Name	RRT (min)	Area	Status	Quan Ions	Result Type
19.850	Sorbitol	1.000	20694	X STg	73.1	Identified
17.900	aGlcp-1OMe	0.902	6329680	X g	73.0	Identified
18.671	BManp-1OTMS	0.941	3005767	X Zg	73.1	Failed
18.671	BGlcp-1OMe	0.941	2584482	X g	204.1	Identified
18.671	BGalL-1OTMS	0.941	3008689	X Zg	73.2	Failed
22.317	BGlcp-1OTMS	1.124	176912	X g	73.1	Identified

Figure E.1.21: Processed GC-MS data for maltotriose.

Sample ID:	mannose	Operator:	HdC
Instrument ID:	Varian CP-3800	Last Calibration:	None
Acquisition Date:	10/23/2009 5:17 PM	Data File:	...ose_1_10-23-2009.sms
Calculation Date:	11/10/2010 9:34 AM	Method:	... 150610_6_101110.mth
Inj. Sample Notes:	mannose methanolysis and silylation with 10uL sorbitol std added after the 20 hour cook		

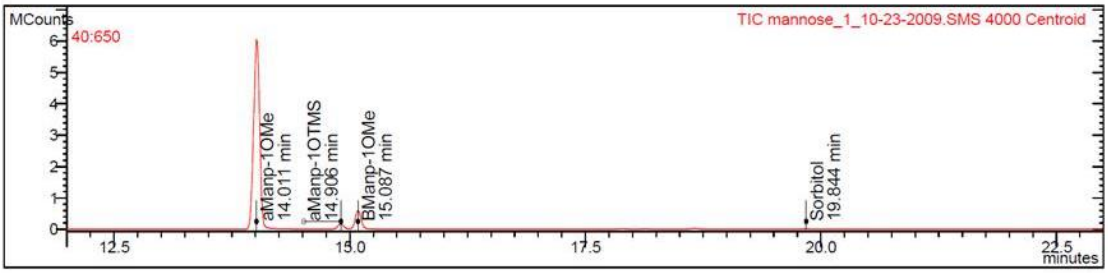

Target Compounds

RT (min)	Peak Name	RRT (min)	Area	Status	Quan Ions	Result Type
19.844	Sorbitol	1.000	9129	X STg	73.1	Identified
14.011	aManp-1OMe	0.706	4706365	X g	204.1	Identified
14.906	aManp-1OTMS	0.751	176812	X g	73.0	Identified
15.087	BManp-1OMe	0.760	507455	X g	73.0	Identified
18.662	BManp-1OTMS	0.940	28969	X Zg	73.1	Failed
18.665	BGlcp-1OMe	0.941	16763	X Zg	204.1	Failed
18.662	BGalL-1OTMS	0.940	28804	X Zg	73.2	Failed

Figure E.1.22: Processed GC-MS data for mannose.

Sample ID:	melibiose	Operator:	HdC
Instrument ID:	Varian CP-3800	Last Calibration:	11/10/2010 10:00 AM
Acquisition Date:	10/28/2009 6:51 AM	Data File:	...ose_1_10-28-2009.sms
Calculation Date:	11/10/2010 10:18 AM	Method:	... 150610_6_101110.mth
Inj. Sample Notes:	melibiose methanolysis silylation with 10 uL of the sorbitol solution added BEFORE the 20hr cook		

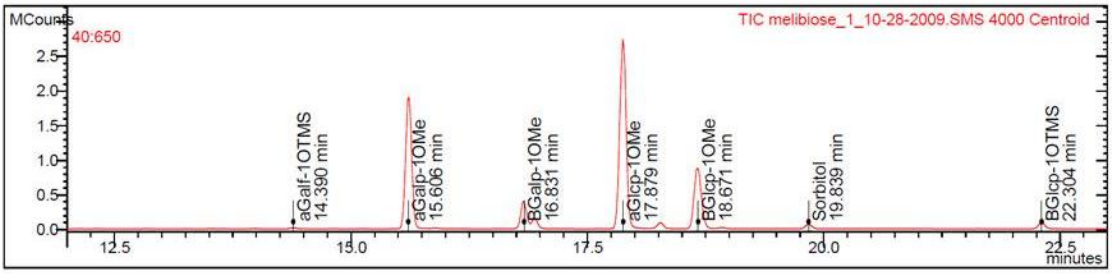

Target Compounds

RT (min)	Peak Name	RRT (min)	Area	Status	Quan Ions	Result Type
19.839	Sorbitol	1.000	74450	ST	73.1	Identified
13.987	aManp-1OMe	0.705	2327	X Zg	204.1	Failed
14.390	aGalf-1OTMS	0.725	16198	X g	73.1	Identified
15.606	aGalp-1OMe	0.787	1876911	X g	73.0	Identified
16.831	BGalp-1OMe	0.848	364946	X g	73.0	Identified
17.879	aGlcp-1OMe	0.901	2692811		73.0	Identified
18.671	BManp-1OTMS	0.941	1067979	X Z	73.1	Failed
18.671	BGlcp-1OMe	0.941	778235		204.1	Identified
18.671	BGalL-1OTMS	0.941	1064650	X Z	73.2	Failed
22.304	BGlcp-1OTMS	1.124	113605		73.1	Identified

Figure E.1.23: Processed GC-MS data for melibiose.

Sample ID:	stachyose	Operator:	HdC
Instrument ID:	Varian CP-3800	Last Calibration:	11/10/2010 10:00 AM
Acquisition Date:	10/28/2009 9:28 AM	Data File:	...ose_1_10-28-2009.sms
Calculation Date:	11/10/2010 10:16 AM	Method:	...101110 stachyose.mth
Inj. Sample Notes:	stachyose methanolysis silylation with 10 uL of the sorbitol solution added BEFORE the 20hr cook		

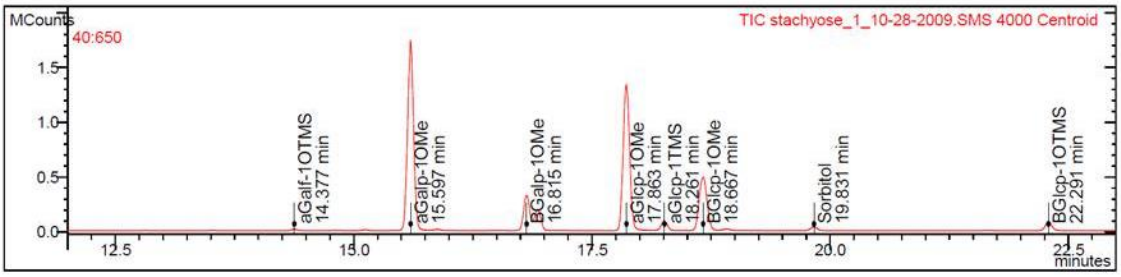

Target Compounds

RT (min)	Peak Name	RRT (min)	Area	Status	Quan Ions	Result Type
19.831	Sorbitol	1.000	40941	ST	73.1	Identified
14.377	aGalf-1OTMS	0.725	13975	X g	73.1	Identified
15.597	aGalp-1OMe	0.787	1685721	X g	73.0	Identified
16.815	BGalp-1OMe	0.848	321592	X g	73.0	Identified
17.863	aGlcp-1OMe	0.901	1346031		73.0	Identified
18.261	aGlcp-1TMS	0.921	101945		73.1	Identified
18.669	BManp-1OTMS	0.941	668141	X Z	73.1	Failed
18.667	BGlcp-1OMe	0.941	448536		204.1	Identified
18.669	BGalL-1OTMS	0.941	666618	X Z	73.2	Failed
22.291	BGlcp-1OTMS	1.124	100586		73.1	Identified

Figure E.1.24: Processed GC-MS data for stachyose.

Sample ID:	locust bean gum	Operator:	ER
Instrument ID:	Varian CP-3800	Last Calibration:	None
Acquisition Date:	6/16/2010 8:49 AM	Data File:	...m_1_6-16-2010_er.sms
Calculation Date:	11/10/2010 10:21 AM	Method:	...cpd tbl 6_141009.mth
Inj. Sample Notes:	locust bean gummethanolysis silylation. solvents freshly dried. 5uL of 0.3 mg/mL sorbitol added before cook.		

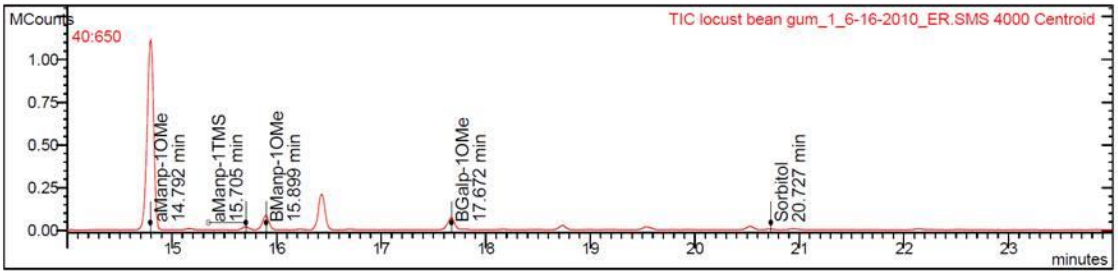

Target Compounds

RT (min)	Peak Name	RRT (min)	Area	Status	Quan Ions	Result Type
20.727	Sorbitol	1.000	4799	X STg	73.1	Identified
14.792	aManp-1OMe	0.714	768885	X g	204.1	Identified
15.705	aManp-1TMS	0.758	17559	X g	73.0	Identified
15.899	BManp-1OMe	0.767	82851	X g	73.0	Identified
16.432	aGalp-1OMe	0.793	216243	X Zg	73.0	Failed
17.672	BGalp-1OMe	0.853	72153	X g	73.0	Identified
18.738	aGlcp-1OMe	0.904	25539	X Zg	73.0	Failed
19.539	BManp-1TMS	0.943	23833	X Zg	73.1	Failed
19.539	BGlcp-1OMe	0.943	17326	X Zg	204.1	Failed
19.539	BGalL-1TMS	0.943	23833	X Zg	73.2	Failed

Figure E.1.25: Processed GC-MS data for locust bean gum.

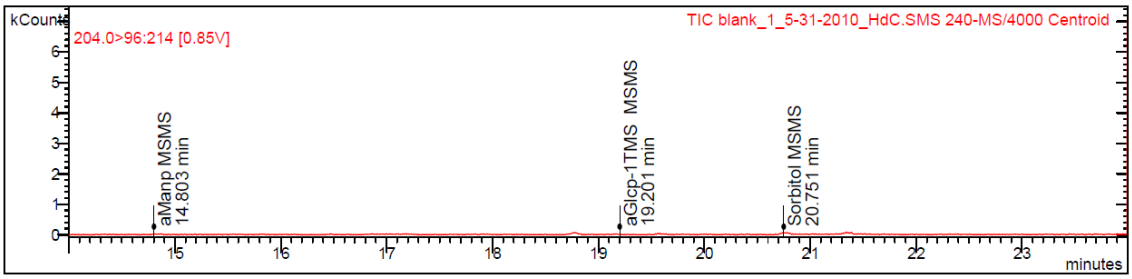

Target Compounds

RT (min)	RRT (min)	Peak Name	Area	Status	Quan Ions	Result Type
20.751		Sorbitol MSMS			RIC	Identified
	1.000		370	X STg		
14.803		aManp MSMS			RIC	Identified
	0.713		24	X g		
14.979		BGalf MSMS			RIC	Failed
	0.722		13	X bg		
19.201		aGlcp-1TMS MSMS			RIC	Identified
	0.925		47	X g		

Figure E.1.26: Processed GC-MS/MS (precursor ion, *m/z* = 204) for a blank sample.

Sample ID:	FB2 F1	Operator:	HdC
Instrument ID:	Varian CP-3800	Last Calibration:	None
Acquisition Date:	5/31/2010 8:35 PM	Data File:	..._1_5-31-2010_hdc.sms
Calculation Date:	3/14/2016 11:01 AM	Method:	...032016 for f1 v4.mth
Inj. Sample Notes:	FB2 F1 methanolysis sample from 190510. MSMS using m/z 204 a s precursor between 13.5-24min.		

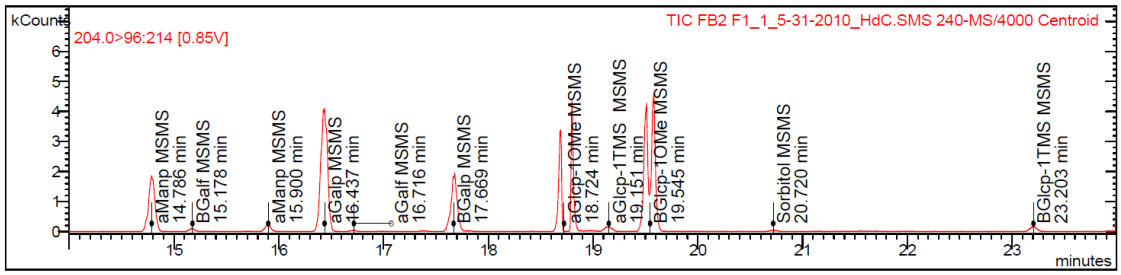

Target Compounds

RT (min)	Peak Name	RRT (min)	Area	Status	Quan Ions	Result Type
20.720	Sorbitol MSMS	1.000	197	X STg	RIC	Identified
14.786	aManp MSMS	0.714	4177	X g	RIC	Identified
15.178	BGalf MSMS	0.733	183	X g	RIC	Identified
15.900	aManp MSMS	0.767	884	X g	RIC	Identified
16.437	aGalp MSMS	0.793	9528	X g	RIC	Identified
16.716	aGalf MSMS	0.807	151	X g	RIC	Identified
17.669	BGalp MSMS	0.853	3442	X g	RIC	Identified
18.724	aGlcp-1OMe MSMS	0.904	13440	X g	RIC	Identified
19.151	aGlcp-1TMS MSMS	0.924	504	X g	RIC	Identified
19.545	BGlcp-1OMe MSMS	0.943	23511	X g	RIC	Identified
23.203	BGlcp-1TMS MSMS	1.120	803	X g	RIC	Identified

Figure E.1.27: Processed GC-MS/MS (precursor ion, *m/z* = 204) for FB2 F1.

Sample ID:	FB2 F2	Operator:	HdC
Instrument ID:	Varian CP-3800	Last Calibration:	None
Acquisition Date:	5/31/2010 9:27 PM	Data File:	..._1_5-31-2010_hdc.sms
Calculation Date:	3/14/2016 11:08 AM	Method:	...032016 for f2 v3.mth
Inj. Sample Notes:	FB2 F2 methanolysis sample from 190510. MSMS using m/z 204 a s precursor between 13.5-24min.		

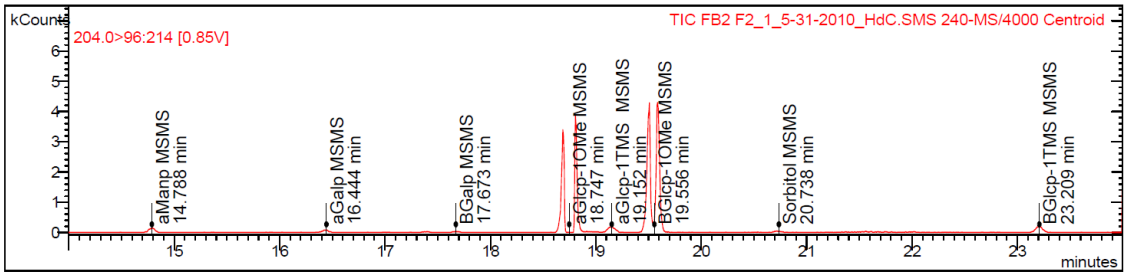

Target Compounds

RT (min)	RRT (min)	Peak Name	Area	Status	Quan Ions	Result Type
20.738		Sorbitol MSMS			RIC	Identified
	1.000		204	X STg		
14.788		aManp MSMS			RIC	Identified
	0.713		102	X g		
16.444		aGalp MSMS			RIC	Identified
	0.793		125	X g		
17.673		BGalp MSMS			RIC	Identified
	0.852		76	X g		
18.747		aGlcp-1OMe MSMS			RIC	Identified
	0.904		12332	X g		
19.152		aGlcp-1TMS MSMS			RIC	Identified
	0.924		906	X g		
19.556		BGlcp-1OMe MSMS			RIC	Identified
	0.943		19786	X g		
23.209		BGlcp-1TMS MSMS			RIC	Identified
	1.119		967	X g		

Figure E.1.28: Processed GC-MS/MS (precursor ion, *m/z* = 204) for FB2 F2.

Sample ID:	FB3 F3	Operator:	HdC
Instrument ID:	Varian CP-3800	Last Calibration:	None
Acquisition Date:	5/31/2010 10:19 PM	Data File:	..._1_5-31-2010_hdc.sms
Calculation Date:	3/14/2016 11:15 AM	Method:	...032016 for f3 v3.mth
Inj. Sample Notes:	FB2 F3 methanolysis sample from 190510. MSMS using m/z 204 a s precursor between 13.5-24min.		

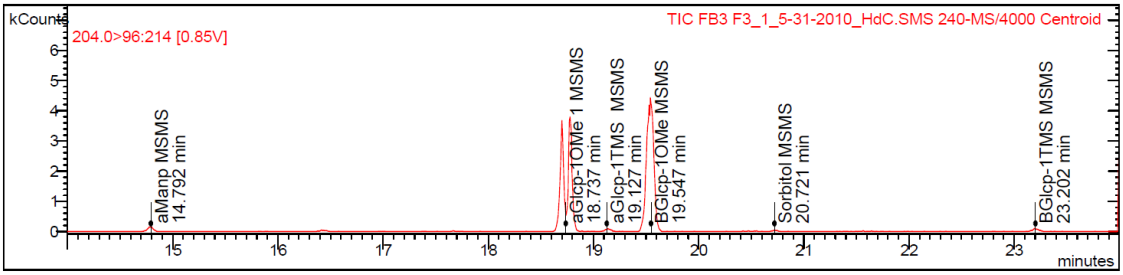

Target Compounds

RT (min)	RRT (min)	Peak Name	Area	Status	Quan Ions	Result Type
20.721	1.000	Sorbitol MSMS	150	X STg	RIC	Identified
14.792	0.714	aManp MSMS	65	X g	RIC	Identified
18.737	0.904	aGlcp-1OMe 1 MSMS	18473	X g	RIC	Identified
19.127	0.923	aGlcp-1TMS MSMS	370	X g	RIC	Identified
19.547	0.943	BGlcp-1OMe MSMS	21298	X g	RIC	Identified
23.202	1.120	BGlcp-1TMS MSMS	423	X g	RIC	Identified

Figure E.1.29: Processed GC-MS/MS (precursor ion, *m/z* = 204) for FB2 F3.

Sample ID:	pullulan	Operator:	HdC
Instrument ID:	Varian CP-3800	Last Calibration:	None
Acquisition Date:	5/31/2010 5:58 PM	Data File:	..._1_5-31-2010_hdc.sms
Calculation Date:	3/14/2016 11:25 AM	Method:	...on_13032016 pull.mth
Inj. Sample Notes:	pullulan methanolysis sample from 190510. MSMS using m/z 204 as precursor between 13.5-24min.		

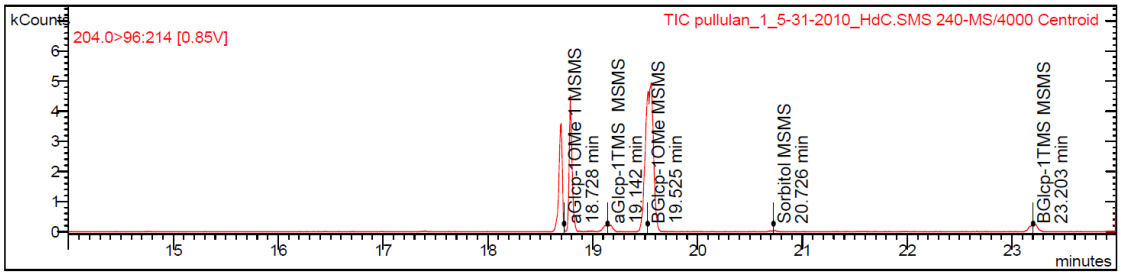

Target Compounds

RT (min)	RRT (min)	Peak Name	Area	Status	Quan Ions	Result Type
20.726		Sorbitol MSMS			RIC	Identified
	1.000		157	X STg		
18.728		aGlcp-1OMe 1 MSMS			RIC	Identified
	0.904		16599	X g		
19.142		aGlcp-1TMS MSMS			RIC	Identified
	0.924		1309	X g		
19.525		BGlcp-1OMe MSMS			RIC	Identified
	0.942		25961	X g		
23.203		BGlcp-1TMS MSMS			RIC	Identified
	1.120		1316	X g		

Figure E.1.30: Processed GC-MS/MS (precursor ion, *m/z* = 204) for pullulan.

Sample ID:	galactose	Operator:	HdC
Instrument ID:	Varian CP-3800	Last Calibration:	None
Acquisition Date:	5/31/2010 7:42 PM	Data File:	..._1_5-31-2010_hdc.sms
Calculation Date:	3/14/2016 11:37 AM	Method:	...ion_13032016 gal.mth
Inj. Sample Notes:	D-(+)-galactose methanolysis sample from 190510. MSMS using m/z 204 as precursor between 13.5-24min.		

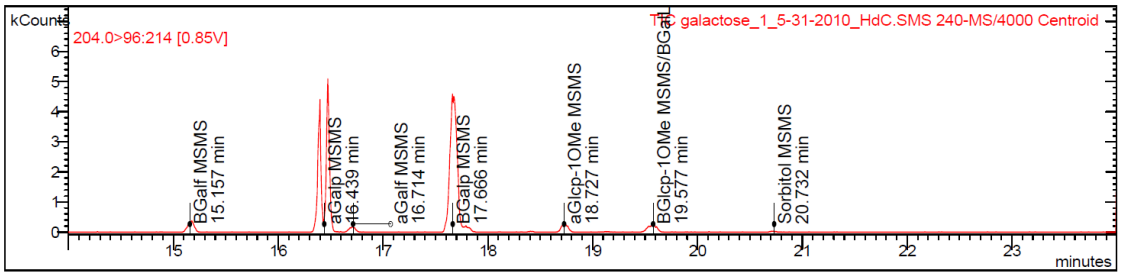

Target Compounds

RT (min)	RRT (min)	Peak Name	Area	Status	Quan Ions	Result Type
20.732		Sorbitol MSMS			189.0	Identified
	1.000		70	X STg		
15.157		BGalf MSMS			149.1	Identified
	0.731		665	X g		
16.439		aGalp MSMS			189.0	Identified
	0.793		12638	X g		
16.714		aGalf MSMS			149.1	Identified
	0.806		300	X g		
17.666		BGalp MSMS			189.0	Identified
	0.852		14589	X g		
18.727		aGlcp-1OMe MSMS			189.0	Identified
	0.903		232	X g		
19.577		BGlcp-1OMe MSMS/BGalL-1OMe			189.0	Identified
	0.944		428	X g		

Figure E.1.31: Processed GC-MS/MS (precursor ion, *m/z* = 204) for galactose.

Sample ID:	mannose	Operator:	HdC
Instrument ID:	Varian CP-3800	Last Calibration:	None
Acquisition Date:	5/31/2010 6:50 PM	Data File:	..._1_5-31-2010_hdc.sms
Calculation Date:	3/14/2016 11:44 AM	Method:	...ion_13032016 man.mth
Inj. Sample Notes:	D-(+)-mannose methanolysis sample from 190510. MSMS using m/z 204 as precursor between 13.5-24min.		

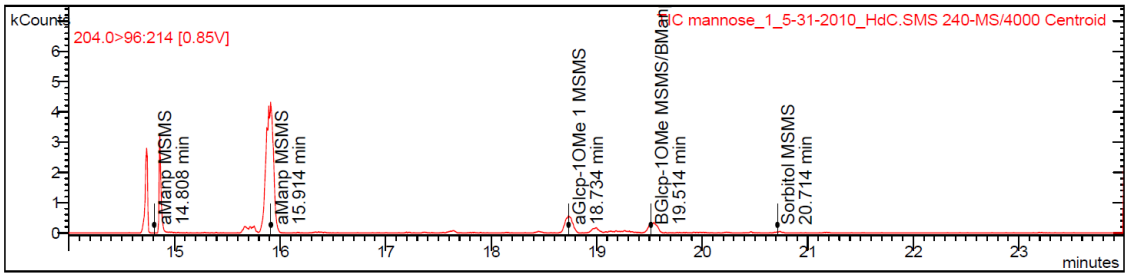

Target Compounds

RT (min)	RRT (min)	Peak Name	Area	Status	Quan Ions	Result Type
20.714	1.000	Sorbitol MSMS	204	X STg	RIC	Identified
14.808	0.715	aManp MSMS	8627	X g	RIC	Identified
15.914	0.768	aManp MSMS	20622	X g	RIC	Identified
18.734	0.904	aGlcp-1OMe 1 MSMS	850	X g	RIC	Identified
19.514	0.942	BGlcp-1OMe MSMS/BManp-1TMS	888	X g	RIC	Identified

Figure E.1.32: Processed GC-MS/MS (precursor ion, *m/z* = 204) for mannose.

Sample ID:	xylose	Operator:	HdC
Instrument ID:	Varian CP-3800	Last Calibration:	11/10/2010 10:00 AM
Acquisition Date:	10/23/2009 7:54 PM	Data File:	...se _1_10-23-2009.sms
Calculation Date:	5/2/2016 3:22 PM	Method:	... analysis_xylose.mth
Inj. Sample Notes:	xylose methanolysis and silylation with 10uL sorbitol std ad ded after the 20 hour cook		

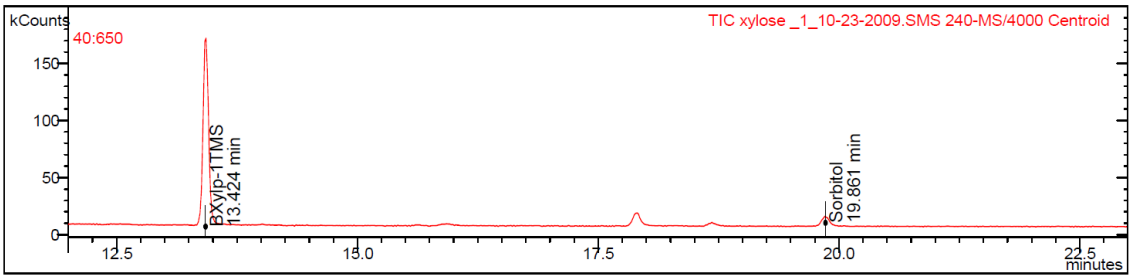

Target Compounds

RT (min)	RRT (min)	Peak Name	Area	Status	Quan Ions	Result Type
19.861	1.000	Sorbitol	10618	ST	73.1	Identified
9.878	0.497	aXylp-1OMe	3352613	X g	73.1	Identified
10.454	0.526	BXylp-1OMe	1540901	X g	73.1	Identified
11.581	0.583	aXylp-1TMS	128476	X g	73.2	Identified
13.424	0.676	BXylp-1TMS	160742	X g	73.2	Identified
17.902	0.901	aGlcp-1OMe	12418	X Z	73.0	Failed
18.680	0.941	BGalL-1OTMS	3277	X Z	73.2	Failed
18.683	0.941	BGlcp-1OMe	2379	X Z	204.1	Failed

Figure E.1.33: Processed GC-MS data for xylose.

E.2 Absolute configuration analysis

Sample ID:	Blank	Operator:	HdC
Instrument ID:	Varian CP-3800	Last Calibration:	None
Acquisition Date:	10/23/2015 9:02 PM	Data File:	...1_10-23-2015_hdc.sms
Calculation Date:	3/12/2016 1:13 PM	Method:	...sing\comp dl pb2.mth
Inj. Sample Notes:	1-2mg with 0.5mg sorbitol in 1M (+)-2-butanolic HCl, cooked for 24hr at 85C (sample) or 8h 80C (std). Neutralised Ag2CO3 . Silylated.		

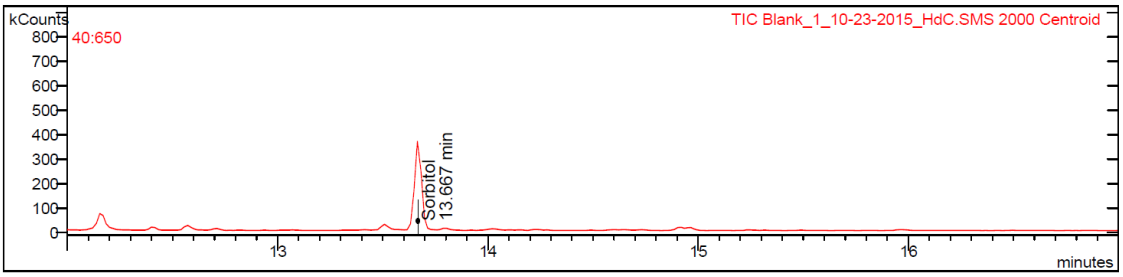

Target Compounds

RT (min)	RRT (min)	Peak Name	Area	Status	Quan Ions	Result Type
13.667	1.000	Sorbitol	155003	X STg	319.3	Identified
14.040	1.027	B-L-Galf #1	2698	X Zg	204.5	Failed
14.915	1.091	B-D-Galp #4	1428	X Zg	204.5	Failed
14.966	1.095	B-L-Galp #4	762	X Zg	204.5	Failed

Figure E.2.1: Processed GC-MS data for a blank sample.

Sample ID:	FB2-2	Operator:	HdC
Instrument ID:	Varian CP-3800	Last Calibration:	None
Acquisition Date:	10/23/2015 6:27 PM	Data File:	...1_10-23-2015_hdc.sms
Calculation Date:	3/31/2016 12:21 PM	Method:	...\comp dl fb2 v2a.mth
Inj. Sample Notes:	1-2mg with 0.5mg sorbitol in 1M (+)-2-butanolic HCl, cooked for 24hr at 85C (sample) or 8h 80C (std). Neutralised Ag2CO3 . Silylated.		

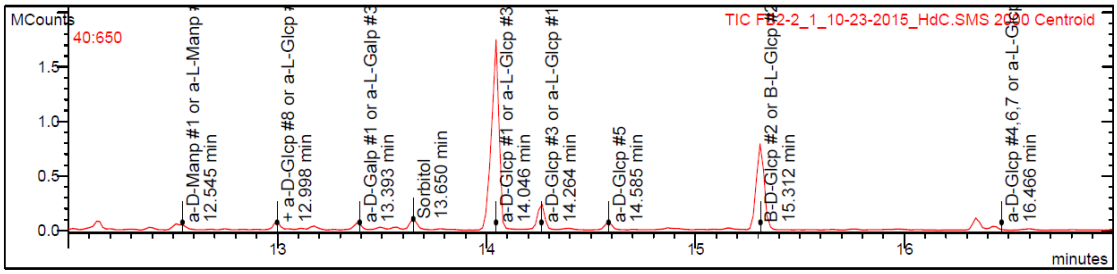

Target Compounds

RT (min)	RRT (min)	Peak Name	Area	Status	Quan Ions	Result Type
13.650	1.000	Sorbitol	45544	X STg	319.3	Identified
12.545	0.919	a-D-Manp #1 or a-L-Manp #2	9165	X g	73.2	Identified
12.998	0.952	a-D-Glcp #8 or a-L-Glcp #8	38645	X g	204.3	Identified
13.172	0.965	a-D-Galf #3	12469	X g	217.5	Identified
13.393	0.981	a-D-Galp #1 or a-L-Galp #3	18384	X g	204.5	Identified
14.046	1.029	a-D-Glcp #1 or a-L-Glcp #3	994835	X g	204.6	Identified
14.046	1.029	B-L-Galf #1	901458	X Zg	204.5	Failed
14.046	1.029	a-L-Manp #4	430439	X Zg	204.3	Failed
14.264	1.045	a-D-Glcp #3 or a-L-Glcp #1	150418	X g	204.5	Identified
14.263	1.045	a/B-D-Manf #5	23235	X Zg	217.3	Failed
14.585	1.069	B-L-Manp #3	32721	X Zg	204.4	Failed
14.585	1.069	a-D-Glcp #5	32845	X g	204.3	Identified
15.312	1.122	B-D-Glcp #2 or B-L-Glcp #2	540323	X g	204.5	Identified
16.466	1.206	a-D-Glcp #4,6,7 or a-L-Glcp #7,6,4	118737	X g	204.5	Identified

Figure E.2.2: Processed GC-MS data for FB2.

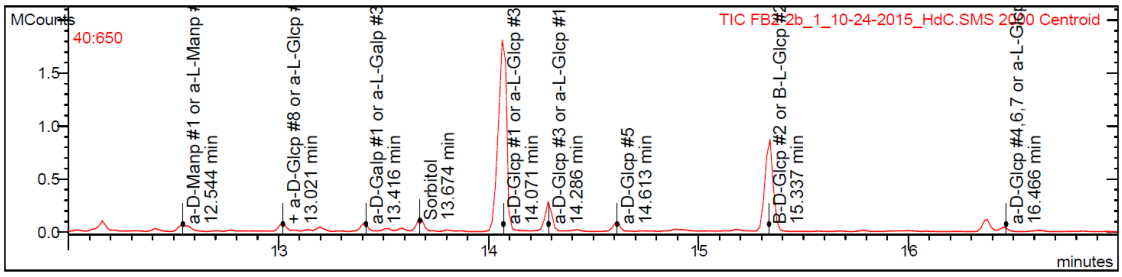

Target Compounds

RT (min)	RRT (min)	Peak Name	Area	Status	Quan Ions	Result Type
13.674		Sorbitol			319.3	Identified
	1.000		52046	X STg		
12.544		a-D-Manp #1 or a-L-Manp #2			73.2	Identified
	0.917		9183	X g		
13.021		a-D-Glcp #8 or a-L-Glcp #8			204.3	Identified
	0.952		43993	X g		
13.196		a-D-Galf #3			217.5	Identified
	0.965		17909	X g		
13.416		a-D-Galp #1 or a-L-Galp #3			204.5	Identified
	0.981		20559	X g		
14.071		a-D-Glcp #1 or a-L-Glcp #3			204.6	Identified
	1.029		1139060	X g		
14.071		B-L-Galf #1			204.5	Failed
	1.029		1138807	X Zg		
14.071		a-L-Manp #4			204.3	Failed
	1.029		1069872	X Zg		
14.286		a-D-Glcp #3 or a-L-Glcp #1			204.5	Identified
	1.045		168836	X g		
14.286		a/B-D-Manf #5			217.3	Failed
	1.045		26630	X Zg		
14.286		a-L-Galf #5			204.5	Failed
	1.045		161662	X Zg		
14.613		B-L-Manp #3			204.4	Failed
	1.069		36678	X Zg		
14.613		a-D-Glcp #5			204.3	Identified
	1.069		38970	X g		
15.337		B-D-Glcp #2 or B-L-Glcp #2			204.5	Identified
	1.122		614952	X g		
16.466		a-D-Glcp #4,6,7 or a-L-Glcp #7,6,4			204.5	Identified
	1.204		132793	X g		

Figure E.2.3: Processed GC-MS data for FB2.

Sample ID:	FB2	Operator:	HdC
Instrument ID:	Varian CP-3800	Last Calibration:	None
Acquisition Date:	10/23/2015 5:48 PM	Data File:	...1_10-23-2015_hdc.sms
Calculation Date:	3/31/2016 12:36 PM	Method:	...\comp dl fb2 v2b.mth
Inj. Sample Notes:	1-2mg with 0.5mg sorbitol in 1M (+)-2-butanolic HCl, cooked for 24hr at 85C (sample) or 8h 80C (std). Neutralised Ag2CO3 . Silylated.		

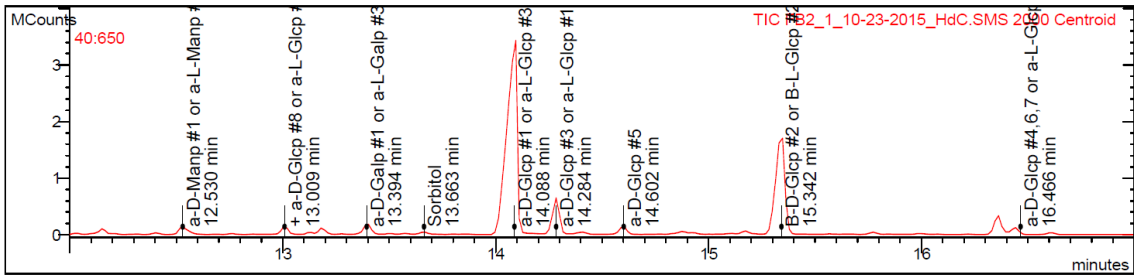

Target Compounds

RT (min)	RRT (min)	Peak Name	Area	Status	Quan Ions	Result Type
13.663		Sorbitol			319.3	Identified
	1.000		16856	X STg		
12.530		a-D-Manp #1 or a-L-Manp #2			73.2	Identified
	0.917		24182	X g		
13.009		a-D-Glcp #8 or a-L-Glcp #8			204.3	Identified
	0.952		75867	X g		
13.129		a-D-Galf #3			217.5	Identified
	0.961		20625	X g		
13.394		a-D-Galp #1 or a-L-Galp #3			217.0	Identified
	0.980		64778	X g		
14.088		a-D-Glcp #1 or a-L-Glcp #3			204.6	Identified
	1.031		2348042	X g		
14.088		B-L-Galf #1			204.5	Failed
	1.031		2304052	X Zg		
14.088		a-L-Manp #4			204.3	Failed
	1.031		2105618	X Zg		
14.284		a-D-Glcp #3 or a-L-Glcp #1			204.5	Identified
	1.045		368525	X g		
14.284		a-L-Galf #5			204.5	Failed
	1.045		331864	X Zg		
14.410		B-D-Galp #2			204.5	Failed
	1.055		25920	X Zg		
14.602		B-L-Manp #3			204.4	Failed
	1.069		63629	X Zg		
14.602		a-D-Glcp #5			204.3	Identified
	1.069		64227	X g		
15.342		B-D-Glcp #2 or B-L-Glcp #2			204.5	Identified
	1.123		1370182	X g		
16.466		a-D-Glcp #4,6,7 or a-L-Glcp #7,6,4			204.5	Identified
	1.205		356825	X g		

Figure E.2.4: Processed GC-MS data for FB2.

Sample ID:	FB2b	Operator:	HdC
Instrument ID:	Varian CP-3800	Last Calibration:	None
Acquisition Date:	10/24/2015 3:31 AM	Data File:	...1_10-24-2015_hdc.sms
Calculation Date:	3/31/2016 12:44 PM	Method:	...\comp dl fb2 v2a.mth
Inj. Sample Notes:	1-2mg with 0.5mg sorbitol in 1M (+)-2-butanolic HCl, cooked for 24hr at 85C (sample) or 8h 80C (std). Neutralised Ag2CO3 . Silylated.		

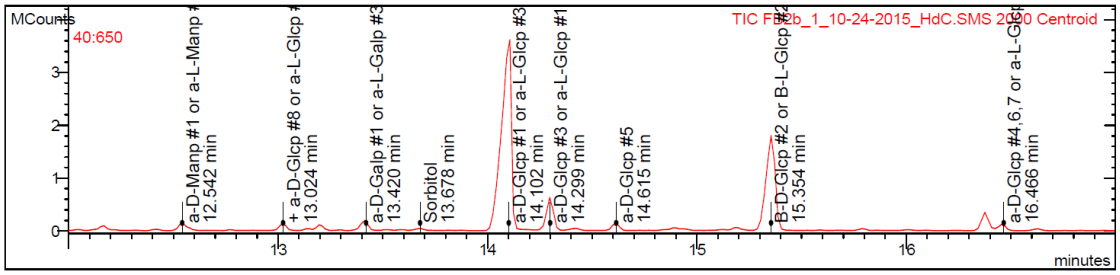

Target Compounds

RT (min)	RRT (min)	Peak Name	Area	Status	Quan Ions	Result Type
13.678		Sorbitol			319.3	Identified
	1.000		18514	X STg		
12.542		a-D-Manp #1 or a-L-Manp #2			73.2	Identified
	0.917		30302	X g		
13.024		a-D-Glcp #8 or a-L-Glcp #8			204.3	Identified
	0.952		76143	X g		
13.200		a-D-Galf #3			217.5	Identified
	0.965		42604	X g		
13.420		a-D-Galp #1 or a-L-Galp #3			204.5	Identified
	0.981		29269	X g		
14.102		a-D-Glcp #1 or a-L-Glcp #3			204.6	Identified
	1.031		2276818	X g		
14.102		B-L-Galf #1			204.5	Failed
	1.031		2272478	X Zg		
14.102		a-L-Manp #4			204.3	Failed
	1.031		2218792	X Zg		
14.299		a-D-Glcp #3 or a-L-Glcp #1			204.5	Identified
	1.045		353867	X g		
14.299		a-L-Galf #5			204.5	Failed
	1.045		349389	X Zg		
14.615		B-L-Manp #3			204.4	Failed
	1.068		56314	X Zg		
14.615		a-D-Glcp #5			204.3	Identified
	1.068		60247	X g		
15.354		B-D-Glcp #2 or B-L-Glcp #2			204.5	Identified
	1.123		1332320	X g		
16.466		a-D-Glcp #4,6,7 or a-L-Glcp #7,6,4			204.5	Identified
	1.204		352980	X g		

Figure E.2.5: Processed GC-MS data for FB2.

Sample ID:	FB2F2 03	Operator:	HdC
Instrument ID:	Varian CP-3800	Last Calibration:	None
Acquisition Date:	12/4/2015 1:01 PM	Data File:	..._1_12-4-2015_hdc.sms
Calculation Date:	3/25/2016 2:26 PM	Method:	...mp dl fb2fr2 v2b.mth
Inj. Sample Notes:	0.8mg with 1mg sorbitol in 1M (+)-2-butanolic HCl, cooked for 24hr at 85C (sample) or 8h 80C (std). Neutralised Ag2CO3. Silylated.		

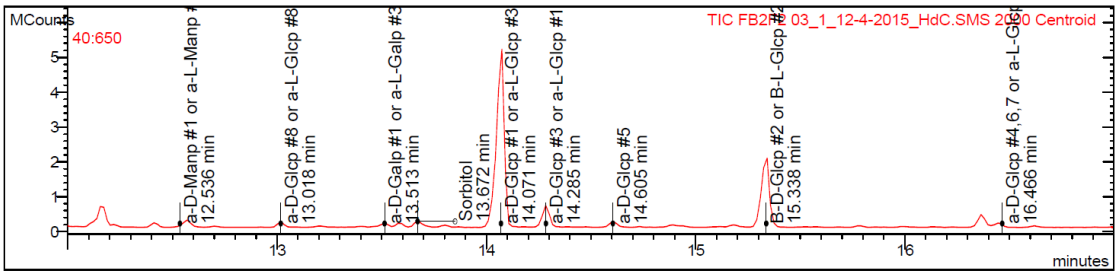

Target Compounds

RT (min)	RRT (min)	Peak Name	Area	Status	Quan Ions	Result Type
13.672		Sorbitol			319.3	Identified
	1.000		37493	X STg		
12.536		a-D-Manp #1 or a-L-Manp #2			204.5	Identified
	0.917		3845	X g		
13.018		a-D-Glcp #8 or a-L-Glcp #8			204.3	Identified
	0.952		45611	X g		
13.513		a-D-Galp #1 or a-L-Galp #3			204.5	Identified
	0.988		1548	X g		
14.071		a-D-Glcp #1 or a-L-Glcp #3			204.6	Identified
	1.029		1475564	X g		
14.071		B-L-Galf #1			204.5	Failed
	1.029		1455118	X Zg		
14.071		a-L-Manp #4			204.3	Failed
	1.029		1372683	X Zg		
14.285		a-D-Glcp #3 or a-L-Glcp #1			204.5	Identified
	1.045		251292	X g		
14.285		a/B-D-Manf #5			217.3	Failed
	1.045		37997	X Zg		
14.416		B-D-Galp #2			204.5	Failed
	1.054		1771	X Zg		
14.285		B-L-Manp #3			204.4	Failed
	1.045		251292	X Zg		
14.605		a-D-Glcp #5			204.3	Identified
	1.068		45057	X g		
15.338		B-D-Glcp #2 or B-L-Glcp #2			204.5	Identified
	1.122		810571	X g		
16.466		a-D-Glcp #4,6,7 or a-L-Glcp #7,6,4			204.5	Identified
	1.204		242795	X g		

Figure E.2.6: Processed GC-MS data for FB2 F2.

Sample ID:	PB2	Operator:	HdC
Instrument ID:	Varian CP-3800	Last Calibration:	None
Acquisition Date:	10/23/2015 7:06 PM	Data File:	...1_10-23-2015_hdc.sms
Calculation Date:	3/21/2016 3:22 PM	Method:	...\comp dl pb2 v2a.mth
Inj. Sample Notes:	1-2mg with 0.5mg sorbitol in 1M (+)-2-butanolic HCl, cooked for 24hr at 85C (sample) or 8h 80C (std). Neutralised Ag2CO3 . Silylated.		

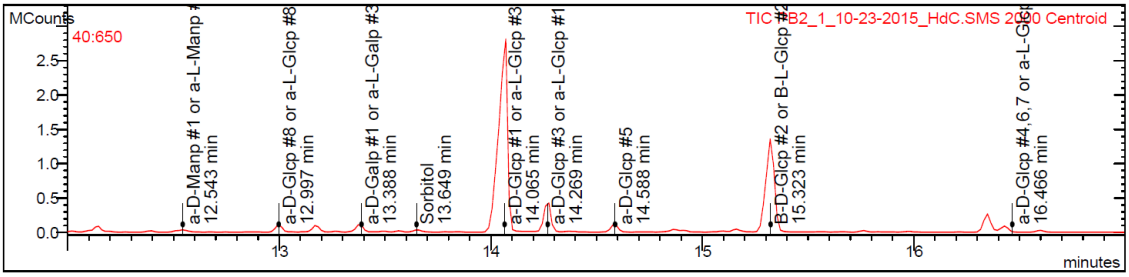

Target Compounds

RT (min)	RRT (min)	Peak Name	Area	Status	Quan Ions	Result Type
13.649		Sorbitol			319.3	Identified
	1.000		14506	X STg		
12.543		a-D-Manp #1 or a-L-Manp #2			73.2	Identified
	0.919		7162	X g		
12.997		a-D-Glcp #8 or a-L-Glcp #8			204.3	Identified
	0.952		59630	X g		
13.388		a-D-Galp #1 or a-L-Galp #3			204.5	Identified
	0.981		7744	X g		
14.065		a-D-Glcp #1 or a-L-Glcp #3			204.6	Identified
	1.031		1624063	X g		
14.065		B-L-Galf #1			204.5	Failed
	1.031		1563930	X Zg		
14.065		a-L-Manp #4			204.3	Failed
	1.031		1400237	X Zg		
14.269		a-D-Glcp #3 or a-L-Glcp #1			204.5	Identified
	1.045		265999	X g		
14.588		B-L-Manp #3			204.4	Failed
	1.069		50145	X Zg		
14.583		a/B-L-Manf #5			217.3	Failed
	1.068		17959	X Zg		
14.588		a-D-Glcp #5			204.3	Identified
	1.069		50324	X g		
15.323		B-D-Glcp #2 or B-L-Glcp #2			204.5	Identified
	1.123		956966	X g		
16.466		a-D-Glcp #4,6,7 or a-L-Glcp #7,6,4			204.5	Identified
	1.206		278754	X g		

Figure E.2.7: Processed GC-MS data for PB2.

Sample ID:	PB2b	Operator:	HdC
Instrument ID:	Varian CP-3800	Last Calibration:	None
Acquisition Date:	10/24/2015 4:48 AM	Data File:	...1_10-24-2015_hdc.sms
Calculation Date:	3/21/2016 4:11 PM	Method:	...\comp dl pb2 v2c.mth
Inj. Sample Notes:	1-2mg with 0.5mg sorbitol in 1M (+)-2-butanolic HCl, cooked for 24hr at 85C (sample) or 8h 80C (std). Neutralised Ag2CO3 . Silylated.		

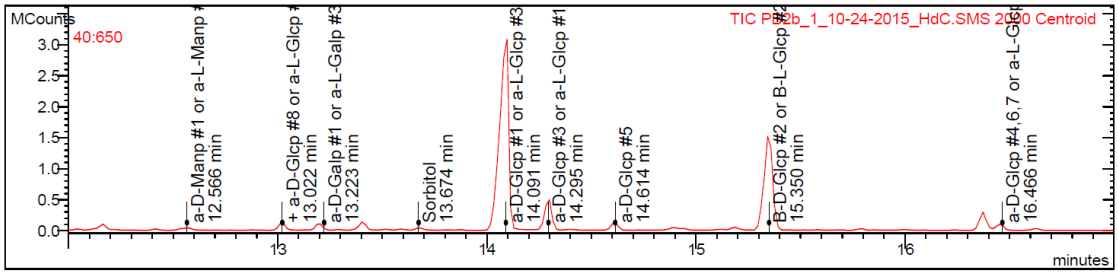

Target Compounds

RT (min)	RRT (min)	Peak Name	Area	Status	Quan Ions	Result Type
13.674		Sorbitol			319.3	Identified
	1.000		16691	X STg		
12.566		a-D-Manp #1 or a-L-Manp #2			73.0	Identified
	0.919		12843	X g		
12.677		B-D-Manp #2 or B-L-Manp #1			204.5	Failed
	0.927		159	X Zg		
13.022		a-D-Glcp #8 or a-L-Glcp #8			204.3	Identified
	0.952		69537	X g		
13.144		a-D-Galf #3			217.5	Identified
	0.961		1237	X g		
13.223		a-D-Galp #1 or a-L-Galp #3			204.5	Identified
	0.967		4376	X g		
14.091		a-D-Glcp #1 or a-L-Glcp #3			204.6	Identified
	1.031		1824111	X g		
14.091		B-L-Galf #1			204.5	Failed
	1.031		1824650	X Zg		
14.091		a-L-Manp #4			204.3	Failed
	1.031		1740046	X Zg		
14.295		a-D-Glcp #3 or a-L-Glcp #1			204.5	Identified
	1.045		308355	X g		
14.295		a/B-D-Manf #5			217.3	Failed
	1.045		45113	X Zg		
14.295		a-L-Galf #5			204.5	Failed
	1.045		257843	X Zg		
14.422		B-D-Galp #2			204.5	Failed
	1.055		2604	X Zg		
14.614		B-L-Manp #3			204.4	Failed
	1.069		54007	X Zg		
14.611		a/B-L-Manf #5			217.3	Failed
	1.069		20750	X Zg		
14.614		a-D-Glcp #5			204.3	Identified
	1.069		58202	X g		
15.350		B-D-Glcp #2 or B-L-Glcp #2			204.5	Identified
	1.123		1111219	X g		
16.466		a-D-Glcp #4,6,7 or a-L-Glcp #7,6,4			204.5	Identified
	1.204		311495	X g		

Figure E.2.8: Processed GC-MS data for PB2.

Sample ID:	PB2 03	Operator:	HdC
Instrument ID:	Varian CP-3800	Last Calibration:	None
Acquisition Date:	12/4/2015 1:40 PM	Data File:	..._1_12-4-2015_hdc.sms
Calculation Date:	3/21/2016 4:37 PM	Method:	...\comp dl pb2 v3a.mth
Inj. Sample Notes:	1.2mg with 1mg sorbitol in 1M (+)-2-butanolic HCl, cooked for 24hr at 85C (sample) or 8h 80C (std). Neutralised Ag2CO3. Silylated.		

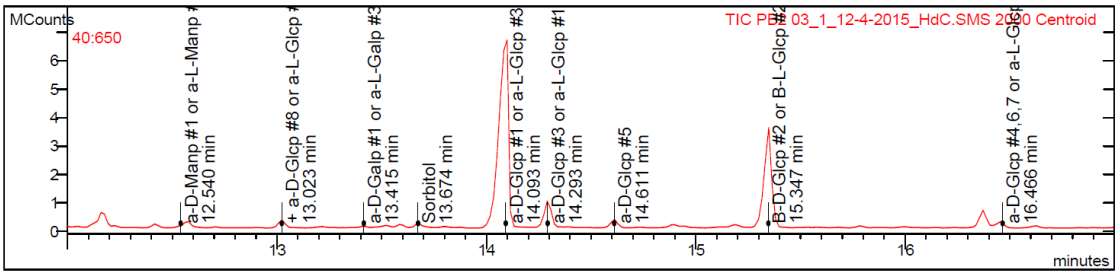

Target Compounds

RT (min)	RRT (min)	Peak Name	Area	Status	Quan Ions	Result Type
13.674	1.000	Sorbitol	26069	X STg	319.3	Identified
12.540	0.917	a-D-Manp #1 or a-L-Manp #2	18624	X g	204.0	Identified
13.023	0.952	a-D-Glcp #8 or a-L-Glcp #8	88174	X g	204.3	Identified
13.201	0.965	a-D-Galf #3	8885	X g	217.5	Identified
13.415	0.981	a-D-Galp #1 or a-L-Galp #3	15564	X g	204.5	Identified
14.093	1.031	a-D-Glcp #1 or a-L-Glcp #3	2056848	X g	204.6	Identified
14.093	1.031	B-L-Galf #1	2047806	X Zg	204.5	Failed
14.093	1.031	a-L-Manp #4	1818893	X Zg	204.3	Failed
14.293	1.045	a-D-Glcp #3 or a-L-Glcp #1	376726	X g	204.5	Identified
14.293	1.045	a/B-D-Manf #5	51862	X Zg	217.3	Failed
14.293	1.045	a-L-Galf #5	341057	X Zg	204.5	Failed
14.419	1.054	B-D-Galp #2	4486	X Zg	204.5	Failed
14.611	1.069	B-L-Manp #3	80004	X Zg	204.4	Failed
14.611	1.069	a-D-Glcp #5	85576	X g	204.3	Identified
15.347	1.122	B-D-Glcp #2 or B-L-Glcp #2	1192452	X g	204.5	Identified
16.466	1.204	a-D-Glcp #4,6,7 or a-L-Glcp #7,6,4	404221	X g	204.5	Identified

Figure E.2.9: Processed GC-MS data for PB2.

Sample ID:	PB7	Operator:	HdC
Instrument ID:	Varian CP-3800	Last Calibration:	None
Acquisition Date:	10/23/2015 7:45 PM	Data File:	...1_10-23-2015_hdc.sms
Calculation Date:	3/21/2016 4:03 PM	Method:	...\comp dl pb7 v2a.mth
Inj. Sample Notes:	1-2mg with 0.5mg sorbitol in 1M (+)-2-butanolic HCl, cooked for 24hr at 85C (sample) or 8h 80C (std). Neutralised Ag2CO3 . Silylated.		

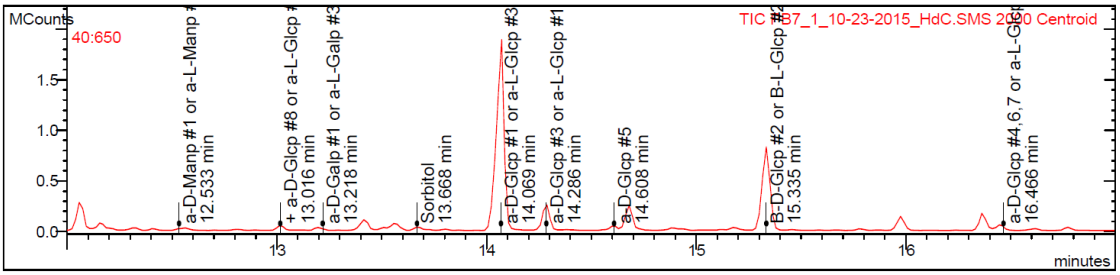

Target Compounds

RT (min)	RRT (min)	Peak Name	Area	Status	Quan Ions	Result Type
13.668		Sorbitol			319.3	Identified
	1.000		11883	X STg		
12.533		a-D-Manp #1 or a-L-Manp #2			204.0	Identified
	0.917		8331	X g		
13.016		a-D-Glcp #8 or a-L-Glcp #8			204.3	Identified
	0.952		28227	X g		
13.193		a-D-Galf #3			217.5	Identified
	0.965		17025	X g		
13.218		a-D-Galp #1 or a-L-Galp #3			204.5	Identified
	0.967		3376	X g		
14.069		a-D-Glcp #1 or a-L-Glcp #3			204.6	Identified
	1.029		1040355	X g		
14.069		B-L-Galf #1			204.5	Failed
	1.029		1038252	X Zg		
14.069		a-L-Manp #4			204.3	Failed
	1.029		1007120	X Zg		
14.286		a-D-Glcp #3 or a-L-Glcp #1			204.5	Identified
	1.045		167921	X g		
14.285		a/B-D-Manf #5			217.3	Failed
	1.045		23349	X Zg		
14.286		a-L-Galf #5			204.5	Failed
	1.045		144194	X Zg		
14.416		B-D-Galp #2			204.5	Failed
	1.055		2708	X Zg		
14.286		B-L-Manp #3			204.4	Failed
	1.045		167921	X Zg		
14.608		a-D-Glcp #5			204.3	Identified
	1.069		19062	X g		
15.335		B-D-Glcp #2 or B-L-Glcp #2			204.5	Identified
	1.122		559113	X g		
16.466		a-D-Glcp #4,6,7 or a-L-Glcp #7,6,4			204.5	Identified
	1.205		174621	X g		

Figure E.2.10: Processed GC-MS data for PB7.

Sample ID:	PB7b	Operator:	HdC
Instrument ID:	Varian CP-3800	Last Calibration:	None
Acquisition Date:	10/24/2015 5:27 AM	Data File:	...1_10-24-2015_hdc.sms
Calculation Date:	3/21/2016 4:05 PM	Method:	...\comp dl pb7 v2a.mth
Inj. Sample Notes:	1-2mg with 0.5mg sorbitol in 1M (+)-2-butanolic HCl, cooked for 24hr at 85C (sample) or 8h 80C (std). Neutralised Ag2CO3 . Silylated.		

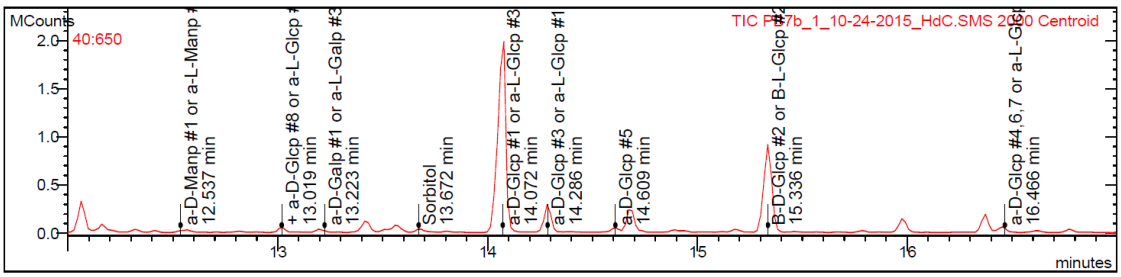

Target Compounds

RT (min)	RRT (min)	Peak Name	Area	Status	Quan Ions	Result Type
13.672		Sorbitol			319.3	Identified
	1.000		12888	X STg		
12.537		a-D-Manp #1 or a-L-Manp #2			204.0	Identified
	0.917		9196	X g		
13.019		a-D-Glcp #8 or a-L-Glcp #8			204.3	Identified
	0.952		30074	X g		
13.195		a-D-Galf #3			217.5	Identified
	0.965		17992	X g		
13.223		a-D-Galp #1 or a-L-Galp #3			204.5	Identified
	0.967		3500	X g		
14.072		a-D-Glcp #1 or a-L-Glcp #3			204.6	Identified
	1.029		1148585	X g		
14.072		B-L-Galf #1			204.5	Failed
	1.029		1149826	X Zg		
14.072		a-L-Manp #4			204.3	Failed
	1.029		1106577	X Zg		
14.286		a-D-Glcp #3 or a-L-Glcp #1			204.5	Identified
	1.045		182208	X g		
14.286		a/B-D-Manf #5			217.3	Failed
	1.045		26653	X Zg		
14.419		B-D-Galp #2			204.5	Failed
	1.055		3122	X Zg		
14.286		B-L-Manp #3			204.4	Failed
	1.045		182208	X Zg		
14.609		a-D-Glcp #5			204.3	Identified
	1.069		20405	X g		
15.336		B-D-Glcp #2 or B-L-Glcp #2			204.5	Identified
	1.122		645507	X g		
16.466		a-D-Glcp #4,6,7 or a-L-Glcp #7,6,4			204.5	Identified
	1.204		192424	X g		

Figure E.2.11: Processed GC-MS data for PB7.

Sample ID:	PB7 03	Operator:	HdC
Instrument ID:	Varian CP-3800	Last Calibration:	None
Acquisition Date:	12/4/2015 2:19 PM	Data File:	..._1_12-4-2015_hdc.sms
Calculation Date:	3/21/2016 4:41 PM	Method:	...\comp dl pb2 v3a.mth
Inj. Sample Notes:	1.2mg with 1mg sorbitol in 1M (+)-2-butanolic HCl, cooked for 24hr at 85C (sample) or 8h 80C (std). Neutralised Ag2CO3. Silylated.		

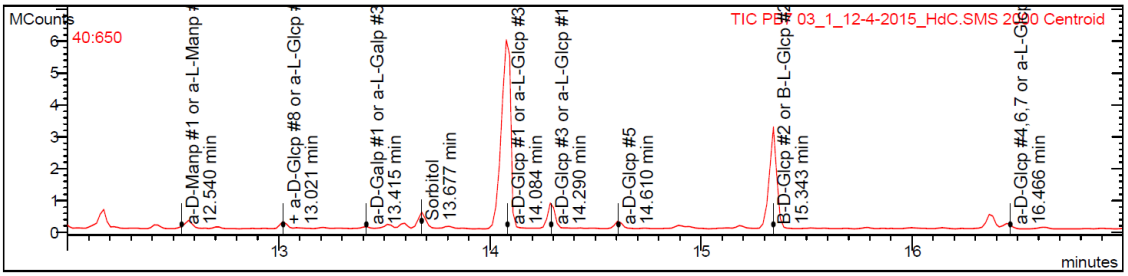

Target Compounds

RT (min)	RRT (min)	Peak Name	Area	Status	Quan Ions	Result Type
13.677		Sorbitol			319.3	Identified
	1.000		118804	X STg		
12.540		a-D-Manp #1 or a-L-Manp #2			204.0	Identified
	0.917		19571	X g		
13.021		a-D-Glcp #8 or a-L-Glcp #8			204.3	Identified
	0.952		68422	X g		
13.199		a-D-Galf #3			217.5	Identified
	0.965		8354	X g		
13.415		a-D-Galp #1 or a-L-Galp #3			204.5	Identified
	0.981		20078	X g		
14.084		a-D-Glcp #1 or a-L-Glcp #3			204.6	Identified
	1.030		2005284	X g		
14.084		B-L-Galf #1			204.5	Failed
	1.030		2000488	X Zg		
14.084		a-L-Manp #4			204.3	Failed
	1.030		1933736	X Zg		
14.290		a-D-Glcp #3 or a-L-Glcp #1			204.5	Identified
	1.045		333535	X g		
14.290		a/B-D-Manf #5			217.3	Failed
	1.045		46646	X Zg		
14.290		a-L-Galf #5			204.5	Failed
	1.045		319264	X Zg		
14.610		B-L-Manp #3			204.4	Failed
	1.068		67615	X Zg		
14.610		a-D-Glcp #5			204.3	Identified
	1.068		69779	X g		
15.343		B-D-Glcp #2 or B-L-Glcp #2			204.5	Identified
	1.122		1193747	X g		
16.466		a-D-Glcp #4,6,7 or a-L-Glcp #7,6,4			204.5	Identified
	1.204		331461	X g		

Figure E.2.12: Processed GC-MS data for PB7.

Sample ID:	D-Glc	Operator:	HdC
Instrument ID:	Varian CP-3800	Last Calibration:	None
Acquisition Date:	10/23/2015 10:20 PM	Data File:	...1_10-23-2015_hdc.sms
Calculation Date:	3/12/2016 4:01 PM	Method:	...sing\comp dl glc.mth
Inj. Sample Notes:	1-2mg with 0.5mg sorbitol in 1M (+)-2-butanolic HCl, cooked for 24hr at 85C (sample) or 8h 80C (std). Neutralised Ag2CO3 . Silylated.		

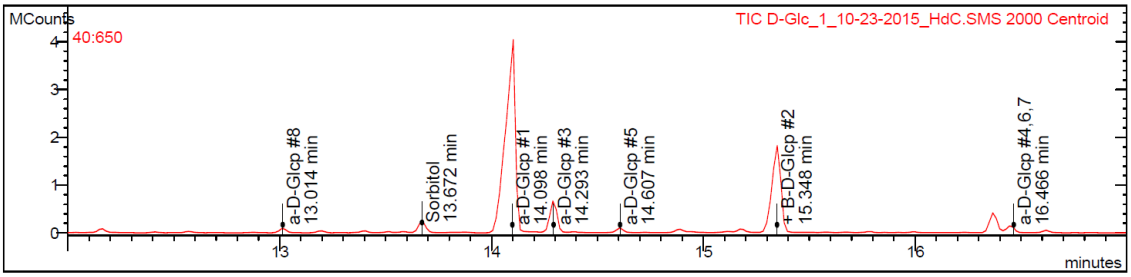

Target Compounds

RT (min)	RRT (min)	Peak Name	Area	Status	Quan Ions	Result Type
13.672	1.000	Sorbitol	103755	X STg	319.3	Identified
13.014	0.952	B-D-Galf #5	49924	X Zg	204.5	Failed
13.014	0.952	a-D-Glcp #8	49960	X g	204.3	Identified
14.098	1.031	a-D-Glcp #1	2457072	X g	204.6	Identified
14.098	1.031	B-L-Galf #1	2455365	X Zg	204.5	Failed
14.098	1.031	a-L-Manp #4	2410027	X Zg	204.3	Failed
14.293	1.045	a-D-Glcp #3	382566	X g	204.5	Identified
14.293	1.045	a/B-D-Manf #5	62350	X Zg	217.3	Failed
14.293	1.045	a-L-Galf #5	353222	X Zg	204.5	Failed
14.293	1.045	B-L-Manp #3	382566	X Zg	204.4	Failed
14.607	1.068	a-D-Glcp #5	41281	X g	204.3	Identified
15.348	1.123	B-D-Glcp #2	1277010	X g	204.5	Identified
15.348	1.123	B-L-Glcp #2	1277010	X g	204.6	Identified
16.466	1.204	a-D-Glcp #4,6,7	426862	X g	204.5	Identified

Figure E.2.13: Processed GC-MS data for D-(+)-glucose.

Sample ID:	L-(-)-Glc 03	Operator:	HdC
Instrument ID:	Varian CP-3800	Last Calibration:	None
Acquisition Date:	12/4/2015 12:22 PM	Data File:	..._1_12-4-2015_hdc.sms
Calculation Date:	3/12/2016 4:17 PM	Method:	...ng\comp dl l-glc.mth
Inj. Sample Notes:	1.3mg with 1mg sorbitol in 1M (+)-2-butanolic HCl, cooked for 24hr at 85C (sample) or 8h 80C (std). Neutralised Ag2CO3. Silylated.		

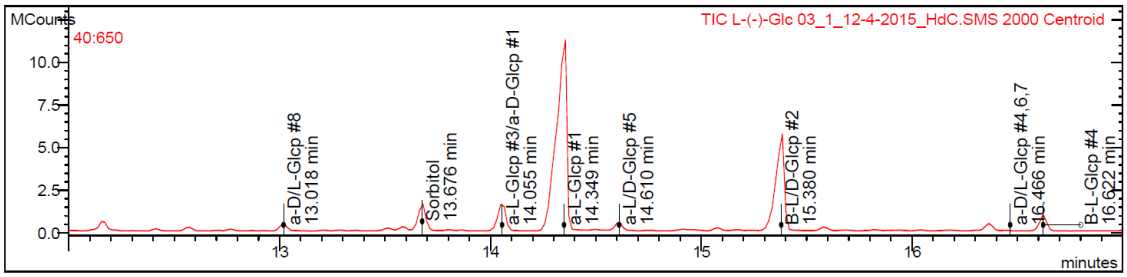

Target Compounds

RT (min)	RRT (min)	Peak Name	Area	Status	Quan Ions	Result Type
13.676		Sorbitol			319.3	Identified
	1.000		387959	X STg		
13.018		a-D/L-Glcp #8			204.3	Identified
	0.952		145171	X g		
14.055		a-L-Glcp #3/a-D-Glcp #1			RIC	Identified
	1.028		4320322	X g		
14.349		a-L-Glcp #1			204.5	Identified
	1.049		3117052	X g		
14.610		a-L/D-Glcp #5			204.3	Identified
	1.068		137521	X g		
15.380		B-L/D-Glcp #2			204.5	Identified
	1.125		1767760	X g		
16.466		a-D/L-Glcp #4,6,7			204.5	Identified
	1.204		615596	X g		
16.622		B-L-Glcp #4			204.6	Identified
	1.215		375563	X g		

Figure E.2.14: Processed GC-MS data for L-(-)-glucose.

Sample ID:	D-Gal	Operator:	HdC
Instrument ID:	Varian CP-3800	Last Calibration:	None
Acquisition Date:	10/23/2015 10:59 PM	Data File:	...1_10-23-2015_hdc.sms
Calculation Date:	3/12/2016 3:35 PM	Method:	...sing\comp dl gal.mth
Inj. Sample Notes:	1-2mg with 0.5mg sorbitol in 1M (+)-2-butanolic HCl, cooked for 24hr at 85C (sample) or 8h 80C (std). Neutralised Ag2CO3 . Silylated.		

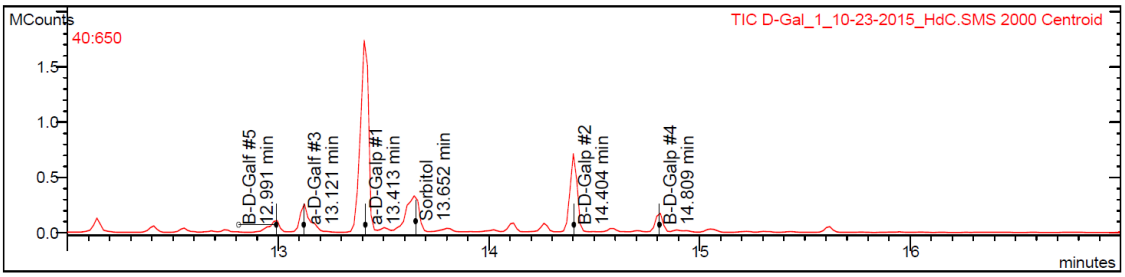

Target Compounds

RT (min)	RRT (min)	Peak Name	Area	Status	Quan Ions	Result Type
13.652	1.000	Sorbitol	134872	X STg	319.3	Identified
12.991	0.952	B-D-Galf #5	40819	X g	204.5	Identified
13.121	0.961	a-D-Galf #3	142941	X g	217.5	Identified
13.413	0.983	a-L-Galp #3	1030495	X Zg	204.5	Failed
13.413	0.983	a-D-Galp #1	1030495	X g	204.5	Identified
14.404	1.055	a-L-Galf #5	412154	X Zg	204.5	Failed
14.404	1.055	B-D-Galp #2	412154	X g	204.5	Identified
14.809	1.085	B-D-Galp #4	89790	X g	204.5	Identified

Figure E.2.15: Processed GC-MS data for D-(+)-galactose.

Sample ID:	L-Gal	Operator:	HdC
Instrument ID:	Varian CP-3800	Last Calibration:	None
Acquisition Date:	10/24/2015 12:17 AM	Data File:	...1_10-24-2015_hdc.sms
Calculation Date:	3/12/2016 3:50 PM	Method:	...ng\comp dl l-gal.mth
Inj. Sample Notes:	1-2mg with 0.5mg sorbitol in 1M (+)-2-butanolic HCl, cooked for 24hr at 85C (sample) or 8h 80C (std). Neutralised Ag2CO3 . Silylated.		

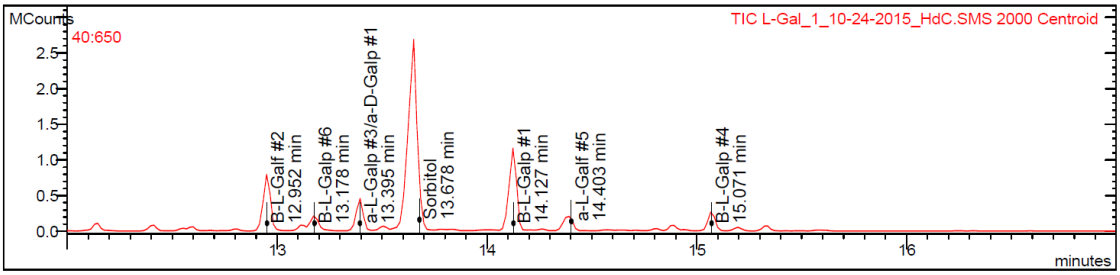

Target Compounds

RT (min)	RRT (min)	Peak Name	Area	Status	Quan Ions	Result Type
13.678		Sorbitol			319.3	Identified
	1.000		219850	X STg		
12.952		B-L-Galf #2			217.5	Identified
	0.947		366459	X g		
13.175		B-D-Galf #5			204.5	Failed
	0.963		89990	X Zg		
13.178		B-L-Galp #6			217.5	Identified
	0.963		34086	X g		
13.395		a-L-Galp #3/a-D-Galp #1			204.5	Identified
	0.979		256966	X g		
14.127		B-L-Galp #1			204.5	Identified
	1.033		636450	X g		
14.403		a-L-Galf #5			204.5	Identified
	1.053		80913	X g		
14.403		B-D-Galp #2			204.5	Failed
	1.053		80913	X Zg		
15.071		B-L-Galp #4			204.5	Identified
	1.102		129209	X g		

Figure E.2.16: Processed GC-MS data for L-(-)-galactose.

Sample ID:	D-Man	Operator:	HdC
Instrument ID:	Varian CP-3800	Last Calibration:	None
Acquisition Date:	10/23/2015 11:38 PM	Data File:	...1_10-23-2015_hdc.sms
Calculation Date:	3/12/2016 3:19 PM	Method:	...sing\comp dl man.mth
Inj. Sample Notes:	1-2mg with 0.5mg sorbitol in 1M (+)-2-butanolic HCl, cooked for 24hr at 85C (sample) or 8h 80C (std). Neutralised Ag2CO3 . Silylated.		

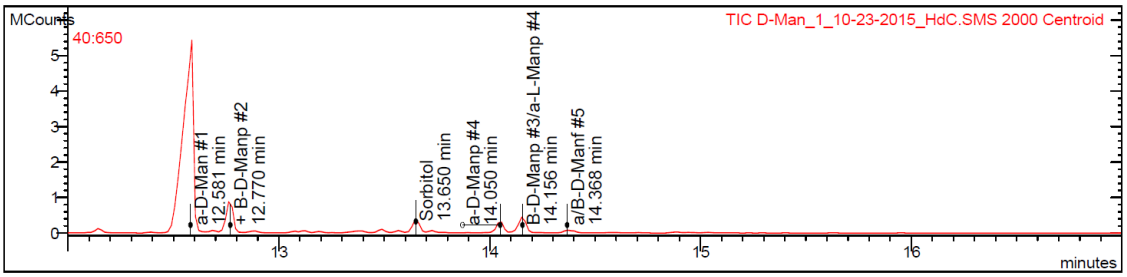

Target Compounds

RT (min)	RRT (min)	Peak Name	Area	Status	Quan Ions	Result Type
13.650		Sorbitol			319.3	Identified
	1.000		166988	X STg		
12.581		a-L-Manp #2			204.5	Failed
	0.922		2990470	X Zg		
12.581		a-D-Man #1			204.5	Identified
	0.922		3001837	X g		
12.770		B-D-Manp #2			204.5	Identified
	0.935		484072	X g		
12.770		B-L-Manp #1			204.5	Identified
	0.935		484072	X g		
14.050		a-D-Manp #4			204.3	Identified
	1.029		200922	X g		
14.156		B-D-Manp #3/a-L-Manp #4			204.5	Identified
	1.037		286004	X g		
14.368		a/B-D-Manf #5			217.3	Identified
	1.053		44962	X g		
14.400		B-L-Manp #3			204.4	Failed
	1.055		29465	X Zg		

Figure E.2.17: Processed GC-MS data for D-(+)-mannose.

Sample ID:	L-Man	Operator:	HdC
Instrument ID:	Varian CP-3800	Last Calibration:	None
Acquisition Date:	10/24/2015 12:55 AM	Data File:	...1_10-24-2015_hdc.sms
Calculation Date:	3/12/2016 3:25 PM	Method:	...sing\comp dl man.mth
Inj. Sample Notes:	1-2mg with 0.5mg sorbitol in 1M (+)-2-butanolic HCl, cooked for 24hr at 85C (sample) or 8h 80C (std). Neutralised Ag2CO3 . Silylated.		

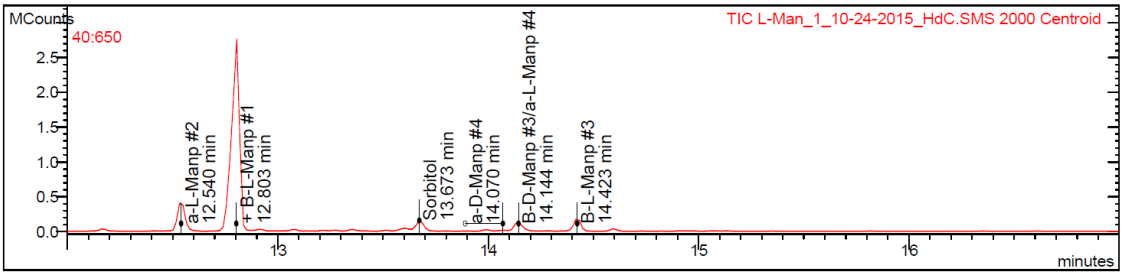

Target Compounds

RT (min)	RRT (min)	Peak Name	Area	Status	Quan Ions	Result Type
13.673	1.000	Sorbitol	58436	X STg	319.3	Identified
12.540	0.917	a-L-Manp #2	271778	X g	204.5	Identified
12.803	0.936	B-D-Manp #2	1468613	X g	204.5	Identified
12.803	0.936	B-L-Manp #1	1502348	X g	204.5	Identified
14.070	1.029	a-D-Manp #4	4163	X g	204.3	Identified
14.144	1.034	B-D-Manp #3/a-L-Manp #4	100497	X g	204.5	Identified
14.422	1.055	a/B-D-Manf #5	25961	X Zg	217.3	Failed
14.423	1.055	B-L-Manp #3	130358	X g	204.4	Identified

Figure E.2.18: Processed GC-MS data for L-(-)-mannose.

Sample ID:	Mix	Operator:	HdC
Instrument ID:	Varian CP-3800	Last Calibration:	None
Acquisition Date:	10/24/2015 1:34 AM	Data File:	...1_10-24-2015_hdc.sms
Calculation Date:	3/12/2016 2:13 PM	Method:	...sing\comp dl mix.mth
Inj. Sample Notes:	1-2mg with 0.5mg sorbitol in 1M (+)-2-butanolic HCl, cooked for 24hr at 85C (sample) or 8h 80C (std). Neutralised Ag2CO3 . Silylated.		

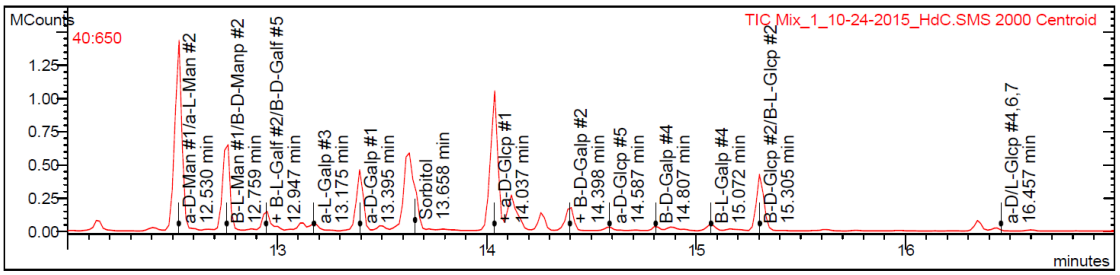

Target Compounds

RT (min)	RRT (min)	Peak Name	Area	Status	Quan Ions	Result Type
13.658		Sorbitol			319.3	Identified
	1.000		128606	X STg		
12.530		a-D-Man #1/a-L-Man #2			204.5	Identified
	0.917		764008	X g		
12.759		B-L-Man #1/B-D-Manp #2			204.5	Identified
	0.934		393691	X g		
12.947		B-L-Galf #2/B-D-Galf #5			RIC	Identified
	0.948		350519	X g		
13.118		a-D-Galf #3			217.5	Identified
	0.960		23536	X g		
13.175		a-L-Galp #3			RIC	Identified
	0.965		66599	X g		
13.395		a-D-Galp #1			204.5	Identified
	0.981		248134	X g		
14.037		a-D-Glcp #1			RIC	Identified
	1.028		2228357	X g		
14.118		B-L-Galp #1/B-D-Manp #4			RIC	Identified
	1.034		569037	X g		
14.262		a-D-Glcp #3/a-L-Glcp #1			RIC	Identified
	1.044		287796	X g		
14.398		B-D-Galp #2			RIC	Identified
	1.054		479328	X g		
14.587		a-D-Glcp #5			204.3	Identified
	1.068		6803	X g		
14.807		B-D-Galp #4			204.3	Identified
	1.084		18202	X g		
15.072		B-L-Galp #4			204.5	Identified
	1.103		30454	X g		
15.305		B-D-Glcp #2/B-L-Glcp #2			RIC	Identified
	1.121		1041799	X g		
16.457		a-D/L-Glcp #4,6,7			RIC	Identified
	1.205		257540	X g		

Figure E.2.19: Processed GC-MS data for a mixture of D-(+)- and L-(-)-galactose, D-(+)- and L-(-)-mannose and D-(+)-glucose.

E.3 Structure analysis

Sample ID:	pullulan	Operator:	hdc
Instrument ID:		Last Calibration:	None
Acquisition Date:	11/23/2011 5:44 AM	Data File:	...1_11-23-2011_hdc.sms
Calculation Date:	3/31/2016 8:48 AM	Method:	...0032016 pullulan.mth
Inj. Sample Notes:	Pullulan permethylated, methanolysis and silylated. 5uL sorb itol (0.0375g/25mL) added before 20hr cook.		

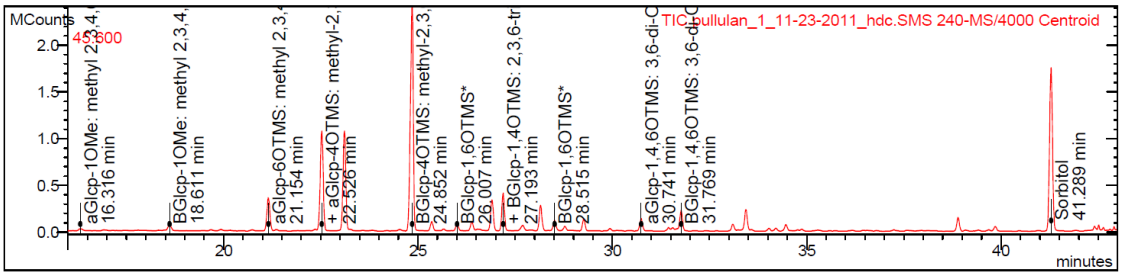

Target Compounds

RT (min)	RRT (min)	Peak Name	Area	Status	Quan Ions	Result Type
41.289		Sorbitol			73.1	Identified
	1.000		1808341	X STg		
16.316		aGlcp-1OMe: methyl 2,3,4,6-tetra-O			88.1	Identified
	0.395		44866	X g		
18.611		BGlcp-1OMe: methyl 2,3,4,6-tetra-O-methy			88.1	Identified
	0.451		110999	X g		
21.154		aGlcp-6OTMS: methyl 2,3,4-tri-O-methyl-6			88.1	Identified
	0.512		310950	X g		
22.526		aGlcp-4OTMS: methyl-2,3,6-tri-O-methyl-4			88.0	Identified
	0.546		946313	X g		
23.109		BGlcp-6OTMS: methyl 2,3,4-tri-O-methyl-6			88.1	Identified
	0.560		912361	X g		
24.852		BGlcp-4OTMS: methyl-2,3,6-tri-O-methyl-4			88.0	Identified
	0.602		1843255	X g		
26.007		BGlcp-1,6OTMS*			73.1	Identified
	0.630		67841	X g		
26.385		aGlcp-1,6OTMS			73.1	Identified
	0.639		48063	X g		
26.906		aGlcp-1,4OTMS: 2,3,6-tri-O-methyl-1,4-bi			73.1	Identified
	0.652		251167	X g		
27.193		BGlcp-1,4OTMS: 2,3,6-tri-O-methyl-1,4-bi			73.1	Identified
	0.659		285463	X g		
27.707		aGlcp-1,6OTMS*			146.1	Identified
	0.671		17212	X g		
28.153		BGlcp-1,6OTMS			73.1	Identified
	0.682		181908	X g		
28.515		BGlcp-1,6OTMS*			146.1	Identified
	0.691		87534	X g		
30.741		aGlcp-1,4,6OTMS: 3,6-di-O-methyl-1,4,6-t			146.2	Identified
	0.745		100342	X g		
31.769		BGlcp-1,4,6OTMS: 3,6-di-O-methyl-1,4,6-t			146.2	Identified
	0.769		140813	X g		

Figure E.3.1: Processed GC-MS data for pullulan.

Sample ID:	Pullulan	Operator:	HdC
Instrument ID:	Varian CP-3800	Last Calibration:	None
Acquisition Date:	3/8/2010 10:47 PM	Data File:	...n_1_3-8-2010_hdc.sms
Calculation Date:	3/30/2016 9:38 AM	Method:	...8032016 pullulan.mth
Inj. Sample Notes:	Pullulan permethylated methanolysis and silylated with sorbitol.		

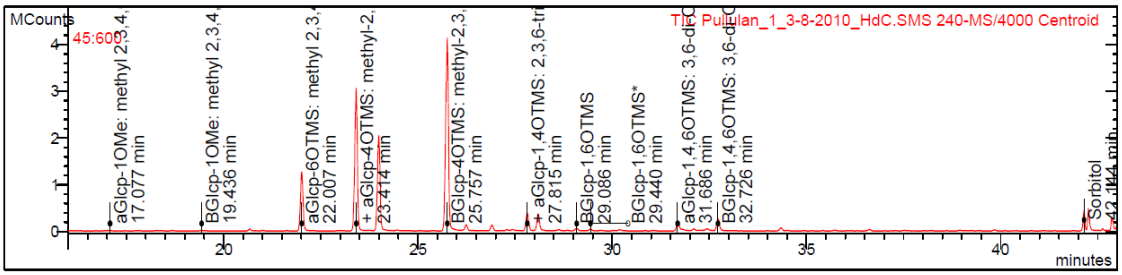

Target Compounds

RT (min)	RRT (min)	Peak Name	Area	Status	Quan Ions	Result Type
42.144		Sorbitol			73.1	Identified
	1.000		301347	X STg		
17.077		aGlcp-1OMe: methyl 2,3,4,6-tetra-O			88.1	Identified
	0.405		14250	X g		
19.436		BGlcp-1OMe: methyl 2,3,4,6-tetra-O-methy			88.1	Identified
	0.461		19764	X g		
20.362		BGalp-1OMe: methyl 2,3,4,6-tetra-O-methy			88.1	Failed
	0.483		178	X Zg		
22.007		aGlcp-6OTMS: methyl 2,3,4-tri-O-methyl-6			88.1	Identified
	0.522		1033047	X g		
23.414		aGlcp-4OTMS: methyl-2,3,6-tri-O-methyl-4			88.0	Identified
	0.556		2610674	X g		
23.995		BGlcp-6OTMS: methyl 2,3,4-tri-O-methyl-6			88.1	Identified
	0.569		1949849	X g		
25.757		BGlcp-4OTMS: methyl-2,3,6-tri-O-methyl-4			88.0	Identified
	0.611		3221079	X g		
26.910		BGlcp-1,6OTMS*			73.1	Identified
	0.639		90643	X g		
27.295		aGlcp-1,6OTMS			73.1	Identified
	0.648		15212	X g		
27.815		aGlcp-1,4OTMS: 2,3,6-tri-O-methyl-1,4-bi			73.1	Identified
	0.660		269043	X g		
28.098		BGlcp-1,4OTMS: 2,3,6-tri-O-methyl-1,4-bi			73.1	Identified
	0.667		242697	X g		
28.642		aGlcp-1,6OTMS*			146.1	Identified
	0.680		10240	X g		
29.086		BGlcp-1,6OTMS			73.1	Identified
	0.690		38109	X g		
29.440		BGlcp-1,6OTMS*			146.1	Identified
	0.699		27716	X g		
31.686		aGlcp-1,4,6OTMS: 3,6-di-O-methyl-1,4,6-t			146.2	Identified
	0.752		173311	X g		
32.726		BGlcp-1,4,6OTMS: 3,6-di-O-methyl-1,4,6-t			146.2	Identified
	0.777		183108	X g		

Figure E.3.2: Processed GC-MS data for pullulan.

Sample ID:	Pullulan	Operator:	HdC
Instrument ID:	Varian CP-3800	Last Calibration:	None
Acquisition Date:	9/21/2012 1:42 PM	Data File:	..._1_9-21-2012_hdc.sms
Calculation Date:	3/31/2016 10:19 AM	Method:	...0032016 pullulan.mth
Inj. Sample Notes:	Pullulan 1:10 split after septum & liner changed		

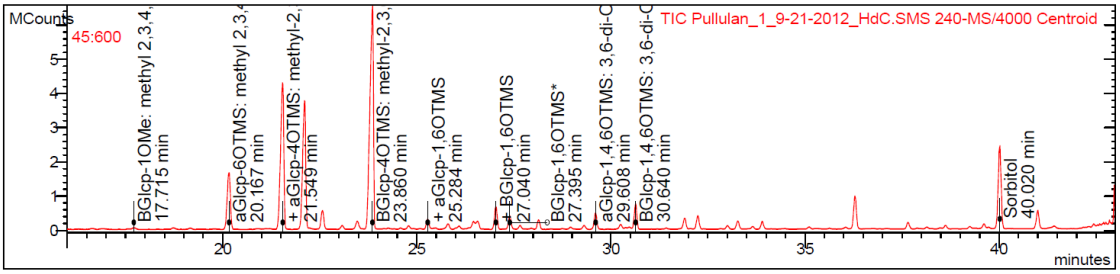

Target Compounds

RT (min)	RRT (min)	Peak Name / Area	Status	Quan Ions	Result Type
40.020		Sorbitol		73.1	Identified
	1.000	2577788	X STg		
15.468		aGlcp-1OMe: methyl 2,3,4,6-tetra-O		88.1	Identified
	0.387	17023	X g		
17.546		aManp-1OMe: Methyl 2,3,4,6 tetra-O-methl		87.9	Failed
	0.438	3193	X Zg		
17.715		BGlcp-1OMe: methyl 2,3,4,6-tetra-O-methy		88.1	Identified
	0.443	76481	X g		
20.167		aGlcp-6OTMS: methyl 2,3,4-tri-O-methyl-6		88.1	Identified
	0.504	1782472	X g		
21.549		aGlcp-4OTMS: methyl-2,3,6-tri-O-methyl-4		88.0	Identified
	0.538	4830557	X g		
22.115		BGlcp-6OTMS: methyl 2,3,4-tri-O-methyl-6		88.1	Identified
	0.553	3678392	X g		
23.860		BGlcp-4OTMS: methyl-2,3,6-tri-O-methyl-4		88.0	Identified
	0.596	7119325	X g		
25.284		aGlcp-1,6OTMS		73.1	Identified
	0.632	189855	X g		
25.802		aGlcp-1,4OTMS: 2,3,6-tri-O-methyl-1,4-bi		73.1	Identified
	0.645	128953	X g		
26.095		BGlcp-1,4OTMS: 2,3,6-tri-O-methyl-1,4-bi		73.1	Identified
	0.652	92734	X g		
26.581		aGlcp-1,6OTMS*		146.1	Identified
	0.664	109598	X g		
27.040		BGlcp-1,6OTMS		73.1	Identified
	0.676	445805	X g		
27.395		BGlcp-1,6OTMS*		146.1	Identified
	0.685	302735	X g		
29.608		aGlcp-1,4,6OTMS: 3,6-di-O-methyl-1,4,6-t		146.2	Identified
	0.740	383059	X g		
30.640		BGlcp-1,4,6OTMS: 3,6-di-O-methyl-1,4,6-t		146.2	Identified
	0.766	481384	X g		

Figure E.3.3: Processed GC-MS data for pullulan.

Sample ID:	pullulan 3133	Operator:	HdC
Instrument ID:	Varian CP-3800	Last Calibration:	None
Acquisition Date:	3/2/2012 8:58 PM	Data File:	...3_1_3-2-2012_hdc.sms
Calculation Date:	3/31/2016 9:24 AM	Method:	...0032016 pullulan.mth
Inj. Sample Notes:	pullulan wk 31 33 structural analysis. 0.0375g/25ml sorbitol		
	IS 5uL added before cook.		

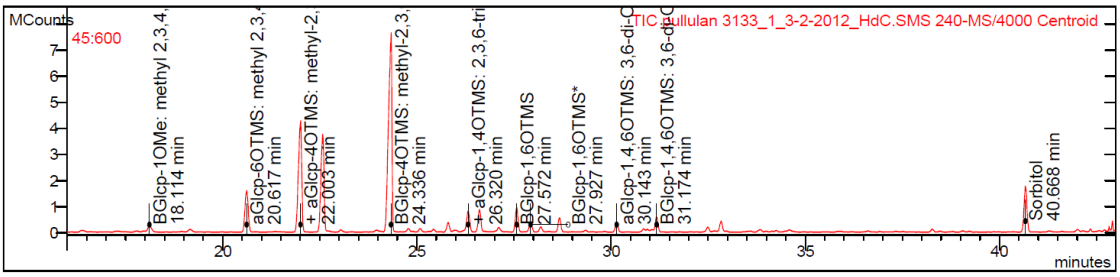

Target Compounds

RT (min)	RRT (min)	Peak Name	Area	Status	Quan Ions	Result Type
40.668		Sorbitol			73.1	Identified
	1.000		1909637	X STg		
15.837		aGlcp-1OMe: methyl 2,3,4,6-tetra-O			88.1	Identified
	0.389		79809	X g		
18.114		BGlcp-1OMe: methyl 2,3,4,6-tetra-O-methy			88.1	Identified
	0.445		435311	X g		
20.617		aGlcp-6OTMS: methyl 2,3,4-tri-O-methyl-6			88.1	Identified
	0.507		1627750	X g		
22.003		aGlcp-4OTMS: methyl-2,3,6-tri-O-methyl-4			88.0	Identified
	0.541		4604279	X g		
22.575		BGlcp-6OTMS: methyl 2,3,4-tri-O-methyl-6			88.1	Identified
	0.555		3967583	X g		
24.336		BGlcp-4OTMS: methyl-2,3,6-tri-O-methyl-4			88.0	Identified
	0.598		7851088	X g		
25.806		aGlcp-1,6OTMS			73.1	Identified
	0.635		237415	X g		
26.320		aGlcp-1,4OTMS: 2,3,6-tri-O-methyl-1,4-bi			73.1	Identified
	0.647		682354	X g		
26.612		BGlcp-1,4OTMS: 2,3,6-tri-O-methyl-1,4-bi			73.1	Identified
	0.654		628281	X g		
27.111		aGlcp-1,6OTMS*			146.1	Identified
	0.667		146403	X g		
27.572		BGlcp-1,6OTMS			73.1	Identified
	0.678		641316	X g		
27.927		BGlcp-1,6OTMS*			146.1	Identified
	0.687		299196	X g		
30.143		aGlcp-1,4,6OTMS: 3,6-di-O-methyl-1,4,6-t			146.2	Identified
	0.741		259787	X g		
31.174		BGlcp-1,4,6OTMS: 3,6-di-O-methyl-1,4,6-t			146.2	Identified
	0.767		353067	X g		

Figure E.3.4: Processed GC-MS data for pullulan.

Sample ID:	FB2 Batch1 Fr1	Operator:	HdC
Instrument ID:	Varian CP-3800	Last Calibration:	None
Acquisition Date:	3/9/2010 12:31 AM	Data File:	...1_1_3-9-2010_hdc.sms
Calculation Date:	3/30/2016 9:19 AM	Method:	...0_28032016 f1 v2.mth
Inj. Sample Notes:	FB2 batch 1 fraction 1 permethylated methanolysis and silylated with sorbitol.		

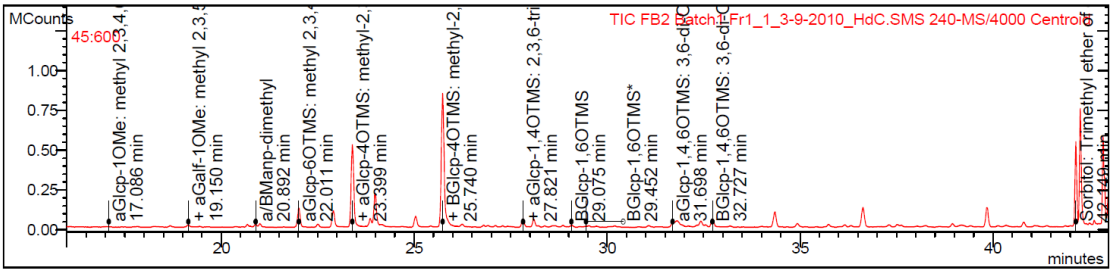

Target Compounds

RT (min)	RRT (min)	Peak Name / Area	Status	Quan Ions	Result Type
42.149	1.000	Sorbitol: Trimethyl ether of glucitol 352223	X STg	73.1	Identified
17.086	0.405	aGlcp-1OMe: methyl 2,3,4,6-tetra-O 3176	X g	88.1	Identified
19.150	0.454	aGalf-1OMe: methyl 2,3,5,6-tetra-O-methy 27785	X g	101.1	Identified
19.437	0.461	BGlcp-1OMe: methyl 2,3,4,6-tetra-O-methy 6494	X g	88.1	Identified
20.382	0.484	BGalp-1OMe: methyl 2,3,4,6-tetra-O-methy 1599	X Zg	88.1	Failed
20.892	0.496	a/BManp-dimethyl 8792	X g	159.1	Identified
22.011	0.522	aGlcp-6OTMS: methyl 2,3,4-tri-O-methyl-6 116753	X g	88.1	Identified
22.507	0.534	aGalp-1TMS 14760	X g	88.1	Identified
22.905	0.543	aGalf-1TMS*: methyl-2,3,4-tris-O-methyl- 84178	X g	101.0	Identified
23.399	0.555	aGlcp-4OTMS: methyl-2,3,6-tri-O-methyl-4 435464	X g	88.0	Identified
23.866	0.566	BGalp-1TMS*: methyl-2,3,4-tris-O-methyl- 14405	X g	88.0	Identified
23.992	0.569	BGlcp-6OTMS: methyl 2,3,4-tri-O-methyl-6 182132	X g	88.1	Identified
25.036	0.594	BGalf-1TMS*: methyl-2,3,4-tris-O-methyl- 84204	X g	101.0	Identified
25.740	0.611	BGlcp-4OTMS: methyl-2,3,6-tri-O-methyl-4 585548	X g	88.0	Identified
26.908	0.638	BGlcp-1,6OTMS* 4312	X g	73.1	Identified
27.298	0.648	aGlcp-1,6OTMS 4228	X g	73.1	Identified
27.821	0.660	aGlcp-1,4OTMS: 2,3,6-tri-O-methyl-1,4-bi 36467	X g	73.1	Identified
28.101	0.667	BGlcp-1,4OTMS: 2,3,6-tri-O-methyl-1,4-bi 33851	X g	73.1	Identified
28.629	0.679	aGlcp-1,6OTMS* 3758	X g	146.1	Identified
29.075	0.690	BGlcp-1,6OTMS 6674	X g	73.1	Identified
29.452	0.699	BGlcp-1,6OTMS* 4285	X g	146.1	Identified

Figure E.3.5: Processed GC-MS data for FB2 F1.

Sample ID:	FB2 batch 2 Fr1	Operator:	HdC
Instrument ID:	Varian CP-3800	Last Calibration:	None
Acquisition Date:	3/9/2010 2:14 AM	Data File:	...1_1_3-9-2010_hdc.sms
Calculation Date:	3/30/2016 9:16 AM	Method:	...0_28032016 f1 v3.mth
Inj. Sample Notes:	FB2 batch 2 fraction 1permethylated methanolysis and silylated with sorbitol.		

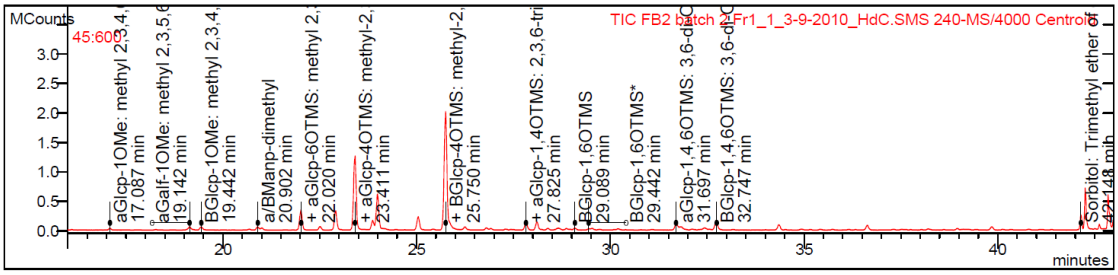

Target Compounds

RT (min)	RRT (min)	Peak Name / Area	Status	Quan Ions	Result Type
42.148		Sorbitol: Trimethyl ether of glucitol		73.1	Identified
	1.000	166381	X STg		
17.087		aGlcp-1OMe: methyl 2,3,4,6-tetra-O		88.1	Identified
	0.405	41176	X g		
19.071		aManp-1OMe: Methyl 2,3,4,6 tetra-O-methl		87.9	Failed
	0.452	11883	X Zg		
19.142		aGalf-1OMe: methyl 2,3,5,6-tetra-O-methy		101.1	Identified
	0.454	60490	X g		
19.442		BGlcp-1OMe: methyl 2,3,4,6-tetra-O-methy		88.1	Identified
	0.461	81895	X g		
20.902		a/BManp-dimethyl		159.1	Identified
	0.496	35349	X g		
22.020		aGlcp-6OTMS: methyl 2,3,4-tri-O-methyl-6		88.1	Identified
	0.522	317033	X g		
22.507		aGalp-1TMS		88.1	Identified
	0.534	45410	X g		
22.911		aGalf-1TMS*: methyl-2,3,4-tris-O-methyl-		101.0	Identified
	0.544	265237	X g		
23.411		aGlcp-4OTMS: methyl-2,3,6-tri-O-methyl-4		88.0	Identified
	0.555	1052248	X g		
23.870		BGalp-1TMS*: methyl-2,3,4-tris-O-methyl-		88.0	Identified
	0.566	14151	X g		
23.991		BGlcp-6OTMS: methyl 2,3,4-tri-O-methyl-6		88.1	Identified
	0.569	421167	X g		
25.040		BGalf-1TMS*: methyl-2,3,4-tris-O-methyl-		101.0	Identified
	0.594	211850	X g		
25.750		BGlcp-4OTMS: methyl-2,3,6-tri-O-methyl-4		88.0	Identified
	0.611	1465265	X g		
26.915		BGlcp-1,6*OTMS		73.1	Identified
	0.639	18531	X g		
27.305		aGlcp-1,6OTMS		73.1	Identified
	0.648	10561	X g		
27.825		aGlcp-1,4OTMS: 2,3,6-tri-O-methyl-1,4-bi		73.1	Identified
	0.660	94084	X g		
28.107		BGlcp-1,4OTMS: 2,3,6-tri-O-methyl-1,4-bi		73.1	Identified
	0.667	90103	X g		
28.637		aGlcp-1,6OTMS*		146.1	Identified
	0.679	11591	X g		
29.089		BGlcp-1,6OTMS		73.1	Identified
	0.690	18185	X g		
29.442		BGlcp-1,6OTMS*		146.1	Identified
	0.699	8106	X g		

Figure E.3.6: Processed GC-MS data for FB2 F1.

Sample ID:	FB2 F1	Operator:	ER
Instrument ID:	Varian CP-3800	Last Calibration:	None
Acquisition Date:	6/17/2010 3:08 AM	Data File:	...1_1_6-17-2010_er.sms
Calculation Date:	3/30/2016 9:00 AM	Method:	...0_28032016 f1 v2.mth
Inj. Sample Notes:	FB2 F1 140410 permethylated methanolysis silylated. all solv ents freshly dried. 5uL 0.3 mg/mL sorbitol added before cook .		

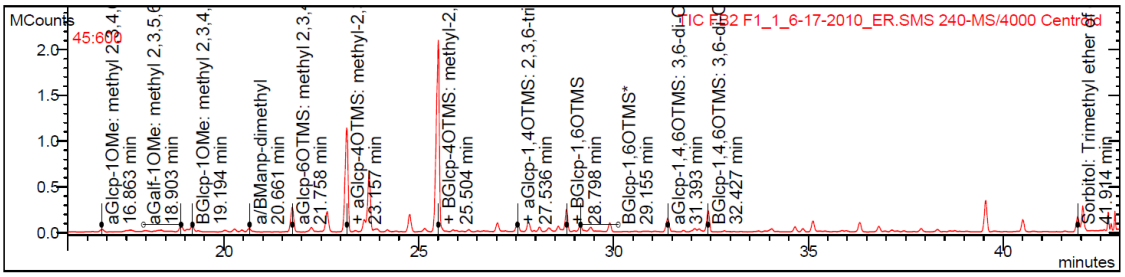

Target Compounds

RT (min)	RRT (min)	Peak Name / Area	Status	Quan Ions	Result Type
41.914		Sorbitol: Trimethyl ether of glucitol		73.1	Identified
	1.000	200404	X STg		
16.863		aGlcp-1OMe: methyl 2,3,4,6-tetra-O		88.1	Identified
	0.402	57946	X g		
18.855		aManp-1OMe: Methyl 2,3,4,6 tetra-O-methl		87.9	Failed
	0.450	17385	X Zg		
18.903		aGalf-1OMe: methyl 2,3,5,6-tetra-O-methy		101.1	Identified
	0.451	107313	X g		
19.194		BGlcp-1OMe: methyl 2,3,4,6-tetra-O-methy		88.1	Identified
	0.458	108505	X g		
20.661		a/BManp-dimethyl		159.1	Identified
	0.493	24163	X g		
21.758		aGlcp-6OTMS: methyl 2,3,4-tri-O-methyl-6		88.1	Identified
	0.519	262947	X g		
22.251		aGalp-1TMS		88.1	Identified
	0.531	38819	X g		
22.653		aGalf-1TMS*: methyl-2,3,4-tris-O-methyl-		101.0	Identified
	0.540	242688	X g		
23.157		aGlcp-4OTMS: methyl-2,3,6-tri-O-methyl-4		88.0	Identified
	0.552	1130673	X g		
23.603		BGalp-1TMS*: methyl-2,3,4-tris-O-methyl-		88.0	Identified
	0.563	8053	X g		
23.730		BGlcp-6OTMS: methyl 2,3,4-tri-O-methyl-6		88.1	Identified
	0.566	487974	X g		
24.763		BGalf-1TMS*: methyl-2,3,4-tris-O-methyl-		101.0	Identified
	0.591	232213	X g		
25.504		BGlcp-4OTMS: methyl-2,3,6-tri-O-methyl-4		88.0	Identified
	0.608	1820014	X g		
27.025		aGlcp-1,6OTMS		73.1	Identified
	0.645	59620	X g		
27.536		aGlcp-1,4OTMS: 2,3,6-tri-O-methyl-1,4-bi		73.1	Identified
	0.657	85608	X g		
27.819		BGlcp-1,4OTMS: 2,3,6-tri-O-methyl-1,4-bi		73.1	Identified
	0.664	69296	X g		
28.340		aGlcp-1,6OTMS*		146.1	Identified
	0.676	15616	X g		
28.798		BGlcp-1,6OTMS		73.1	Identified
	0.687	114805	X g		
29.155		BGlcp-1,6OTMS*		146.1	Identified
	0.696	40050	X g		

Figure E.3.7: Processed GC-MS data for FB2 F1.

Sample ID:	FB2 Batch 2 Fr2	Operator:	HdC
Instrument ID:	Varian CP-3800	Last Calibration:	None
Acquisition Date:	3/9/2010 3:06 AM	Data File:	...2_1_3-9-2010_hdc.sms
Calculation Date:	3/30/2016 9:26 AM	Method:	...0_28032016 f2 v2.mth
Inj. Sample Notes:	FB2 batch 2 fraction 2 permethylated methanolysis and silyla ted with sorbitol.		

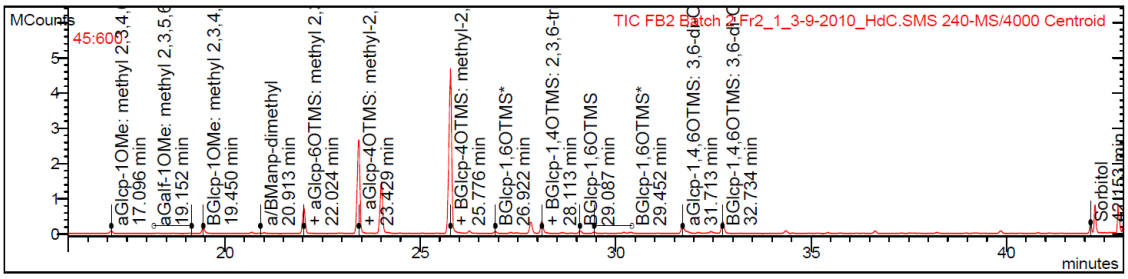

Target Compounds

RT (min)	RRT (min)	Peak Name / Area	Status	Quan Ions	Result Type
42.153	1.000	Sorbitol 263019	X STg	73.1	Identified
17.096	0.406	aGlcp-1OMe: methyl 2,3,4,6-tetra-O 116963	X g	88.1	Identified
19.081	0.453	aManp-1OMe: Methyl 2,3,4,6 tetra-O-methl 904	X Zg	87.9	Failed
19.152	0.454	aGalf-1OMe: methyl 2,3,5,6-tetra-O-methy 1930	X g	101.1	Identified
19.450	0.461	BGlcp-1OMe: methyl 2,3,4,6-tetra-O-methy 254664	X g	88.1	Identified
20.381	0.484	BGalp-1OMe: methyl 2,3,4,6-tetra-O-methy 507	X Zg	88.1	Failed
20.913	0.496	a/BManp-dimethyl 4781	X g	159.1	Identified
22.024	0.522	aGlcp-6OTMS: methyl 2,3,4-tri-O-methyl-6 663541	X g	88.1	Identified
22.913	0.544	aGalf-1TMS*: methyl-2,3,4-tris-O-methyl- 6216	X g	101.0	Identified
23.429	0.556	aGlcp-4OTMS: methyl-2,3,6-tri-O-methyl-4 2354656	X g	88.0	Identified
24.007	0.570	BGlcp-6OTMS: methyl 2,3,4-tri-O-methyl-6 1207376	X g	88.1	Identified
25.044	0.594	BGalf-1TMS*: methyl-2,3,4-tris-O-methyl- 5042	X g	101.0	Identified
25.776	0.612	BGlcp-4OTMS: methyl-2,3,6-tri-O-methyl-4 3716108	X g	88.0	Identified
26.922	0.639	BGlcp-1,6OTMS* 39765	X g	73.1	Identified
27.314	0.648	aGlcp-1,6OTMS 19028	X g	73.1	Identified
27.835	0.660	aGlcp-1,4OTMS: 2,3,6-tri-O-methyl-1,4-bi 231598	X g	73.1	Identified
28.113	0.667	BGlcp-1,4OTMS: 2,3,6-tri-O-methyl-1,4-bi 247390	X g	73.1	Identified
28.647	0.680	aGlcp-1,6OTMS* 18195	X g	146.1	Identified
29.087	0.690	BGlcp-1,6OTMS 25969	X g	73.1	Identified
29.452	0.699	BGlcp-1,6OTMS* 25527	X g	146.1	Identified
31.713	0.752	aGlcp-1,4,6OTMS: 3,6-di-O-methyl-1,4,6-t 171414	X g	146.2	Identified

Figure E.3.8: Processed GC-MS data for FB2 F2.

Sample ID:	FB2 F2	Operator:	ER
Instrument ID:	Varian CP-3800	Last Calibration:	None
Acquisition Date:	6/17/2010 3:59 AM	Data File:	...2_1_6-17-2010_er.sms
Calculation Date:	3/30/2016 8:04 AM	Method:	...0_28032016 f2 v2.mth
Inj. Sample Notes:	FB2 F2 030310 permethylated methanolysis silylated. all solvents freshly dried. 5uL 0.3 mg/mL sorbitol added before cook		

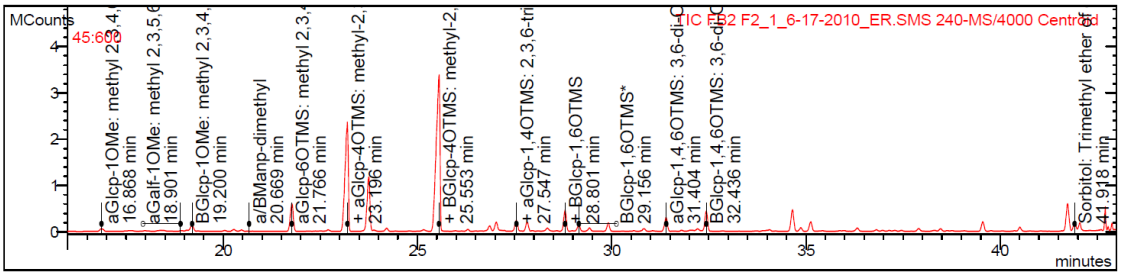

Target Compounds

RT (min)	RRT (min)	Peak Name / Area	Status	Quan Ions	Result Type
41.918		Sorbitol: Trimethyl ether of glucitol		73.1	Identified
	1.000	199935	X STg		
16.868		aGlcp-1OMe: methyl 2,3,4,6-tetra-O		88.1	Identified
	0.402	121007	X g		
18.901		aGalf-1OMe: methyl 2,3,5,6-tetra-O-methy		101.1	Identified
	0.451	5157	X g		
19.200		BGlcp-1OMe: methyl 2,3,4,6-tetra-O-methy		88.1	Identified
	0.458	214651	X g		
20.669		a/BManp-dimethyl		159.1	Identified
	0.493	2674	X g		
21.766		aGlcp-6OTMS: methyl 2,3,4-tri-O-methyl-6		88.1	Identified
	0.519	683094	X g		
22.250		aGalp-1TMS		88.1	Identified
	0.531	795	X g		
22.642		aGalf-1TMS*: methyl-2,3,4-tris-O-methyl-		101.0	Identified
	0.540	1799	X g		
23.196		aGlcp-4OTMS: methyl-2,3,6-tri-O-methyl-4		88.0	Identified
	0.553	2758970	X g		
23.747		BGlcp-6OTMS: methyl 2,3,4-tri-O-methyl-6		88.1	Identified
	0.567	1267123	X g		
24.770		BGalf-1TMS*: methyl-2,3,4-tris-O-methyl-		101.0	Identified
	0.591	2607	X g		
25.553		BGlcp-4OTMS: methyl-2,3,6-tri-O-methyl-4		88.0	Identified
	0.610	3924085	X g		
26.642		BGlcp-1,6*OTMS		73.1	Identified
	0.636	1610	X g		
27.034		aGlcp-1,6OTMS		73.1	Identified
	0.645	101400	X g		
27.547		aGlcp-1,4OTMS: 2,3,6-tri-O-methyl-1,4-bi		73.1	Identified
	0.657	178294	X g		
27.819		BGlcp-1,4OTMS: 2,3,6-tri-O-methyl-1,4-bi		73.1	Identified
	0.664	129183	X g		
28.352		aGlcp-1,6OTMS*		146.1	Identified
	0.676	32437	X g		
28.801		BGlcp-1,6OTMS		73.1	Identified
	0.687	207338	X g		
29.156		BGlcp-1,6OTMS*		146.1	Identified
	0.696	66902	X g		
31.404		aGlcp-1,4,6OTMS: 3,6-di-O-methyl-1,4,6-t		146.2	Identified
	0.749	230963	X g		

Figure E.3.9: Processed GC-MS data for FB2 F2.

Sample ID:	FB2 Batch2 Fr3	Operator:	HdC
Instrument ID:	Varian CP-3800	Last Calibration:	None
Acquisition Date:	3/9/2010 3:58 AM	Data File:	...3_1_3-9-2010_hdc.sms
Calculation Date:	3/30/2016 4:59 PM	Method:	...0_28032016 f3 v3.mth
Inj. Sample Notes:	FB2 batch 2 fraction 3 permethylated methanolysis and silyla ted with sorbitol.		

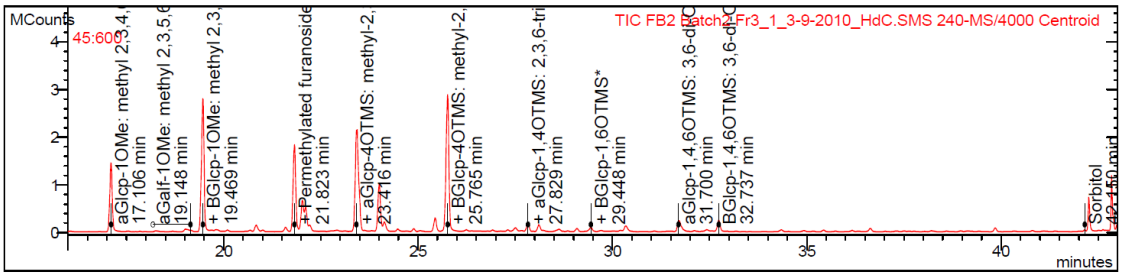

Target Compounds

RT (min)	RRT (min)	Peak Name	Area	Status	Quan Ions	Result Type
42.150	1.000	Sorbitol	24052	X STg	73.1	Identified
17.106	0.406	aGlcp-1OMe: methyl 2,3,4,6-tetra-O	1933812	X g	88.1	Identified
19.078	0.453	aManp-1OMe: Methyl 2,3,4,6 tetra-O-methl	4839	X Zg	87.9	Failed
19.148	0.454	aGalf-1OMe: methyl 2,3,5,6-tetra-O-methy	12192	X g	101.1	Identified
19.469	0.462	BGlcp-1OMe: methyl 2,3,4,6-tetra-O-methy	3891123	X g	88.1	Identified
20.381	0.484	BGalp-1OMe: methyl 2,3,4,6-tetra-O-methy	2639	X g	88.1	Identified
20.900	0.496	a/BManp-dimethyl	8244	X g	159.1	Identified
22.026	0.523	aGlcp-6OTMS: methyl 2,3,4-tri-O-methyl-6	575801	X g	88.1	Identified
22.915	0.544	aGalf-1TMS*: methyl-2,3,4-tris-O-methyl-	16092	X g	101.0	Identified
23.416	0.556	aGlcp-4OTMS: methyl-2,3,6-tri-O-methyl-4	1772150	X g	88.0	Identified
24.002	0.569	BGlcp-6OTMS: methyl 2,3,4-tri-O-methyl-6	833731	X g	88.1	Identified
25.044	0.594	BGalf-1TMS*: methyl-2,3,4-tris-O-methyl-	11633	X g	101.0	Identified
25.765	0.611	BGlcp-4OTMS: methyl-2,3,6-tri-O-methyl-4	2198969	X g	88.0	Identified
26.920	0.639	BGlcp-1,6OTMS*	21724	X g	73.1	Identified
27.314	0.648	aGlcp-1,6OTMS	18175	X g	73.1	Identified
27.829	0.660	aGlcp-1,4OTMS: 2,3,6-tri-O-methyl-1,4-bi	115001	X g	73.1	Identified
28.109	0.667	BGlcp-1,4OTMS: 2,3,6-tri-O-methyl-1,4-bi	95472	X g	73.1	Identified
28.639	0.679	aGlcp-1,6OTMS*	38682	X g	146.1	Identified
29.092	0.690	BGlcp-1,6OTMS	41107	X g	73.1	Identified
29.448	0.699	BGlcp-1,6OTMS*	58404	X g	146.1	Identified
31.700	0.752	aGlcp-1,4,6OTMS: 3,6-di-O-methyl-1,4,6-t	155617	X g	146.2	Identified

Figure E.3.10: Processed GC-MS data for FB2 F3.

Sample ID:	FB2 a	Operator:	ER
Instrument ID:	Varian CP-3800	Last Calibration:	None
Acquisition Date:	11/5/2012 12:31 PM	Data File:	...a_1_11-5-2012_er.sms
Calculation Date:	3/30/2016 3:26 PM	Method:	...012_30032016 fb2.mth
Inj. Sample Notes:	None		

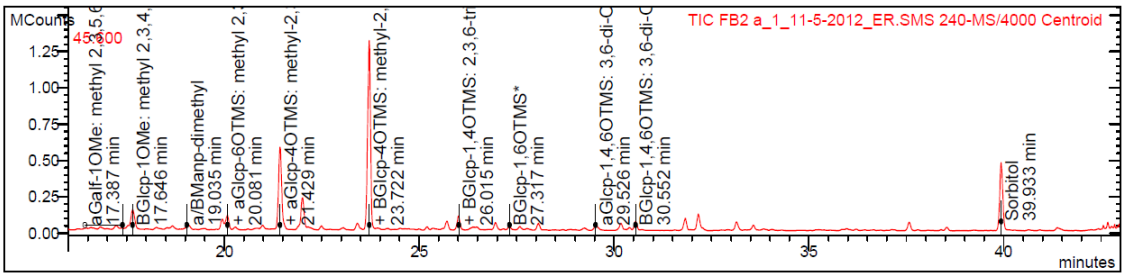

Target Compounds

RT (min)	RRT (min)	Peak Name / Area	Status	Quan Ions	Result Type
39.933		Sorbitol		73.1	Identified
	1.000	529380	X STg		
15.416		aGlcp-1OMe: methyl 2,3,4,6-tetra-O		88.1	Identified
	0.386	101955	X g		
17.336		aManp-1OMe: Methyl 2,3,4,6 tetra-O-methl		87.9	Failed
	0.434	7909	X Zg		
17.387		aGalf-1OMe: methyl 2,3,5,6-tetra-O-methy		101.1	Identified
	0.435	6120	X g		
17.646		BGlcp-1OMe: methyl 2,3,4,6-tetra-O-methy		88.1	Identified
	0.442	252239	X g		
19.035		a/BManp-dimethyl		159.1	Identified
	0.477	12078	X g		
20.081		aGlcp-6OTMS: methyl 2,3,4-tri-O-methyl-6		88.1	Identified
	0.503	111567	X g		
20.599		aGalp-1TMS		88.1	Identified
	0.516	2578	X g		
20.985		aGalf-1TMS*: methyl-2,3,4-tris-O-methyl-		101.0	Identified
	0.526	21597	X g		
21.429		aGlcp-4OTMS: methyl-2,3,6-tri-O-methyl-4		88.0	Identified
	0.537	391969	X g		
22.007		BGlcp-6OTMS: methyl 2,3,4-tri-O-methyl-6		88.1	Identified
	0.551	244553	X g		
23.063		BGalf-1TMS*: methyl-2,3,4-tris-O-methyl-		101.0	Identified
	0.578	12690	X g		
23.722		BGlcp-4OTMS: methyl-2,3,6-tri-O-methyl-4		88.0	Identified
	0.594	900825	X g		
25.201		aGlcp-1,6OTMS		73.1	Identified
	0.631	16464	X g		
25.714		aGlcp-1,4OTMS: 2,3,6-tri-O-methyl-1,4-bi		73.1	Identified
	0.644	29581	X g		
26.015		BGlcp-1,4OTMS: 2,3,6-tri-O-methyl-1,4-bi		73.1	Identified
	0.651	43498	X g		
26.502		aGlcp-1,6OTMS*		146.1	Identified
	0.664	9480	X g		
26.961		BGlcp-1,6OTMS		73.1	Identified
	0.675	36058	X g		
27.317		BGlcp-1,6OTMS*		146.1	Identified
	0.684	21103	X g		
29.526		aGlcp-1,4,6OTMS: 3,6-di-O-methyl-1,4,6-t		146.2	Identified
	0.739	32529	X g		
30.552		BGlcp-1,4,6OTMS: 3,6-di-O-methyl-1,4,6-t		146.2	Identified
	0.765	46160	X g		

Figure E.3.11: Processed GC-MS data for FB2.

Sample ID:	FB2b	Operator:	ER
Instrument ID:	Varian CP-3800	Last Calibration:	None
Acquisition Date:	11/5/2012 1:26 PM	Data File:	...b_1_11-5-2012_er.sms
Calculation Date:	3/30/2016 4:21 PM	Method:	...12_30032016 fb2b.mth
Inj. Sample Notes:	None		

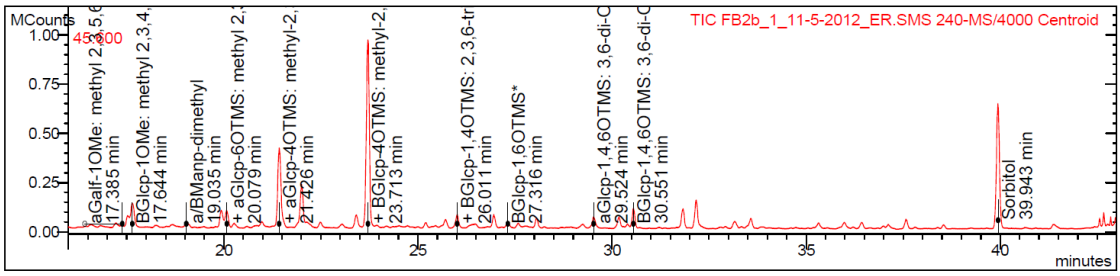

Target Compounds

RT (min)	RRT (min)	Peak Name	Area	Status	Quan Ions	Result Type
39.943		Sorbitol			73.1	Identified
	1.000		746821	X STg		
15.412		aGlcp-1OMe: methyl 2,3,4,6-tetra-O			88.1	Identified
	0.386		97495	X g		
17.385		aGalf-1OMe: methyl 2,3,5,6-tetra-O-methy			101.1	Identified
	0.435		4445	X g		
17.644		BGlcp-1OMe: methyl 2,3,4,6-tetra-O-methy			88.1	Identified
	0.442		205386	X g		
19.035		a/BManp-dimethyl			159.1	Identified
	0.477		12239	X g		
20.079		aGlcp-6OTMS: methyl 2,3,4-tri-O-methyl-6			88.1	Identified
	0.503		90278	X g		
20.979		aGalf-1TMS*: methyl-2,3,4-tris-O-methyl-			101.0	Identified
	0.525		20626	X g		
21.426		aGlcp-4OTMS: methyl-2,3,6-tri-O-methyl-4			88.0	Identified
	0.536		388295	X g		
22.004		BGlcp-6OTMS: methyl 2,3,4-tri-O-methyl-6			88.1	Identified
	0.551		232005	X g		
23.059		BGalf-1TMS*: methyl-2,3,4-tris-O-methyl-			101.0	Identified
	0.577		10987	X g		
23.713		BGlcp-4OTMS: methyl-2,3,6-tri-O-methyl-4			88.0	Identified
	0.594		735738	X g		
25.209		aGlcp-1,6OTMS			73.1	Identified
	0.631		18272	X g		
25.722		aGlcp-1,4OTMS: 2,3,6-tri-O-methyl-1,4-bi			73.1	Identified
	0.644		40179	X g		
26.011		BGlcp-1,4OTMS: 2,3,6-tri-O-methyl-1,4-bi			73.1	Identified
	0.651		54410	X g		
26.499		aGlcp-1,6OTMS*			146.1	Identified
	0.663		12855	X g		
26.958		BGlcp-1,6OTMS			73.1	Identified
	0.675		41401	X g		
27.316		BGlcp-1,6OTMS*			146.1	Identified
	0.684		27469	X g		
29.524		aGlcp-1,4,6OTMS: 3,6-di-O-methyl-1,4,6-t			146.2	Identified
	0.739		49314	X g		
30.551		BGlcp-1,4,6OTMS: 3,6-di-O-methyl-1,4,6-t			146.2	Identified
	0.765		72532	X g		

Figure E.3.12: Processed GC-MS data for FB2.

Sample ID:	PB2	Operator:	HdC
Instrument ID:	Varian CP-3800	Last Calibration:	None
Acquisition Date:	9/24/2012 11:30 PM	Data File:	..._1_9-24-2012_hdc.sms
Calculation Date:	3/30/2016 5:10 PM	Method:	...012_30032016 pb2.mth
Inj. Sample Notes:	SACPOL Batch2. IS=0.0398G/25ml. Structural		

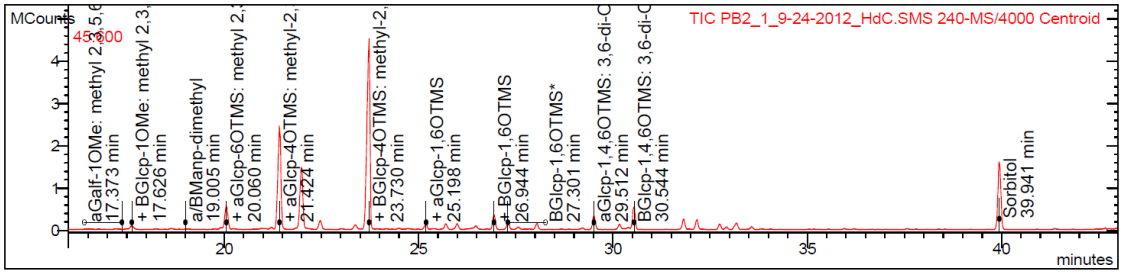

Target Compounds

RT (min)	RRT (min)	Peak Name	Area	Status	Quan Ions	Result Type
39.941		Sorbitol			73.1	Identified
	1.000		1791870	X STg		
15.390		aGlcp-1OMe: methyl 2,3,4,6-tetra-O			88.1	Identified
	0.385		53429	X g		
17.323		aManp-1OMe: Methyl 2,3,4,6 tetra-O-methl			87.9	Failed
	0.434		2187	X Zg		
17.373		aGalf-1OMe: methyl 2,3,5,6-tetra-O-methy			101.1	Identified
	0.435		1684	X g		
17.626		BGlcp-1OMe: methyl 2,3,4,6-tetra-O-methy			88.1	Identified
	0.441		144233	X g		
18.001		aManf-1OMe: Methyl 2,3,4,6-tetra-O-methl			101.2	Identified
	0.451		4254	X g		
19.005		a/BManp-dimethyl			159.1	Identified
	0.476		1758	X g		
20.060		aGlcp-6OTMS: methyl 2,3,4-tri-O-methyl-6			88.1	Identified
	0.502		382204	X g		
20.580		aGalp-1TMS			88.1	Identified
	0.515		4086	X g		
20.963		aGalf-1TMS*: methyl-2,3,4-tris-O-methyl-			101.0	Identified
	0.525		26752	X g		
21.424		aGlcp-4OTMS: methyl-2,3,6-tri-O-methyl-4			88.0	Identified
	0.536		2388651	X g		
21.993		BGlcp-6OTMS: methyl 2,3,4-tri-O-methyl-6			88.1	Identified
	0.551		1547237	X g		
23.037		BGalf-1TMS*: methyl-2,3,4-tris-O-methyl-			101.0	Identified
	0.577		21417	X g		
23.730		BGlcp-4OTMS: methyl-2,3,6-tri-O-methyl-4			88.0	Identified
	0.594		3975138	X g		
25.198		aGlcp-1,6OTMS			73.1	Identified
	0.631		99355	X g		
25.704		aGlcp-1,4OTMS: 2,3,6-tri-O-methyl-1,4-bi			73.1	Identified
	0.644		87563	X g		
25.995		BGlcp-1,4OTMS: 2,3,6-tri-O-methyl-1,4-bi			73.1	Identified
	0.651		111129	X g		
26.480		aGlcp-1,6OTMS*			146.1	Identified
	0.663		66844	X g		
26.944		BGlcp-1,6OTMS			73.1	Identified
	0.675		240272	X g		
27.301		BGlcp-1,6OTMS*			146.1	Identified
	0.684		124313	X g		
29.512		aGlcp-1,4,6OTMS: 3,6-di-O-methyl-1,4,6-t			146.2	Identified
	0.739		275305	X g		

Figure E.3.13: Processed GC-MS data for PB2.

Sample ID:	PB7D7	Operator:	HdC
Instrument ID:	Varian CP-3800	Last Calibration:	None
Acquisition Date:	9/25/2012 6:47 AM	Data File:	..._1_9-25-2012_hdc.sms
Calculation Date:	3/30/2016 5:12 PM	Method:	...012_30032016 pb2.mth
Inj. Sample Notes:	SACPOL Batch7 Day7. IS=0.0398g/25ml. Structural		

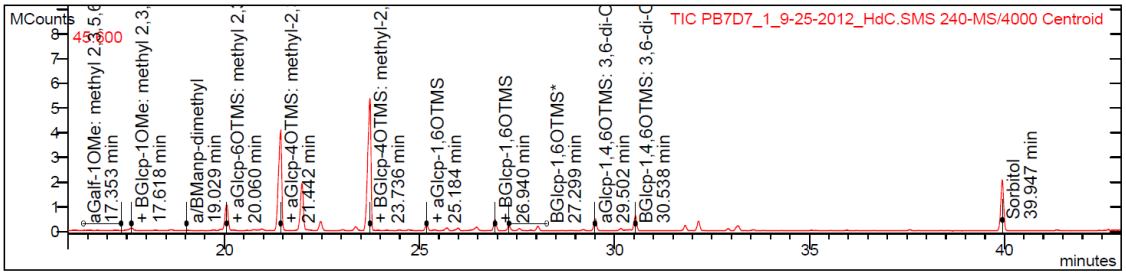

Target Compounds

RT (min)	RRT (min)	Peak Name	Area	Status	Quan Ions	Result Type
39.947	1.000	Sorbitol	2246806	X STg	73.1	Identified
15.389	0.385	aGlcp-1OMe: methyl 2,3,4,6-tetra-O	101095	X g	88.1	Identified
17.332	0.434	aManp-1OMe: Methyl 2,3,4,6 tetra-O-methl	1398	X Zg	87.9	Failed
17.353	0.434	aGalf-1OMe: methyl 2,3,5,6-tetra-O-methy	2888	X g	101.1	Identified
17.618	0.441	BGlcp-1OMe: methyl 2,3,4,6-tetra-O-methy	186738	X g	88.1	Identified
17.976	0.450	aManf-1OMe: Methyl 2,3,4,6-tetra-O-methl	7779	X g	101.2	Identified
19.029	0.476	a/BManp-dimethyl	3833	X g	159.1	Identified
20.060	0.502	aGlcp-6OTMS: methyl 2,3,4-tri-O-methyl-6	696079	X g	88.1	Identified
20.584	0.515	aGalp-1TMS	6478	X g	88.1	Identified
20.958	0.525	aGalf-1TMS*: methyl-2,3,4-tris-O-methyl-	58483	X g	101.0	Identified
21.442	0.537	aGlcp-4OTMS: methyl-2,3,6-tri-O-methyl-4	4401676	X g	88.0	Identified
21.994	0.551	BGlcp-6OTMS: methyl 2,3,4-tri-O-methyl-6	2000070	X g	88.1	Identified
23.037	0.577	BGalf-1TMS*: methyl-2,3,4-tris-O-methyl-	52832	X g	101.0	Identified
23.736	0.594	BGlcp-4OTMS: methyl-2,3,6-tri-O-methyl-4	5172124	X g	88.0	Identified
25.184	0.630	aGlcp-1,6OTMS	157526	X g	73.1	Identified
25.706	0.644	aGlcp-1,4OTMS: 2,3,6-tri-O-methyl-1,4-bi	80179	X g	73.1	Identified
25.992	0.651	BGlcp-1,4OTMS: 2,3,6-tri-O-methyl-1,4-bi	97289	X g	73.1	Identified
26.480	0.663	aGlcp-1,6OTMS*	107948	X g	146.1	Identified
26.940	0.674	BGlcp-1,6OTMS	307704	X g	73.1	Identified
27.299	0.683	BGlcp-1,6OTMS*	153710	X g	146.1	Identified
29.502	0.739	aGlcp-1,4,6OTMS: 3,6-di-O-methyl-1,4,6-t	426741	X g	146.2	Identified

Figure E.3.14: Processed GC-MS data for PB7.

Sample ID:	dextran sigma	Operator:	ER
Instrument ID:	Varian CP-3800	Last Calibration:	None
Acquisition Date:	6/16/2010 9:58 PM	Data File:	...a_1_6-16-2010_er.sms
Calculation Date:	11/10/2010 12:18 PM	Method:	...or 150610_101110.mth
Inj. Sample Notes:	dextran sigma permethylated methanolysis silylated. all solv ents freshly dried. 5uL 0.3 mg/mL sorbitol added before cook .		

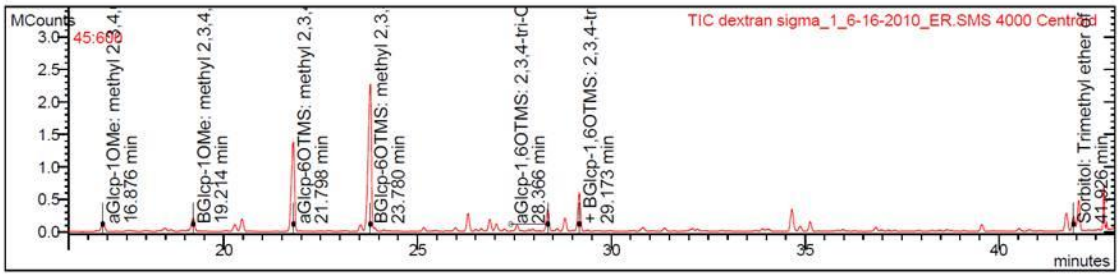

Target Compounds

RT (min)	Peak Name	Quan Ions	Result Type
RRT (min)	Area	Status	
41.926	Sorbitol: Trimethyl ether of glucitol	73.1	Identified
1.000	261469	X STg	
16.876	aGlcp-1OMe: methyl 2,3,4,6-tetra-O	88.1	Identified
0.403	243451	X g	
19.214	BGlcp-1OMe: methyl 2,3,4,6-tetra-O-methy	88.1	Identified
0.458	340373	X g	
21.798	aGlcp-6OTMS: methyl 2,3,4-tri-O-methyl-6	88.1	Identified
0.520	1736150	X g	
23.780	BGlcp-6OTMS: methyl 2,3,4-tri-O-methyl-6	88.1	Identified
0.567	2899923	X g	
28.366	aGlcp-1,6OTMS: 2,3,4-tri-O-methyl-1,6-bi	146.1	Identified
0.677	298193	X g	
28.805	BGlcL-1,6OTMS	159.3	Identified
0.687	70732	X g	
29.173	BGlcp-1,6OTMS: 2,3,4-tri-O-methyl-1,6-bi	146.1	Identified
0.696	474150	X g	
32.437	BGlcp-1,4,6OTMS: 3,6-di-O-methyl-1,4,6-t	146.2	Failed
0.774	4639	X Zg	

Status and Errors:

X : Error
S : Internal Standard Peak.
T : Relative Retention Time Peak.
Z : Ion Ratio failed. Check Qualifier parameters.
g : No Calibration Data. Reporting Peak Size.

Figure E.3.15: Processed GC-MS data for dextran.

Sample ID:	D(+)-galactose	Operator:	ER
Instrument ID:	Varian CP-3800	Last Calibration:	None
Acquisition Date:	6/17/2010 12:33 AM	Data File:	...e_1_6-17-2010_er.sms
Calculation Date:	11/10/2010 12:20 PM	Method:	...or 150610_101110.mth
Inj. Sample Notes:	D(+)-galactose permethylated methanolysis silylated. all sol vents freshly dried. 5uL 0.3 mg/mL sorbitol added before coo k.		

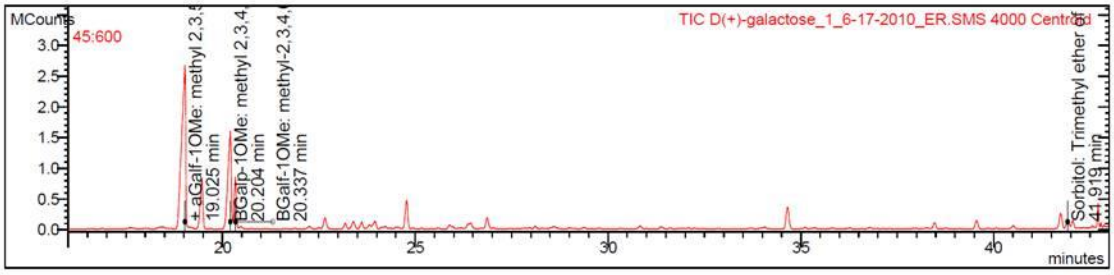

Target Compounds

RT (min)	Peak Name	Quan Ions	Result Type
RRT (min)	Area	Status	
41.919	Sorbitol: Trimethyl ether of glucitol	73.1	Identified
1.000	169513	X STg	
19.025	aGalf-1OMe: methyl 2,3,5,6-tetra-O-methy	101.1	Identified
0.454	5253244	X g	
19.464	aGalp-1OMe: methyl 2,3,4,6-tetra-O-methy	88.1	Identified
0.464	1226941	X g	
20.204	BGalp-1OMe: methyl 2,3,4,6-tetra-O-methy	88.1	Identified
0.482	2846509	X g	
20.337	BGalf-1OMe: methyl-2,3,4,6-tetra-O-methy	101.1	Identified
0.485	926119	X g	

Status and Errors:
X : Error
S : Internal Standard Peak.
T : Relative Retention Time Peak.
g : No Calibration Data. Reporting Peak Size.

Figure E.3.16: Processed GC-MS data for galactose.

Sample ID:	D(+)-mannose	Operator:	ER
Instrument ID:	Varian CP-3800	Last Calibration:	None
Acquisition Date:	6/17/2010 1:24 AM	Data File:	...e_1_6-17-2010_er.sms
Calculation Date:	11/10/2010 12:22 PM	Method:	...or 150610_101110.mth
Inj. Sample Notes:	D(+)-mannose permethylated methanolysis silylated. all solve nts freshly dried. 5uL 0.3 mg/mL sorbitol added before cook.		

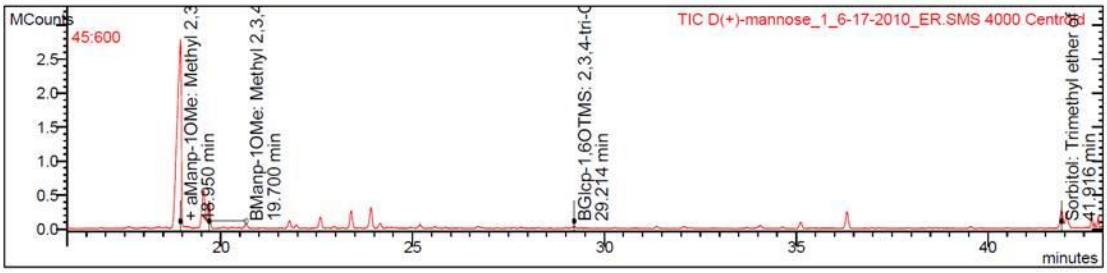

Target Compounds

RT (min)	Peak Name	Quan Ions	Result Type
RRT (min)	Area	Status	
41.916	Sorbitol: Trimethyl ether of glucitol	73.1	Identified
1.000	362847	X STg	
18.950	aManp-1OMe: Methyl 2,3,4,6 tetra-O-methl	88.0	Identified
0.452	6638513	X g	
19.558	aManf-1OMe: Methyl 2,3,4,6-tetra-O-methl	101.2	Identified
0.467	726329	X g	
19.700	BManp-1OMe: Methyl 2,3,4,6-tetra-O-methl	88.1	Identified
0.470	468505	X g	
21.790	aGlcp-6OTMS: methyl 2,3,4-tri-O-methyl-6	88.1	Failed
0.520	14174	X Zg	
29.214	BGlcp-1,6OTMS: 2,3,4-tri-O-methyl-1,6-bi	146.1	Identified
0.697	18147	X g	

Status and Errors:

X : Error
S : Internal Standard Peak.
T : Relative Retention Time Peak.
Z : Ion Ratio failed. Check Qualifier parameters.
g : No Calibration Data. Reporting Peak Size.

Figure E.3.17: Processed GC-MS data for mannose.

Sample ID:	Amylose Potatoe	Operator:	HdC
Instrument ID:	Varian CP-3800	Last Calibration:	None
Acquisition Date:	3/19/2010 6:52 PM	Data File:	..._1_3-19-2010_hdc.sms
Calculation Date:	11/15/2010 3:19 PM	Method:	...cpd tbl 5_091110.mth
Inj. Sample Notes:	Amylose potatoe permethylated, methanolysis, silylation wit h sorbitol internal std		

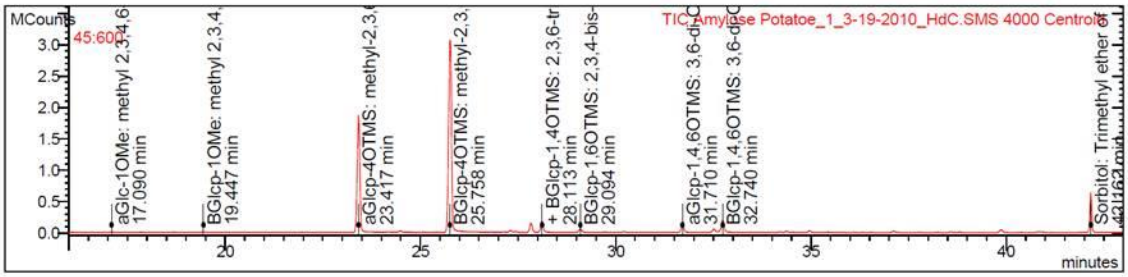

Target Compounds

RT (min)	Peak Name	Quan Ions	Result Type
RRT (min)	Area	Status	
42.162	Sorbitol: Trimethyl ether of glucitol	73.1	Identified
1.000	456119	X STg	
17.090	aGlc-1OMe: methyl 2,3,4,6-tetra-O-	88.1	Identified
0.405	9811	X g	
19.447	BGlcp-1OMe: methyl 2,3,4,6-tetra-O-methy	88.1	Identified
0.461	12766	X g	
23.417	aGlcp-4OTMS: methyl-2,3,6-tri-O-methyl-4	88.0	Identified
0.555	1625191	X g	
25.758	BGlcp-4OTMS: methyl-2,3,6-tri-O-methyl-4	88.0	Identified
0.611	2361369	X g	
27.310	aGlcp-1,6OTMS: 2,3,4-bis-O-methyl-1,6-bi	73.1	Identified
0.648	11077	X g	
27.831	aGlcp-1,4OTMS: 2,3,6-tri-O-methyl-1,4-bi	73.1	Identified
0.660	93232	X g	
28.113	BGlcp-1,4OTMS: 2,3,6-tri-O-methyl-1,4-bi	73.1	Identified
0.667	111342	X g	
29.094	BGlcp-1,6OTMS: 2,3,4-bis-O-methyl-1,6-bi	73.1	Identified
0.690	37886	X g	
31.710	aGlcp-1,4,6OTMS: 3,6-di-O-methyl-1,4,6-t	146.2	Identified
0.752	107001	X g	
32.740	BGlcp-1,4,6OTMS: 3,6-di-O-methyl-1,4,6-t	146.2	Identified
0.777	136776	X g	

Figure E.3.18: Processed GC-MS data for amylose.

Sample ID:	Amylopectin Potato	Operator:	HdC
Instrument ID:	Varian CP-3800	Last Calibration:	None
Acquisition Date:	3/19/2010 6:01 PM	Data File:	..._1_3-19-2010_hdc.sms
Calculation Date:	11/15/2010 3:17 PM	Method:	...cpd tbl 5_091110.mth
Inj. Sample Notes:	Amylopectin from potatoe permethylated, methanolysis, silyl ation with sorbitol internal std		

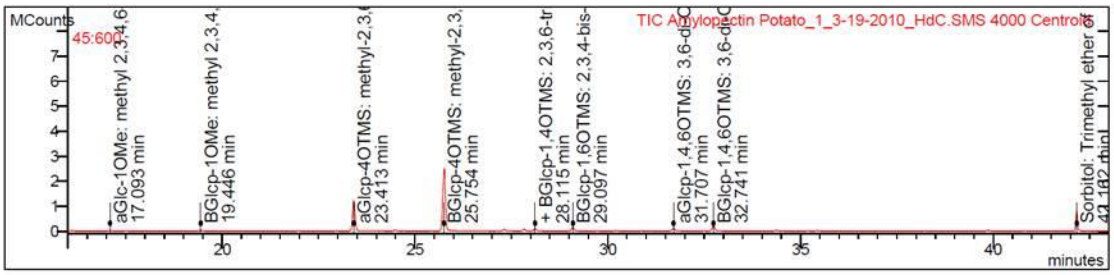

Target Compounds

RT (min)	Peak Name	Quan Ions	Result Type
RRT (min)	Area	Status	
42.162	Sorbitol: Trimethyl ether of glucitol	73.1	Identified
1.000	580343	X STg	
17.093	aGlc-1OMe: methyl 2,3,4,6-tetra-O-	88.1	Identified
0.405	19414	X g	
19.446	BGlcp-1OMe: methyl 2,3,4,6-tetra-O-methy	88.1	Identified
0.461	34663	X g	
23.413	aGlcp-4OTMS: methyl-2,3,6-tri-O-methyl-4	88.0	Identified
0.555	1045203	X g	
25.754	BGlcp-4OTMS: methyl-2,3,6-tri-O-methyl-4	88.0	Identified
0.611	1854405	X g	
27.313	aGlcp-1,6OTMS: 2,3,4-bis-O-methyl-1,6-bi	73.1	Identified
0.648	25226	X g	
27.841	aGlcp-1,4OTMS: 2,3,6-tri-O-methyl-1,4-bi	73.1	Identified
0.660	46294	X g	
28.115	BGlcp-1,4OTMS: 2,3,6-tri-O-methyl-1,4-bi	73.1	Identified
0.667	62092	X g	
29.097	BGlcp-1,6OTMS: 2,3,4-bis-O-methyl-1,6-bi	73.1	Identified
0.690	98647	X g	
31.707	aGlcp-1,4,6OTMS: 3,6-di-O-methyl-1,4,6-t	146.2	Identified
0.752	94698	X g	
32.741	BGlcp-1,4,6OTMS: 3,6-di-O-methyl-1,4,6-t	146.2	Identified
0.777	139816	X g	

Figure E.3.19: Processed GC-MS data for amylopectin.

Sample ID:	cellobiose	Operator:	HdC
Instrument ID:	Varian CP-3800	Last Calibration:	None
Acquisition Date:	7/15/2009 2:09 AM	Data File:	...iose_1_7-15-2009.sms
Calculation Date:	11/9/2010 2:56 PM	Method:	...pd tbl 8 _091110.mth
Inj. Sample Notes:	cellobiose methylation, methanolysis, silylation		

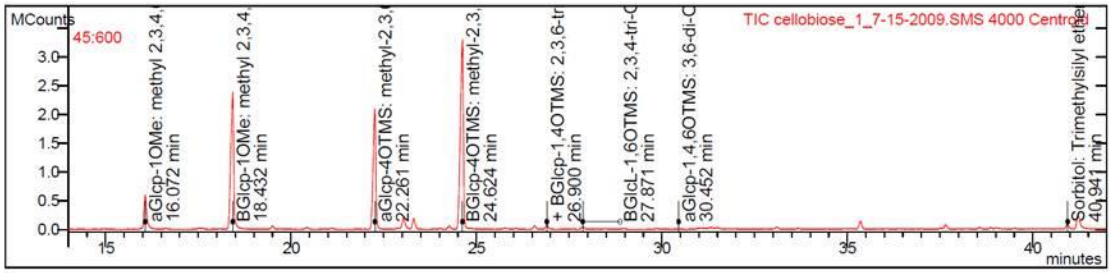

Target Compounds

RT (min)	Peak Name	Quan Ions	Result Type
RRT (min)	Area	Status	
40.941	Sorbitol: Trimethylsilyl ether of glucit	73.0	Identified
1.000	112186	X STg	
16.072	aGlcp-1OMe: methyl 2,3,4,6-tetra-O-methy	88.0	Identified
0.393	940953	X g	
18.072	aManp-1OMe: Methyl 2,3,4,6 tetra-O-methl	88.0	Failed
0.441	9888	X Zg	
18.432	BGlcp-1OMe: methyl 2,3,4,6-tetra-O-methy	88.0	Identified
0.450	3979513	X g	
22.261	aGlcp-4OTMS: methyl-2,3,6-tri-O-methyl-4	88.0	Identified
0.544	2019324	X g	
24.274	BGlcp-3OTMS: methyl 3,4,6-tri-O-methyl-3	146.0	Failed
0.593	32497	X Zg	
24.624	BGlcp-4OTMS: methyl-2,3,6-tri-O-methyl-4	88.0	Identified
0.601	3162716	X g	
26.572	aGlcp-1,4OTMS: 2,3,6-tri-O-methyl-1,4-bi	73.1	Identified
0.649	58049	X g	
26.900	BGlcp-1,4OTMS: 2,3,6-tri-O-methyl-1,4-bi	73.1	Identified
0.657	70566	X g	
27.871	BGlcL-1,6OTMS: 2,3,4-tri-O-methyl-1,6-bi	73.0	Identified
0.681	31488	X g	
30.452	aGlcp-1,4,6OTMS: 3,6-di-O-methyl-1,4,6-t	146.1	Identified
0.744	7896	X g	

Figure E.3.20: Processed GC-MS data for cellobiose.

Sample ID:	galactose	Operator:	HdC
Instrument ID:	Varian CP-3800	Last Calibration:	None
Acquisition Date:	7/15/2009 5:36 AM	Data File:	...tose_1_7-15-2009.sms
Calculation Date:	11/9/2010 2:54 PM	Method:	...pd tbl 8 _091110.mth
Inj. Sample Notes:	galactose methylation, methanolysis, silylation		

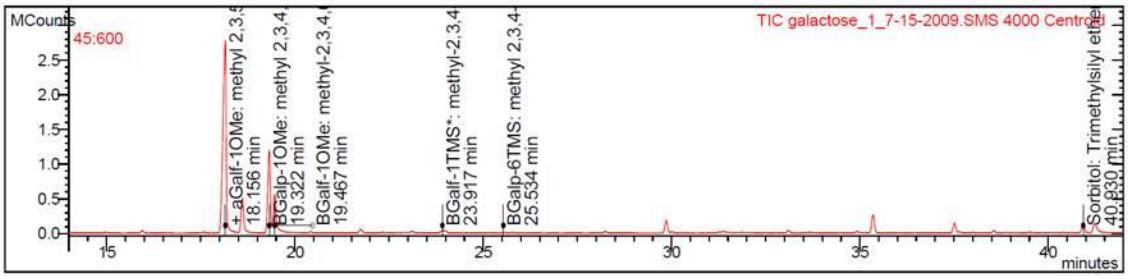

Target Compounds

RT (min)	Peak Name	Quan Ions	Result Type
RRT (min)	Area	Status	
40.930	Sorbitol: Trimethylsilyl ether of glucit	73.0	Identified
1.000	182620	X STg	
18.156	aGalf-1OMe: methyl 2,3,5,6-tetra-O-methy	101.0	Identified
0.444	6445975	X g	
18.606	aGalp-1OMe: methyl 2,3,4,6-tetra-O-methy	88.0	Identified
0.455	696737	X g	
19.322	BGalp-1OMe: methyl 2,3,4,6-tetra-O-methy	88.0	Identified
0.472	1666563	X g	
19.467	BGalf-1OMe: methyl-2,3,4,6-tetra-O-methy	101.0	Identified
0.476	805783	X g	
23.917	BGalf-1TMS*: methyl-2,3,4-tris-O-methyl-	101.1	Identified
0.584	58301	X g	
25.534	BGalp-6TMS: methyl 2,3,4-tri-O-methyl-6-	88.0	Identified
0.624	9094	X g	

Figure E.3.21: Processed GC-MS data for galactose.

Sample ID:	glucose	Operator:	HdC
Instrument ID:	Varian CP-3800	Last Calibration:	None
Acquisition Date:	7/14/2009 6:24 PM	Data File:	...cose_1_7-14-2009.sms
Calculation Date:	11/9/2010 2:58 PM	Method:	...pd tbl 8 _091110.mth
Inj. Sample Notes:	glucose methylation, methanolysis, silylation		

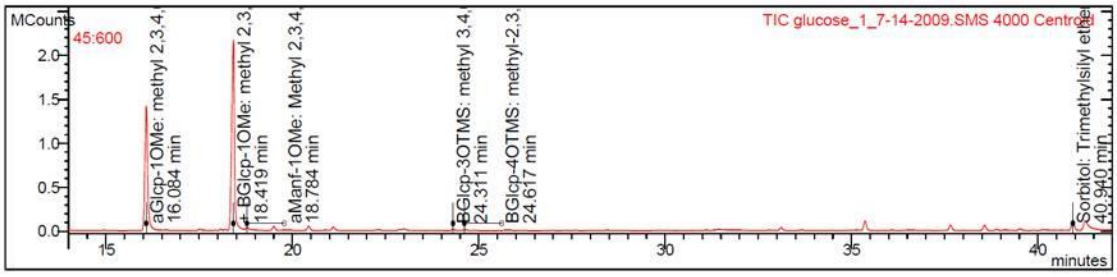

Target Compounds

RT (min)	Peak Name	Quan Ions	Result Type
RRT (min)	Area	Status	
40.940	Sorbitol: Trimethylsilyl ether of glucit	73.0	Identified
1.000	149225	X STg	
16.084	aGlcp-1OMe: methyl 2,3,4,6-tetra-O-methy	88.0	Identified
0.393	2235720	X g	
18.081	aManp-1OMe: Methyl 2,3,4,6 tetra-O-methl	88.0	Identified
0.442	20550	X g	
18.419	BGlcp-1OMe: methyl 2,3,4,6-tetra-O-methy	88.0	Identified
0.450	3419933	X g	
18.784	aManf-1OMe: Methyl 2,3,4,6-tetra-O-methl	101.0	Identified
0.459	26793	X g	
22.882	BGlcp-6OTMS: methyl 2,3,4-tri-O-methyl-6	88.0	Failed
0.559	10139	X Zg	
22.993	aGlcp-3OTMS: methyl 3,4,6-tri-O-methyl-3	146.0	Failed
0.562	3883	X Zg	
24.311	BGlcp-3OTMS: methyl 3,4,6-tri-O-methyl-3	146.0	Identified
0.594	9985	X g	
24.617	BGlcp-4OTMS: methyl-2,3,6-tri-O-methyl-4	88.0	Identified
0.601	8543	X g	

Figure E.3.22: Processed GC-MS data for glucose.

Sample ID:	lichenan	Operator:	HdC
Instrument ID:	Varian CP-3800	Last Calibration:	None
Acquisition Date:	7/15/2009 1:17 AM	Data File:	...enan_1_7-15-2009.sms
Calculation Date:	11/9/2010 3:02 PM	Method:	...pd tbl 8 _091110.mth
Inj. Sample Notes:	lichenan methylation, methanolysis, silylation		

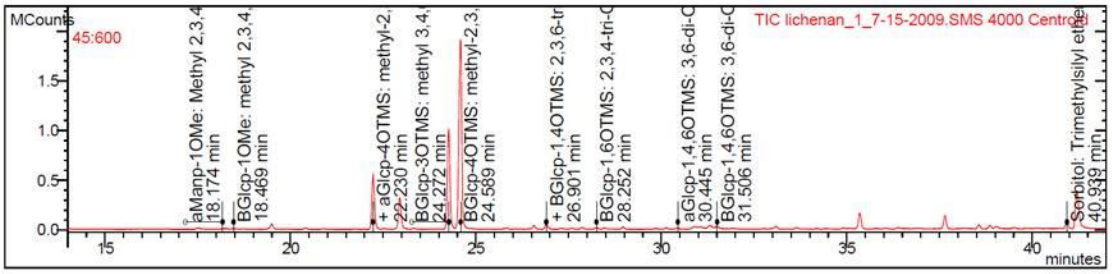

Target Compounds

RT (min)	Peak Name	Quan Ions	Result Type
RRT (min)	Area	Status	
40.939	Sorbitol: Trimethylsilyl ether of glucit	73.0	Identified
1.000	96257	X STg	
18.174	aManp-1OMe: Methyl 2,3,4,6 tetra-O-methl	88.0	Identified
0.444	6971	X g	
18.469	BGlcp-1OMe: methyl 2,3,4,6-tetra-O-methy	88.0	Identified
0.451	9428	X g	
19.407	BGalp-1OMe: methyl 2,3,4,6-tetra-O-methy	88.0	Failed
0.474	6164	X Zg	
22.230	aGlcp-4OTMS: methyl-2,3,6-tri-O-methyl-4	88.0	Identified
0.543	476476	X g	
22.952	aGlcp-3OTMS: methyl 3,4,6-tri-O-methyl-3	146.0	Identified
0.561	255926	X g	
24.272	BGlcp-3OTMS: methyl 3,4,6-tri-O-methyl-3	146.0	Identified
0.593	821624	X g	
24.589	BGlcp-4OTMS: methyl-2,3,6-tri-O-methyl-4	88.0	Identified
0.601	1568055	X g	
26.564	aGlcp-1,4OTMS: 2,3,6-tri-O-methyl-1,4-bi	73.1	Identified
0.649	33383	X g	
26.901	BGlcp-1,4OTMS: 2,3,6-tri-O-methyl-1,4-bi	73.1	Identified
0.657	55394	X g	
28.252	BGlcp-1,6OTMS: 2,3,4-tri-O-methyl-1,6-bi	146.1	Identified
0.690	9992	X g	
30.445	aGlcp-1,4,6OTMS: 3,6-di-O-methyl-1,4,6-t	146.1	Identified
0.744	7531	X g	
31.506	BGlcp-1,4,6OTMS: 3,6-di-O-methyl-1,4,6-t	73.0	Identified
0.770	19285	X g	

Figure E.3.23: Processed GC-MS data for lichenan.

Sample ID:	maltotriose	Operator:	HdC
Instrument ID:	Varian CP-3800	Last Calibration:	None
Acquisition Date:	7/15/2009 3:52 AM	Data File:	...iose_1_7-15-2009.sms
Calculation Date:	11/9/2010 3:05 PM	Method:	...pd tbl 8 _091110.mth
Inj. Sample Notes:	maltotriose methylation, methanolysis, silylation		

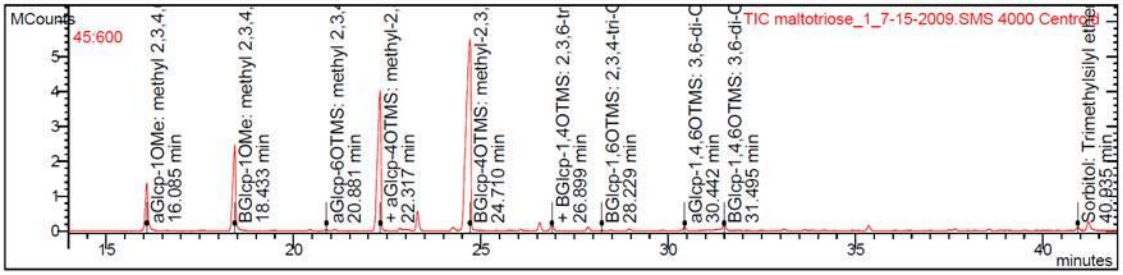

Target Compounds

RT (min)	Peak Name	Quan Ions	Result Type
RRT (min)	Area	Status	
40.935	Sorbitol: Trimethylsilyl ether of glucit	73.0	Identified
1.000	137715	X STg	
16.085	aGlcp-1OMe: methyl 2,3,4,6-tetra-O-methy	88.0	Identified
0.393	2191803	X g	
18.087	aManp-1OMe: Methyl 2,3,4,6 tetra-O-methl	88.0	Failed
0.442	2865	X Zg	
18.433	BGlcp-1OMe: methyl 2,3,4,6-tetra-O-methy	88.0	Identified
0.450	4243823	X g	
19.385	BGalp-1OMe: methyl 2,3,4,6-tetra-O-methy	88.0	Failed
0.474	9178	X Zg	
20.881	aGlcp-6OTMS: methyl 2,3,4-tri-O-methyl-6	88.0	Identified
0.510	28871	X g	
22.317	aGlcp-4OTMS: methyl-2,3,6-tri-O-methyl-4	88.0	Identified
0.545	5330482	X g	
22.967	aGlcp-3OTMS: methyl 3,4,6-tri-O-methyl-3	146.0	Identified
0.561	16170	X g	
24.287	BGlcp-3OTMS: methyl 3,4,6-tri-O-methyl-3	146.0	Failed
0.593	33161	X Zg	
24.710	BGlcp-4OTMS: methyl-2,3,6-tri-O-methyl-4	88.0	Identified
0.604	9036351	X g	
26.572	aGlcp-1,4OTMS: 2,3,6-tri-O-methyl-1,4-bi	73.1	Identified
0.649	207420	X g	
26.899	BGlcp-1,4OTMS: 2,3,6-tri-O-methyl-1,4-bi	73.1	Identified
0.657	224021	X g	
27.866	BGlcL-1,6OTMS: 2,3,4-tri-O-methyl-1,6-bi	73.0	Identified
0.681	85320	X g	
28.229	BGlcp-1,6OTMS: 2,3,4-tri-O-methyl-1,6-bi	146.1	Identified
0.690	1622	X g	
30.442	aGlcp-1,4,6OTMS: 3,6-di-O-methyl-1,4,6-t	146.1	Identified
0.744	98274	X g	
31.495	BGlcp-1,4,6OTMS: 3,6-di-O-methyl-1,4,6-t	73.0	Identified
0.769	190323	X g	

Figure E.3.24: Processed GC-MS data for maltotriose.

Sample ID:	D-(+)-mannose	Operator:	HdC
Instrument ID:	Varian CP-3800	Last Calibration:	None
Acquisition Date:	7/15/2009 4:44 AM	Data File:	...nose_1_7-15-2009.sms
Calculation Date:	11/9/2010 3:33 PM	Method:	...pd tbl 8 _091110.mth
Inj. Sample Notes:	D-(+)-mannose methylation, methanolysis, silylation		

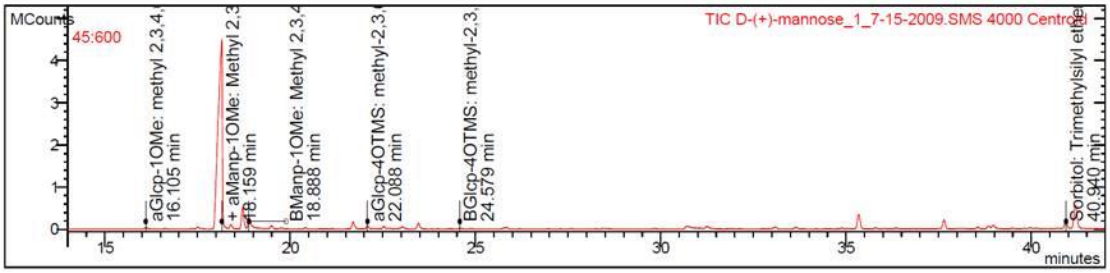

Target Compounds

RT (min)	Peak Name	Quan Ions	Result Type
RRT (min)	Area	Status	
40.940	Sorbitol: Trimethylsilyl ether of glucit	73.0	Identified
1.000	209744	X STg	
16.105	aGlcp-1OMe: methyl 2,3,4,6-tetra-O-methy	88.0	Identified
0.393	57742	X g	
18.159	aManp-1OMe: Methyl 2,3,4,6 tetra-O-methl	88.0	Identified
0.444	10969955	X g	
18.721	aManf-1OMe: Methyl 2,3,4,6-tetra-O-methl	101.0	Identified
0.457	637795	X g	
18.888	BManp-1OMe: Methyl 2,3,4,6-tetra-O-methl	88.0	Identified
0.461	362148	X g	
22.088	aGlcp-4OTMS: methyl-2,3,6-tri-O-methyl-4	88.0	Identified
0.540	55230	X g	
24.276	BGlcp-3OTMS: methyl 3,4,6-tri-O-methyl-3	146.0	Failed
0.593	5048	X Zg	
24.579	BGlcp-4OTMS: methyl-2,3,6-tri-O-methyl-4	88.0	Identified
0.600	13877	X g	

Figure E.3.25: Processed GC-MS data for mannose.

Sample ID:	melibiose	Operator:	HdC
Instrument ID:	Varian CP-3800	Last Calibration:	None
Acquisition Date:	7/14/2009 8:59 PM	Data File:	...iose_1_7-14-2009.sms
Calculation Date:	11/9/2010 3:07 PM	Method:	...pd tbl 8 _091110.mth
Inj. Sample Notes:	melibiose methylation, methanolysis, silylation		

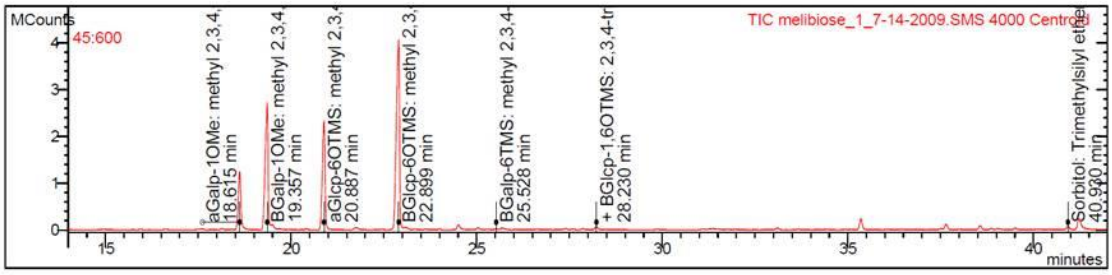

Target Compounds

RT (min)	Peak Name	Quan Ions	Result Type
RRT (min)	Area	Status	
40.930	Sorbitol: Trimethylsilyl ether of glucit	73.0	Identified
1.000	96592	X STg	
18.127	aManp-1OMe: Methyl 2,3,4,6 tetra-O-methl	88.0	Failed
0.443	4396	X Zg	
18.127	aGalf-1OMe: methyl 2,3,5,6-tetra-O-methy	101.0	Failed
0.443	44802	X Zg	
18.615	aGalp-1OMe: methyl 2,3,4,6-tetra-O-methy	88.0	Identified
0.455	1929452	X g	
19.357	BGalp-1OMe: methyl 2,3,4,6-tetra-O-methy	88.0	Identified
0.473	4390285	X g	
20.887	aGlcp-6OTMS: methyl 2,3,4-tri-O-methyl-6	88.0	Identified
0.510	2540686	X g	
22.899	BGlcp-6OTMS: methyl 2,3,4-tri-O-methyl-6	88.0	Identified
0.559	5422658	X g	
25.036	aGalp-6TMS: methyl 2,3,4-tri-O-methyl-6-	88.0	Failed
0.612	26746	X Zg	
25.528	BGalp-6TMS: methyl 2,3,4-tri-O-methyl-6-	88.0	Identified
0.624	12117	X g	
27.396	aGlcp-1,6OTMS: 2,3,4-tri-O-methyl-1,6-bi	146.1	Identified
0.669	22699	X g	
28.230	BGlcp-1,6OTMS: 2,3,4-tri-O-methyl-1,6-bi	146.1	Identified
0.690	47288	X g	

Figure E.3.26: Processed GC-MS data for melibiose.

Sample ID:	panose	Operator:	HdC
Instrument ID:	Varian CP-3800	Last Calibration:	None
Acquisition Date:	7/14/2009 11:34 PM	Data File:	...nose_1_7-14-2009.sms
Calculation Date:	11/9/2010 3:17 PM	Method:	...pd tbl 8 _091110.mth
Inj. Sample Notes:	panose methylation, methanolysis, silylation		

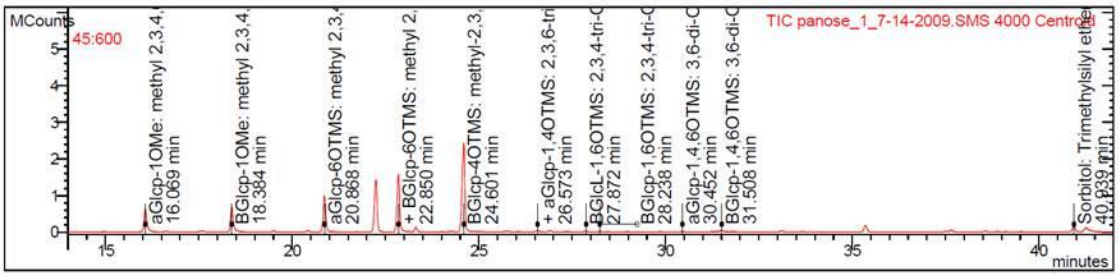

Target Compounds

RT (min)	Peak Name	Quan Ions	Result Type
RRT (min)	Area	Status	
40.939	Sorbitol: Trimethylsilyl ether of glucit	73.0	Identified
1.000	226760	X STg	
16.069	aGlcp-1OMe: methyl 2,3,4,6-tetra-O-methy	88.0	Identified
0.393	1007494	X g	
18.384	BGlcp-1OMe: methyl 2,3,4,6-tetra-O-methy	88.0	Identified
0.449	1024005	X g	
20.868	aGlcp-6OTMS: methyl 2,3,4-tri-O-methyl-6	88.0	Identified
0.510	973591	X g	
22.243	aGlcp-4OTMS: methyl-2,3,6-tri-O-methyl-4	88.0	Identified
0.543	1328493	X g	
22.850	BGlcp-6OTMS: methyl 2,3,4-tri-O-methyl-6	88.0	Identified
0.558	1601343	X g	
24.276	BGlcp-3OTMS: methyl 3,4,6-tri-O-methyl-3	146.0	Failed
0.593	10828	X Zg	
24.601	BGlcp-4OTMS: methyl-2,3,6-tri-O-methyl-4	88.0	Identified
0.601	2078593	X g	
26.573	aGlcp-1,4OTMS: 2,3,6-tri-O-methyl-1,4-bi	73.1	Identified
0.649	38582	X g	
26.904	BGlcp-1,4OTMS: 2,3,6-tri-O-methyl-1,4-bi	73.1	Identified
0.657	36625	X g	
27.872	BGlcL-1,6OTMS: 2,3,4-tri-O-methyl-1,6-bi	73.0	Identified
0.681	19789	X g	
27.403	aGlcp-1,6OTMS: 2,3,4-tri-O-methyl-1,6-bi	146.1	Identified
0.669	8319	X g	
28.238	BGlcp-1,6OTMS: 2,3,4-tri-O-methyl-1,6-bi	146.1	Identified
0.690	13797	X g	
30.452	aGlcp-1,4,6OTMS: 3,6-di-O-methyl-1,4,6-t	146.1	Identified
0.744	16888	X g	
31.508	BGlcp-1,4,6OTMS: 3,6-di-O-methyl-1,4,6-t	73.0	Identified
0.770	34591	X g	

Figure E.3.27: Processed GC-MS data for panose.

Sample ID:	Arabinogalactan	Operator:	ER
Instrument ID:	Varian CP-3800	Last Calibration:	None
Acquisition Date:	3/4/2014 9:16 PM	Data File:	...an_1_3-4-2014_er.sms
Calculation Date:	5/2/2016 3:35 PM	Method:	...with water peaks.mth
Inj. Sample Notes:	1MG STRUCTURE ANALYSIS		

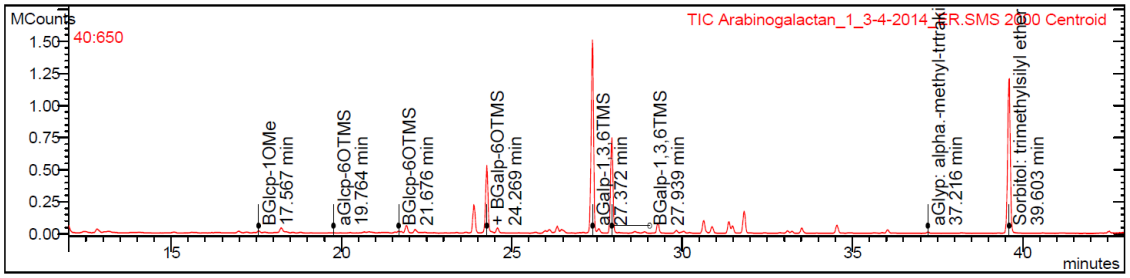

Target Compounds

RT (min)	Peak Name	Area	Status	Quan Ions	Result Type
39.603	Sorbitol: trimethylsilyl ether of glucit	1058536	X Sg	319.2	Identified
17.567	BGlcp-1OMe	11980	X g	88.1	Identified
19.764	aGlcp-6OTMS	2504	X g	88.1	Identified
21.676	BGlcp-6OTMS	7931	X g	88.1	Identified
23.891	aGalp-6OTMS	235266	X g	88.1	Identified
24.269	BGalp-6OTMS	505393	X g	88.1	Identified
27.372	aGalp-1,3,6TMS	1681722	X g	146.2	Identified
27.939	BGalp-1,3,6TMS	910690	X g	146.1	Identified
37.216	aGlyp: alpha.-methyl-trtrakis-O-(trimeth	9675	X g	204.2	Identified

Figure E.3.28: Processed GC-MS data for arabinogalactan.

Sample ID:	stachyose	Operator:	HdC
Instrument ID:	Varian CP-3800	Last Calibration:	None
Acquisition Date:	7/14/2009 8:07 PM	Data File:	...yose_1_7-14-2009.sms
Calculation Date:	11/9/2010 3:19 PM	Method:	...pd tbl 8 _091110.mth
Inj. Sample Notes:	stachyose methylation, methanolysis, silylation		

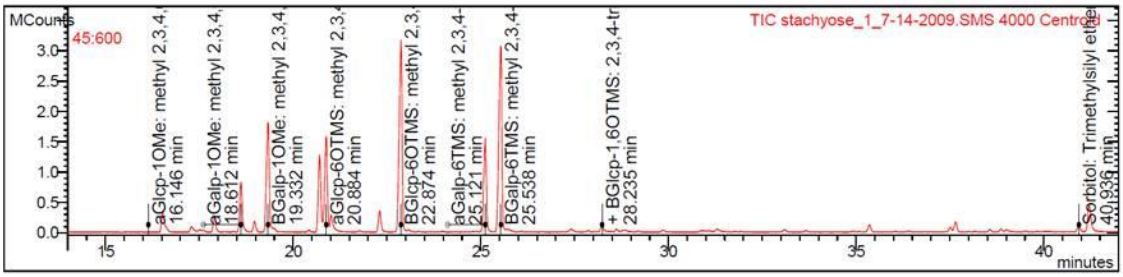

Target Compounds

RT (min)	Peak Name	RRT (min)	Area	Status	Quan Ions	Result Type
40.936	Sorbitol: Trimethylsilyl ether of glucit	1.000	151658	X STg	73.0	Identified
16.146	aGlcp-1OMe: methyl 2,3,4,6-tetra-O-methy	0.394	5460	X g	88.0	Identified
18.612	aGalp-1OMe: methyl 2,3,4,6-tetra-O-methy	0.455	1215402	X g	88.0	Identified
19.332	BGalp-1OMe: methyl 2,3,4,6-tetra-O-methy	0.472	2727669	X g	88.0	Identified
20.884	aGlcp-6OTMS: methyl 2,3,4-tri-O-methyl-6	0.510	1524504	X g	88.0	Identified
22.874	BGlcp-6OTMS: methyl 2,3,4-tri-O-methyl-6	0.559	3599373	X g	88.0	Identified
25.121	aGalp-6TMS: methyl 2,3,4-tri-O-methyl-6-	0.614	1786094	X g	88.0	Identified
25.538	BGalp-6TMS: methyl 2,3,4-tri-O-methyl-6-	0.624	3909646	X g	88.0	Identified
27.401	aGlcp-1,6OTMS: 2,3,4-tri-O-methyl-1,6-bi	0.669	39711	X g	146.1	Identified
28.235	BGlcp-1,6OTMS: 2,3,4-tri-O-methyl-1,6-bi	0.690	87113	X g	146.1	Identified

Figure E.3.29: Processed GC-MS data for stachyose.

Sample ID:	Lactose	Operator:	HdC
Instrument ID:	Varian CP-3800	Last Calibration:	None
Acquisition Date:	9/4/2009 7:55 PM	Data File:	...ctose_1_9-4-2009.sms
Calculation Date:	5/2/2016 3:29 PM	Method:	...is 040909_091110.mth
Inj. Sample Notes:	lactose methylated, methanolysis, silylated.		

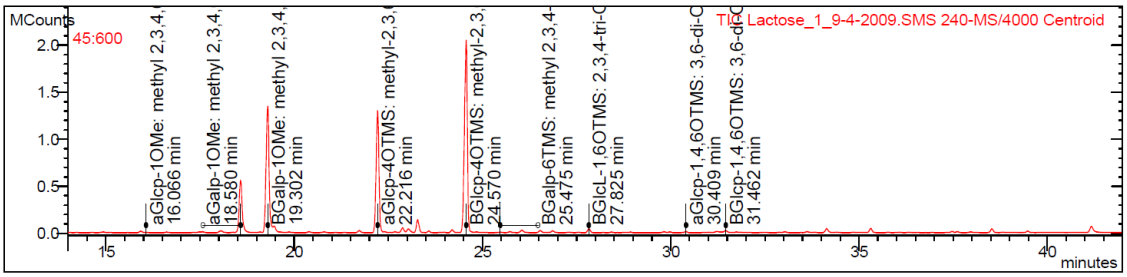

Target Compounds

RT (min)	RRT (min)	Peak Name / Area	Status	Quan Ions	Result Type
16.066	0.392	aGlcp-1OMe: methyl 2,3,4,6-tetra-O-methy 4174	X gj	88.0	Identified
18.060	0.441	aManp-1OMe: Methyl 2,3,4,6 tetra-O-methl 3148	X Zgj	88.0	Failed
18.075	0.442	aGalf-1OMe: methyl 2,3,5,6-tetra-O-methy 22922	X Zgj	101.0	Failed
18.580	0.454	aGalp-1OMe: methyl 2,3,4,6-tetra-O-methy 885618	X gj	88.0	Identified
19.302	0.471	BGalp-1OMe: methyl 2,3,4,6-tetra-O-methy 2105267	X gj	88.0	Identified
22.216	0.543	aGlcp-4OTMS: methyl-2,3,6-tri-O-methyl-4 1239655	X gj	88.0	Identified
24.570	0.600	BGlcp-4OTMS: methyl-2,3,6-tri-O-methyl-4 1764640	X gj	88.0	Identified
25.475	0.622	BGalp-6TMS: methyl 2,3,4-tri-O-methyl-6- 5784	X gj	88.0	Identified
27.825	0.680	BGlcL-1,6OTMS: 2,3,4-tri-O-methyl-1,6-bi 32365	X gj	73.0	Identified
30.409	0.743	aGlcp-1,4,6OTMS: 3,6-di-O-methyl-1,4,6-t 9570	X gj	146.1	Identified
31.462	0.769	BGlcp-1,4,6OTMS: 3,6-di-O-methyl-1,4,6-t 16425	X gj	73.0	Identified

Figure E.3.30: Processed GC-MS data for lactose.

Appendix F
Nuclear magnetic resonance spectra

This appendix provides the accompanying 1D and 2D NMR spectra for all the samples analysed as well as information on the impurity peaks identified in both the D_2O and $CDCl_3$ analyses.

F.1 Analysis of native polysaccharides in D_2O

The NMR spectra for underivatised samples of pullulan and the fractionated FB2 F1 and FB2 F2 EPSs are presented below. All spectra recorded in D_2O were referenced to δ_H 4.73 ppm. and all spectra recorded in $CDCl_3$ were referenced to δ_H 7.26 ppm and δ_C 77.36 ppm.

F.1.1 Pullulan

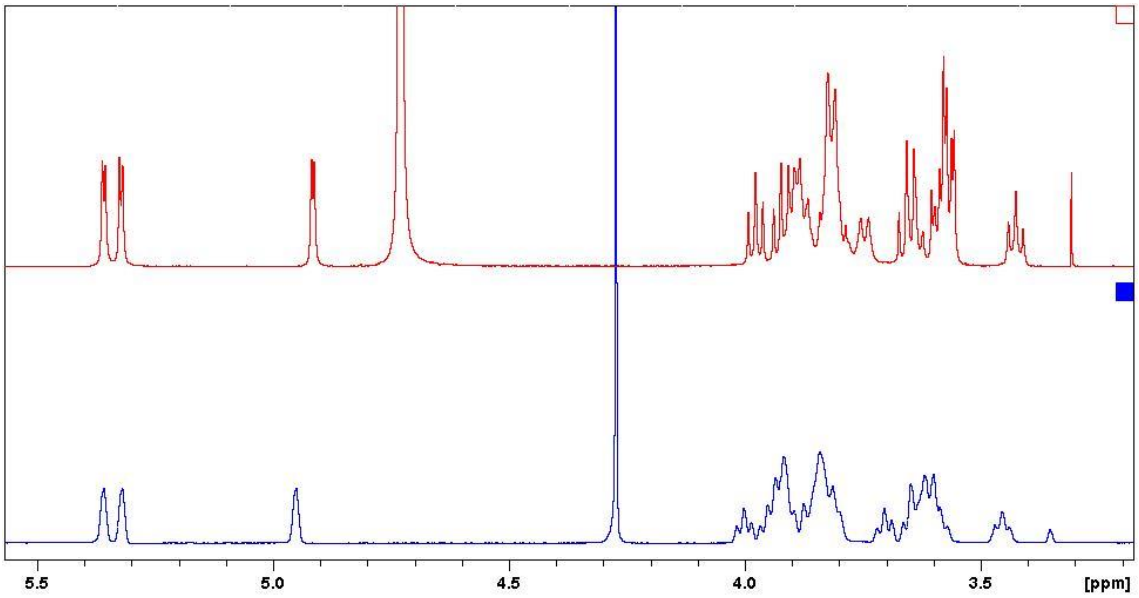

Figure F.1.1: Comparison of the resolution provided by spectra obtained at 600.1 MHz for the proton NMR of pullulan at 25 °C (top) and 70 °C (bottom) in D_2O. The improved resolution of the cooler temperature resulted in all the NMR experiments to be performed at either ambient (400 MHz) or 25 °C (600 MHz) temperatures. The singlet at δ_H 3.31 ppm is due to contamination with methanol (Fulmer *et al.*, 2010).

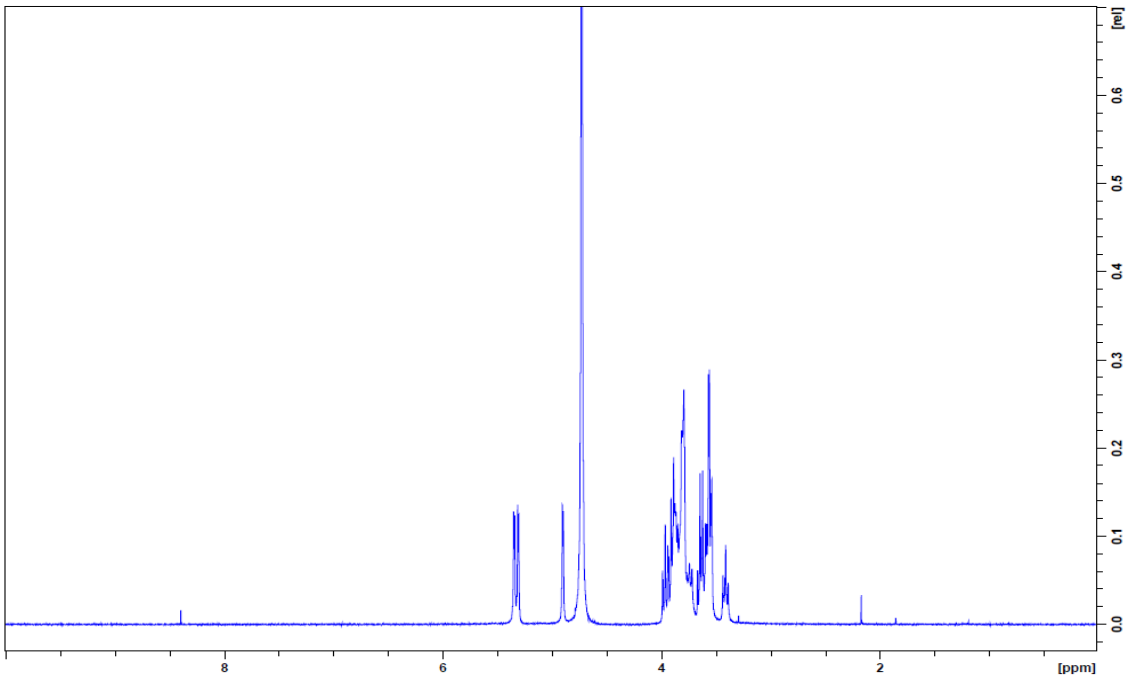

Figure F.1.2: Proton NMR spectrum of pullulan (replicate 1) in D_2O recorded at 400 MHz. Impurities appear as singlets at δ_H 8.40ppm (unknown, 0.024H), 3.31 ppm (methanol, 0.016H), 2.17 ppm (acetone, 0.038H), 1.86 ppm (unknown, 0.008H) and 1.20 ppm (unknown, 0.003H) (Fulmer *et al.,* 2010).

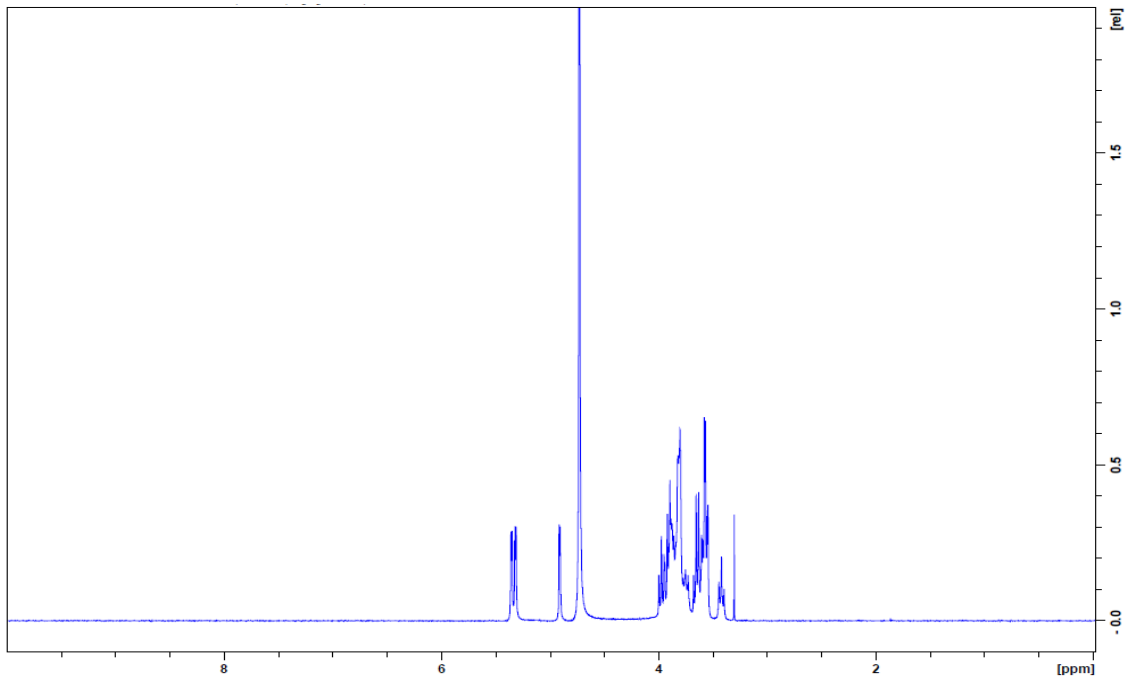

Figure F.1.3: Proton NMR spectrum of pullulan (replicate 2) in D_2O recorded at 400 MHz. Impurities appear as singlets at δ_H 3.31 ppm (methanol, 0.203H) and 1.86 ppm (unknown, 0.002H) (Fulmer *et al.,* 2010).

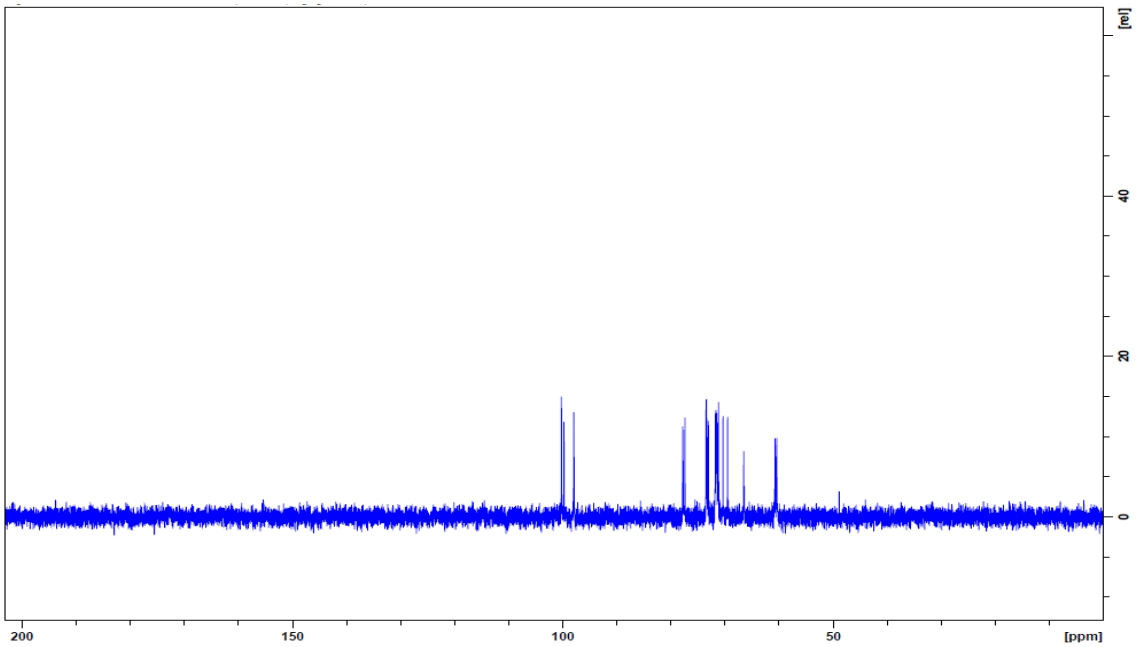

Figure F.1.4: Carbon NMR spectrum of pullulan (replicate 2) recorded in D_2O at 101 MHz. The small peak at δ_C 48.9 ppm is due the methanol contaminant (Fulmer *et al*., 2010).

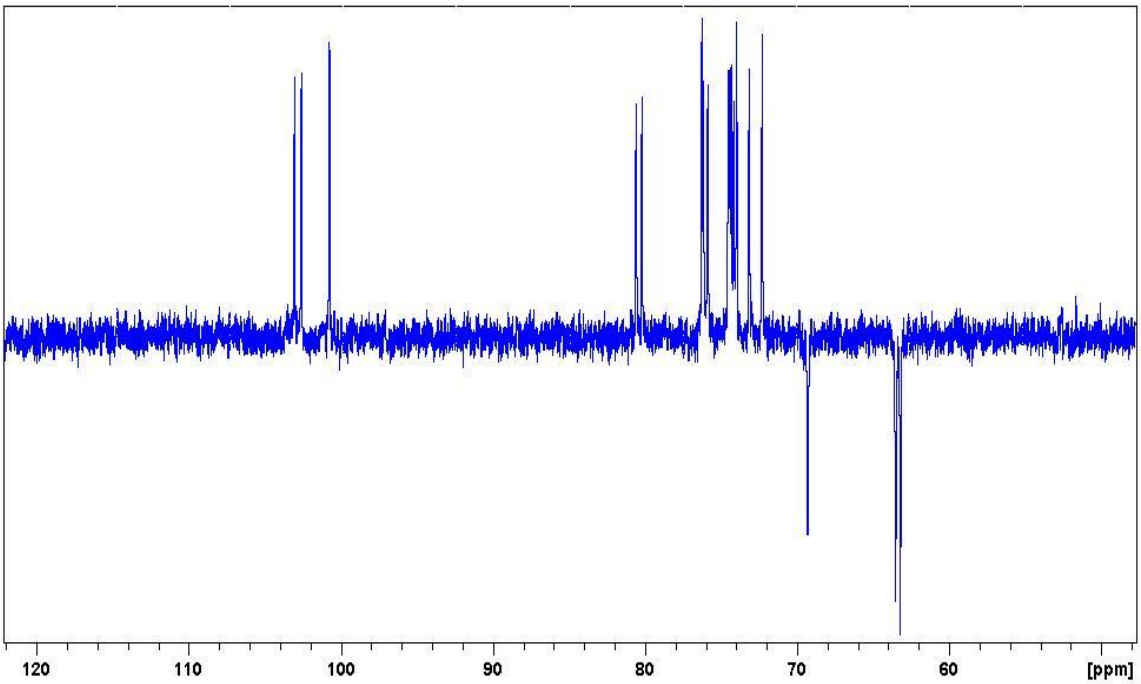

Figure F.1.5: DEPT135 spectrum of pullulan recorded in D_2O at 101 MHz.

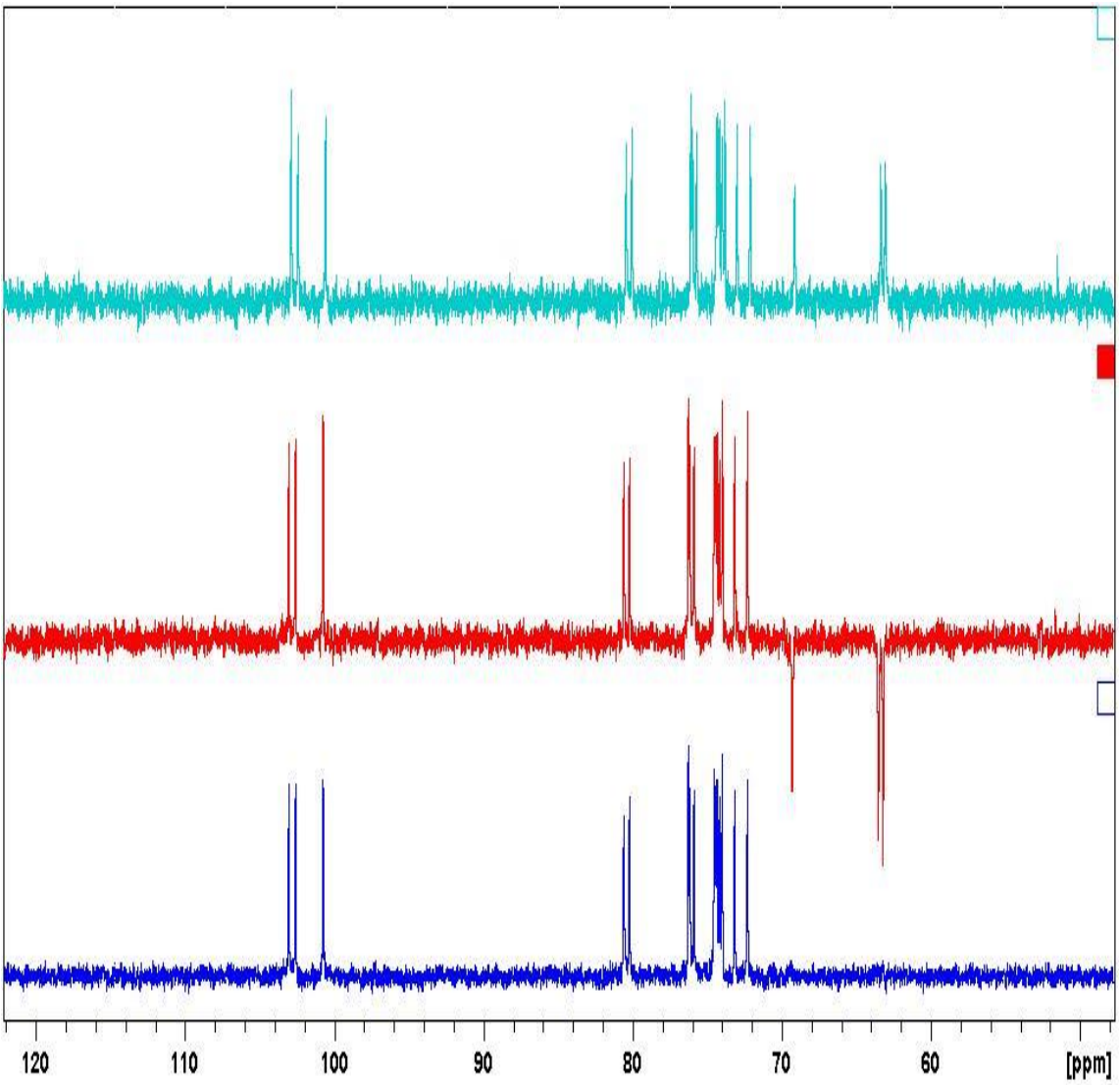

Figure F.1.6: Comparison between the carbon (top), DEPT135 (middle), and DEPT90 (bottom) spectra of pullulan recorded in D_2O at 101 MHz.

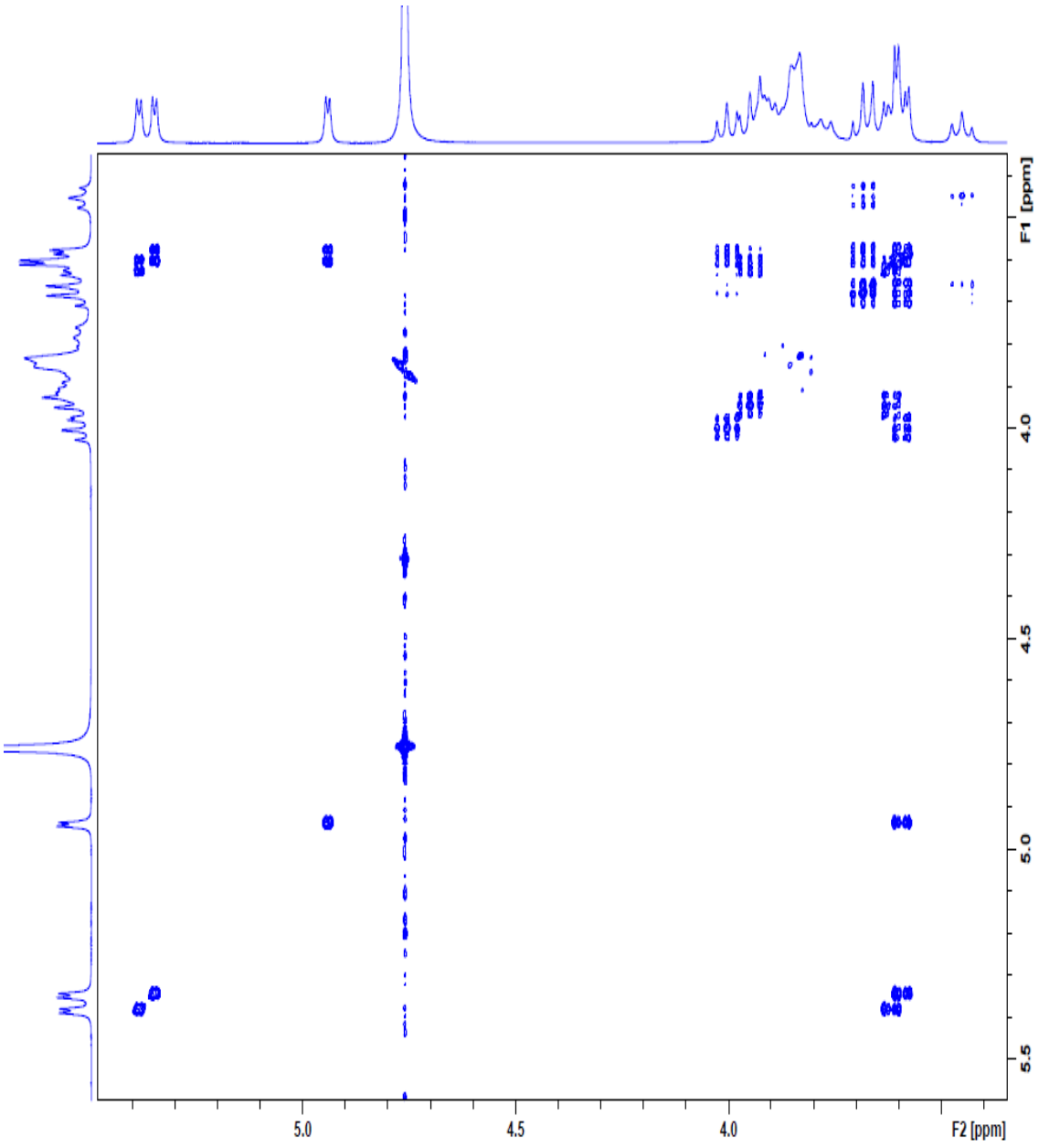

Figure F.1.7: COSY spectrum for pullulan (replicate 2) in D_2O.

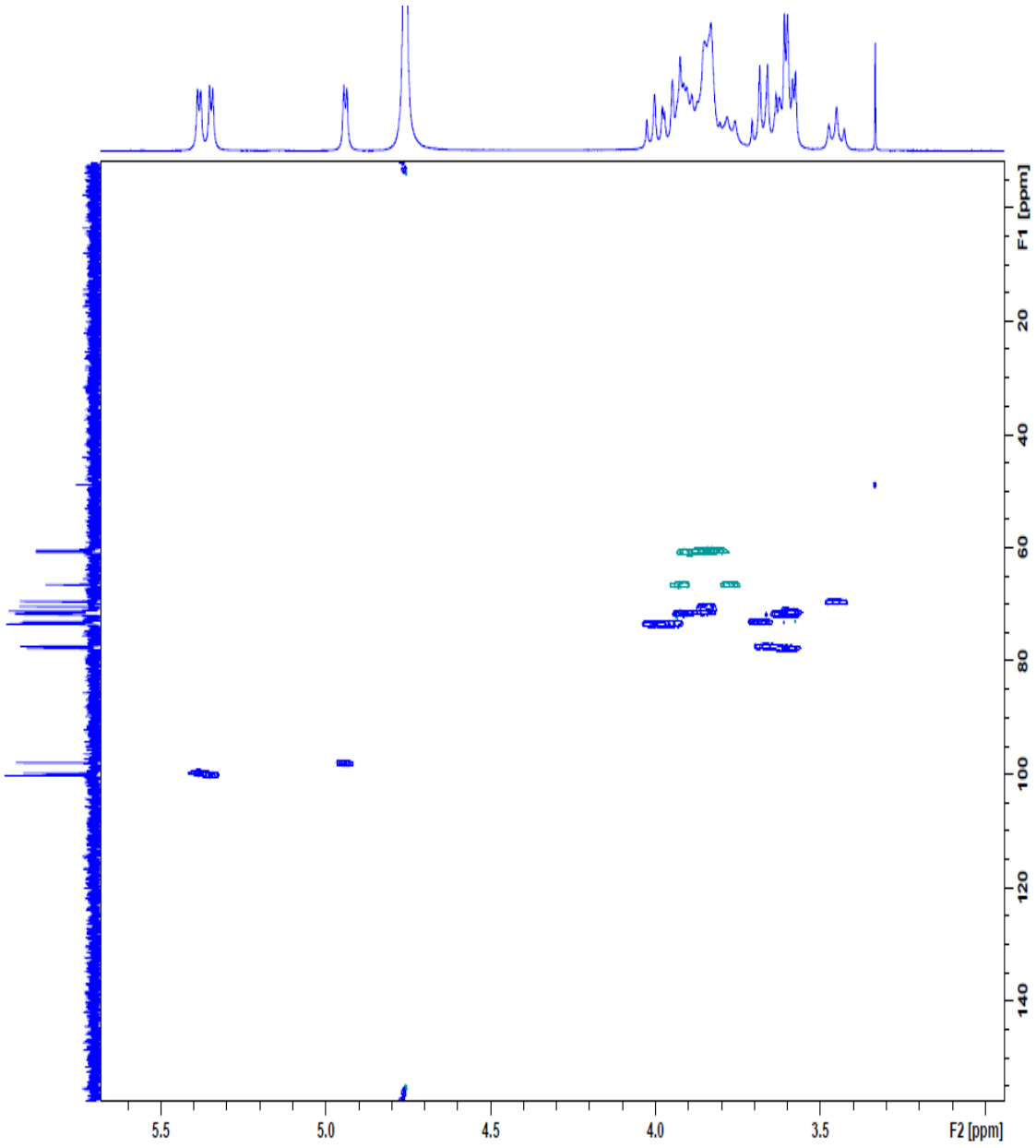

Figure F.1.8: HSQC spectrum for pullulan (replicate 2) in D_2O.

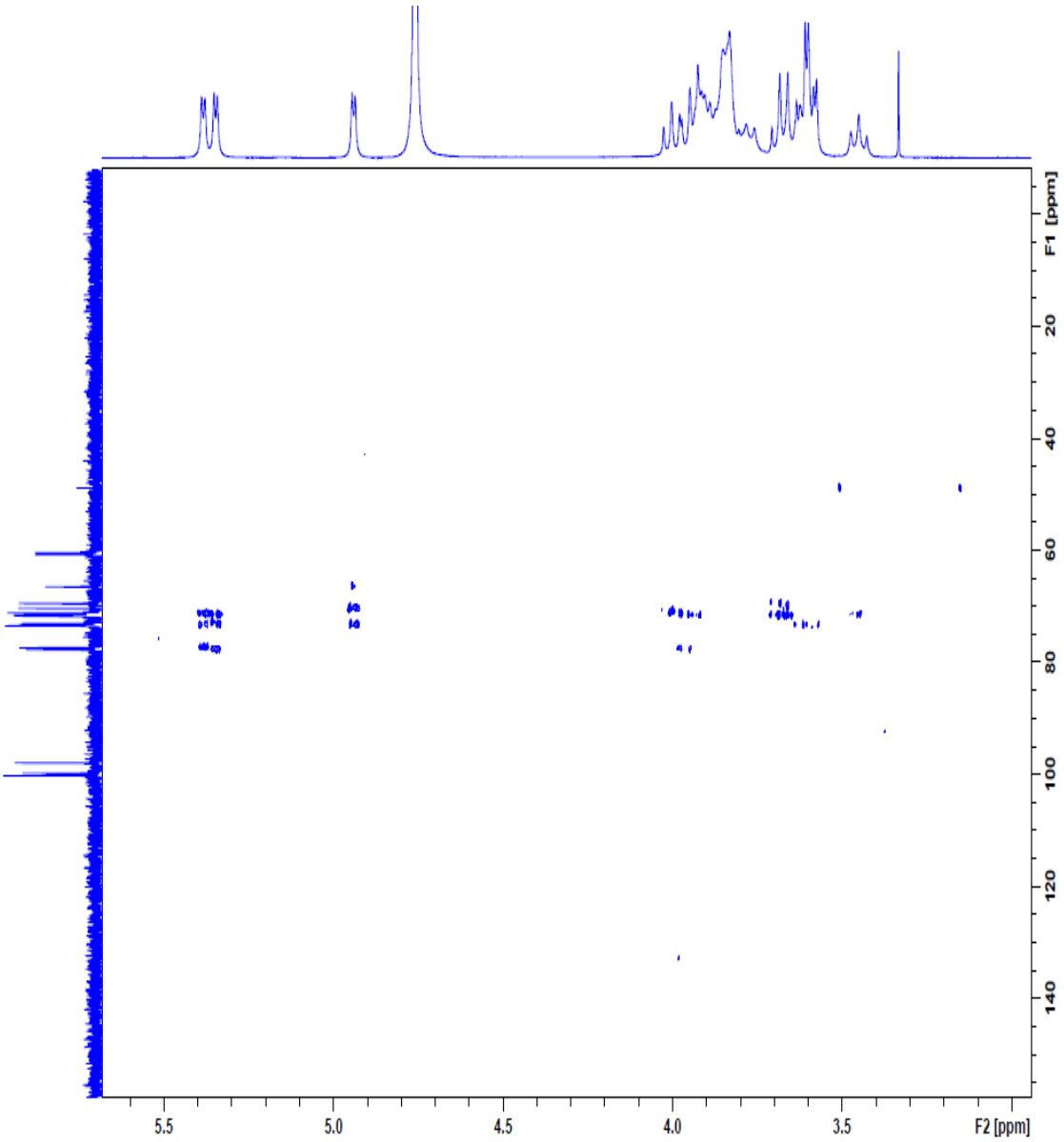

Figure F.1.9: HMBC spectrum for pullulan (replicate 2) in D_2O.

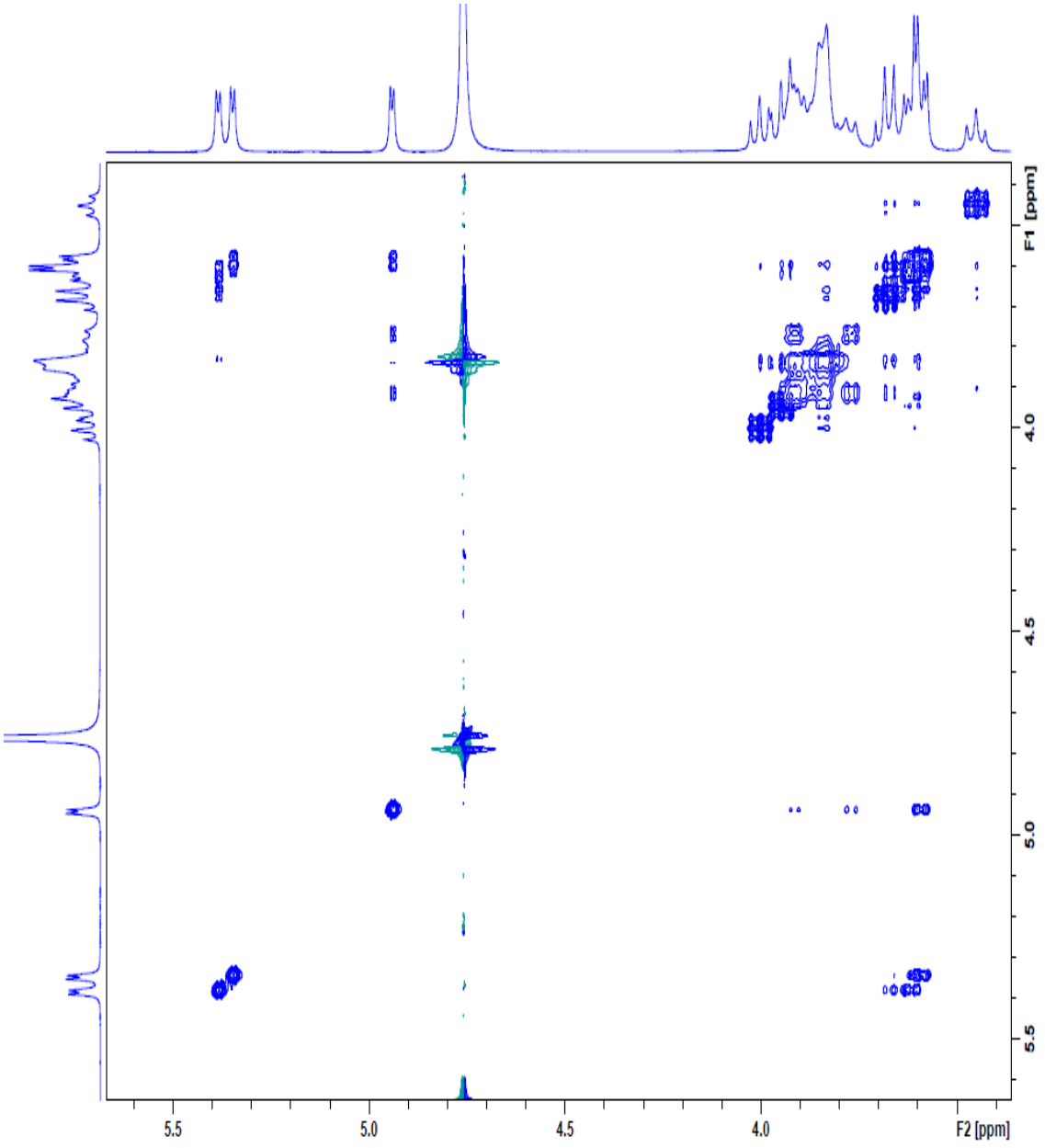

Figure F.1.10: NOESY spectrum for pullulan (replicate 2) in D_2O.

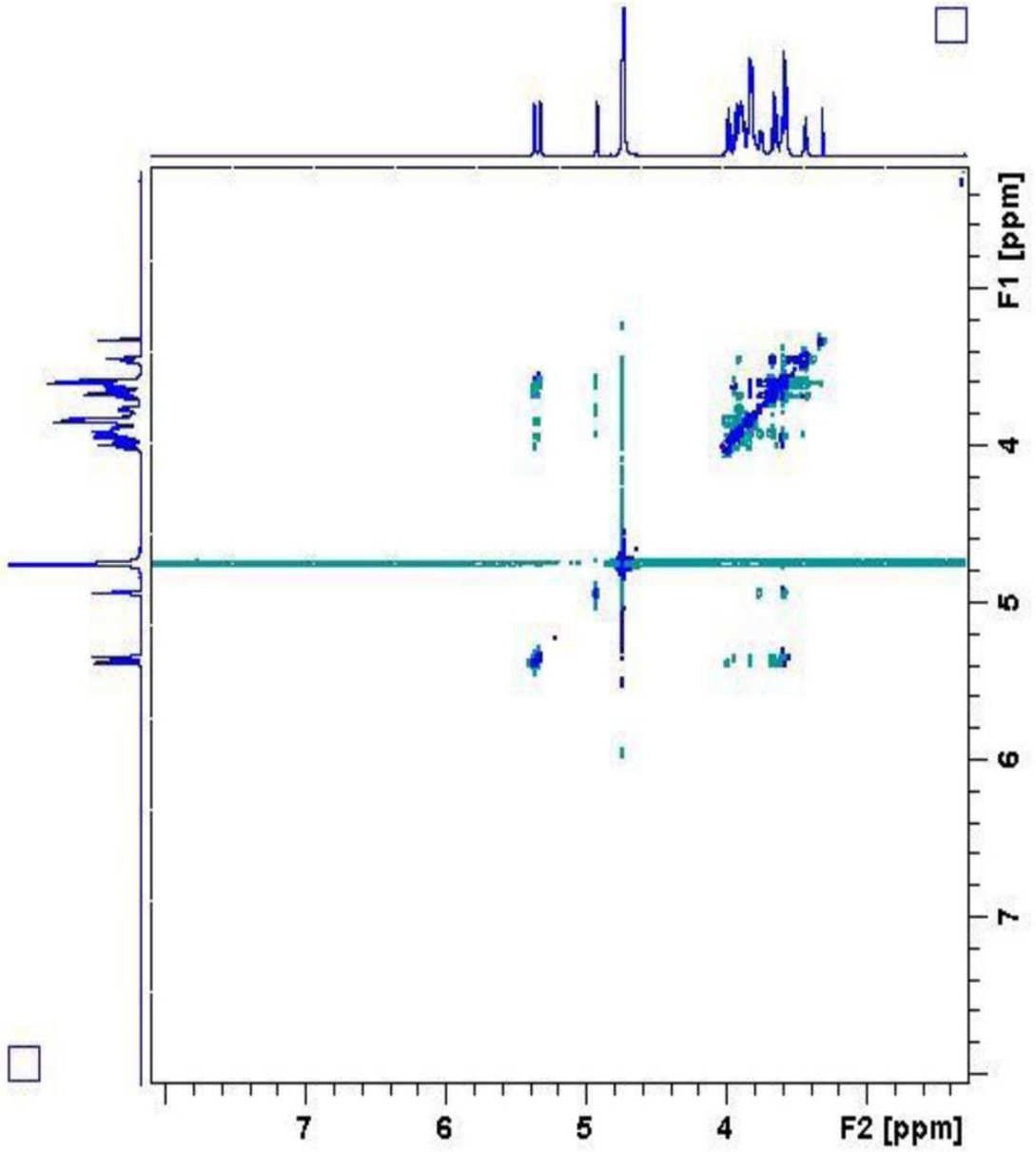

Figure F.1.11: ROESY spectrum for pullulan (replicate 2) in D_2O.

F.1.2 FB2 F1

The NMR spectra for the purified FB2 F1 fraction of the FB2 *P. sacchari* EPS are provided.

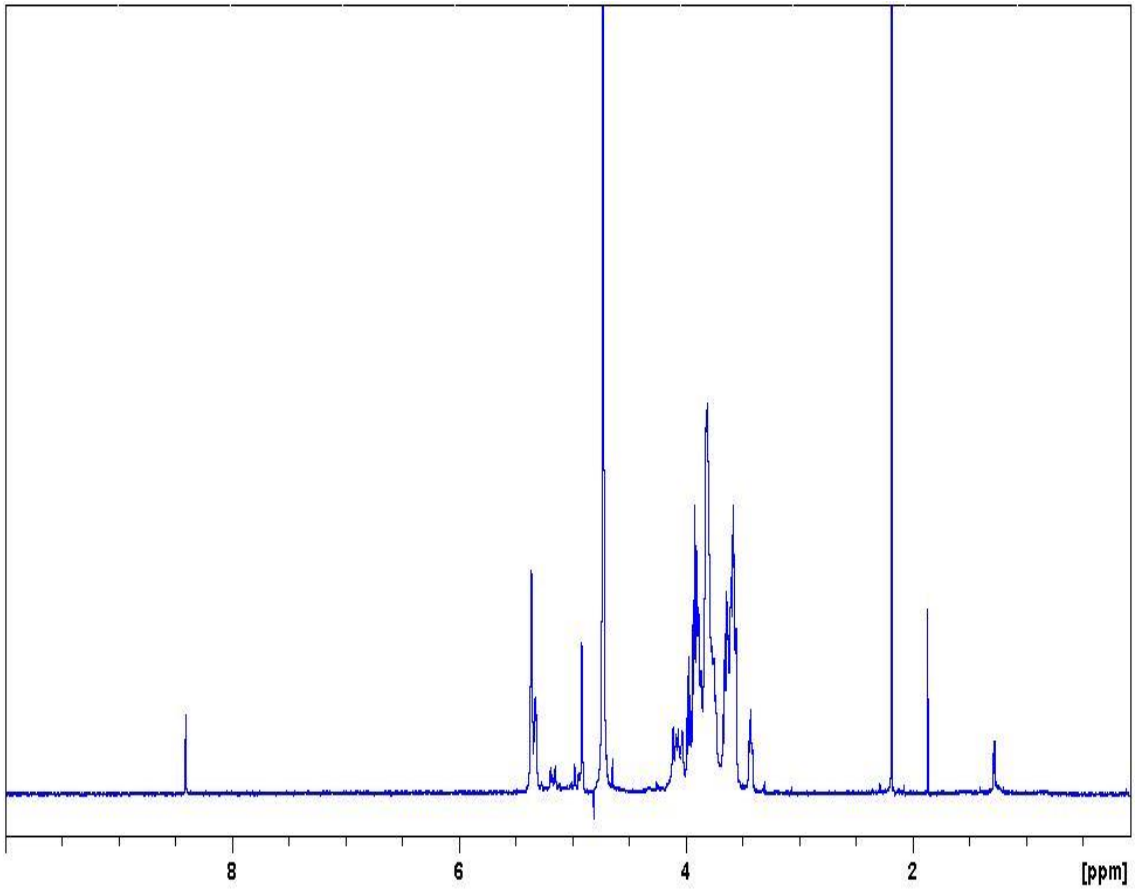

Figure F.1.12: Proton spectrum for FB2 F1 recorded in D_2O at 600 MHz. Impurity peaks were detected at δ_H 8.40 ppm, 3.31 ppm (methanol), 2.17 ppm (acetone), 1.86 ppm (unknown), and 1.20 ppm (unknown) as seen in a similarly prepared pullulan sample (Figure F.1.2) (Fulmer *et al.*, 2010).

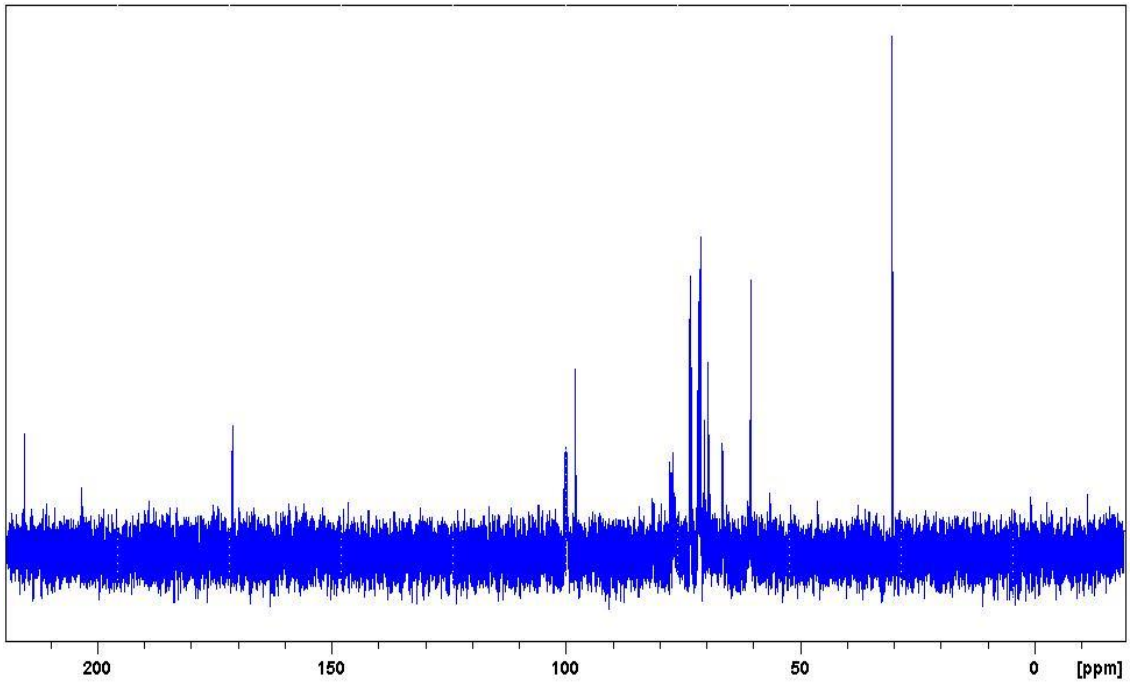

Figure F.1.13: Carbon spectrum for FB2 F1 in D_2O at 151 MHz. Impurity peaks were detected at δ_C 215.5 ppm (CO, acetone), 202.7 ppm, 171.7 ppm and 30.9 ppm (CH_3, acetone) (Fulmer *et al.*, 2010).

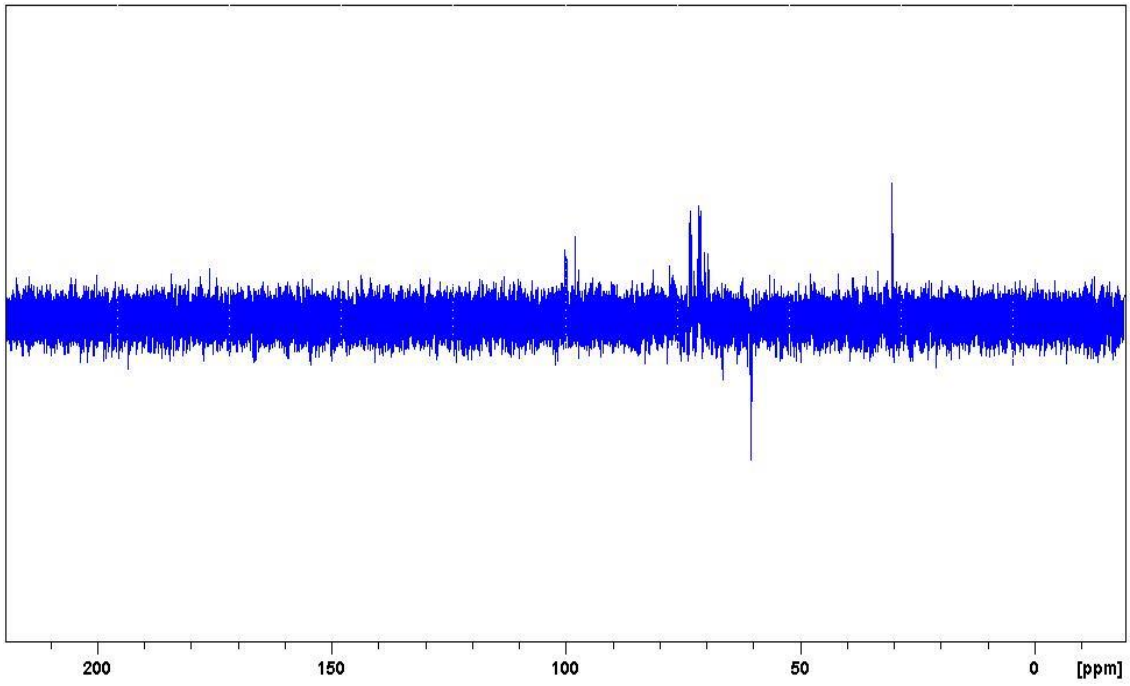

Figure F.1.14: DEPT135 spectrum for FB2 F1 recorded in D_2O at 151 MHz.

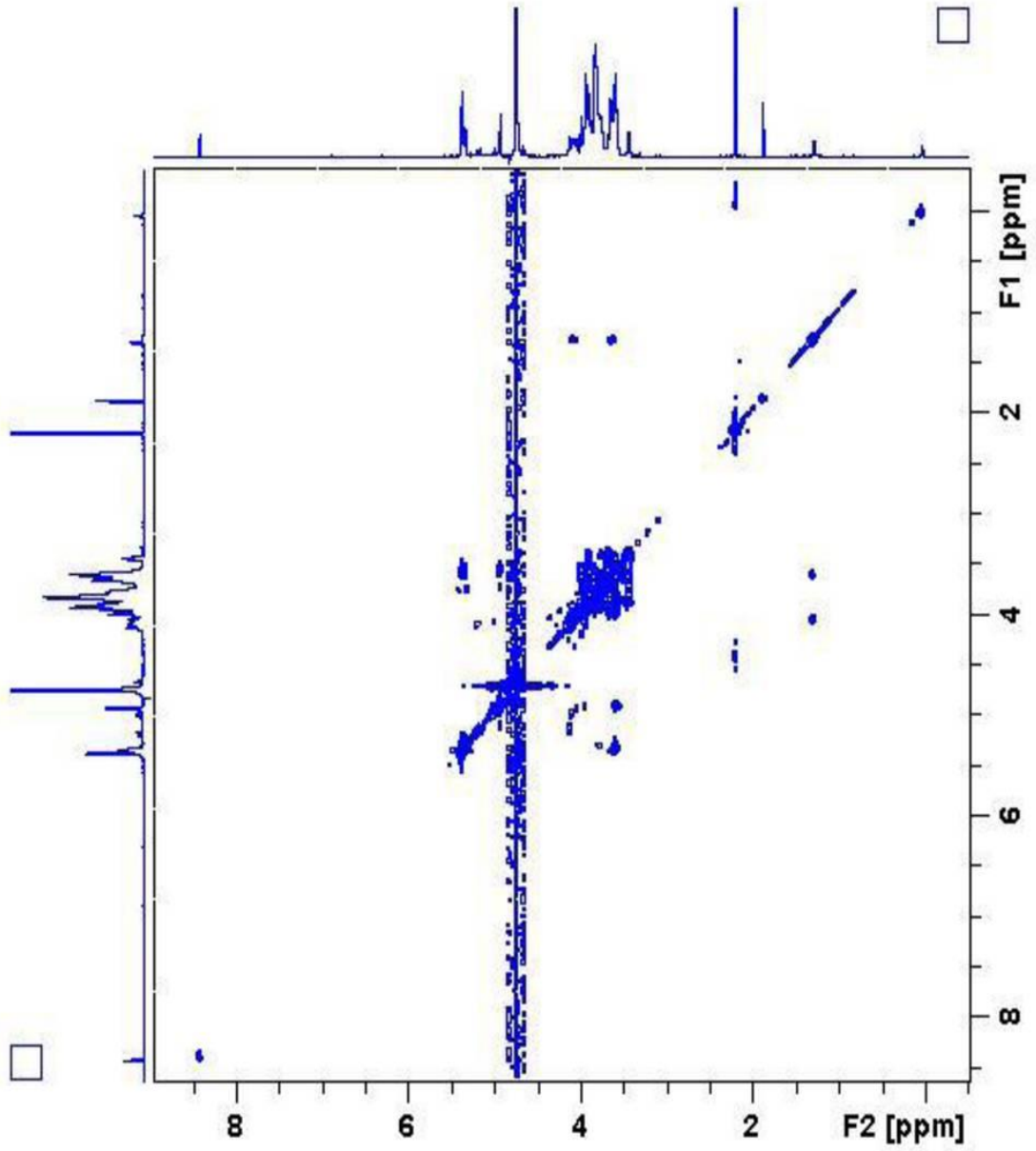

Figure F.1.15: COSY spectrum of FB2 F1 in D_2O.

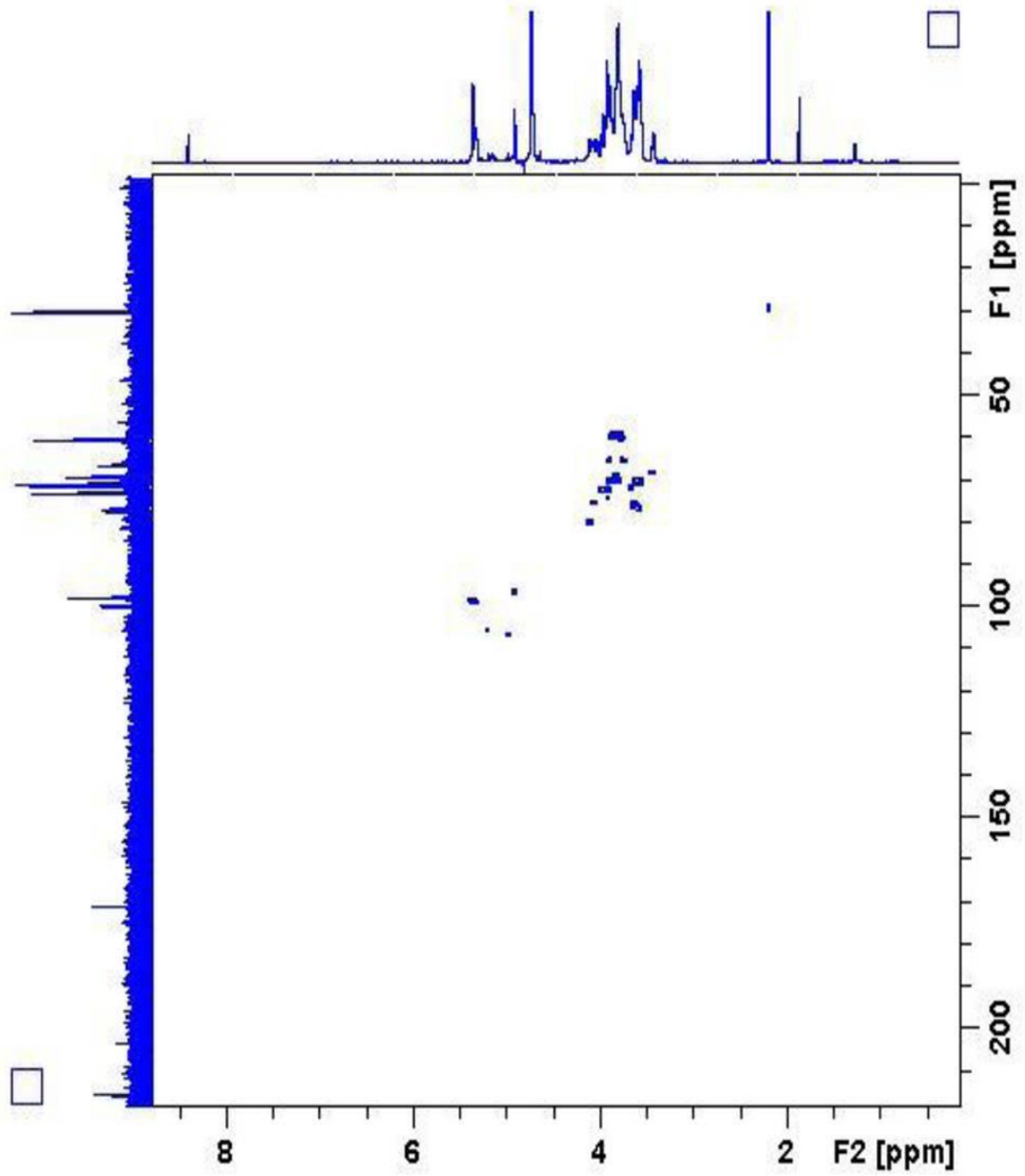

Figure F.1.16: HSQC spectrum of FB2 F1 in D_2O. A correlation is observed for the acetone impurity at δ_H 2.17 ppm and δ_C 30.9 ppm (Fulmer *et al.*, 2010).

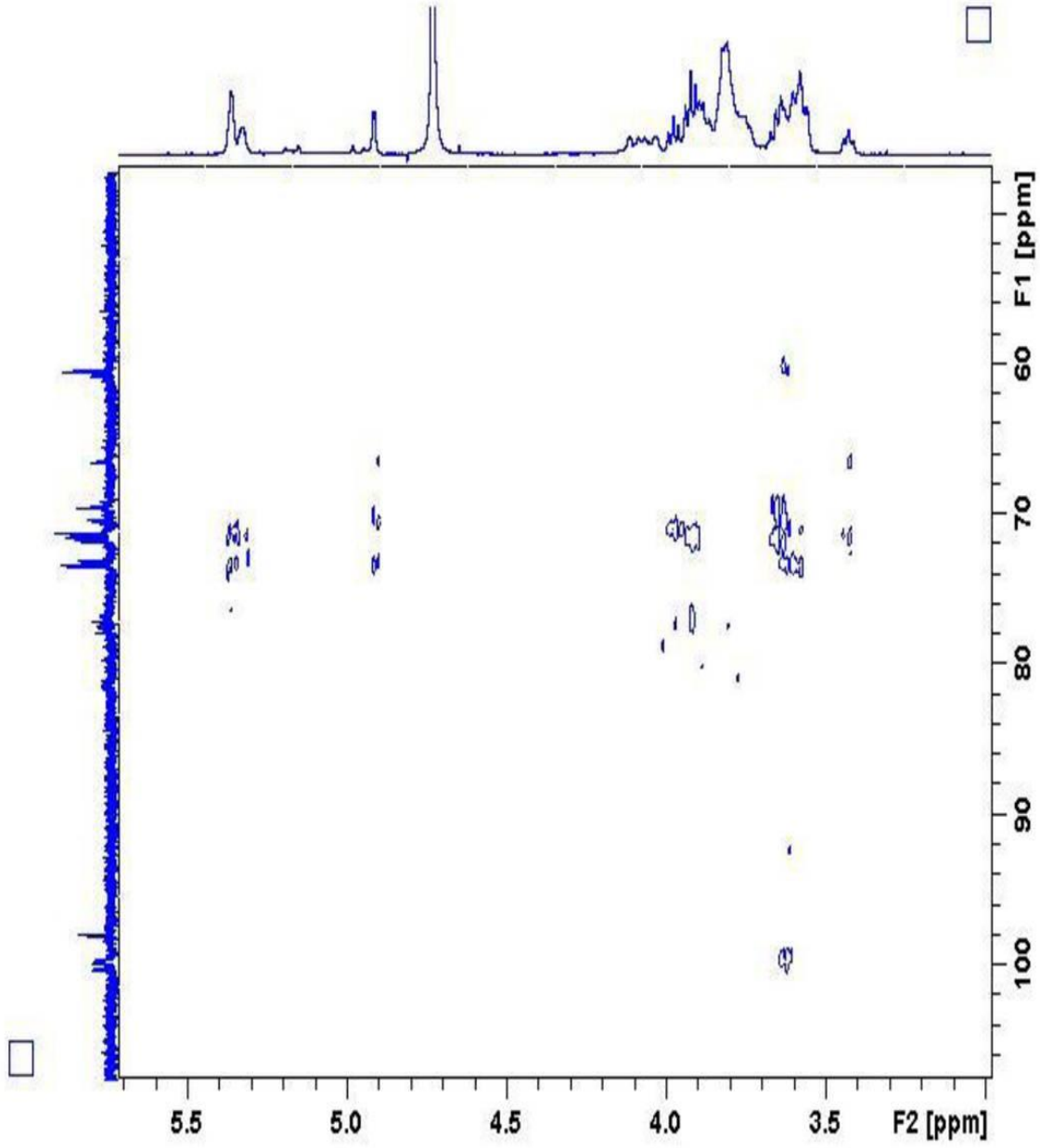

Figure F.1.17: HMBC spectrum of FB2 F1 in D_2O.

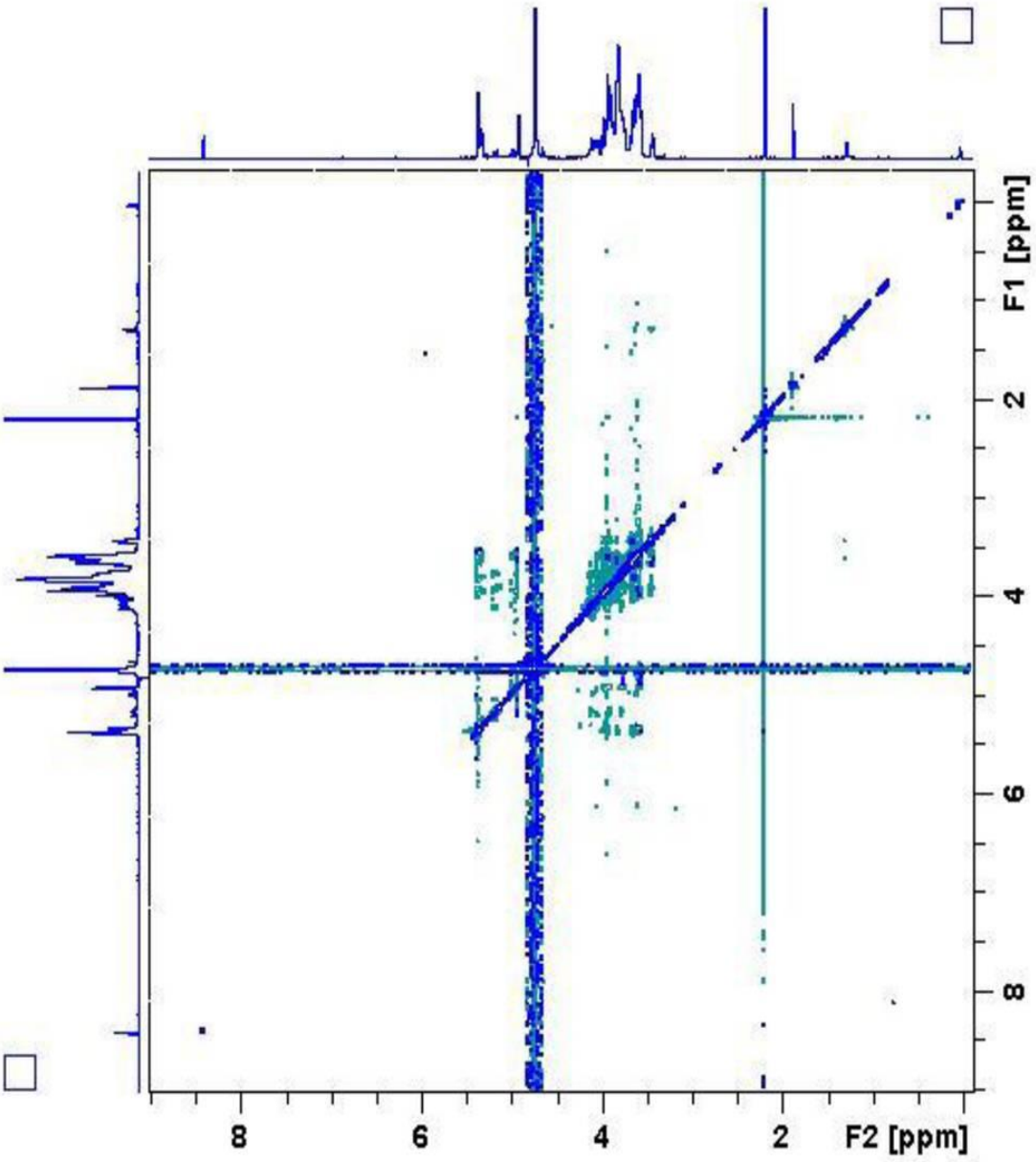

Figure F.1.18: ROESY spectrum of FB2 F1 in D_2O.

F.1.3 FB2 F2

The NMR spectra for the purified FB2 F2 fraction of the FB2 *P. sacchari* EPS are provided.

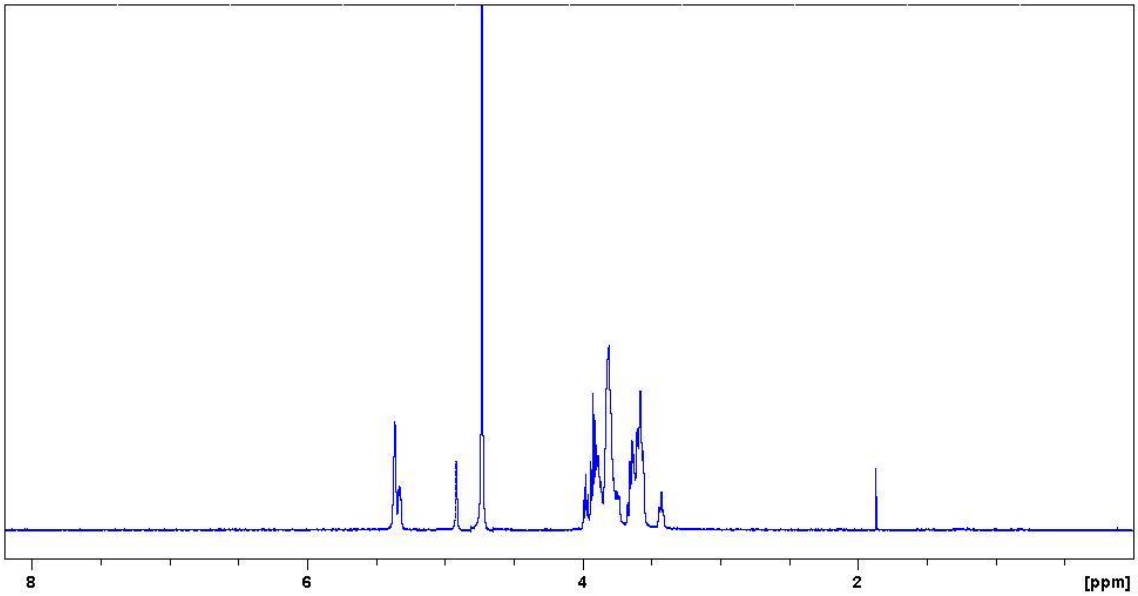

Figure F.1.19: Proton spectrum for FB2 F2a recorded in D_2O at 600 MHz. An impurity peak is observed at δ_H 1.86 ppm (unknown) as was previously observed in a pullulan sample (Figure F.1.2).

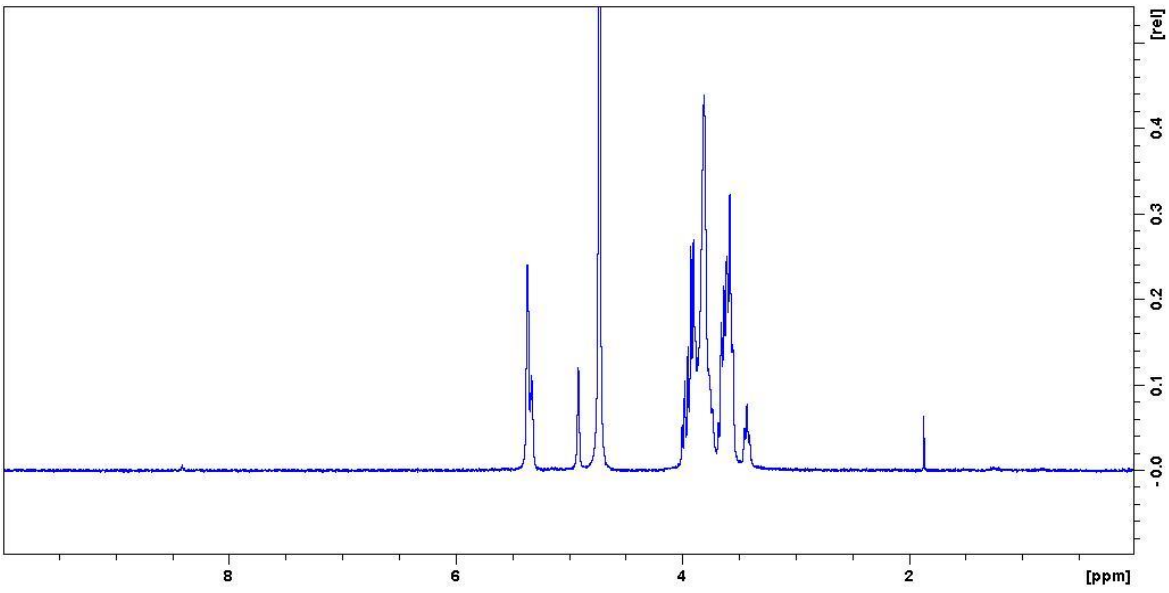

Figure F.1.20: Proton spectrum for FB2 F2b recorded in D_2O at 400 MHz. Impurity peaks are seen at δ_H 8.40 ppm (unknown) and 1.86 ppm (unknown) as was previously observed in a pullulan sample (Figure F.1.2).

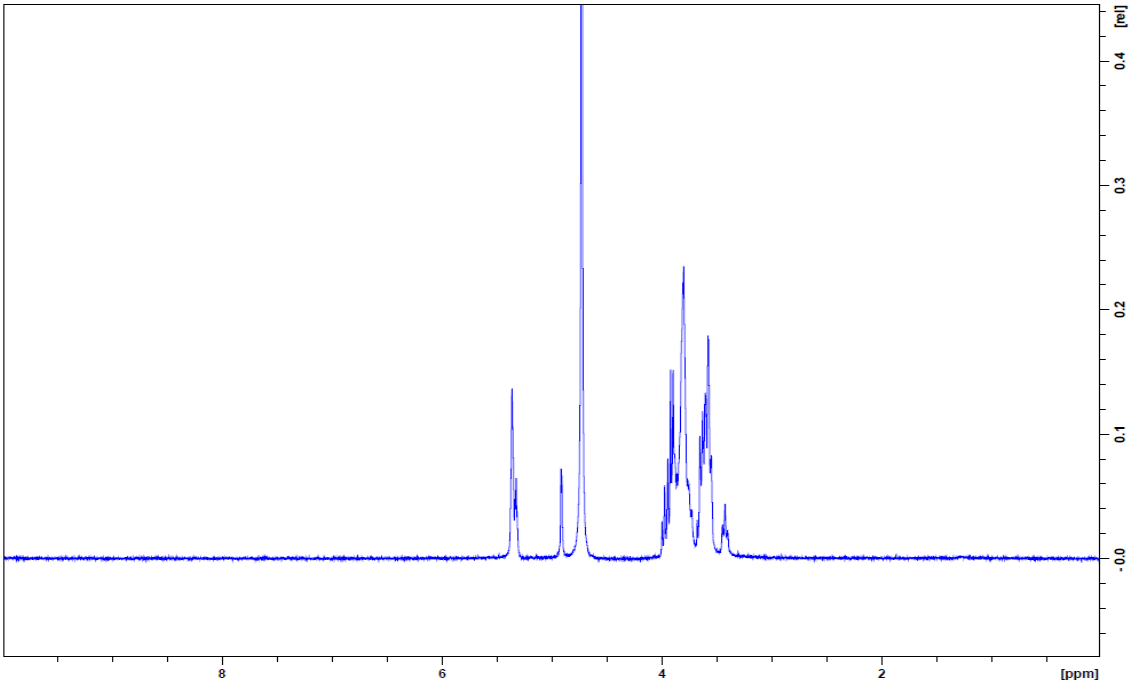

Figure F.1.21: Proton spectrum for FB2 F2c recorded in D_2O at 400 MHz. Unlike FB2 F2a and FB2 F2b, this separately prepared sample has no detectable impurity peaks and provides evidence that the unknown impurities (δ_H 8.40 and 1.86 ppm) arise from contamination during the preparation of the EPS samples for NMR analyses.

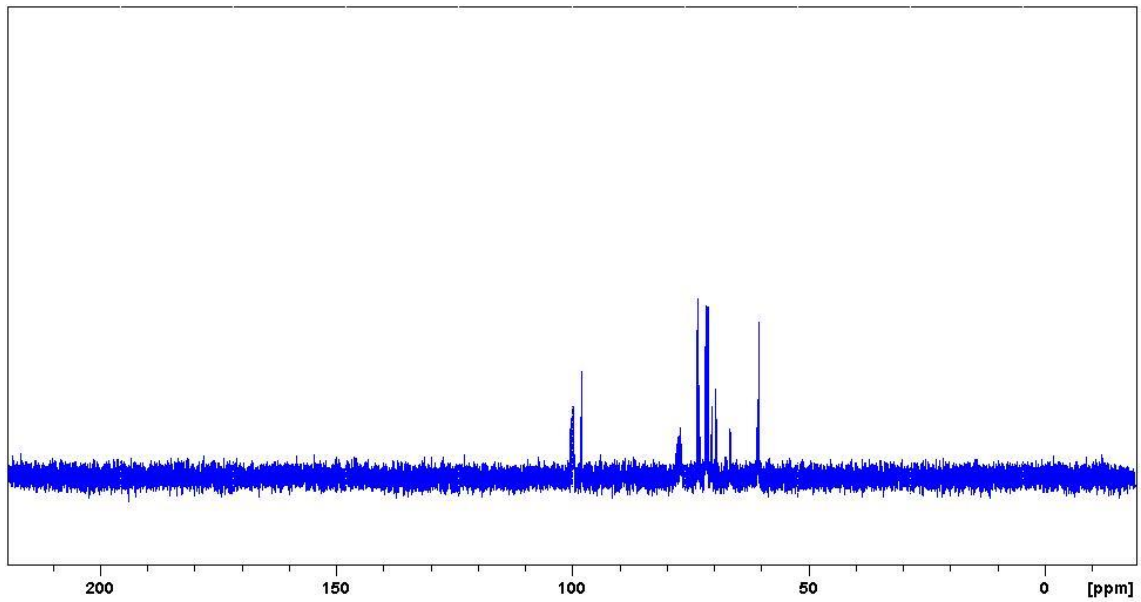

Figure F.1.22: Carbon spectrum for FB2 F2c recorded in D_2O at 151 MHz.

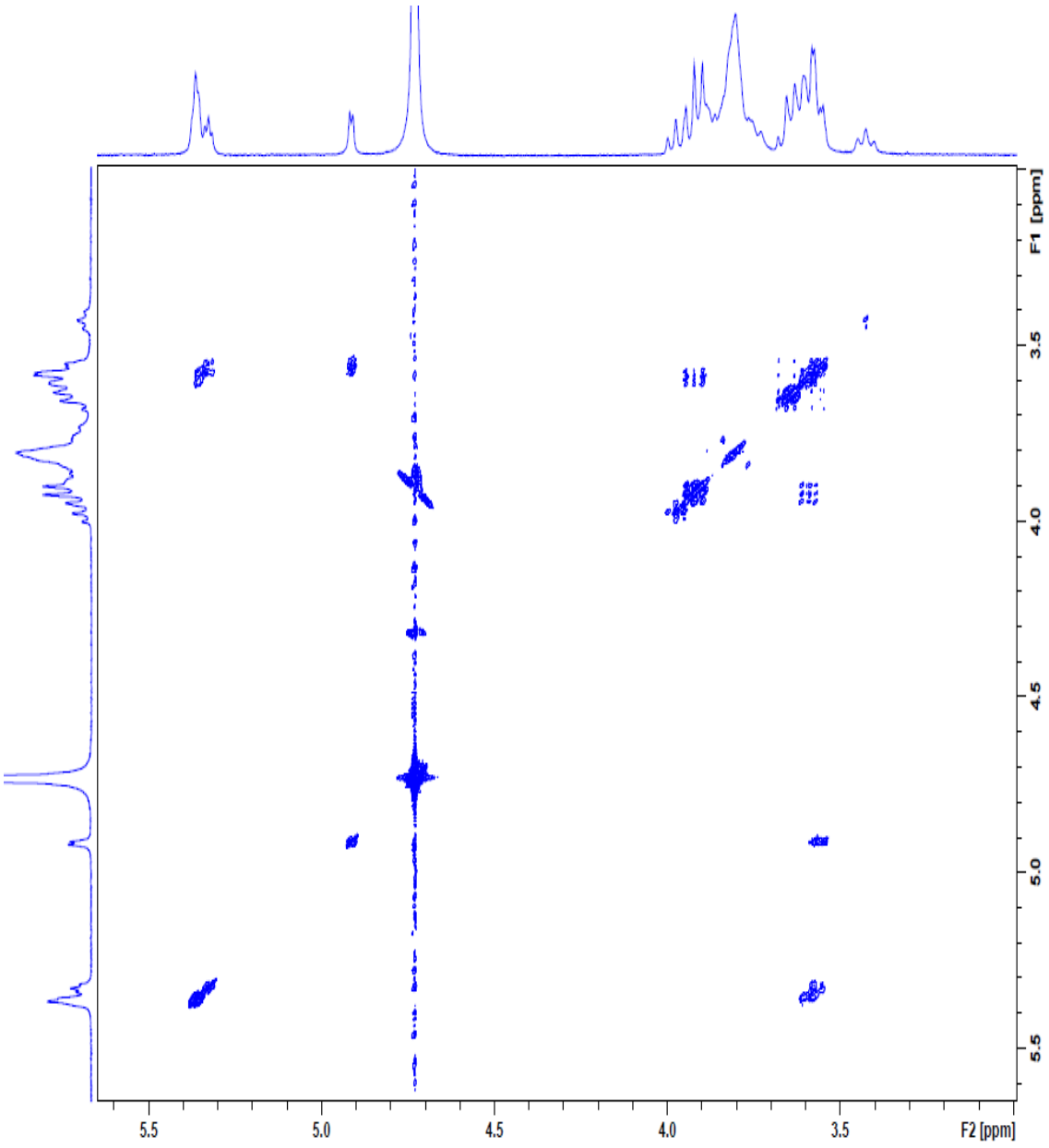

Figure F.1.23: COSY spectrum for FB2 F2c in D_2O.

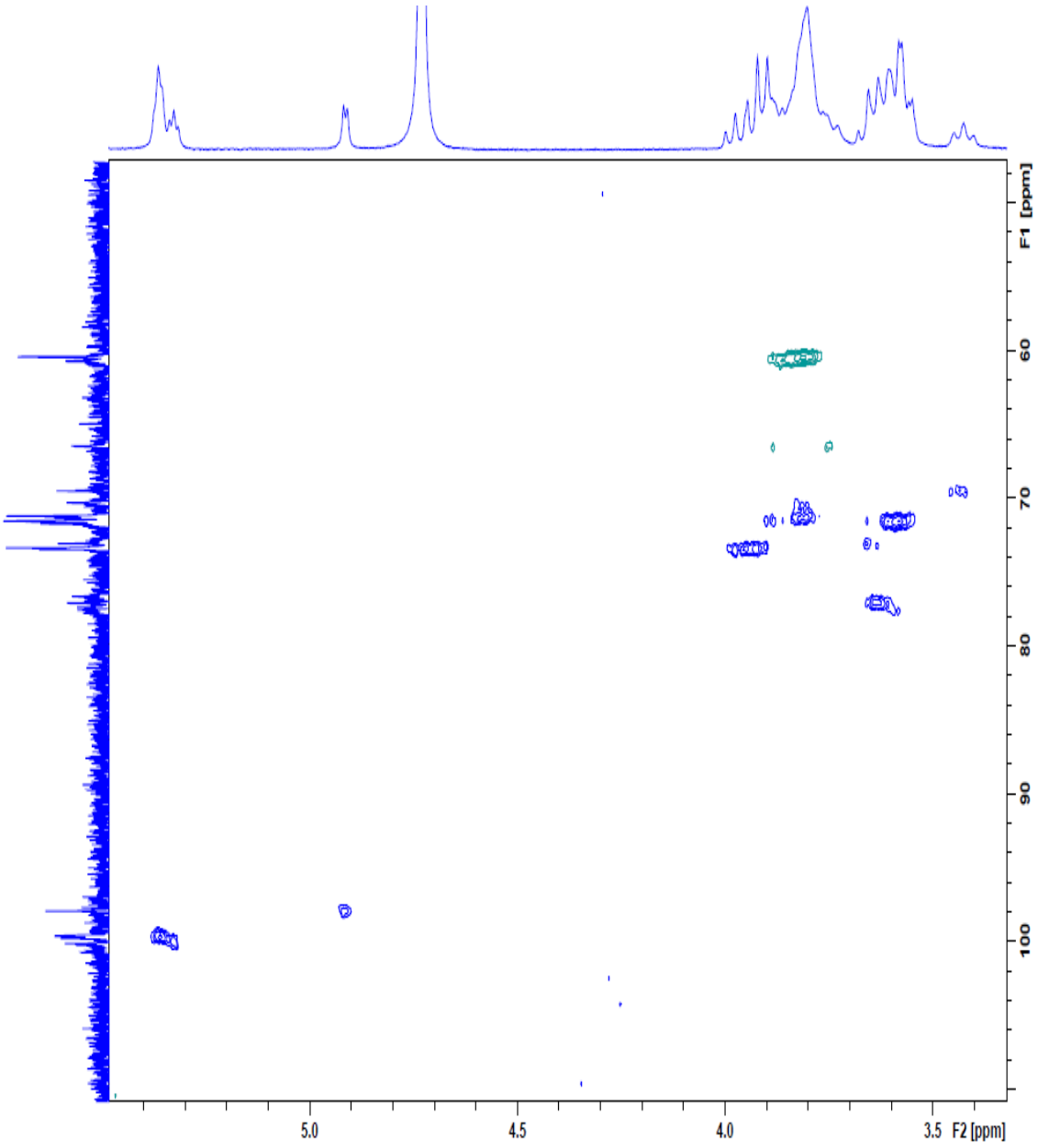

Figure F.1.24: HSQC spectrum for FB2 F2c in D_2O.

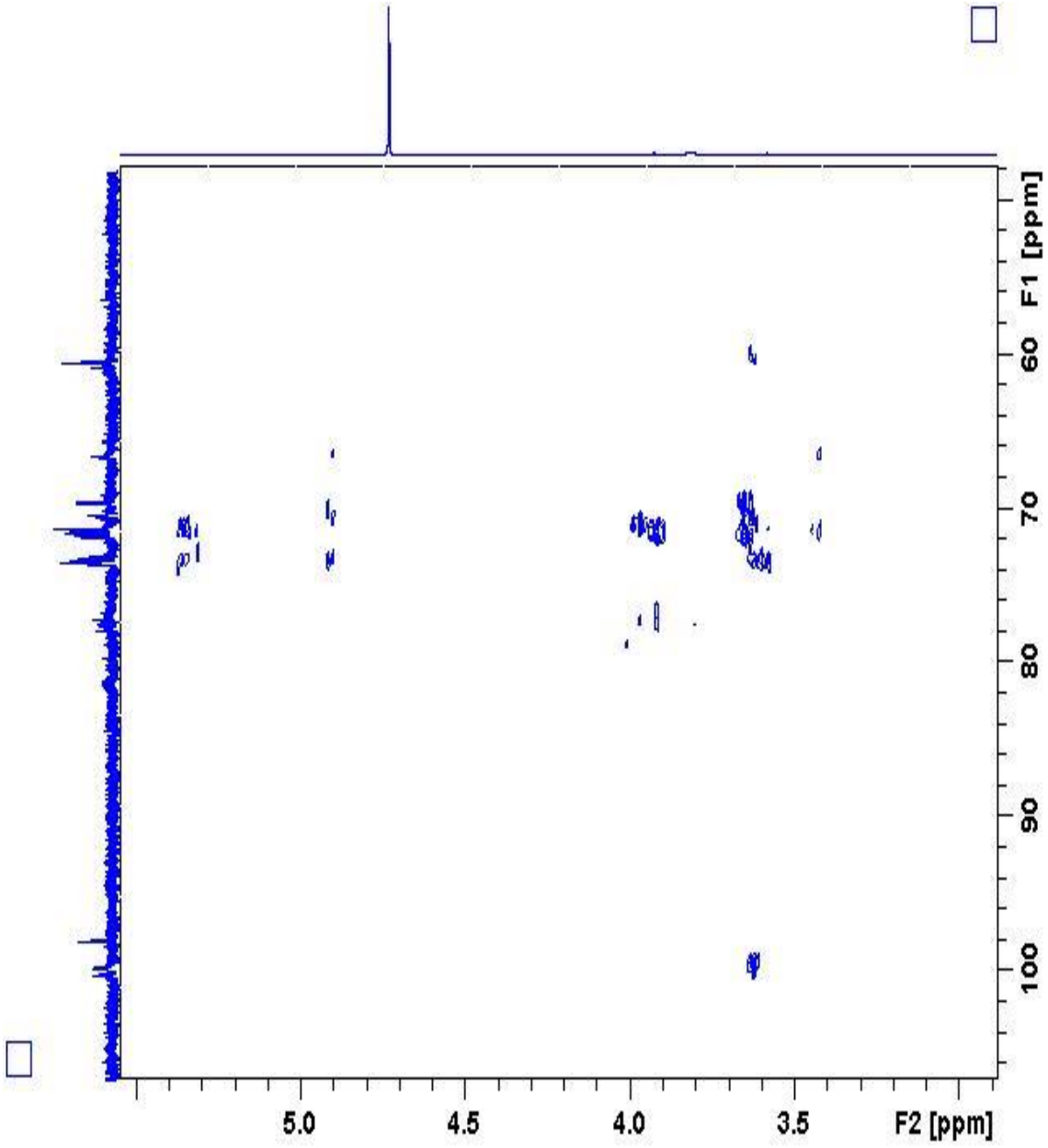

Figure F.1.25: HMBC spectrum for FB2 F2a in D_2O.

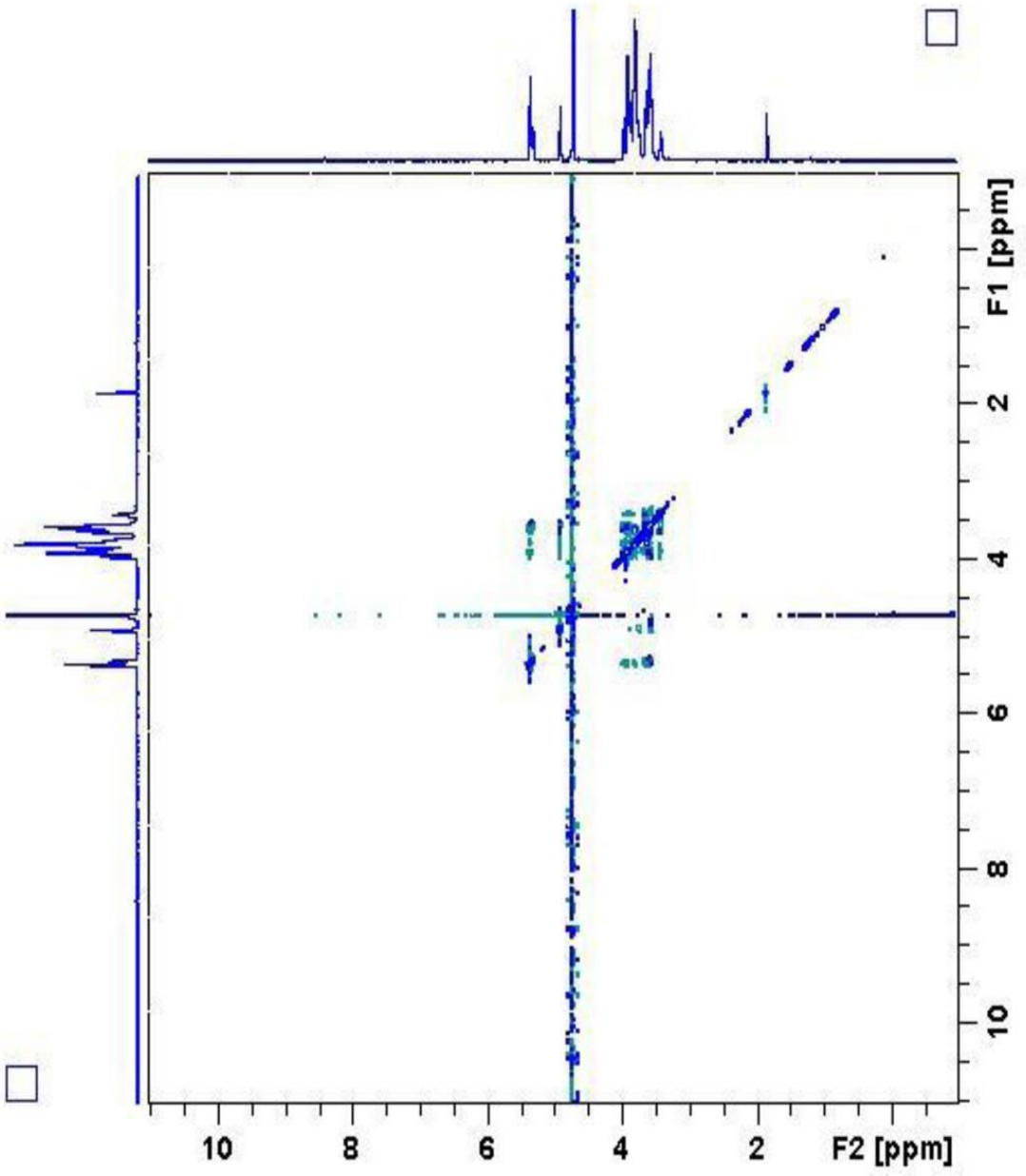

Figure F.1.26: ROESY spectrum for FB2 F2a in D_2O.

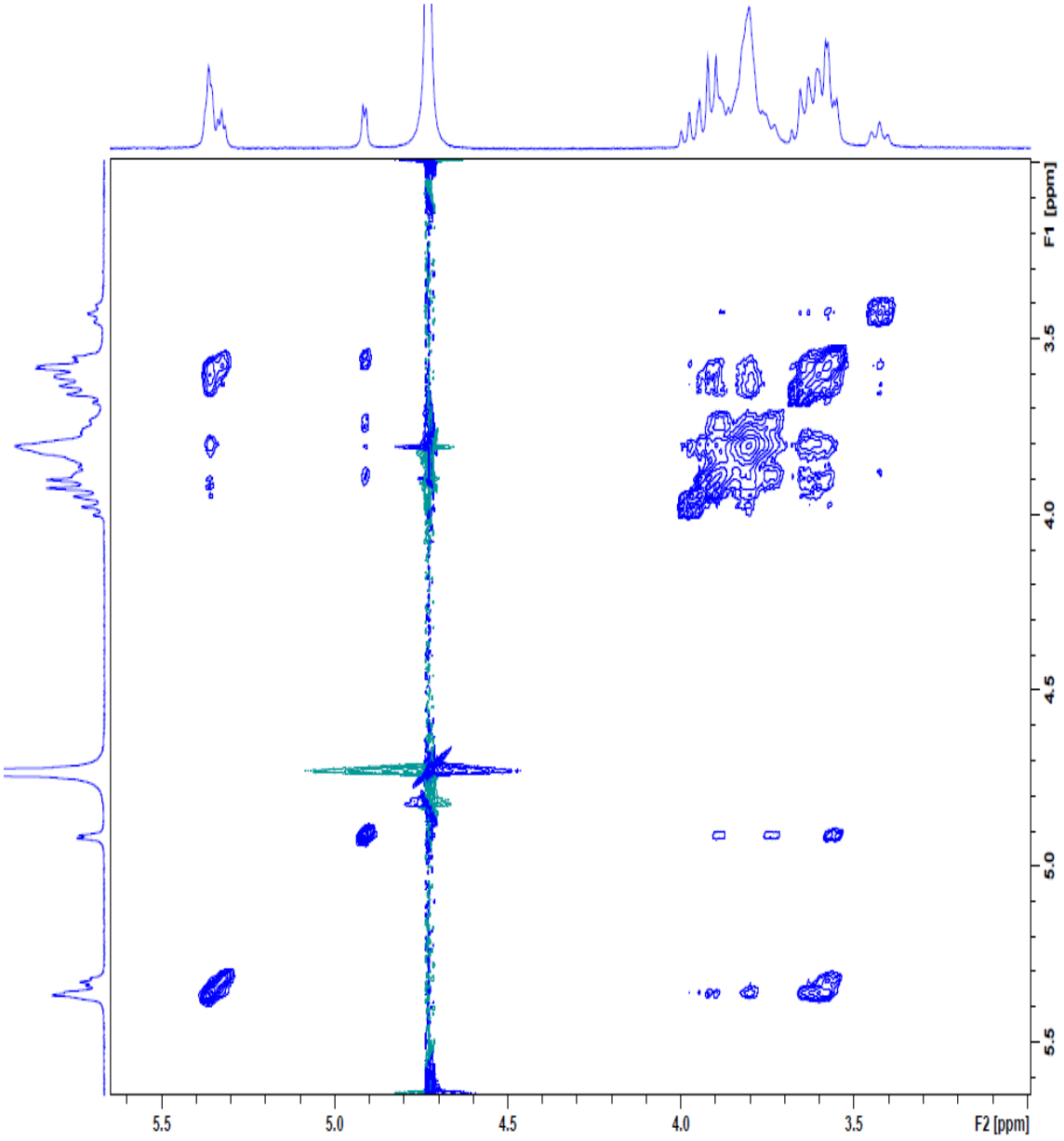

Figure F.1.27: NOESY spectrum for FB2 F2c in D_2O.

F.1.4 FB2, PB2 and PB7

The proton NMR spectra for the crude FB2, PB2 and PB7 *P. sacchari* EPSs are provided.

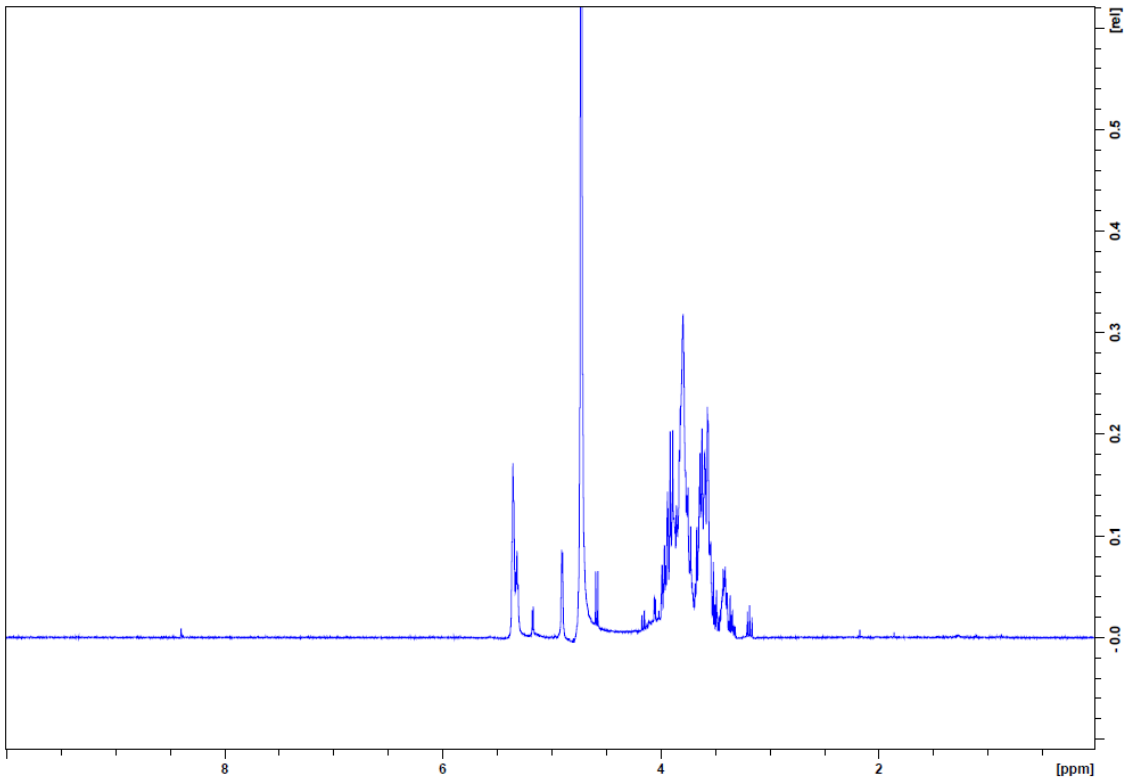

Figure F.1.28: Proton spectrum for crude FB2 in D_2O. Trace impurity peaks are evident at δ_H 8.40 ppm (unknown), 2.17 ppm (acetone) and 1.86 ppm (unknown) (Fulmer *et al.*, 2010).

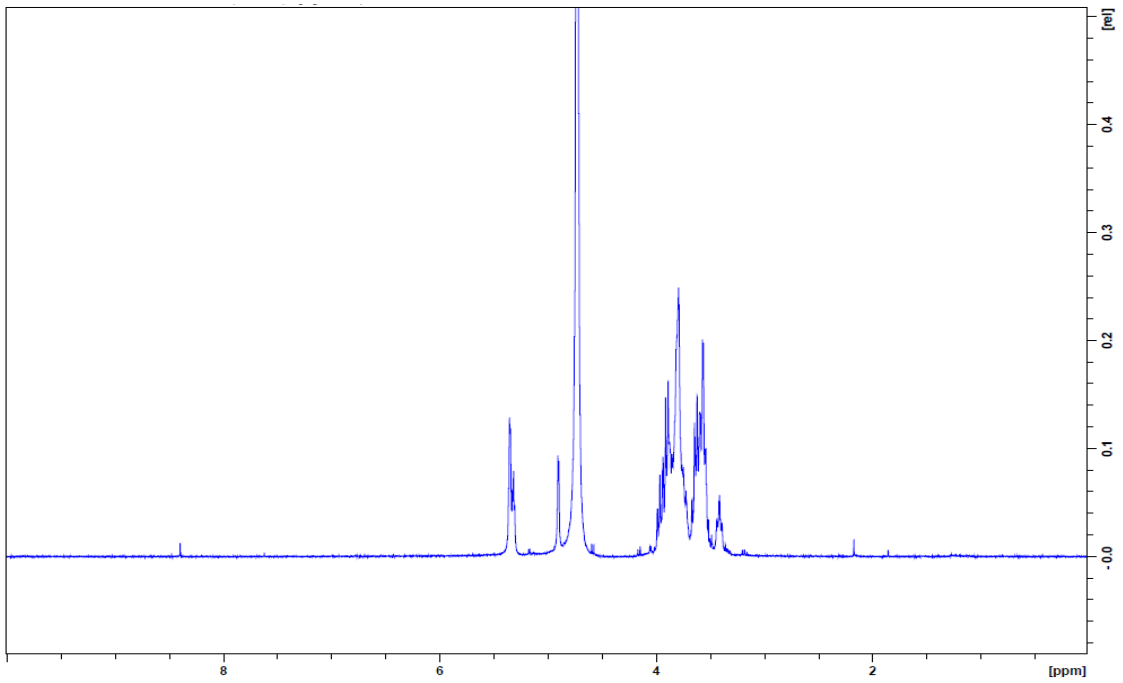

Figure F.1.29: Proton spectrum for crude PB2 in D_2O. Trace impurity peaks are evident at δ_H 8.40 ppm (unknown), 2.17 ppm (acetone) and 1.86 ppm (unknown) (Fulmer *et al.*, 2010).

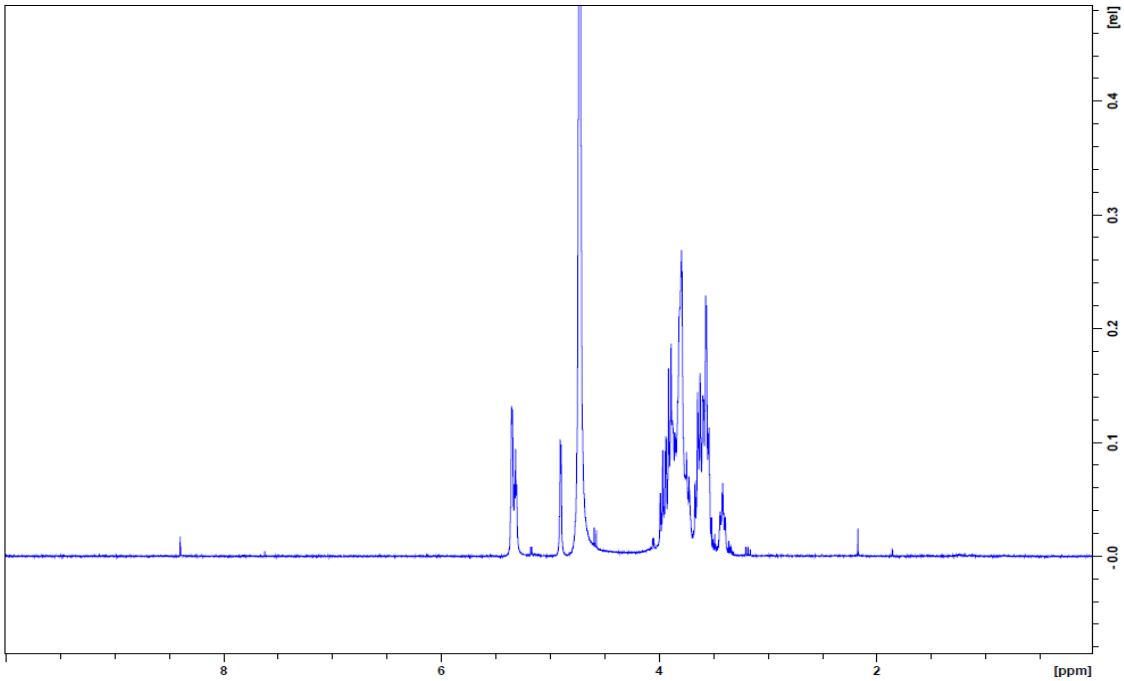

Figure F.1.30: Proton spectrum for crude PB7 in D_2O. Trace impurity peaks are evident at δ_H 8.40 ppm (unknown), 2.17 ppm (acetone) and 1.86 ppm (unknown) (Fulmer *et al.*, 2010).

Discussion on the impurities in the D_2O NMR analyses

In the NMR analyses of the native samples in D_2O, several impurity peaks were detected. In the ^1H NMR spectra there were singlets appearing at δ_H 8.40, 3.31, 2.17, 1.86 and 1.20 ppm. In the ^{13}C spectra, impurity peaks were evident at δ_C 215.5, 202.7, 171.7, 48.9 and 30.9 ppm. It was established that δ_H 2.17 ppm and δ_C 215.5, 30.9 ppm resonances are from acetone, and confirmed with HSQC correlations (Fulmer *et al*., 2010). Likewise, it was established that the δ_H 3.31 ppm and δ_C 48.9 ppm resonances are due to methanol (Fulmer *et al*., 2010). Initially, the resonance appearing at δ_H 8.40 ppm was believed to belong to protein in the FB2 EPSs, as it corresponds to a downfield amide singlet. This peak, however, did not show any correlations with the atoms determined in the purified EPSs of FB2. After several replicate analyses for pullulan and FB2 F2 were carried out, it was observed that none, some, or all of these impuritities were present – including that of δ_H 8.40 ppm. Therefore, it was concluded that these resonances are not associated with the structure of the EPS samples or pullulan. Whilst these impurities were not further characterised, it was postulated that the additional unknown impurities are either likely due to contamination from pyridine and/or the constituents of the cleaning agent Extran® MA02 when glassware used may have not been sufficiently rinsed. The glassware used to dissolve the samples in D_2O were the same vials that were used for the GC-MS silylations, which were carried out in pyridine solution. These vials are cleaned with Extran® MA02, which contains sodium metaphosphate, Marlipal SU, Marlon A375, Marlopan AT 50, Kathon ICP and NaOH (Anonymous, 2006). The structures of Kathon ICP and pyridine are shown in Figure F.1.31 and Figure F.1.32, respectively. The possible structures of derivatives of these contaminants, which may give rise to a combination of some of the resonances seen in the ^1H and ^{13}C NMR, are shown in Figure F.1.33 and Figure F.1.34.

Although the NMR impurities were not fully elucidated, it was important to determine that these resonances in the spectra were not from the samples. Understanding that the initial glassware used for NMR sample preparation was a possible source of contamination, these were not used in the preparation of the peracetylated samples. The NMR spectra for the peracetylated samples are presented next, together with a similar assessment of any impurities detected.

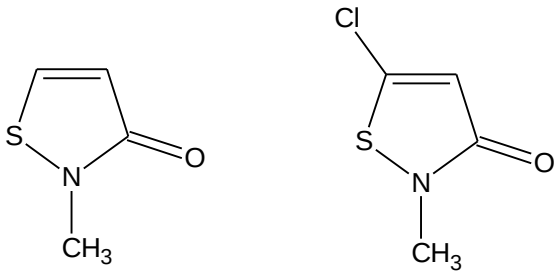

Figure F.1.31: Structures for Kathon ICP found in Extran®.

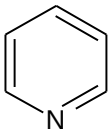

Figure F.1.32: Structure of pyridine.

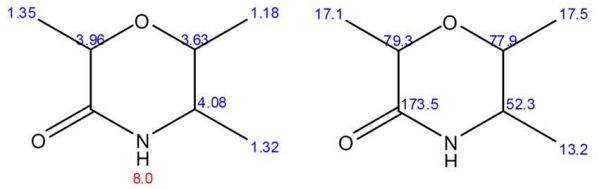

2,5,6-trimethylmorpholin-3-one

Figure F.1.33: A possible analogue of pyridine and/or Kathon ICP that may give rise to some of the resonances seen in the NMR spectra of pullulan and the *P. sacchari* EPSs in D_2O.

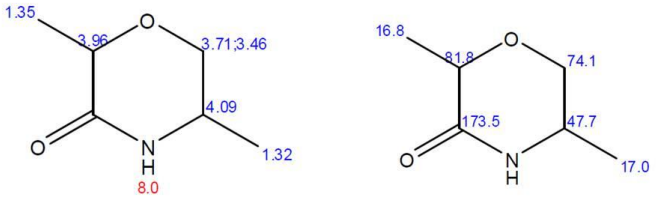

2,5-dimethylmorpholin-3-one

Figure F.1.34: A possible analogue of pyridine and/or Kathon ICP that may give rise to some of the resonances seen in the NMR spectra of pullulan and the *P. sacchari* EPSs in D_2O.

F.2 Analysis of peracetylated polysaccharides in $CDCl_3$

The NMR spectra for peracetylated samples of pullulan and the crude EPSs (FB2, PB2 and PB7) are presented below. All samples were dissolved in $CDCl_3$ and the spectra were referenced to δ_H 7.26 ppm and δ_C 77.36 ppm.

F.2.1 Pullulan peracetate

The NMR spectra for pullulan peracetate are presented. The sample was dissolved in $CDCl_3$. All proton spectra were recorded at 600 MHz and all carbon spectra were recorded at 151 MHz.

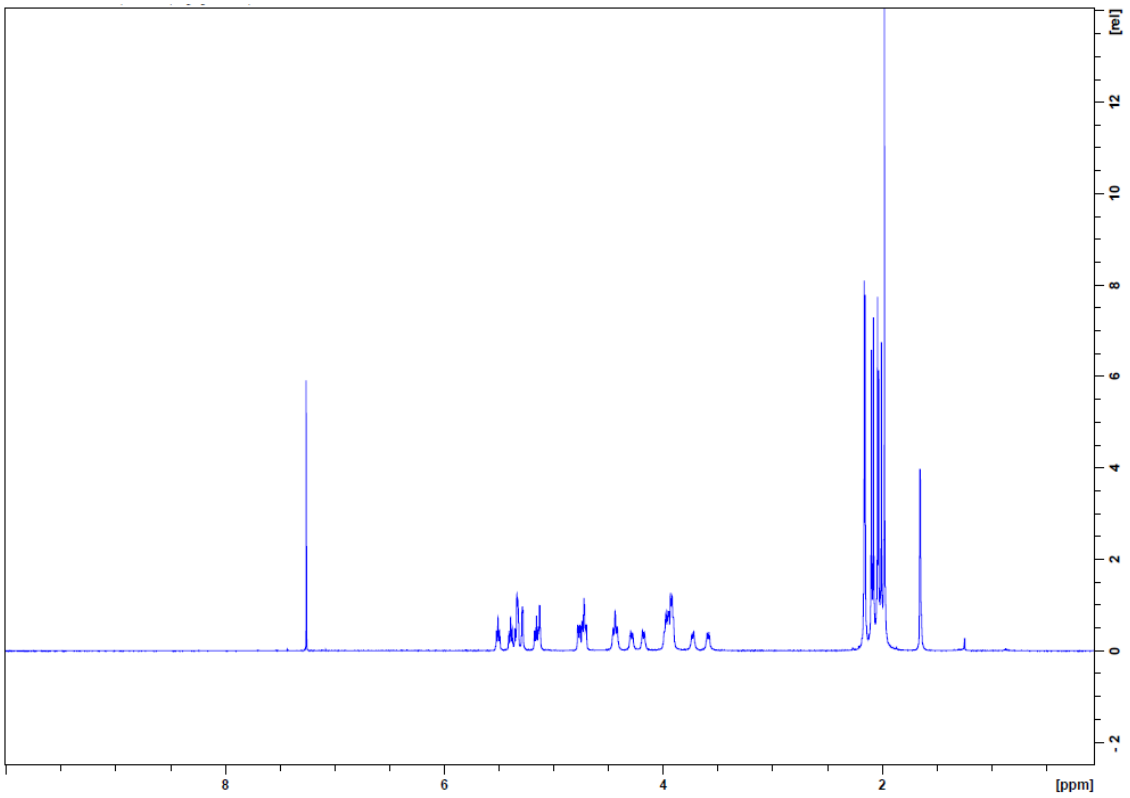

Figure F.2.1: Proton NMR of pullulan peracetate. A water (OH) and/or acetate (OAc) anomeric peak is detected at δ_H 1.66 ppm and an unknown impurity at δ_H 1.25 ppm (Farkas *et al.*, 1997; Fulmer *et al.*, 2010).

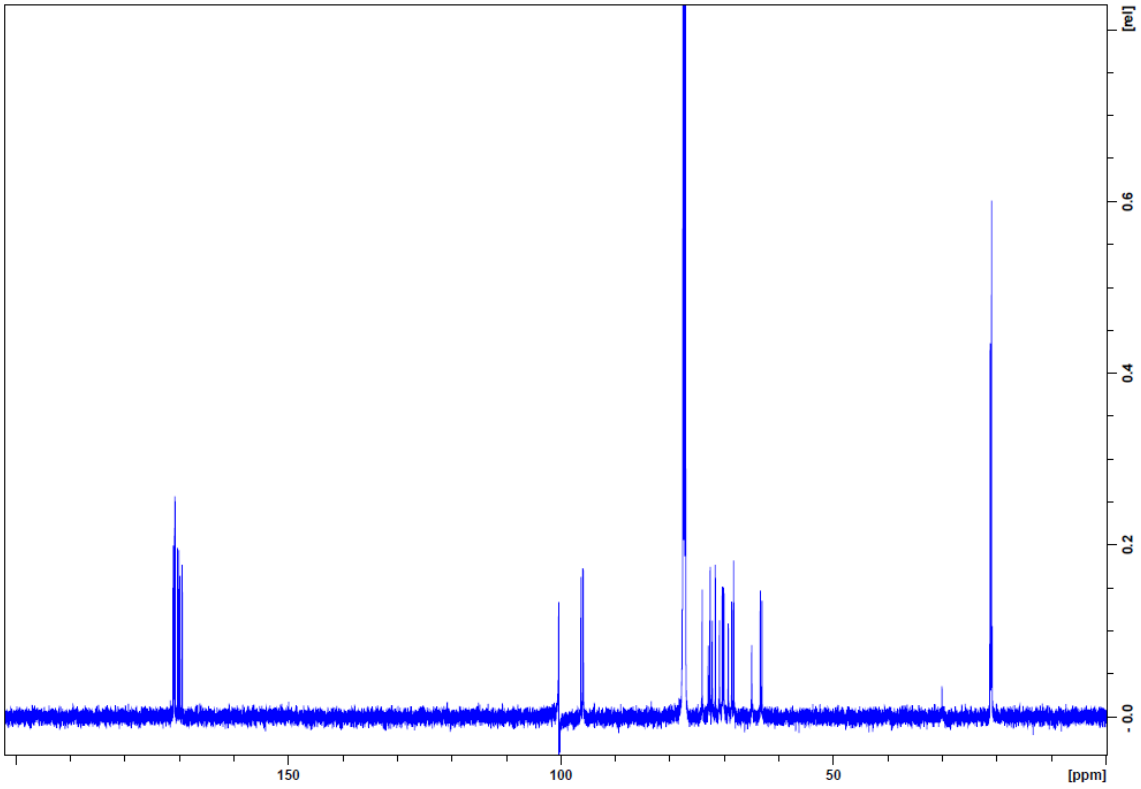

Figure F.2.2: Carbon spectrum for pullulan peracetate. An acetone peak is visible at δ_C 30.1 ppm (Fulmer *et al.*, 2010).

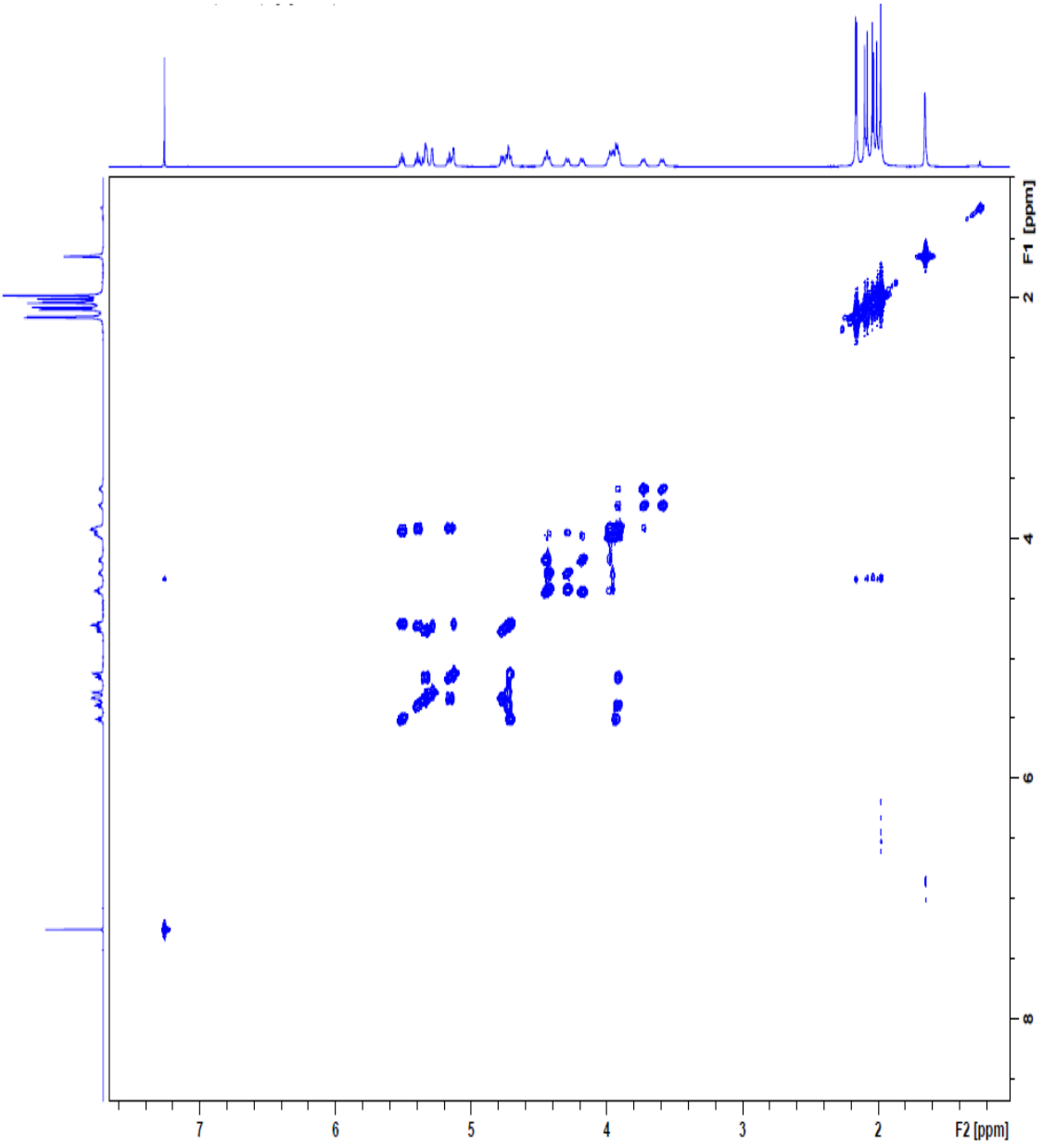

Figure F.2.3: COSY spectrum of pullulan peracetate.

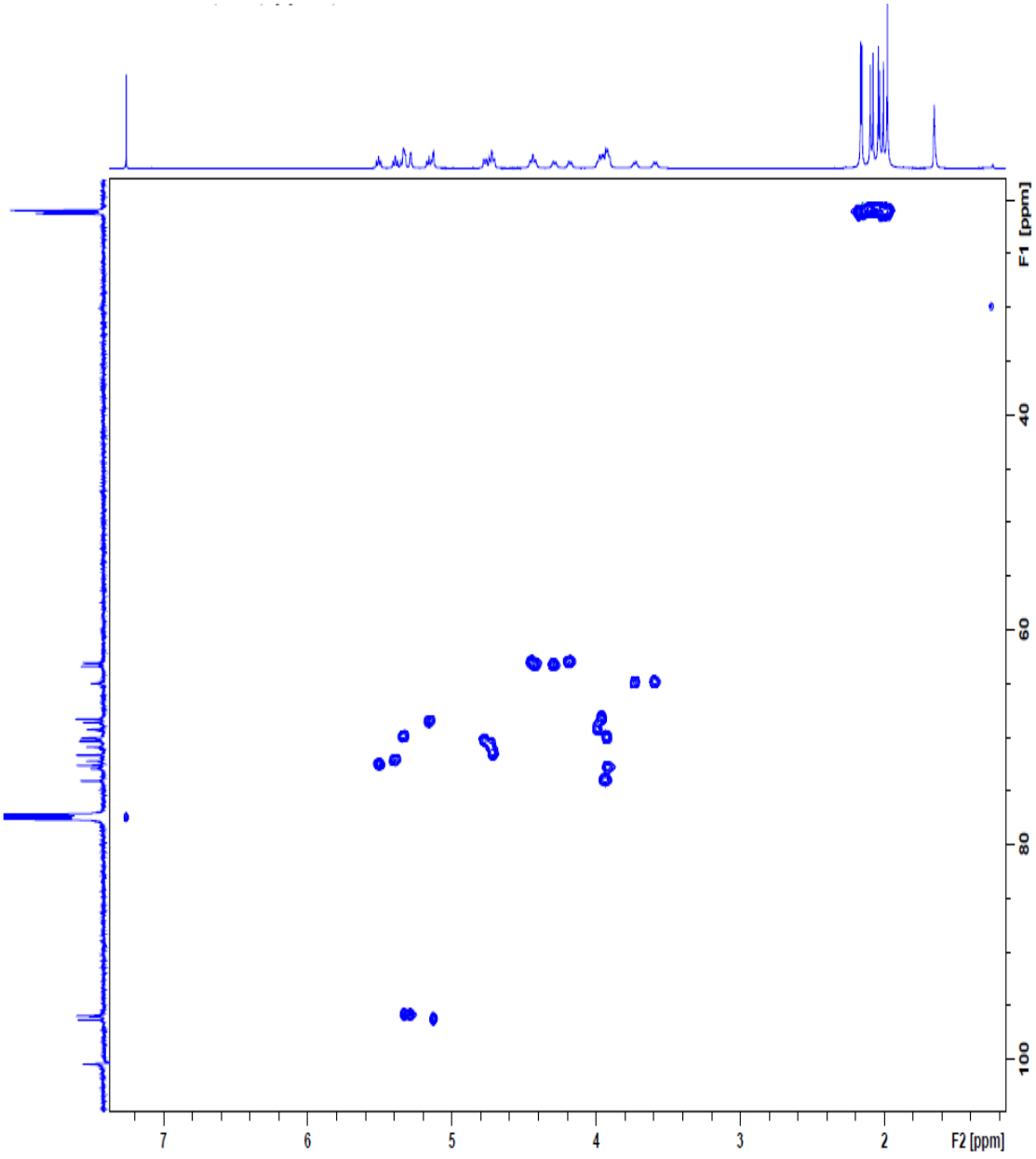

Figure F.2.4: HSQC spectrum of pullulan peracetate.

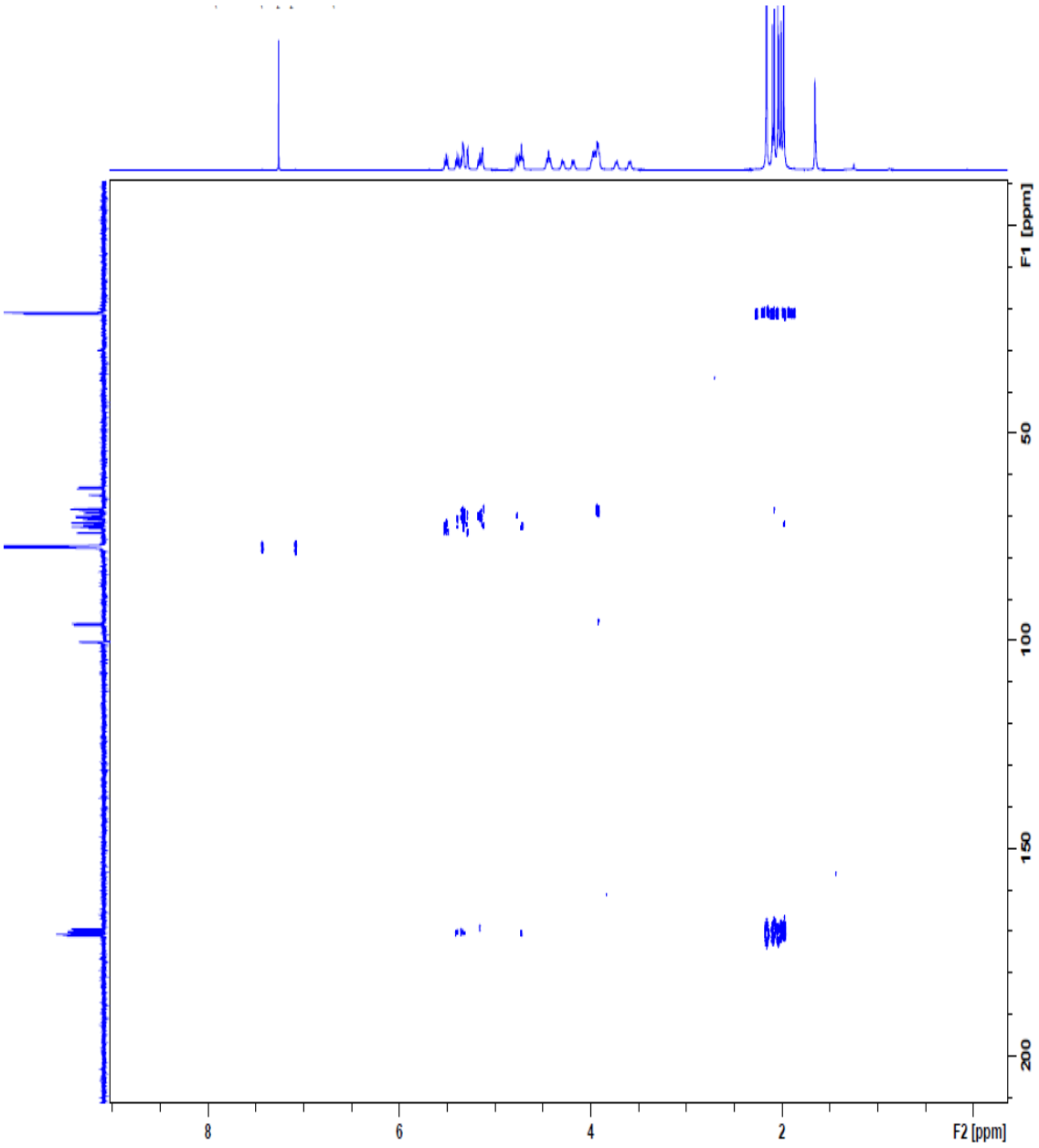

Figure F.2.5: HMBC spectrum of pullulan peracetate.

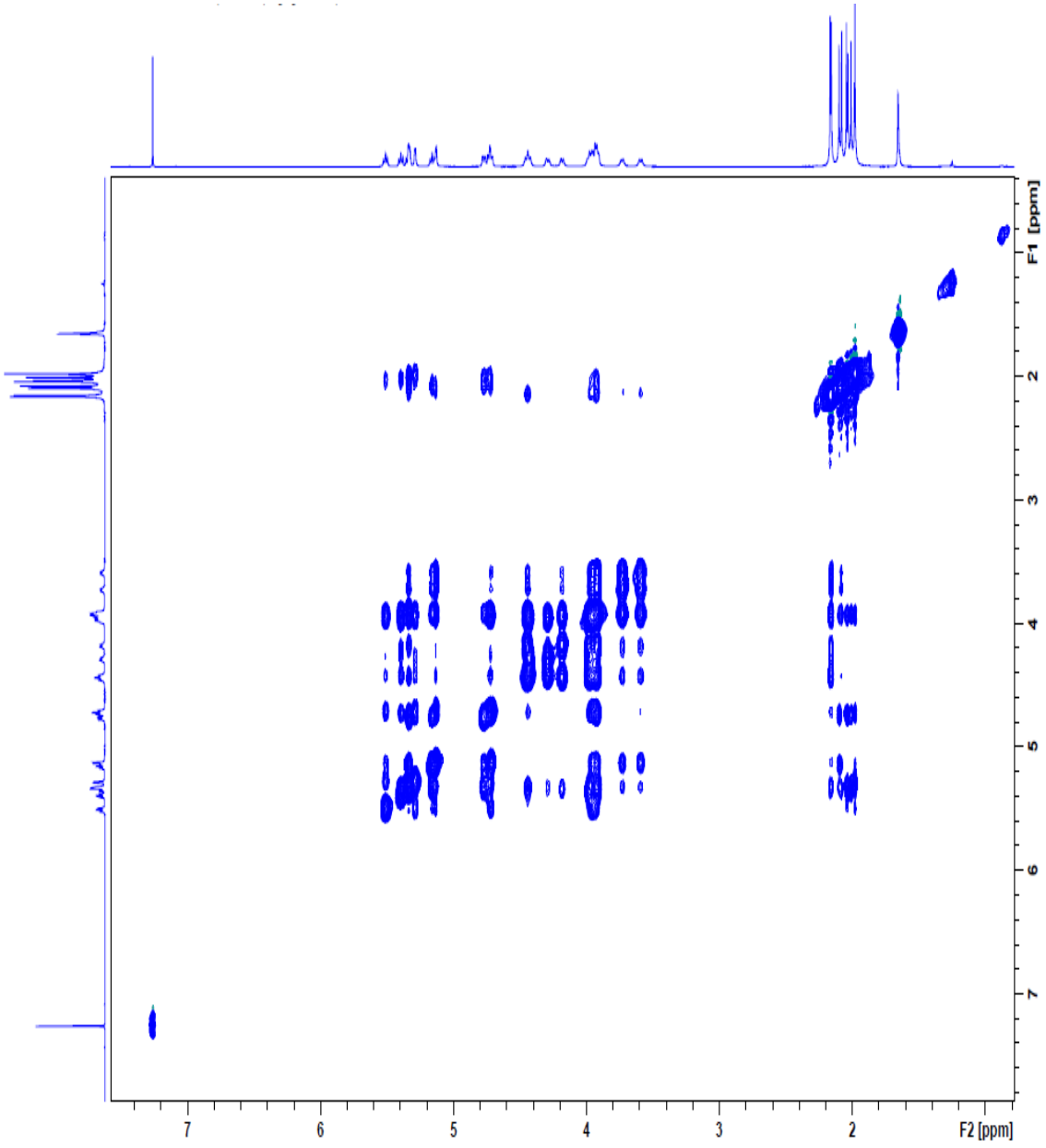

Figure F.2.6: NOESY spectrum of pullulan peracetate.

F.2.2 PB2 peracetate

The NMR spectra for the crude PB2 peracetate sample are presented. The sample was dissolved in $CDCl_3$. All proton spectra were recorded at 600 MHz and all carbon spectra were recorded at 151 MHz.

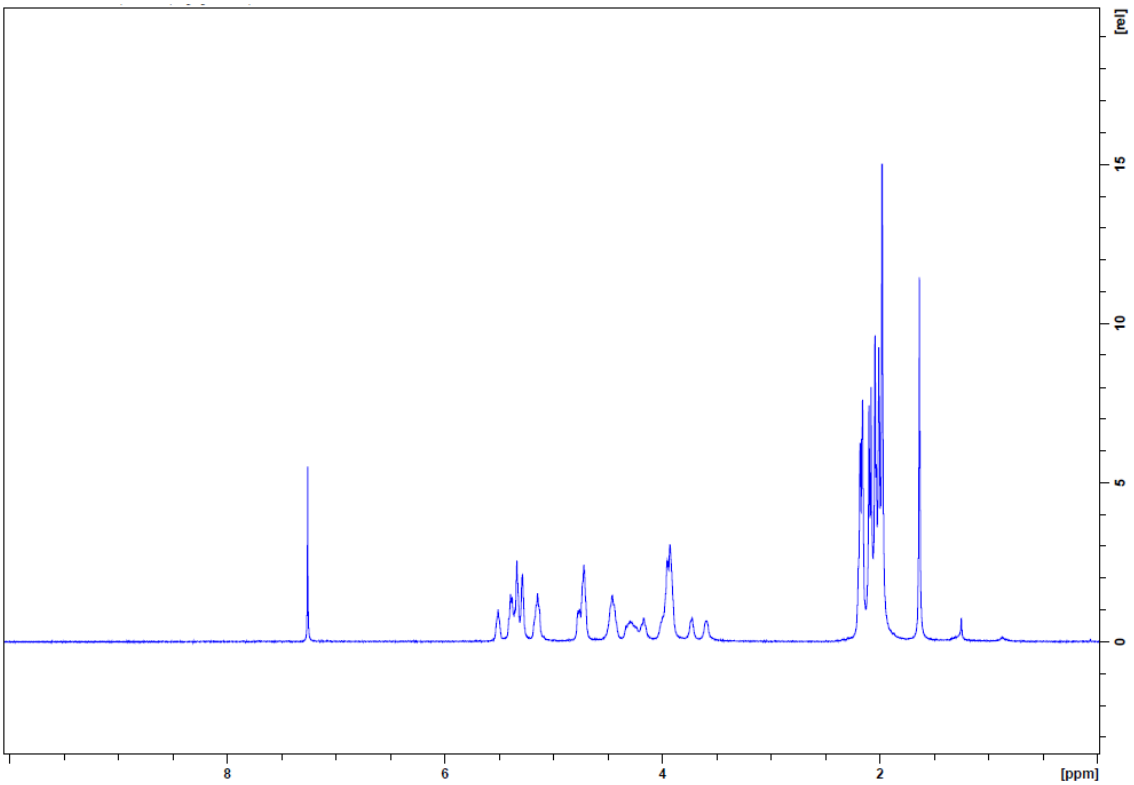

Figure F.2.7: Proton spectrum of PB2 peracetate. A water (OH) and/or acetate (OAc) anomeric peak is detected at δ_H 1.66 ppm (Farkas *et al.*, 1997; Fulmer *et al.*, 2010). Another peak is visible at δ_H 1.25 ppm, found to have an HSQC correlation with the acetone peak at δ_C 30.1 ppm (Figure F.2.10).

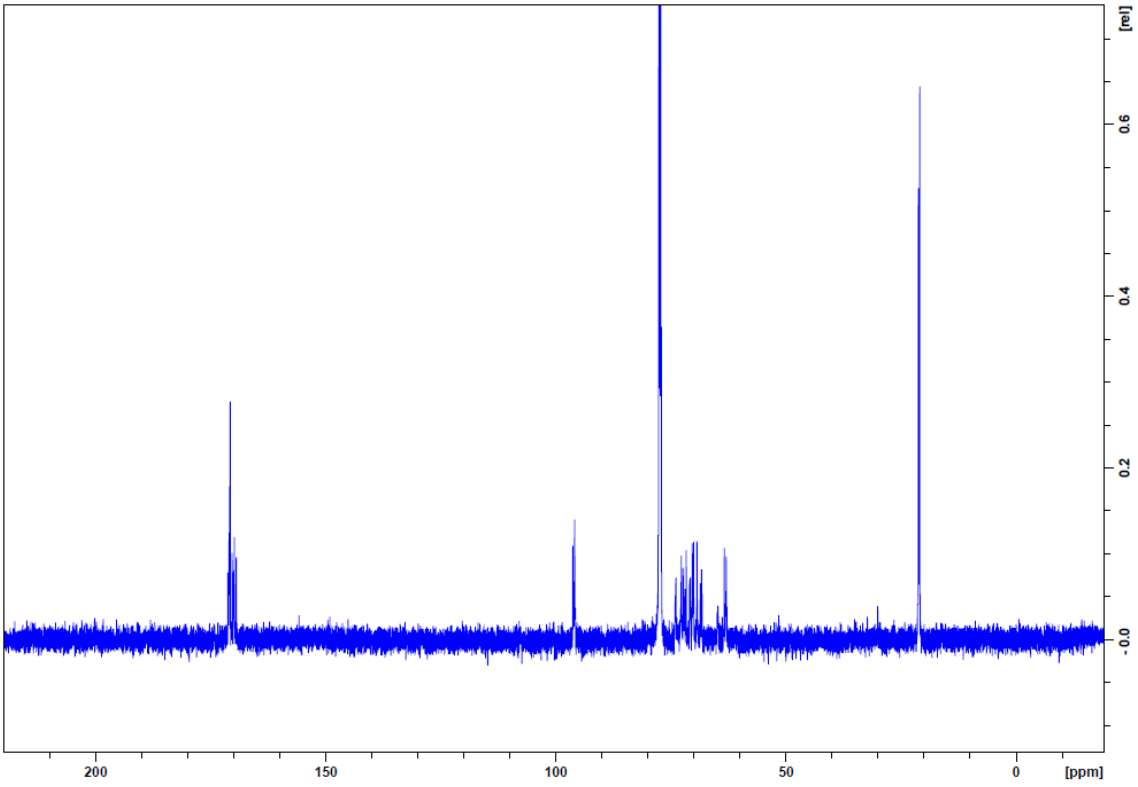

Figure F.2.8: Carbon spectrum for PB2 peracetate. An acetone peak is visible at δ_C 30.1 ppm (Fulmer *et al.*, 2010).

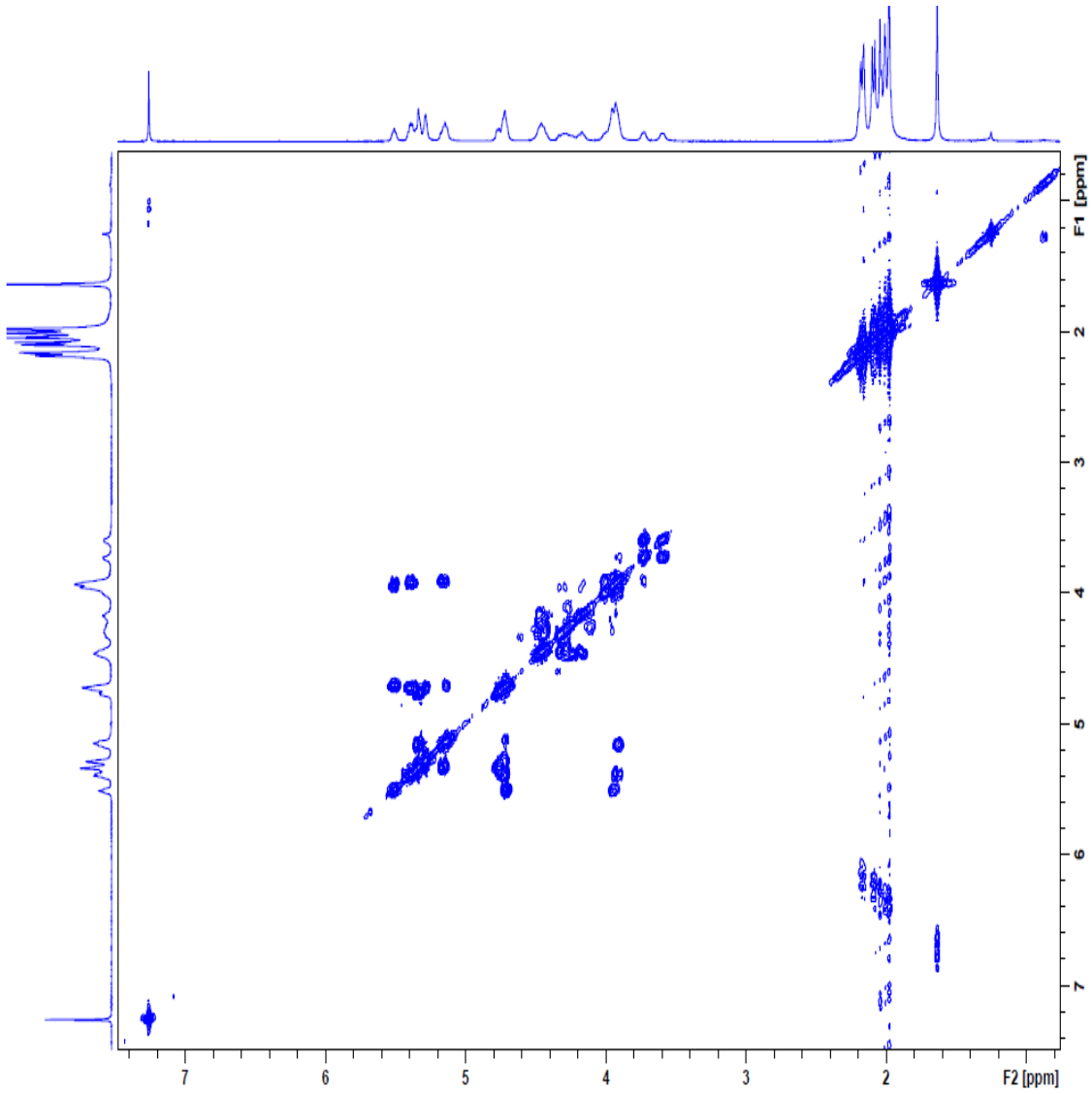

Figure F.2.9: COSY spectrum for PB2 peracetate.

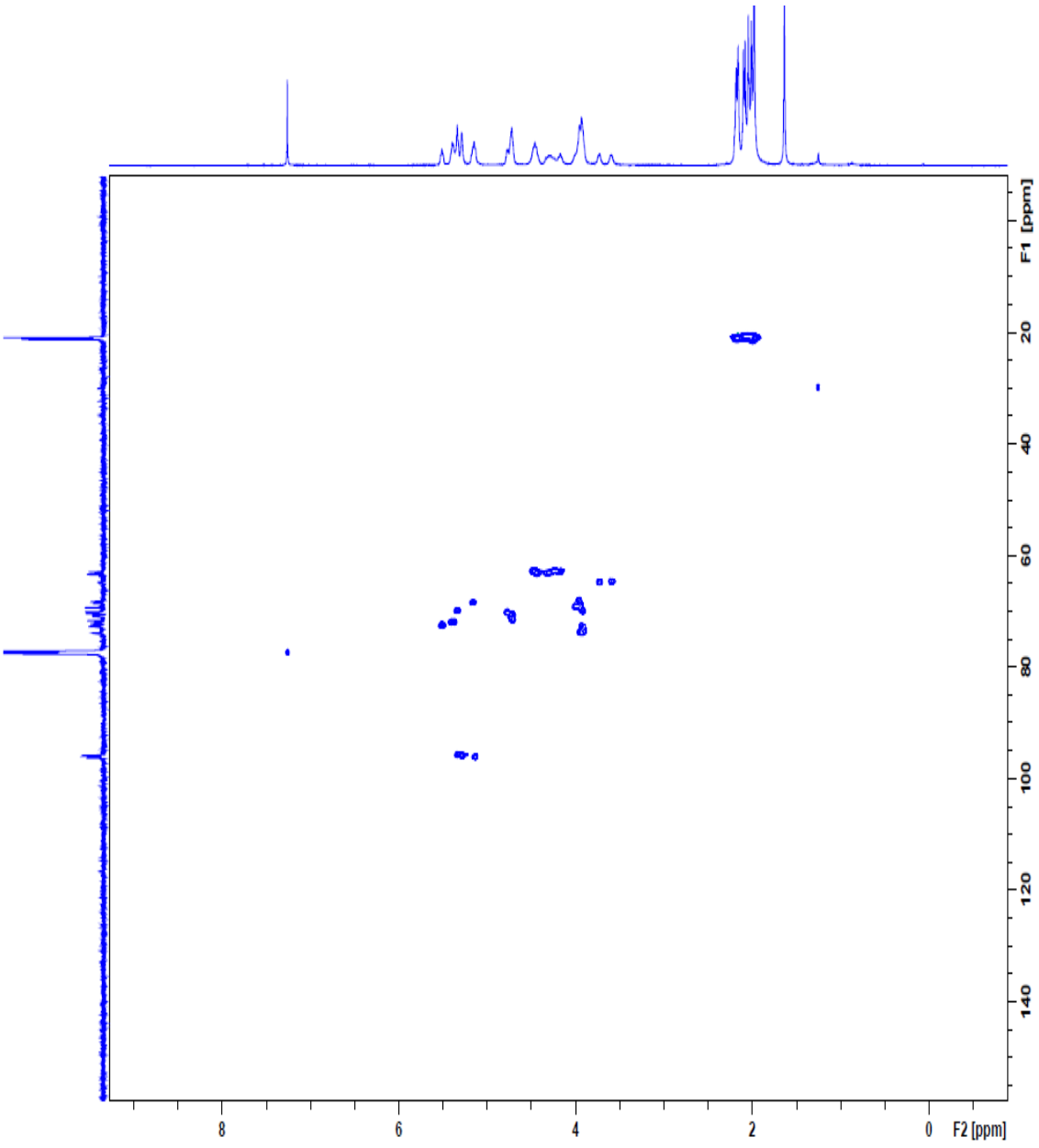

Figure F.2.10: HSQC spectrum of PB2 peracetate. There is a correlation between the acetone peak at δ_C 30.1 ppm and the singlet at δ_H 1.25 ppm.

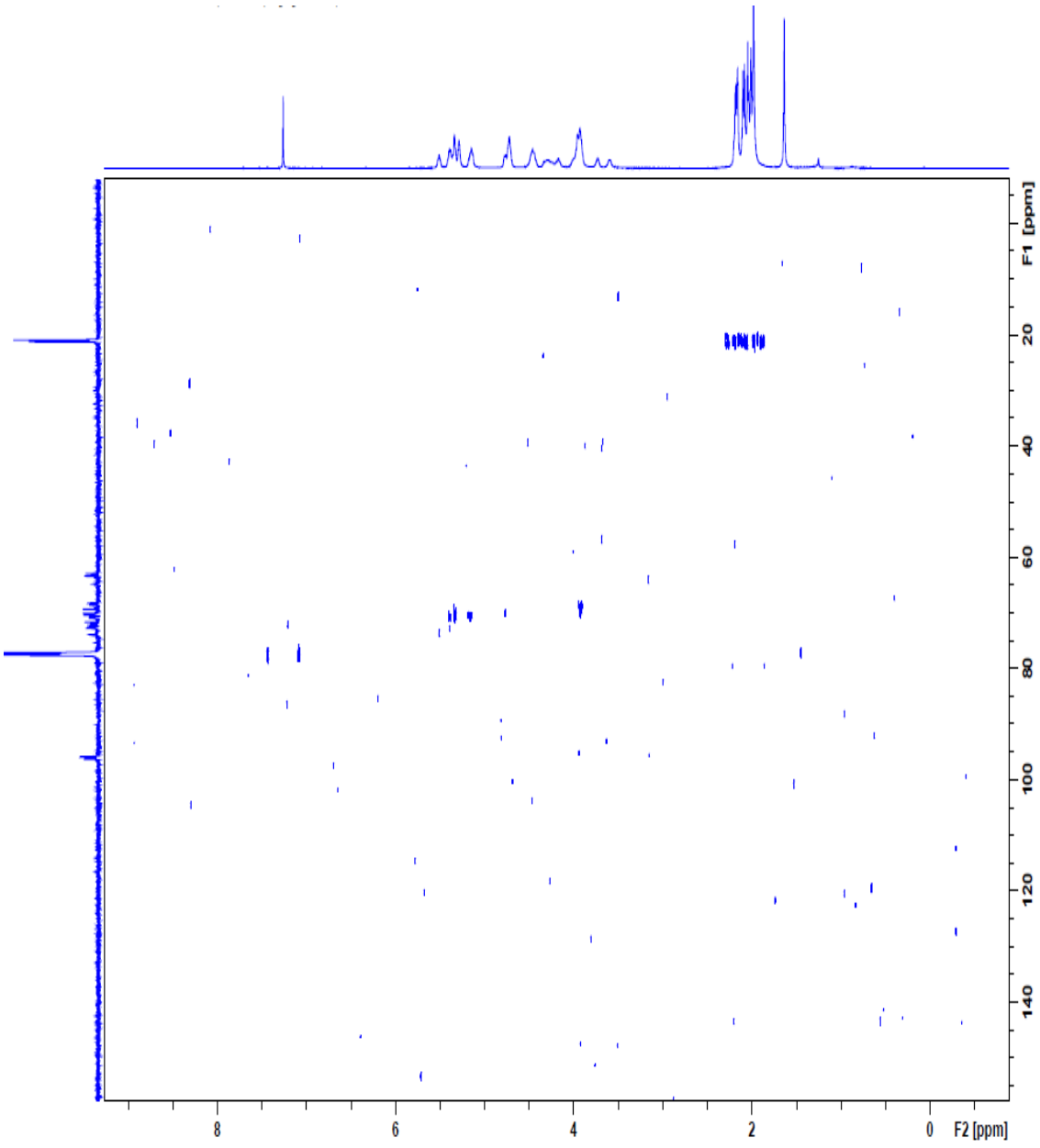

Figure F.2.11: HMBC spectrum of PB2 peracetate.

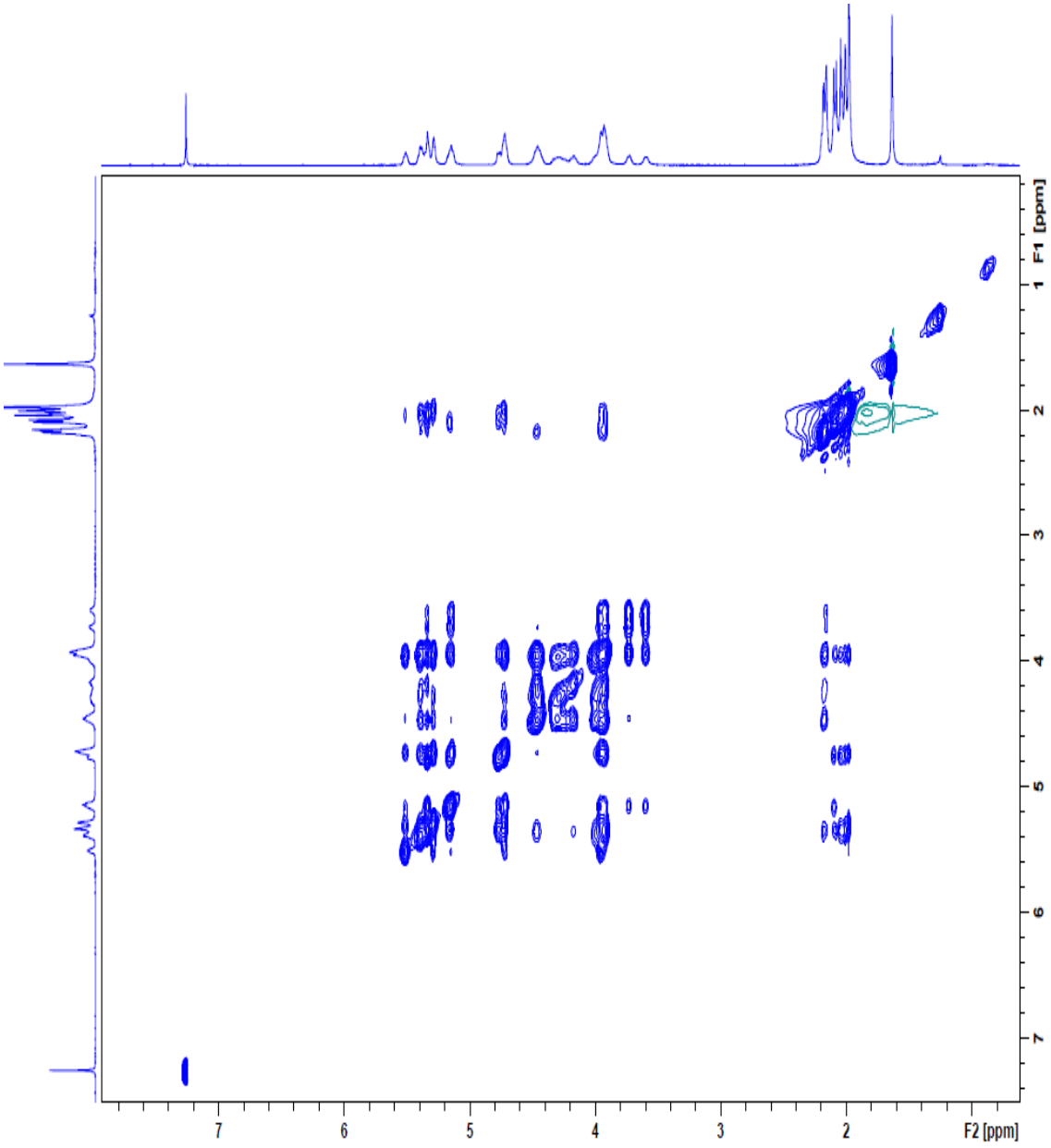

Figure F.2.12: NOESY spectrum of PB2 peracetate.

F.2.3 PB7 peracetate

The NMR spectra for the crude PB7 peracetate sample are presented. The sample was dissolved in $CDCl_3$. All proton spectra were recorded at 600 MHz and all carbon spectra were recorded at 151 MHz.

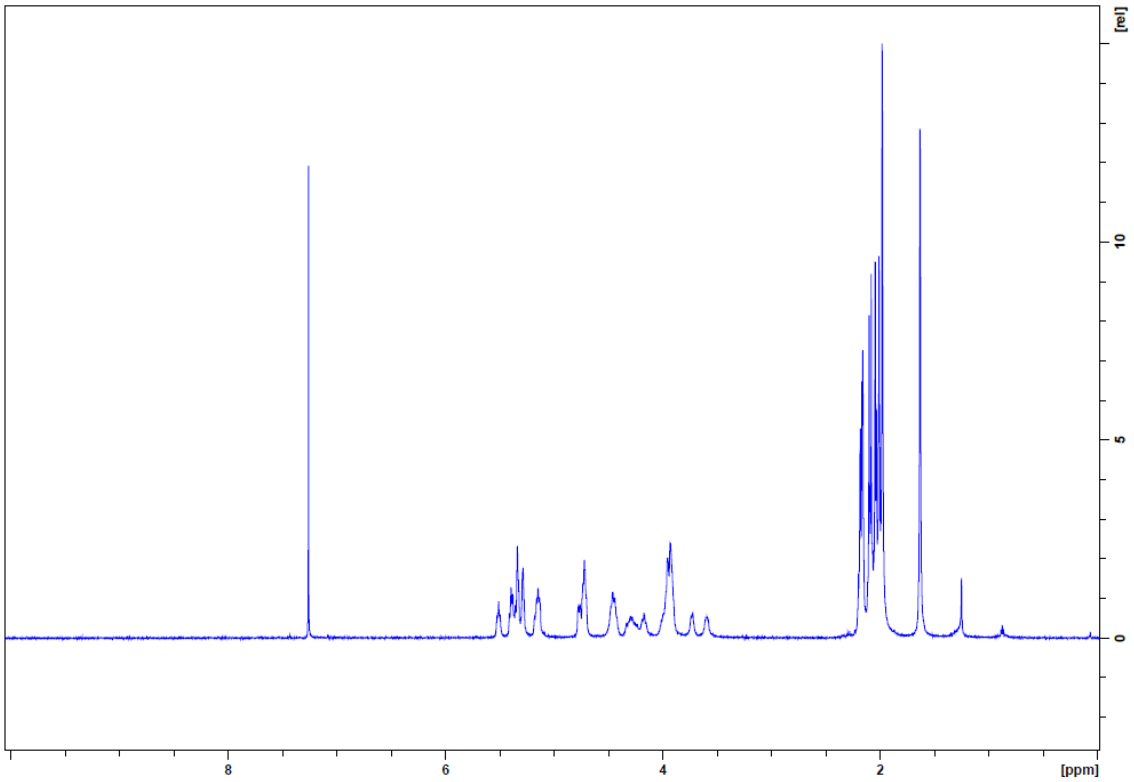

Figure F.2.13: Proton spectrum of PB7 peracetate. A water (OH) and/or acetate (OAc) anomeric peak is detected at δ_H 1.66 ppm (Farkas *et al.*, 1997; Fulmer *et al.*, 2010). Another peak is visible at δ_H 1.25 ppm, found to have an HSQC (Figure F.2.16) and HMBC (Figure F.2.17) correlation with the acetone peak at δ_C 30.1 ppm.

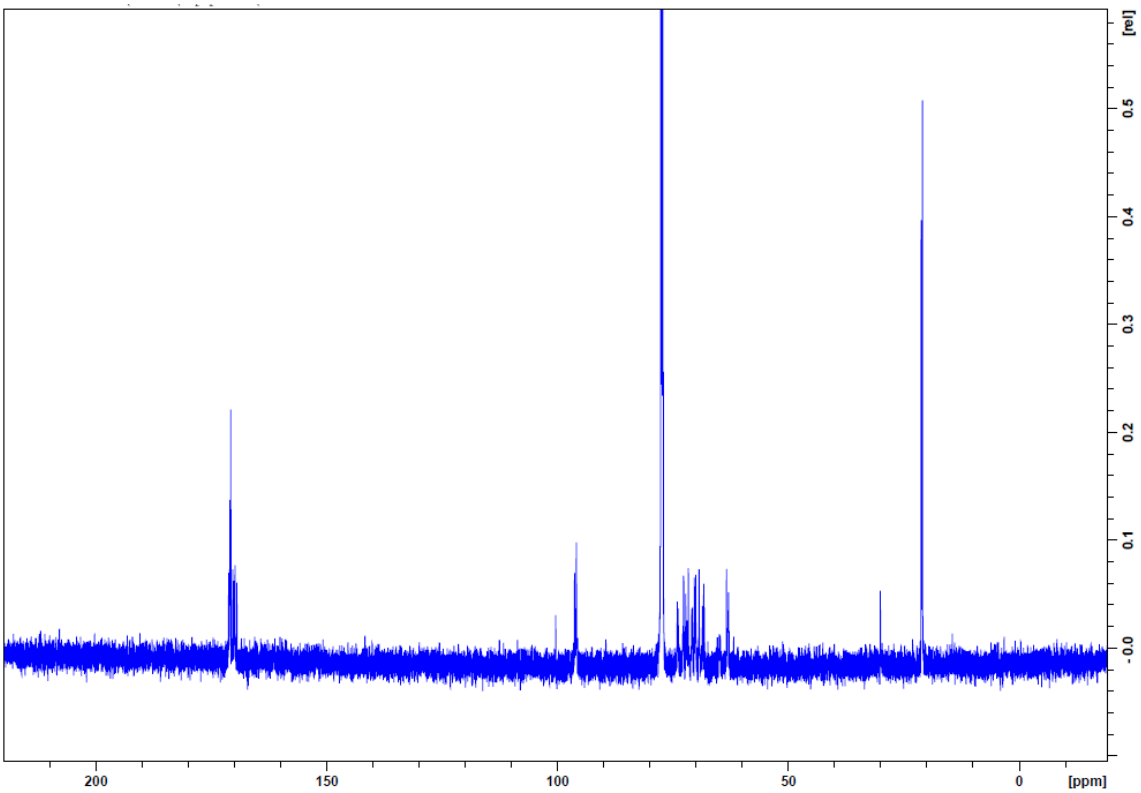

Figure F.2.14: Carbon spectrum for PB7 peracetate. An acetone peak is visible at δ_C 30.1 ppm (Fulmer *et al.*, 2010).

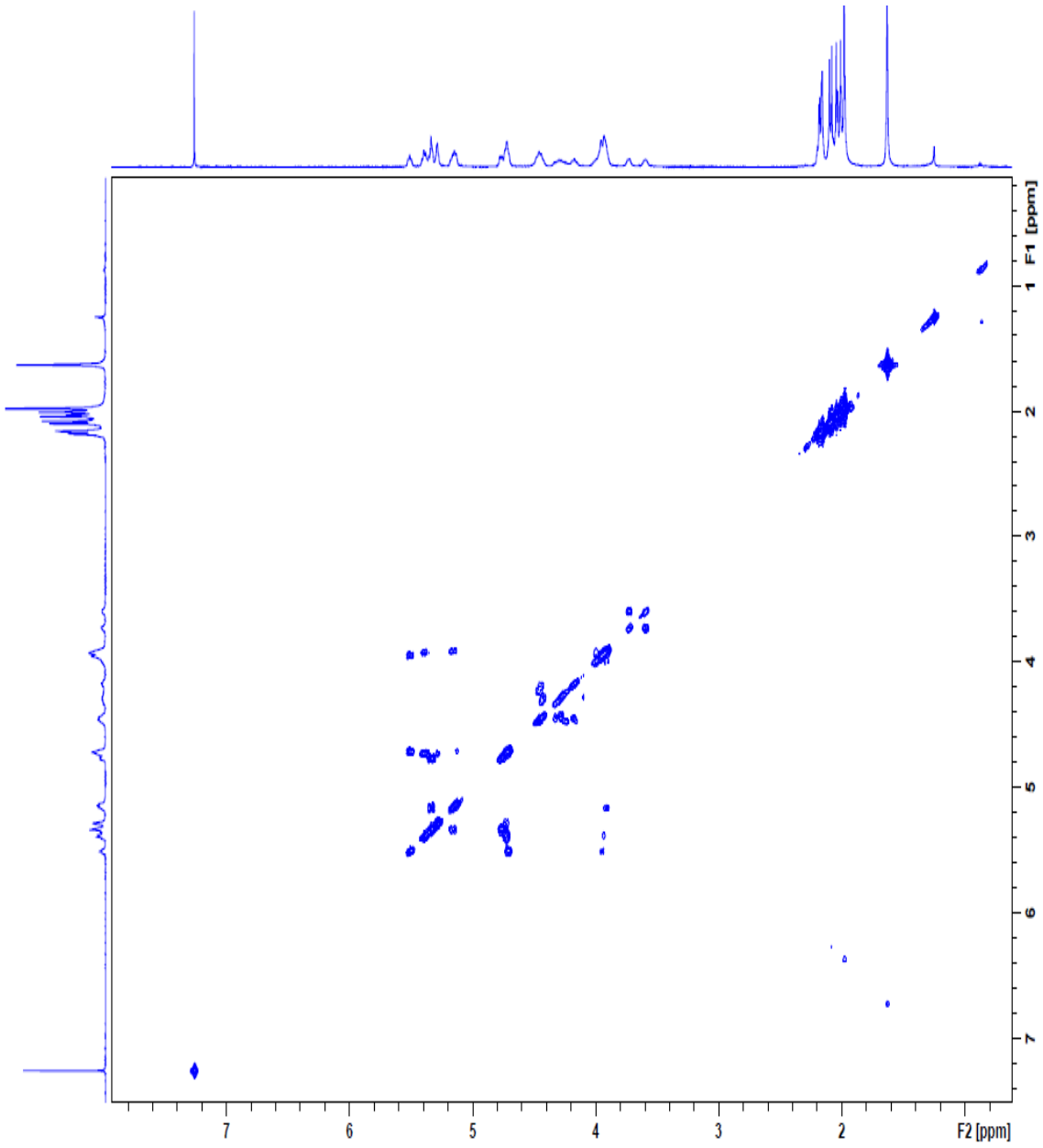

Figure F.2.15: COSY spectrum of PB7 peracetate.

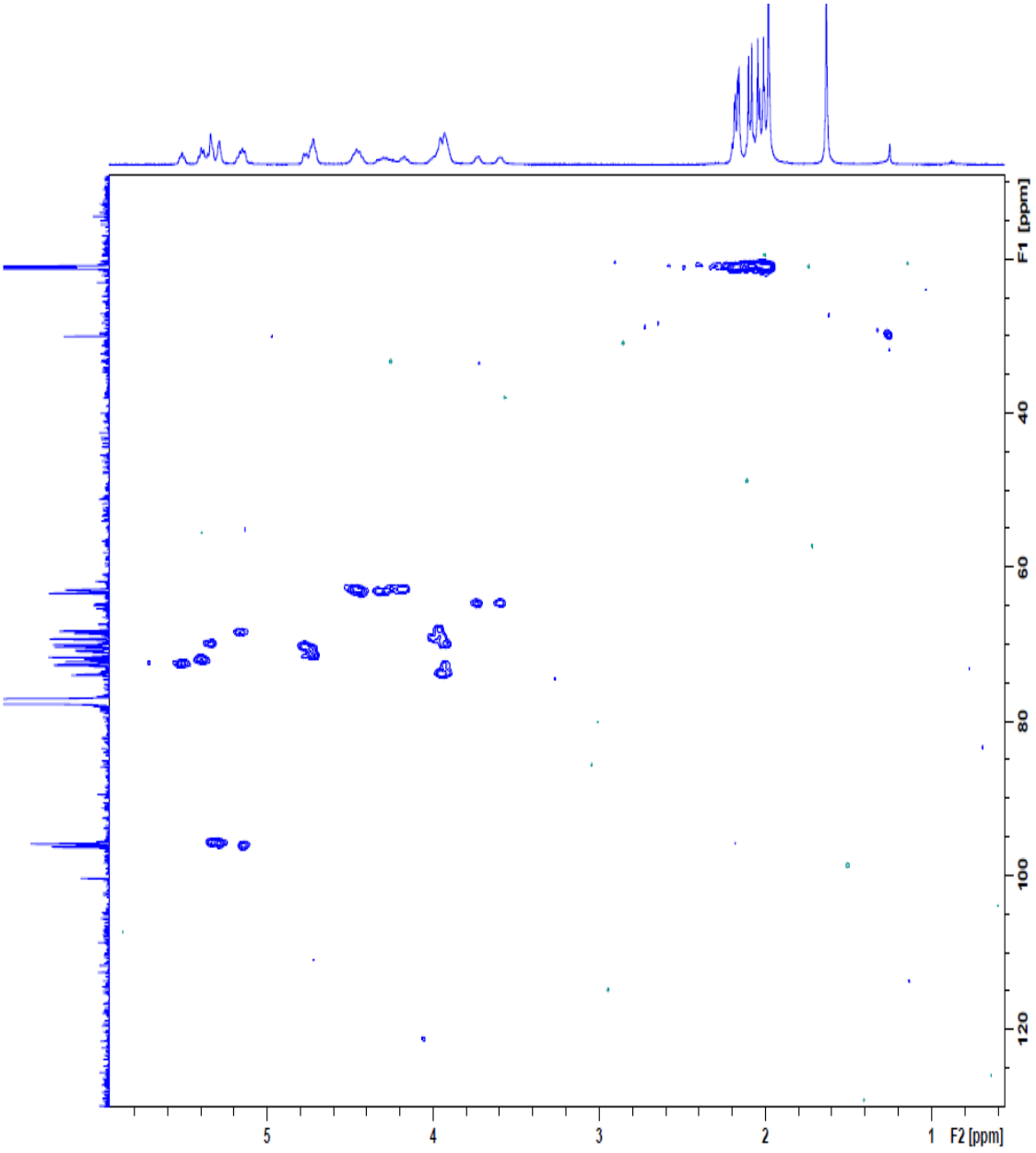

Figure F.2.16: HSQC spectrum of PB7 peracetate. There is a correlation between the acetone peak at δ_C 30.1 ppm and the singlet at δ_H 1.25 ppm.

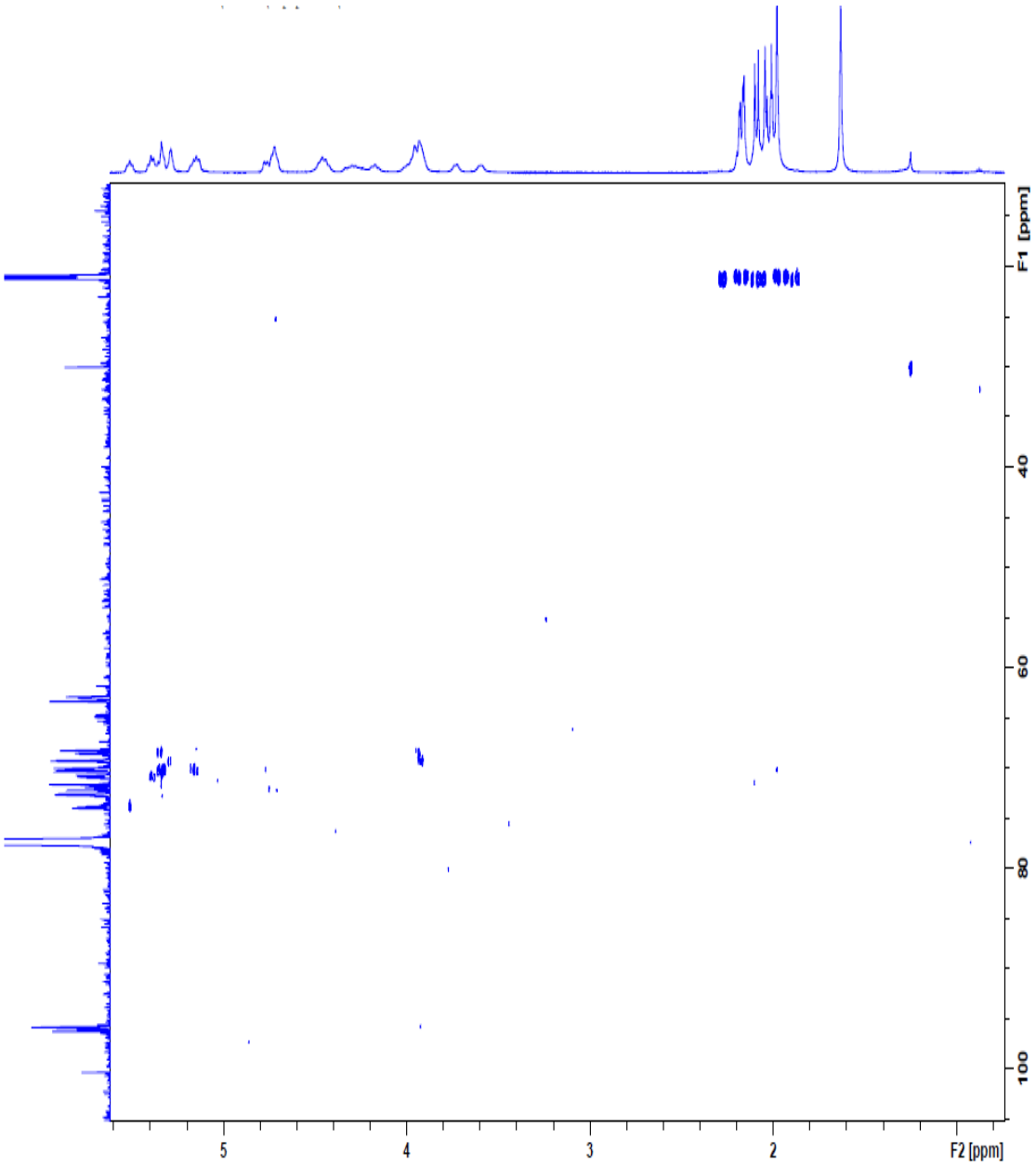

Figure F.2.17: HMBC spectrum of PB7 peracetate. There is a correlation between the acetone peak at δ_C 30.1 ppm and the singlet at δ_H 1.25 ppm.

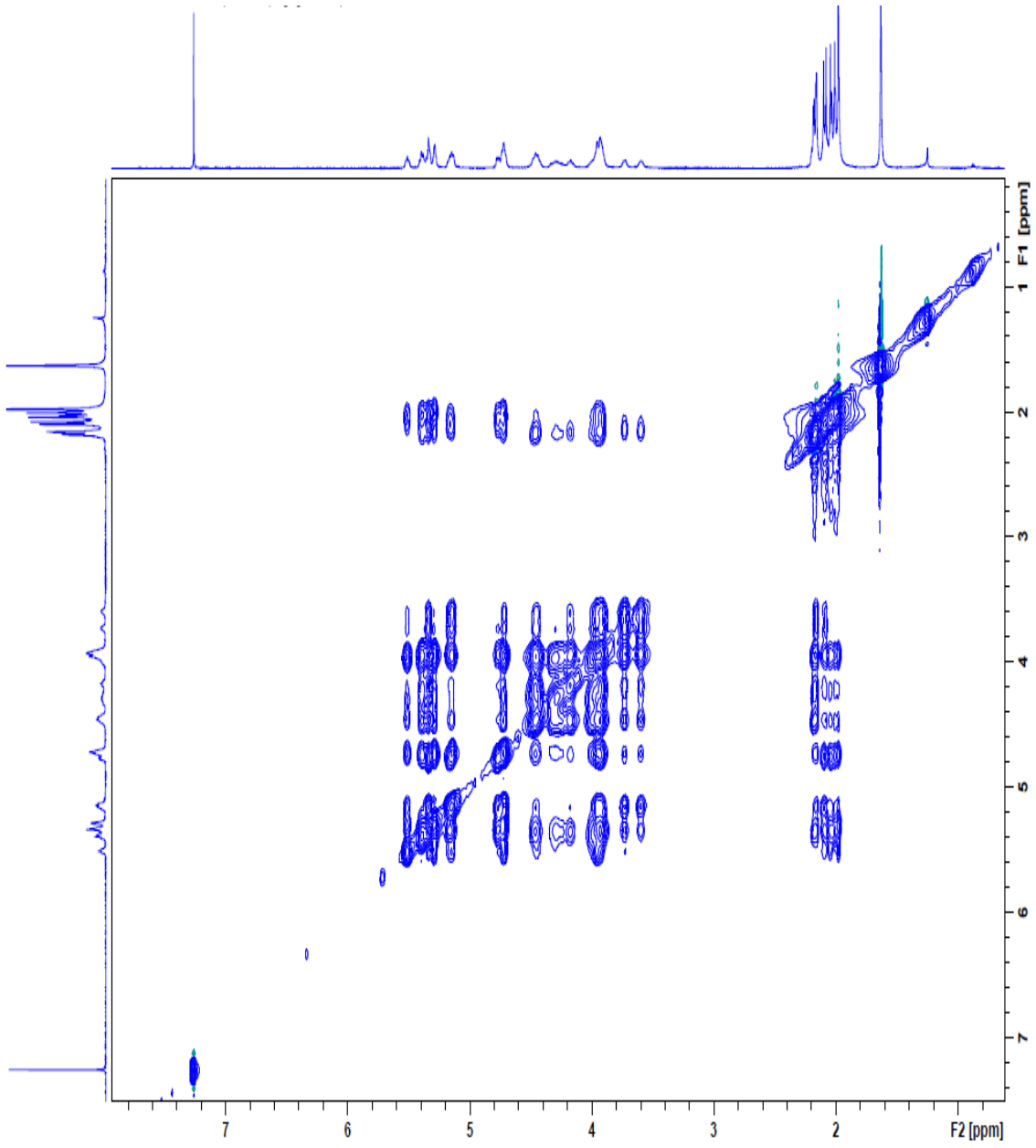

Figure F.2.18: NOESY spectrum of PB7 peracetate.

F.2.4 FB2 peracetate

The NMR spectra for the crude FB2 peracetate sample are presented. The sample was dissolved in $CDCl_3$. All proton spectra were recorded at 600 MHz and all carbon spectra were recorded at 151 MHz.

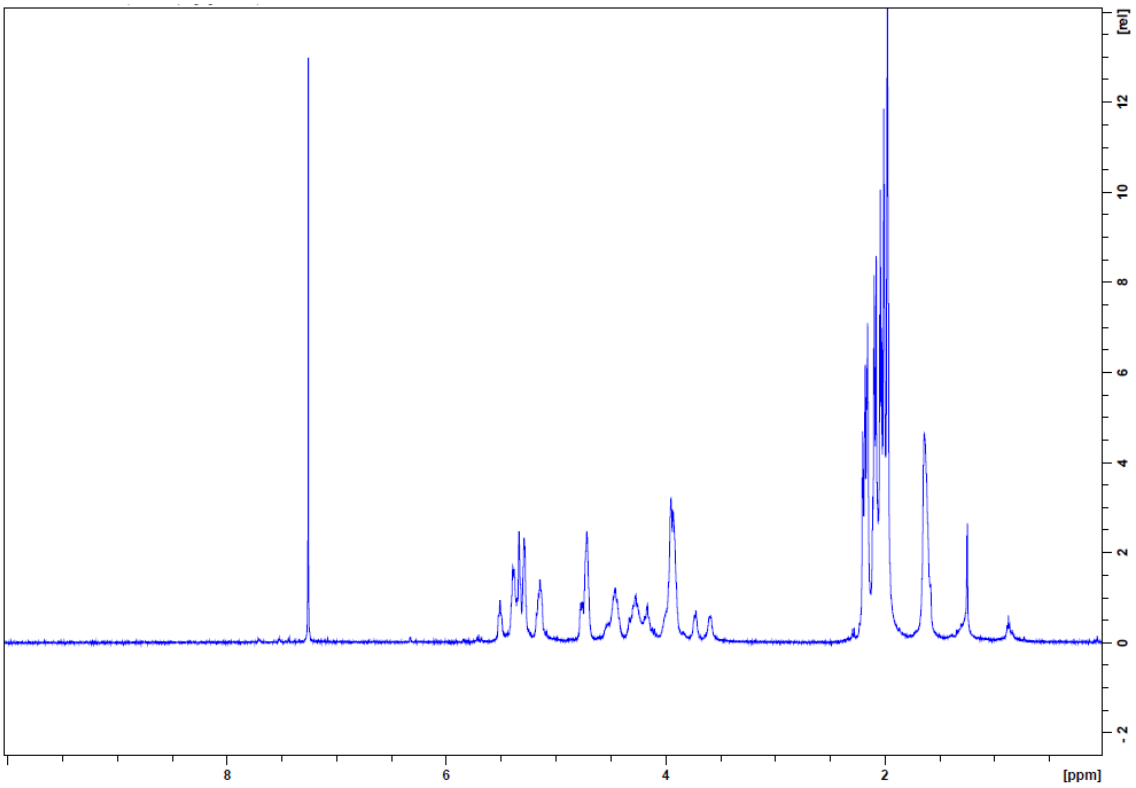

Figure F.2.19: Proton spectrum of FB2 peracetate. A water (OH) and/or acetate (OAc) anomeric peak is detected at δ_H 1.66 ppm (Farkas *et al.*, 1997; Fulmer *et al.*, 2010). Another peak is visible at δ_H 1.25 ppm, found to have an HSQC correlation with the acetone peak at δ_C 30.1 ppm (Figure F.2.22).

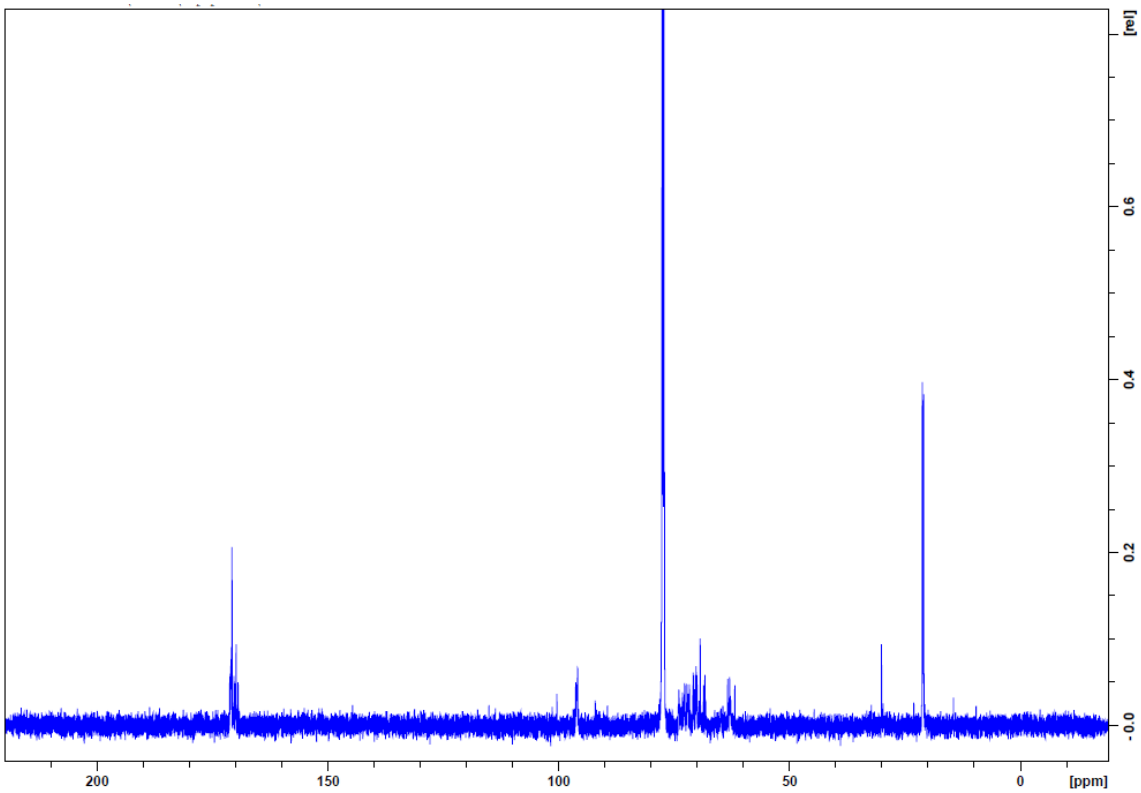

Figure F.2.20: Carbon spectrum of FB2 peracetate. An acetone peak is visible at δ_C 30.1 ppm (Fulmer *et al.*, 2010).

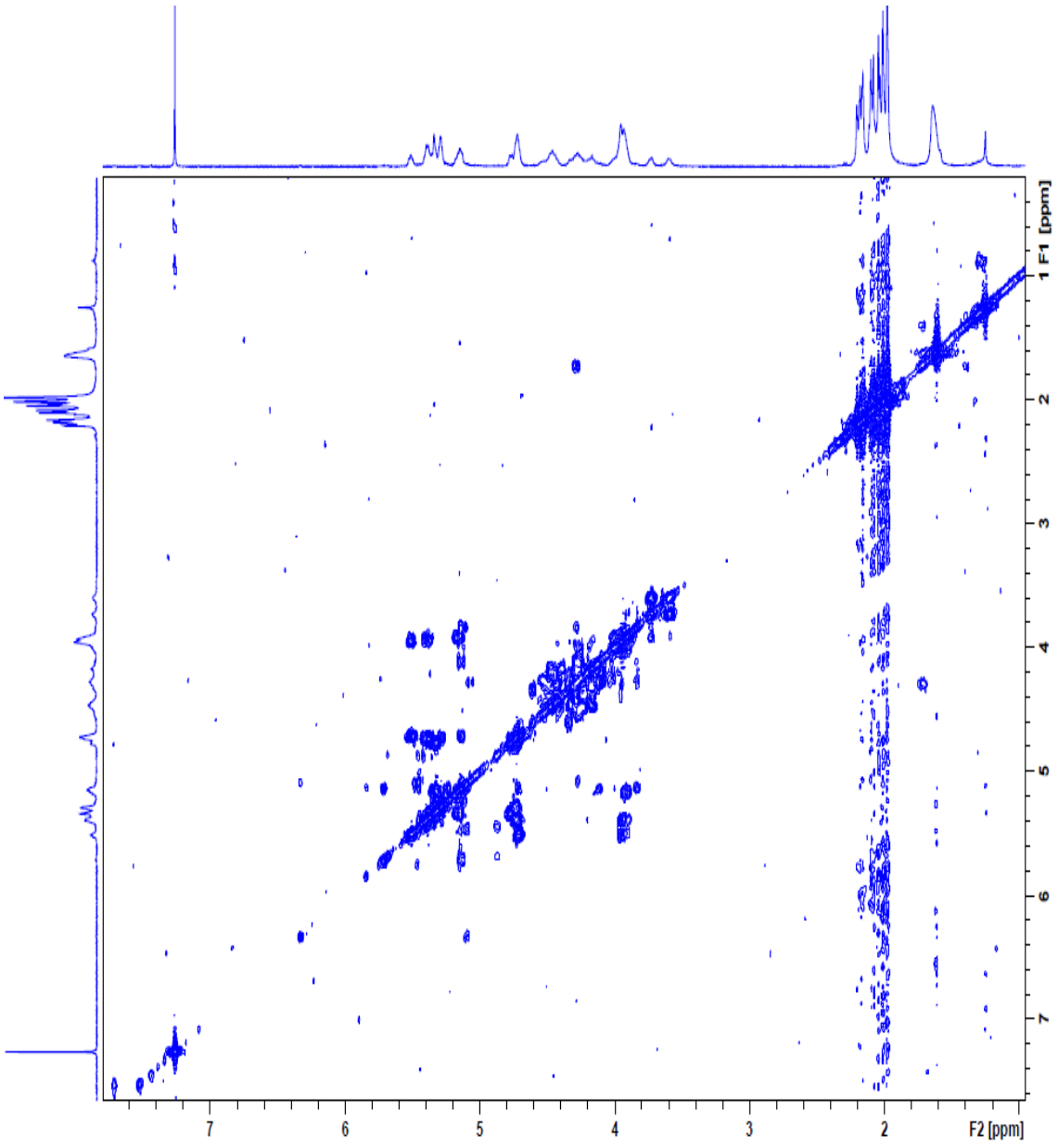

Figure F.2.21: COSY spectrum of FB2 peracetate.

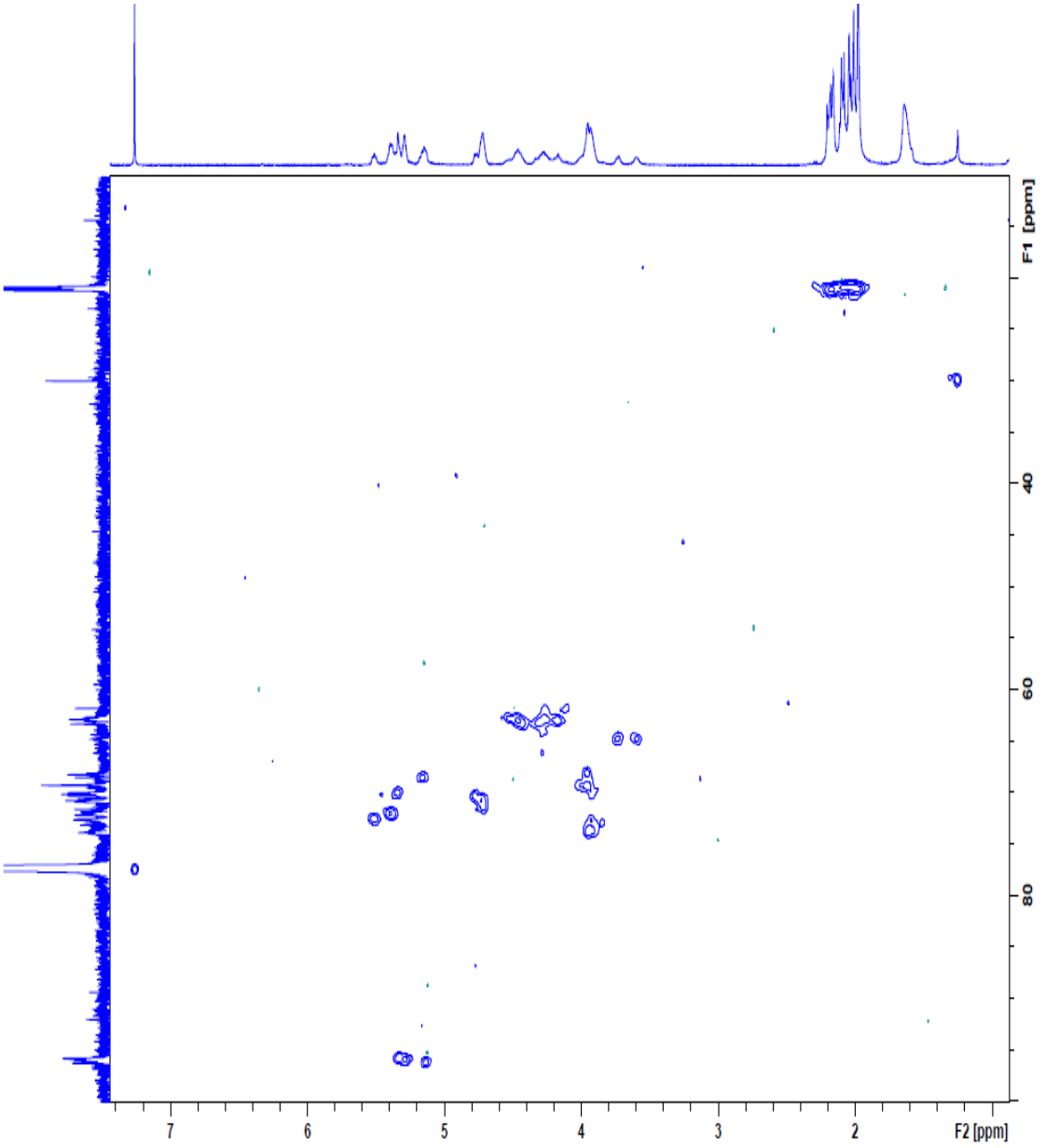

Figure F.2.22: HSQC spectrum of FB2 peracetate. There is a correlation between the acetone peak at δ_C 30.1 ppm and the singlet at δ_H 1.25 ppm.

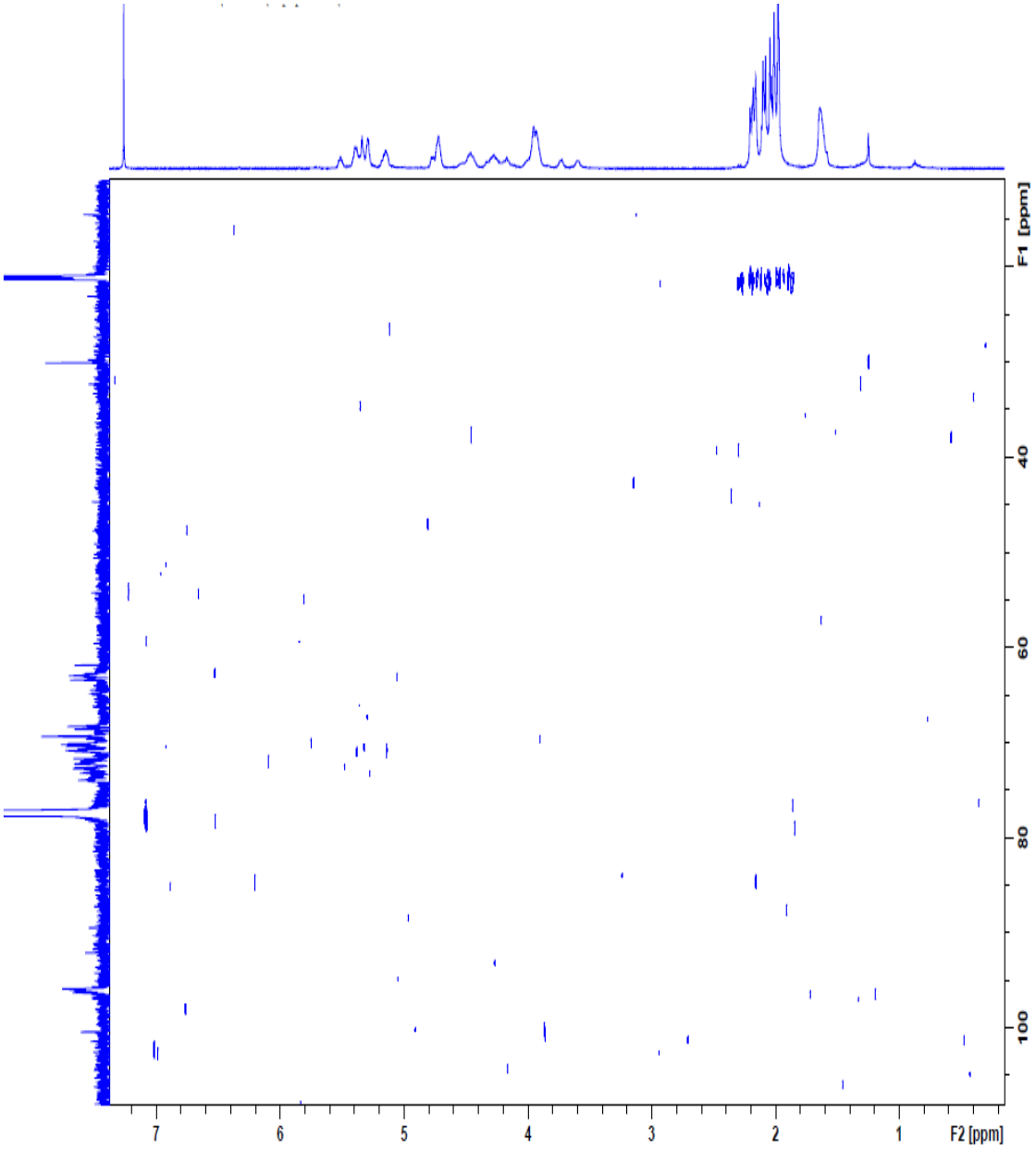

Figure F.2.23: HMBC spectrum of FB2 peracetate.

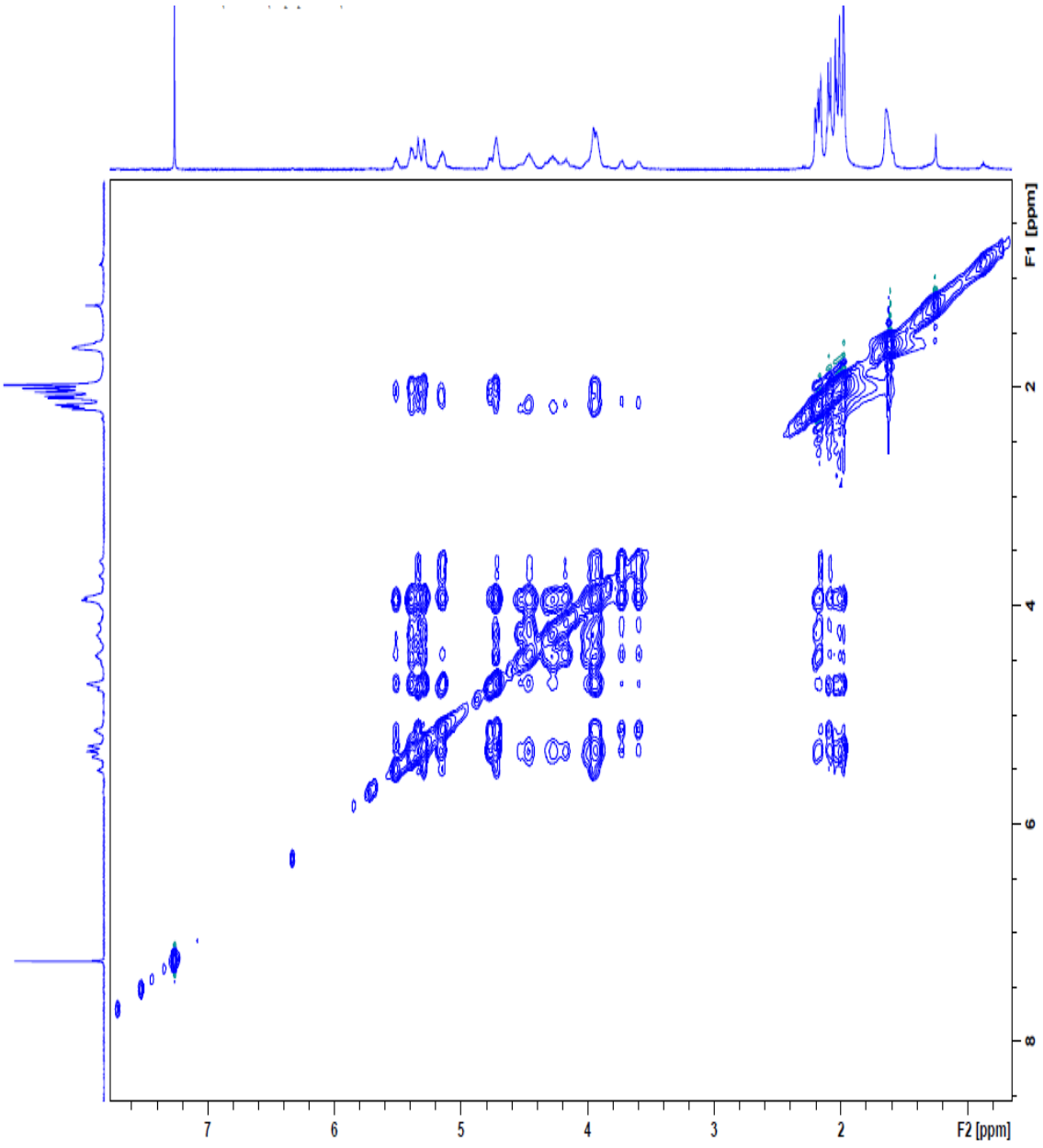

Figure F.2.24: NOESY spectrum of FB2 peracetate.

Discussion on the impurities in the $CDCl_3$ NMR analyses

In the NMR analyses of the peracetylated samples in $CDCl_3$, several impurity peaks were detected. In the ^1H NMR spectra of both the pullulan and EPS peracetates there were singlets appearing at δ_H 1.66, 1.25 and 0.89 ppm. In the ^{13}C spectra, an impurity peak due to acetone was present at δ_C 30.1 ppm (Fulmer *et al.*, 2010). It was established that the resonance at δ_H 1.66 ppm was due to either water (OH) and/or acetate (OAc) anomeric peaks (Farkas *et al*., 1997; Fulmer *et al*., 2010). HSQC (PB7 and FB2) and HMBC (PB7) correlations between δ_C 30.1 ppm and δ_H 1.66 ppm indicated that the latter resonance belongs to acetone. The most upfield resonance (and smallest impurity) is likely due contaminants such as pump oil, grease, ethane, *n*-hexane or *n*-propane (Fulmer *et al*., 2010). Since the intensity was so small, the possible related δ_C resonances could not be detected, and the nature of the impurity could not be confirmed. Most of the impurities identified from the D_2O analyses were also absent, hence the glassware used in the sample preparation was the most likely source of those impurities. Furthermore, the impurities identified in the $CDCl_3$ analyses had no bearing on the assessment of the polysaccharide structures.

F.3 Estimation of the repeat sequence ratios from nuclear magnetic resonance data

Together with the areas of the anomeric protons of A, B and C, the area attributable to all possible malto-oligomers within the repeating subunits were calculated in relation to maltotriose.

Repeat sequence ratio

It is apparent from the spectra of both the crude and the fractionated EPS samples, that the *P. sacchari* polysaccharides all contain DP3, DP4, and possibly > DP4 repeat sequences. In order to calculate the percentage of DP4 and > DP4 in each sample, the method as described by Delben and co-workers was used (2006). Together with the ^1H NMR data, the areas occupied by the anomeric protons were investigated. For all calculations, the areas of peaks due to the resonance of the anomeric protons for the $A + A'$ (Area_A), and $C + C'$ (Area_C) were assumed to be equal for any malto-oligosaccharide sequence. Thus, the average area (Area_{AC}) can be found by the following expression:

$$\mathrm{Area}_{AC} = \frac{1}{2}[\mathrm{Area}_A + \mathrm{Area}_C] \tag{7.3}$$

Since the resonances for the B, B' and B'' anomeric protons all occur at about 5.39 ppm, and since the area in addition to unity at this signal is indicative of the percentage DP4 (or > DP4) in the polysaccharides, the percentage X can be found as follows:

$$X = 100\frac{[\mathrm{Area}_B - \mathrm{Area}_{AC}]}{\mathrm{Area}_{AC}} \tag{7.4}$$

where Area_B is the peak area for the anomeric proton resonances for B, B' and B''. But since the peaks for B, B' and $B''$and $A + A'$overlap extensively, X was found as follows, instead.

$$X = 100\frac{[\text{Area}_{AB} - 2\text{Area}_C]}{\text{Area}_C} \quad (7.5)$$

where Area_{AB} is the total area for the B, B' and B, and A and A' peaks. The results for pullulan, and all the *P. sacchari* EPS samples are shown in Table F.3.1.

Table F.3.1 Calculated value for the area percent (X) of the DP4 and >DP4 contribution in each of the repeat sequences of pullulan, FB2 F1, FB2 F2, and the crude FB2, PB2 and PB7 *P. sacchari* EPSs.

Sample	$Area_{AB}$	$Area_C$	X /%
Pullulan	2.0112	1.000	1.1
FB2 F1	3.3479	1.000	134.8
FB2 F2	3.3899	1.000	139.0
FB2	3.7151	1.000	171.5
PB7	2.5625	1.000	56.3
PB2	2.7782	1.000	77.8

From Table F.3.1, the calculated value of the DP4 portion in the pullulan sample is 1.1%. This amount is well within 7% for pullulans from *A. pullulans*. The calculated results for FB2 F1 (134.8%) and FB2 F2 (139.0%) reveal that there is a vast abundance of DP4 and > DP4 subunits in the purified EPSs, far in excess of pullulan. The distribution and quantitation of these higher malto-oligosaccharides were determined by enzymatic-HPLC analysis (see Section 5.4)

F.4 References

Anonymous (2006). Material safety and data sheet: Extran(R) MA02. 1-6.

Delben F, Forabosco A, Guerrini M, Liut G and Torri G (2006). Pullulans produced by strains of *Cryphonectria parasitica*-II. Nuclear magnetic resonance evidence. *Carbohydrate Polymers*. **63** 545-554.

Farkas E, Janossy L, Harangi J, Kandra L and Liptak A (1997). Synthesis of chromogenic substrates of a-amylases on a cyclodextrin basis *Carbohydrate Research*. **303** 407-415.

Fulmer GR, Miller AJM, Sherden NH, Gottlieb HE, Nudelman A, Stoltz BM, Bercaw JE and Goldberg KI (2010). NMR Chemical shifts of trace impurities: Common laboratory solvents, organics, and gases in deuterated solvents relevant to the organometallic chemist. *Organometallics*. **29** (9):2176-2179.

Appendix G
Enzymatic analysis: data and chromatograms

This Appendix provides the enzymatic analysis data and HPLC chromatograms used for pullulan and the EPS samples. The Appendix is divided into two main sections – one section for each set of enzyme experiments carried out; namely, E1 and E2.

G.1 Enzyme treatment E1

The calibration data, recovery of pullulan, determination of mannose and galactose and the relevant chromatograms for the E1 experiments are found in the sections that follow.

G.1.1 Calibration data

The DP3 and DP4 calibration data is found in Table G.1.1 and the calibration curves are found in Figure G.1.1.

Table G.1.1 Calibration data for maltotriose and maltotetraose.

Standard	Average Height /mV	Concentration /mg L^{-1}	Average RF /mV L mg^{-1}	R^2
DP3	67.575	25	2.703	0.9969
	266.800	100	2.668	
	536.996	200	2.685	
	983.096	400	2.458	
	1202.253	500	2.405	
DP4	108.715	50	2.174	0.9968
	215.928	100	2.159	
	380.324	200	1.902	
	705.147	400	1.763	
	844.851	500	1.690	

RF – response factor, R^2 – coefficient of determination,
DP3 – maltotriose, DP4 – maltotetraose

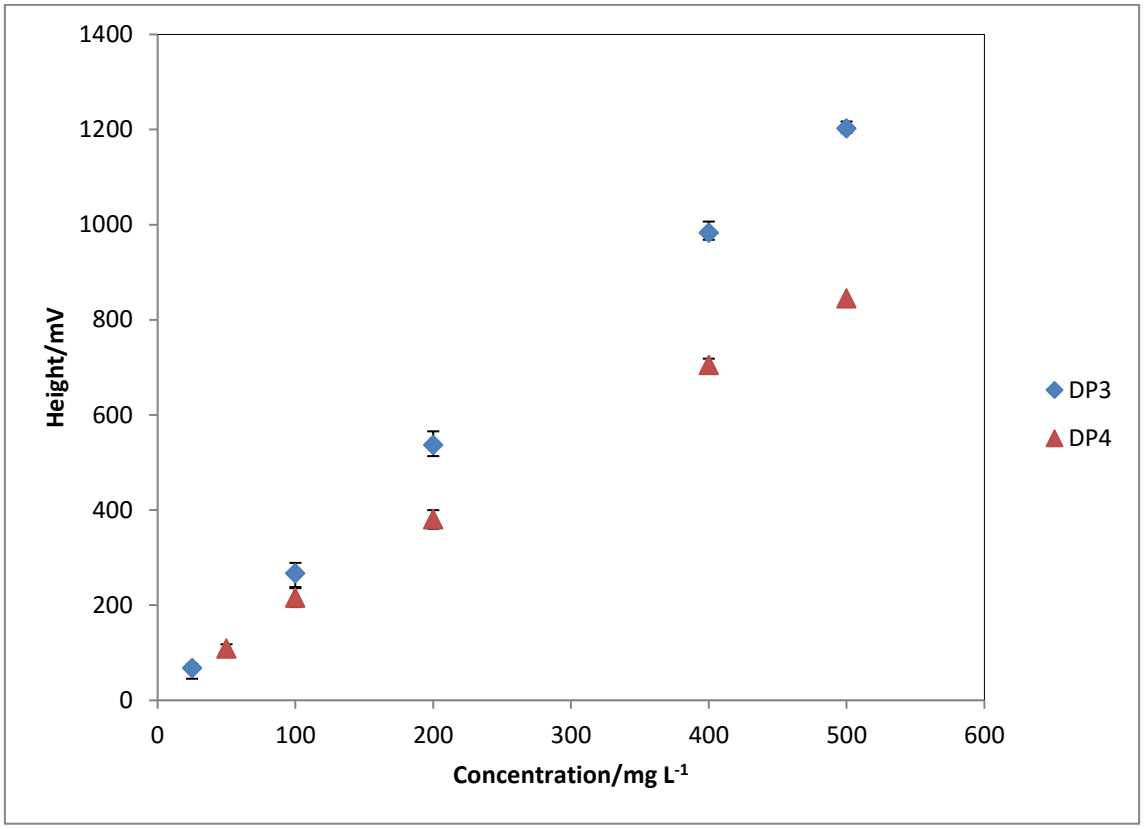

Figure G.1.1: Calibration curves for maltotriose (DP3) and maltotetraose (DP4). The average height and standard error of the duplicate injections are depicted.

The calibrations for DP3 (25 – 500 mg L^{-1}) and DP4 (50 – 500 mg L^{-1}) were carried out in duplicate. The calibrations are found to be linear across the range investigated, with an acceptable coefficient of variation (R^2) of 0.997. The average response factor (RF) for each of the standards were then used to quantify the DP3 and DP4 hydrolysate products in pullulan, FB2 F1 and FB2 F2 after reaction with the E1 pullulanase. The next section provides the pullulan recovery data, the estimation of mannose and galactose in FB2 F1, as well as the chromatograms for some of the standards and the samples analysed.

G.1.2 Pullulan recovery

The pullulan recovery data is provided in Table G.1.2. The result provides that the E1 pullulanase effectively hydrolysed the pullulan samples after 19 hours of incubation, with a recovery of 101.9 ± 1.7%.

Table G.1.2 Recovery data for the pullulan samples hydrolysed with E1 pullulanase for 19 hours.

Pullulan Sample	Concentration /mg L^{-1}	Height DP3/mV	RF /mV L mg^{-1}	Recovery DP3 /mg L^{-1}	Recovery DP3/%
A1	428	1062.249	2.458	432	101.0
A2	428	1059.232	2.458	431	100.7
B1	404	1009.712	2.458	411	101.7
B2	404	1011.191	2.458	411	101.8
C1	220	611.593	2.685	228	103.5
C2	220	618.970	2.685	231	104.8
E	260	698.462	2.685	260	100.1
Average					**101.9**
Standard deviation					**1.7**
Relative standard deviation					**1.6**

RF – response factor, DP3 – maltotriose, DP4 – maltotetraose

G.1.3 Mannose and galactose determination

The GC-MS composition and structure analysis of FB2 F1 revealed that the sample contains mannose (Man) and galactose (Gal) components. A 50 mg L^{-1} standard of mannose and a 25 mg L^{-1} standard of galactose were prepared in deionised water and analysed alongside all the samples to confirm their presence. The retention times of these components are within the region where the pullulanase matrix appears and so accurate quantitation posed a challenge. Furthermore, a full set of calibration standards was not prepared. However, the relative amounts of these components were estimated. To do so, the change in the respective peak heights from the pullulanase blank and hydrolysed pullulan samples, to that of FB2 F1 and FB F2 was determined. This section provides the relevant chromatograms and a summary of these results.

For the following chromatograms, peaks that were identified against authentic standards include man, gal, maltose (DP2), maltotriose (DP3), maltotetraose (DP4), maltopentaose (DP5), maltohexaose (DP6) and maltoheptaose (DP7). Maltooctaose (DP8), maltononaose (DP9) and maltodecaose (DP10) are inferred in the elution profiles. The insert in each chromatogram provides the corresponding retention times and integrated peak heights for the identified components.

The Man and Gal peaks were found to co-elute in the region of the enzyme matrix. To estimate the quantity of these components present in the samples, their height differences to the enzyme peaks were compared. From the GC-MS data, FB2 F1 is the only sample expected to contain quantifiable amounts of these monosaccharides. The HPLC chromatograms confirm that FB2 F1 (Figure G.1.6) is the only sample with increased peak heights in the enzyme matrix region. The average heights of the coinciding peaks for Man and Gal were determined for the enzyme blank and pullulan (Table G.1.3). The Man and Gal peak heights in FB2 F1 were then corrected, by subtracting the average heights from Table G.1.3. The results in Table G.1.4 provide that FB2 F1 contains 1.8% Man and 19.9% Gal. The value for Gal approximates the result as determined by NMR (refer to Section 5.3.2). However, the value for Man is underestimated as the result obtained by NMR suggests that there is ~10% present in FB2 F1 (refer to Section 5.3.2). If it were necessary to determine these components more accurately, then the samples would have to

be subjected to a cleanup step prior to analysis. For example, microdialysis could be used to remove the enzyme matrix from the samples prior to HPAEC-PAD analysis (Nilsson *et al.*, 2001; Torto *et al.*, 2000). Nonethless, addition of the accounted for Gal, Man and glucan components increases the pullulanase hydrolysis efficiency from 66.3% to 86.2% (refer to Section 5.4.1). Addition of the anticipated Man deficit of ~8.2% increases the total hydrolysis to ~94.4% for FB2 F1.

Table G.1.3 Average heights determined in the mannose and galactose region where the enzyme peak co-elutes.

Sample	Galactose or Enzyme /mV	Mannose or Enzyme /mV
Enzyme blank	1087.436	36.301
Pullulan	1031.428	28.389
Average	1059.432	32.345

Table G.1.4 The estimated amount of mannose and galactose determined in FB2 F1 through correcting the peak heights for the co-eluting average heights of the enzyme matrix.

Component	Total peak height /mV	Corrected peak height /mV	RF /mV L mg^{-1}	Amount /mg L^{-1}	Total DPs /mg L^{-1}	Relative amount /%
Mannose	67.53	35.185	4.697	7.5	414	1.8
Galactose	1858.85	799.418	9.715	82.3	414	19.9

G.1.4 High performance liquid chromatograms

The HPAEC-PAD chromatograms for mannose, galactose, enzyme blank, one pullulan and each EPS sample can be seen in Figure G.1.2 to Figure G.1.7. Also provided is one each of the DP3 and DP4 chromatograms (see Figure G.1.8 and Figure G.1.9). The table insert in each chromatogram provides the retention times and integrated heights for each identified component.

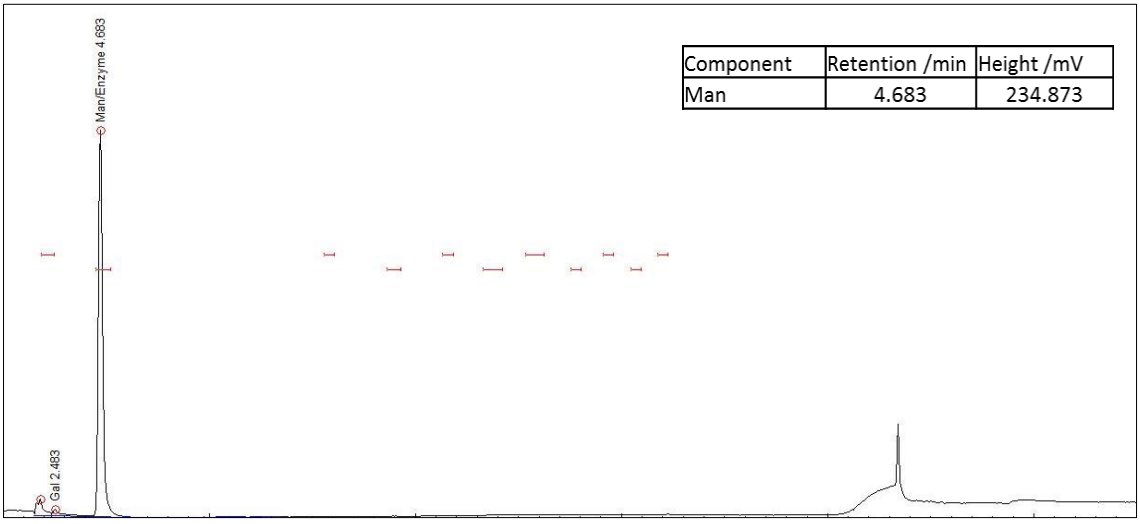

Figure G.1.2: A chromatogram of 50 mg L^{-1} mannose (Man) in deionised water shown to elute in the region of the enzyme matrix. The response factor (RF) is found to be 4.697 mV L mg^{-1}. The area displayed is 0-55 minutes, and 80-400 mV.

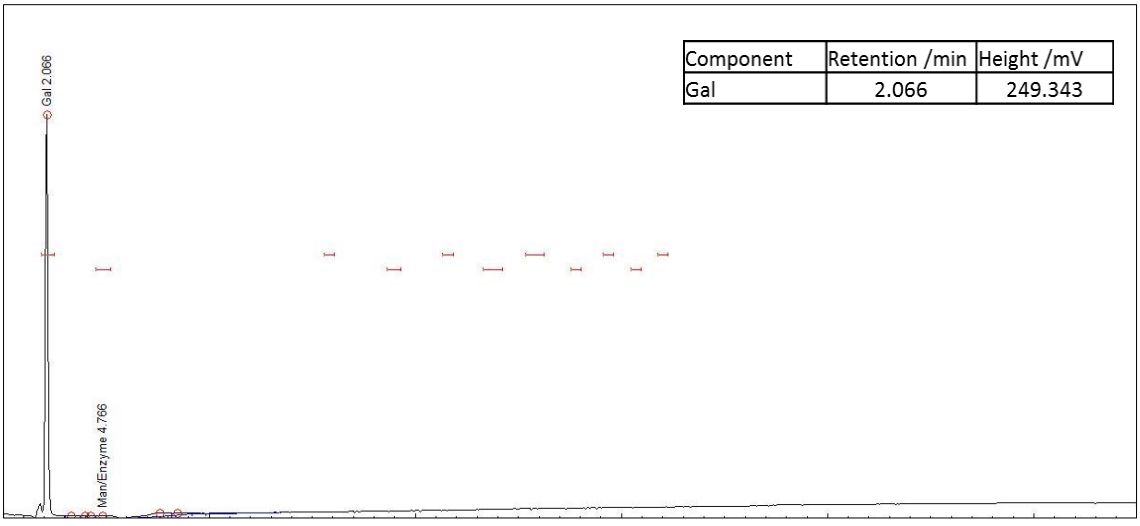

Figure G.1.3: A chromatogram of 25 mg L^{-1} galactose (Gal) in deionised water shown to elute in the region of the enzyme matrix. The response factor (RF) is found to be 9.715 mV L mg^{-1}. The area displayed is 0-55 minutes, and 80-400 mV.

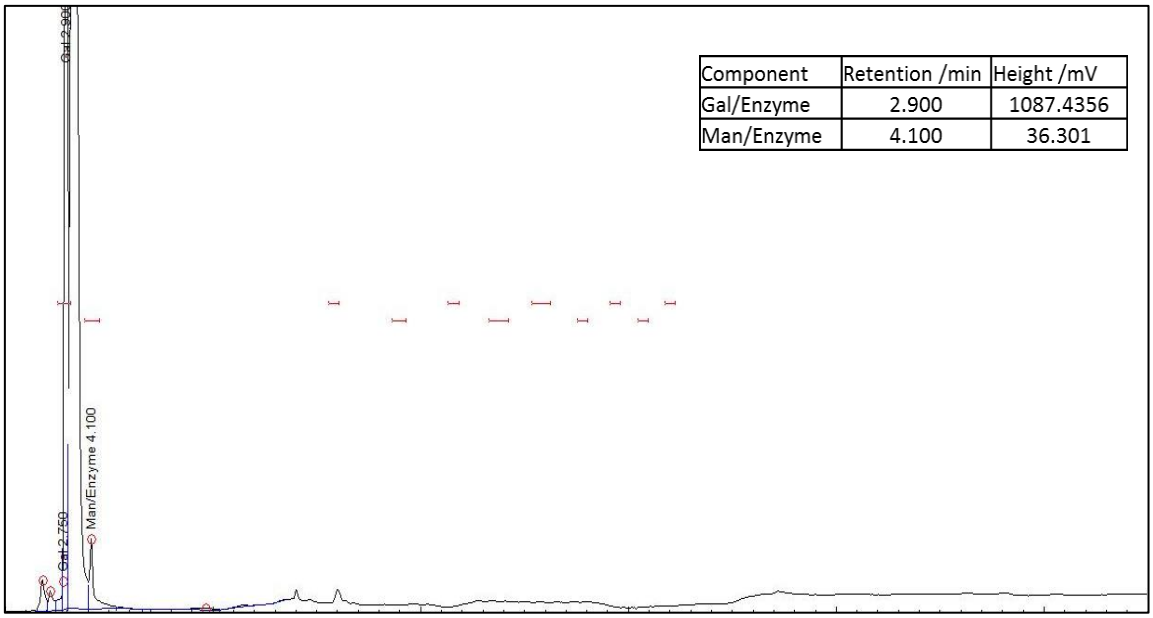

Component	Retention /min	Height /mV
Gal/Enzyme	2.900	1087.4356
Man/Enzyme	4.100	36.301

Figure G.1.4: Blank sample containing only E1 pullulanase. The blank was incubated along with the samples. It appears that two of these matrix peaks coincide with galactose (Gal) and mannose (Man) as indicated. The area displayed is 0-55 minutes, and 80-400 mV.

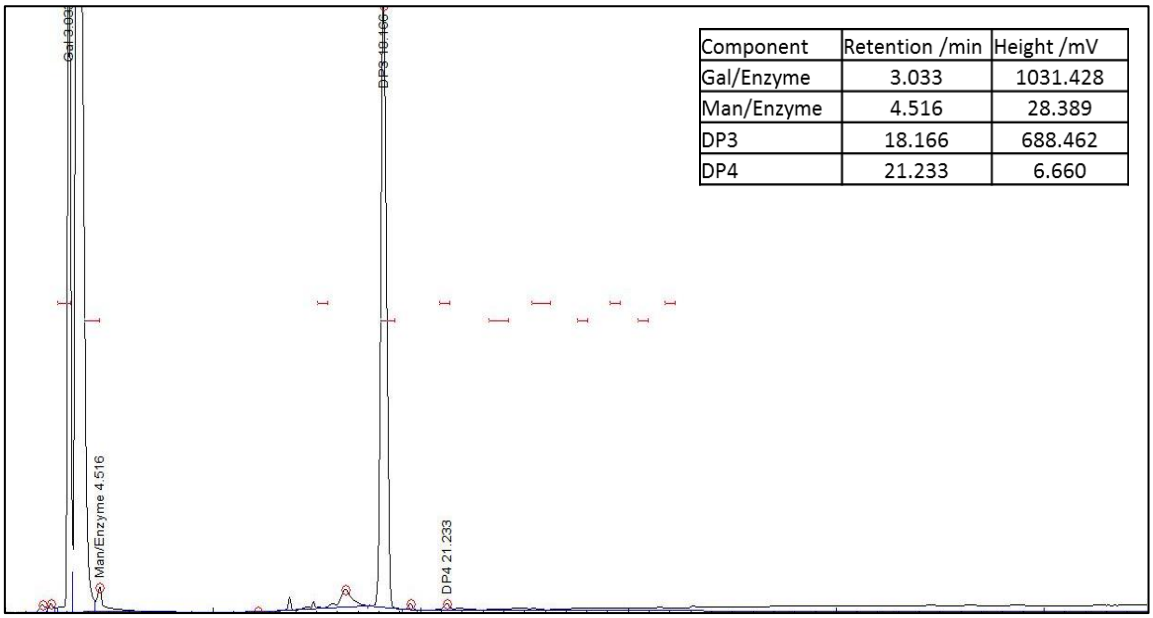

Component	Retention /min	Height /mV
Gal/Enzyme	3.033	1031.428
Man/Enzyme	4.516	28.389
DP3	18.166	688.462
DP4	21.233	6.660

Figure G.1.5: Chromatogram of 260 mg L^{-1} pullulan treated with E1 pullulanase. It appears that two of the enzyme matrix peaks coincide with galactose (Gal) and mannose (Man) as indicated. DP3 and DP4 peaks are also detected and integrated. The area displayed is 0-55 minutes, and 80-800 mV.

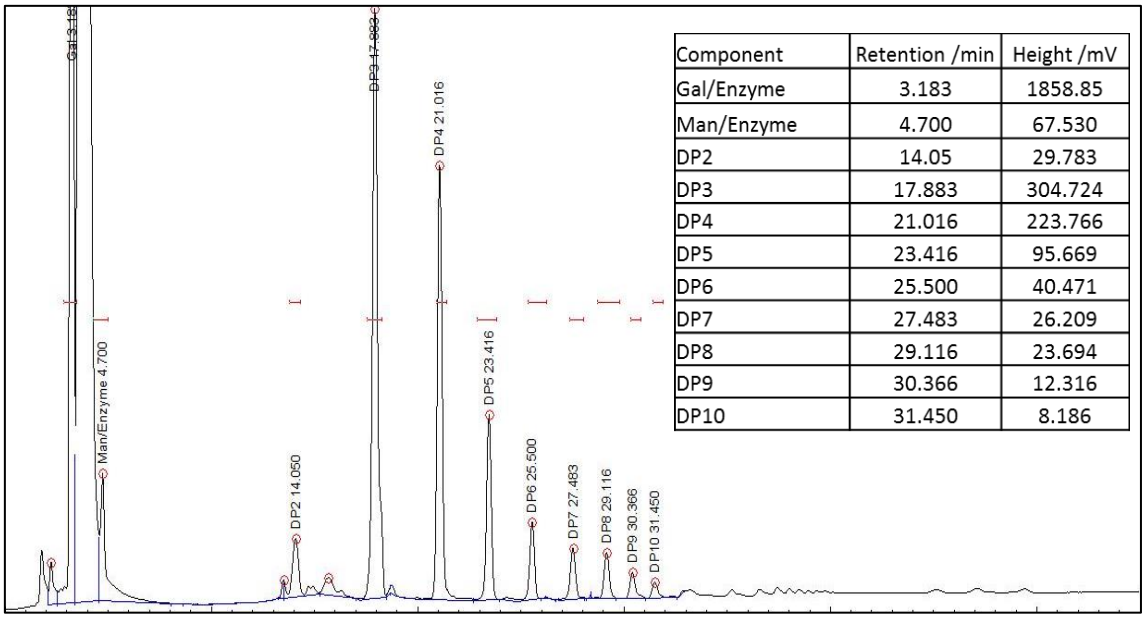

Component	Retention /min	Height /mV
Gal/Enzyme	3.183	1858.85
Man/Enzyme	4.700	67.530
DP2	14.05	29.783
DP3	17.883	304.724
DP4	21.016	223.766
DP5	23.416	95.669
DP6	25.500	40.471
DP7	27.483	26.209
DP8	29.116	23.694
DP9	30.366	12.316
DP10	31.450	8.186

Figure G.1.6: The FB2 F1 fraction treated with E1 pullulanase. The area shown is 0-55 minutes and 80-400 mV.

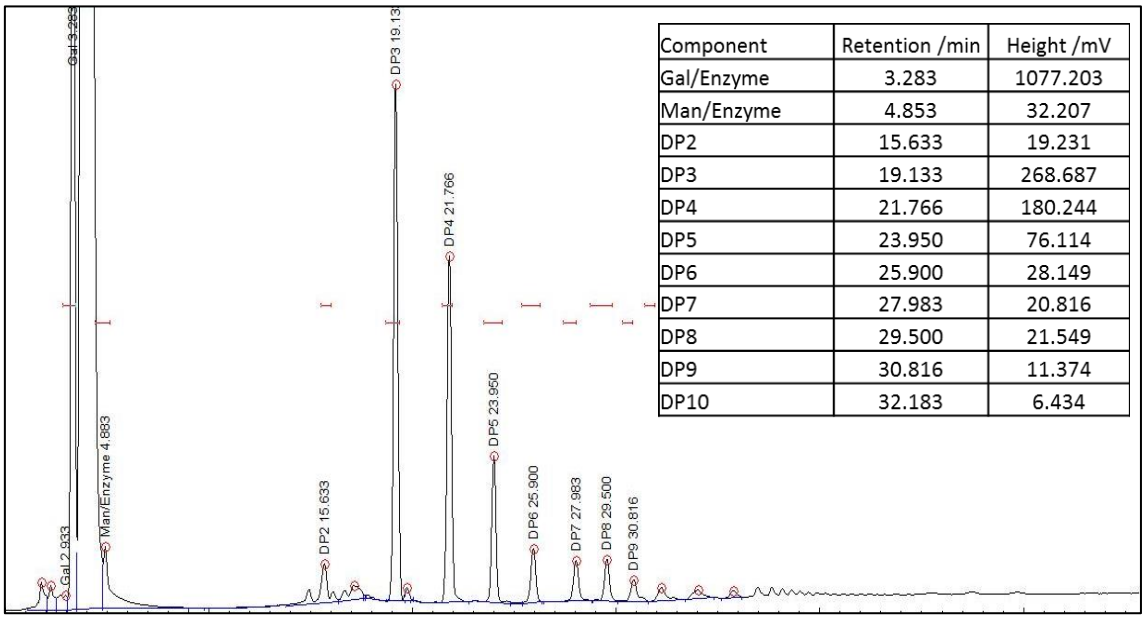

Component	Retention /min	Height /mV
Gal/Enzyme	3.283	1077.203
Man/Enzyme	4.853	32.207
DP2	15.633	19.231
DP3	19.133	268.687
DP4	21.766	180.244
DP5	23.950	76.114
DP6	25.900	28.149
DP7	27.983	20.816
DP8	29.500	21.549
DP9	30.816	11.374
DP10	32.183	6.434

Figure G.1.7: The FB2 F2 fraction treated with E1 pullulanase. The area shown is 0-55 minutes and 80-400 mV.

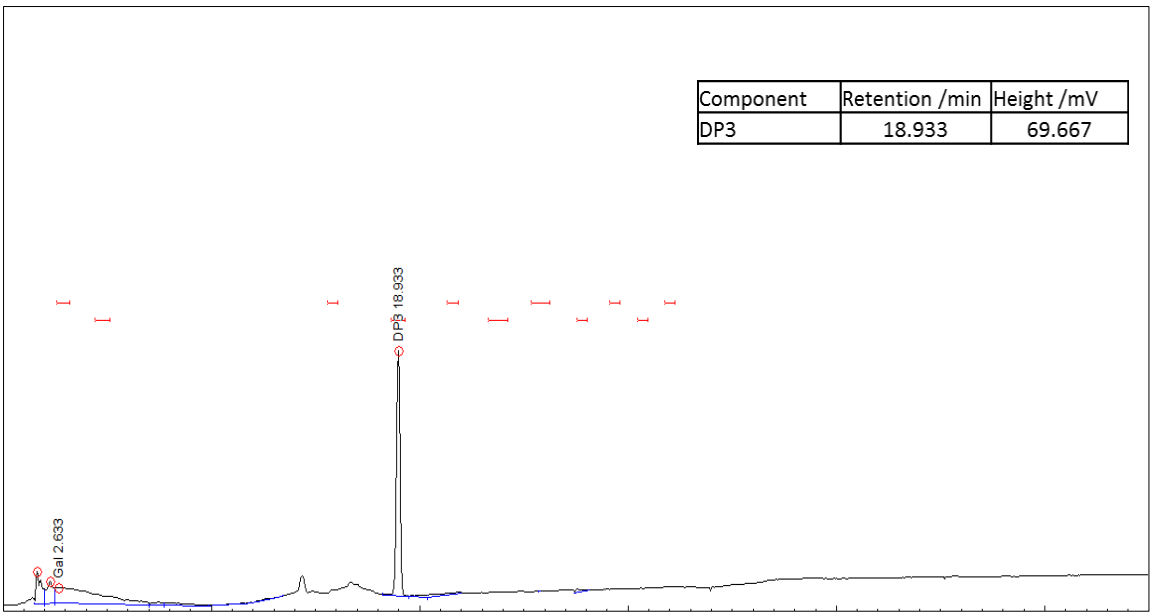

Figure G.1.8: A chromatogram of 25 mg L^{-1} maltotriose (DP3) in deionised water. The area displayed is 0-55 minutes, and 80-250 mV.

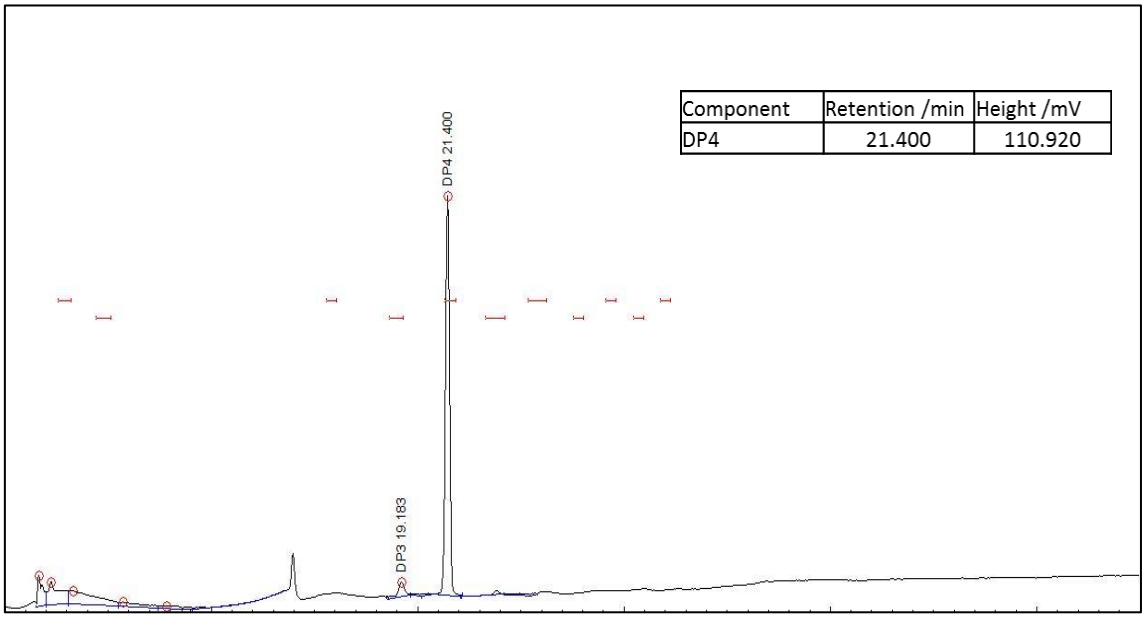

Figure G.1.9: A chromatogram of 50 mg L^{-1} maltotetraose (DP4) in deionised water. The area displayed is 0-55 minutes, and 80-250 mV.

G.2 Enzyme treatment E2

This section provides all the E2 data. First, the principle, experimental outline and results of the E2 enzyme activity are detailed. Second, the calibration data, calibration curves and example chromatograms are presented. Finally, all the HPLC chromatograms of the samples analysed are presented.

G.2.1 Enzyme activity determination

The Somogyi-Nelson assay is employed to determine the enzyme activity of the E2 pullulanase. The principle, experimental outline and results of the assay are detailed herein.

Principle

The Somogyi-Nelson (S/N) assay is widely used to measure carbohydrase (*e.g.*, cellulose, mannanase, pullulanase, glucanase, pectinase, *etc*.) activities against appropriate polysaccharides. Reducing sugars arise from the hydrolysis of glycosidic bonds between carbohydrates or carbohydrate and non-carbohydrate moieties (Gusakov *et al.*, 2011). Methods such as the 3,5-dinitrosalicylic acid (DNS) and S/N assay measure the reducing sugar hydrolysis products to determine carbohydrase activities. The S/N assay makes use of copper and arsenomolybdate reagents to form a coloured complex with the reducing sugars and measuring the absorbance at 540 nm (Anonymous, 1996; Nelson, 1944; Somogyi, 1945). The amount of reducing sugars present is determined against a calibration curve prepared from glucose standards.

Experimental

The S/N method as outlined by Sigma (Anonymous, 1996; Nelson, 1944; Somogyi, 1945) was followed in order to determine the activity of the E2 pullulanase. The reagents used in the procedure are outlined in Table G.2.1. Three separate tests (T1, T2 and T3) were carried out at a 1000× dilution of the enzyme. Each test was performed in triplicate (replicates are denoted as a, b and c) and the measurements were determined at 546 nm on a Perkin Elmer Lamda 25 UV/VIS Spectrometer.

Table G.2.1 Supplier and lot number details for the reagents used to carry out the Somogyi-Nelson determination of the Sigma pullulanase activity.

Reagent	Supplier	Lot number
Sodium acetate trihydrate	Merck	1033486
Hydrochloric acid	Merck	104261
Pullulan	Sigma-Aldrich	40K1170
D-(+)-Glucose	Sigma-Aldrich	129K0051
Sodium sulfate anhydrous	Merck	3455 D
Sodium carbonate anhydrous	BDH	BB102404H
Sodium potassium tartrate	Merck	1044639
Cupric sulfate pentahydrate	Merck	1040768
Sodium bicarbonate	Merck	42 B
Ammonium molybdate tetrahydrate	Sigma-Aldrich	BCBD2746V
Sulfuric acid	Merck	1045579
Pullulanase (E2)	Sigma-Aldrich	SLBB6227

Results

This section provides the results for the S/N determination of the E2 pullulanase activity.

Table G.2.2 Triplicate glucose standard absorbance values for the Somogyi-Nelson determination of the E2 pullulanase activity.

Standards	Glucose /µmole	Absorbance at 546 nm /AU	Absorbance – blank /AU
S0a	0.0000	0.0336	0.0000
S1a	0.2002	0.1317	0.0981
S2a	0.4004	0.2309	0.1973
S3a	0.6006	0.3628	0.3292
S4a	0.8008	0.4642	0.4306
S5a	1.0010	0.5723	0.5387
S0b	0.0000	0.0338	0.0000
S1b	0.2002	0.1437	0.1099
S2b	0.4004	0.2619	0.2281
S3b	0.6006	0.3959	0.3621
S4b	0.8008	0.4995	0.4657
S5b	1.0010	0.6216	0.5878
S0c	0.0000	0.0340	0.0000
S1c	0.2002	0.1313	0.0973
S2c	0.4004	0.2367	0.2027
S3c	0.6006	0.3522	0.3182
S4c	0.8008	0.4768	0.4428
S5c	1.0010	0.6130	0.5790

S – standard, a/b/c – replicate, AU – absorbance units

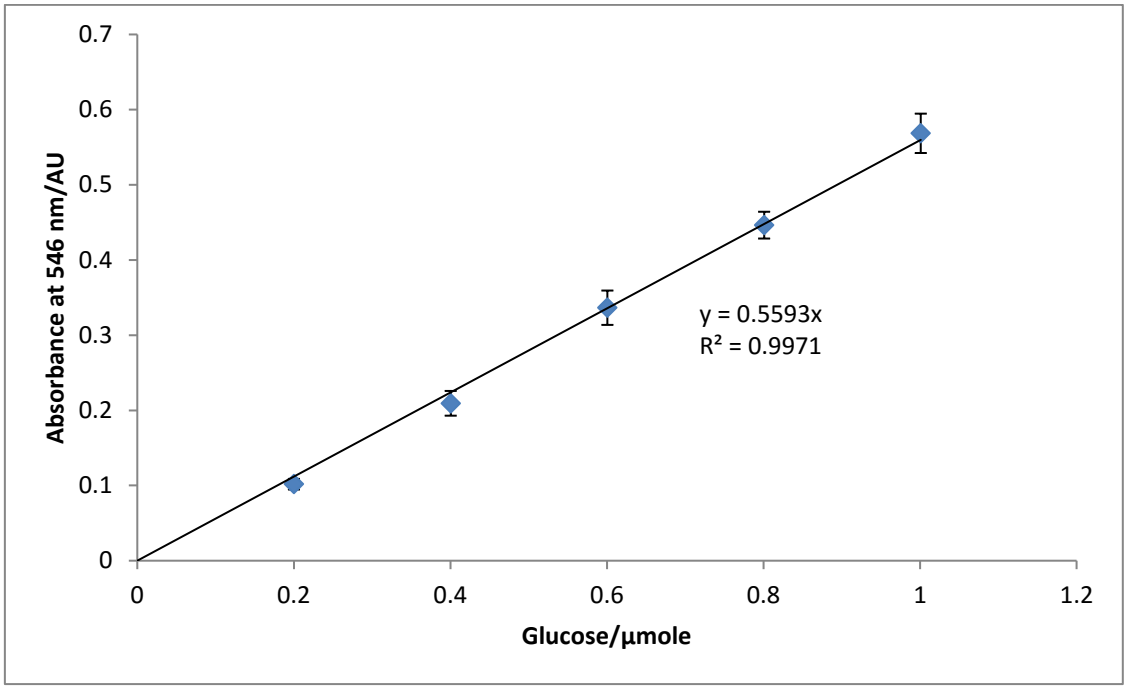

Figure G.2.1: Calibration curve derived from the average of three triplicate analyses of glucose released from pullulan substrate to determine the E2 pullulanase activity by the Somogyi-Nelson method.

Table G.2.3 Absorbance results and determined enzyme activity units by the Somogyi-Nelson method for the E2 pullulanase.

Test	Glucose /µmole	Absorbance – enzyme blank /AU	Test activity /U mL^{-1}	Undiluted activity /U mL^{-1}
T1a	0.1797	0.1005	1.8	1797
T1b	0.1736	0.0971	1.7	1736
T1c	0.1888	0.1056	1.9	1888
T2a	0.1999	0.1118	2.0	1999
T2b	0.1738	0.0972	1.7	1738
T2c	0.1759	0.0984	1.8	1759
T3a	0.1718	0.0961	1.7	1718
T3b	0.2001	0.1119	2.0	2001
T3c	0.1965	0.1099	2.0	1965
Range			1.7 - 2.0	1718 – 2001
Average			1.8	1845
Standard deviation			0.1	119
Relative standard deviation/%			6.5	6.5

T – test, a/b/c – replicate, AU – absorbance unit, U – enzyme activity unit

The averaged results of the three tests, each performed in triplicate, of the enzyme activity for the E2 pullulanase by the Somogyi-Nelson assay is 1845 U mL^{-1}; where, one unit is said to liberate 1.0 µmole of maltotriose (measured as glucose) from pullulan per minute at pH 5.0 at 25 °C (Anonymous, 1996).

G.2.2 Calibration data

The details for the calibration standards, preparation of solutions and calibration curves are provided below.

Preparation of standards

Several sets of standards (labelled S1-S9) were each prepared from authentic malto-oligosaccharide standards ranging from DP2-DP7. The ranges covered the expected values of hydrolysate products in each of the samples treated with E2. The calibration ranges were also analysed to ensure that the ranges were within linear calibration regions for accurate determination of the hydrolysate products in the samples. Each of the standards used to prepare the stock solutions was dried *in vacuo*, over di-phosphorus pentoxide, at 40 °C for a minimum of 24 hours before preparation. The masses of the standards and the volumes and final concentrations of the stock solutions are provided in Table G.2.4. The stock solutions were prepared with A-grade volumetric flasks and the masses were recorded on an analytical balance (Denver Instruments SI-234) correct to 0.1 mg, which had been calibrated on the day of weighing. Aliquots of the stock solutions were then transferred to volumetric flasks with variable Eppendorf® pipettors (10-100 µL and 100-1000 µL) or A-grade graduated glass pipettes according to Table G.2.5. The solutions were again made to the mark with the sodium acetate buffer (20 mM), to prepare solutions S1-S9 with the concentrations detailed in Table G.2.6.

Table G.2.4 Preparation of calibration standards' stock solutions.

Standard	Dry mass /g	Stock /mL	Stock /mg L^{-1}
Gal	0.1016	100.0	1016
Man	0.0996	100.0	996
DP2	0.0993	100.0	993
DP3	0.1018	100.0	1018
DP4	0.0118	10.0	1180
DP5	0.0110	10.0	1100
DP6	0.0115	10.0	1150
DP7	0.0114	10.0	1140

Gal – galactose, Man – mannose, DP2 – maltose, DP3 – maltotriose, DP4 – maltotetraose, DP5 – maltopentaose, DP6 – maltohexaose, DP7 – maltoheptaose

Table G.2.5 Volumes of stock solutions pipetted and made to volume (25.0 mL) in 20 mM sodium acetate buffer to prepare calibration standards S1 – S9.

Standard	Volume pipetted/mL								
	S1[a]	S2	S3	S4	S5	S6	S7	S8	S9
Gal	0.200	0.125	0.625	1.250	2.000	1.990	4.000	4.000	0
Man	0.200	0.100	0.175	0.250	0.375	0.375	1.125	0	2.500
DP2	0.200	0.125	0.150	0.250	0.375	0.375	0.500	0	0
DP3	0.200	2.000	2.625	3.250	4.500	4.510	5.000	0	0
DP4	0.200	1.250	1.875	2.750	3.400	0	0	0	0
DP5	1.000	0.625	0.875	1.125	1.500	1.500	0	0	0
DP6	0.300	0.125	0.250	0.450	0.700	0.700	0	0	0
DP7	0.200	0.050	0.125	0.250	0.400	0.400	0	0.550	0.550

[a] Prepared to 100.0 mL instead of 25.0 mL

Gal – galactose, Man – mannose, DP2 – maltose, DP3 – maltotriose, DP4 – maltotetraose, DP5 – maltopentaose, DP6 – maltohexaose, DP7 – maltoheptaose

Table G.2.6 Final concentrations of calibration standards S1-S9 prepared in 20 mM sodium acetate buffer.

Standard	Final concentration/mg L^{-1}								
	S1	S2	S3	S4	S5	S6	S7	S8	S9
Gal	2.0	5.1	25.4	50.8	81.3	81.3	163	163	0
Man	2.0	4.0	7.0	10.0	14.9	14.9	44.8	0	99.6
DP2	2.0	5.0	6.0	9.9	14.9	14.9	19.9	0	0
DP3	2.0	81.4	107	132	183	183	204	0	0
DP4	2.4	59.0	88.5	130	160	0.0	0	0	0
DP5	11.0	27.5	38.5	49.5	66.0	66.0	0	0	0
DP6	3.4	5.7	11.5	20.7	32.2	32.2	0	0	0
DP7	2.3	2.3	5.7	11.4	18.2	18.2	0	25.1	25.1

Gal – galactose, Man – mannose, DP2 – maltose, DP3 – maltotriose, DP4 – maltotetraose, DP5 – maltopentaose, DP6 – maltohexaose, DP7 – maltoheptaose

Calibrations

The HPAEC-PAD data and calibration curves are provided in this section. An HPAEC-PAD chromatogram is provided for the various calibration standards used for each set of analyses. The calibration standards were injected at the beginning and the end of each set of samples analyses. A total of five sample sets and five standard sets were analysed. The average RF of the standards injected before and after each sample set was used to determine the concentration of the respective peaks in the bracketed sample set. Calibration A represents the average of Set 1 and Set 2 of the standards, Calibration B the average of Set 2 and Set 3, whilst Calibration C is the average of Set 4 and Set 5. The calibration data and curves for Calibration A are found

in Table G.2.7 and Figure G.2.2, respectively. The calibration data and curves for Calibration B are found in Table G.2.8 and Figure G.2.4, respectively. The calibration data and curves for Calibration C are found in Table G.2.9 and Figure G.2.6, respectively. An example of three of the calibration standards is given in Figure G.2.3, Figure G.2.5 and Figure G.2.7 to illustrate the peak separation, heights, retention time identification, and integration parameters used to determine the calibration responses.

Table G.2.7 Average calibration data for the Calibration A standards. The calibration data for galactose and mannose are not included as they were not used for quantitation.

Standard	Height /mV	Concentration /mg L^{-1}	RF /mV L mg^{-1}	R^2
DP2	2.951	2.0	1.475	0.9990
	6.772	5.0	1.354	
	7.629	6.0	1.271	
	11.954	9.9	1.207	
	18.023	14.9	1.210	
DP3	59.755	81.4	0.734	0.9826
	75.676	107	0.708	
	80.998	132	0.612	
	107.190	183	0.585	
DP4	3.032	2.4	1.2633	0.9958
	34.859	59.0	0.5908	
	51.695	88.5	0.5841	
	69.476	130	0.5353	
DP5	7.676	11.0	0.6978	0.9952
	14.544	27.5	0.5289	
	21.309	38.5	0.5535	
	25.336	49.5	0.5118	
	32.420	66.0	0.4912	
DP6	2.266	3.4	0.6665	0.9946
	3.542	5.7	0.6213	
	6.495	11.5	0.5647	
	11.295	20.7	0.5457	
	15.646	32.2	0.4859	
DP7	1.854	2.3	0.8062	0.9826
	3.004	5.7	0.5270	
	6.411	11.4	0.5624	
	8.578	18.2	0.4713	

RF – response factor, R^2 – coefficient of determination, DP2 – maltose,
DP3 – maltotriose, DP4 – maltotetraose, DP5 – maltopentaose, DP6 – maltohexaose,
DP7 – maltoheptaose

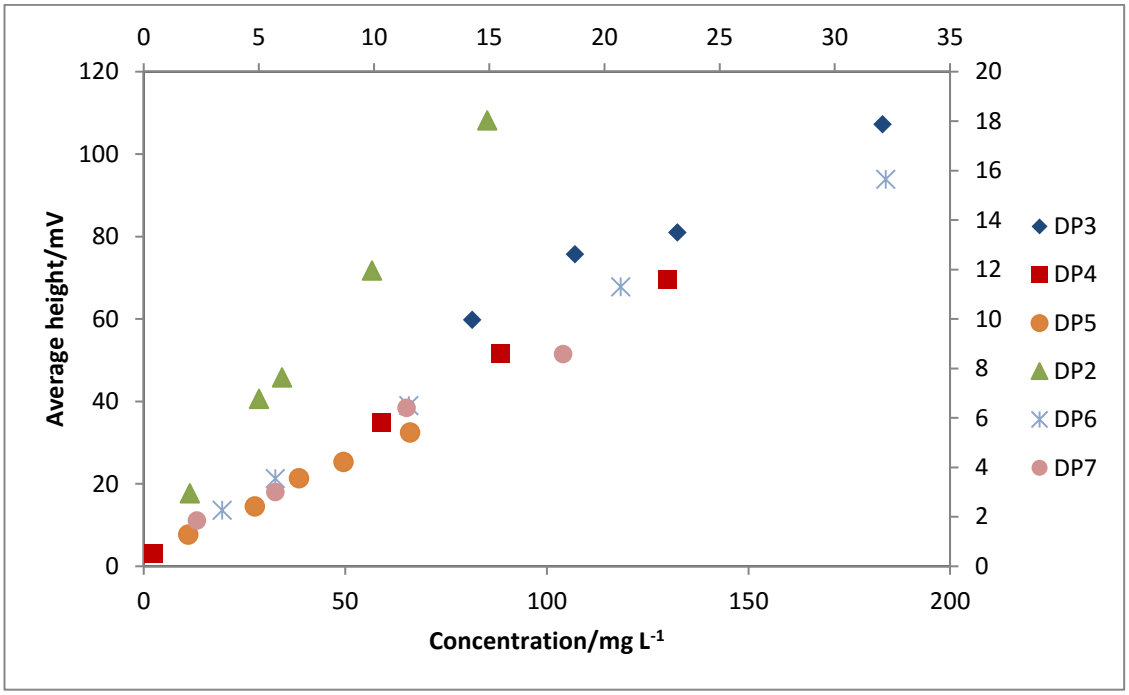

Figure G.2.2: HPAEC-PAD calibration curves for the averaged data collected for the standards making up Calibration A. These standards include maltose (DP2), maltotriose (DP3), maltotetraose (DP4), maltopentaose (DP5), maltohexaose (DP6) and maltoheptaose (DP7). These data were used to determine the quantities of the same hydrolysate products in the first set of samples analysed.

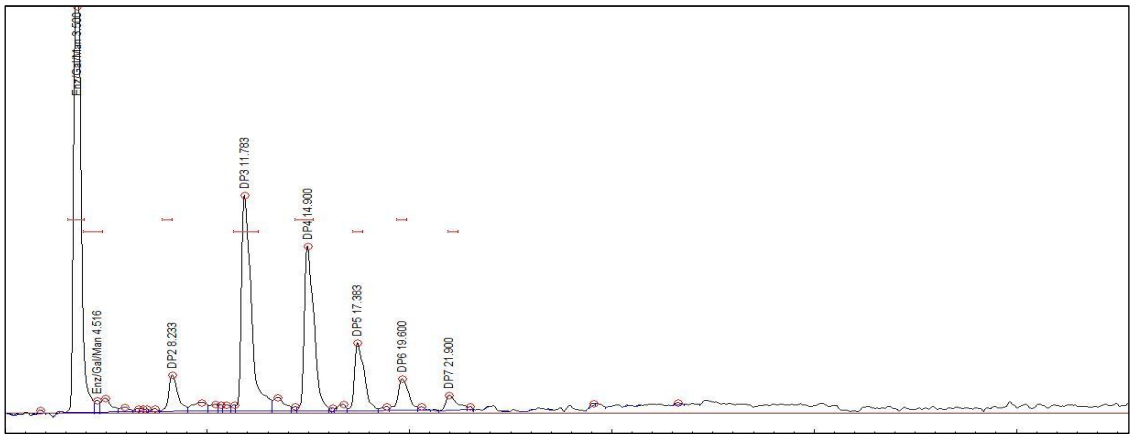

Figure G.2.3: Chromatogram for standard S5 run in the first set of the Calibration A standards. This standard contains galactose (Gal, 81.3 mg L^{-1}), mannose (Man, 14.9 mg L^{-1}), maltose (DP2, 14.9 mg L^{-1}), maltotriose (DP3, 183 mg L^{-1}), maltotetraose (DP4, 160 mg L^{-1}), maltopentaose (DP5, 66.0 mg L^{-1}), maltohexaose (DP6, 32.2 mg L^{-1}) and maltoheptaose (DP7, 18.2 mg L^{-1}). Man and galactose co-elute in the region of the enzyme (Enz) matrix as indicated. The area displayed is 0-55 minutes and −10-200 mV, with the detector sensitivity set at 1000 nA.

Table G.2.8 Average calibration data for the Calibration B standards. The calibration data for galactose and mannose are not included as they were not used for quantitation.

Standard	Height /mV	Concentration /mg L^{-1}	RF /mV L mg^{-1}	R^2
DP2	3.027	2.0	1.514	0.9940
	7.255	5.0	1.451	
	8.789	6.0	1.465	
	11.865	9.9	1.198	
	17.482	14.9	1.173	
	24.063	19.9	1.209	
DP3	60.793	81.4	0.747	0.9937
	79.753	107	0.746	
	88.562	132	0.669	
	120.047	183	0.655	
	134.696	204	0.662	
DP4	3.676	2.4	1.5317	0.9851
	36.449	59.0	0.6178	
	53.011	88.5	0.5990	
	71.342	130	0.5496	
	79.710	161	0.4966	
DP5	8.643	11.0	0.7857	0.9932
	15.309	27.5	0.5567	
	21.915	38.5	0.5692	
	26.799	49.5	0.5414	
	32.774	66.0	0.4966	
DP6	2.242	3.4	0.6594	0.9840
	3.856	5.7	0.6765	
	7.311	11.5	0.6357	
	11.386	20.7	0.5500	
	15.284	32.2	0.4747	
DP7	1.609	2.3	0.6997	0.9893
	3.404	5.7	0.5971	
	6.293	11.4	0.5520	
	8.611	18.2	0.4732	

RF – response factor, R^2 – coefficient of determination, DP2 – maltose, DP3 – maltotriose, DP4 – maltotetraose, DP5 – maltopentaose, DP6 – maltohexaose, DP7 – maltoheptaose

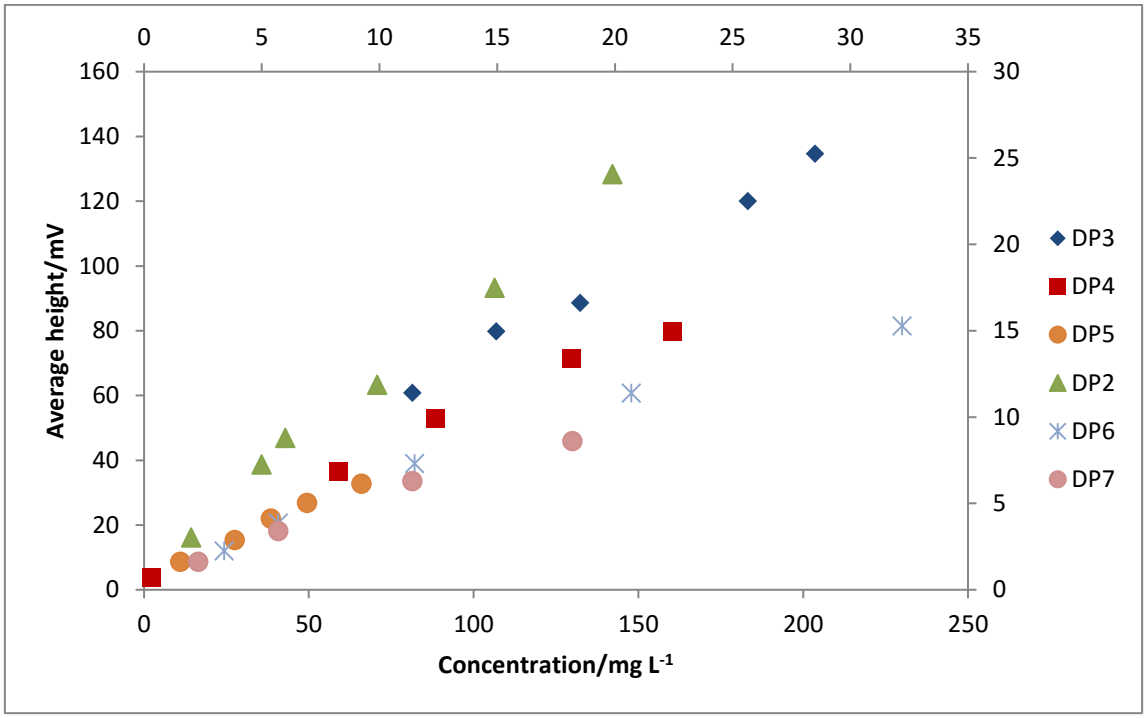

Figure G.2.4: HPAEC-PAD calibration curves for the averaged data collected for the standards making up Calibration B. These standards include maltose (DP2), maltotriose (DP3), maltotetraose (DP4), maltopentaose (DP5), maltohexaose (DP6) and maltoheptaose (DP7). These data were used to determine the quantities of the same hydrolysate products in the second and third set of samples run concurrently.

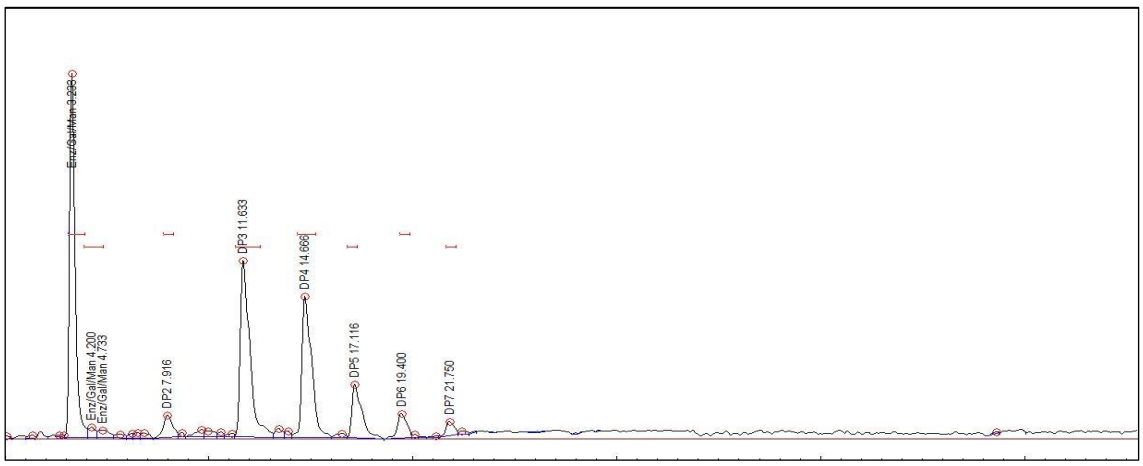

Figure G.2.5: Chromatogram for standard S4 run after the third set of samples in Calibration B. This standard contains galactose (Gal, 50.8 mg L^{-1}), mannose (Man, 10.0 mg L^{-1}), maltose (DP2, 9.9 mg L^{-1}), maltotriose (DP3, 132 mg L^{-1}), maltotetraose (DP4, 130 mg L^{-1}), maltopentaose (DP5, 49.5 mg L^{-1}), maltohexaose (DP6, 20.7 mg L^{-1}) and maltoheptaose (DP7, 11.4 mg L^{-1}). Man and galactose co-elute in the region of the enzyme (Enz) matrix as indicated. The area displayed is 0-55 minutes, and −10-200 mV, with the detector sensitivity set at 1000 nA.

Table G.2.9 Average calibration data for the Calibration C standards. The calibration data for galactose and mannose are not included as they were not used for quantitation.

Standard	Height /mV	Concentration /mg L^{-1}	RF /mV L mg^{-1}	R^2
DP2	17.971	5.0	3.594	0.9971
	21.421	6.0	3.570	
	31.0095	9.9	3.284	
	46.885	14.9	3.147	
	65.121	19.9	3.272	
DP3	202.912	81.4	2.493	0.9867
	250.024	107	2.339	
	291.811	132	2.206	
	491.097	204	2.412	
DP4	106.8095	59.0	1.8103	0.9978
	153.022	88.5	1.7291	
	206.8715	130	1.5938	
	258.078	161	1.6080	
DP5	42.718	27.5	1.5534	0.9922
	58.127	38.5	1.5098	
	66.966	49.5	1.3528	
	85.241	66.0	1.2915	
DP6	10.996	5.7	1.9290	0.9891
	17.362	11.5	1.5097	
	30.649	20.7	1.4806	
	40.788	32.2	1.2667	
DP7	3.033	2.3	1.3187	0.9951
	8.101	5.7	1.4211	
	15.022	11.4	1.3177	
	21.360	18.2	1.1736	
	31.153	25.1	1.2412	

RF – response factor, R^2 – coefficient of determination, DP2 – maltose,
DP3 – maltotriose, DP4 – maltotetraose, DP5 – maltopentaose, DP6 – maltohexaose,
DP7 – maltoheptaose

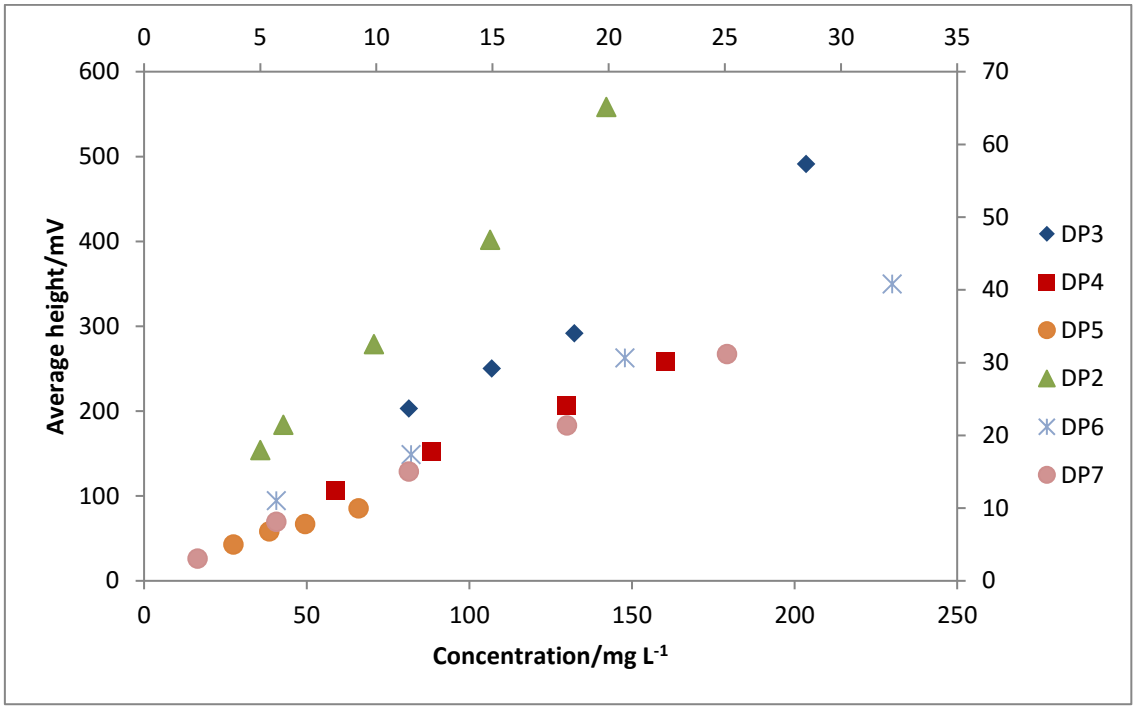

Figure G.2.6: HPAEC-PAD calibration curves for the averaged data collected for the standards making up Calibration C. These standards include maltose (DP2), maltotriose (DP3), maltotetraose (DP4), maltopentaose (DP5), maltohexaose (DP6) and maltoheptaose (DP7). These data were used to determine the quantities of the same hydrolysate products in the fourth and fifth set of samples run concurrently.

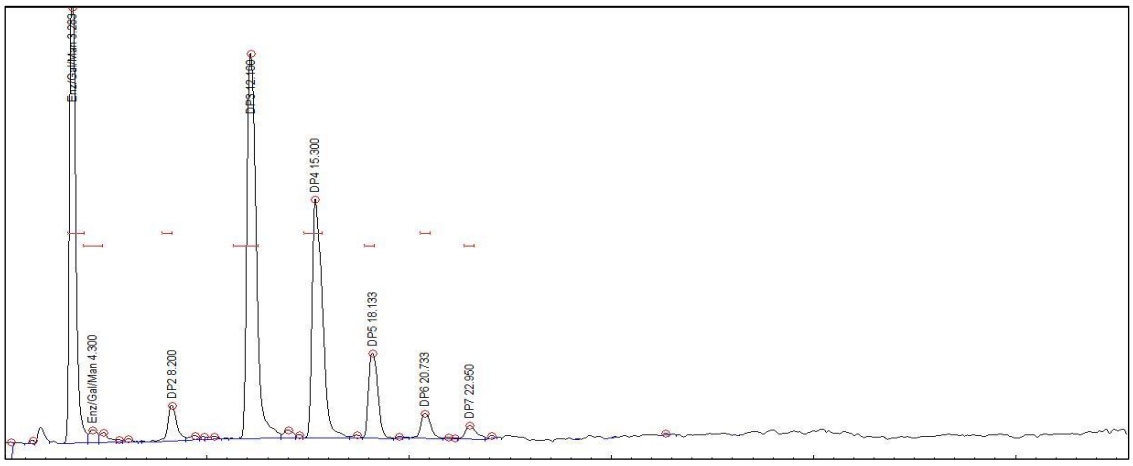

Figure G.2.7: Chromatogram for standard S3 run before the fourth set of samples in Calibration C. This standard contains galactose (Gal, 25.4 mg L^{-1}), mannose (Man, 7.0 mg L^{-1}), maltose (DP2, 6.0 mg L^{-1}), maltotriose (DP3, 107 mg L^{-1}), maltotetraose (DP4, 88.5 mg L^{-1}), maltopentaose (DP5, 38.5 mg L^{-1}), maltohexaose (DP6, 11.5 mg L^{-1}) and maltoheptaose (DP7, 5.7 mg L^{-1}). Man and galactose co-elute in the region of the enzyme (Enz) matrix as indicated. The area displayed is 0-55 minutes, and 30-300 mV, with the detector sensitivity set at 300 nA.

G.2.3 High performance liquid chromatograms

This section provides one each of the chromatograms for a blank and the five samples analysed in E2 at a detector response of either 1000 nA or 300 nA. The peaks are identified against authentic standards; including, maltose (DP2), maltotriose (DP3), maltotetraose (DP4), maltopentaose (DP5), maltohexaose (DP6) and maltoheptaose (DP7). Maltooctaose (DP8), maltononaose (DP9) and maltodecaose (DP10) are inferred in the elution profiles. The insert in each chromatogram provides the corresponding retention times and integrated peak heights for the identified components in Figure G.2.8 to Figure G.2.19. In all cases, the enzyme matrix, galactose and mannose components co-eluted and were labelled and identified as Enz/Gal/Man in each sample. The individual components within the co-eluting peaks could not be quantified. Figure G.2.20 provides an illustration comparing five chromatograms of the elution profiles of a galactose and DP7 standard, a mannose and DP7 standard, against an enzyme blank, a S5 standard (containing both galactose and mannose along with the DP2-DP7 standards) and the FB2 F2 sample. The accompanying Table G.2.10 provides a summary of the respective chromatogram retention times and integrated peak heights for the co-eluting peaks.

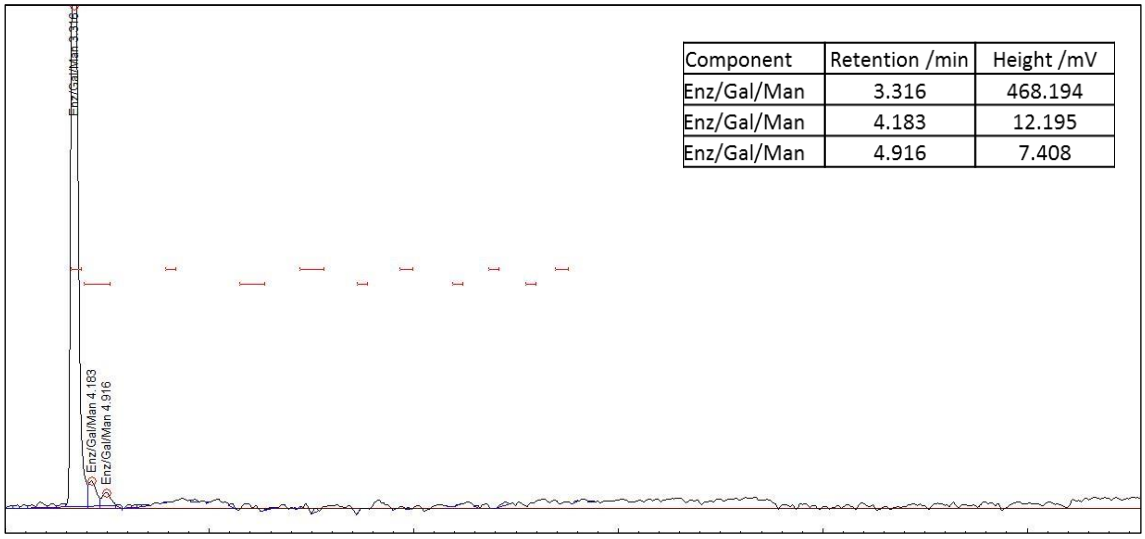

Component	Retention /min	Height /mV
Enz/Gal/Man	3.316	468.194
Enz/Gal/Man	4.183	12.195
Enz/Gal/Man	4.916	7.408

Figure G.2.8: Chromatogram of a blank sample containing 15 U of E2 pullulanase in 20 mM sodium acetate buffer. The chromatogram area displayed is 0-55 minutes and −10-200 mV, with the detector sensitivity set at 1000 nA.

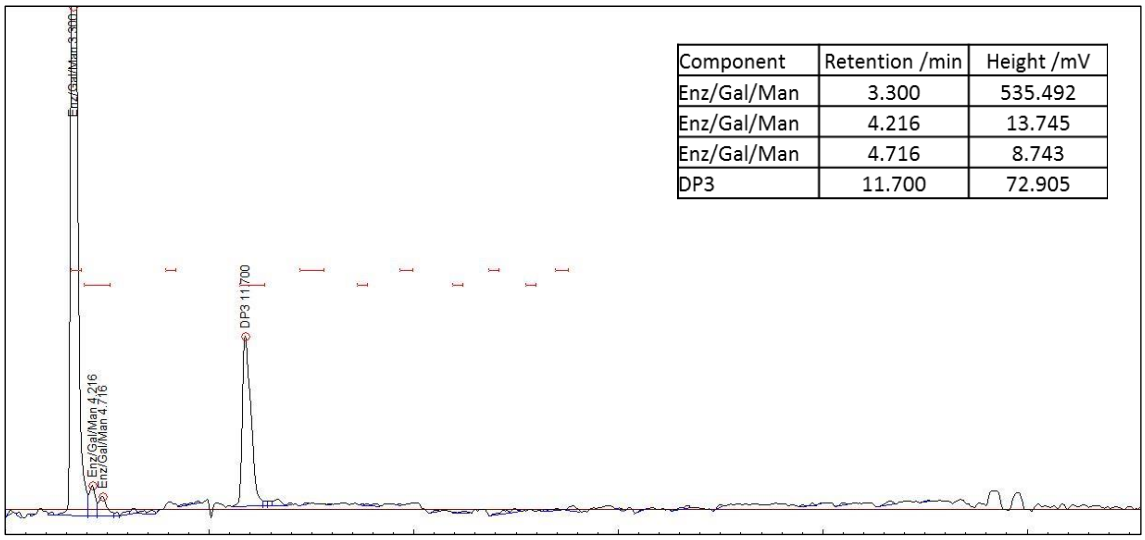

Component	Retention /min	Height /mV
Enz/Gal/Man	3.300	535.492
Enz/Gal/Man	4.216	13.745
Enz/Gal/Man	4.716	8.743
DP3	11.700	72.905

Figure G.2.9: Chromatogram of a 101 mg L^{-1} pullulan sample (from sample set 1) hydrolysed with 15 U of E2 pullulanase in 20 mM sodium acetate buffer. The chromatogram area displayed is 0-55 minutes and −10-200 mV, with the detector sensitivity set at 1000 nA.

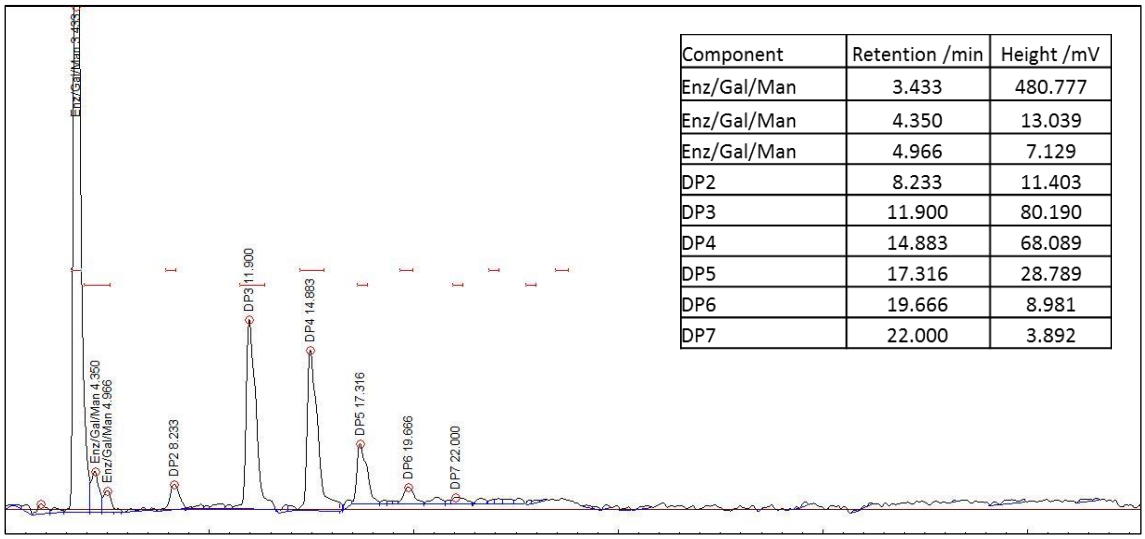

Component	Retention /min	Height /mV
Enz/Gal/Man	3.433	480.777
Enz/Gal/Man	4.350	13.039
Enz/Gal/Man	4.966	7.129
DP2	8.233	11.403
DP3	11.900	80.190
DP4	14.883	68.089
DP5	17.316	28.789
DP6	19.666	8.981
DP7	22.000	3.892

Figure G.2.10: Chromatogram of a 360 mg L^{-1} PB2 sample (from sample set 1) hydrolysed with 15 U of E2 pullulanase in 20 mM sodium acetate buffer. The chromatogram area displayed is 0-55 minutes and −10-200 mV, with the detector sensitivity set at 1000 nA.

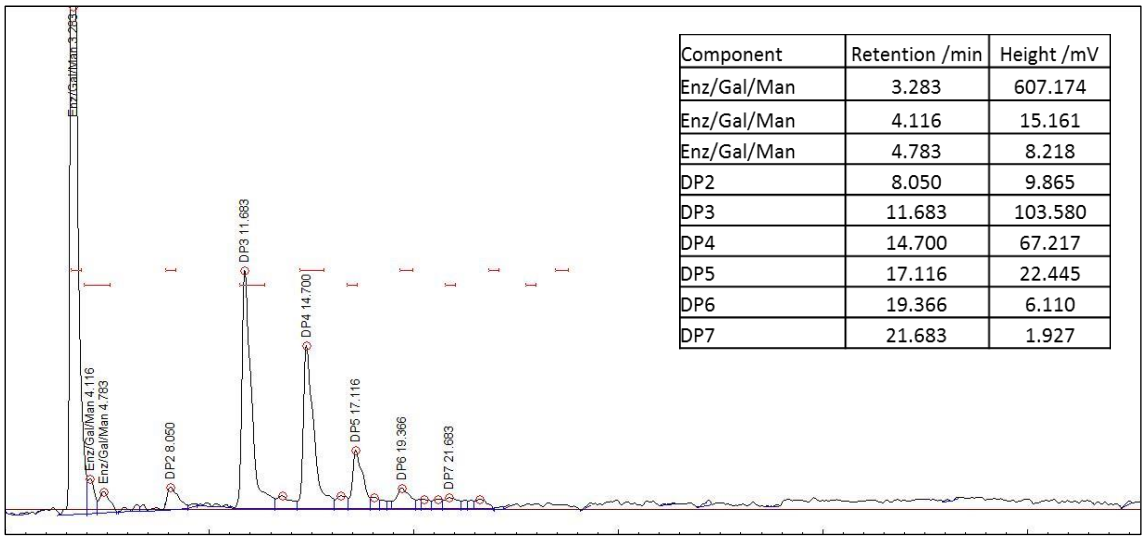

Component	Retention /min	Height /mV
Enz/Gal/Man	3.283	607.174
Enz/Gal/Man	4.116	15.161
Enz/Gal/Man	4.783	8.218
DP2	8.050	9.865
DP3	11.683	103.580
DP4	14.700	67.217
DP5	17.116	22.445
DP6	19.366	6.110
DP7	21.683	1.927

Figure G.2.11: Chromatogram of a 374 mg L^{-1} PB7 sample (from sample set 3) hydrolysed with 15 U of E2 pullulanase in 20 mM sodium acetate buffer. The chromatogram area displayed is 0-55 minutes and −10-200 mV, with the detector sensitivity set at 1000 nA.

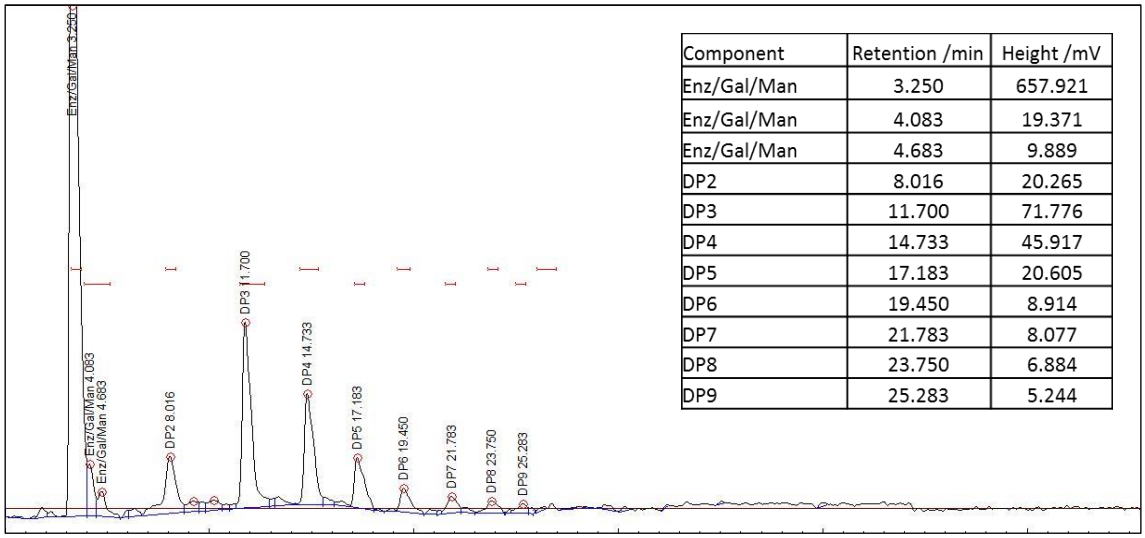

Component	Retention /min	Height /mV
Enz/Gal/Man	3.250	657.921
Enz/Gal/Man	4.083	19.371
Enz/Gal/Man	4.683	9.889
DP2	8.016	20.265
DP3	11.700	71.776
DP4	14.733	45.917
DP5	17.183	20.605
DP6	19.450	8.914
DP7	21.783	8.077
DP8	23.750	6.884
DP9	25.283	5.244

Figure G.2.12: Chromatogram of a 379 mg L^{-1} FB2 sample (from sample set 3) hydrolysed with 15 U of E2 pullulanase in 20 mM sodium acetate buffer. The chromatogram area displayed is 0-55 minutes and −10-200 mV, with the detector sensitivity set at 1000 nA.

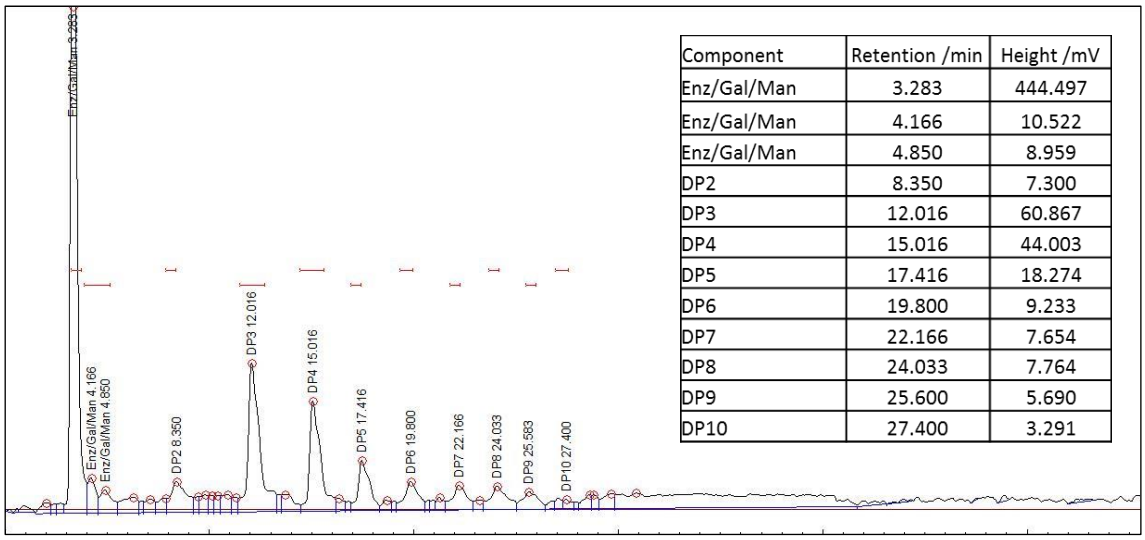

Component	Retention /min	Height /mV
Enz/Gal/Man	3.283	444.497
Enz/Gal/Man	4.166	10.522
Enz/Gal/Man	4.850	8.959
DP2	8.350	7.300
DP3	12.016	60.867
DP4	15.016	44.003
DP5	17.416	18.274
DP6	19.800	9.233
DP7	22.166	7.654
DP8	24.033	7.764
DP9	25.600	5.690
DP10	27.400	3.291

Figure G.2.13: Chromatogram of a 357 mg L^{-1} FB2 F2 sample (from sample set 3) hydrolysed with 15 U of E2 pullulanase in 20 mM sodium acetate buffer. The chromatogram area displayed is 0-55 minutes and −10-200 mV, with the detector sensitivity set at 1000 nA.

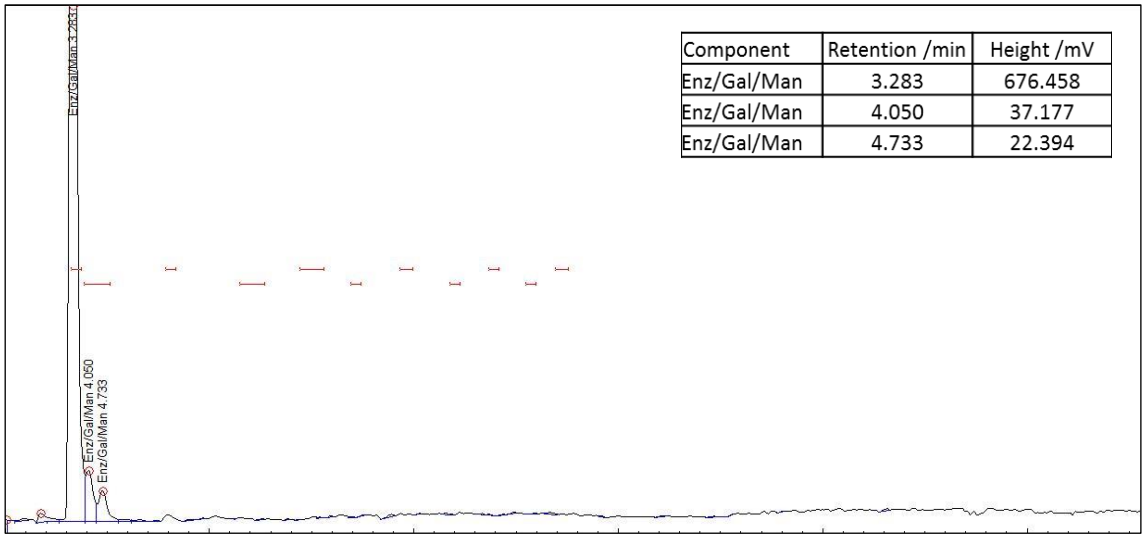

Component	Retention /min	Height /mV
Enz/Gal/Man	3.283	676.458
Enz/Gal/Man	4.050	37.177
Enz/Gal/Man	4.733	22.394

Figure G.2.14: Chromatogram of a blank sample (from sample set 4) hydrolysed with 15 U of E2 pullulanase in 20 mM sodium acetate buffer. The chromatogram area displayed is 0-55 minutes and 30-400 mV, with the detector sensitivity set at 300 nA.

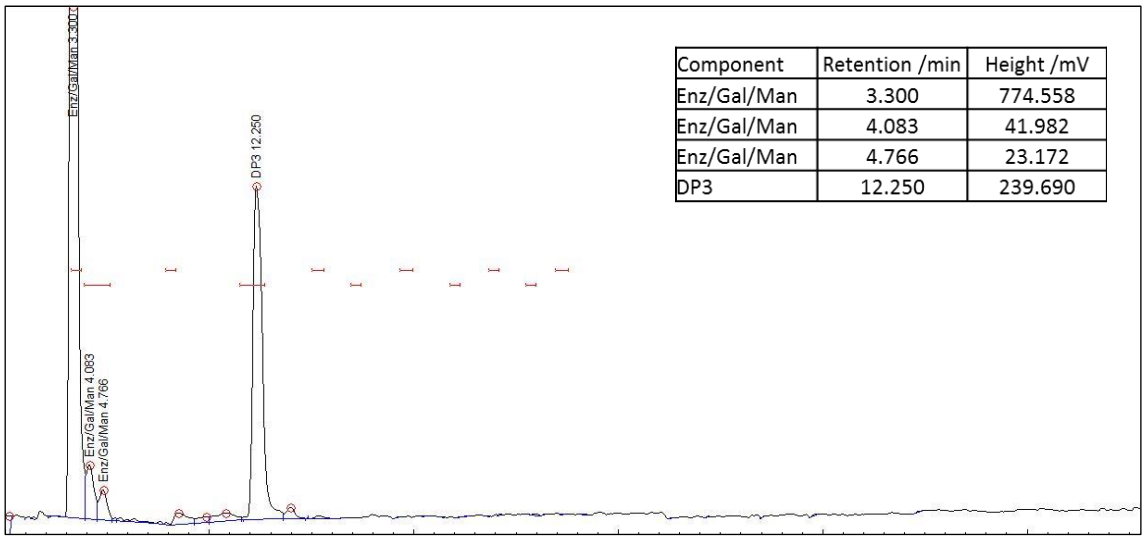

Component	Retention /min	Height /mV
Enz/Gal/Man	3.300	774.558
Enz/Gal/Man	4.083	41.982
Enz/Gal/Man	4.766	23.172
DP3	12.250	239.690

Figure G.2.15: Chromatogram of a 101 mg L^{-1} pullulan sample (from sample set 4) hydrolysed with 15 U of E2 pullulanase in 20 mM sodium acetate buffer. The chromatogram area displayed is 0-55 minutes and 30-400 mV, with the detector sensitivity set at 300 nA.

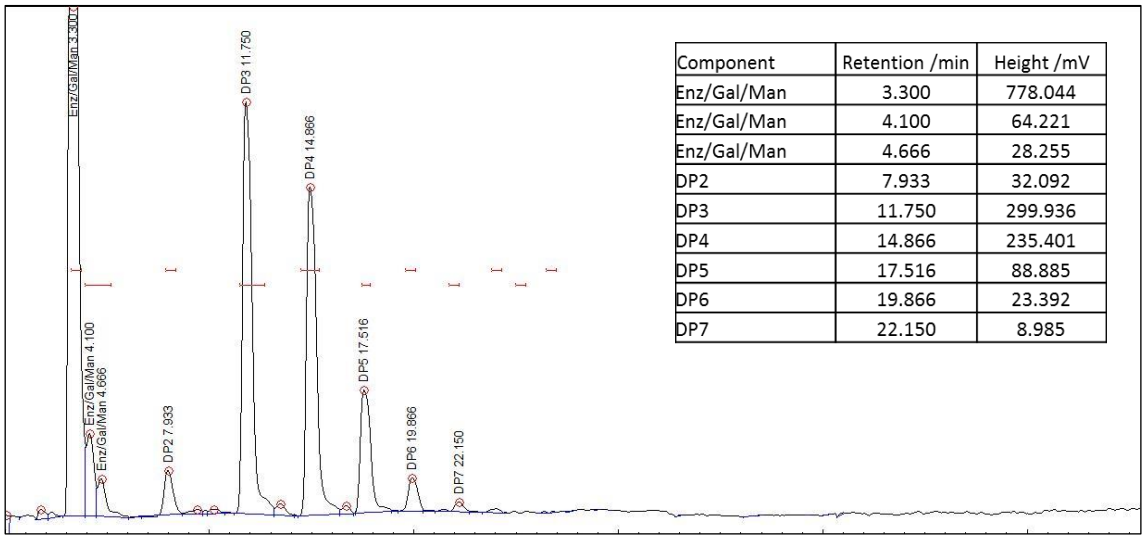

Component	Retention /min	Height /mV
Enz/Gal/Man	3.300	778.044
Enz/Gal/Man	4.100	64.221
Enz/Gal/Man	4.666	28.255
DP2	7.933	32.092
DP3	11.750	299.936
DP4	14.866	235.401
DP5	17.516	88.885
DP6	19.866	23.392
DP7	22.150	8.985

Figure G.2.16: Chromatogram of a 360 mg L^{-1} PB2 sample (from sample set 5) hydrolysed with 15 U of E2 pullulanase in 20 mM sodium acetate buffer. The chromatogram area displayed is 0-55 minutes and 30-400 mV, with the detector sensitivity set at 300 nA.

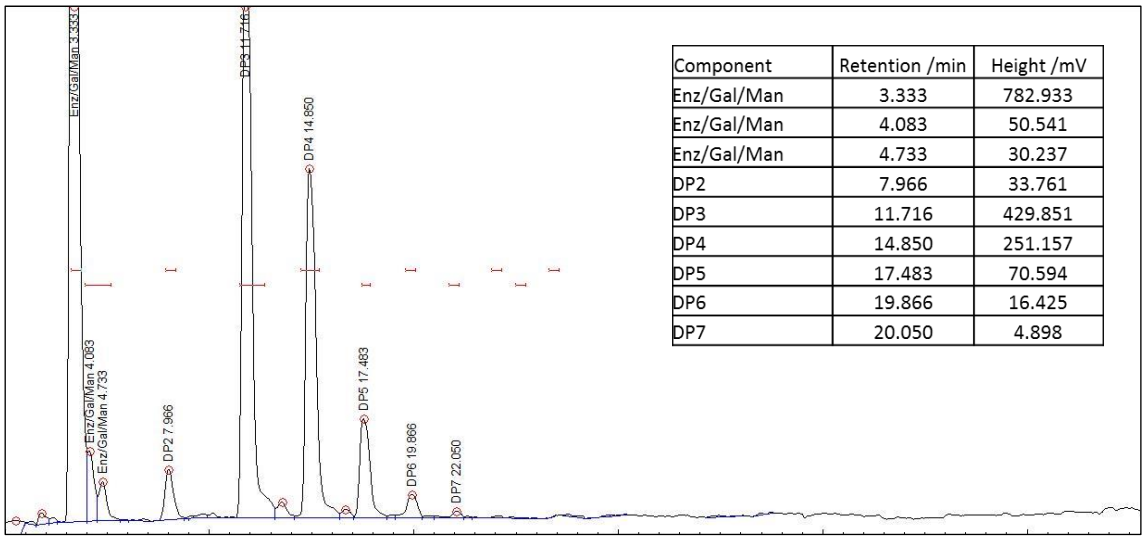

Component	Retention /min	Height /mV
Enz/Gal/Man	3.333	782.933
Enz/Gal/Man	4.083	50.541
Enz/Gal/Man	4.733	30.237
DP2	7.966	33.761
DP3	11.716	429.851
DP4	14.850	251.157
DP5	17.483	70.594
DP6	19.866	16.425
DP7	20.050	4.898

Figure G.2.17: Chromatogram of a 374 mg L^{-1} PB7 sample (from sample set 5) hydrolysed with 15 U of E2 pullulanase in 20 mM sodium acetate buffer. The chromatogram area displayed is 0-55 minutes and 30-400 mV, with the detector sensitivity set at 300 nA.

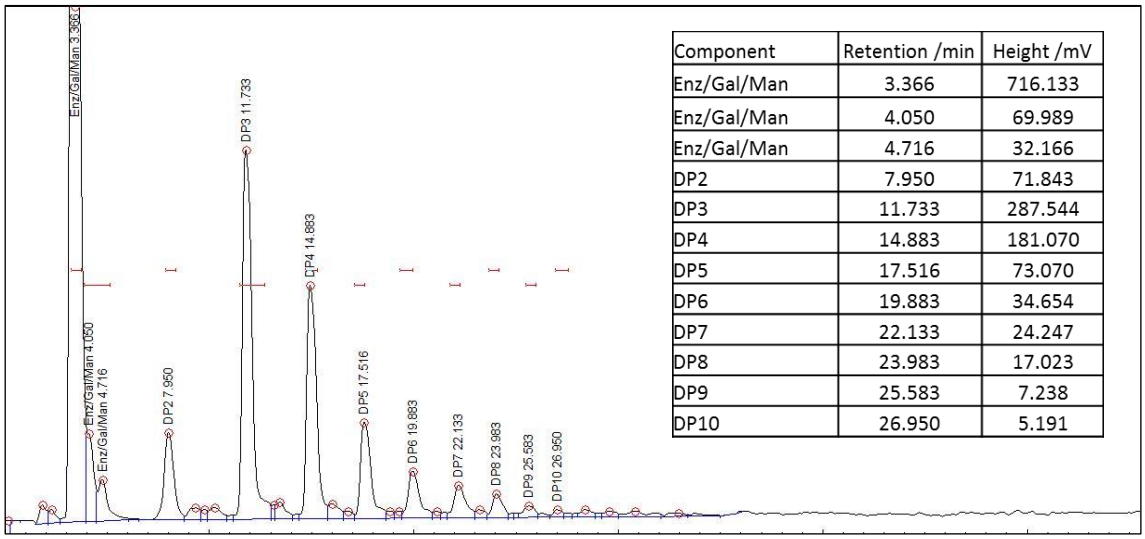

Component	Retention /min	Height /mV
Enz/Gal/Man	3.366	716.133
Enz/Gal/Man	4.050	69.989
Enz/Gal/Man	4.716	32.166
DP2	7.950	71.843
DP3	11.733	287.544
DP4	14.883	181.070
DP5	17.516	73.070
DP6	19.883	34.654
DP7	22.133	24.247
DP8	23.983	17.023
DP9	25.583	7.238
DP10	26.950	5.191

Figure G.2.18: Chromatogram of a 379 mg L^{-1} FB2 sample (from sample set 5) hydrolysed with 15 U of E2 pullulanase in 20 mM sodium acetate buffer. The chromatogram area displayed is 0-55 minutes and 30-400 mV, with the detector sensitivity set at 300 nA.

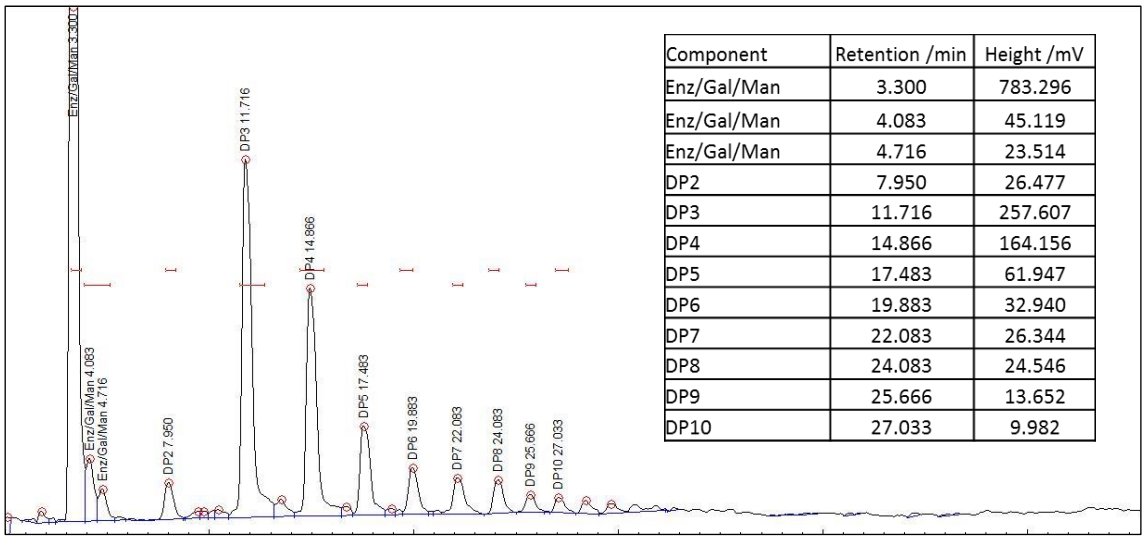

Component	Retention /min	Height /mV
Enz/Gal/Man	3.300	783.296
Enz/Gal/Man	4.083	45.119
Enz/Gal/Man	4.716	23.514
DP2	7.950	26.477
DP3	11.716	257.607
DP4	14.866	164.156
DP5	17.483	61.947
DP6	19.883	32.940
DP7	22.083	26.344
DP8	24.083	24.546
DP9	25.666	13.652
DP10	27.033	9.982

Figure G.2.19: Chromatogram of a 357 mg L^{-1} FB2 F2 sample (from sample set 5) hydrolysed with 15 U of E2 pullulanase in 20 mM sodium acetate buffer. The chromatogram area displayed is 0-55 minutes and 30-400 mV, with the detector sensitivity set at 300 nA.

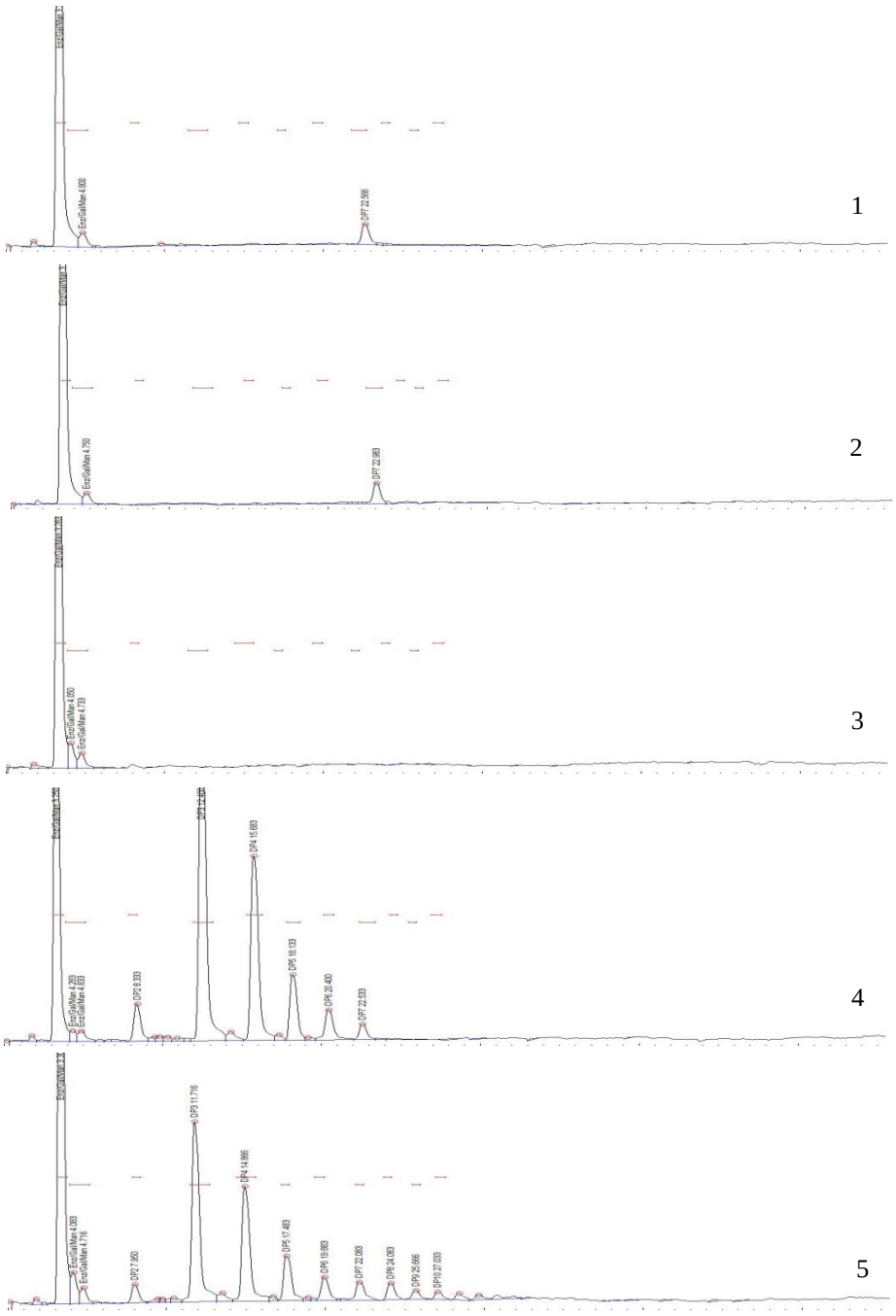

Figure G.2.20: Chromatograms comparing the elution profiles of galactose (1: 163 mg L^{-1} Gal and DP7), mannose (2: 99.6 mg L^{-1} Man and DP7), an enzyme blank (3: 15 U E2 pullulanase), a mixed standard (4: 81.3 mg L^{-1} Gal + 14.9 mg L^{-1} Man + DP2 + DP3 + DP4 + DP5 + DP6 + DP7) and a sample (5: 357 mg L^{-1} FB2 F2).

Table G.2.10 Applicable component amount and respective peak retention times and response heights for chromatograms 1-5 from Figure G.2.20.

Chromatogram	Components	Amounts	RT /min	Height /mV
1	Galactose + DP7	163 mg L^{-1}	3.350	663.110
			4.860	20.899
			20.916	30.533
2	Mannose + DP7	99.6 mg L^{-1}	3.250	738.052
			4.750	16.753
			22.983	23.513
3	Enzyme blank	15 U	3.283	674.971
			4.050	35.201
			4.733	20.680
4	Galactose + Mannose + DP2-DP7	81.3 mg L^{-1} + 14.9 mg L^{-1}	3.250	739.958
			4.283	15.698
			4.883	14.657
5	FB2 F2	357 mg L^{-1}	3.300	783.300
			4.083	45.119
			4.716	23.513

RT – retention time

G.3 References

Anonymous (1996) Enzymatic Assay of Pullulanase. Sigma-Aldrich, 14 October 2014, <https://www.sigmaaldrich.com/content/dam/sigma-aldrich/docs/Sigma/Enzyme_Assay/pullulanase.pdf>

Gusakov AV, Kondratyeva EG and Sinitsyn AP (2011). Comparison of Two Methods for Assaying Reducing Sugars in the Determination of Carbohydrase Activities. *International Journal of Analytical Chemistry*. **2011** 4.

Nelson N (1944). A photometric adaptation of the Somogyi method for the determination of glucose. *The Journal of Biological Chemistry*. **153** 375-380.

Nilsson GS, Richardson S, Huber A, Torto N, Laurell T and Gorton L (2001). Microdialysis clean-up and sampling in enzyme-based methods for the characterisation of starch. *Carbohydrate Polymers*. **46** (1):59-68.

Somogyi M (1945). A new reagent for the determination of sugars. *Journal of Biological Chemistry*. **160** 61-68.

Torto N, Lobelo B and Gorton L (2000). Determination of saccharides in wastewater from the beverage industry by microdialysis sampling, microbore high performance anion exchange chromatography and integrated pulsed electrochemical detection. *Analyst*. **125** (8):1379-1381.